Non-Isocyanate Polyurethanes (NIPUs) Recycling and Upcycling

A manuscript submitted to the

University of Liège (Uliege) & University of the Basque Country (UPV/EHU)

Liège, Belgium, September 2025

PhD Thesis

Presented by

Maliheh Razavi-Esfali

Under the supervision of

Dr. Christophe Detrembleur (Uliege)

Dr. Haritz Sardon (UPV/EHU)

LIÈGE université

eman ta zabal zazu

Universidad del País Vasco

Euskal Herriko Unibertsitatea

Thesis Jury

Prof. Christophe Detrembleur	University of Liege (Promoter)
Prof. Haritz Sardon	UPV/EHU (Co-promoter)
Prof. Loïc Quinton	University of Liege (President)
Prof. Lourdes Irusta	UPV/EHU (Secretary)
Prof. Steven De Meester	Ghent University
Prof. Zeljko Tomovic	Eindhoven University of Technology
Dr. Bruno Grignard	University of Liege

Abstract

This thesis tackles two critical challenges in polymer science: the urgent need to eliminate toxic isocyanates from polyurethane (PU) synthesis, and the limited advancement of efficient strategies for producing non-isocyanate polyurethanes (NIPUs) from recycled conventional polymers or existing NIPU materials. These challenges extend beyond chemistry and engineering-they are also deeply environmental and societal, as plastic waste continues to accumulate in landfills and natural ecosystems. In response, this work aims to develop high-performance NIPUs directly from polymer waste, thereby contributing to the creation of sustainable materials engineered for circularity. This research was carried out within the framework of the NIPU-EJD European project, which is dedicated to advancing the field of non-isocyanate polyurethanes.

The thesis begins with the design of poly(oxazolidone-co-thioether) materials using CO_2-based poly(oxo-carbonates) as precursors. Through a mild, catalyst-free depolymerization via aminolysis, followed by UV-initiated thiol-ene click chemistry, functional poly(oxazolidones) with high thermal stability and post-functionalization potential were synthesized. This process illustrates a promising upcycling route that transforms CO_2-based polymer waste into chemically rich, structurally diverse NIPUs.

The focus then shifts to the chemical recycling of polyhydroxyurethane (PHU) foams, which were depolymerized under both acidic and alkaline aqueous conditions to recover key monomers- namely, polyglycerol and diamines. These recovered building blocks were reintegrated into foam formulations to create second-generation NIPU foams with up to 63% recycled content, without compromising structural integrity or thermal properties. This approach demonstrates, for the first time, that true closed-loop recycling is achievable for NIPU foams under mild, scalable conditions. Recognizing that technical feasibility alone is insufficient to evaluate sustainability, a comprehensive cradle-to-grave Life Cycle Assessment (LCA) was conducted to quantify the environmental trade-offs associated with NIPU recycling. This analysis identified several environmental hotspots- particularly related to electricity use, solvent recovery, and neutralization agents- where optimization was necessary. Based on these findings, a refined process was developed that significantly reduced the environmental impacts of foam recycling, particularly in terms of climate change and resource use.

Overall, this work demonstrates that the synthesis of functional, high-performance NIPUs from polymer waste is not only possible, but also scalable and environmentally improvable. It offers a blueprint for combining green chemistry, waste valorization, and systems thinking to build sustainable polymer technologies from the ground up.

Résumé

Cette thèse aborde deux défis majeurs de la science des polymères : la nécessité urgente d'éliminer les isocyanates toxiques dans la synthèse des polyuréthanes (PU) et l'insuffisance de stratégies efficaces pour produire des polyuréthanes non isocyanates (NIPU) à partir de polymères conventionnels ou de matériaux NIPU recyclés. Ces enjeux dépassent le cadre de la chimie et de l'ingénierie ; ils sont également profondément environnementaux et sociétaux, dans un contexte où les déchets plastiques continuent de s'accumuler dans les décharges et les écosystèmes naturels. En réponse, ce travail vise à développer des NIPU de haute performance directement à partir de déchets polymères, contribuant ainsi à la création de matériaux durables conçus pour l'économie circulaire. Cette recherche a été menée dans le cadre du projet européen NIPU-EJD, dédié à l'avancement du domaine des polyuréthanes non isocyanates.

La thèse débute par la conception de matériaux à base de poly(oxazolidone-co-thioéther), en utilisant des poly(oxo-carbonates) issus du CO_2 comme précurseurs. Grâce à une dépolymérisation douce, sans catalyseur, par aminolyse, suivie d'une chimie "click" thiol-ène initiée par UV, des poly(oxazolidones) fonctionnels à haute stabilité thermique et à fort potentiel de post-fonctionnalisation ont été synthétisés. Ce procédé illustre une voie prometteuse de surcyclage, transformant des déchets polymères à base de CO_2 en NIPU chimiquement riches et structurellement diversifiés.

L'attention se porte ensuite sur le recyclage chimique des mousses de polyhydroxyuréthane (PHU), dépolymérisées dans des conditions aqueuses acides et basiques pour récupérer les monomères clés- à savoir, le polyglycérol et les diamines. Ces éléments constitutifs récupérés ont été réintégrés dans de nouvelles formulations de mousses, donnant naissance à des mousses NIPU de seconde génération contenant jusqu'à 63 % de matière recyclée, sans compromettre leur intégrité structurelle ni leurs propriétés thermiques. Cette approche démontre, pour la première fois, qu'un recyclage en boucle fermée est réalisable pour les mousses NIPU dans des conditions douces et évolutives.

Conscients que la faisabilité technique ne suffit pas à évaluer la durabilité, une Analyse de Cycle de Vie (ACV) complète, de type "du berceau à la tombe", a été réalisée pour quantifier les compromis environnementaux liés au recyclage des NIPU. Cette analyse a mis en évidence plusieurs points critiques- notamment l'utilisation d'électricité, la récupération des solvants et les agents de neutralisation- qui ont nécessité des optimisations. À partir de ces résultats, un procédé amélioré a été développé, réduisant significativement les impacts environnementaux du recyclage des mousses, en particulier en termes de changement climatique et d'utilisation des ressources. Dans l'ensemble, ce travail démontre que la synthèse de NIPU fonctionnels et performants à partir de déchets polymères est non seulement réalisable, mais également évolutive et améliorable sur le plan environnemental. Il propose une feuille de route pour combiner chimie verte, valorisation des déchets et pensée systémique afin de construire des technologies polymères durables dès leur conception.

Resumen

Esta tesis aborda dos desafíos fundamentales en la ciencia de los polímeros: la urgente necesidad de eliminar los isocianatos tóxicos en la síntesis de los poliuretanos (PU), y el desarrollo limitado de estrategias eficaces para producir poliuretanos no-isocianatos (NIPU) a partir del reciclaje de polímeros convencionales o de materiales NIPU ya existentes. Estos retos no solo son de carácter químico y técnico, sino también profundamente ambientales y sociales, ya que los residuos plásticos siguen acumulándose en vertederos y ecosistemas naturales. En respuesta a ello, este trabajo tiene como objetivo desarrollar NIPU de alto rendimiento directamente a partir de residuos poliméricos, contribuyendo así a la creación de materiales sostenibles diseñados para la circularidad. Esta investigación se realizó en el marco del proyecto europeo NIPU-EJD, dedicado al avance del campo de los poliuretanos no-isocianatos.

La tesis comienza con el diseño de materiales de tipo poli(oxazolidona-co-tioéter), utilizando poli(oxo-carbonatos) derivados del CO_2 como precursores. Mediante una despolimerización suave y sin catalizador por aminólisis, seguida de una reacción tipo click tiol-eno iniciada por radiación UV, se sintetizaron poli(oxazolidonas) funcionales con alta estabilidad térmica y gran potencial de post-funcionalización. Este proceso representa una vía prometedora de suprarreciclaje, transformando residuos poliméricos derivados del CO_2 en NIPU estructuralmente diversos y químicamente enriquecidos.

El enfoque se traslada luego al reciclaje químico de espumas de poli(hidroxiuretano) (PHU), las cuales fueron despolimerizadas en condiciones acuosas ácidas y alcalinas para recuperar monómeros clave: poliglicerol y diaminas. Estos bloques de construcción recuperados se reintrodujeron en nuevas formulaciones para producir espumas NIPU de segunda generación, con hasta un 63 % de contenido reciclado, sin comprometer la integridad estructural ni las propiedades térmicas. Esta estrategia demuestra, por primera vez, que el reciclaje en circuito cerrado es posible para espumas NIPU bajo condiciones suaves y escalables.

Conscientes de que la viabilidad técnica por sí sola no basta para evaluar la sostenibilidad, se llevó a cabo un Análisis de Ciclo de Vida (ACV) completo, desde la cuna hasta la tumba, para cuantificar los impactos ambientales asociados al reciclaje de NIPU. Este análisis identificó varios puntos críticos- en particular el consumo de electricidad, la recuperación de disolventes y el uso de agentes de neutralización- que requerían optimización. A partir de estos hallazgos, se desarrolló un proceso mejorado que redujo significativamente los impactos ambientales del reciclaje de espumas, especialmente en lo relativo al cambio climático y al uso de recursos. En conjunto, este trabajo demuestra que la síntesis de NIPU funcionales y de alto rendimiento a partir de residuos poliméricos no solo es posible, sino también escalable y ambientalmente optimizable. Ofrece una hoja de ruta para combinar la química verde, la valorización de residuos y el pensamiento sistémico con el fin de construir tecnologías poliméricas sostenibles desde su origen.

“Just when the caterpillar thought the world was over, it became a butterfly.” ~ Chuang Tzu

ACKNOWLEDGEMENTS

Three years and six months have passed- a journey marked not only by scientific exploration but also by profound personal growth. Throughout the course of this thesis (thanks to the European Union, which funded this work through the NIPU-EJD 955700 MSCA project), I had the unique privilege of living in three different places across two countries. This experience extended far beyond the lab bench, shaping me in ways I never anticipated. Each place introduced new challenges, new people, and new perspectives that helped shape who I am today- not only as a researcher, but as a human being.

I began my PhD at CERM in Belgium, where I took my first steps into the world of polymer chemistry research. It was a time of intense learning- scientifically, emotionally, and mentally- as I began to navigate the layered realities of academic life. I moved across borders to a new continent, stepping into a different language, lifestyle, and working culture. This transition was both demanding and deeply enriching. It stretched me far beyond the technical dimensions of research and taught me to embrace uncertainty, develop resilience, and grow through transformation. Now, as I look back on this extraordinary journey, I realize that the completion of this thesis would not have been possible without the unwavering support, guidance, and kindness of many people. To each of you, I offer my deepest gratitude.

First and foremost, I would like to express my sincere gratitude to my supervisors, Dr. Christophe Detrembleur and Prof. Haritz Sardon, for their invaluable support throughout the course of my doctoral studies. Their scientific expertise and thoughtful guidance, have been fundamental in shaping both the direction and quality of this work. It has been a privilege to work under their supervision. I am equally thankful to my co-supervisor, Dr. Bruno Grignard, for his constructive feedback, and insightful discussions at every stage of this research. I would like to thank all the jury members: Dr. Loïc Quinton, Dr. Lourdes Irusta, Dr. Steven De Meester, Dr. Zeljko Tomovic, Dr. Bruno Grignard for doing me the honor of being part of this thesis jury and for taking the time to evaluate my work.

A big thank you to the technicians at CERM (Belgium)- Grégory Cartigny, Valérie Collard, Charlotte Dannemark, and Martine Dejeneffe. Your technical support, and patience, helped a lot in my daily lab work.

To my dear friends in CERM, Lionel and Manas- thank you for being there through all the ups and downs. Whether we were celebrating small victories or dragging ourselves through long, exhausting days, we shared it all with a cup of coffee or tea. Those moments of venting, laughing, and simply being there for each other made this journey bearable, even meaningful. To my office-mates at CERM-Anna, Charlene, François, Sofia, Lilas, Dagmara, and Oscar- thank you for the laughter, the shared frustrations, and the small daily moments that made those early PhD years more enjoyable. Some of the best memories of that period were made in our shared space, and I'll always be grateful for that.

I also wish to thank all CERM colleagues who were part of this chapter of my journey: Pascal, Thomas, Maksimov, Maksim, Raphaël, Hamid, Laétitia, and Victor- thank you for the discussions, the occasional

help, and for simply being part of the experience. And a special thanks to Fabiana, whose kind presence and support during the very first month of my PhD helped me settle in and find my footing when everything still felt new and uncertain.

Out of lab, to Yasi and Sahar, this year marks the 11th anniversary of our friendship. Yasi, I still can't believe how lucky I was to have you by my side- not only from afar, but right here in Belgium during some of the most difficult moments of this journey. Your presence, your help, and simply your being there meant more than words can express. Thank you for being a true friend- through time, distance, and everything in between. To Sahar, it's hard to believe that it's been seven years since we last met in person, and yet, our friendship has remained as alive and meaningful as ever. Through our weekly talks, shared memories, and the way we've stood by each other in difficult times, you've shown me the true essence of lasting friendship. No distance can weaken what we've built, and I'm so grateful to still walk this journey of life with you by my side.

The second chapter of my PhD took place at my second university in Spain, a place that felt like home from the very beginning. I had the privilege of meeting truly amazing people who made this phase of my journey both joyful and inspiring. Among those I shared an office with, Akshaya, who started this journey alongside me, was a constant companion through it all. Flore and Alice, whose determination to learn Persian always brought a smile to my face, added a touch of warmth and curiosity to our daily life. Ainhoa introduced me to the hidden gems of San Sebastián, while Aritz and Oihane never hesitated to help me whenever I needed a hand- your kindness did not go unnoticed. To Md Shafi, who always called me a workaholic (though he himself was working until 8 PM!)- thank you for the friendly banter and shared motivation. Marta Mestre, your energy was simply contagious and lifted the mood of everyone around you. Jaya, thank you not only for introducing me to the incredible culture of India, but also for the good memories we shared along the way. Ekta, always on the move from lab to lab, your presence brought such dynamism to the group. To Gabriela and Ander, although we didn't spend much time together, I truly admire you both. To Beatriz, always with a smile, and Claire, who brought a sense of calm and positivity- thank you. Ane, with whom I shared so much of this time online, and Jon, a technical expert and someone you could always count on- I appreciate you both deeply. Gabby, your kindness and gentle soul left a lasting impression. Bigge, your quiet determination was always inspiring. Tansu, and Giulia thank you for never hesitating to help and for the good moments we shared- your support meant a lot. Aitor, your calmness was so comforting.

I also had the pleasure of working alongside a group of brilliant postdocs- individuals so humble and approachable that it was easy to forget I was surrounded by minds that could easily be future Nobel Prize nominees. To Ion, I call you the man who knows everything! You always helped all of us. To Gabriel, thank you for never hesitating to help whenever I reached out- your enthusiasm whenever you were making a new foam was amazing! Lucas, your sharp intellect combined with your activism was always inspiring. I'm still waiting for the day we show up at a manifestation- scooters and all! Louis, I honestly don't know how you managed to keep a smile in literally every situation- your calm positivity

was contagious, and I have no doubt you'll make an amazing professor. Xabier, you always carried the wisdom and confidence of someone who had seen it all- thank you for the quiet strength and knowledge you brought into every conversation. And to Letizia, your passion for organic chemistry and the way you carried yourself in science truly motivated me- thank you for the inspiration. Thank you to Daniele, for your generous technical help and for opening a window into the wider technical world beyond the lab.

I would also like to warmly thank Dr. Marta Ximenis, whose kindness, encouragement, and practical support meant a great deal to me. Beyond your scientific advice and your remarkable talent for organizing and managing the lab, you offered guidance that extended far beyond technical matters. I learned so much from your unique blend of leadership and friendship, and I feel truly fortunate to have shared this journey with you.

A heartfelt thank you to Elena, the artistic soul behind the templates, figures, and the cover of this thesis. Your fresh perspective, creativity, and thoughtful design brought beauty and clarity to the science. You are truly an artist with a brilliant mind, and I'm so grateful our paths crossed.

To Fateme, my dear friend outside the lab- thank you for being my weekend companion during my time in San Sebastián. From cooking together to playing games, and even canceling more trips than we actually took, the time we spent was full of laughter and comfort. The moments we shared were simple, honest, and unforgettable. I'll always cherish them.

During my industrial secondment at Materia Nova, I had the privilege of working under the supervision of Olivier Talon, who introduced me to the world of Life Cycle Assessment (LCA). Every minute spent with him felt like an entire day of hands-on training- clear, insightful, and deeply educational. His guidance not only sharpened my technical understanding but also gave me a broader and more meaningful perspective on sustainability in science.

During the NIPU-EJD project, I had the chance to meet incredible people who made this scientific journey so much more than just research. To Connie and Anne Goldberg, the heart and mind behind the project- your leadership, clarity, and wisdom were a constant source of inspiration. Anne, You are a truly motivated and wise woman, and I often found myself thinking, "If I could one day be as influential as Anne..."

We were twelve PhD students, coming from different corners of the world, united by a common goal and shared curiosity. Among them, I want to express my deepest gratitude to Luca, with whom I shared the first two years of this journey. From that first invitation to grab a coffee, to the last moment when you turned off the light of our shared hood- you were there. We shared experiments, frustrations, jokes, silence, and endless conversations. You were not just a colleague- you were my everyday companion, a true friend, and someone whose presence made everything lighter and more meaningful. To Marco, thank you for all your help- and for showing me what it means to live a truly sustainable life. To Florent- you were a kind one since the beginning! Keep diving my friend! To Christy, from day one I felt a deep connection with you- you have a rare and profound soul that stays with people. To Francesca, your

resilience and your love of nature inspired me. To Katherine, your energy was unmatched, you are a very strong girl. Federico, I always remember you on a motorcycle exploring the world; Nicholas, I understand more than anyone the difficulties you faced, and your resilience is admiring; Pavithra, your smile and warm friendship; Guillem, your endless humor- thank you all for making this project unforgettable. And Pauline, though we shared only a few coffees in San Sebastián, they somehow tasted different, and I'll remember them fondly.

To my father, whose absence I've felt deeply- I wish you were here to witness this milestone. Your memory has accompanied me silently through every step of this journey, and I carry your strength with me always. To my family, the heart behind everything I do: my mother, Tahere, whose love, and quiet strength have been my constant anchor; thanks for providing all the spices and dried vegetable to make cooking easier and tastier. To me my sister Mahbi, your energy, our daily talks, and the emotions we've shared go far beyond sisterhood- what we have is a true and irreplaceable friendship; and Najme, I always miss sitting down for a simple cup of tea with you- and I always, always love you. To Arian, Benita, and Delana, my beloved nephew and nieces- your laughter, your joy, and your innocence were a healing force during the most stressful days. To Aran, thank you for bringing happiness into Mahbi's life, and by doing so, into mine as well. Your presence has added warmth and joy to our family. And thank you for always keeping a room ready for me in your house- I know it's symbolic… or maybe not! To Artemis and Arta, thank you for the joy and love you brought into my life, for your understanding, and for reminding me what truly matters beyond the world of research. To my relatives in Iran, thank you for surrounding me with love, warmth, and the comfort of delicious homemade food every time I had the chance to see you. Your care grounded me and reminded me of where I come from. To my friends across the world- Samira, Mahshid, Razie, Maryam, and many others- thank you for staying connected despite the distance, for cheering me on from afar, and for reminding me that friendship has no borders. Your presence in my life, even across time zones, brought me joy and strength during this journey.

And finally, to Babak- my love, my rock, my constant. You were with me through every moment of this journey: in every failure, every sleepless night, every moment of doubt. You were always there, steady and calm, with one sentence that I never stopped hearing: "I believe in you." Thank you for being my home through it all.

The number of people with whom I've shared this journey- and who have supported, inspired, or helped me along the way- is far greater than I could list here. It is truly impossible to name them all, but their presence has not gone unnoticed, and I carry their kindness and influence with deep gratitude.

از همگی سپاسگزارم!

Thank you all, Eskerrik asko danontzat, Gracias a todos, Merci a tous, Danke an alle!, Grazie a tutti! 谢谢你们所有人, তোমাদের সবাইকে ধন্যবাদ।, आप सभी का धन्यवाद।.

1 Table of Contents

List of Acronyms and Symbols

5CC: 5-membered cyclic carbonate

Bis(aCC): Bis(α-alkylidene cyclic carbonate)s

CAN: Covalent adaptable network

CC: Cyclic carbonate (except chapters 4 & 5)

CC: Climate Change (Chapters 4 & 5)

CO_2: Carbon dioxide

DBU: 1,8-diazabicyclo[5.4.0]undec-7-ene

DCM: Dichloromethane

DMC: dimethyl carbonate

DMF: Dimethylformamide

DMSO: Dimethylsulfoxide

DSC: Differential scanning calorimetry

EoL: End-of-Life

EU: European Union

EWG: Electro-withdrawing group

FTIR: Fourier Transform Infrared Spectroscopy

GC: Gel Content

GWP: Global Warming Potential

H_2SO_4: Sulfuric acid

HCl: Hydrochloric acid

LCA: Life cycle assessment

LCI: Life Cycle Inventory

LCIA: Life Cycle Impact Assessment

M_n: Number average molecular weight

M_w: Weight average molecular weight

***m*-XDA:** Metaxylylene diamine

NaOH: Sodium Hydroxide

NIPU: Non-isocyanate polyurethane

NIPUF: Non-isocyanate polyurethane foam

NMR: Nuclear Magnetic Resonance

PC: Polycarbonate

PG: Polyglycerol

PGC: Polyglycerol carbonate

PHU: Poly (hydroxy urethane)

POXa: Polyoxazolidone

PU: Polyurethane

PUF: Polyurethane foam

SEC: Size Exclusion Chromatography

SEM: Scanning Electron Microscopy

TBD: 1,5,7-Triazabicyclo[4.4.0]dec-5-ene

T_g: Glass-transition temperature

TGA: Thermogravimetric Analysis

THF: Tetrahydrofuran

TMPTC: trimethylolpropane tris-cyclic carbonate

αCC: 4,4-Dimethyl-5-methylene-1,3-dioxolan-2-one

Chapter 1. Introduction

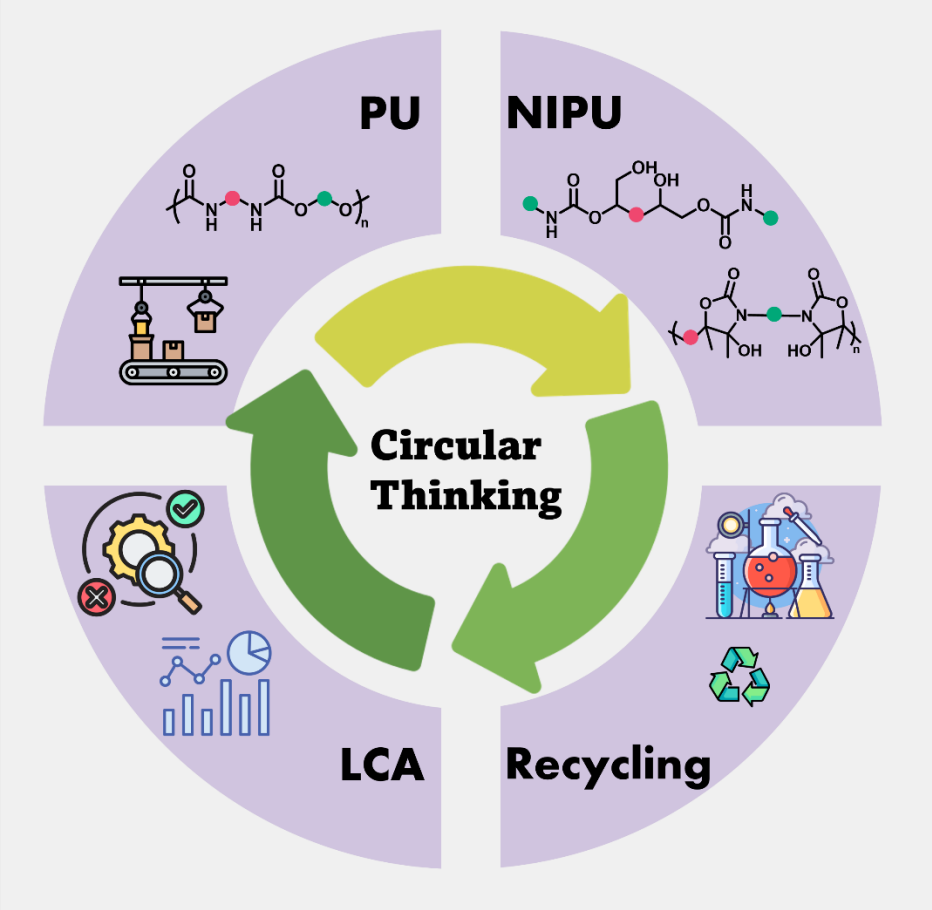

1 Circular Thinking

"Don't plant anything but integrity. You'll harvest what you sow." *Rumi, Persian philosopher*

Every action has a consequence. This fundamental principle, inspired by ancient wisdom and validated by modern scientific inquiry, teaches us that no system operates in isolation. From minor gestures to major innovation, each act has a series of reactions- some immediate, some extend through several generations.

This widely accepted principle indicates that our decisions - what we build, consume, and discard- echo through time. In the modern world, where human impact flows into nearly every corner of the biosphere, these consequences are visible and measurable. Recent progress has made major improvements in daily living standards but also inserted intense pressure on Earth's natural systems. The Earth now has a population of over 8 billion people which pushes both consumption and waste to levels never seen before. This puts immense pressure on ecosystems and necessitates a systematic rethinking of human lifestyles and consumption patterns.

With this in mind, the framework of sustainability emerges as both a necessity and an ethical obligation. The goal of sustainability is to harmonize human development with the planet's ecological boundaries, ensuring that today's actions do not deplete the resources so that the future generations could meet their needs. It integrates environmental, economic, and social dimensions and emphasizes that these pillars are deeply interconnected as represented in **Fig. 1**.

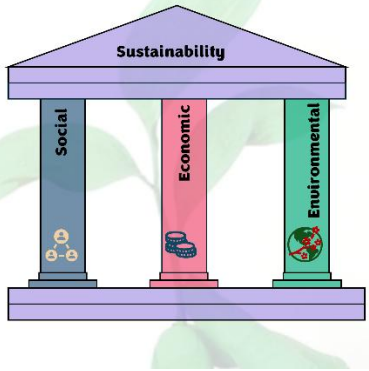

Fig. 1. Three pillars of sustainability.

True sustainability exists in the intersection of these three pillars. It requires balancing environmental limits with the basic rights and dignity of the entire population. This framework functions as the basis for policy creation and innovation methods while directing consumption habits across both global and local scales. In 2015, a key step was taken to put sustainability into practice, when the United Nations adopted the 2030 Agenda for Sustainable Development [1]. They introduced 17 Sustainable Development Goals (SDGs), a comprehensive roadmap addressing everything from poverty and clean water to climate action and responsible production (**Fig. 2**). These goals emphasize that environmental sustainability is inseparable from social justice and economic transformation.

Fig. 2. 17 sustainable development goals (https://www.globalgoals.org/).

Plastics sit at the heart of this sustainability agenda. People used to see plastics as revolutionary materials because they were durable and versatile yet cheap, but they now function as the complicated relationship between convenience in consumption and environmental harm. The production and use of plastics have grown dramatically since the 1950s. By 2022, global output had climbed to 400 million metric tons, with more than two-thirds composed of disposable products that quickly become waste and their production is estimated to increase by 2–3 times by 2050 [2]. Data indicate that approximately 7.0 billion tons of plastic waste have accumulated globally - 19% has been incinerated, 50% buried in landfills, 22% dispersed into the natural environment, and a mere 9% successfully recycled [3]. Plastics demonstrate a dual reality:

technological progress and ecological threat. Although it extends food shelf life, decreases transport emissions, and helps healthcare initiatives, its long-lasting nature results in continuing environmental pollution. Every year, 8 million tons of plastic are released into oceans, affecting over 700 marine species [4]. Their fabrication, utilization, and disposal require reconsideration through a lifecycle perspective. To contribute to sustainability, plastics need well-considered design and responsible organization from cradle to grave. Lifecycle thinking is important to mitigate their impacts and increase their utility without compromising future needs [5]. Instead of assessing environmental impact at a single stage- like production or use- life cycle thinking considers the whole product life span: from raw material extraction and processing, through manufacturing and use, to disposal, recycling, or reuse [3, 6].

Without this big-picture view, interventions made with good motives can have unintended outcomes. This is known as burden shifting. For example, polylactic acid (PLA), a bio-based plastic- often perceived as sustainable- is produced from renewable crops like corn or sugarcane and has a relatively low carbon footprint during manufacturing [7]. However, intensive agriculture needed for PLA feedstock cultivation can result in water stress, pesticide pollution, and land-use conflicts. Moreover, PLA's compostability only happens under industrial conditions rarely accessible in global waste systems, thus, it often ends up persisting like conventional plastics. In contrast, polyethylene (PE), derived from fossil fuels, is not biodegradable but is more widely and efficiently recycled in existing infrastructure [8, 9]. This explains how materials that initially appear sustainable, may transfer environmental burdens to other stages, pointing out the importance of comprehensive, life cycle-based evaluations [7, 10, 11].

This insight is also important when considering recycling. Recycling is often divided into two categories: closed-loop and open-loop systems (**Fig. 3**) [12]. Closed-loop recycling keeps the material’s composition and reuses it in the same or equivalent product- such as recycling PET bottles into new PET bottles [13]. Open-loop recycling, or downcycling, converts materials into lower-value products, which are usually non-recyclable at the next cycle [14]. Even though both approaches reduce virgin resource demand, it is closed-loop systems that preserve material’s quality and value over time.

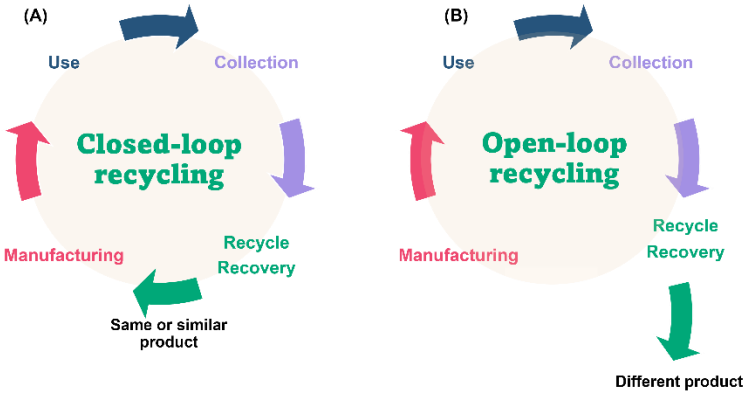

Fig. 3. Schematic representing (A) closed-loop recycling; (B) open-loop recycling.

Together, these approaches merge within a larger goal of the circular economy. Unlike the linear model of "take–make–use–dispose," (**Fig. 4A**) the circular model (**Fig. 4B**) attempts to keep material value by prolonging their life through reuse, repair, remanufacture, and recycling. The goal is not only to reduce environmental damage but to structure systems in which waste does not exist intentionally [6]. A key part of this model is the opinion that materials must be designed for their next life since the beginning- by careful choice of feedstocks, modular system architecture, and alignment with current recovery systems (design to recycle approach) [15].

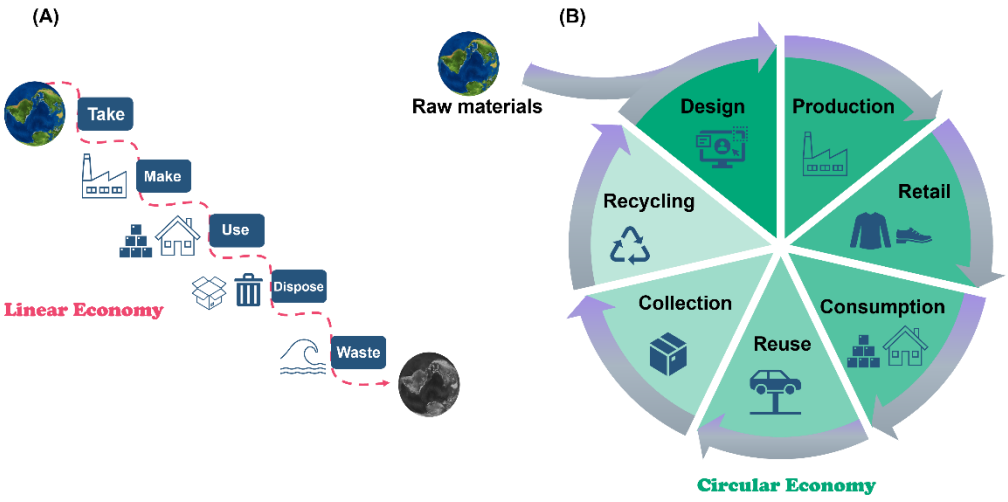

Fig. 4. Schematic representing (A) linear economy; (B) circular economy.

To transition to a circular economy for plastics, fundamental change across the whole value chain is needed- from raw material choice and product design to consumer behavior and end-of-life management. Bioplastics and bio-based materials are promising but must be evaluated with full life-cycle assessments to avoid burden-shifting.

These interconnected strategies- sustainability, life cycle thinking, recycling, and circular economy- form the conceptual foundation of this thesis. They provide a necessary lens through which the environmental impacts of materials can be evaluated, mitigated, and ultimately redesigned. The challenge is not only replacing harmful materials, but in transforming the entire system of material flow- from design to disposal- into one that is regenerative, resilient, and aligned with the needs of both people and planet.

2 Polyurethane Chemistry and Application

The development of polyurethanes (PUs) is nearly as old as that of synthetic polymers themselves. In 1937 Otto Bayer together with his German colleagues initiated the base of PU chemistry [16]. Its industrial applicability rapidly expanded during World War II, when PU-based coatings were employed to impregnate paper and manufacture protective clothing resistant to chemical warfare agents, such as mustard gas. Following the war, the exceptional combination of chemical resistance and mechanical durability demonstrated by PUs, enabled their widespread use in high-gloss aircraft finishes and chemically and corrosion-resistant coatings for diverse substrates such as metals, wood, and masonry [17]. These early successes enhanced the versatility and robustness of PU materials, which led to their widespread industrial and consumer market growth over the next decades [18].

The success of PU materials rests on the exceptional reactivity of isocyanates combined with the wide variety of available monomers (**Fig. 5**), allowing for highly versatile synthetic strategies. The electrophilic character of the isocyanate carbon, enhanced by the strong electron-withdrawing effects of adjacent nitrogen and oxygen atoms, makes it highly vulnerable to nucleophilic attack [19]. Reaction of isocyanates with alcohols results in the formation of urethane linkages (**Fig. 5A**), whereas reaction with amines yields urea functionalities (**Fig. 5B**) [20]. Water can also react with isocyanates, initially forming an unstable carbamic acid intermediate that rapidly decomposes into a primary amine and carbon dioxide (CO_2) [21]. The amine formed from the reaction proceeds to react with another

isocyanate, thus creating a urea linkage and enabling chain extension. The carbon dioxide produced during the hydrolysis of isocyanates functions as a blowing agent which is crucial in PU foam production (**Fig. 5C**) [22, 23].

The mechanical properties of the resulting PUs are strongly dependent on the types and structures of the starting materials: aromatic isocyanates like TDI and MDI are more reactive than aliphatic types like IPDI and HMDI (**Fig. 5D**) [24]. Polyols are other key components in PU chemistry: flexible, soft polymers arise from long-chain polyols (such as polyethylene glycol (PEG), polypropylene glycol (PPG), or polytetramethylene glycol (PTMG) with varying molecular weights) with low crosslinking, whereas rigid and tough materials are produced through short chain polyols (typically monoethylene glycol, and 1,4-butanediol) and contain higher degrees of crosslinking (**Fig. 5E**) [25]. Moreover, polyether polyols based on propylene oxide offer good flexibility but lower oxidative stability, while polycarbonate polyols provide superior strength but at higher costs [26, 27]. Additionally, the molar ratio between soft and hard segments also plays a key role in determining PU properties, being foams or elastomer. Having a higher content of hard blocks leads to rigid PU, applied in civil construction and domestic appliances, while a higher soft-block content leads to soft foams and elastomers, used in cushioning, adhesives, heat and sound-proofing applications [28]. Therefore, the broad scope of precursors and their combinations, together with incorporation of various additives and the careful selection of processing conditions leads to a wide range of PU properties and applications [24]. Ultimately, those properties can be finely adjusted by the precise selection of monomers, their relative content, synthetic route, processing conditions, and additive incorporation [29]. For an in-depth discussion on the wide range of properties PU materials can obtain, and consequently their vast application range, the readers are directed to fundamental textbooks of the field, such as the one by Mark F. Sonnenschein, Polyurethanes: Science, Technology, Markets, and Trends [28], and The Polyurethanes Book, by D. Randall and S. Lee [30].

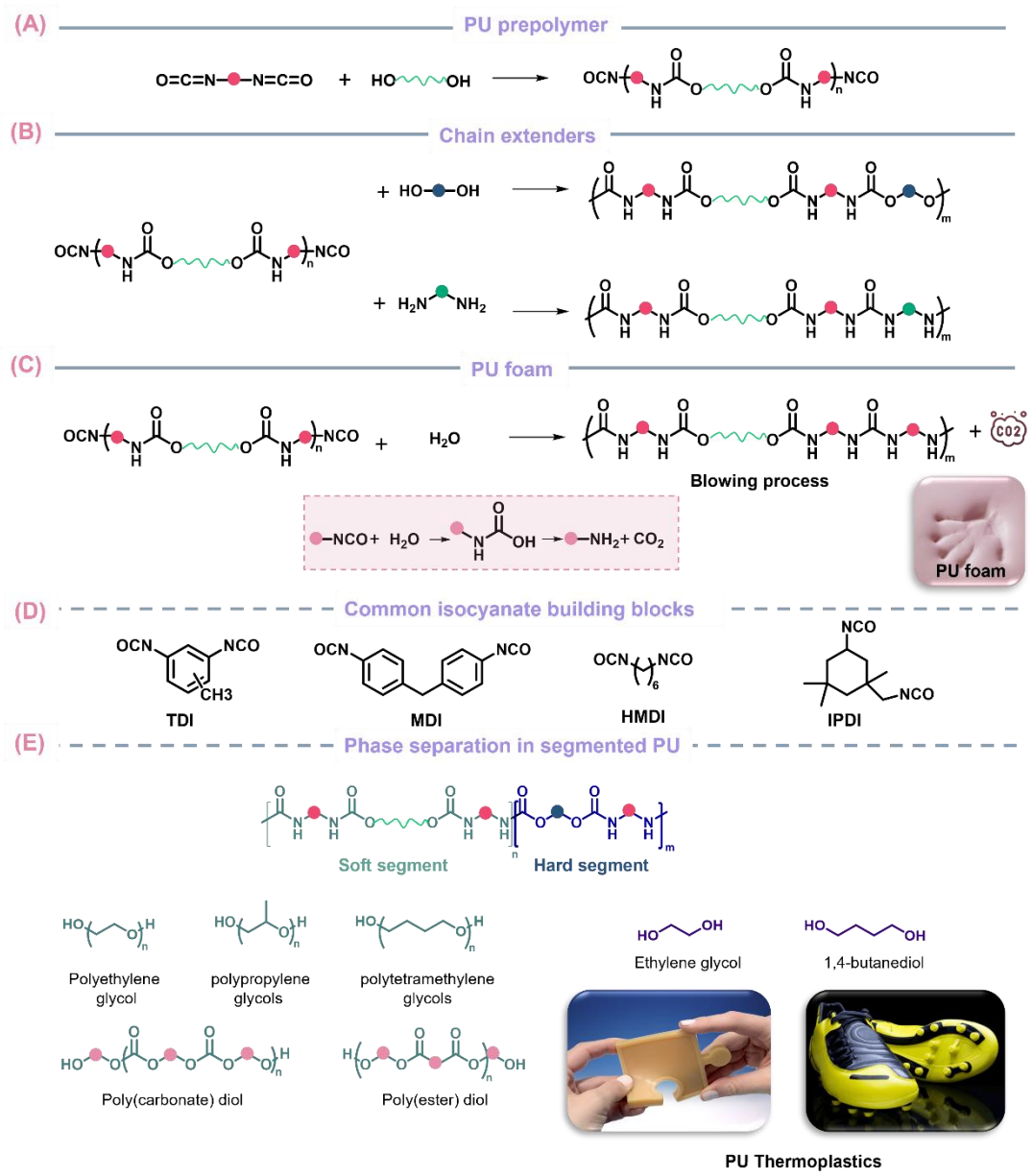

Fig. 5. Schematic representing (A) synthesis of PU pre-polymer; (B) chain-extenders used in the preparation of PU; (C) PU foam formulation; (D) common isocyanate-building blocks used in the synthesis of PU (E) soft and hard segments in PU resulting in phase separation.

In fact, PU ranks as the seventh most widely utilized polymer globally, with an estimated production of around 27 million tons per year [31]. The PU market is typically divided into five main segments of varying sizes: foams, which dominate with approximately 65% of the market share; coatings, accounting for 13%; elastomers, representing 12%; adhesives, making up 7%; and biomedical applications, comprising the remaining 3%, as illustrated in **Fig. 6** [32-35].

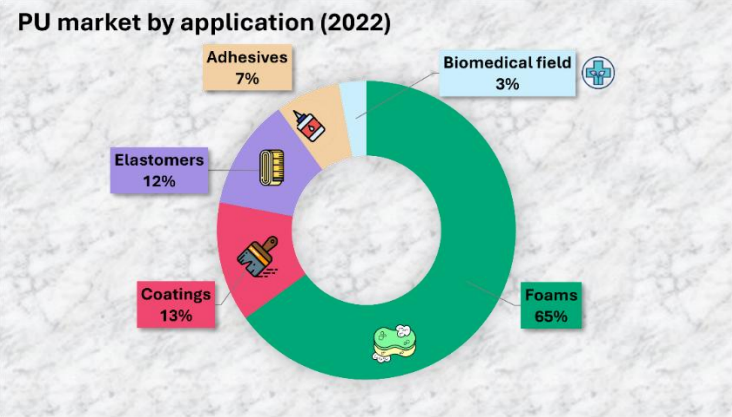

Fig. 6. PU market by application, obtained in 2022.

2.1 PU challenges

Despite their numerous benefits, the production and disposal processes of PUs face environmental, health, and legislative issues which researchers have explored extensively throughout the last ten years. Most PUs are derived from petroleum-based feedstocks and, upon disposal, typically follow one of two pathways: incineration, where they are used as an energy source but contribute to global warming through carbon dioxide (CO_2) emissions, or landfilling, which constitutes about 50% of PU waste disposal and presents soil and ecosystem pollution threats [36, 37]. From a health perspective, the synthesis of PU generates serious health concerns because multiple essential chemicals used in the process are toxic. While alcohol monomers are generally considered safe, other critical components such as isocyanates and catalysts raise significant health concerns. From a health perspective, PU synthesis raises serious concerns because several key chemicals involved are toxic. While alcohol-based polyols are generally regarded as safe, the use of isocyanates remains problematic, as these compounds are highly reactive and hazardous even at low exposure levels. In addition, PU formulations typically require catalysts, most commonly tertiary amines such as 1,4-diazabicyclo[2.2.2]octane (DABCO) and dimethylcyclohexylamine, or in some cases organotin compounds such as dibutyltin dilaurate (DBTDL). Importantly, DBTDL itself is highly toxic and environmentally persistent, and like isocyanates, it is classified among substances of concern due to carcinogenic, mutagenic, or reprotoxic (CMR) effects [38-40]. Additionally, the industrial production of isocyanates depends on highly hazardous reagents such as phosgene, a lethal gas that can cause severe lung irritation and death when inhaled at

concentrations above 4 ppm [41]. In use, isocyanates pose significant risks, including respiratory and skin irritations. Growing public awareness and increasing regulatory pressure surrounding the hazards associated with these substances have led to stricter legal frameworks- for example, since 2009, consumer PU formulations in many regions are required to contain no more than 0.1% w/w of residual isocyanate [42-44].

2.2 Strategies to enhance the sustainability of PUs

To elevate the overall sustainability of PUs, the majority of research have targeted two critical stages of their life cycle: the production phase, focusing on the advancement of environmentally friendly raw materials and synthesis methods [45], and the end-of-life phase, where recycling strategies seek to reduce environmental impact and enhance circularity [46]. Recent advancements in isocyanate synthesis have increasingly placed emphasis on green chemistry, trying to reduce the need for hazardous reagents, such as phosgene, upon various chemical strategies [47].

Moreover, significant advancement has been made toward the synthesis of bio-based isocyanates to further enhance sustainability. Aromatic diisocyanates have been synthesized from lignin-derived building blocks such as syringic and vanillic acids through Curtius rearrangement strategies [48]. Guaiacol and vanillic alcohol, derived from lignocellulosic biomass, have been used to prepare novel biomass-based diisocyanates via Friedel–Crafts alkylation followed by amine functionalization and diisocyanate formation [49]. Furthermore, p-menthane-1,8-diisocyanate (PMDI), structurally analogous to petroleum-derived isophorone diisocyanate (IPDI), has been synthesized from terpene-derived p-menthane-1,8-diamine [50].

Despite numerous advancements in phosgene-free synthetic routes and the increasing interest in renewable monomer sources, the industrial synthesis of isocyanates via phosgene remains highly optimized and cost-effective, posing a significant barrier to alternative technologies. Moreover, while several biobased isocyanates have been proposed, their commercial availability remains limited, and most are restricted to aliphatic structures, with minimal penetration into large-scale production. Given the intrinsic toxicity and handling hazards associated with isocyanates- regardless of their origin- there has been growing interest over the past decade in developing alternative chemistries for PU synthesis that entirely bypass isocyanates. These emerging non-isocyanate approaches not only offer potential improvements

in safety but also align more closely with the principles of a circular economy. These developments will be further discussed in section 3.

2.2.1 Recycling of PUs

In terms of end-of-life management, the complex chemical structure of PUs poses serious challenges. The majority of applications- particularly coatings, adhesives, and foams- are based on thermoset formulations, whose crosslinked nature makes recycling especially difficult. **Fig. 7** provides a comprehensive overview of the PU life cycle, explaining the source of raw materials (petroleum-based and bio-based), manufacturing, product use, and the various end-of-life options. This schematic clearly illustrates the fundamental differences between linear and circular pathways in PU material flows. The upper section of the figure shows recycling strategies, which are designed to reintegrate waste PUs into the value chain, either through mechanical recycling (e.g., rebonding foam scraps), chemical recycling (e.g., depolymerization into monomers or polyols), or reuse in secondary applications. These methods try to stop PU waste from going through normal disposal routes such as landfilling and incineration, depicted on the lower right. The goal is to reduce the environmental burden and carbon footprint associated with PU products by closing the material loop. However, only 29.7% of PU waste is recycled, 39.5% undergoes energy recovery, and 30.8% ends up in landfills [51]. Low-density PU foams, in particular, occupy substantial landfill space. With global PU production reaching nearly 26 million metric tons in 2022 and estimated to reach 31 million by 2030, urgent intervention is needed to reduce its environmental impact [52].

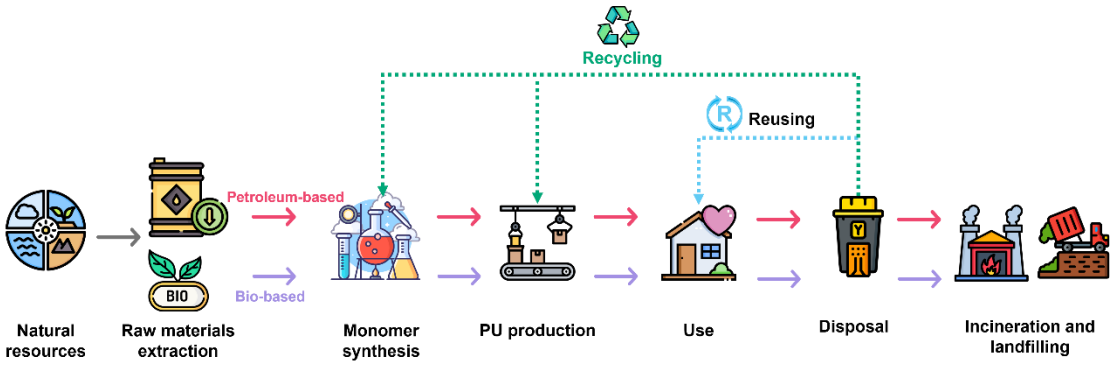

Fig. 7. General scheme of PU life cycle.

Thermoset PUs cannot be reprocessed through conventional melting and remolding techniques used for thermoplastics. As a result, mechanical recycling of PU is primarily limited to physical

methods such as shredding, followed by rebonding with polyisocyanates under heat and pressure. This process is commonly applied to flexible PU foam scrap and slabstock production waste, yielding rebonded materials typically used in low-value applications such as carpet underlay and foam panels for sound insulation. However, the recycled products often do not perform as well as the original PU materials [53]. While mechanical recycling offers a way to temporarily extend the life of PU materials, it finally only delays their disposal through landfilling or incineration, as mechanical properties degrade after a finite number of rebonding cycles [42].

Importantly, current data suggests that the European market for low-value rebonded PU materials has reached saturation, suggesting that future PU waste streams will not be readily absorbed by this recycling pathway [54]. Thus, alternative recycling strategies are urgently necessary to valorize these materials and prevent their premature disposal [42, 55]. In response, recent research efforts have increasingly investigated the development of improved chemical recycling techniques and novel approaches to effectively address both current and anticipated PU waste challenges. In principle, polymers with backbones linked by C-O and C-N bonds exhibit relatively low reaction barriers and near-neutral reaction-free energies, making them suitable for chemical depolymerization [56]. Activation of stable carbamates typically requires the use of a catalyst, most commonly a strong base such as potassium hydroxide (KOH) or 1,8-diazabicyclo[5.4.0]undec-7-ene (DBU). These bases facilitate the deprotonation or nucleophilic activation of the carbamate intermediate, enabling subsequent transformations [57]. A variety of chemical methods can be utilized for the depolymerization of PUs including hydrolysis [58-60], acidolysis [61-65], glycolysis [66-69], and aminolysis [70-72] (**Fig. 8**).

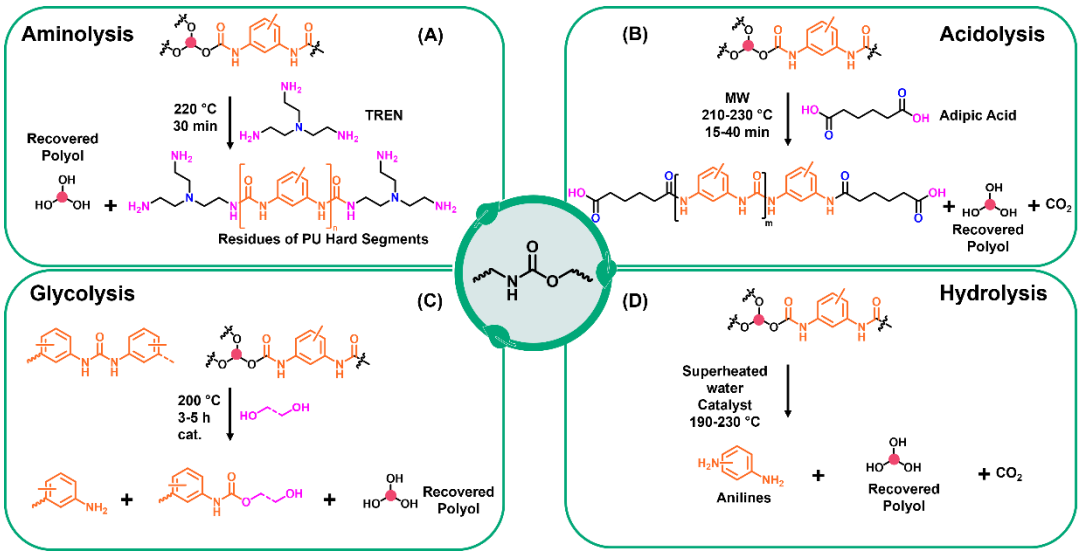

Fig. 8. Chemical recycling methods implemented to PUs.

2.2.1.1 Aminolysis

Aminolysis is an effective chemical recycling route for PUs, exploiting nucleophilic cleavage of urethane linkages by primary or secondary amines (**Fig. 8A**) [72]. Examples of typical aminolysis agents are primary amines (ethylenediamine, ethanolamine) [72, 73], secondary amines (diethanolamine, morpholine) [74, 75], and bio-derived amines such as butane-1,4-diamine (BDA) [73]. The selectivity of aminolysis significantly relies on the type of amine; primary amines generally cleave both C-O and C-N urethane bonds, producing polyols, substituted ureas, and potentially amines, while secondary amines selectively cleave the C-O bond [75]. The aminolysis process efficiency is significantly improved by utilizing catalytic systems such as metal hydroxides, alkali salts, or organic catalysts like acid-base pairs (e.g., TBD:MSA) [75]. Recent advancements in microwave-assisted aminolysis have shown substantial improvements in reaction kinetics and energy efficiency for PU recycling [76]. Studies have shown that microwave energy promotes urethane bond cleavage and enhances process control while reducing operational temperatures which results in more efficient outcomes and decreased environmental impact [70]. Moreover, microwave heating reduces both reaction time and energy use in comparison to traditional heating methods. Additionally, microwave-assisted aminolysis enables the use of lower amounts of degradation reagents while facilitating total degradation of urethane groups, resulting in recovered polyols comparable to

their virgin counterparts [76]. However, careful control of the reaction setup is important for producing pure products and reducing unwanted by-products.

2.2.1.2 Acidolysis

This method involves the depolymerization of urethane linkages using dicarboxylic acids (e.g., adipic, succinic, maleic, or phthalic acid), typically under solvent-free conditions and elevated temperatures (190–230 °C) [63, 77, 78]. The reaction breaks the PU network into functionalized polyols and urea/amide derivatives, with the possibility of selective recovery of both soft and hard segments (**Fig. 8B**). Lately, it has been shown that catalyst-assisted acidolysis-especially using zinc acetate-significantly enhances degradation efficiency, achieving up to 97% depolymerization within 3 h at 200 °C [63]. The use of microwave heating further enhance kinetics, shortening reaction durations to less than one hour, while keeping the quality of recovered polyols [77]. More recently, vapor-phase acidolysis using dicarboxylic acids or their anhydrides was introduced, enabling efficient polyol recovery at lower temperatures (<150 °C), thus reducing energy consumption and side reactions such as esterification [79]. Moreover, studies have demonstrated that the recovered polyols after the acidolysis of PU foams can be reused not only in the production of flexible and rigid PU foams but also in PU adhesives (PUAs), with mechanical properties comparable or superior to virgin materials [62]. Through acidolysis, hard segment residues can be valorized, and aromatic diamines such as toluene diamine can be recovered, which can be isolated via hydrolysis or hydrogenation [65].

2.2.1.3 Glycolysis

Glycolysis is currently the most developed chemical recycling strategy especially for PU foams, both flexible and rigid. It involves the depolymerization of PU via a transurethanization-like reaction between the urethane bonds and glycols such as diethylene glycol (DEG) or ethylene glycol (**Fig. 8C**) [80]. Industrially, glycolysis is typically performed at elevated temperatures (170–220 °C) with the aid of basic catalysts like KOH or organometallic compounds such as stannous octoate [67]. Split-phase glycolysis, using an excess of glycolysis

agent, allows the reaction mixture to separate into two liquid phases: an upper phase rich in recovered polyol and a bottom phase containing carbamates, excess glycol, and degradation byproducts [66, 81]. This facilitates the purification of the recovered polyols, making them reusable in flexible and rigid foam applications. Recent innovations include microwave-assisted glycolysis, which significantly shortens reaction times while achieving high-purity polyol recovery [82, 83]. Moreover, approaches like pentaerythritol-assisted glycolysis aim to enhance depolymerization efficiency and yield polyols suitable for both flexible and rigid PU foam formulations [84, 85]. Although glycolysis can efficiently recover polyols of acceptable quality, it still requires high temperatures and significant energy input, and some life cycle assessments (LCA) have reported that the environmental benefits can be offset if the need for virgin isocyanates to compensate property loss is too high [86].

2.2.1.4 Hydrolysis

Hydrolysis is a well-established chemical recycling strategy for PUs, involving the cleavage of urethane linkages through reaction with water, typically under high-temperature and high-pressure conditions (150–250 °C, 5–30 MPa) [60]. This approach enables the depolymerization of PU into polyols, amines, and CO_2 while avoiding the use of organic solvents or toxic reagents (**Fig. 8D**). Hydrolytic depolymerization can be conducted using superheated water or steam (wet or dry), and is often performed in batch or tubular reactors [87, 88]. In superheated steam systems at atmospheric pressure (230–316 °C), toluene diamines (TDAs) and high-quality polyols have been recovered in yields exceeding 80% [89]. Furthermore, novel systems using pressurized CO_2-water mixtures exploit the in situ formation of carbonic acid to catalyze hydrolysis, offering milder reaction pathways with excellent monomer recovery and no byproduct formation [90]. Despite the simplicity of its mechanism, hydrolysis remains technically challenging, often necessitating harsh conditions or catalytic assistance. Zinc acetate, lead acetate, and CO_2-based catalysts such as carbonic acid have shown enhanced reaction rates and selectivity [60, 91]. The reaction kinetics typically follow pseudo-first-order behavior, and the degradation mechanism differs between urethane and urea linkages: urethanes hydrolyze directly, while ureas thermally dissociate before hydrolysis [87]. Enzyme-assisted hydrolysis using cutinases has also recently gained attention as a green alternative for

polyester-PU systems, demonstrating efficient depolymerization at mild temperatures (e.g., 50 °C) under aqueous conditions [92].

While these recycling methods provide a renewed purpose for materials that would otherwise be discarded through incineration or landfilling, they are not truly circular, as they generate a secondary feed of lower quality. Additionally, PUs present significant challenges due to the high reactivity of polyisocyanates, which lead not only to the formation of urea groups, but also allophanate, biuret, and isocyanurate linkages [93, 94]. Compared to urethane bonds, these thermodynamically stable groups are less susceptible to chemical cleavage. Moreover, as most commercial PUs products are composed of co-polymers that often include various isocyanates and polyols, separating these components after depolymerization poses a greater challenge than identifying a suitable depolymerization method [65]. Thus, the opportunity for creating recycled materials with virgin-like properties is still mostly unexplored, and when recycling is carried out, the proportion of recycled material integrated into new formulations is often quite low (10-40%) [63, 95]. Overcoming these limitations is crucial for advancing truly sustainable and circular PU recycling techniques. Overall, no single method is universally optimal; trade-offs exist between efficiency, product quality, energy input, and scalability, highlighting the need for process integration, selective catalysis, and life cycle optimization in future developments.

2.2.1.5 Industrial implementation of PU chemical recycling

In addition to academic research, several industrial actors have initiated pilot or commercial projects on the chemical recycling of PUs, with a strong emphasis on foam applications. This is not surprising, as foams represent the largest share of PU consumption and constitute a particularly problematic waste stream due to their low density and high volume. RAMPF Group has developed chemical recycling technologies based on glycolysis, acidolysis, and aminolysis to recover polyols from post-consumer flexible PU foams (e.g., mattresses, furniture, automotive seats). The company reports that these recycled polyols exhibit performance comparable to virgin polyols and can be reintegrated into new formulations for adhesives, coatings, sealants, and foams [96]. Dow, in collaboration with Gruppo Fiori, has demonstrated a process for recovering PU foams from end-of-life vehicles without the need for manual disassembly. The recovered foams can then be directed to chemical depolymerization

processes for polyol recovery, illustrating efforts to lower the logistical and economic barriers associated with foam recycling [97]. Covestro has invested in large-scale projects such as PUReSmart and Circular Foam, which target both flexible (e.g., mattresses) and rigid (e.g., building insulation) PU foams. These initiatives focus on chemolysis routes for high-purity recovery of polyols and diamines, with the goal of reintroducing them into new foam formulations [98]. BASF is advancing continuous depolymerization technologies for rigid PU foams from end-of-life appliances, particularly refrigerators and freezers. The recovered polyols are intended for reuse in insulation materials, thereby creating a closed-loop system within the appliance sector [99]. Huntsman, together with Shincell, has recently introduced a fully recyclable thermoplastic polyurethane (TPU) foam for footwear applications. Unlike conventional thermoset foams, TPU foams are designed for reprocessing through mechanical or chemical recycling, demonstrating how product design can facilitate end-of-life management [100].

Collectively, these industrial efforts emphasise two important trends: (i) the transition from proof-of-concept chemistry toward scalable recycling processes with demonstrated industrial relevance, and (ii) the increasing recognition that design-for-recycling- whether through more homogeneous formulations, or the use of thermoplastic analogues- can greatly facilitate downstream processing and maximize recovery yields. While significant challenges remain in terms of cost, purity of recovered feedstocks, and infrastructure, these developments indicate that recycling of PUs is progressing from the laboratory toward practical implementation, thereby contributing to the emergence of more circular PU value chains.

3 Non-Isocyanate Polyurethanes: A Sustainable Evolution in PU Chemistry

Despite advances in sustainable manufacturing and recycling for conventional PUs, their dependence on toxic isocyanates remains a critical problem for environmental safety and sustainable use. Non-isocyanate polyurethanes (NIPUs) have become a promising substitute in response to the current limitations of traditional PU materials. NIPUs do not rely on toxic isocyanates and they can be synthesized using CO_2-based feedstocks and/or renewable resources. Subsequent sections will present the developmental processes for NIPUs alongside

their production methodologies and recycling opportunities as innovative approaches to more sustainable PU materials.

3.1 Different ways to synthesize NIPUs

Literature delineates four principal synthetic strategies for the preparation of NIPUs: polycondensation, molecular rearrangement, ring-opening polymerization and copolymerization, polyaddition of polycyclic carbonates to polyamines. Recent review articles deliver extensive examinations of these synthetic methods while providing essential evaluations of their functional mechanisms and applicability within various NIPU architectures [101, 102]. Moreover, a recently introduced emerging strategy involves the use of alkylidene oxazolidone chemistry to produce recyclable NIPUs. These pathways are briefly discussed in the following section.

3.1.1 Polycondensation strategies

Polycondensation typically proceeds via step-growth polymerization between diols and carbamate-functionalized monomers such as dicarbamates, dichloroformates, or carbamoyl chlorides. Although these approaches are synthetically versatile, routes involving chlorinated intermediates (e.g., dichloroformates or carbamoyl chlorides) produce low-molecular-weight by-products such as HCl, which complicate purification and hinder industrial scalability [103, 104]. To overcome these drawbacks, phosgene-free strategies have been introduced- for instance, the reaction of diamines with dimethyl carbonate (DMC), a CO_2-derived reagent, to afford dicarbamate intermediates [105]. The transurethanization of polycarbamates with polyols and the reaction of polycarbonates with polyamines typically release alcohols as by-products (e.g., methanol), whereas the reaction of polycarbamates with polyaldehydes route generate water (**Fig. 9A**).

3.1.2 Rearrangement-based pathways

Rearrangement reactions- namely the Curtius, Hofmann, and Lossen rearrangements-constitute another route for the synthesis of PU structures through the in situ generation of isocyanates from precursors such as acyl azides, carboxamides, and hydroxamic acids (**Fig. 9B**) [106-110]. The fundamental operation of these methods depends on the temporary creation of isocyanates which conflicts with the goal of fully eliminating isocyanates despite their classification under NIPU chemistry. Furthermore, the initial materials required for these chemical rearrangements possess significant toxicity and thermal instability which complicates their safe handling [111]. In fact, the decision to classify these pathways within the NIPU framework faces disagreement from both regulatory and green chemistry perspectives.

3.1.3 Ring-opening polymerization (ROP)

The ring-opening polymerization (ROP) of strained cyclic monomers such as cyclic carbamates has been explored as a method for synthesizing NIPU frameworks [112, 113] (**Fig. 9C**). These reactions offer high atom economy and avoid the formation of stoichiometric by-products. However, they typically require elevated temperatures and hazardous starting materials, often derived from phosgene, such as phenyl chloroformate.

3.1.4 Ring-opening copolymerization (ROCOP)

In contrast, aziridines undergo ring-opening copolymerization (ROCOP) with carbon dioxide, forming PUs through a different mechanism [114] (**Fig. 9D**). Although this approach has been recognized as innovative and offers potential for direct CO_2 utilization, it suffers from limitations in accessible polymer architectures [115]. Furthermore, the high toxicity and handling risks of aziridines significantly hinder their industrial application.

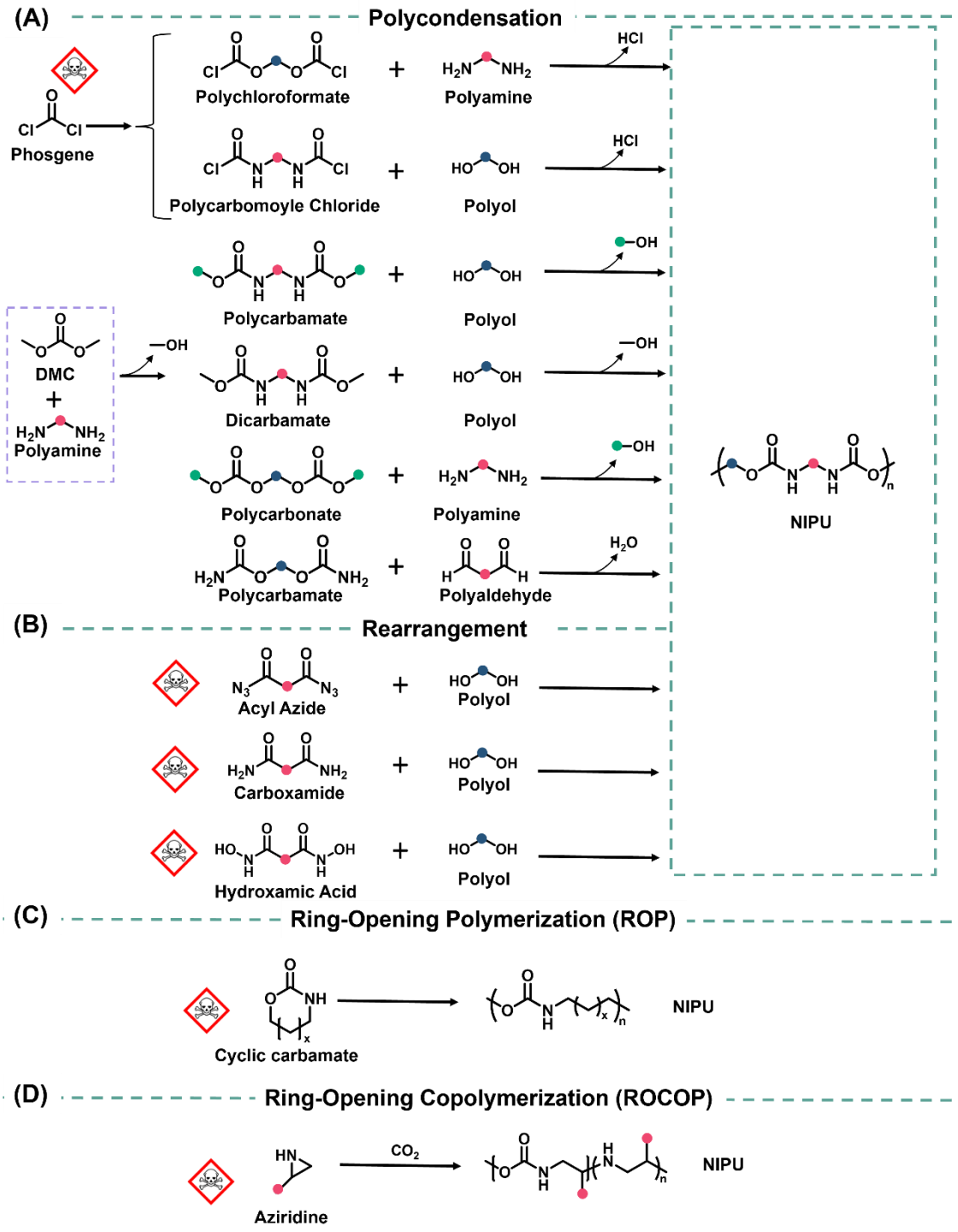

Fig. 9. Schematic representing different ways to synthesize NIPUs, (A) polycondensation method; (B) rearrangement method; (C) ring opening polymerization (ROP) strategy; (D) ring-opening copolymerization (ROCOP).

3.1.5 Polyaddition of cyclic carbonates with amines: a greener route to NIPUs

The most industrially and environmentally promising route to NIPUs is the polyaddition of cyclic carbonates (CC)s with diamines [116, 117]. This reaction offers a truly isocyanate-free approach, proceeding without the formation of volatile by-products and under relatively mild conditions. Unlike other NIPU synthesis routes, this method relies on readily accessible CC monomers and structurally diverse diamines, and benefits from excellent atom economy, functional versatility, and potential for full bio-based sourcing [118-120]. It has therefore emerged as the benchmark reaction for potentially greener PU chemistry. The coupling of CO_2 and epoxides is the most widespread and scalable route to 5-membered CCs (5CCs) [121]. Other carbonate types are obtained via alternative carboxylation or cyclization pathways. These classes and their implications for polymer design will be discussed in the following sections.

3.1.5.1 Five- to eight-membered cyclic carbonates to produce PHU-type NIPUs

Among the various routes employed for NIPU synthesis, polyaddition of five-, six-, seven-, and eight-membered CCs with polyamines are by far the most extensively investigated providing the so-called poly(hydroxyurethane)s (PHUs). Six-, seven-, and eight-membered cyclic carbonates (6CCs, 7CCs, and 8CCs; **Fig. 10**) exhibit superior reactivity compared to their five-membered counterparts (5CCs) [122, 123]. However, their synthesis is limited by the need for complex, often costly or toxic precursors, restricting their structural diversity.

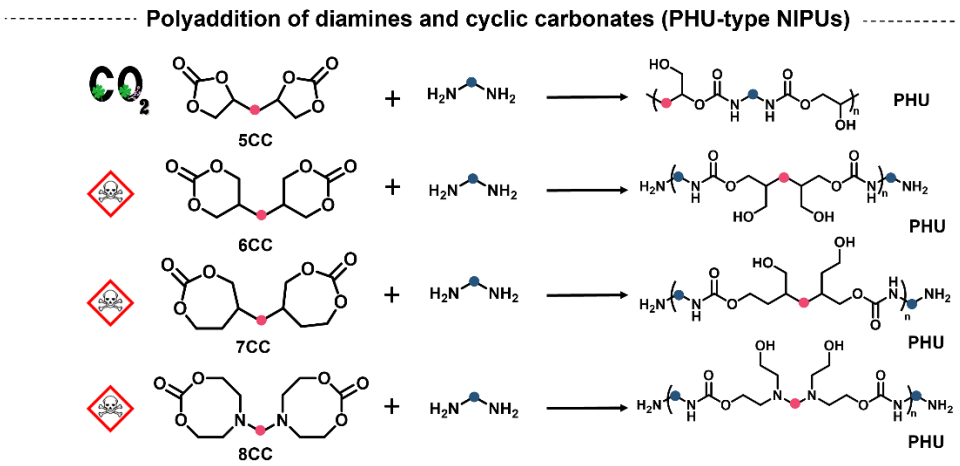

Fig. 10. Schematic representing different monomers to synthesize PHU-type NIPUs through polyaddition of diamine with dicyclic carbonates.

In contrast, 5CCs provide broad molecular versatility and are readily accessible from inexpensive and non-toxic starting materials, including renewable resources such as vegetable oils and polysaccharides [124]. These monomers are typically synthesized via the catalytic coupling of CO_2 with epoxides, a reaction that is both atom-efficient and scalable, enabling the valorization of CO_2 as a renewable C1 feedstock [125-127]. The aminolysis of 5CCs with primary amines proceeds via nucleophilic ring opening, yielding a mixture hydroxyurethane linkages (**Fig. 11**) [128].

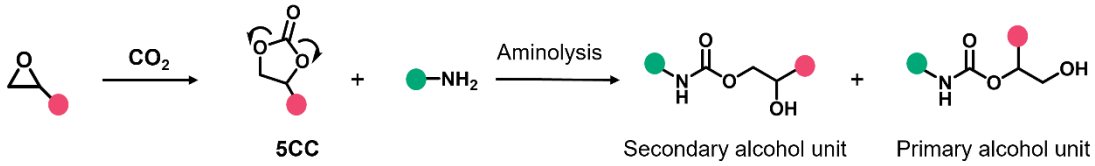

Fig. 11. Schematic representing the synthesis of 5CC from epoxy and CO_2, and the aminolysis of 5CCs resulting in the production of PHUs furnished with secondary and primary alcohols.

From a sustainability perspective, 5CCs are particularly attractive because both the carbonate core and the epoxide precursor can be derived from bio-based resources. For example, epoxidized triglycerides (e.g., from soybean or linseed oil), glycerol, sorbitol, vanillin, or cellulose derivatives can be converted into 5CCs, enabling bio-based content up to 100% in the final PHUs [129-131]. This opens the door to fully renewable, non-toxic, and side-product-free PU alternatives.

Despite these advantages, the practical implementation of 5CCs in polymer synthesis is limited by their high thermodynamic stability as five-membered rings, which makes the aminolysis reaction with primary amines relatively sluggish, especially under ambient conditions [132]. This kinetic limitation has prompted extensive research to optimize reaction conditions and molecular structures to facilitate high-yield polyaddition and improve the properties of resulting PHUs.

The nature of the solvent plays a crucial role in modulating the reactivity of 5CCs with amines (**Fig. 12A**). In aprotic solvents, the nucleophilic attack of the amine on the carbonate carbonyl- the rate-determining step- is slow due to limited polarization of the carbonyl group [133-135]. Conversely, protic solvents such as ethanol and methanol enhance electrophilicity via hydrogen bonding with the carbonyl oxygen, thereby accelerating the initial nucleophilic attack [136,

137]. However, as most industrial processes involve bulk polymerization, solvent effects are often marginal under practical conditions, and alternative approaches such as internal activation or plasticizer-assisted mobility enhancement are required [138].

Moreover, the substitution pattern on 5CCs significantly affects their reactivity. Electron-withdrawing groups (EWG) such as trifluoromethyl (CF_3), vinyl, and ester groups enhance the electrophilic character of the carbonate, facilitating aminolysis (**Fig. 12B**) [132]. Among these, CF_3-substituted carbonates yield nearly quantitative conversions but remain synthetically underexplored [134]. Ester-functionalized 5CCs offer high reactivity but may participate in side-reactions like amidation. Ether-functionalized 5CCs are less reactive but are preferred in many cases due to their synthetic accessibility and negligible side reactions [139]. Moreover, the aminolysis reaction of 5CCs benefits from an EWG near the cyclic carbonate because it strengthens the electrophilic character of the carbonyl group (**Fig. 12B**).

Additionally, amine structure is another determining factor (**Fig. 12C**). Primary aliphatic amines connected to primary carbons demonstrate superior reactivity [140]. Electron-withdrawing substituents when positioned adjacent to the amine group lead to increased nucleophilicity and faster reaction rates [141]. In contrast, secondary amines and aromatic amines display little to no reactivity when maintained at ambient temperature conditions [142]. Additionally, the reactivity of amines decreases as the alkyl chain length increases due to both steric hindrance and electronic effects [143].

The ring size of cyclic carbonates also influences reactivity. Different CCs with various ring size is shown in **Fig. 12D**. Comparative studies show that 6CC, 7CC, and 8CC cyclic carbonates are more reactive that 5CC, primarily due to increasing ring strain [122, 135, 139, 144]. However, the synthesis of larger-ring carbonates often relies on toxic or hazardous precursors such as phosgene or carbon disulfide, restricting their suitability in sustainable chemistry [133, 144]. In contrast, 5CCs present environmental and economic benefits as they can be derived from bio-based feedstocks like glycerol or through carbonation of vegetable oil derived epoxides even though they demonstrate less intrinsic reactivity [145, 146].

Catalysis serves as a potent strategy to overcome the natural reactivity constraints of the 5CC-amine reaction. Rection efficiency improves through catalysts which enhance carbonate electrophilicity and amine nucleophilicity while also may directly participate as nucleophilic activators. Among various catalytic systems investigated- Lewis acids [147, 148], organobases [149], phosphines [150], enzymes [151]- thioureas and guanidines such as TBD have emerged

as the most effective [152] (**Fig. 12E**). These catalysts accelerate the aminolysis of 5CCs with amines, enabling higher conversions and therefore access to higher molar mass PUs. In the absence of catalysts, the reaction often stalls at oligomers that display broad and multimodal SEC traces. While dispersities in step-growth polymerizations are fundamentally governed by Carothers' law and approach 2 at full conversion, the use of catalysts ensures that this theoretical regime can be reached in practice. In fact, Monmagnon et al. [153] showed that TBD-catalyzed NIPU synthesis yields polymers with tighter molar mass profiles compared to non-catalyzed reactions. Moreover, mechanistic studies by Bossion et al. [154] highlight how TBD's dual hydrogen-bonding activation fosters a more homogeneous step-growth process, further enhancing structural contro

Beyond reactivity, achieving high molar mass PHUs remains a fundamental obstacle. Hydroxyurethane formation is a reversible reaction, and the polymerization is often limited by an equilibrium that prevents complete conversion. This limitation is further exacerbated in bulk polymerizations, where extensive hydrogen bonding between hydroxyl and urethane groups markedly increases viscosity and restricts molecular mobility, hindering further chain growth [155]. This is particularly evident in bulk polymerizations, where hydrogen bonding between hydroxyl and urethane groups produces a noticeable increase in viscosity [156]. Additionally, stoichiometric imbalances caused by side reactions- such as amine carbonation by atmospheric CO_2 [157], urea formation via transurethanization [158], amidation of ester-substituted carbonates [158], and formation of oxazolidinones [159]- prevent full conversion and restrict polymer chain growth. Higher reaction temperatures help overcome diffusion barriers and enhance molar mass, yet lead to more unwanted side reactions.

In summary, 5CCs present a practical and sustainable approach to NIPU synthesis yet demand precise adjustments of several parameters such as solvent environment, carbonate and amine structure, catalytic system, and reaction temperature. Breakthroughs in monomer engineering together with improved catalytic control methods remain crucial to fully utilize 5CC-based PHUs within industrial settings.

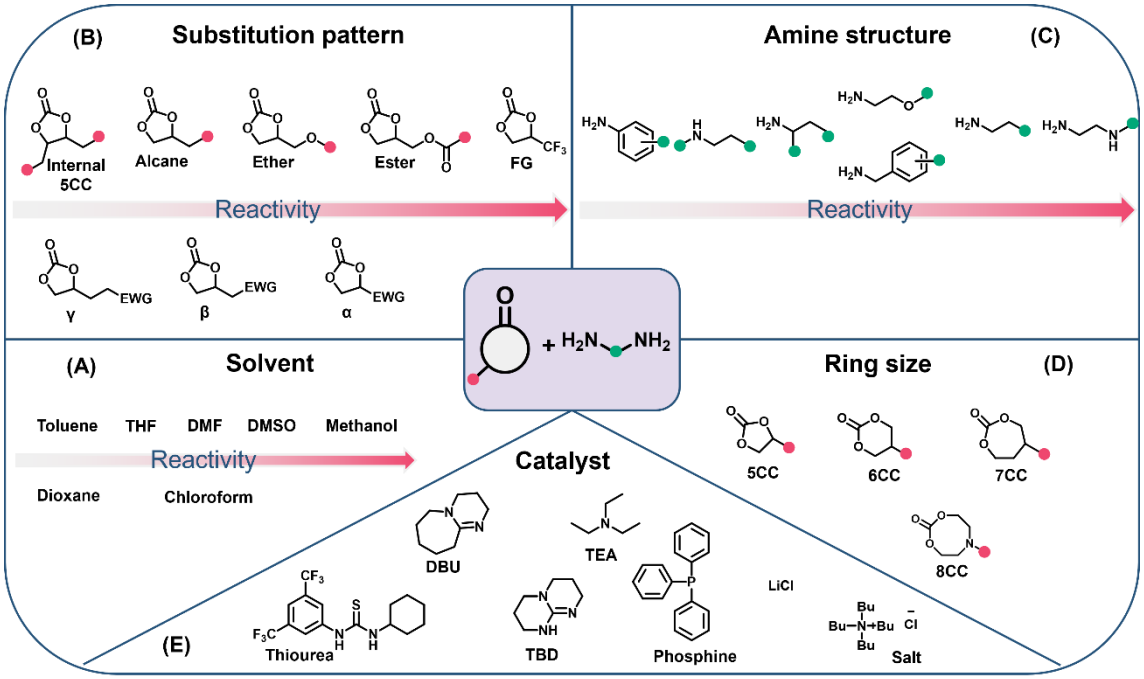

Fig. 12. Schematic representing the factors that affect the reactivity of CCs and amines; (A) the effect of solvent; (B) the effect of substitution pattern of 5CCs; (C) the effect of amine structure; (D) the effect of ring size; and (E) the effect of catalyst.

3.1.5.2 Exovinylene cyclic carbonates: a divergent CO_2-based platform toward NIPUs and beyond

Exovinylene bis-cyclic carbonates (BisαCCs) represent an innovative class of CO_2-derived monomers synthesized via organocatalyzed carboxylative coupling of CO_2 with bis(propargylic alcohol)s [119, 160]. **Fig. 13** shows the setup of the CO_2 reactor that can be utilized to prepare BisαCCs in one batch under controlled temperature and pressure. The synthesis process is explained in details by Detrembleur and coworkers [119, 161].

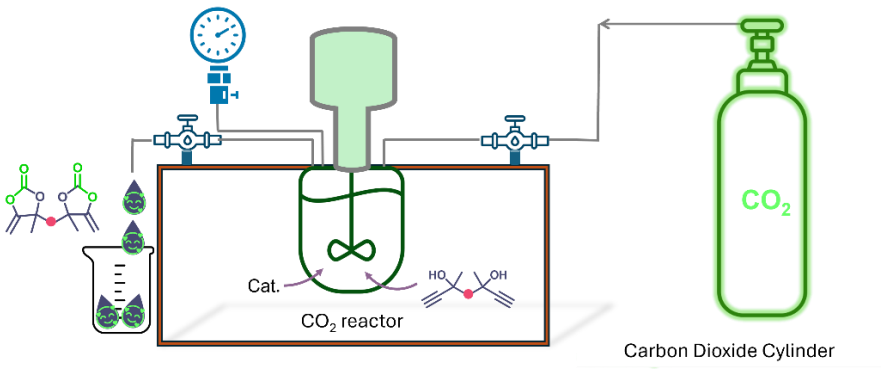

Fig. 13. Schematic representing CO_2 reactor utilized to produce BisαCCs.

Distinguished from traditional epoxide-derived cyclic carbonates by their exocyclic olefinic functionality, BisαCCs exhibit enhanced reactivity toward various nucleophiles such as amines, diols and thiols through regioselective ring-opening mechanisms (**Fig. 14**).

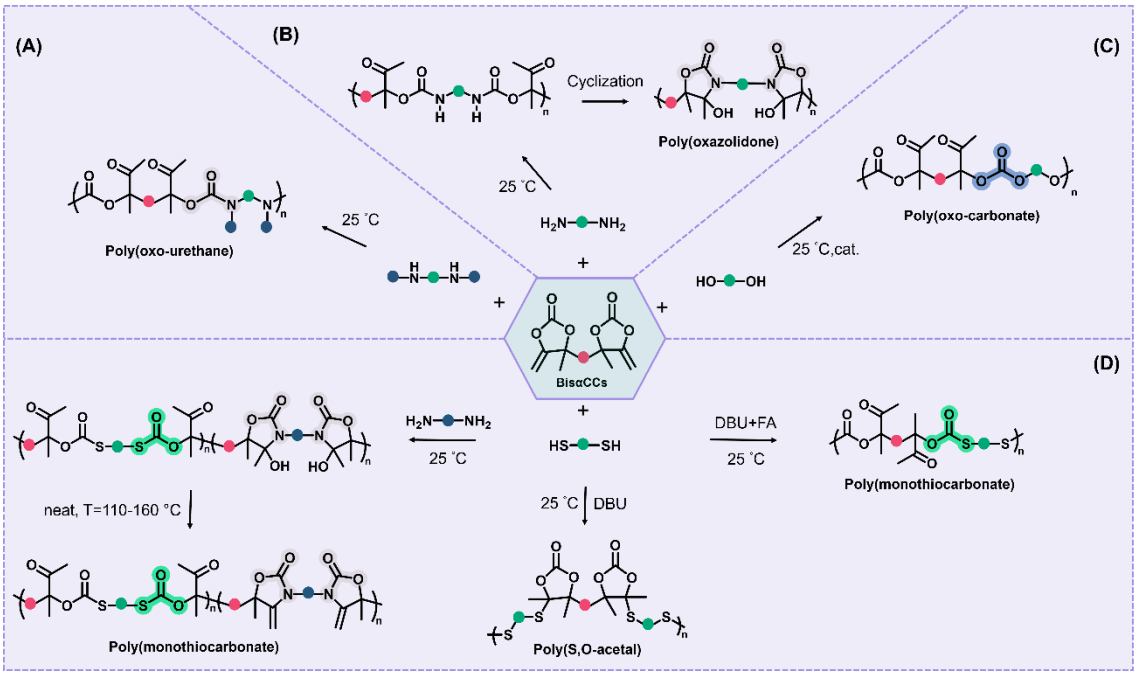

Fig. 14. Schematic representing various polymers obtained from BisαCCs; (A) poly(oxo-urethane); (B) poly(hydroxy-oxazolidone); (C) poly(oxo-carbonate); (D) poly(monothiocarbonate) and poly(S,O-acetal).

From the perspective of CO_2-based NIPUs, BisαCCs are of particular interest due to their ability to furnish two structurally distinct PU analogues: poly(oxo-urethane)s (**Fig. 14A**) and poly(hydroxyoxazolidone)s (PHOxs) (**Fig. 14B**), depending on the nature of the diamine employed. Gennen et al. studied the polymerization of BisαCC monomers with secondary diamines at room temperature using $CHCl_3$ and DMF as solvents to achieve poly(oxo-urethane)s [119]. Polymerizations in DMF yielded significantly higher molecular weights- up to three times greater- compared to $CHCl_3$, with M_n reaching 13,500 g·mol^{-1} (M_w 40,000 g·mol^{-1}). The addition of catalytic DBU further increased molecular weights to M_n 25,000 g·mol^{-1} (M_w 73,000 g·mol^{-1}).

In contrast, polyaddition of BisαCCs with primary diamines (e.g., 1,8-octanediamine) proceeds quantitatively at room temperature, yielding PHOxs through a two-step cascade: initial aminolysis, followed by intramolecular cyclization to form the oxazolidone ring (**Fig. 14B**).

Less hindered diamines (aliphatic and benzylic) rapidly cyclize to form defect-free PHOxs, while bulky cycloaliphatic diamines yield polymers containing both oxo-urethane and hydroxyoxazolidone linkages due to a slower cyclization [162]. These polymers display high glass transition temperatures (90–130 °C) and thermal stability (T_d > 360 °C), making them suitable for demanding applications [162].

What sets BisαCCs apart is not merely their applicability to NIPUs, but their unparalleled versatility in producing structurally and functionally diverse polymers from a single CO_2-derived precursor. This divergent reactivity is governed by the nucleophile and has been harnessed to create an extensive library of materials with distinct properties:

Poly(oxo-carbonates). Poly(oxo-carbonates) are synthesized via DBU-catalyzed step-growth polyaddition of BisαCCs with various (bio-based) diols (e.g., isosorbide, 1,4-butanediol) at ambient temperature (25 °C) (**Fig. 14C**). The resulting polycarbonates achieve high molar masses (M_w up to ~27,000 g mol^{-1}; M_n typically around 13,000–17,000 g mol^{-1}), exhibit a semicristalline behavior, and display glass transition temperatures ranging approximately from −20 to 95 °C, with thermal decomposition temperatures above 250 °C [163]. Interestingly, this class of polycarbonates, exhibited easy recyclability through a catalyst-free chemical recycling [164]. In this process, aminolysis with propylamine at room temperature under catalyst-free conditions led to complete depolymerization, yielding the original diol and a previously unreported bis(oxazolidone). The process was tolerant to alcohol groups; using aminopropanol afforded a hydroxyl-functional bis(oxazolidone) in high yield. This building block was then co-polymerized with BisαCC to produce a poly(oxazolidone-co-carbonate) containing both oxazolidone and oxo-carbonate linkages.

Poly(monothiocarbonate)s and Poly(S,O-acetal)s. The organocatalyzed thiol-addition to BisαCCs offers a robust and sustainable platform for synthesizing sulfur-containing polymers with tunable architectures. The resulting polymer structure is governed by the choice of catalyst and reaction conditions, thereby allowing fine control over material functionality and recyclability (**Fig. 14D**). Ouhib et al. [165] demonstrated that BisαCCs undergo rapid thiol addition in the presence of DBU, initiating a switchable domino mechanism that converts β-oxothiocarbonate intermediates into cyclic S,O-acetals under thermodynamic control. The rearrangement is driven by the nucleophilicity of the thiolate and the basicity of the medium, resulting in poly(S,O-acetal)s characterized by densely functionalized backbones. Notably, when the reaction is quenched shortly after initiation or conducted in the presence of

fluorinated alcohol as a co-catalyst (DBU/FA), the rearrangement is effectively suppressed. Under these conditions, the β-oxothiocarbonate intermediates are kinetically trapped, leading to the exclusive formation of poly(monothiocarbonate)s in quantitative yield and with 100% atom economy.

In contrast, Maes et al. [166] exploited the DBU-catalyzed rearrangement pathway to synthesize CO_2-sourced covalent adaptable networks (CANs) incorporating dynamic S,O-acetal linkages. CANs are a class of crosslinked polymer networks that can reversibly undergo bond exchange reactions, allowing the material to be reprocessed or healed without permanent degradation. In this specific system, the dynamic nature arises from an associative thiol-exchange mechanism, in which free thiolates attack the cyclic S,O-acetal bonds, triggering a substitution reaction without breaking the network connectivity. These materials exhibit dynamic behavior at elevated temperatures, enabling thermal reprocessing over multiple cycles and demonstrating efficient self-healing in proof-of-concept coating applications. Mechanistic and rheological studies confirmed the reversible exchange of S,O-acetal bonds under basic conditions, with bond dynamics tunable by temperature and the presence of nucleophilic catalysts such as DBU.

Further control over the polymer structure can be achieved by completely omitting the catalyst. Habets et al. [167] reported a catalyst-free terpolymerization of BisαCC with stoichiometric amounts of dithiols and diamines, yielding poly(monothiocarbonate-co-oxazolidone)s under ambient conditions. In this system, primary amines act as weak bases to promote selective thiol ring-opening, while the absence of strong base prevents further rearrangement. The resulting copolymers display dual glass transitions, good solubility, and can be readily dehydrated to introduce pendant α-alkylidene oxazolidone moieties, which are amenable to post-polymerization modification via thiol-ene chemistry.

To sum up, the ability of exovinylene cyclic carbonates to access such a broad spectrum of polymer classes- ranging from thermoplastics and elastomers to CANs and sulfur-functional materials- through simple variation in nucleophile and reaction conditions, positions them as one of the most strategically potent CO_2-derived monomers available today. Their modular design and high-performance profiles makes them a cornerstone for future materials innovation rooted in carbon circularity. Further research into scalable synthesis, catalyst systems, and reactive extrusion will likely accelerate the integration of αCC-derived polymers into

mainstream industrial applications, from sustainable coatings and biomedical devices to dynamic construction materials and electronic packaging.

3.1.6 Dynamic NIPUs from alkylidene oxazolidone chemistry

A very recent innovation in the field of NIPUs involves the use of CO_2-derived alkylidene oxazolidone monomers as versatile building blocks for constructing dynamic polymer networks. These alkylidene oxazolidones, synthesized via aminolysis of α-alkylidene cyclic carbonates (αCC) followed by dehydration, possess an exovinylene group that enables cationic thiol-ene addition with thiols to form N,S-acetal linkages. This chemistry was employed by Habets *et al.* [168] to produce highly dynamic, dissociative covalent adaptable networks (CANs) that can undergo mechanical recycling, chemical depolymerization, and upcycling, all under mild conditions (**Fig. 15A**). The highly dissociative nature of the N,S-acetal bonds was harnessed to enable three distinct recycling pathways for the NIPU thermosets: (1) mechanical recycling via compression molding, extrusion, or injection molding- repeated at least 10 times without property loss; (2) chemical recycling through thermal depolymerization and subsequent closed-loop repolymerization, applicable even to dyed or composite materials; and (3) upcycling by mixing two different oxazolidone-based networks into a new material with altered properties. Expanding on this platform, Caliari *et al.* [169] demonstrated the dual functionality of alkylidene oxazolidone monomers, which can participate in both radical and cationic thiol-ene reactions (**Fig. 15B**). This allows the formation of hybrid polymer networks featuring a mix of permanent (thioether) and reversible (N,S-acetal) linkages, which exhibit pluripotent mechanical properties and are compatible with 3D printing technologies such as fused deposition modeling (FDM). These systems highlight the unique potential of alkylidene oxazolidone motifs in designing next-generation recyclable thermosets, combining sustainability, tunability, and processability.

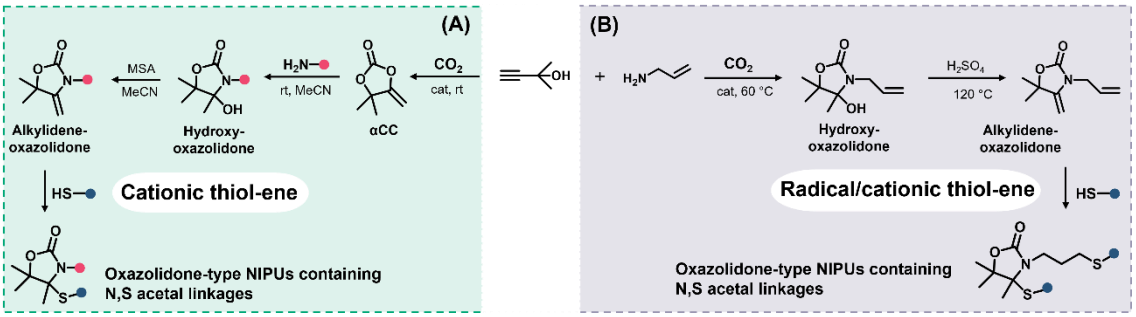

Fig. 15. Schematic representing two oxazolidone-type NIPUs; (A) Aminolysis of αCC, followed by dehydration, and subsequent cationic thiol-ene; (B) One-step protocol reaction between propargyl alcohol, allyl amine, and CO_2 followed by dehydration and subsequent radical/cationic thiol-ene.

4 Applications of NIPUs

NIPUs are increasingly investigated for applications in adhesives [170, 171], coatings [172-174], and foams [175], owing to their reported mechanical robustness, chemical resistance, and greener synthetic routes. These characteristics have positioned NIPUs as promising alternatives to conventional PUs. However, in spite of this growing interest, systematic comparisons with commercial PUs are still relatively scarce, and further validation is needed to confirm consistent performance advantages. In this thesis, particular emphasis is placed on foams providing the basis for the subsequent studies presented in this work. The following sections outline different synthetic strategies for the preparation of NIPU foams. Readers interested in other application areas of NIPUs are referred to dedicated reviews and fundamental references [176-180].

4.1 NIPU foams

Foamed polymers represent a major application of PUs, particularly in areas such as thermal insulation, cushioning, and protective packaging. The foaming of NIPUs differs from traditional PU foams (PUFs) mainly due to (1) the absence of isocyanate hydrolysis for CO_2 generation, and (2) the high energy needed for CO_2 release from cyclic carbonate decarboxylation [175]. As in PU foaming, balancing the rates of blowing and polymerization is important. A fast foaming rate with slow polymerization leads to cell wall rupture and foam collapse, while excessive cross-linking hinders proper foam expansion [181]. In response to

the challenge of foaming NIPUs without traditional isocyanate chemistry, several strategies have been developed using physical or chemical blowing procedures and are discussed here. In this section, some of the most relevant approaches are outlined, with particular emphasis on strategies based on cyclic carbonate decarboxylation, which are central to the studies presented in this thesis. For a broader overview of NIPU foaming methods-including alternative physical and chemical routes- the reader is referred to the recent comprehensive review by Orabona et al [182].

4.1.1 NIPUFs using physical blowing procedures

Physical blowing agents (PBAs) are volatile compounds- mostly low-boiling-point liquids or compressed gases- that are mixed within the foam formulation. During foam processing, these agents undergo a phase change (e.g., vaporization) upon heating or depressurization, leading to gas expansion and the formation of a cellular structure. Unlike chemical blowing agents, PBAs do not participate in chemical reactions with the polymer matrix, and their foaming effect is purely driven by physical mechanisms. In one approach, fluorocarbon blowing agents like Solkane are incorporated into the formulation to produce NIPUFs [183] (**Fig. 16A, NIPUF1**). During polymerization, the evaporation of fluorocarbon leads to the formation of a flexible PHU foam of 83 kg m^{-3} with an open-cell morphology (**Fig. 16A)** characterized by a hysteresis value of 13.3% and hardness of 3.0 kPa. A more controlled method employs supercritical CO_2 foaming, where thermoplastic PHUs are saturated with CO_2 in a high-pressure batch reactor [184]. Upon rapid depressurization, the matrix undergoes gas expansion, forming low-density, microcellular foams (**Fig. 16B, NIPUF2**). This approach was applied to the preparation of the first bio- and CO_2-sourced NIPU foams with potential thermal insulating properties. CO_2-derived cyclic carbonates, obtained by coupling CO_2 with epoxides such as poly(ethylene glycol) diglycidyl ether (PEG) and epoxidized soybean oil (ESBO) using a bicomponent organocatalyst, were polymerized with a bio-sourced amino-telechelic oligoamide. The resulting foams, prepared via a two-step batch foaming process (CO_2 impregnation under supercritical conditions followed by expansion at 80 °C or 100 °C), exhibited close porosity, microcellular morphology with pore sizes of 1–20 μm, low density (~110 kg m^{-3}), and low thermal conductivity (λ = 50 mW m^{-1} K^{-1}).

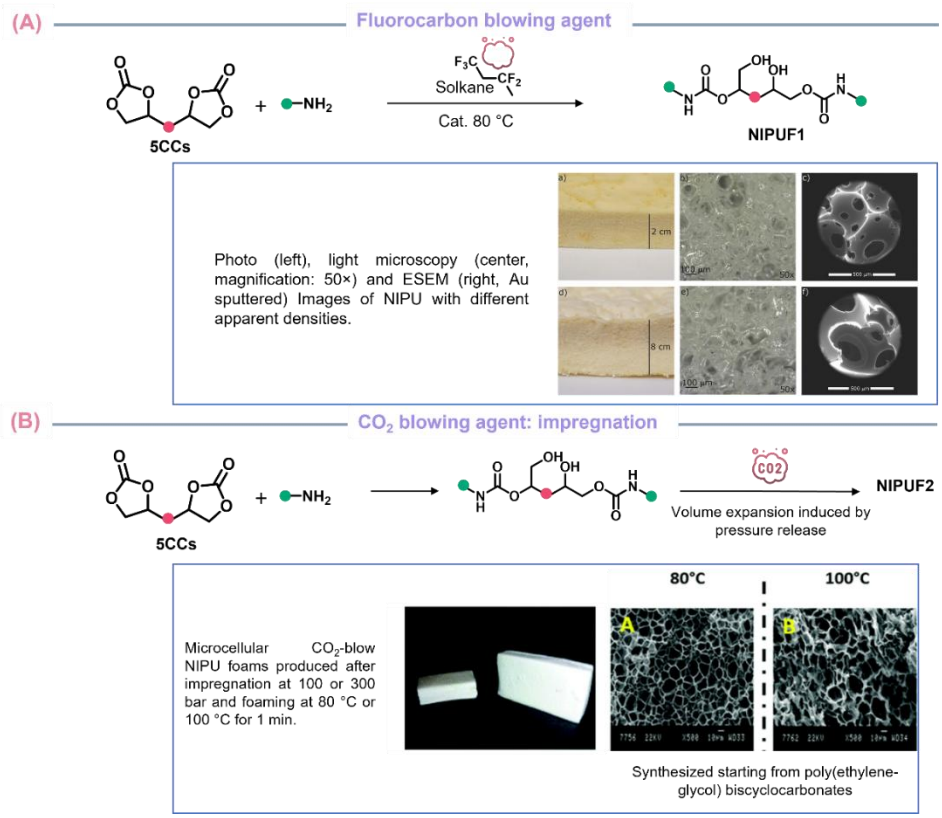

Fig. 16. Schematic representation of the foaming process for PHU-based materials using physical blowing agents; (A) Using fluorocarbon blowing agent, along with digital and ESEM images of NIPU foams with different formulations [183]; (B) Impregnation of CO_2 as blowing agent along with photographs and SEM images of the resulting foams [184].

4.1.2 NIPUFs using chemical blowing procedures

Chemical blowing agents (CBAs) are compounds that decompose or react during polymerization- often triggered by the exothermic nature of the reaction, external heating, or processing conditions- to generate gases such as CO_2 or H_2. These gaseous byproducts create porosity within the polymer matrix, resulting in foam formation [182].

4.1.2.1 Foaming based on siloxane/amine condensation

NIPU foams were prepared by exploiting the reactivity of polyamines with poly(methylhydrogenosiloxane) (PMH, MOMENTIVE MH15), generating H_2 as the blowing agent [185, 186] (**Fig. 17A**). Cornille et al. combined trifunctional 5CC (TMPTC) and difunctional 5CC (polypropylene oxide biscyclic carbonate, PPO-bis5CC) with diamines

(Jeffamine EDR148 or Priamine 1073) (**Fig. 17B**). The 5CC mixture and TBD catalyst were first blended, followed by diamine and finally PMH, and the mixture was foamed at 80 °C for 12 h and 120 °C for 4 h, yielding foams of 194-295 kg·m^{-3} (T_g= 18–19 °C) (**Fig. 17C**). The properties of NIPU foams were governed by the functionality of the cyclic carbonates as well as by the structural characteristics of both the carbonates and the amines. Later, they replaced TBD with a fluorinated thiourea catalyst enabled room-temperature foaming (3 days) using Jeffamine EDR148, 5CC, catalyst and MOMENTIVE MH15 [187], which yielded foams of 195–382 kg·m^{-3} (T_g = 0-11 °C). Sternberg et al. employed cyclocarbonated lignin with fatty-acid diamines, TBD, and DMSO, affording foams (240–331 kg·m^{-3}, T_g ~100 °C) [188]. Ahmad et al. proposed an alternative using amine-terminated hydroxyurethane precursors from carbonated castor oil and diamines, combined with epoxy resin/hardener and PMH, producing foams at 90 °C (1 h) [189]. To lower curing temperatures, Coste et al. used tetrafunctional 6CC precursors, liquid at room temperature, mixed with diamines and PMH without catalyst, under mild conditions (4 h, 50 °C), yielding foams (170–530 kg·m^{-3}) with properties tuned by diamine structure [190].

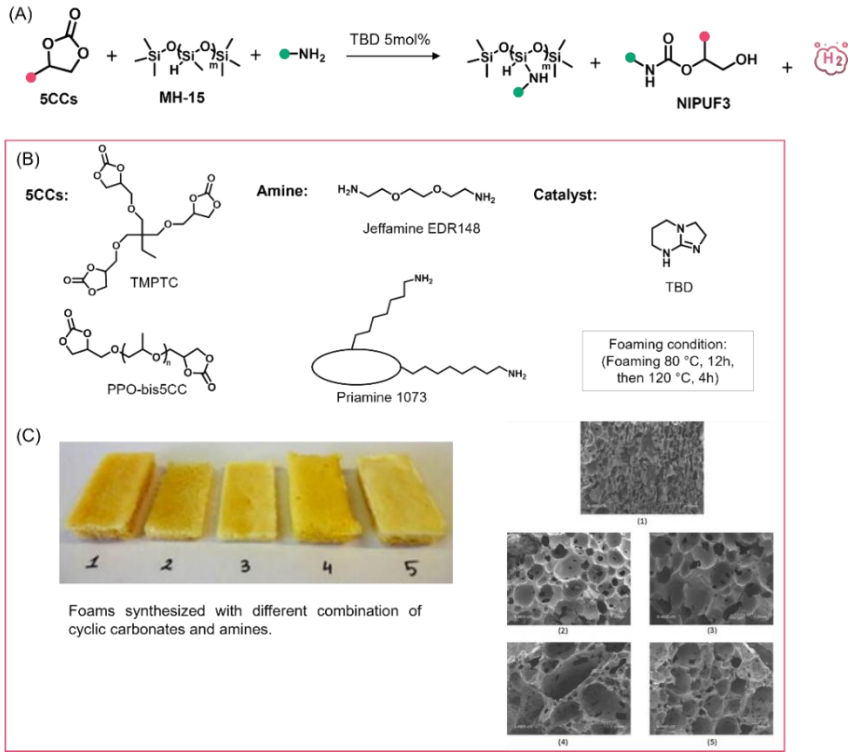

Fig. 17. (A) Schematic illustration of the foaming process of PHU-based materials via siloxane/amine condensation; (B) The formulation of the first reported PHU self-foaming system relied on a siloxane-amine reaction that released H_2 as the blowing agent [185, 186], (C) Photographs and SEM micrographs of the same foams with different formulations. See reference [185] for more details.

4.1.2.2 Foaming based on maleic/citric acid blowing

Another foaming technique involves organic acid-based chemical blowing, using maleic or citric acid with glutaraldehyde (**Fig. 18, NIPUF4**) [191, 192]. While effective foam formation is observed, the exact foaming mechanism remains poorly understood.

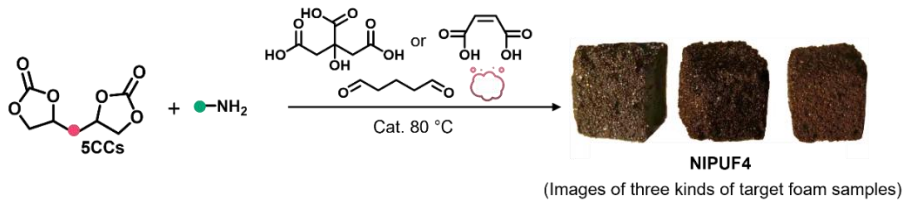

Fig. 18. Schematic representation of the foaming process for PHU-based materials using maleic/citric acid chemical blowing agent, and photographs of the resulting foams.

Each method offer unique benefits and drawbacks regarding safety measures as well as morphology control and sustainability which highlights the necessity for customized formulations in NIPU foam technology development.

4.1.2.3 Foaming based on decarboxylation of 5CC

In conventional PU systems, the ability of isocyanates to release CO_2 upon exposure to moisture is a major asset. Industrially, even when co-blowing agents such as HFCs or pentane isomers are added, water-induced foaming remains an important mechanism in self-foaming formulations. To mimic this intrinsic foaming ability, Clark et al. [193] were the first to report the decarboxylation of a biobased 5CC precursor as a strategy to promote gas cell formation within a PHU matrix (**Fig. 19A, NIPUF5**). This decarboxylation pathway arises from the aminolysis of a sorbitol-derived difunctional 5CC, producing the two common PHU isomers. A key point is that the isomer containing a primary hydroxyl group- which is more reactive- is prone to intramolecular rearrangement as a secondary process that releases CO_2. However, precise control over the ratio of these PHU isomers remains challenging, resulting in an uncontrolled extent of decarboxylation. This work initiated a new approach in the development of NIPU foams by showing that 5CC precursors can have a dual function: contributing to the formation of the PHU backbone and at the same time generating CO_2 for foam expansion. Building on this concept, Monie et.al [194] developed a tricomponent system exploiting the orthogonal reactivity of (i) amine and (ii) thiol precursors with a trifunctional 5CC (**Fig. 19B1,**

NIPUF6). Under controlled temperature and catalytic conditions, this system enables simultaneous curing and decarboxylation processes. They proved that the S-alkylation reaction between thiol monomers and tri-cyclic carbonates proceeds efficiently in the presence of DBU as a catalyst. Applied to reactive formulations containing a tri(cyclic carbonate), a diamine, and a dithiol, this strategy produced homogeneous microcellular PHU foams with open-cell morphology (**Fig. 19B2**) under mild curing and ambient atmosphere. Importantly, the formation of thioether linkages during CO_2 release contributed to network construction and fixed the thiol units into the polymer matrix. The resulting foams were highly flexible and could incorporate additives such as clay and PDMS, demonstrating compatibility with formulation tuning. Building on the S-alkylation foaming platform, Torkelson and colleagues introduced a rheology-guided formulation strategy in which the aminolysis (gelling) and thiol-decarboxylation (foaming) reactions were decoupled. This approach allowed them to optimize network strength prior to gas release, enabling rapid, catalyst-free self-blowing while reducing the synthesis time from ~20 h to 30 min without sacrificing foam morphology or properties [195], later extending this to bio-based systems derived from cashew nutshells [196]. Their subsequent studies elucidated how thiol structure and dynamic covalent chemistry govern foam performance, thereby enhancing both the sustainability and tunability of PHU foams [197].

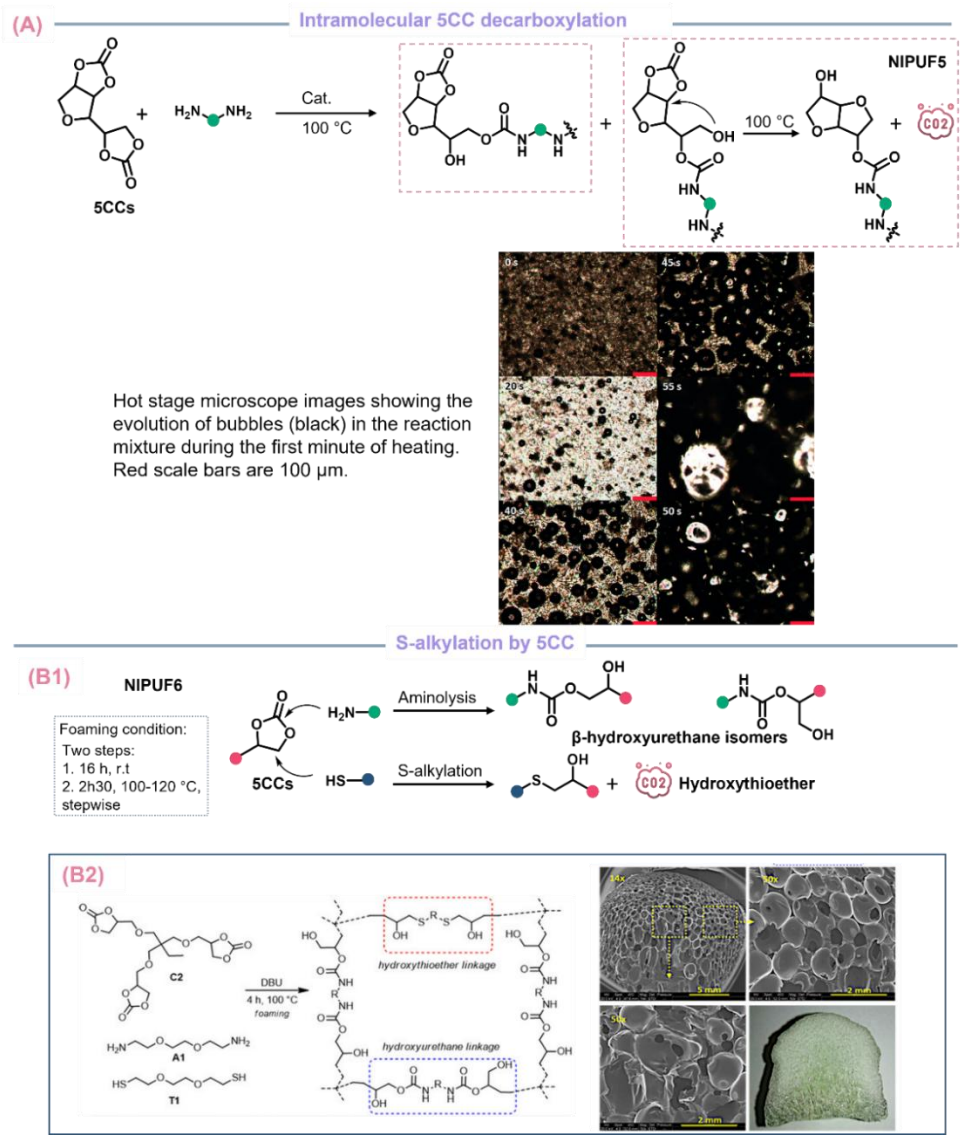

Fig. 19. (A) at the top, general foaming process for thermally driven decarboxylation of bis-cyclic carbonates derived from sorbitol, at the bottom, hot stage microscope images of the foams; (B1) general foaming process for S-alkylation of 5CC, and (B2) PHU formulation and SEM characterizations of corresponding self-blown foams.

Later, Monie et.al reported a one-pot method for producing self-blown, NIPUFs by combining amines with cyclic carbonates to form the polymer matrix, along with thiolactone. The aminolysis of the latter generates a thiol that react with the cyclic carbonates to release CO_2 as the blowing agent [198] (**Fig. 20, NIPUF7**). This process enables the simultaneous formation of multiple linkages within the polymer network, such as amides, hydroxyurethanes, and thioethers. The obtained foams exhibit an open cell morphology and can be controlled from flexible to rigid by adjusting the formulation parameters. Use of masked thiols (thiolactones) improves handling by reducing odor and safety concerns, while allowing catalyst-free polymerization and foam formation [199].

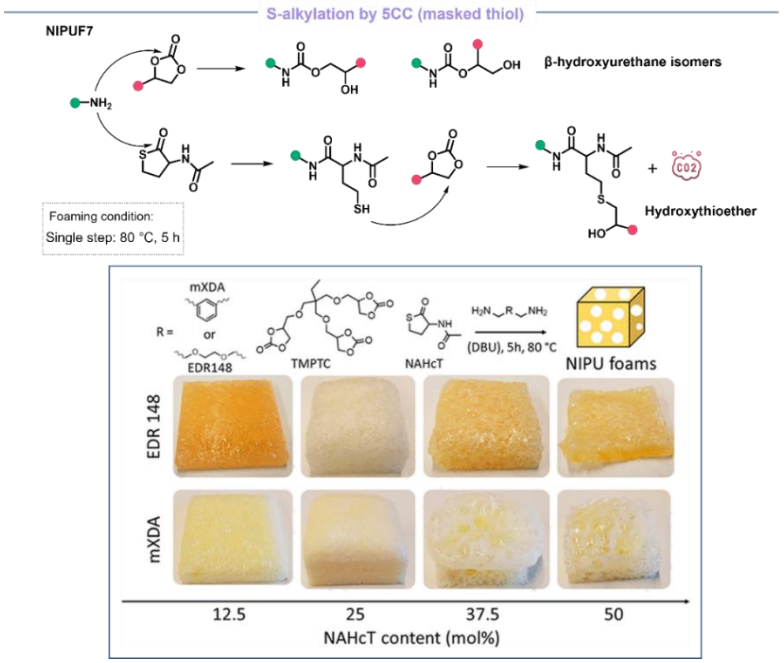

Fig. 20. (Top) Schematic illustration of the foaming process of PHU-based materials via S-alkylation of 5CCs. (Bottom) Formulations of different foams and their corresponding photographs.

Building upon the selective decarboxylation of 5CCs for blowing agent generation, a major breakthrough was made by utilizing the susceptibility of 5CCs to hydrolysis in basic environments. By carefully controlling water content, temperature, and catalyst (DBU) loading, a self-foaming PHU system was developed that closely mimics conventional PUFs (**Fig. 21, NIPUF8**) [181]. In addition to the aminolysis forming the PHU network, partial hydrolysis of 5CCs releases CO_2, which acts as the blowing agent. In terms of chemistry, the authors generated a series of NIPU foams from a conventional tris(cyclic carbonate), exploring the influence of different amines (aromatic and aliphatic), reaction temperatures (80 and 100 °C), curing times (3 and 5 h), and water contents. Under the chosen conditions, aminolysis yields surpassed 90% within 30 min. Depending on the formulation, both flexible and rigid foams were produced. The incorporation of clays, such as hydrotalcite, was particularly important for achieving uniform cellular structures (**Fig. 21B**). The self-blown foams exhibited compressive strengths in the range of 0.10–0.20 MPa at 40% strain. (**Fig. 21C**, top images). Crucially, the method was also validated at a larger scale into preheated closed molds of defined geometries to mimic the reaction injection molding (RIM) process (**Fig. 21C**, bottom images). This solvent-free route provided foams at 100 °C, whose properties closely matched those prepared on a smaller scale. Altogether, this work represents the first demonstration of NIPU

foam scale-up in closed molds mimicking the RIM process, offering a practical route toward industrial application.

This hydrolysis-induced foaming strategy was further extended by Trojanowska et al. [200], who incorporated moisture-containing biofillers- such as proteins, lignosulfonate, and polysaccharides- into the formulation. The intrinsic water in these fillers, together with water from the co-monomer mixture, was sufficient to partially hydrolyze CO_2-based cyclic carbonates in the presence of DBU as catalyst, triggering in situ CO_2 release and enabling uniform self-blown PHU foams. This approach allowed the fabrication of foams with up to 97% theoretical bio-based content by selecting bio-based monomers, while offering tunable mechanical properties and maintaining recyclability.

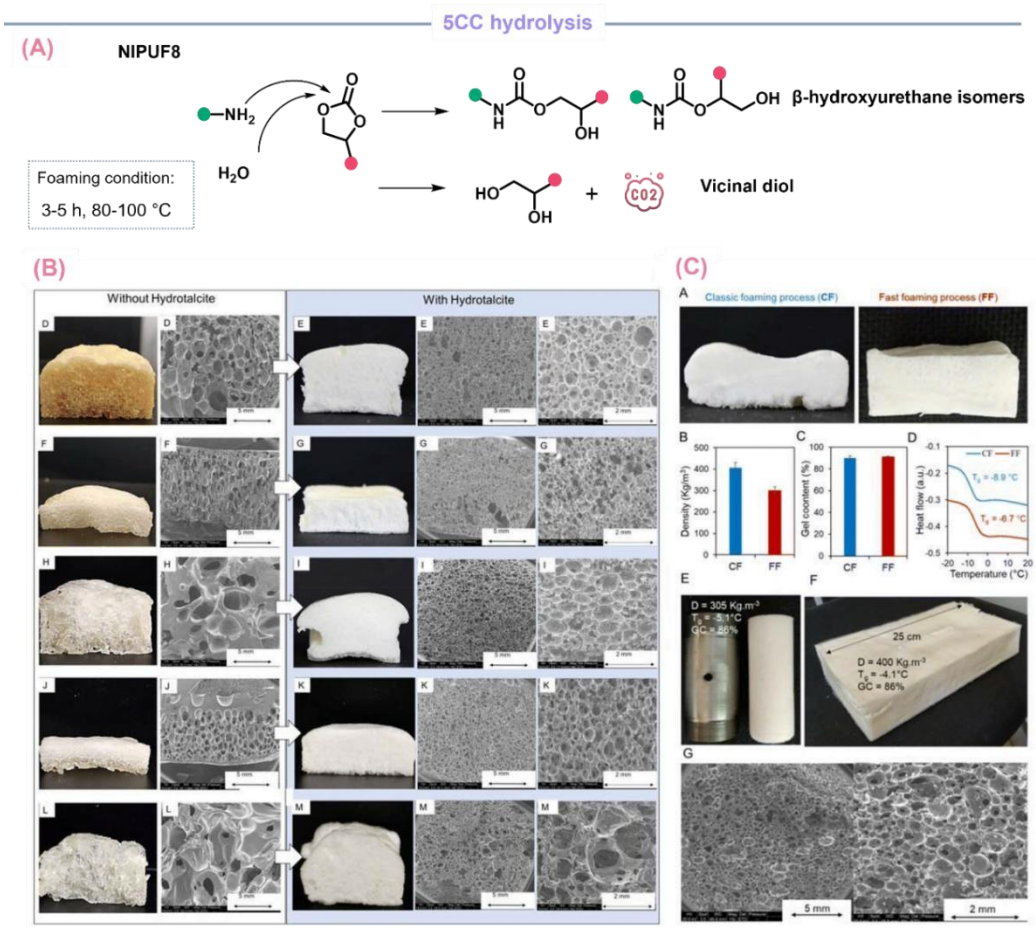

Fig. 21. (A) Schematic illustration of the foaming process of PHU-based materials via 5CC hydrolysis; (B) Morphological characterization of the foams in the presence and absence of hydrotalcite as reinforcing filler; (C) Comparison between the classic foaming process (left) and the fast foaming process (right): density, gel content, and thermal properties (top). Upscaling of NIPU foam production up to 650 g in a closed mold, with SEM images of the scaled-up formulation (bottom) [181].

Moreover, the same group developed a rapid room-temperature method to produce hybrid NIPUFs using cascade exothermic reactions from a diamine/triamine mixture, poly(cyclic carbonate) and polyepoxide combined with water and a catalyst (KOH) as follows: (1) aminolysis of CC, (2) hydrolysis of CC and (3) aminolysis of the epoxy precursor (e.g., trimethylolpropane triglycidyl ether, TMPTE) (**Fig. 22, NIPUF9)** [201]. By varying the diamine in TMPTE-based formulations, the platform yielded both flexible and rigid foams that demolded in ~15 min with high gel contents and overall densities of ~200–300 $kg \cdot m^{-3}$ (**Fig. 22A–C**). Substituting petro-based TMPTC/TMPTE and the synthetic filler with glycerol-derived GTC/GTE and natural clay (Cloisite Na) provided foams of similar quality while increasing the bio-based content to ~70–90 wt% (**Fig. 22B,D**).

In a distinct yet conceptually related approach, they also revisited the thiol-cyclic carbonate foaming system and addressed its slow reactivity by substituting aliphatic thiols with more acidic aromatic thiols [202]. This modification allowed the amine co-monomer to promote the S-alkylation reaction without the need for an external organobase catalyst. While this catalyst-free formulation was not sufficiently reactive to foam at room temperature alone, the integration of epoxides enabled a cascade of exothermic reactions that rapidly elevated the temperature into the foaming window. As a result, homogeneous, crosslinked NIPUFs were obtained within 5 minutes, with tunable mechanical properties ranging from flexible to rigid depending on the amine and epoxide combination.

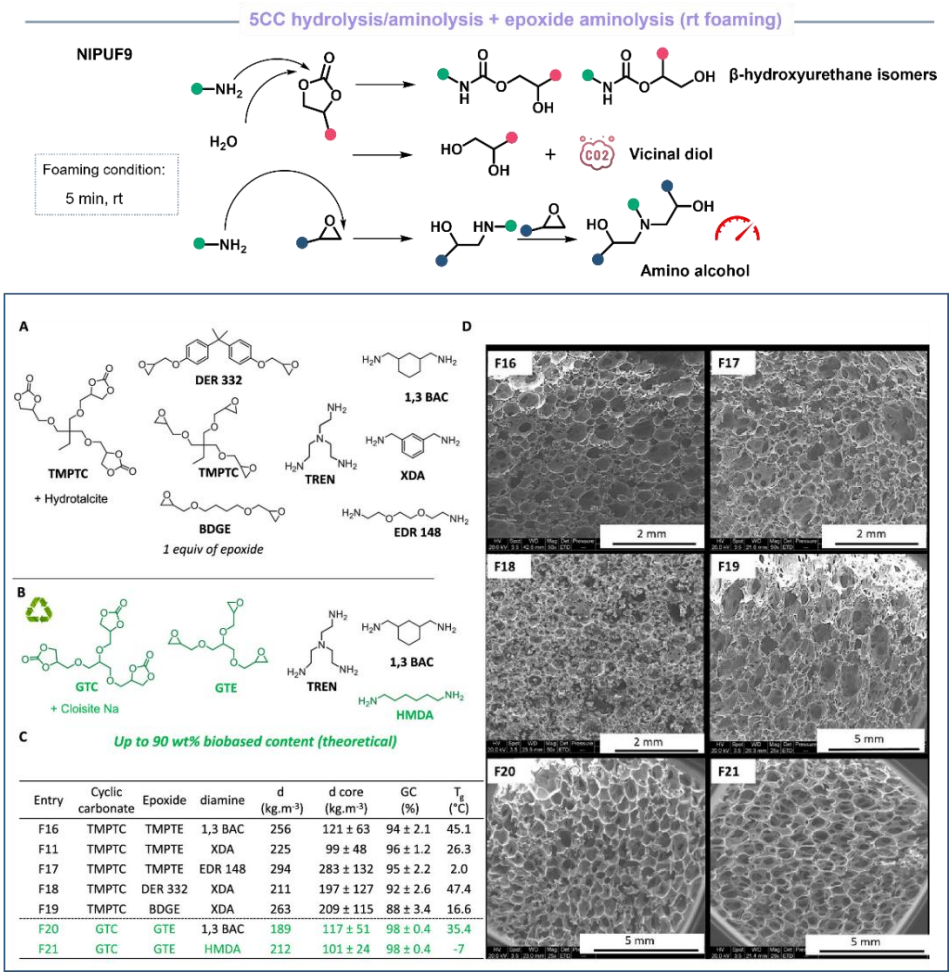

Entry	Cyclic carbonate	Epoxide	diamine	d (kg.m^{-3})	d core (kg.m^{-3})	GC (%)	T_g (°C)
F16	TMPTC	TMPTE	1,3 BAC	256	121 ± 63	94 ± 2.1	45.1
F11	TMPTC	TMPTE	XDA	225	99 ± 48	96 ± 1.2	26.3
F17	TMPTC	TMPTE	EDR 148	294	283 ± 132	95 ± 2.2	2.0
F18	TMPTC	DER 332	XDA	211	197 ± 127	92 ± 2.6	47.4
F19	TMPTC	BDGE	XDA	263	209 ± 115	88 ± 3.4	16.6
F20	GTC	GTE	1,3 BAC	189	117 ± 51	98 ± 0.4	35.4
F21	GTC	GTE	HMDA	212	101 ± 24	98 ± 0.4	-7

Fig. 22. (Top) Schematic illustration of the foaming process of PHU-based materials via 5CC hydrolysis/aminolysis plus epoxide aminolysis. (Bottom) (A) List of monomers used for producing PHU hybrid foams from RT formulations; (B) structure of the monomers used for preparing foams with high theoretical biobased content; (C) formulations and foams properties (D) SEM images of the different foams. for detailed explanation see [187] .

More recently, Makarov et al. [203] introduced a hybrid foaming system combining conventional 5CCs and exo-vinylene-substituted analogues (αCCs), which undergo rapid and highly exothermic aminolysis at room temperature (**Fig. 23, NIPUF10)**. The αCC-driven cascade exotherm enables fast, catalyst-free foaming without the need for epoxides or external blowing agents, while selectively generating pendant hydroxyoxazolidone structures within the NIPU network. This modular approach allows fine-tuning of foam morphology and mechanical properties- from flexible to rigid- through adjustments in αCC/5CC ratio, water content, and amine composition, marking a significant step toward next-generation, NIPUFs.

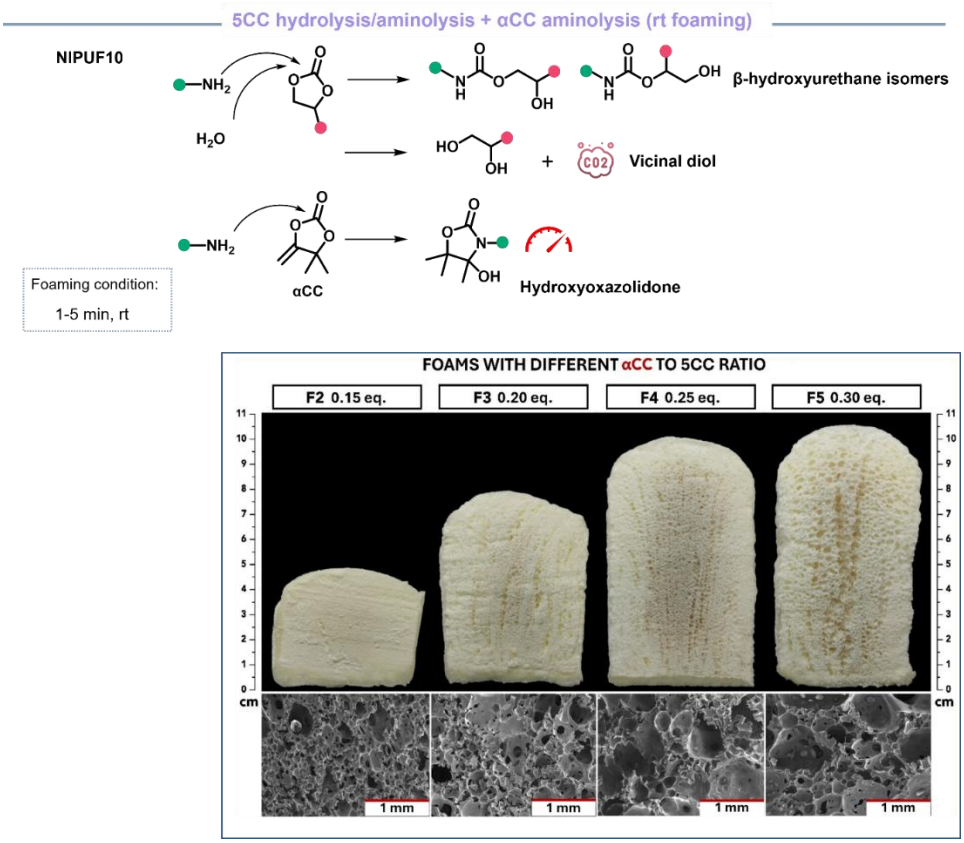

Fig. 23. (Top) Schematic illustration of the foaming process of PHU-based materials via 5CC hydrolysis/aminolysis plus αCC aminolysis; (Bottom) Formulations of different foams and their corresponding photographs [189].

These studies collectively demonstrate that self-blown NIPUFs are advancing quickly, with growing engagement across research groups. Recent innovations in formulation design, benign blowing strategies, and crosslinking chemistry have markedly improved cell morphology, compressive performance, and thermal insulation. Although challenges remain- most notably matching the performance-to-cost ratio of conventional PUFs and addressing the inherent hydrophilicity of NIPUFs. Compared to conventional PUFs, NIPUFs exhibit a higher degree of hydrophilicity, owing to the abundance of polar hydroxyl and carbamate groups. This increased affinity for water leads to hydroplasticization of the polymer matrix, which can alter mechanical properties upon moisture uptake [204]. While this presents a challenge for durability, it also underscores the need for targeted strategies (e.g., crosslinking density optimization, hydrophobic co-monomers, surface treatments) to balance sustainability with performance [204]. Nevertheless, NIPUFs with very high bio-based content (>90%) can now be prepared readily, underscoring their upward trajectory as next-generation sustainable foams. With continued optimization of reactivity, cure profiles, and foam stabilization, NIPUFs are poised to become viable and competitive alternatives in targeted commercial applications,

while aligning with sustainability goals and regulatory momentum to limit or phase out isocyanates.

From an environmental and techno-economic perspective, NIPUFs exchange some processing convenience for substantial gains in hazard reduction and circularity. Eliminating diisocyanates addresses worker-exposure and end-of-life concerns and enables the use of CO_2-derived cyclic carbonates and other bio-based feedstocks. At the same time, realizing net sustainability benefits depends on solvent-free routes, lower-temperature cures, efficient catalysts, and design-for-recycling- elements best verified via rigorous cradle-to-gate/-grave LCA. Economically, PUFs still benefit from decades of scale, fast cure cycles, and optimized supply chains; NIPUFs face higher unit costs today due to slower kinetics and newer value chains [205]. However, learning-curve effects, process intensification (e.g., continuous foaming/RIM adaptations), and regulatory and market pull for safer, low-hazard materials are rapidly narrowing this gap.

4.2 Toxicity considerations of NIPU monomers and precursors

While NIPUs avoid the use of highly toxic isocyanates, their synthesis still relies on precursors whose toxicological profiles vary considerably. The assumption that NIPUs are inherently safe is therefore misleading; instead, the toxicity of individual building blocks must be carefully considered.

Amines. Aliphatic and aromatic diamines are widely used in NIPU synthesis, yet some are known to exhibit significant hazards. For example, tris(2-aminoethyl)amine (TREN) is corrosive and acutely toxic upon inhalation (see product safety data sheet), while toluene-2,4-diamine (TDA) is classified as a probable human carcinogen (IARC Group 2B) [206]. Conversely, some aliphatic diamines such as hexamethylene diamine (HMDA) or isophorone diamine (IPDA) are less acutely hazardous but still require strict handling measures. Other diamines relevant to NIPU chemistry include *m*-xylylenediamine (*m*-XDA) has been associated with allergic contact dermatitis and occupational sensitization in exposed workers [207, 208], and Jeffamine EDR-148 (1,2-bis(2-aminoethoxy)ethane), a low-molecular-weight polyetherdiamines used in foaming reactions, for which peer-reviewed toxicological data are scarce. Preliminary in vitro studies on related Jeffamine polyetherdiamines suggest

comparatively lower cytotoxicity than polyethylenimine [209], but dedicated evaluations for EDR-148 are still lacking. This highlights that the selection of the diamine is a critical determinant of the overall safety profile of a given NIPU system.

Epoxides. Epoxides are the key intermediates for cyclic carbonate synthesis via CO_2/epoxide coupling, but their toxicological profile is a major limitation. Industrial production focuses on ethylene oxide and propylene oxide, derived from petroleum-based ethylene and propylene, respectively [210]. Both are volatile and hazardous: ethylene oxide is classified by IARC as Group 1 carcinogenic to humans, while propylene oxide is Group 2B possibly carcinogenic. Acute exposure causes eye, skin, and respiratory irritation, and their high reactivity toward DNA and proteins underpins their mutagenic and carcinogenic potential. Epichlorohydrin, another widely used epoxide (sometimes bio-sourced from glycerol), is also toxic and classified as Group 2A probably carcinogenic [211, 212]. Although epoxides are transient precursors to cyclic carbonates rather than components of the final NIPU foams that was synthesized in this thesis, their use raises occupational and environmental concerns, especially given their volatility and reactivity.

To address these limitations, several sustainable alternatives have been explored. These include (i) producing propylene and ethylene from bio-based ethanol or other renewable feedstocks [213]; (ii) using bio-derived epoxides such as limonene oxide or fatty acid epoxides from vegetable oils [214-217]; and (iii) employing glycerol-based epichlorohydrin or glycerol carbonate routes [218, 219]. Importantly, one-pot processes are under investigation that combine alkene epoxidation and CO_2 cycloaddition in situ, thus avoiding isolation and handling of toxic epoxides while improving process sustainability [220]. Although catalytic and selectivity challenges remain, such strategies aim to reconcile safety, renewability, and cost-competitiveness in cyclic carbonate production.

Propargylic alcohol derivatives. Propargyl alcohol (PA) and its derivatives are important precursors for CO_2-sourced α-alkylidene cyclic carbonates (αCCs), which in turn are polymerized with diamines to form NIPUs as discussed in section 3.1. However, their toxicological profile raises concerns. Inhalation studies in rats and mice showed that PA causes acute toxicity at concentrations ≥125 ppm, with the liver identified as the primary target organ and the nasal epithelium as a secondary site of injury. Chronic exposures led to non-neoplastic lesions and an increased incidence of nasal adenomas [221]. Weak mutagenic activity was also observed in bacterial and mammalian systems. Although PA is structurally distinct from

isocyanates and lacks the potent sensitization hazards of the latter, its hepatotoxic and carcinogenic potential underline the need for strict exposure control. When considering NIPU pathways based on bisαCC monomers, it is therefore important to acknowledge that their upstream synthesis involves hazardous intermediates, and comprehensive safety evaluations remain essential.

Cyclic carbonates. Toxicological data for multifunctional cyclic carbonates (di- or tricyclic) are scarce. For monofunctional cyclic carbonates such as ethylene carbonate or propylene carbonate, available studies indicate relatively low acute toxicity compared to isocyanates, and these compounds are often used as solvents [222, 223]. Based on structural analogy, it is frequently assumed that polycyclic carbonates exhibit similarly moderate toxicity, but such assumptions remain speculative until validated by dedicated studies.

Alkylidene cyclic carbonates. For alkylidene-based carbonates, which display higher chemical reactivity than conventional cyclic carbonates, no systematic toxicological studies are currently available. Their increased reactivity suggests a potentially higher toxicity, but this remains a hypothesis requiring confirmation.

In summary, although NIPUs eliminate the well-documented risks associated with isocyanates, their synthesis involves precursors whose safety profiles range from relatively benign (e.g., propylene carbonate) to highly concerning (e.g., aromatic diamines, reactive epoxides). The routes investigated in this thesis- namely the cyclic carbonate/amine/water foaming approach based on multifunctional cyclic carbonates, as well as the synthesis of α-alkylidene cyclic carbonates explored in a separate chapter- were therefore the focus of the present toxicological discussion. For these systems, preliminary evidence suggests lower overall occupational hazards than conventional isocyanate chemistry, yet comprehensive toxicological data remain lacking. Future research should thus prioritize systematic evaluation of these emerging monomers to validate their sustainability and safety claims.

5 NIPU Recycling

Having reviewed different synthetic methods and some applications of NIPUs, we now investigate their end-of-life management- a critical dimension of sustainable polymer development. Effective recycling strategies are essential for reducing environmental impact and obtaining material circularity consistent with the framework of circular economy. In recent

years, the rise of sustainable polymer science has catalyzed significant interest in recyclable NIPU systems, focusing on two principal end-of-life strategies (1) using dynamic covalent chemistry for reprocessing, and (2) depolymerization of NIPU through solvolysis.

Dynamic covalent chemistry (DCC) offers a powerful, molecularly engineered approach for NIPU recycling. By incorporating reversible covalent bonds such as imine, disulfide, or acetal linkages, NIPU networks can participate in bond exchange reactions when exposed to certain controlled conditions [224-226]. This design has inspired the vision of mechanical reprocessing of covalent adaptable networks (CANs), allowing reshaping and re-use. For example, recent studies by Detrembleur and coworkers [198, 201] and Torkelson and coworkers [227, 228] have demonstrated successful foam-to-film recycling of self-blowing PHU foams, with reprocessed materials exhibiting full recovery of crosslink density and mechanical integrity in some cases across multiple reprocessing cycles. However, major bottleneck persists: in general, during mechanical grinding and repeated reprocessing cycles, some side reactions occur, leading to substantial deterioration of mechanical performance [229, 230]. While this issue is particularly critical for crosslinked thermosets, it is increasingly being addressed, and several CANs have now progressed beyond the lab to first market introductions [231].

In parallel, depolymerization through solvolysis presents an extrinsic, reagent-driven strategy that does not depend on the presence of dynamic bonds. It involves the irreversible cleavage of labile bonds using nucleophilic reactants (for example water or alcohol), utilizing depolymerization strategies such as alkaline hydrolysis, glycolysis, or hydroglycolysis [232]. These processes yield low-molecular-weight products such as polyols, diamines, or short-chain oligomers, which can be purified and reused as feedstocks for the synthesis of new materials. Thus, depolymerization not only breaks down crosslinked networks but also enables recycling, either by closing the loop through molecular recovery and repolymerization or by valorizing the fragments into other classes of polymers. In this thesis, we focus specifically on chemical recycling as the central strategy under investigation.

5.1 Depolymerization of NIPUs through solvolysis

Solvolysis-based depolymerization serves as a promising sustainable method for breaking down NIPUs which do not have dynamic covalent bonds built into their structure. Unlike

dynamic chemistry, which enables reversible bond exchange, solvolysis works by breaking labile bonds within polymer networks through irreversible reactions with external nucleophiles like water and alcohols under specific thermal or catalytic controls. These labile bonds may include not only β-hydroxyurethane linkages, but also carbonate, ester, or thioether bonds, depending on the structure of the NIPU formulation.

This technique breaks down crosslinked or thermoset NIPU substances into retrievable monomers as well as oligomers and functional intermediates for repolymerization or other high-value applications. A small number of systematic research efforts have explored the solvolysis-based depolymerization of NIPUs for chemical recycling despite the favorable reactivity of their labile bonds. The next section provides an analysis of essential contributions which examines their operational mechanisms and effectiveness while considering their impact on future circular material design.

5.1.1 Alcoholysis

Zhang et al. [233] demonstrated a fully bio-based NIPU network that achieved chemical recycling through reaction between urethane bonds and ethanol. The polymer network was constructed from CO_2-derived cyclic carbonate and Priamine 1074, resulting in a highly crosslinked PHU structure (**Fig. 24**). To depolymerize this material, the authors employed a catalyst-free alcoholysis approach, immersing shredded NIPU samples in anhydrous ethanol at 160 °C for 8 hours in a sealed reactor. Under these conditions, ethanol acted as a nucleophile, attacking the carbamate carbonyl in a transurethanization process that resulted in cleavage of urethane linkages and formation of small oligomers. The ethanol was removed post-reaction, and the resulting fragments were reprocessed by hot pressing at 170 °C for 24 hours, regenerating a second-generation NIPU. Structural analysis (FTIR and NMR) confirmed successful restoration of the polymer backbone. Impressively, the recycled film retained 91% of its original tensile strength (31.3 MPa vs. 34.9 MPa), and even after three recycling cycles, mechanical performance remained above 20 MPa- indicating robust, repeatable recyclability.

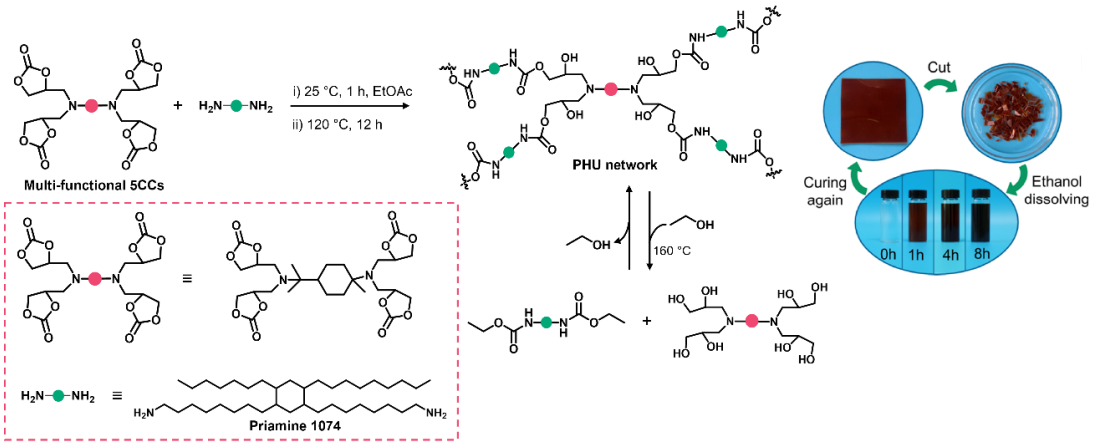

Fig. 24. Schematic representation of the crosslinked PHUs and the closed-loop recycling process through transurethanization [233].

In another study, Chen et al. [234] demonstrated the use of dynamic covalent chemistry of transcarbamoylation to achieve chemical depolymerization and monomer recovery from both linear and crosslinked PHUs. In this study, PHUs were synthesized from CO_2-derived 5CCs and p-xylylenediamine (pXDA), forming networks rich in urethane and hydroxyl groups, an ideal platform for dynamic bond exchange (**Fig. 25**). Depolymerization was achieved by treating the PHUs with methanol (MeOH) in the presence of potassium tert-butoxide (tBuOK, 3 equiv.) in a THF/MeOH (1:1 v/v) solvent system at 80 °C for 24 hours. This triggered transcarbamoylation reactions, whereby methanol reversibly exchanged with the urethane carbonyl to form dimethylcarbamate monomers and polyol byproducts. The process yielded up to 45 mol% dimethylcarbamate from linear PHUs and 15 mol% from crosslinked networks, with the recovered products confirmed to be predominantly monomeric via NMR analysis.

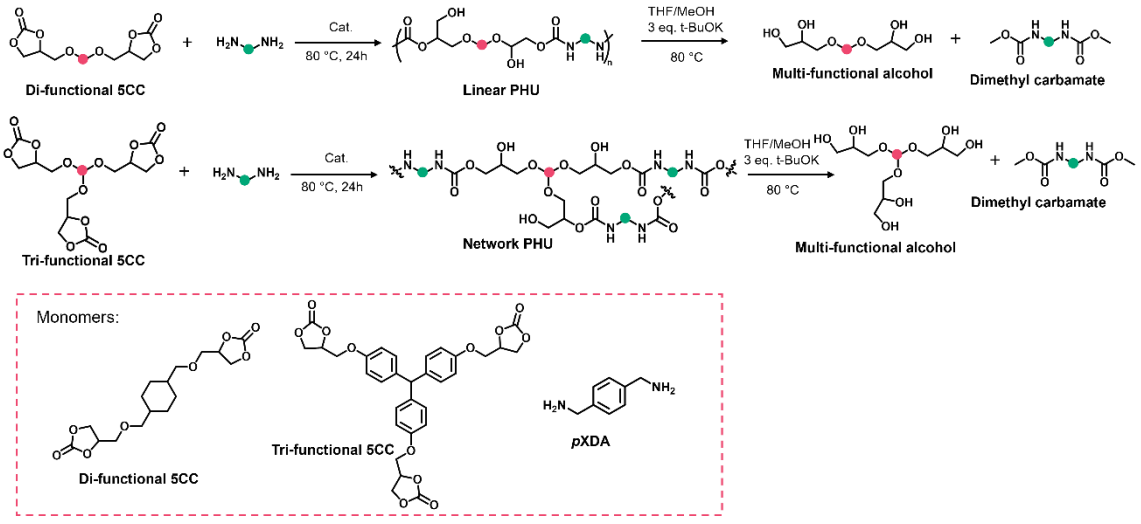

Fig. 25. Schematic representation of the linear and crosslinked PHUs and the chemical recycling process through dissociative transcarbamoylation [234].

Miao et al. [235] recently reported highly recyclable NIPUs based on resveratrol-derived 6CCs, crosslinked with multifunctional amines. The resulting rigid network, notable for its high tensile strength (up to 92 MPa), was chemically depolymerized by alcoholysis using 20 wt% sodium hydroxide (NaOH) as a catalyst in methanol under reflux for 3 h. Under these conditions, the urethane bonds were selectively cleaved, affording the original multi-1,3-propanediol monomer in 93% yield with >95% purity (**Fig. 26**). The recovered diol was further reacted with CO_2 in the presence of p-toluenesulfonyl chloride (TsCl) and N,N,N′,N′-tetramethylethylenediamine (TMEDA) to regenerate the cyclic carbonate precursor, and the subsequent second-generation NIPU exhibited nearly identical structure and mechanical properties to the original.

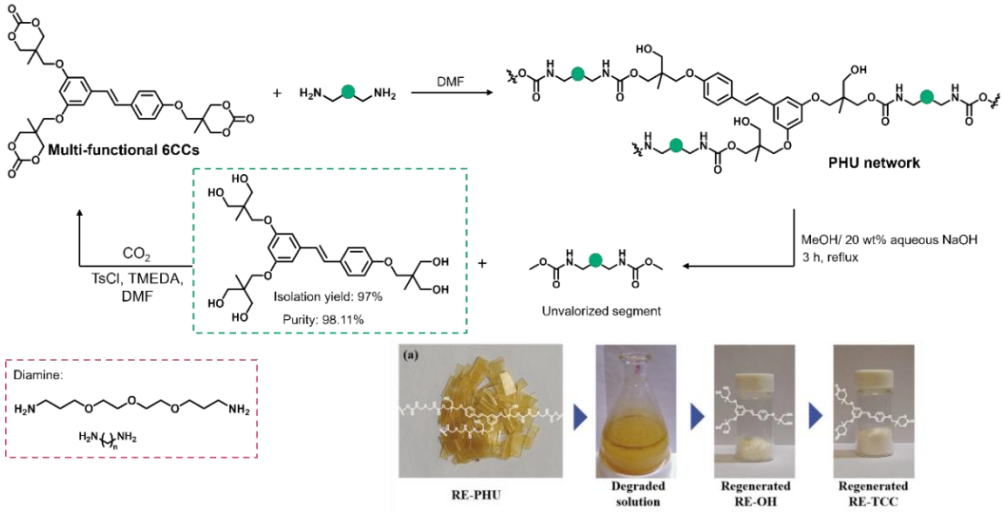

Fig. 26. Synthesis of PHU and consecutive reprocessing through alcoholysis, and conversion of recovered monomer to poly (cyclic carbonates) [235].

In a related study from the same group, Liu et al. [118] developed a series of high-strength NIPUs from CO_2-derived 6CCs based on isoeugenol, cured with multifunctional amines. These materials were chemically depolymerized under mild basic conditions (30 wt% NaOH in ethanol at 90 °C for 4 h) to yield the pre-monomer in >90% recovery and 99.6% purity, as confirmed by FTIR, NMR, and MS. The recovered monomer was converted back into the cyclic carbonate (multifunctional 6CCs) and reused to produce new NIPUs. Impressively, the recycled NIPUs exhibited >98% recovery in tensile strength and identical thermal properties (T_g = 51 °C) compared to the original, highlighting the material's excellent chemical circularity.

In a complementary approach, Wybo et al. [236] synthesized lignin-based, crosslinked aromatic NIPUs via transurethanization between dimethyl dicarbamates and liquid lignin polyols. Despite the thermoset nature of the final material, effective depolymerization was achieved via transurethanization inverse reaction in neat methanol at 140 °C for 24 h in a sealed reactor under autogenous pressure (~10 bar), without any added catalyst (**Fig. 27**). This treatment yielded a brown homogeneous liquid from which the initial carbamate and polyol building blocks were recovered. FTIR and NMR analysis confirmed the reformation of dimethyl dicarbamates and hydroxyl-rich lignin polyols, with approximately 90% of urethane bonds cleaved. Although the repolymerized material exhibited slightly reduced mechanical performance, attributed to minor urea formation and water sensitivity, it retained its urethane network structure, illustrating the feasibility of partial monomer regeneration from aromatic, bio-based NIPU thermosets.

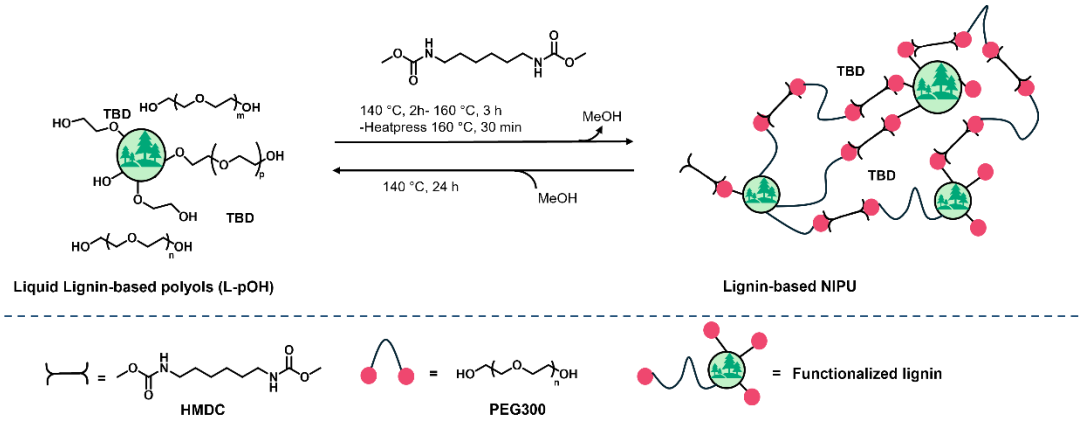

Fig. 27. Reaction scheme for the polymerization of Lignin-based NIPU with HMDC, and its depolymerization with methanol [236].

5.1.2 Hydrolysis

Hydrolysis has emerged as a viable strategy for the chemical depolymerization of NIPUs, particularly those containing hydrolytically labile carbonate. This approach typically involves the cleavage of polymer linkages through reaction with water under acidic or basic conditions, resulting in the formation of polyols, amines, CO_2, or other low-molecular-weight fragments. Mechanistically, hydrolysis proceeds through nucleophilic attack of water on the electrophilic carbon in either the urethane or carbonate group, followed by proton transfers and bond cleavage. When properly designed, this strategy enables the selective degradation of NIPU

networks, particularly for the recovery of embedded bio-based components such as lignin or hydroxyl-functional polyols, and can complement dynamic recycling strategies when dissociative bond scission is desired.

Wu et al. [224] developed a self-healing, reprocessable, and partially degradable NIPU elastomer by synthesizing a dual crosslinked network based on low-molecular-weight amino-terminated nitrile rubber (ATBN) and 6CCs derived from di(trimethylolpropane). Because the terminal amine groups of ATBN are sterically hindered by the long rubber chains, the authors first prepared a prepolymer via nucleophilic addition with bis(6-membered cyclic carbonate) (6CCs) in N-methyl-2-pyrrolidone (NMP) at 100 °C for 24 h under nitrogen. This prepolymer was then crosslinked by further reacting with additional 6CCs and titanium isopropoxide catalyst ($C_{16}H_{36}O_4Ti$) in THF at 25 °C, resulting in a polymer with both covalent urethane bonds and physical crosslinks from hydrogen bonds formed by hydroxyl and carbonate groups (**Fig. 28**). To chemically depolymerize the network, the polymer was treated with 1 M HCl at 100 °C for 24 h, which selectively cleaved the carbonate-linkage introduced from the 6CC units. The urethane bonds remained intact, allowing for the selective recovery of di(trimethylolpropane) in up to 75% isolated yield. No recovery of the amine-based ATBN component was attempted, and the authors did not demonstrate repolymerization of the recovered monomer.

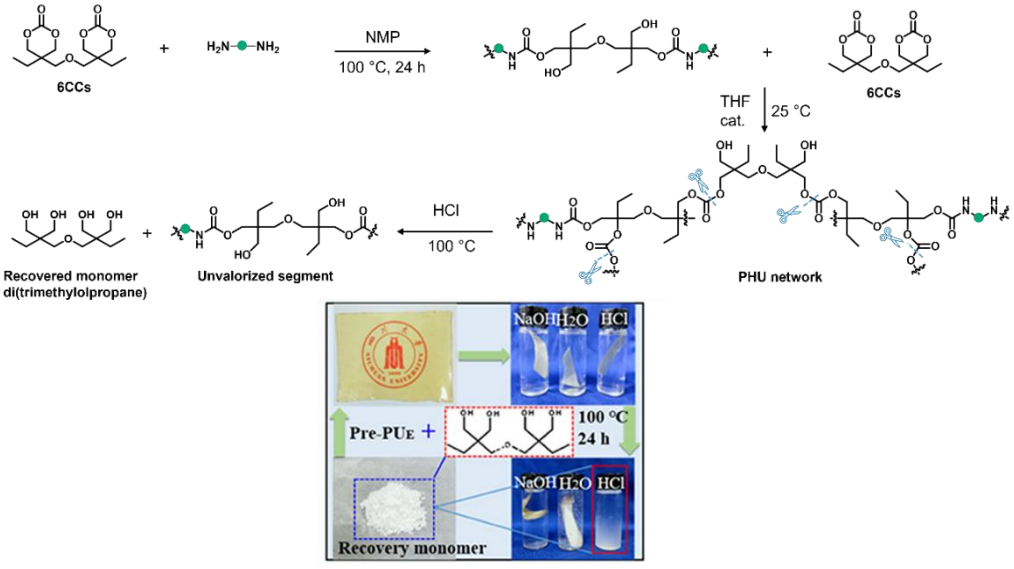

Fig. 28. The chemical synthesis route and molecular design of PHU network and subsequent hydrolysis depolymerization [224].

Sternberg et al. [232] demonstrated a chemical recycling process for lignin-based NIPU foams, emphasizing selective recovery and reuse of lignin. The NIPU foams were synthesized from glycerol carbonate-oxyalkylated Kraft lignin, cyclocarbonated with dimethyl carbonate (DMC), and cured with bio-based Priamine 1074 (**Fig. 29**). The cyclocarbonated lignin monomer possesses additional labile ether and acyclic carbonate linkages, which facilitate its decomposition within the foam matrix. Glycolysis with ethylene glycol alone exhibits limited degradation efficiency- even at 220 °C- achieving only 30-40% foam breakdown after 3-6 hours. In contrast, alkaline hydrolysis using 0.1 M KOH under the same conditions results in a significantly higher degradation rate of approximately 65-70%. The most effective strategy, however, involves a hybrid hydroglycolysis process, which combines 10 wt% ethylene glycol with a 0.2 M aqueous KOH solution. This approach enhances foam decomposition efficiency up to 90%. In this study, the authors specifically focused on the recovery, characterization, and reuse of lignin to fabricate second-generation foams. Detailed structural analysis revealed that the hydroglycolysis treatment yields an ethylene glycol-modified lignin with high hydroxyl functionality- favorable for the reformation of cyclic carbonates via condensation with dimethyl carbonate (DMC)- and a molar mass comparable to that of native lignin. This structural preservation ensures full solubility of the recycled lignin in new foam formulations.

Unlike lignin recovered via alkaline hydrolysis, which could only be reintegrated at 10-20 wt% due to solubility issues stemming from extensive structural modifications, the lignin obtained from hydroglycolysis was revalorized entirely. It enabled the fabrication of foams with physical properties- density (251 kg/m^3), compressive modulus (1.51 MPa), and compressive strength at 10% deformation (0.126 MPa)- that are virtually identical to those of the original foams.

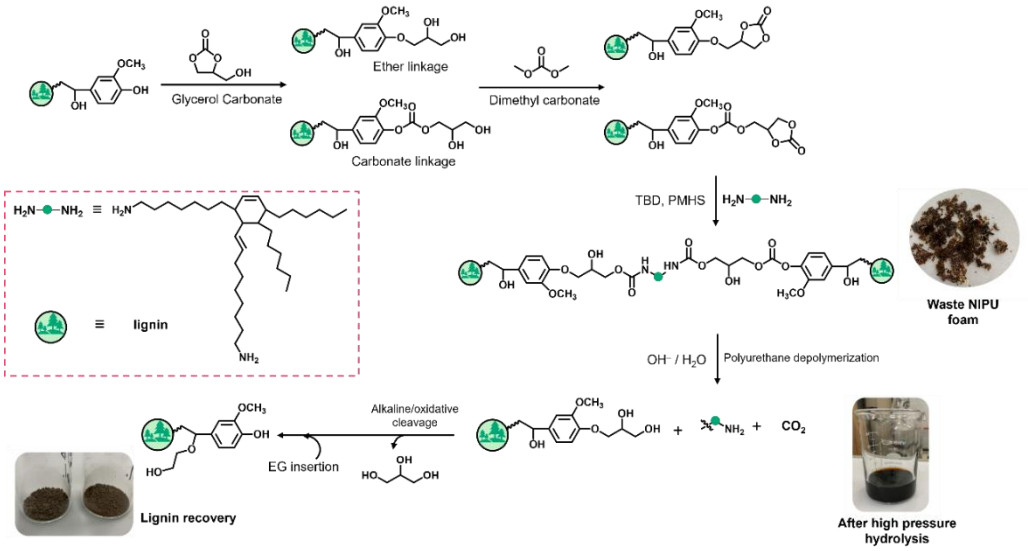

Fig. 29. Chemical recycling of the lignin-based NIPUFs, side products, and recovery of hydroxy-functionalized lignin fragments [232].

6 Life Cycle Assessment: A Tool for Navigating the Sustainability Challenges of Polymers

After investigating the synthesis methods, applications, and recycling techniques of NIPUs, we should now assess their environmental relevance beyond laboratory performance. Although innovative chemistries and recycling techniques improve the circularity of NIPUs, a thorough evaluation of their true sustainability demands quantifiable and systematic metrics. Sustainability in polymer science comes from a complex interaction between functional performance, environmental impact, and economic feasibility throughout the material's whole life cycle. Polymers need technical properties such as durability and thermal stability but also require minimized resource use and impacts associated with emissions and toxicity throughout their life-cycle. Sustainability have an inherent multidimensionality and its measurement by a single parameter is not possible. This section examines different methods for sustainability evaluation in polymer science while emphasizing on life cycle assessment (LCA).

6.1 How can we measure sustainability in polymer science?

A variety of tools have been developed to assess environmental performance, each having specific advantages but also some limitations. Historically, two of the most influential metrics-

Atom Economy (1991) [237] and the Environmental Factor (E-factor) (1992) [238]- established the basis of sustainable chemical fabrication. Interestingly, the introduction of these metrics occurred even before the formal establishment of the twelve principles of Green Chemistry in 1998. This shows that the necessity for quantitative measures of process efficiency and waste minimization was understood earlier. However, by time it became evident that reaction-level metrics did not sufficiently cover all environmental issues including toxicity, energy usage, and life cycle impacts (**Fig. 30**).

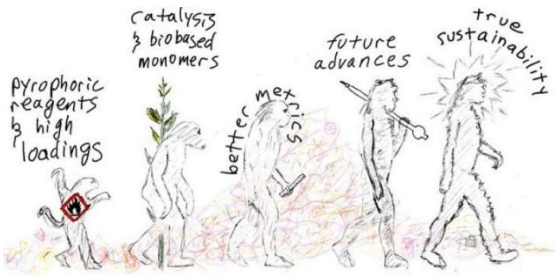

Fig. 30. Sustainable Polymers: Our Evolving Understanding, adapted from [239].

This realization resulted in the development of more organized and comprehensive methodologies expanding from process-specific indicators to system-wide assessment frameworks. According to Vaccaro et al. [240], green chemistry metrics are generally divided into three principal groups: (1) mass-related metrics, (2) non-mass-related metrics, and (3) systemic tools, including life cycle assessment (LCA) and circularity metrics.

This classification presents a structured and unified framework for assessing sustainability at multiple levels- from single chemical reactions to entire product systems- and will be used in this thesis to structure both theoretical discussion and applied analysis.

6.1.1 Mass-related metrics

Mass-based green chemistry metrics are one of the earliest-established and most widely used tools for evaluating the efficiency of chemical processes. They quantify how effectively raw materials are transformed into final products, pointing out waste minimization and resource efficiency at the molecular and reaction scales. Some examples of mass-related green metrics are selected and explained in this section.

Atom Economy (AE), introduced by Trost in 1991 [237], is a theoretical measure of the percentage of reactant atoms that remain in the final product. While AE is useful in concept design, it neglects the reaction yield, excess reagents, solvents, and auxiliaries, making it insufficient to use in real situations.

The Environmental Factor (E-factor), developed by Sheldon in 1992 [238], enables a more complete and systematic view by calculating the mass of waste generated per unit mass of product. It accounts for solvents, purification materials, and side products- making it more representative of actual industrial operations.

Process Mass Intensity (PMI) expands on the E-factor by evaluating the total input mass required (including reactants, solvents, catalysts, and auxiliaries) per mass of product [241]. Unlike AE, PMI can be applied to real process data, and unlike the E-factor, it retains a non-subtractive format that enables clear material flow accounting.

Reaction Mass Efficiency (RME) combines yield, stoichiometry, and AE to provide a normalized percentage of starting reactants converted into the final product [241]. It is specifically useful for comparing various synthetic routes for the production of the same target molecule.

These metrics are particularly used in pharmaceutical and fine chemical industries because they are simple to implement specifically for small- and mid-scale experimental settings. However, they remain process-centered and do not account for toxicity, energy consumption, or life cycle impacts, which are critical to evaluating sustainability in polymer systems where starting materials, additives, and recycling choices vary significantly in environmental burden [242].

6.1.2 Non-mass-related metrics

To deal with the limitations of mass-only metrics, more holistic tools have been developed that incorporate toxicity, safety, hazard potential, and environmental impact. These non-mass-related metrics reflect a deeper consideration of chemical risk and benign design. For example, the benign index (BI), developed by Andraos [243], integrates multiple environmental impact criteria- such as persistence, bioaccumulation, and acute toxicity-into a single normalized score from 0 (most harmful) to 1 (least harmful). Each chemical used in the process is weighed by its molar contribution. The safety hazard index (SHI) is also similar, but concentrates on physical and safety risks, such as flammability, explosiveness, and occupational hazards [244].

It facilitates the assessment and identification of safer reagents, solvents, and intermediates. Other compound-level hazard metrics, such as the GHS-based hazard scores, or Globally Harmonized System ratings, can be applied to assess substitution options and process safety in early-stage polymer formulation and scale-up [242]. When designing polymers and additives that have minimized toxicity to humans and ecosystems, these metrics become vital as they address the growing concerns regarding persistent plastics and dangerous degradation products. However, these evaluation tools are limited to qualitative measures and rankings- which prevents their straightforward integration into material flow models and circularity analysis frameworks.

6.1.3 Systemic tools: life cycle assessment (LCA)

For more comprehensive evaluation of environmental performance beyond single chemical reaction, system-wide tools such as LCA and circularity metrics have proven essential. It is the most comprehensive and internationally standardized tool for environmental assessment and has become important in polymer science for comparing materials, technologies, and strategies on a common basis. The following section will therefore introduce LCA in detail- its definition, methodological structure, and application for evaluating NIPU production and recycling- helping prepare for how it will be used later in this thesis.

6.2 LCA definition

LCA began in the late 1960s because industries were concerned about how they used energy and materials. In 1969 Harry Teasley from the Coca-Cola company launched one of the earliest formal environmental life cycle analyses which examined the resource and energy needs of multiple beverage containers [245]. Researchers conducted this groundbreaking study to evaluate energy consumption and material use throughout the entire existence of beverage containers while creating the first documented example of LCA application. This early work predated the 1973-74 oil crisis but already reflected concerns about efficient resource use and associated environmental impacts, paving the way for the subsequent evolution from linear to circular industrial frameworks.

In the 1970s and 1980s, U.S. environmental legislation such as the Resource Conservation and Recovery Act (RCRA, 1976) formalized the idea of evaluating products from “cradle to grave,”

requiring analyses of waste and material recovery across entire systems [246]. However, during this era various industries used different methods for life cycle assessments which lacked coordination. The 1990s represented an essential milestone for the development and standardization of LCA methodology. The Society of Environmental Toxicology and Chemistry (SETAC) together with the International Organization for Standardization (ISO) took crucial roles in shaping and standardizing life cycle assessment methods [247]. SETAC's 1993 Code of Practice emphasized objectivity and full-system analysis, while ISO 14040 and 14044 standards (published in 1997 and updated in 2006) defined LCA as the "compilation and evaluation of the inputs, outputs, and the potential environmental impacts of a product system throughout its life cycle" [248-250]. According to these standards, LCA consists of four main phases of (1) goal and scope definition, (2) life cycle inventory (LCI), (3) life cycle impact assessment (LCIA), and (4) interpretation (**Fig. 31**). The iterative nature of these phases requires adaptations according to the intended application, data availability and necessary detail level. The combination of these elements provides transparency and reproducibility while maintaining methodological rigor [251, 252].

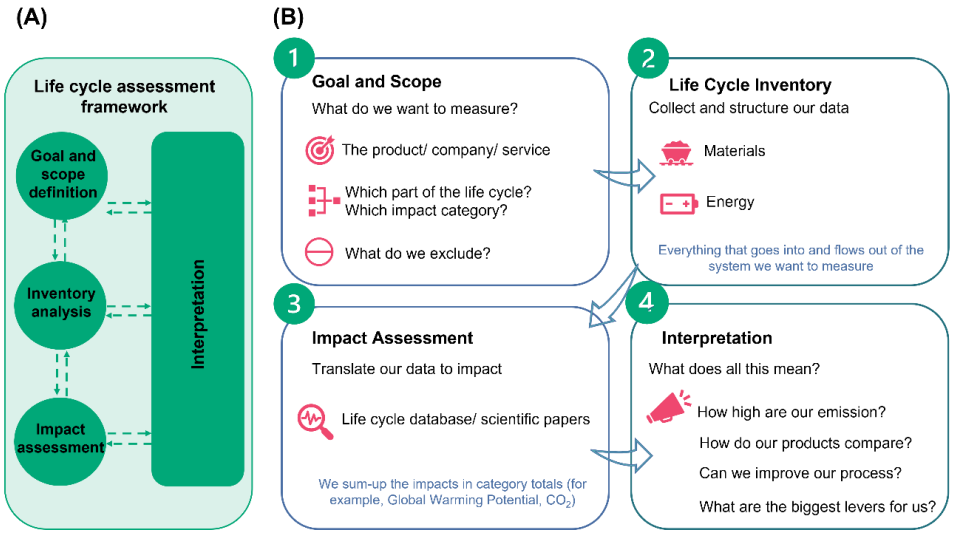

Fig. 31. LCA framework, Explanation of different stages of LCA.

6.2.1 Goal and scope definition

The initial segment of the study holds primary importance because it sets up essential elements like the objective, scope, and primary hypotheses which define the analysis framework. The study begins with the establishment of its objectives and the underlying motivations for its execution. Then it should be determined whether the results will serve internal purposes (such

as company use) or external objectives (like informing the public or institutions). Then, the scope of the study is established. This includes defining the system and its boundaries (conceptual, geographical, and temporal), the quality of the data employed, the primary hypotheses, and the study's limitations [253].

An important part of the scope is the definition of the *functional unit* (FU) of the system under study. It establishes a common reference by which all material and energy flows, emissions, and outputs are normalized, enabling consistent comparison in different systems and scenarios [254].

In alignment with the goal definition, the *system boundary* details which unit processes are included in the analysis, thereby defining the extent and depth of the study [255]. The system boundary defines the limits of the system under study and must be defined in accordance with the established goal and scope. It incorporates geographical, technological, and temporal parameters, with its correct definition being essential to determine the study's breadth and workload.

Additionally, *allocation* is the methodological procedure used to partition the input or output flows of a process or product system among the system under study and one or more associated product systems. According to ISO standards, when addressing systems involving joint co-production or recycling, allocation should be avoided whenever possible by subdividing processes into distinct sub-processes or by expanding the system boundaries to account for the additional functions of co-products (ISO, 2006c) [256]. If allocation cannot be avoided, inputs and outputs should be partitioned based on the relative significance of the co-products, typically using physical relationships such as mass or volume to ensure consistency [257].

6.2.2 Inventory analysis

The life cycle inventory (LCI) phase involves systematic collection and quantification of material and energy flows for all unit processes within the defined system boundary. This includes [258]:

- Inputs: Raw materials, energy use, water consumption, chemicals.
- Outputs: Emissions to air, water, and soil; solid waste; co-products.

This part of the process is resource-intensive in terms of data requirements, often requiring collection of data from multiple references (e.g., primary lab or industrial data, secondary datasets from databases like Ecoinvent). For polymer systems, this might include quantifying monomer production, polymerization, processing energy, and end-of-life treatment. Data quality, temporal and geographical relevance, and completeness must be assessed. Software such as SimaPro, GaBi, or OpenLCA is usually utilized for modeling and managing complex inventories.

6.2.3 Life cycle impact assessment (LCIA)

After completing the inventory stage, the life cycle impact assessment (LCIA) phase analyzes how the gathered data might affect the environment. Various environmental indicators such as climate change, acidification, eutrophication, and resource depletion help quantify and categorize impacts to better understand the environmental performance of the system [259]. Goal and scope determine which categories should be selected. In the field of polymer recycling research, scientists frequently focus on environmental impacts involving energy consumption as well as carbon emissions and toxic substances.

6.2.4 Interpretation

The final phase brings together all findings while identifying significant contributors and generating conclusions and recommendations that adhere to the established goal and scope [259]. It includes:

Hotspot analysis: Identifying stages or processes with dominant impacts.

Sensitivity and uncertainty analysis: Evaluates the influence of altered assumptions and data quality on the research findings.

Consistency check: Requires that data sources match with methodologies and assumptions while maintaining full transparency.

Interpretation allows practitioners to develop improvement strategies such as choosing less impactful feedstocks or changing the end-of-life process while delivering practical guidance for decision-making in design, policies, and research development.

Collectively, a robust LCA framework results from the integration of these four fundamental phases. The ISO framework ensures that the results maintain scientific validity while remaining transparent and reproducible so stakeholders can compare materials alongside technologies and process scenarios effectively. The LCA framework allows polymer systems to measure the balance between energy consumption, recyclability potential, longevity, and toxic effects which helps direct innovation to create sustainable solutions.

6.3 Environmental assessments of isocyanate-based PUs and NIPUs

The environmental sustainability of PU products has garnered increasing scrutiny recently, especially as it applies to green chemistry, circular materials, and the transition to NIPU alternatives. LCA has been widely applied to evaluate PU systems, including thermal insulation panels [260], bedding foams, dispersions [261], coatings [262], and composite aerogels [263]. While LCAs have spanned a diverse range of PU applications, most studies focus on foam-based systems because of their significant environmental footprint and potential use-phase benefits. Early LCA studies primarily focused on fossil-based PUFs used in thermal insulation, often comparing them with other conventional insulation materials such as expanded polystyrene (EPS), extruded polystyrene (XPS), mineral wool, and glass wool. For example, Nicolae et.al [264] applied LCA in the context of building refurbishment and showed that rigid PUFs offered considerable operational energy savings (up to 55%) when compared to EPS and XPS, though they also exhibited higher embodied impacts due to isocyanate production. Similarly, Pargana et al. [265] conducted a cradle-to-gate comparative LCA of insulation materials and found that while PUFs had favorable thermal performance, their production stage dominated global warming potential (GWP) and toxicity categories. With growing interest in improving the environmental profile of PUFs, several LCA studies have shifted focus to chemically recycled, bio-based, and carbon-capture-utilized (CCU) alternatives. Marson et al. [86] investigated chemically recycled polyols obtained via glycolysis for use in PU foams. Their LCA indicated that while recycled polyols could reduce environmental burdens associated with virgin polyol synthesis, the net benefit was highly dependent on energy source and yield during depolymerization. Manzardo et al. [250] developed a robust LCA framework to compare fossil-based and six bio-based rigid PU formulations using azelaic acid and lignin-derived polyols. Although some bio-based foams achieved up to 30-44% reductions in GWP and eutrophication potential, others showed marginal or even worse impacts due to higher density or inefficient polymerization. Isocyanate use (MDI) remained the dominant contributor

across all formulations. Bachmann et al. [266] examined the synergistic use of biomass and CO_2 (via CCU) as feedstocks for polyol production in flexible PU supply chains. Their bottom-up modeling of 47 production scenarios revealed that combined biomass-CO_2 strategies outperformed single-source approaches, achieving up to 13% additional GHG savings and 25% reduction in biomass demand, while also reducing burden shifting to categories like land use and metal depletion. Kulas et al. [267] analyzed lignin fractionation and valorization via techno-economic and LCA modeling. They found that despite the environmental promise of lignin-based PUs, trade-offs arise when energy-intensive pretreatments are involved, especially in GWP and human toxicity categories. Zhang et al. [268] and Tortoioli et al. [269] assessed bio-based PUFs derived from thistle oil and lignin respectively, confirming the environmental viability of renewable polyol pathways under optimized conditions. However, the impacts varied depending on agricultural inputs, catalyst loadings, and thermal performance of final foams. Quinteiro et al. [270] offered an important comparison between fossil-based and waste cooking oil (WCO)-based polyols in PUFs. Their results revealed that replacing 100% of fossil polyol with WCO-based alternatives can reduce GWP and fossil depletion by over 40%, but only if the functional performance and processing yield are preserved.

Despite the variety of functional units and system boundaries used, several clear conclusions can be drawn across this growing body of LCA literature in PUs:

Isocyanates (MDI and TDI) are consistently the largest single contributors to environmental impact- accounting for up to 50-60% of GWP, 91-99% of human toxicity, and dominant shares in ozone depletion and acidification [271].

Polyol origin significantly influences environmental performance. Bio-based polyols can reduce climate and resource impacts, but may increase eutrophication, land use, and freshwater ecotoxicity depending on the feedstock and processing method [250].

End-of-life treatments, such as landfilling and incineration, contribute marginally to total LCA scores unless incineration burdens or chemical recycling processes are considered in detail.

The evolving body of LCA research indicates important opportunities for innovation and comparison in the development of next-generation NIPUs. The overwhelming contribution of isocyanates and fossil-based polyols to environmental impacts in traditional PUs emphasizes the importance of NIPU systems- particularly those based on bio-based cyclic carbonates and recyclable architectures- to address current sustainability challenges.

In the case of NIPUs, few studies have conducted LCA studies. A research was done by Liang and co-workers [272] that investigated a comprehensive LCA and techno-economic analysis (TEA) of PHU and non-isocyanate polythiourethanes (NIPTUs) production and reprocessing pathways, using data from patents, literature, and experimental work. The LCA focused on three key impact categories: greenhouse gas (GHG) emissions, fossil energy use, and water consumption. Four production routes were analyzed: (1) bio-based PHU, (2) second-generation PHU via depolymerization, (3) bio-based NIPTU, and (4) second-generation NIPTU via depolymerization. While the analysis was performed on bulk materials (not foams), it provided valuable insights into the contribution of individual precursors to environmental impacts. Virgin PHU and NIPTU production consumed significantly more water and fossil energy than conventional PU foams, though PHU exhibited lower GHG emissions and NIPTU only slightly higher (**Fig. 32**). Reprocessing reduced GHG emissions and fossil energy use for both NIPUs, particularly NIPTU, but increased water use due to solvent-intensive steps. Importantly, replacing fossil methanol with bio-methanol and improving amine synthesis efficiency substantially reduced fossil energy demand.

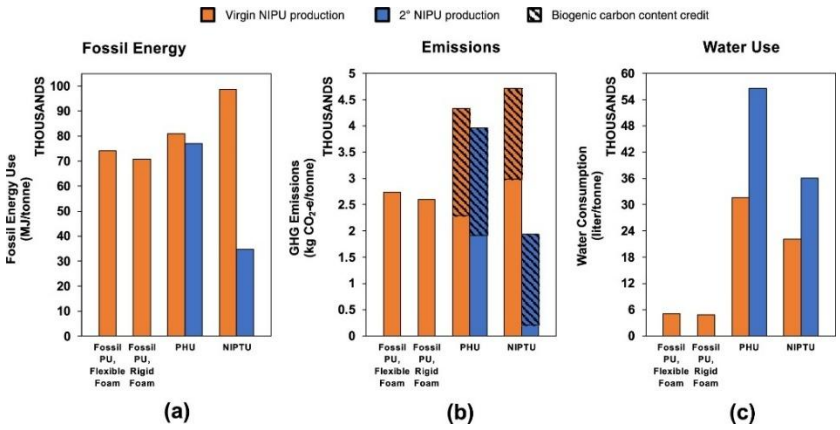

Fig. 32. Environmental impacts of NIPU production and reprocessing, presented in three categories: (a) fossil energy consumption, (b) greenhouse gas (GHG) emissions, and (c) water consumption. Results are shown for bio-based PHU and NIPTU, as well as their reprocessed counterparts (2° NIPUs), and benchmarked against conventional PU flexible and rigid foams. Orange bars represent virgin PU/NIPU production, while blue bars indicate impacts from NIPU reprocessing. Adapted from ref [272]. Copyright (2024) American Chemical Society. Licensed under CC BY-NC-ND 4.0.

Another LCA study by Bron et al. [273] compared PHUs synthesized from bio-based 5CCs and petrochemical-derived 6CCs. Their findings showed that 5CC-based systems had significantly lower environmental impacts, owing to lower solvent use, renewable feedstocks,

and milder reaction conditions. This study emphasized the decisive role of carbonate ring size, solvent usage, and synthetic route in shaping the overall sustainability of NIPUs (**Fig. 33**). Further advancing this field, Seychal et al. conducted an LCA study to assess the environmental benefits of PHU-derived covalent adaptable networks (CANs) in composite applications [274]. Their analysis revealed that although the production of PHU itself, particularly due to its energy-intensive curing process, could impose higher environmental impacts compared to conventional epoxy resins, the implementation of PHU-epoxy hybrid CANs significantly mitigated these impacts. In particular, hybrid composites reinforced with natural fibers exhibited up to a 15% reduction in climate change (CC) indicators and fossil resource depletion compared to standard epoxy systems. Moreover, the dynamic nature of CANs enabled more sustainable end-of-life scenarios through mechanical and chemical recycling strategies, offering notable environmental gains, especially for carbon fiber-reinforced composites. These findings reinforce the potential of PHU-based dynamic matrices as promising candidates for sustainable composite materials.

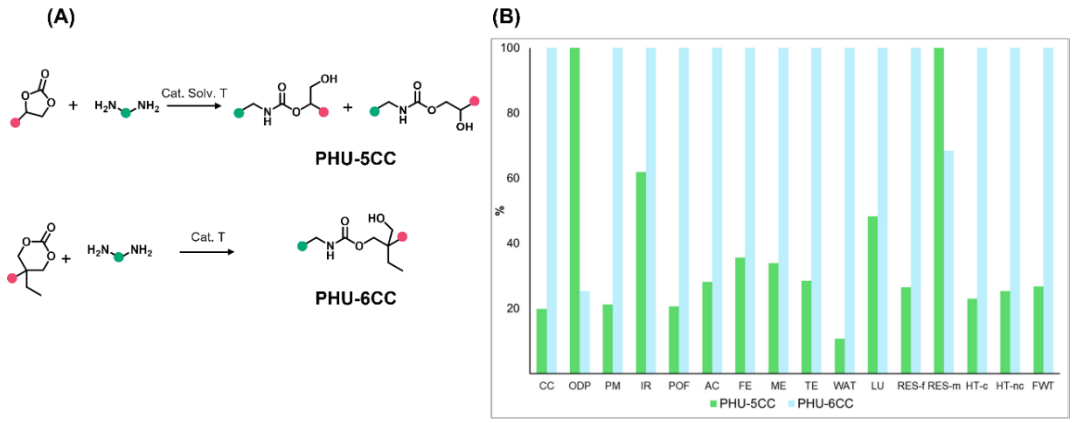

Fig. 33. (A) The chemistry of two PHUs produced from polyaddition of diamines with 5CCs and 8CCs; (B) Environmental impacts assessment- compared cradle-to-gate impacts of PHU-5CC and PHU-6CC [273]. The definition of abbreviations is explained in **Table 1**.

Table 1. Recommended life cycle impact assessment methods and their indicators, as outlined by the Joint Research Centre of the European Commission [275]

Impact Category	Acronym	Unit	Indicator
Climate Change	CC	Kg CO_2 eq	Radiative forcing as Global Warming Potential (GWP100)
Ozone Depletion	ODP	kg CFC-11eq	Ozone Depletion Potential (ODP)
Particulate Matter	PM	Disease incidences	Human health effects associated with exposure to PM2.5
Ionizing Radiation	IR	kBq U235	Human exposure efficiency relative to U235
Photochemical ozone formation	POF	kg NMVOC eq	Tropospheric ozone concentration increase
Acidification	AC	mol H^+eq	Accumulated Exceedance (AE)
Eutrophication, freshwater	FE	kg Peq	Fraction of nutrients reaching freshwater end compartment (P)
Eutrophication, marine	ME	kg Neq	Fraction of nutrients reaching marine end compartment (N)
Eutrophication, terrestrial	TE	mol Neq	Accumulated Exceedance (AE)
Water use	WAT	m3 world eq. deprived water	User deprivation potential (deprivation-weighted water consumption)
Land use	LU	Dimensionless (pt)	Soil quality index
Resource use, fossils	RES-f	MJ	Abiotic resource depletion – fossil fuels (ADP-fossil)
Resource use, minerals and metals	RES-m	kg Sbeq	Abiotic resource depletion (ADP ultimate reserves)
Human toxicity, cancer	HT-c	CTUh	Comparative Toxic Unit for humans (CTUh)
Human toxicity, non-cancer	HT-nc	CTUh	Comparative Toxic Unit for humans (CTUh)
Ecotoxicity, freshwater	FWT	CTUe	Comparative Toxic Unit for ecosystems (CTUe)

7 Conclusion

In this chapter, we began with the concept of sustainability as both a moral imperative and a practical necessity, and circular thinking as a strategy to reconcile material innovation with ecological responsibility. Within this framework, we examined the chemistry, challenges, and evolving potential of polyurethanes (PUs), with particular emphasis on non-isocyanate polyurethanes (NIPUs) as a sustainable alternative. Conventional PUs, while widely used, pose significant health and environmental risks due to their reliance on toxic isocyanates. In contrast, NIPUs can be synthesized through greener pathways- most notably the polyaddition of CO_2-based five-membered cyclic carbonates with diamines- which has emerged as the most widely employed and industrially viable route. Nevertheless, it is important to recognize that some precursors involved in NIPU synthesis (e.g., certain diamines or epoxides) also present toxicity

concerns, and further investigation and molecular design improvements are required to ensure their safe and sustainable deployment. Despite these challenges, such chemistries have already enabled applications in coatings, adhesives, and especially self-blown foams, demonstrating that performance and sustainability can indeed coexist.

A core theme of this review has been circularity, with an investigation into NIPU recycling. Depolymerization via solvolysis (e.g., hydrolysis, alcoholysis) has provided opportunities for molecular regeneration. However, even though these techniques show great promise, the field still lacks extensive studies on scalable and efficient recycling of NIPUs, which can be an important area for further research.

Importantly, sustainability must not only be pursued- but it must also be measured. Life Cycle Assessment (LCA) offers a comprehensive tool to assess environmental impacts among a material's life cycle. Existing LCA studies on NIPUs suggest that, despite the relatively high resource demands of virgin synthesis, recycled or reprocessed NIPUs can significantly reduce fossil energy use and greenhouse gas emissions- sometimes even having superior performance compared to conventional PUs. Nonetheless, notable challenges remains in areas such as water use, catalyst toxicity, and depolymerization efficiency, all of which require targeted innovation.

Ultimately, NIPUs are not only a safer alternative to isocyanate-based PUs- they show a significant evolution toward materials science focused on circularity and circular design. By combining material science and circular thinking and integrating tools like LCA, we can move forward to a polymer economy that supports environmental stability and intergenerational equity. Progressing in this field needs not only scientific advancements, but also a commitment to design with foresight- because every action has a consequence, and we must learn to measure those consequences before we act.

8 References

1. Colglazier, W., *Sustainable development agenda: 2030.* Science, 2015. **349**(6252): p. 1048-1050.

2. Agenda, I. *The new plastics economy rethinking the future of plastics*. in *World Economic Forum*. 2016.

3. Yang, S., et al., *Lifecycle management for sustainable plastics: Recent progress from synthesis, processing to upcycling.* Advanced Materials, 2024. **36**(33): p. 2404115.

4. Jambeck, J.R., et al., *Plastic waste inputs from land into the ocean.* science, 2015. **347**(6223): p. 768-771.

5. Balaji, A.B. and X. Liu, *Plastics in circular economy: a sustainable progression*, in *An introduction to circular economy*. 2020, Springer. p. 159-178.

6. Liu, L. and S. Ramakrishna, *An introduction to circular economy*. 2021: Springer.

7. Morão, A. and F. De Bie, *Life cycle impact assessment of polylactic acid (PLA) produced from sugarcane in Thailand.* Journal of Polymers and the Environment, 2019. **27**(11): p. 2523-2539.

8. Li, H., et al., *Recycling of waste polyethylene in asphalt and its performance enhancement methods: A critical literature review.* Journal of Cleaner Production, 2024: p. 142072.

9. Selvin, M., et al., *Review on recycling of cross-linked polyethylene.* Industrial & Engineering Chemistry Research, 2024. **63**(3): p. 1200-1214.

10. Fonseca, A., et al., *Life cycle assessment of PLA products: A systematic literature review.* Sustainability, 2023. **15**(16): p. 12470.

11. Shen, J.J., *Comparative life cycle assessment of polylactic acid (PLA) and polyethylene terephthalate (PET).* Comparative Assessment of PLA and PET, 2011.

12. Huysman, S., et al., *The recyclability benefit rate of closed-loop and open-loop systems: A case study on plastic recycling in Flanders.* Resources, Conservation and Recycling, 2015. **101**: p. 53-60.

13. Ügdüler, S., et al., *Towards closed-loop recycling of multilayer and coloured PET plastic waste by alkaline hydrolysis.* Green chemistry, 2020. **22**(16): p. 5376-5394.

14. Huysveld, S., et al., *Advancing circular economy benefit indicators and application on open-loop recycling of mixed and contaminated plastic waste fractions.* Journal of Cleaner Production, 2019. **211**: p. 1-13.

15. Perli, G., H. Sardon, and F. Vidal, *Reaction: Is a circular economy for chemicals and materials possible?* Chem, 2024. **10**(7): p. 1961-1962.

16. Bayer, O., *Das di-isocyanat-polyadditionsverfahren (polyurethane).* Angewandte Chemie, 1947. **59**(9): p. 257-272.

17. Brzeska, J. and A. Piotrowska-Kirschling, *A brief introduction to the polyurethanes according to the principles of green chemistry.* Processes, 2021. **9**(11): p. 1929.

18. Engels, H.W., et al., *Polyurethanes: Versatile materials and sustainable problem solvers for today's challenges.* Angewandte Chemie International Edition, 2013. **52**(36): p. 9422-9441.

19. Zavarise, C., et al., *Isocyanate-based multicomponent reactions.* RSC advances, 2024. **14**(53): p. 39253-39267.

20. Ephraim, S., A. Woodward, and R. Mesrobian, *Kinetic Studies of the Reaction of Phenyl Isocyanate with Alcohols in Various Solvents1.* Journal of the American Chemical Society, 1958. **80**(6): p. 1326-1328.

21. Bernardini, J., et al., *Exploitation of Arundo donax L. hydrolysis residue for the green synthesis of flexible polyurethane foams.* BioResources, 2017. **12**(2): p. 3630-3655.

22. Willocq, B., et al., *Advances in intrinsic self-healing polyurethanes and related composites.* RSC advances, 2020. **10**(23): p. 13766-13782.

23. Ates, M., et al., *Polyurethane foam materials and their industrial applications.* Polymer International, 2022. **71**(10): p. 1157-1163.

24. Akindoyo, J.O., et al., *Polyurethane types, synthesis and applications–a review.* Rsc Advances, 2016. **6**(115): p. 114453-114482.

25. Xu, C. and Y. Hong, *Rational design of biodegradable thermoplastic polyurethanes for tissue repair.* Bioactive Materials, 2022. **15**: p. 250-271.

26. Moyano-Vallejo, A., et al., *Enhanced Green Strength in a Polycarbonate Polyol-Based Reactive Polyurethane Hot-Melt Adhesive.* Polymers, 2024. **16**(23): p. 3356.

27. Xu, J., et al., *Synthesis and characterization of polyurethane with poly (ether-ester) diols soft segments consisted by ether and ester linkages in one repeating unit.* European Polymer Journal, 2022. **179**: p. 111553.

28. Sonnenschein, M.F., *Polyurethanes: science, technology, markets, and trends*. 2021: John Wiley & Sons.

29. de Souza, F.M., P.K. Kahol, and R.K. Gupta, *Introduction to polyurethane chemistry*, in *Polyurethane chemistry: Renewable polyols and isocyanates*. 2021, ACS Publications. p. 1-24.

30. Randall, D. and S. Lee, *The polyurethanes book.* Huntsman Polyurethanes, 2010.

31. Mendiburu-Valor, E., et al., *Synthesis and characterization of sustainable polyurethanes from renewable and recycled feedstocks.* Journal of Cleaner Production, 2023. **400**: p. 136749.

32. Holden, G., *Thermoplastic elastomers*, in *Applied Plastics Engineering Handbook*. 2024, Elsevier. p. 97-113.

33. Peyrton, J. and L. Averous, *Structure-properties relationships of cellular materials from biobased polyurethane foams.* Materials Science and Engineering: R: Reports, 2021. **145**: p. 100608.

34. Detrembleur, C., B. Grignard, and F. Monie, *Self-blowing isocyanate-free polyurethane foams*. 2023.

35. Sahoo, S., S. Mohanty, and S.K. Nayak, *Biobased polyurethane adhesive over petroleum based adhesive: Use of renewable resource.* Journal of Macromolecular Science, Part A, 2018. **55**(1): p. 36-48.

36. Wojnowska-Baryła, I., K. Bernat, and M. Zaborowska, *Plastic waste degradation in landfill conditions: the problem with microplastics, and their direct and indirect environmental effects.* International Journal of Environmental Research and Public Health, 2022. **19**(20): p. 13223.

37. Kemona, A. and M. Piotrowska, *Polyurethane recycling and disposal: Methods and prospects.* Polymers, 2020. **12**(8): p. 1752.

38. PETERS, J.M. and R.L. MURPHY, *Pulmonary toxicity of isocyanates*. 1970, American College of Physicians. p. 654-655.

39. Varma, D., J. Ferguson, and Y. Alarie, *Reproductive toxicity of methyl isocyanate in mice.* Journal of Toxicology and Environmental Health, Part A Current Issues, 1987. **21**(3): p. 265-275.

40. Salmon, A., M.K. Muir, and N. Andersson, *Acute toxicity of methyl isocyanate: a preliminary study of the dose response for eye and other effects.* Occupational and Environmental Medicine, 1985. **42**(12): p. 795-798.

41. Cucinell, S.A. and E. Arsenal, *Review of the toxicity of long-term phosgene exposure.* Archives of Environmental Health: An International Journal, 1974. **28**(5): p. 272-275.

42. Rossignolo, G., G. Malucelli, and A. Lorenzetti, *Recycling of polyurethanes: where we are and where we are going.* Green Chemistry, 2024. **26**(3): p. 1132-1152.

43. Liang, C., et al., *Material flows of polyurethane in the United States.* Environmental science & technology, 2021. **55**(20): p. 14215-14224.

44. Di, J., et al., *United States plastics: Large flows, short lifetimes, and negligible recycling.* Resources, Conservation and Recycling, 2021. **167**: p. 105440.

45. Vargas, J.A.M., et al., *Innovations in isocyanate synthesis for a sustainable future.* Organic & Biomolecular Chemistry, 2025. **23**(3): p. 487-505.

46. Fonseca, L.P., et al., *Reducing the carbon footprint of polyurethanes by chemical and biological depolymerization: Fact or fiction?* Current Opinion in Green and Sustainable Chemistry, 2023. **41**: p. 100802.

47. Vargas, J.A.M., et al., *Innovations in isocyanate synthesis for a sustainable future.* Organic & Biomolecular Chemistry, 2025. **23**(3): p. 487-505.

48. Wadgaonkar, P.P., *Bio-Based Aromatic Diisocyanates for Preparation of Polyurethanes.* 2015: p. US9950996B2-US9950996B2.

49. Lemouzy, S., et al., *Lignin-based bisguaiacol diisocyanate: a green route for the synthesis of biobased polyurethanes.* Green Chemistry, 2023. **25**(12): p. 4833-4839.

50. Delavarde, A., et al., *Paving the Way towards Sustainability of Polyurethanes: Synthesis and Properties of Terpene-Based Diisocyanate.* Molecules, 2023. **28**(20): p. 7133.

51. Gadhave, R.V., et al., *Recycling and disposal methods for polyurethane wastes: A review.* Open Journal of Polymer Chemistry, 2019. **9**(2): p. 39-51.

52. Gama, N., et al., *Polyurethane recycling through acidolysis: current status and prospects for the future.* Journal of Polymers and the Environment, 2024. **32**(10): p. 4777-4793.

53. Roobankumar, R. and M. SenthilPandian, *A review of utilization of waste polyurethane foam as lightweight aggregate in concrete.* Heliyon, 2024.

54. Zhao, L. and V. Semetey, *Recycling polyurethanes through transcarbamoylation.* ACS omega, 2021. **6**(6): p. 4175-4183.

55. Kemona, A. and M. Piotrowska, *Polyurethane recycling and disposal: methods and prospects. Polymers 12 (8): 1752*. 2020.

56. Fonseca, L.P., et al., *Reducing the carbon footprint of polyurethanes by chemical and biological depolymerization: Fact or fiction?* Current Opinion in Green and Sustainable Chemistry, 2023. **41**: p. 100802.

57. Chen, X.-C., et al., *Synergetic activation of CO 2 by the DBU-organocatalyst and amine substrates towards stable carbamate salts for synthesis of oxazolidinones.* Catalysis Science & Technology, 2021. **11**(21): p. 7072-7082.

58. Mahoney, L.R., S.A. Weiner, and F.C. Ferris, *Hydrolysis of polyurethane foam waste.* Environmental Science & Technology, 1974. **8**(2): p. 135-139.

59. Campbell, G.A. and W.C. Meluch, *Polyurethane foam recycling. Superheated steam hydrolysis.* Environmental Science & Technology, 1976. **10**(2): p. 182-185.

60. Motokucho, S., et al., *Hydrolysis of aromatic polyurethane in water under high pressure of CO2.* Journal of Polymer Science Part A: Polymer Chemistry, 2017. **55**(12): p. 2004-2010.

61. Gama, N., et al., *Recycling of polyurethane by acidolysis: The effect of reaction conditions on the properties of the recovered polyol.* Polymer, 2021. **219**: p. 123561.

62. Godinho, B., et al., *Recycling of polyurethane wastes using different carboxylic acids via acidolysis to produce wood adhesives.* Journal of Polymer Science, 2021. **59**(8): p. 697-705.

63. He, H., et al., *Chemical recycling of waste polyurethane foams: Efficient acidolysis under the catalysis of zinc acetate.* ACS Sustainable Chemistry & Engineering, 2023. **11**(14): p. 5515-5523.

64. Gama, N., et al., *Recycling of polyurethane scraps via acidolysis.* Chemical Engineering Journal, 2020. **395**: p. 125102.

65. Bech, T.B., et al., *Chemical separation of polyurethane via acidolysis–combining acidolysis with hydrolysis for valorisation of aromatic amines.* Green Chemistry, 2024. **26**(14): p. 8395-8404.

66. Nikje, A., et al., *"Split-phase" glycolysis of flexible PUF wastes and application of recovered phases in rigid and flexible foams production.* Polymer-Plastics Technology and Engineering, 2007. **46**(3): p. 265-271.

67. Molero, C., et al., *Glycolysis of flexible polyurethane wastes using stannous octoate as the catalyst.* Journal of material cycles and waste management, 2009. **11**: p. 130-132.

68. Murai, M., et al., *Glycolysis of rigid polyurethane foam under various reaction conditions.* Journal of cellular plastics, 2003. **39**(1): p. 15-27.

69. Wu, C.-H., et al., *Glycolysis of waste flexible polyurethane foam.* Polymer Degradation and Stability, 2003. **80**(1): p. 103-111.

70. Grdadolnik, M., et al., *Chemical recycling of flexible polyurethane foams by aminolysis to recover high-quality polyols.* ACS sustainable chemistry & engineering, 2023. **11**(29): p. 10864-10873.

71. Chen, X., et al., *Reprocessable polyhydroxyurethane networks exhibiting full property recovery and concurrent associative and dissociative dynamic chemistry via transcarbamoylation and reversible cyclic carbonate aminolysis.* Polymer Chemistry, 2017. **8**(41): p. 6349-6355.

72. Bhandari, S. and P. Gupta, *Chemical depolymerization of polyurethane foam via ammonolysis and aminolysis*, in *Recycling of Polyurethane Foams*. 2018, Elsevier. p. 77-87.

73. Recupido, F., et al., *Efficient recycling pathway of bio-based composite polyurethane foams via sustainable diamine.* Ecotoxicology and environmental safety, 2024. **269**: p. 115758.

74. Watando, H., et al., *Improving chemical recycling rate by reclaiming polyurethane elastomer from polyurethane foam.* Polymer Degradation and Stability, 2006. **91**(12): p. 3354-3359.

75. Olazabal, I., et al., *Upgrading polyurethanes into functional ureas through the asymmetric chemical deconstruction of carbamates.* ACS Sustainable Chemistry & Engineering, 2022. **11**(1): p. 332-342.

76. Figueira-Magalhães, M., D. Martinez-Hernandez, and I. Julian, *Microwave-Assisted PUF Aminolysis: Experimental Validation, Scaling Process Assessment and LCA Evaluation.* Sustainability, 2025. **17**(9): p. 4091.

77. Grdadolnik, M., et al., *Insight into chemical recycling of flexible polyurethane foams by acidolysis.* ACS sustainable chemistry & engineering, 2022. **10**(3): p. 1323-1332.

78. Gama, N., et al., *Polyurethane recycling through acidolysis: current status and prospects for the future.* Journal of Polymers and the Environment, 2024. **32**(10): p. 4777-4793.

79. Liu, B., et al., *Vapor-Phase Dicarboxylic Acids and Anhydrides Drive Depolymerization of Polyurethanes.* ACS Macro Letters, 2024. **13**(4): p. 435-439.

80. Heiran, R., et al., *Glycolysis: An efficient route for recycling of end of life polyurethane foams.* Journal of Polymer Research, 2021. **28**: p. 1-19.

81. Molero, C., A. de Lucas, and J.F. Rodríguez, *Recovery of polyols from flexible polyurethane foam by "split-phase" glycolysis: Study on the influence of reaction parameters.* Polymer Degradation and Stability, 2008. **93**(2): p. 353-361.

82. Alavi Nikje, M.M. and M. Nikrah, *Microwave-assisted glycolysis of polyurethane cold cure foam wastes from automotive seats in "split-phase" condition.* Polymer-Plastics Technology and Engineering, 2007. **46**(4): p. 409-415.

83. Donadini, R., et al., *Chemical recycling of polyurethane waste via a microwave-assisted glycolysis process.* ACS omega, 2023. **8**(5): p. 4655-4666.

84. Wieczorek, K., et al., *Recycling of Polyurethane Foams via Glycolysis: A Review.* Materials, 2024. **17**(18): p. 4617.

85. ALAVI, N.M. and G.A. BAGHERI, *Regeneration of polyol by pentaerythritol-assisted glycolysis of flexible polyurethane foam wastes.* 2010.

86. Marson, A., et al., *Life cycle assessment of polyurethane foams from polyols obtained through chemical recycling.* ACS omega, 2021. **6**(2): p. 1718-1724.

87. Gerlock, J., et al., *Reaction of polyurethane foam with dry steam: Kinetics and mechanism of reactions.* Journal of Polymer Science: Polymer Chemistry Edition, 1980. **18**(2): p. 541-557.

88. Dai, Z., et al., *Effect of diaminotoluene on the decomposition of polyurethane foam waste in superheated water.* Polymer Degradation and Stability, 2002. **76**(2): p. 179-184.

89. Zamani, S., et al., *Polyurethane recycling: Conversion of carbamates—Catalysis, side-reactions and mole balance.* Polymers, 2022. **14**(22): p. 4869.

90. Motokucho, S., et al., *Environment-friendly chemical recycling of aliphatic polyurethanes by hydrolysis in a CO 2-water system.* Journal of Applied Polymer Science, 2018. **135**(8): p. 45897.

91. Nemade, A., S. Mishra, and V. Zope, *Kinetics and thermodynamics of neutral hydrolytic depolymerization of polyurethane foam waste using different catalysts at higher temperature and autogenious pressures.* Polymer-Plastics Technology and Engineering, 2009. **49**(1): p. 83-89.

92. Di Bisceglie, F., et al., *Cutinase-catalyzed polyester-polyurethane degradation: elucidation of the hydrolysis mechanism.* Polymers, 2022. **14**(3): p. 411.

93. Lapprand, A., et al., *Reactivity of isocyanates with urethanes: Conditions for allophanate formation.* Polymer degradation and stability, 2005. **90**(2): p. 363-373.

94. Fonseca, L.P., et al., *Reducing the carbon footprint of polyurethanes by chemical and biological depolymerization: Fact or fiction?* Current Opinion in Green and Sustainable Chemistry, 2023. **41**: p. 100802.

95. Miguel-Fernández, R., et al., *Recovery of Green Polyols from Rigid Polyurethane Waste by Catalytic Depolymerization.* Polymers, 2022. **14**(14): p. 2936.

96. Group, R. 2024; Available from: https://www.rampf-group.com/en/news/2024/formulating-a-greener-future-chemical-recycling-solutions-by-rampf/.

97. Corporate, D.; Available from: https://corporate.dow.com/en-us/news/press-releases/dow-and-gruppo-fiori-develop-breakthrough-recycling-process.html.

98. Covestro.

99. BASF.

100. Huntsman.

101. Kathalewar, M.S., et al., *Non-isocyanate polyurethanes: from chemistry to applications.* Rsc Advances, 2013. **3**(13): p. 4110-4129.

102. Maisonneuve, L., et al., *Isocyanate-free routes to polyurethanes and poly (hydroxy urethane) s.* Chemical reviews, 2015. **115**(22): p. 12407-12439.

103. Ghasemlou, M., et al., *Bio-based routes to synthesize cyclic carbonates and polyamines precursors of non-isocyanate polyurethanes: A review.* European Polymer Journal, 2019. **118**: p. 668-684.

104. Anderson, J.R., et al., *Ambient temperature curable isocyanate-free compositions for preparing crosslinked polyurethanes*. 2014, Google Patents.

105. Duval, C., et al., *Synthesis and properties of renewable nonisocyanate polyurethanes (NIPU s) from dimethylcarbonate.* Journal of Polymer Science Part A: Polymer Chemistry, 2015. **53**(11): p. 1351-1359.

106. Masuyama, A., K. Tsuchiya, and M. Okahara, *Preparation and thermolysis of N-ammonioamidates containing hydroxyl group in acyl moiety.* Bulletin of the Chemical Society of Japan, 1985. **58**(10): p. 2855-2859.

107. Ghatge, N. and J. Jadhav, *Synthesis, characterization, and properties of novel poly (ether urethanes).* Journal of Polymer Science: Polymer Chemistry Edition, 1983. **21**(7): p. 1941-1950.

108. Scriven, E.F. and K. Turnbull, *Azides: their preparation and synthetic uses.* Chemical Reviews, 1988. **88**(2): p. 297-368.

109. Palaskar, D.V., et al., *Synthesis of biobased polyurethane from oleic and ricinoleic acids as the renewable resources via the AB-type self-condensation approach.* Biomacromolecules, 2010. **11**(5): p. 1202-1211.

110. Neumann, C.N., et al., *Water-Free Synthesis of Polyurethane Foams Using Highly Reactive Diisocyanates Derived from 5-Hydroxymethylfurfural.* Macromolecular Rapid Communications, 2011. **32**(17): p. 1373-1378.

111. Suryawanshi, Y., P. Sanap, and V. Wani, *Advances in the synthesis of non-isocyanate polyurethanes.* Polymer Bulletin, 2019. **76**: p. 3233-3246.

112. Neffgen, S., H. Keul, and H. Höcker, *Ring-opening polymerization of cyclic urethanes and ring-closing depolymerization of the respective polyurethanes.* Macromolecular rapid communications, 1996. **17**(6): p. 373-382.

113. Kušan, J., H. Keul, and H. Höcker, *Cationic ring-opening polymerization of tetramethylene urethane.* Macromolecules, 2001. **34**(3): p. 389-395.

114. Ihata, O., Y. Kayaki, and T. Ikariya, *Synthesis of thermoresponsive polyurethane from 2-methylaziridine and supercritical carbon dioxide.* Angewandte Chemie, 2004. **116**(6): p. 735-737.

115. Gu, L., et al., *Thermal and pH responsive high molecular weight poly (urethane-amine) with high urethane content.* Journal of Polymer Science Part A: Polymer Chemistry, 2011. **49**(24): p. 5162-5168.

116. Martínez de Sarasa Buchaca, M., et al., *Synthesis of Nonisocyanate Poly (hydroxy) urethanes from Bis (cyclic carbonates) and Polyamines.* Polymers, 2022. **14**(13): p. 2719.

117. Stachak, P., et al., *Recent advances in fabrication of non-isocyanate polyurethane-based composite materials.* Materials, 2021. **14**(13): p. 3497.

118. Liu, J., et al., *Chemically Recyclable Biobased Non-Isocyanate Polyurethane Networks from CO2-Derived Six-membered Cyclic Carbonates.* Macromolecular Rapid Communications, 2023. **44**(19): p. 2300263.

119. Gennen, S., et al., *CO2-Sourced α-Alkylidene Cyclic Carbonates: A Step Forward in the Quest for Functional Regioregular Poly (urethane) s and Poly (carbonate) s.* Angewandte Chemie, 2017. **129**(35): p. 10530-10534.

120. Mundo, F., et al., *On sustainability aspects of the synthesis of five-membered cyclic carbonates.* ACS Sustainable Chemistry & Engineering, 2024. **12**(17): p. 6452-6466.

121. Motokucho, S. and H. Morikawa, *Poly (hydroxyurethane): catalytic applicability for the cyclic carbonate synthesis from epoxides and CO 2.* Chemical Communications, 2020. **56**(73): p. 10678-10681.

122. Yuen, A., et al., *Room temperature synthesis of non-isocyanate polyurethanes (NIPUs) using highly reactive N-substituted 8-membered cyclic carbonates.* Polymer Chemistry, 2016. **7**(11): p. 2105-2111.

123. Fortman, D.J., et al., *Mechanically activated, catalyst-free polyhydroxyurethane vitrimers.* Journal of the American Chemical Society, 2015. **137**(44): p. 14019-14022.

124. Cornille, A., et al., *A perspective approach to sustainable routes for non-isocyanate polyurethanes.* European Polymer Journal, 2017. **87**: p. 535-552.

125. Büttner, H., et al., *Recent developments in the synthesis of cyclic carbonates from epoxides and CO 2.* Chemical Transformations of Carbon Dioxide, 2018: p. 89-144.

126. Blattmann, H., et al., *Isocyanate-and phosgene-free routes to polyfunctional cyclic carbonates and green polyurethanes by fixation of carbon dioxide.* Macromolecular rapid communications, 2014. **35**(14): p. 1238-1254.

127. Turnaturi, R., et al., *CO 2-derived non-isocyanate polyurethanes (NIPUs) and their potential applications.* Green Chemistry, 2023. **25**(23): p. 9574-9602.

128. Rollin, P., et al., *Five-membered cyclic carbonates: Versatility for applications in organic synthesis, pharmaceutical, and materials sciences.* Applied Sciences, 2021. **11**(11): p. 5024.

129. Theerathanagorn, T., et al., *Polyhydroxyurethanes from biobased monomers and CO2: a bridge between sustainable chemistry and CO2 utilization.* Chinese Journal of Chemistry, 2024. **42**(6): p. 652-685.

130. Delavarde, A., et al., *Sustainable polyurethanes: toward new cutting-edge opportunities.* Progress in Polymer Science, 2024: p. 101805.

131. Carré, C., et al., *From the synthesis of biobased cyclic carbonate to polyhydroxyurethanes: a promising route towards renewable non-isocyanate polyurethanes.* ChemSusChem, 2019. **12**(15): p. 3410-3430.

132. Cornille, A., et al., *A perspective approach to sustainable routes for non-isocyanate polyurethanes.* European Polymer Journal, 2017. **87**: p. 535-552.

133. Tomita, H., F. Sanda, and T. Endo, *Reactivity comparison of five-and six-membered cyclic carbonates with amines: Basic evaluation for synthesis of poly (hydroxyurethane).* Journal of Polymer Science Part A: Polymer Chemistry, 2001. **39**(1): p. 162-168.

134. Tomita, H., F. Sanda, and T. Endo, *Model reaction for the synthesis of polyhydroxyurethanes from cyclic carbonates with amines: Substituent effect on the reactivity*

and selectivity of ring-opening direction in the reaction of five-membered cyclic carbonates with amine. Journal of Polymer Science Part A: Polymer Chemistry, 2001. **39**(21): p. 3678-3685.

135. Ochiai, B., et al., *Kinetic and computational studies on aminolysis of bicyclic carbonates bearing alicyclic structure giving alicyclic hydroxyurethanes.* Tetrahedron, 2005. **61**(7): p. 1835-1838.

136. Maisonneuve, L., et al., *Fatty acid-based (bis) 6-membered cyclic carbonates as efficient isocyanate free poly (hydroxyurethane) precursors.* Polymer Chemistry, 2014. **5**(21): p. 6142-6147.

137. Nemirovsky, V. and S. Skorokhodov. *Kinetic study of aminolysis of poly (vinylene carbonate) and related model compounds*. in *Journal of Polymer Science Part C: Polymer Symposia*. 1967. Wiley Online Library.

138. Rayung, M., N. Abd Ghani, and N. Hasanudin, *A review on vegetable oil-based non isocyanate polyurethane: towards a greener and sustainable production route.* RSC advances, 2024. **14**(13): p. 9273-9299.

139. Lamarzelle, O., et al., *Activated lipidic cyclic carbonates for non-isocyanate polyurethane synthesis.* Polymer Chemistry, 2016. **7**(7): p. 1439-1451.

140. Tabushi, I. and R. Oda, *A kinetic study of the reaction of ethylene carbonate and amines.* Nippon Kagaki Zasshi, 1963. **84**(2): p. 162-167.

141. Diakoumakos, C.D. and D.L. Kotzev, *Nanocomposites based on polyurethane or polyurethane-epoxy hybrid resins prepared avoiding isocyanates*. 2012, Google Patents.

142. Diakoumakos, C.D. and D.L. Kotzev. *Non-isocyanate-based polyurethanes derived upon the reaction of amines with cyclocarbonate resins*. in *Macromolecular Symposia*. 2004. Wiley Online Library.

143. Nohra, B., et al., *Aminolysis reaction of glycerol carbonate in organic and hydroorganic medium.* Journal of the American Oil Chemists' Society, 2012. **89**: p. 1125-1133.

144. Tomita, H., F. Sanda, and T. Endo, *Polyaddition of bis (seven-membered cyclic carbonate) with diamines: A novel and efficient synthetic method for polyhydroxyurethanes.* Journal of Polymer Science Part A: Polymer Chemistry, 2001. **39**(23): p. 4091-4100.

145. He, Y., H. Keul, and M. Möller, *Synthesis, characterization, and application of a bifunctional coupler containing a five-and a six-membered ring carbonate.* Reactive and Functional Polymers, 2011. **71**(2): p. 175-186.

146. North, M., *Synthesis of cyclic carbonates from CO2 emissions.* Chimica Oggi, 2012.

147. Lombardo, V.M., et al., *Cooperative catalysis of cyclic carbonate ring opening: application towards non-isocyanate polyurethane materials.* European Journal of Organic Chemistry, 2015. **2015**(13): p. 2791-2795.

148. Soules, A., et al., *Method for preparing a compound comprising at least one beta-hydroxy-urethane unit and/or at least one upsilon-hydroxy-urethane unit*. 2014, Google Patents.

149. Kamber, N.E., et al., *Organocatalytic ring-opening polymerization.* Chemical reviews, 2007. **107**(12): p. 5813-5840.

150. Ashton, P.R., et al., *Using polarization effects to alter chemical reactivity: A simple host which enhances amine nucleophilicity.* Organic letters, 2000. **2**(10): p. 1365-1368.

151. Bisht, K.S., et al., *Lipase-catalyzed ring-opening polymerization of trimethylene carbonate.* Macromolecules, 1997. **30**(25): p. 7735-7742.

152. Lambeth, R.H. and T.J. Henderson, *Organocatalytic synthesis of (poly) hydroxyurethanes from cyclic carbonates and amines.* Polymer, 2013. **54**(21): p. 5568-5573.

153. Monmagnon, A., et al., *Insights on the polymerization kinetics of non-isocyanate polyurethanes (NIPU) using in situ NMR spectroscopy.* Polymer Testing, 2024. **140**: p. 108615.

154. Bossion, A., et al., *Opportunities for organocatalysis in polymer synthesis via step-growth methods.* Progress in Polymer Science, 2019. **90**: p. 164-210.

155. Prömpers, G., H. Keul, and H. Höcker, *Polyurethanes with pendant hydroxy groups: polycondensation of D-mannitol-1, 2: 5, 6-dicarbonate with diamines.* Designed monomers and polymers, 2005. **8**(6): p. 547-569.

156. Fleischer, M., H. Blattmann, and R. Mülhaupt, *Glycerol-, pentaerythritol-and trimethylolpropane-based polyurethanes and their cellulose carbonate composites prepared via the non-isocyanate route with catalytic carbon dioxide fixation.* Green Chemistry, 2013. **15**(4): p. 934-942.

157. Astarita, G., G. Marrucci, and F. Gioia, *The influence of carbonation ratio and total amine concentration on carbon dioxide absorption in aqueous monoethanolamine solutions.* Chemical Engineering Science, 1964. **19**(2): p. 95-103.

158. Besse, V., et al., *How to explain low molar masses in PolyHydroxyUrethanes (PHUs).* European Polymer Journal, 2015. **71**: p. 1-11.

159. Clements, J.H., *Reactive applications of cyclic alkylene carbonates.* Industrial & Engineering Chemistry Research, 2003. **42**(4): p. 663-674.

160. Ngassam Tounzoua, C., B. Grignard, and C. Detrembleur, *Exovinylene cyclic carbonates: Multifaceted CO2-based building blocks for modern chemistry and polymer science.* Angewandte Chemie, 2022. **134**(22): p. e202116066.

161. Grignard, B., et al., *Advances in the use of CO 2 as a renewable feedstock for the synthesis of polymers.* Chemical Society Reviews, 2019. **48**(16): p. 4466-4514.

162. Habets, T., et al., *Advancing the synthesis of isocyanate-free poly (oxazolidones) s: Scope and limitations.* Macromolecules, 2020. **53**(15): p. 6396-6408.

163. Siragusa, F., et al., *Access to biorenewable and CO2-based polycarbonates from exovinylene cyclic carbonates.* ACS Sustainable Chemistry & Engineering, 2021. **9**(4): p. 1714-1728.

164. Siragusa, F., et al., *Catalyst-Free Approach for the Degradation of Bio-and CO2-Sourced Polycarbonates: A Step toward a Circular Plastic Economy.* ACS Sustainable Chemistry & Engineering, 2022. **10**(27): p. 8863-8875.

165. Ouhib, F., et al., *A switchable domino process for the construction of novel CO2-sourced sulfur-containing building blocks and polymers.* Angewandte Chemie, 2019. **131**(34): p. 11894-11899.

166. Maes, S., et al., *Unprecedented associative exchange in CO 2-sourced cyclic S, O-acetal-based covalent adaptable networks.* Polymer Chemistry, 2024. **15**(22): p. 2296-2307.

167. Habets, T., et al., *Facile construction of functional poly (monothiocarbonate) copolymers under mild operating conditions.* Polymer Chemistry, 2022. **13**(21): p. 3076-3090.

168. Habets, T., et al., *Covalent adaptable networks through dynamic N, S-acetal chemistry: toward recyclable CO2-based thermosets.* Journal of the American Chemical Society, 2023.

169. Caliari, M., et al., *Fully Recyclable Pluripotent Networks for 3D Printing Enabled by Dissociative Dynamic Bonds.* Advanced Materials, 2025. **37**(15): p. 2417355.

170. Anitha, S., et al., *CO 2 derived hydrogen bonding spacer: enhanced toughness, transparency, elongation and non-covalent interactions in epoxy-hydroxyurethane networks.* Journal of Materials Chemistry A, 2017. **5**(46): p. 24299-24313.

171. Panchireddy, S., et al., *Catechol containing polyhydroxyurethanes as high-performance coatings and adhesives.* ACS Sustainable Chemistry & Engineering, 2018. **6**(11): p. 14936-14944.

172. Bourguignon, M., et al., *Water-Borne Isocyanate-Free Polyurethane Hydrogels with Adaptable Functionality and Behavior.* Macromolecular Rapid Communications, 2021. **42**(3): p. 2000482.

173. Schmidt, S., et al., *Isocyanate-free route to poly (carbohydrate–urethane) thermosets and 100% bio-based coatings derived from glycerol feedstock.* Macromolecules, 2016. **49**(19): p. 7268-7276.

174. Kalinina, F., D. Mognonov, and L. Radnaeva, *Poly (hydroxy urethane) coatings prepared from copolymers of 3-(2-vinyloxyethoxy)-l, 2-propylene carbonate and N-phenylmaleimide.* Russian Journal of Applied Chemistry, 2008. **81**: p. 1302-1304.

175. Lim, C.C.N.D., et al., *Emerging Trends in Nonisocyanate Polyurethane Foams: A Review.* ACS Engineering Au, 2024. **4**(6): p. 493-518.

176. Gomez-Lopez, A., et al., *Poly (hydroxyurethane) adhesives and coatings: state-of-the-art and future directions.* ACS Sustainable Chemistry & Engineering, 2021. **9**(29): p. 9541-9562.

177. Tenorio-Alfonso, A., M.C. Sánchez, and J.M. Franco, *A review of the sustainable approaches in the production of bio-based polyurethanes and their applications in the adhesive field.* Journal of Polymers and the Environment, 2020. **28**: p. 749-774.

178. Chaudhary, M.L. and R.K. Gupta, *Non-Isocyanate Polyurethanes-Based Adhesives*, in *Non-Isocyanate Polyurethanes: Chemistry, Progress, and Challenges*. 2025, ACS Publications. p. 175-197.

179. Khatoon, H., et al., *A review on the production, properties and applications of non-isocyanate polyurethane: A greener perspective.* Progress in Organic Coatings, 2021. **154**: p. 106124.

180. Chaudhary, M.L., R. Patel, and R.K. Gupta, *Beyond Isocyanates: Advances in Non-Isocyanate Polyurethane Chemistry and Applications.* Polymer, 2025: p. 128553.

181. Bourguignon, M., B. Grignard, and C. Detrembleur, *Water-Induced Self-Blown Non-Isocyanate Polyurethane Foams.* Angewandte Chemie International Edition, 2022. **61**(51): p. e202213422.

182. Orabona, F., et al., *Cutting-Edge Development of Non-Isocyanate Polyurethane (NIPU) Foams: From Sustainable Precursors to Environmental Impact Evaluation.* Green Chemistry, 2025.

183. Blattmann, H., M. Lauth, and R. Mülhaupt, *Flexible and bio-based nonisocyanate polyurethane (NIPU) foams.* Macromolecular Materials and Engineering, 2016. **301**(8): p. 944-952.

184. Grignard, B., et al., *CO 2-blown microcellular non-isocyanate polyurethane (NIPU) foams: from bio-and CO 2-sourced monomers to potentially thermal insulating materials.* Green Chemistry, 2016. **18**(7): p. 2206-2215.

185. Cornille, A., et al., *A new way of creating cellular polyurethane materials: NIPU foams.* European Polymer Journal, 2015. **66**: p. 129-138.

186. Cornille, A., et al., *Room temperature flexible isocyanate-free polyurethane foams.* European Polymer Journal, 2016. **84**: p. 873-888.

187. Blain, M., et al., *Rational investigations in the ring opening of cyclic carbonates by amines.* Green Chemistry, 2014. **16**(9): p. 4286-4291.

188. Sternberg, J. and S. Pilla, *Materials for the biorefinery: high bio-content, shape memory Kraft lignin-derived non-isocyanate polyurethane foams using a non-toxic protocol.* Green Chemistry, 2020. **22**(20): p. 6922-6935.

189. Ahmad, Z.R. and P.A. Mahanwar, *Synthesis and properties of foams from a blend of vegetable oil based polyhydroxyurethane and epoxy resin.* Cellular Polymers, 2022. **41**(4): p. 163-186.

190. Coste, G., et al., *Non-isocyanate polyurethane foams based on six-membered cyclic carbonates.* European Polymer Journal, 2022. **176**: p. 111392.

191. Chen, X., et al., *Condensed tannin-glucose-based NIPU bio-foams of improved fire retardancy.* Polymer Degradation and Stability, 2020. **175**: p. 109121.

192. Xi, X., et al., *Preparation and evaluation of glucose based non-isocyanate polyurethane self-blowing rigid foams.* Polymers, 2019. **11**(11): p. 1802.

193. Clark, J.H., et al., *Renewable self-blowing non-isocyanate polyurethane foams from lysine and sorbitol.* European Journal of Organic Chemistry, 2018. **2018**(31): p. 4265-4271.

194. Monie, F., et al., *Chemo-and regioselective additions of nucleophiles to cyclic carbonates for the preparation of self-blowing non-isocyanate polyurethane foams.* Angewandte Chemie, 2020. **132**(39): p. 17181-17189.

195. Purwanto, N.S., et al., *Rapidly synthesized, self-blowing, non-isocyanate polyurethane network foams with reprocessing to bulk networks via hydroxyurethane dynamic chemistry.* Polymer, 2023. **272**: p. 125858.

196. Purwanto, N.S., Y. Chen, and J.M. Torkelson, *Reprocessable, bio-based, self-blowing non-isocyanate polyurethane network foams from cashew nutshell liquid.* ACS Applied Polymer Materials, 2023. **5**(8): p. 6651-6661.

197. Purwanto, N.S., Y. Chen, and J.M. Torkelson, *Biobased, reprocessable, self-blown non-isocyanate polyurethane foams: Influence of blowing agent structure and functionality.* European Polymer Journal, 2024. **206**: p. 112775.

198. Monie, F., B. Grignard, and C. Detrembleur, *Divergent aminolysis approach for constructing recyclable self-blown nonisocyanate polyurethane foams.* ACS Macro Letters, 2022. **11**(2): p. 236-242.

199. Coste, G., C. Negrell, and S. Caillol, *Cascade (dithio) carbonate ring opening reactions for self-blowing polyhydroxythiourethane foams.* Macromolecular Rapid Communications, 2022. **43**(13): p. 2100833.

200. Trojanowska, D., et al., *Valorization of waste biomass for the fabrication of isocyanate-free polyurethane foams.* Green Chemistry, 2024. **26**(14): p. 8383-8394.

201. Bourguignon, M., B. Grignard, and C. Detrembleur, *Cascade exotherms for rapidly producing hybrid nonisocyanate polyurethane foams from room temperature formulations.* Journal of the American Chemical Society, 2023. **146**(1): p. 988-1000.

202. Bourguignon, M., B. Grignard, and C. Detrembleur, *Fast, catalyst-free room temperature production of isocyanate-free polyurethane foams using aromatic thiols.* Polymer Chemistry, 2025. **16**(2): p. 192-203.

203. Makarov, M., et al., *Advancing Non-isocyanate Polyurethane Foams: exo-Vinylene Cyclic Carbonate–Amine Chemistry Enabling Room-Temperature Reactivity and Fast Self-Blowing.* Macromolecules, 2025.

204. Monie, F., et al., *The multifaceted role of water as an accelerator for the preparation of isocyanate-free polyurethane thermosets.* Macromolecules, 2024. **57**(18): p. 8877-8888.

205. Singh, P., et al., *Non-Isocyanate Polyurethane (NIPU) Foams: Overcoming Challenges and Embracing Sustainability.* Polymer, 2025: p. 128658.

206. Thysen, B., S.K. Varma, and E. Bloch, *Reproductive toxicity of 2, 4-toluenediamlne in the rat. 1. Effect on male fertility.* Journal of Toxicology and Environmental Health, Part A Current Issues, 1985. **16**(6): p. 753-761.

207. Sommer, S. and S. Wilkinson, *Occupational contact dermatitis due to the epoxy hardener m-xylylenediamine.* Contact Dermatitis (01051873), 2001. **44**(6).

208. Richter, G. and H. Kadner, *Allergische Kontaktekzeme durch m-Xylylen-diamin in der Polyurethanseidenproduktion.* Dermatosen in Beruf und Umwelt, 1990. **38**(4): p. 117-120.

209. Castan, L., et al., *Comparative study of cytotoxicity and genotoxicity of commercial Jeffamines® and polyethylenimine in CHO-K1 cells.* Journal of Biomedical Materials Research Part B: Applied Biomaterials, 2018. **106**(2): p. 742-750.

210. Pescarmona, P.P., *Cyclic carbonates synthesised from CO2: Applications, challenges and recent research trends.* Current Opinion in Green and Sustainable Chemistry, 2021. **29**: p. 100457.

211. Manson, M.M., *Epoxides--is there a human health problem?* Occupational and Environmental Medicine, 1980. **37**(4): p. 317-336.

212. Humans, I.W.G.o.t.E.o.C.R.t., *Arsenic, metals, fibres, and dusts.* IARC monographs on the evaluation of carcinogenic risks to humans, 2012. **100**(PT C): p. 11.

213. Kamphuis, A.J., F. Picchioni, and P.P. Pescarmona, *CO 2-fixation into cyclic and polymeric carbonates: principles and applications.* Green chemistry, 2019. **21**(3): p. 406-448.

214. Maltby, K.A., et al., *Selective catalytic synthesis of 1, 2-and 8, 9-cyclic limonene carbonates as versatile building blocks for novel hydroxyurethanes.* Chemistry–A European Journal, 2020. **26**(33): p. 7405-7415.

215. Lueangchaichaweng, W., et al., *High surface area, nanostructured boehmite and alumina catalysts: Synthesis and application in the sustainable epoxidation of alkenes.* Applied Catalysis A: General, 2019. **571**: p. 180-187.

216. Longwitz, L., et al., *Calcium-based catalytic system for the synthesis of bio-derived cyclic carbonates under mild conditions.* ACS Catalysis, 2018. **8**(1): p. 665-672.

217. Carrodeguas, L.P., et al., *Fatty acid based biocarbonates: Al-mediated stereoselective preparation of mono-, di-and tricarbonates under mild and solvent-less conditions.* Green Chemistry, 2017. **19**(15): p. 3535-3541.

218. Huang, K., et al., *Synthesis of porous polymeric catalysts for the conversion of carbon dioxide.* Acs Catalysis, 2018. **8**(10): p. 9079-9102.

219. Christy, S., et al., *Recent progress in the synthesis and applications of glycerol carbonate.* Current Opinion in Green and Sustainable Chemistry, 2018. **14**: p. 99-107.

220. Liu, J., et al., *Metal-free imidazolium hydrogen carbonate ionic liquids as bifunctional catalysts for the one-pot synthesis of cyclic carbonates from olefins and CO2.* Green Chemistry, 2019. **21**(14): p. 3834-3838.

221. Thakur, S.A., et al., *Evaluation of propargyl alcohol toxicity and carcinogenicity in F344/N rats and B6C3F1/N mice following whole-body inhalation exposure.* Toxicology, 2013. **314**(1): p. 100-111.

222. Hanley Jr, T., et al., *Metabolism and disposition of ethylene carbonate in male Fischer 344 rats.* Toxicology and applied pharmacology, 1989. **100**(1): p. 24-31.

223. Cherian, M. and C. Writer, *Amended Safety Assessment of Propylene Carbonate as Used in Cosmetics.* 2024.

224. Wu, H., et al., *A degradable and self-healable vitrimer based on non-isocyanate polyurethane.* Frontiers in Chemistry, 2020. **8**: p. 585569.

225. Bakkali-Hassani, C., et al., *Polyhydroxyurethane covalent adaptable networks: looking for suitable catalysts.* Polymer Chemistry, 2023. **14**(31): p. 3610-3620.

226. Seychal, G., et al., *Can polyhydroxyurethane-derived covalent adaptable networks provide environmental benefits in composite applications?* 2025.

227. Purwanto, N.S., Y. Chen, and J.M. Torkelson, *Reprocessable, bio-based, self-blowing non-isocyanate polyurethane network foams from cashew nutshell liquid.* ACS Applied Polymer Materials, 2023. **5**(8): p. 6651-6661.

228. Purwanto, N.S., Y. Chen, and J.M. Torkelson, *Biobased, reprocessable, self-blown non-isocyanate polyurethane foams: Influence of blowing agent structure and functionality.* European Polymer Journal, 2024. **206**: p. 112775.

229. Caruso, M.M., et al., *Mechanically-induced chemical changes in polymeric materials.* Chemical reviews, 2009. **109**(11): p. 5755-5798.

230. Ragaert, K., L. Delva, and K. Van Geem, *Mechanical and chemical recycling of solid plastic waste.* Waste management, 2017. **69**: p. 24-58.

231. Maes, S., et al., *Taking dynamic covalent chemistry out of the lab and into reprocessable industrial thermosets.* Nature Reviews Chemistry, 2025. **9**(3): p. 144-158.

232. Sternberg, J. and S. Pilla, *Chemical recycling of a lignin-based non-isocyanate polyurethane foam.* Nature Sustainability, 2023. **6**(3): p. 316-324.

233. Zhang, B., et al., *High-strength, self-healing, recyclable, and catalyst-free bio-based non-isocyanate polyurethane.* ACS Sustainable Chemistry & Engineering, 2023. **11**(15): p. 6100-6113.

234. Chen, Y., M. Laporte, and J.M. Torkelson, *Circularity of non-isocyanate polyurethanes: Small-molecule recovery from linear and network polyhydroxyurethanes via transcarbamoylation.* Journal of Polymer Research, 2024. **31**(9): p. 264.

235. Miao, P., et al., *Chemically recyclable and mechanically robust non-isocyanate polyurethanes from resveratrol.* Polymer Chemistry, 2023. **14**(36): p. 4216-4226.

236. Wybo, N., et al., *Unlocking sustainable, aromatic, and versatile materials through transurethanization: development of non-isocyanate polyurethanes from lignins.* Journal of Materials Chemistry A, 2025.

237. Trost, B.M., *The atom economy—a search for synthetic efficiency.* Science, 1991. **254**(5037): p. 1471-1477.

238. Sheldon, R.A., *Organic synthesis-past, present and future.* Chemistry and Industry, 1992(23): p. 903-6.

239. Getzler, Y.D. and R.T. Mathers, *Sustainable polymers: Our evolving understanding.* Accounts of Chemical Research, 2022. **55**(14): p. 1869-1878.

240. Ness, B., et al., *Categorising tools for sustainability assessment.* Ecological economics, 2007. **60**(3): p. 498-508.

241. Curzons, A.D., et al., *So you think your process is green, how do you know?—Using principles of sustainability to determine what is green–a corporate perspective.* Green Chemistry, 2001. **3**(1): p. 1-6.

242. Vaccaro, L. and F. Ferlin, *Green Chemistry Metrics*, in *Encyclopedia of Green Chemistry (First Edition)*, B. Török, Editor. 2025, Elsevier: Oxford. p. 38-46.

243. Andraos, J., *Inclusion of environmental impact parameters in radial pentagon material efficiency metrics analysis: Using benign indices as a step towards a complete assessment of "greenness" for chemical reactions and synthesis plans.* Organic Process Research & Development, 2012. **16**(9): p. 1482-1506.

244. Andraos, J., *Safety/hazard indices: completion of a unified suite of metrics for the assessment of "greenness" for chemical reactions and synthesis plans.* Organic Process Research & Development, 2013. **17**(2): p. 175-192.

245. Hunt, R.G., W.E. Franklin, and R. Hunt, *LCA—How it came about: —Personal reflections on the origin and the development of LCA in the USA.* The international journal of life cycle assessment, 1996. **1**: p. 4-7.

246. Klöpffer, W., *Life cycle assessment: From the beginning to the current state.* Environmental science and pollution research, 1997. **4**: p. 223-228.

247. Horne, R., T. Grant, and K. Verghese, *Life cycle assessment: principles, practice, and prospects*. 2009: Csiro Publishing.

248. Lee, C.K., H.H. Khoo, and R.B. Tan, *Life cyle assessment based environmental performance comparison of batch and continuous processing: a case of 4-D-erythronolactone synthesis.* Organic Process Research & Development, 2016. **20**(11): p. 1937-1948.

249. Wernet, G., et al., *Life cycle assessment of fine chemical production: a case study of pharmaceutical synthesis.* The International Journal of Life Cycle Assessment, 2010. **15**: p. 294-303.

250. Manzardo, A., et al., *Life cycle assessment framework to support the design of biobased rigid polyurethane foams.* ACS omega, 2019. **4**(9): p. 14114-14123.

251. Fava, J.A., S.o.E. Toxicology, and Chemistry, *A technical framework for life cycle assessment: workshop report; August 18-23, 1990*. 1991: SETAC.

252. Diemer, A., *From Life Cycle Assessment (LCA) to Life Cycle Sustainability Assessment (LCSA), methodological issues and prospects for implementing circular business models.* International Journal of Scientific Engineering and Applied Science (IJSEAS), 2023. **9**(12): p. 1-50.

253. Liu, M., G. Zhu, and Y. Tian, *The historical evolution and research trends of life cycle assessment.* Green Carbon, 2024.

254. Hauschild, M.Z., R.K. Rosenbaum, and S.I. Olsen, *Life cycle assessment*. Vol. 2018. 2018: Springer.

255. Iso, I., *14044: 2006.* Environmental management—life cycle assessment—requirements and guidelines, 2006: p. 1-46.

256. Weidema, B., *Avoiding co-product allocation in life-cycle assessment.* Journal of industrial ecology, 2000. **4**(3): p. 11-33.

257. Pelletier, N., et al., *Rationales for and limitations of preferred solutions for multi-functionality problems in LCA: is increased consistency possible?* The International Journal of Life Cycle Assessment, 2015. **20**: p. 74-86.

258. Diemer, A., *From Life Cycle Assessment (LCA) to Life Cycle Sustainability Assessment (LCSA), methodological issues and prospects for implementing circular business models.*

International Journal of Scientific Engineering and Applied Science (IJSEAS), 2023. **9**(12): p. 1-50.

259. Valdivia, S., et al., *Principles for the application of life cycle sustainability assessment.* The International Journal of Life Cycle Assessment, 2021. **26**(9): p. 1900-1905.

260. Guolo, E., et al. *Environmental impacts for polyurethane panels*. in *E3S Web of Conferences*. 2019. EDP Sciences.

261. Klug, V., et al., *Comparative life cycle assessment of different production processes for waterborne polyurethane dispersions.* ACS Sustainable Chemistry & Engineering, 2021. **9**(27): p. 8980-8989.

262. Wray, H.E., et al., *Life cycle environmental impact considerations in the design of novel biobased polyurethane coatings.* ACS Sustainable Chemistry & Engineering, 2023. **11**(21): p. 8065-8074.

263. Aldaghi, S.A., et al., *Environmental Impact of Polyurethane-Based Aerogel Production: Influence of Solvents and Solids Content.* Resources, 2024. **13**(10): p. 138.

264. Nicolae, B. and B. George-Vlad, *Life cycle analysis in refurbishment of the buildings as intervention practices in energy saving.* Energy and Buildings, 2015. **86**: p. 74-85.

265. Pargana, N., et al., *Comparative environmental life cycle assessment of thermal insulation materials of buildings.* Energy and Buildings, 2014. **82**: p. 466-481.

266. Bachmann, M., et al., *Renewable carbon feedstock for polymers: environmental benefits from synergistic use of biomass and CO 2.* Faraday discussions, 2021. **230**: p. 227-246.

267. Kulas, D.G., M.C. Thies, and D.R. Shonnard, *Techno-economic analysis and life cycle assessment of waste lignin fractionation and valorization using the ALPHA process.* ACS Sustainable Chemistry & Engineering, 2021. **9**(15): p. 5388-5395.

268. Zhang, X., et al., *Effects of surface functionalization of lignin on synthesis and properties of rigid bio-based polyurethanes foams.* Polymers, 2018. **10**(7): p. 706.

269. Tortoioli, S., et al., *Environmental assessment of bio-oil transformation from thistle in the Italian context: An LCA study.* Rigas Tehniskas Universitates Zinatniskie Raksti, 2020. **24**(3): p. 430-446.

270. Quinteiro, P., et al., *Environmental assessment of different strategies to produce rigid polyurethane foams using unrefined crude glycerol.* Journal of Cleaner Production, 2022. **371**: p. 133554.

271. Silva, R., A. Barros-Timmons, and P. Quinteiro, *Life cycle assessment of fossil-and bio-based polyurethane foams: a review.* Journal of Cleaner Production, 2023. **430**: p. 139697.

272. Liang, C., et al., *Techno-economic analysis and life cycle assessment of biomass-derived polyhydroxyurethane and nonisocyanate polythiourethane production and reprocessing.* ACS Sustainable Chemistry & Engineering, 2024. **12**(32): p. 12161-12170.

273. Bron, P., et al., *Comparative Life Cycle Assessment of Recyclable Polyhydroxyurethanes Synthesized from Five-and Six-Membered Carbonates.* Macromol, 2025. **5**(1): p. 12.

274. Seychal, G., et al., *Can polyhydroxyurethane-derived covalent adaptable networks provide environmental benefits in composite applications?* 2025.

275. Andreasi Bassi, S., et al., *Updated characterisation and normalisation factors for the Environmental Footprint 3.1 method.* Publications Office of the European Union: Luxembourg, 2023.

Aim of the Thesis

This thesis seeks to advance the development of non-isocyanate polyurethanes (NIPUs) through the use of CO_2-based monomers in their synthesis, while integrating innovative recycling and upcycling strategies supported by comprehensive sustainability assessment methodologies. Building on the review presented in **chapter 1**, which examined developments in NIPU synthesis, recycling approaches, and sustainability metrics, this work brings these domains together to develop viable, high-performance, and environmentally responsible material circularity pathways.

Despite growing interest in NIPUs as safer and more sustainable alternatives to conventional polyurethanes, producing NIPUs out of polymer waste and a truly closed-loop recycling systems remain rare. Most existing efforts- such as mechanical recycling- fail to regenerate materials with performance levels comparable to virgin polymers. Moreover, advances in recyclability must be evaluated not only in terms of technical feasibility but also through rigorous and quantifiable environmental metrics.

To address these gaps, this thesis adopts the principles of circular economy, green chemistry, and systems thinking to design and evaluate emerging recycling and upcycling methods. Central to this approach is the integration of life cycle assessment (LCA), which provides a comprehensive framework for assessing the environmental implications of material design, processing, and recovery. By combining molecular-level innovation with systems-level analysis, this work contributes fundamentally to the interdisciplinary efforts on the development of more sustainable polymer materials that support a circular economy-based future.

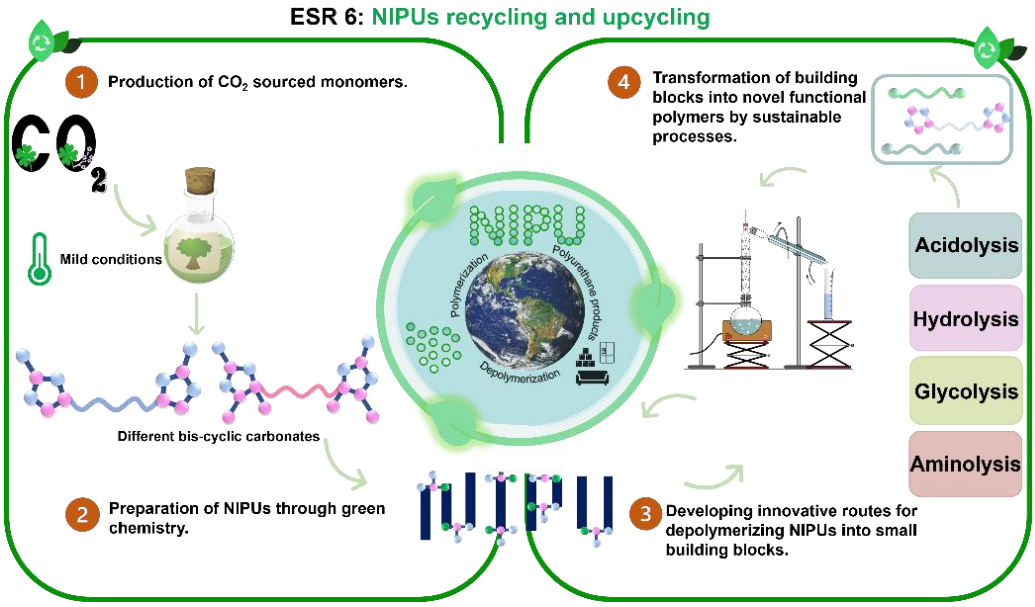

Fig. 1. Graphical abstract of the thesis.

The research conducted in this thesis is organized into four main chapters, each addressing a specific aspect of the NIPU lifecycle- from green synthesis to recycling and sustainability assessment:

Chapter 2 investigates the development of functional non-isocyanate poly(oxazolidone)s (POxas) via upcycling of CO_2-derived poly(oxo-carbonate)s. This chapter explores the catalyst-free aminolysis of polycarbonates using allylamine at room temperature to yield a bis(oxazolidone) monomer functionalized by allyl groups, which is subsequently polymerized with commercial dithiols through UV-induced thiol-ene click chemistry. The chapter studies the influence of monomer structure on polymer molecular weight, thermal stability, and explores post-polymerization functionalization potentials.

Chapter 3 investigates the chemical recycling of NIPU foams of the poly(hydroxyurethane)-type (prepared by the water-induced foaming of poly(cyclic carbonate)/polyamine formulations) via hydrolytic depolymerization under acidic and basic conditions. The study evaluates the efficiency of foam degradation, the mechanism of bond cleavage, and the recovery yields of the various building blocks. Through different characterizations, the full depolymerization of the PHU network into polyglycerol and diamine components is confirmed. We then investigate their re-use for the formation of the second-generation foams using the same self-blowing technology. The chapter also explores the formulation design needed to

maintain foam quality with up to 63% recycled content. This work aims to demonstrate a viable closed-loop recycling strategy for NIPU foams under mild and scalable reaction conditions.

Chapter 4 applies a cradle-to-grave LCA to evaluate the environmental implications of the chemical recycling strategy introduced in Chapter 3. By integrating lab-scale reaction data and experimental yields, the LCA quantifies the environmental trade-offs associated with energy use, raw materials and solvent consumption, and emissions. A comparative analysis is performed between incineration and closed-loop recycling, revealing dominant impact categories. Contribution and sensitivity analyses identify process hotspots and opportunities for greener alternatives, such as renewable energy sources and more benign neutralizing agents. This chapter aims to provide a quantitative framework to assess and guide sustainable material development in the NIPU field.

Chapter 5 explores the optimization potential of the NIPU recycling process by refining the hydrolysis process and monomer isolation strategies. Building on the findings of Chapters 3 and 4, this chapter focuses on improving the recovery yields of key components while simultaneously reducing environmental impacts, as assessed through a comparative LCA. By demonstrating significant environmental performance gains through targeted process modifications, this work strengthens the foundation for a more efficient closed-loop recycling approach and supports the advancement of scalable, sustainable applications in polymer materials.

Chapter 6 synthesizes the key findings from the preceding chapters and outlines the remaining challenges, providing a foundation for future research directions.

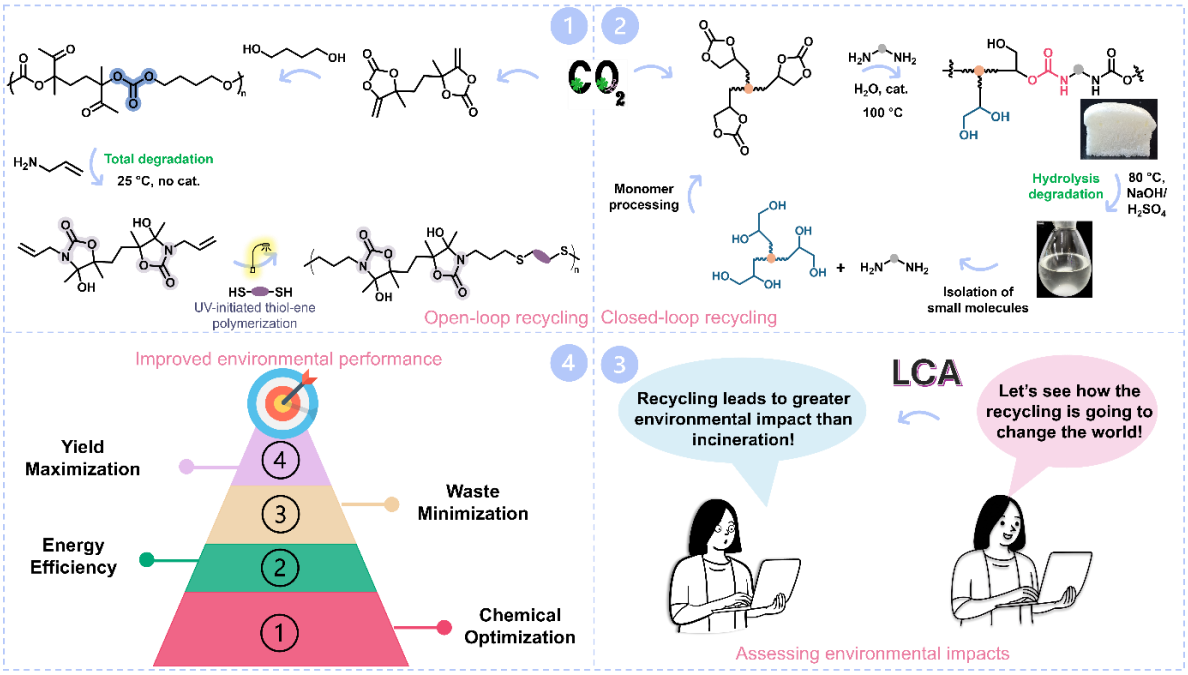

Fig. 2. Objectives of the thesis.

Chapter 2. Design of functional isocyanate-free poly(oxazolidone)s under mild conditions

Maliheh Razavi-Esfali, Thomas Habets, Fabiana Siragusa, Bruno Grignard, Haritz Sardon* and Christophe Detrembleur*

Reference : *Polym. Chem., 2024,15, 1962-1974*

ABSTRACT

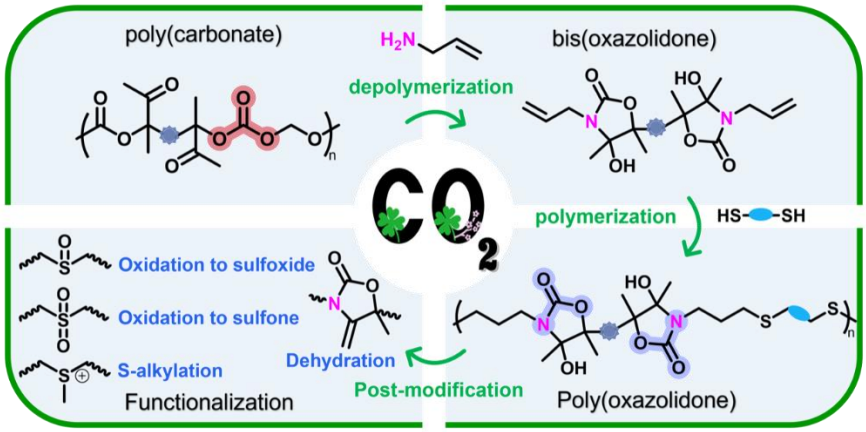

Polyoxazolidones, i.e. high performance polymers bearing cyclic carbamate linkages, were recently accessible by a non-isocyanate route under mild conditions. Herein, we report the preparation of polyoxazolidones bearing thioether linkages, which offers multiple opportunities for facile chain functionalization. The process consists in the chemical upcycling of CO_2-based poly(*oxo*-carbonate)s by aminolysis with allylamine. At room temperature, the poly(*oxo*-carbonate) is completely decomposed into an allyl-functionalized bis(oxazolidone) which is then copolymerized with dithiols by UV-initiated thiol-ene polymerization. The allyl-functionalized bis(oxazolidone) monomer is also quantitatively obtained by reacting allyl amine with a CO_2-based bis(alkylidene cyclic carbonate). A library of poly(oxazolidone-*co*-thioether) copolymers is easily accessible by varying the nature of the dithiol and M_w up to 101,000 g/mol is reached. All polymers are quantitatively dehydrated by simple thermal treatment at a temperature ranging from 120 to 140 °C at the solid state, furnishing poly(oxazolidone-*co*-thioether) copolymers bearing exocyclic vinylene moieties and presenting a high thermal stability ($T_{deg10\%}$ up to 360 °C) and various glass transition temperatures. The post-polymerization modifications by thiol oxidation to sulfoxide or sulfone, or through S-alkylation of the thioether linkages, are realized to deliver unprecedented functional polyoxazolidones. Notably, the introduction of sulfonium groups enables to produce the first example of water-soluble polyoxazolidones. This work describes a simple platform to produce a large panel of functional polyoxazolidones that are not accessible by the current isocyanate-based methods, moreover under mild operating conditions by exploiting CO_2-based monomers.

1 INTRODUCTION

Polyurethanes (PUs), ranking 6th among all polymers, are found in multiple applications such as foams, adhesives, coatings, and elastomers [1-3]. However, most PUs still present a poor resistance to heat which is considered as a serious disadvantage for some high-performance applications requiring high thermal stability [4-6]. In response to this challenge, the solution was found in the development of polyoxazolidones (POxa), a specialized class of PUs distinguished by their exceptional thermal stability thanks to the presence of thermally and chemically resistant five-membered cyclic urethane linkages. Their exceptional heat resistance renders them highly promising for industrial applications that demand elevated thermal durability, e.g. in automotive, aerospace, electrical engineering, and electronics sectors [7-12]. POxa are most often produced by copolymerization of diisocyanates with polyepoxides at high temperature (typically 160 °C) in the presence of suitable catalysts [13-15]. Nevertheless, diisocyanates are toxic compounds and numerous epoxides are classified as CMR (carcinogenic, mutagenic and reprotoxic) products, both causing serious harm to the environment and the human body [16, 17]. The high reactivity of the reagents as well as the harsh reaction conditions are also not compatible with the introduction of many functionalities (e.g. ketones and alcohols) in the polymer chains, restricting the possibilities to tune POxa properties. Although POxa are highly appealing for the development of high-performance materials, more versatile, greener, and safer synthetic approaches are searched for their production. To address this challenge, only few works succeeded to find alternative pathways toward these elusive polymers, such as the polycondensation of diurethanes with diepoxides at 90 °C employing a tertiary amine as a catalyst [18], or the copper-catalyzed 4-component reaction of a dialkyne with a diamine, an aldehyde, and carbon dioxide at temperatures ranging from 75 to 80 °C [19, 20]. Previous work by our group pioneered the utilization of novel CO_2-sourced activated cyclic carbonates, i.e. α-alkylidene carbonates (αCC), for preparing isocyanate-free POxa by copolymerization of bifunctional monomers (bisαCC)s with diamines under mild conditions, i.e. at room temperature (RT) and under catalyst-free conditions [21-23]. The scope of POxa was also extended by Schaub's [24] and Lamb's [25] groups by varying the structure of BisαCC. The functional group tolerance of the reaction was proven to be feasible through copolymerization with mixtures of diamines and dithiols, providing elusive poly(oxazolidone-*co*-monothiocarbonate)s [26]. Recently, circular POxa networks embedding dynamic *N,S*-acetal bonds were produced starting from αCC, diamines, and polythiols [27].

BisαCC also served to prepare poly(*oxo*-carbonate)s by organocatalyzed copolymerization with (biorenewable) diols [28-33], some of them having found applications as solid electrolytes for lithium batteries [34]. Interestingly, this class of polycarbonates, also prepared at RT, displayed easy recyclability. By aminolysis with propylamine, the polymer was totally decomposed into the starting diol and an elusive bis(oxazolidone) at RT under catalyst-free conditions. The process has shown to be tolerant to alcohol functional groups and by utilizing aminopropanol, a hydroxyl functional bis(oxazolidone) was collected at high yield. The building block further served as a comonomer for polymerization with BisαCC to deliver a polymer containing oxazolidone and *oxo*-carbonate linkages (thus, poly(oxazolidone-*co*-carbonate)) [35] (Scheme 1A). The facile depolymerization of poly(*oxo*-carbonate) involved the nucleophilic attack of the primary amine on the pendant ketone groups, leading to an hemiaminal intermediate that could undergo intramolecular cyclization to deliver the five-membered oxazolidone and the leaving alcohol. This approach of polycarbonates upcycling utilizing simple commercially available functional amines thus offered an appealing route to easily produce functional bis(oxazolidone)s re-entering the production of hybrid POxa.

In this work, we exploited this poly(*oxo*-carbonate)s upcycling strategy to deliver an allyl functionalized bis(oxazolidone) by facile aminolysis with allylamine. The monomer was then upcycled into hybrid POxa containing thioether linkages by a radical thiol-ene photopolymerization with various dithiols (Scheme 1B). We showed that various functionalities are easily introduced to the polymer chains, i.e. pendant olefins by dehydration, sulfoxide, or sulfone by partial or total oxidation of the thioethers, or sulfonium by their *S*-alkylation. The successful polymer modifications were demonstrated by NMR and IR spectroscopies, and the thermal properties of the polymers were assessed by thermogravimetric analysis (TGA) and differential scanning calorimetry (DSC). This work enlarged the upcycling possibilities of poly(*oxo*-carbonate)s by utilizing commercially available reagents while giving access to new functional POxa-type polymers of tunable properties. Another alternative route was also proposed to quantitatively deliver the allyl functionalized bis(oxazolidone) needed for the construction of the hybrid POxa by direct aminolysis of a CO_2-based bis(alkylidene cyclic carbonate) with allylamine at RT.

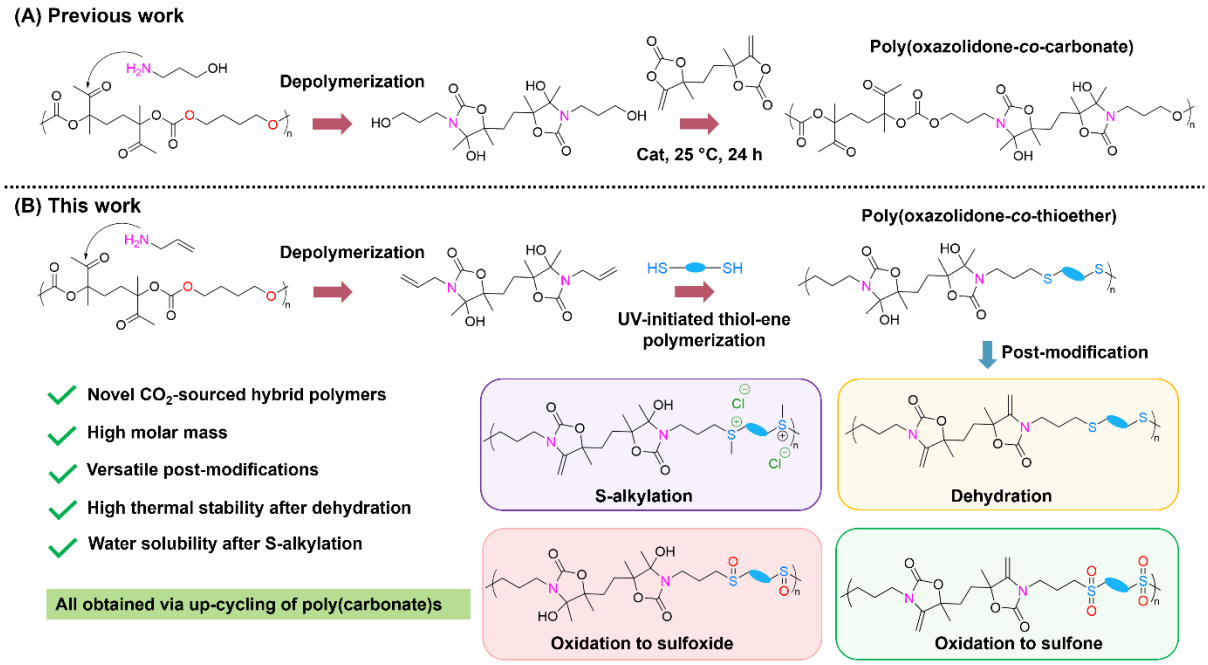

Scheme 1. (A) Depolymerization of PC by aminolysis with propanolamine and its upcycling into a hybrid polyoxazolidone containing carbonate linkages [35]; (B) Depolymerization of PC by aminolysis with allylamine and upcycling into a polyoxazolidone containing thioether bonds via thiol-ene photopolymerization, and further modifications of the polymer.

2 EXPERIMENTAL

2.1 Synthesis of monomer 4,4′-(ethane-1,2-diyl)bis(4-methyl-5-methylene-1,3-dioxolan-2-one) (BisαCC)

BisαCC was synthesized according to a procedure described before (Figure S1) [21]. Ethynylmagnesium bromide solution (800 mL, 0.5 M in THF, 0.4 mol, 3.1 eq.) was charged into a two-necked round-bottom flask under an inert nitrogen atmosphere. 2,5-hexanedione (15 mL, 0.13 mol, 1 eq.) was slowly added dropwise to the solution under stirring. Following 24 h of stirring at room temperature, the reaction was quenched with the addition of a saturated ammonium chloride (NH_4Cl) solution (260 mL). The resulting precipitate was isolated through centrifugation and then removed by filtration. To the filtrate, 300 mL of diethyl ether was added. The aqueous phase was extracted with diethylether (3 x 300 mL). The combined organic layers were dried over $MgSO_4$, filtered, and concentrated under vacuum. The resulting white-orange solid was dissolved in diethyl ether (250 mL) and subjected to silica gel

chromatography with diethyl ether as the eluent. 3,6-dimethyl-1,7-octadiyne-3,6-diol was collected as a white solid after evaporation of the solvent (20 g, isolated yield = 93%).

3,6-dimethyl-1,7-octadiyne-3,6-diol (20 g, 0.12 mol, 1 eq.), tetrabutylammonium phenolate (2 g, 6 mmol, 0.05 eq.), CuI (1.15 g, 6 mmol, 0.05 eq.), and acetonitrile (40 mL) were added in a 250 ml high pressure autoclave. The reactor was pressurized with CO_2 (100 bar) at 40 °C and, after 24 h, depressurized to discharge the gas. The autoclave content was dissolved in CH_2Cl_2 (400 mL) and purified by silica gel chromatography (eluent: CH_2Cl_2). The solvent was evaporated and the obtained yellow solid was dried under vacuum. The obtained solid was dissolved in acetonitrile (300 mL) and subjected to recrystallization at -20 °C for 30 min. The resulting solid was collected by filtration, washed with cold acetonitrile, and dried under vacuum. Thus, the pure product was obtained as a white solid and characterized by ^{1}H, and ^{13}C NMR spectroscopy (Figures S2-S3) (8 g, isolated yield = 26%).

2.2 Synthesis of poly(*oxo*-carbonate) (PC)

PC was synthesized according to a procedure described before [28]. **BisαCC** (2 g, 7.86 mmol, 1 equiv), 1,4-butanediol (0.708 g, 7.86 mmol, 1 equiv) and DBU (60 µL, 0.401 mmol, 0.05 equiv) were added to a reaction tube with dry DMSO (10 mL) and the mixture was stirred at 25 °C for 24 h. Then, the polymer was precipitated in diethyl ether followed by centrifugation at 10,000 rpm for 7 min and then dried under vacuum at 25 °C for 8 h. The solid was then solubilized in THF and dialyzed against THF for 24 h, followed by precipitation in diethyl ether and filtration. Finally, the polymer was dried under vacuum at 40 °C for 8 h and characterized by ^{1}H, ^{13}C, and HSQC NMR spectroscopy (Figures S4-S6) and SEC (Figure S7).

2.3 Depolymerization of poly(*oxo*-carbonate) (PC) by allylamine into bis(oxazolidone) (1).

PC (400 mg) was added in a reaction tube and dissolved in dry THF (1.2 mL). Then, 1,3,5-trimethoxybenzene (TMB) (25 mg) was added as an internal standard, followed by the addition of allylamine (395 mg, 3 equiv *vs* each ketone functionality of the polymer repeating unit). The

mixture was stirred at 25 °C and the depolymerization was monitored by ^{1}H-NMR spectroscopy and SEC by sampling over time. The bis(oxazolidone) (**1**) was isolated by precipitation of the reaction mixture into diethyl ether followed by filtration. The solid was dried under vacuum at 40 °C for 24 h (isolated yield = 63%, 215 mg). The isolated monomer was characterized by ^{1}H, ^{13}C, COSY, HSQC, and HMBC NMR spectroscopy (Figures S10-S14)

2.4 Synthesis of bis(oxazolidone)s (1) by aminolysis of BisαCC

BisαCC (2 g, 7.86 mmol, 1 equiv) was added to an ice bath-cooled glass vial followed by the addition of allylamine (2.24 g, 39.2 mmol, 5 equiv). The reaction was monitored by ^{1}H-NMR. After a 30 min reaction, the monomer was simply purified by removing the solvent under vacuum at 40 °C (isolated yield > 99%). The isolated monomer was characterized by ^{1}H, ^{13}C, COSY, HSQC, and HMBC NMR spectroscopy (see Figures S10-S14)

2.5 General procedure for the synthesis of polymers by radical thiol-ene

Bis(oxazolidone) **1** (400 mg, 1.08 mmol, 1 equiv), dithiol **2** (1.08 mmol, 1 equiv) and 2,2-Dimethoxy-2-phenyl acetophenone (DMPA) (13.9 mg, 0.054 mmol, 0.05 equiv) were added in a glass flask, followed by the addition of DMF (600 µL). The reaction mixture was stirred under irradiation of 365 nm UV light (Omnicure series 2000, 200 W) for 24 h. The distance of the light source to the reaction mixture was kept constant at 10 cm for each polymerization reaction. After 24 h, an aliquot of the crude product was sampled for ^{1}H-NMR and SEC characterizations. The polymer was diluted in a minimum amount of THF, precipitated in diethyl ether, and centrifugated at 10,000 rpm for 7 min. After 4 h of vacuum-drying at RT, the solid was solubilized and dialyzed in THF for 24 h, followed by precipitation in diethyl ether and filtration. The pure polymer was dried under vacuum at 40 °C for 24 h and characterized by ^{1}H, ^{13}C, COSY, HSQC, HMBC NMR spectroscopy (see Figure 1, and Figures S29-S53) and SEC (see Table 2).

2.6 Representative procedure for the dehydration of polymers

All the dehydration temperatures of polymers were determined by TGA and presented in Table 3. The dehydration of polymers was performed according to a procedure described before [26]. The oven was pre-heated to the dehydration temperature, and then 100 mg of the corresponding polymer was poured onto an aluminum plate and was placed in the oven for 2 h under air. The dehydrated polymers were used for characterizations without any further purification. The dehydrated polymers were characterized by ^{1}H, ^{13}C, COSY, HSQC, HMBC NMR spectroscopy (see Figures S65-S89), and SEC (see Figures S90-S94).

2.7 Procedures for polymer post-modification

Oxidation of thioether to sulfoxide. Selective oxidation of **P2b** to sulfoxide was performed following modification of a previous procedure [36]. In a glass vial, polymer **P2b** (100 mg, 0.19 mmol) was dissolved in 2 mL DMF. 395 µL of a 30% (w/w) H_2O_2 aqueous solution (10 equiv *vs* thioether function, 3.84 mmol) was added, and the mixture was stirred for 72 h. The polymer was precipitated in diethyl ether followed by centrifugation at 10,000 rpm for 7 min. The solid was dried under vacuum at 25 °C for 24 h (isolated yield = 90%). The polymer was characterized by ^{1}H, ^{13}C, COSY, HSQC, HMBC NMR spectroscopy (see Figures S116-S121), FTIR (see Figure S122) and SEC (see Figure S123).

Oxidation of thioether to sulfone. Selective oxidation of **P2b** to sulfone was performed following modification of previous procedures [37, 38]. In a glass vial, polymer **P2b** (200 mg, 0.384 mmol) was dissolved in 2 mL DMF. Then, 237 µL (3 equiv *vs* thioether function, 2.3 mmol) of a 30% (w/w) H_2O_2 aqueous solution and 6 mg (0.025 equiv) of diphenyl diselenide (DPDS) were added and the mixture was stirred for 48 h. The polymer was precipitated in diethyl ether followed by centrifugation at 10,000 rpm for 7 min and dried under vacuum at 40 °C for 24 h and then at 60 °C for 16 h (isolated yield = 92%). The polymer was characterized by ^{1}H, ^{13}C, COSY, HSQC, HMBC NMR spectroscopy (see Figures S125-S130), FTIR (Figure S131), and SEC (see Figure S132).

S-Alkylation of thioether. In a glass vial, polymer **P2b** (200 mg, 0.384 mmol) was dissolved in 3 mL DMF. Then, methyl iodide (10 equiv *vs* thioether function, 3.84 mmol) was added, and

the reaction mixture was stirred for 48 h. The resulting solution was dialyzed in a solution of NaCl 0.1 M for 2 days to exchange the counterion I^- to Cl^-, and then dialyzed in water for 1 day. The solution was lyophilized to obtain the polymer as a white solid (isolated yield = 70%). The polymer was characterized by ^1H, ^{13}C, COSY, HSQC, HMBC NMR spectroscopy (see Figures S134-S139).

3 RESULTS AND DISCUSSION

3.1 Monomer synthesis

We first studied the aminolysis of a CO_2-sourced poly(*oxo*-carbonate) (**PC**) using allylamine, to provide a new bis(oxazolidone) with allyl functionality. To this aim, **PC** was synthesized via step-growth copolymerization of **BisαCC** (see Figures S1-S3 reaction scheme and NMR characterization of **BisαCC**) with 1,4-butanediol at 25 °C in the presence of DBU as organocatalyst (5 mol % *vs* **BisαCC**), following a previously described procedure [28] (Scheme 2). The microstructure of **PC** was confirmed by ^1H, ^{13}C and HSQC NMR spectroscopy (Figures S4-S6) and the molar mass was determined by size exclusion chromatography (SEC; M_w = 22,900 g/mol, Figure S7). The aminolysis of **PC** was conducted at RT in THF using allylamine (3 equiv *vs* each ketone functionality of the polymer repeating unit). The formation of the products and the extent of depolymerization were monitored by ^1H-NMR spectroscopy (Figure S8) and SEC (Figure S9). After only 1h, ^1H-NMR revealed that the resonance relative to the methyl adjacent to the ketone group of **PC** (δ = 2.10 ppm) drastically decreased (90% of degradation). This was translated in a huge decrease of molar mass as determined by SEC, reaching a low value in M_w of 850 g/mol. The ^1H-NMR also revealed characteristic resonances corresponding to the expected products: the released alcohol (HO-$\underline{CH_2}$- at 3.39 ppm), the oxazolidone (N-$\underline{CH_2}$- at 3.76 ppm) and the imine side-product (N-$\underline{CH_2}$- at 3.95 ppm; see our previous work for the mechanism of formation of this side-product [35]). After 24 h of reaction, the characteristic signals of **PC** totally disappeared, indicating complete polymer degradation (Figure S8). Interestingly, the determined molar composition of the products alcohol/oxazolidone/imine was 0.5/0.4/0.1. The selectivity in oxazolidone product was thus higher compared to the depolymerization performed with propylamine in our previous

work (alcohol/oxazolidone/imine was 0.5/0.33/0.17) [35]. The formed bis(oxazolidone) was isolated by precipitation in diethyl ether (isolated yield 63%) (Figures S10-S14).

An alternative route to monomer **1** was the direct aminolysis of **BisαCC** by allylamine (Scheme 2). The reaction was monitored by ^{1}H-NMR using 5 equiv of allylamine as both the reagent and solvent, in an ice bath under catalyst-free conditions (Figure S15). The results evidenced a fast aminolysis, reaching completion within 30 min, with the selective and quantitative production of bis(oxazolidone) **1** (isolated yield of >99%).

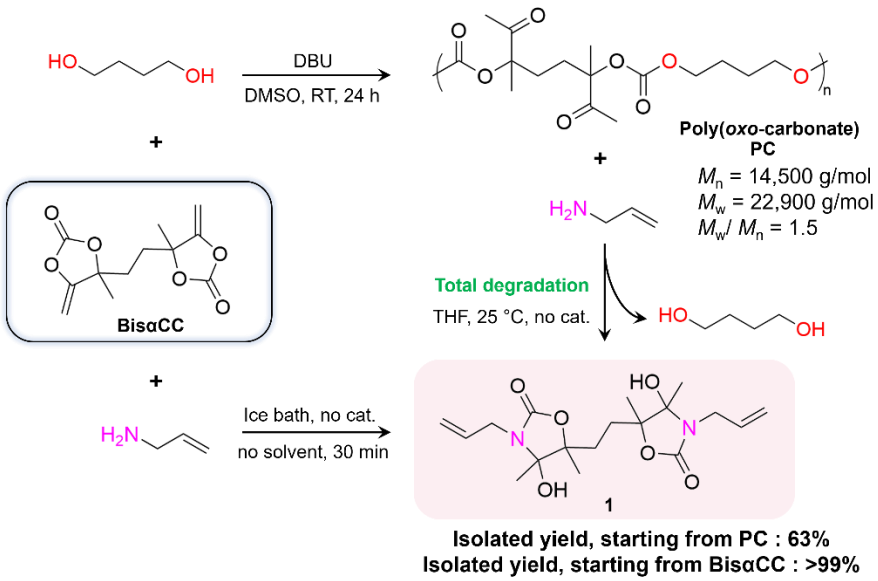

Scheme 2. Aminolysis of PC into **1**, and direct synthesis of **1** by aminolysis of BisαCC

3.2 Synthesis of poly(oxazolidone-*co*-thioether)s

The allyl functionalized bis(oxazolidone) **1** was copolymerized with dithiol **2a** by UV-initiated radical thiol-ene in the presence of a photoinitiator (Scheme 3). The experimental setup is shown in Figures S16-S17. An equimolar ratio between the two comonomers was used and a series of reaction parameters were explored to determine the optimal conditions to reach high monomer conversions and molar masses (solvent, concentration, nature of the photoinitiator). All the polymerizations were carried out at RT, using a 365 nm UV lamp for 24 h. Crude reaction mixtures were analyzed by ^{1}H-NMR spectroscopy (to determine the monomer

conversion, Figure S18, Eq. S1) and SEC (to determine the relative polymer M_w). The results are summarized in Table 1.

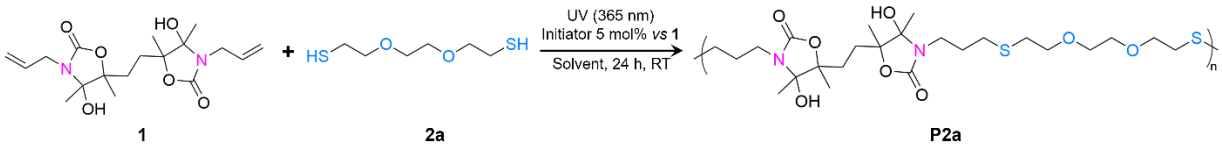

Scheme 3. Reaction scheme for the photoinitiated thiol–ene polymerization of **1** with **2a**

Table 1. Optimization of the reactions conditions for the preparation of poly(oxazolidone-*co*-thioether)s.

Entry	Solvent	Concentration (M)	Initiator [a] (5 mol% *vs* monomer **1**)	M_n (g/mol) [b]	M_w (g/mol) [b]	Dispersity [b]	Conv. [c] (%)
1	DMF	0.5	DMPA	4,500	10,000	2.3	90
2	DMF	1.5	DMPA	16,500	74,000	4.5	>99
3	DMF	1.8	DMPA	27,000	116,000	4.2	>99
4	THF	1.8	DMPA	4,500	7,700	1.7	72
5	Acetonitrile	1.8	DMPA	5,000	12,600	2.4	80
6	DMF	1.8	Omnirad 2100	13,000	38,500	2.9	92
7	DMF	1.8	Omnirad 2022	15,000	38,000	2.5	97

[a] The structure of free-radical initiators is shown in Scheme S1 [b] determined by SEC in DMF/LiBr calibrated with PS standards on crude reaction mixture; [c] conversion of monomer **1** calculated by ^{1}H-NMR spectroscopy on crude reaction mixture. Conditions: 365 nm UV light, 24 h, RT.

As shown in Table 1, the monomer conversion and polymer molar mass were strongly dependent on the nature of the solvent. At same concentration (1.8 M) and with the same photoinitiator (2,2-dimethoxy-2-phenyl acetophenone; DMPA), the conversion and polymer M_w were higher in DMF (> 98%; 116,000 g/mol; entry 3) compared to those obtained in THF (72%; 7,700 g/mol; entry 4) or acetonitrile (80%; 12,600 g/mol; entry 5). Hence, DMF proved to be the optimal solvent for this polymerization process. Decreasing the monomer concentration from 1.8 to 1.5 and 0.5 M was detrimental for the reaction (entries 1-3). Replacing DMPA by alternative photoinitiators such as Omnirad 2100 or Omnirad 2022 had

adverse effects on both the conversions and the polymer molar mass (entries 6-7). It is worth noting that high monomer conversion resulted in highly viscous reaction mixtures, thereby impeding growing chains diffusion and efficient stirring. This phenomenon led to broad molecular weight distributions with dispersity values growing over the theoretical maximum value of 2.

Having the optimized reaction conditions in hand (DMF as solvent, monomer concentration of 1.8M, DMPA as photoinitiator), the time of UV light exposure required to reach complete monomer conversion was determined by monitoring the photopolymerization process over time using monomer **1** and dithiol **2b** (Figure S19a) by ^{1}H-NMR spectroscopy and SEC. The dithiol **2b** was selected to simplify the ^{1}H-NMR spectrum of the reaction compared to dithiol **2a**. As shown in Figure S19b, the resonance associated to allyl moiety of **1** at δ = 5.06-5.22 ppm disappeared after 30 min reaction, confirming nearly total monomer consumption. After 24 h, the viscosity of the reaction medium was high, which prevented any further stirring. The time evolution of the SEC chromatogram, and thus polymer molar mass and dispersity, upon exposure to UV light is shown in Figures S20 and S21. After 5 h of photopolymerization, a moderate M_w of 19,000 g/mol was obtained ($Đ$ = 1.9), and was significantly increased to M_w of 53,000 g/mol ($Đ$ = 2.6) after 24 h of reaction.

Various dithiols **2a-2e** (Scheme 4) were then evaluated for the photopolymerization to illustrate the versatility of the process and to prepare a large scope of polymers (Table 2). All the polymerizations were conducted in the optimized reaction conditions at RT for 24 h. A conversion of more than 99% was obtained for **P2a-d** as determined by ^{1}H-NMR on crude mixtures, evidenced by the almost complete disappearance of the olefinic peak (δ= 5.06-5.22 ppm) of monomer **1** (Figure S22). It is worth noting that a lower conversion of 80% was obtained for polymer **P2e** probably due to the low solubility of dithiol **2e** in DMF. The crude polymers had moderate to high relative M_w, with values ranging from 19,000 (for **P2e**) to 116,000 g/mol (for **P2a**) (Table 2). The molecular characteristics of polymers after purification and their SEC chromatograms are depicted in Table S1 and Figures S23-S28.

The polymers microstructures were fully characterized by NMR spectroscopy, and all ^{1}H- and ^{13}C-NMR spectra are depicted in Figure 1 and Figures S29-S53. ^{1}H-NMR spectra demonstrated the anticipated repeating units consisting of thioether and oxazolidone linkages, with their typical resonances, e.g. S-$\underline{CH_2}$ of thioethers at δ = 2.44-2.50 ppm, and N-$\underline{CH_2}$ of oxazolidones at δ = 3.08-3.19 ppm as well as the resonance of the hydroxyl moiety at δ = 6.01 ppm (Figure

1). The presence of ether linkages in polymer **P2a** was confirmed by the resonance at δ = 3.55 ppm of the methylene group adjacent to ether bond (CH$_2$-O). For **P2c** the presence of the ester linkages was confirmed by the adjacent methylene peak (CH$_2$-COO, δ = 2.61 ppm). The presence of the oxazolidone group was further confirmed by ^{13}C-NMR spectroscopy, with the typical resonance of the carbonyl group at 157 ppm in all synthesized polymers. For **P2c**, in addition to the carbonyl group of oxazolidone, the one of the ester moiety was also present at 171.85 ppm. All the polymers were soluble in DMSO, DMF and THF, and were insoluble in water (Table S2).

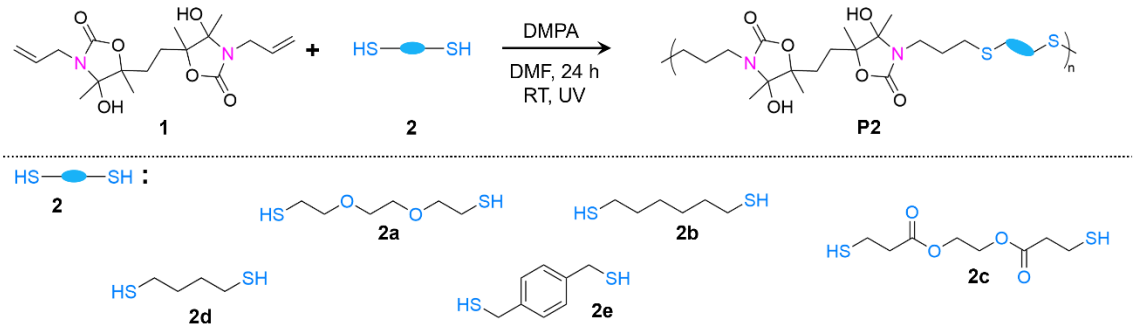

Scheme 4. Synthesis of poly(oxazolidone-*co*-thioether)s **P2a-P2e**

Table 2. Scope of the photoinitiated thiol–ene click polymerization of monomer **1** and different dithiols.

Entry	Polymer	Dithiol	M_n (g/mol)[a]	M_w (g/mol)[a]	Dispersity[a]	Conv.[b] (%)
1	P2a	2a	27,000	116,000	4.2	>99
2	P2b	2b	19,000	71,000	3.7	>99
3	P2c	2c	18,000	54,000	2.9	>99
4	P2d	2d	22,000	55,000	2.5	>99
5	P2e	2e	7,000	19,000	2.7	80

Condition: DMF (1.8 M), 2,2-dimethoxy-2-phenyl acetophenone (DMPA) 5 mol% *vs* monomer **1**, 365 nm UV light, 24 h, RT.

[a] determined on crude products by SEC in DMF/LiBr calibrated with PS standards; [b] determined by ^{1}H-NMR spectroscopy on crude reaction mixtures. The calculations were detailed in the supporting information.

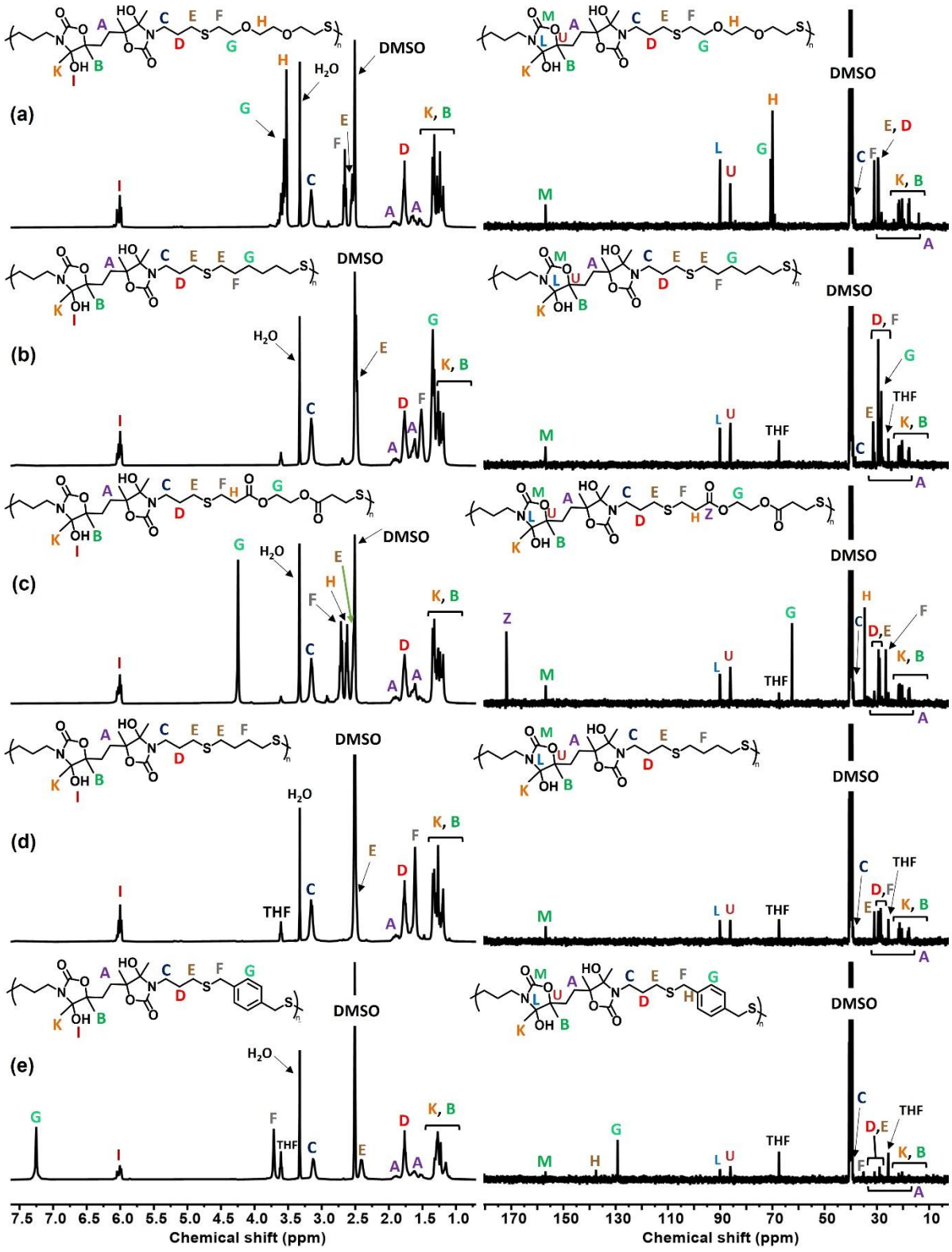

Figure 1. ^{1}H-NMR spectra (left, 400 MHz, DMSO-d_6) and ^{13}C-NMR spectra (right, 100 MHz, DMSO-d_6) of purified polymers (a) **P2a**, (b) **P2b**, (c) **P2c**, (d) **P2d**, (e) **P2e**.

3.3 Polymers dehydration and thermal properties

The thermal stability of all polymers was investigated using thermogravimetric analysis (TGA, Figures S54-S58). A two-step thermal degradation behavior was observed (see Figure 2b, TGA curve of **P2b** as a representative example), a typical feature of poly(hydroxyoxazolidone)s [26]. The first weight loss corresponded to the release of volatile traces and most importantly to the dehydration of hydroxyoxazolidone units in the range of 120 to 140 °C, resulting in the formation of an exocyclic vinylene moiety (Figure 2a). The dehydration temperature (T_{dehy}) was precisely determined by applying a slow heating ramp (2 K/min; Figures S59-S63), as already reported for POxa of the hydroxyoxazolidone-type [26]. The second weight loss was attributed to the degradation of the polymer backbone. The degradation temperature at 10% mass loss ($T_{deg,10\%}$) of the polymers was determined after the dehydration event and was in the range of 320 to 365 °C (Table 3; Figures S54-S58).

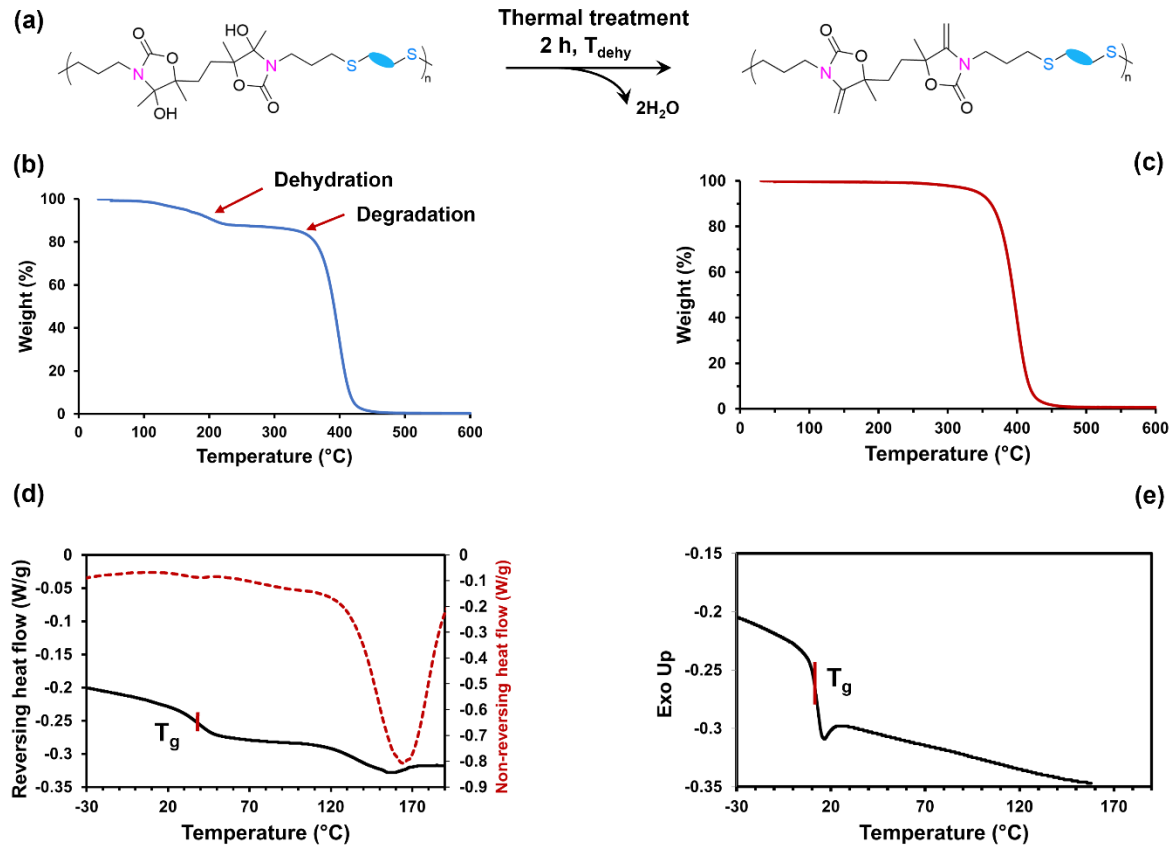

Figure 2. (a) schematic representation of POxa dehydration; (b) TGA pattern of POxa (**P2b**); (c) TGA thermogram of POxa-dehydrated (**P2b-dehydrated**); (d) mDSC thermogram for POxa (**P2b**); (e) DSC thermogram of POxa-dehydrated (**P2b-dehydrated**).

As dehydration affected the polymers functionality, their properties were studied and compared to polymers before dehydration. The quantitative dehydration of POxa was previously reported by treating the polymers with acetic acid [23] or *p*-Toluene sulfonic acid [25], and more recently by simple neat thermal treatment [26]. Herein, we adopted the thermal treatment methodology as it permitted to quantitatively produce the dehydrated polymers by heating POxa at their T_{dehy} for 2 h under air. As the dehydration process was carried out on neat POxa without requiring any dehydrating agent nor solvent, no purification step was needed after the thermal treatment to provide dehydrated POxa (coined POxa-dehydrated). The complete dehydration was confirmed by NMR spectroscopy (Figure S64-S89). The ^{1}H-NMR spectra of **P2b** and **P2b-dehydrated** are depicted in Figures S61a and S61b as representative examples, which confirmed that the proton signal of tertiary alcohol at δ = 5.95-6.1 ppm completely disappeared, and the characteristic resonance of exocyclic olefinic protons appeared at δ = 4.07-4.36 ppm. The ^{13}C-NMR spectra of **P2b-dehydrated** evidenced the typical olefinic resonance at around δ = 80 ppm and δ = 148 ppm. The SEC chromatograms for dehydrated polymers, displayed in Figures S90-S94, revealed a shift to lower molar mass (Table S3). Although chain scission may have occurred following dehydration, the variation in molecular weight observed before and after dehydration could also be attributed to changes in the hydrodynamic volume of the polymers in the solvent used for SEC analysis.

The TGA analyses of all dehydrated polymers showed a single-step degradation pattern with $T_{deg,10\%}$ in the range of 305 to 361 °C (see Figure 2c, TGA curve of **P2b-dehydrated** as a representative example and Figures S95-S99 for the other polymers). The overlay of TGA thermograms for both hydrated and dehydrated **P2b** copolymers (Figure S100) further confirmed that the first degradation step of hydrated polymers was attributed to their dehydration. Overall, the TGA analyses demonstrated the high thermal stability of the dehydrated hybrid POxa, which is significantly higher than conventional non-isocyanate polyurethanes of the polyhydroxyurethane-type ($T_{deg,\ 10\%}$ around 170-285 °C)[39-43].

POxa polymers were characterized by modulated DSC (mDSC) analyses as the T_g was difficult to detect using conventional DSC analyses (Figures S101-S105). This feature was already observed for other hydroxy-oxazolidone-containing polymers, i.e., poly(hydroxyoxazolidone-*co*-thiocarbonate)s [26] and poly(oxazolidone-*co*-carbonate)s [35], which were characterized by two broad and weak T_gs. For the herein synthesized polymers, no second T_g could be determined due to possible overlapping with early dehydration. As observed in Figure 2d, the reversing contribution of the heat flow allows the determination of the T_g of all polymers, in

the range of 7 to 39 °C, and the dehydration event is observed at higher temperature in the non-reversing contribution of the heat flow. For POxa-dehydrated, one strong T_g could be detected by conventional DSC, ranging from 2 to 53 °C depending on the polymer structure (Figures S106-S110). Although a rational trend is not trivial between T_g and the chemical structure in hydrated polymers, the T_g of dehydrated analogs seemed directly related to the rigidity of the dithiol structures, i.e. a low T_g for **P2a** containing ether linkages bringing increased chain flexibility and the highest for **P2e** containing an aromatic moiety.

Table 3. Thermal properties of POxa and POxa-dehydrated.

POxa-hydrated					POxa-dehydrated	
Entry	Polymer	$T_{deg,\ 10\%}$ [a] (°C)	T_{dehy} [a] (°C)	T_g [b] (°C)	$T_{deg,\ 10\%}$ [a] (°C)	T_g [c] (°C)
1	P2a	356	120	7	348	2
2	P2b	364	140	39	361	12
3	P2c	341	130	31	338	7
4	P2d	360	120	37	354	24
5	P2e	324	130	38	305	53

[a] The degradation and dehydration temperatures were determined by TGA. For POxa-hydrated, the $T_{deg,10\%}$ of the polymers was determined after the first weight loss. [b] Glass transition temperatures were determined by modulated DSC (using the reversing heat flow curve). [c] Glass transition temperatures were determined by conventional DSC.

3.4 Mechanical properties

Insights into the mechanical properties of poly(oxazolidone)s before and after dehydration were gained through tensile testing. **P2a**, selected for its high molecular weight as determined by SEC, underwent compression molding at 70 °C, a temperature below the dehydration threshold. Testing dogbone-shaped specimens were further obtained via die-cutting (Figure 3a-3b). Despite its low T_g (7 °C as determined by DSC), **P2a** exhibited elastic behavior with a Young's modulus value of 398 MPa and a yield strength of 11.4 MPa. The material then underwent plastic deformation until rupture, with a stress at break of 7.6 MPa and a strain at break of 314% (Figure 3e). Interestingly, the same experiment conducted on the dehydrated polymer **P2a-dehydrated** revealed flow when exposed to stress, rendering tensile testing impossible (Figure 3c-3d). This striking difference between hydrated and dehydrated polymers

might be ascribed to intermolecular hydrogen bonding exclusively present in the hydroxyl-containing material.

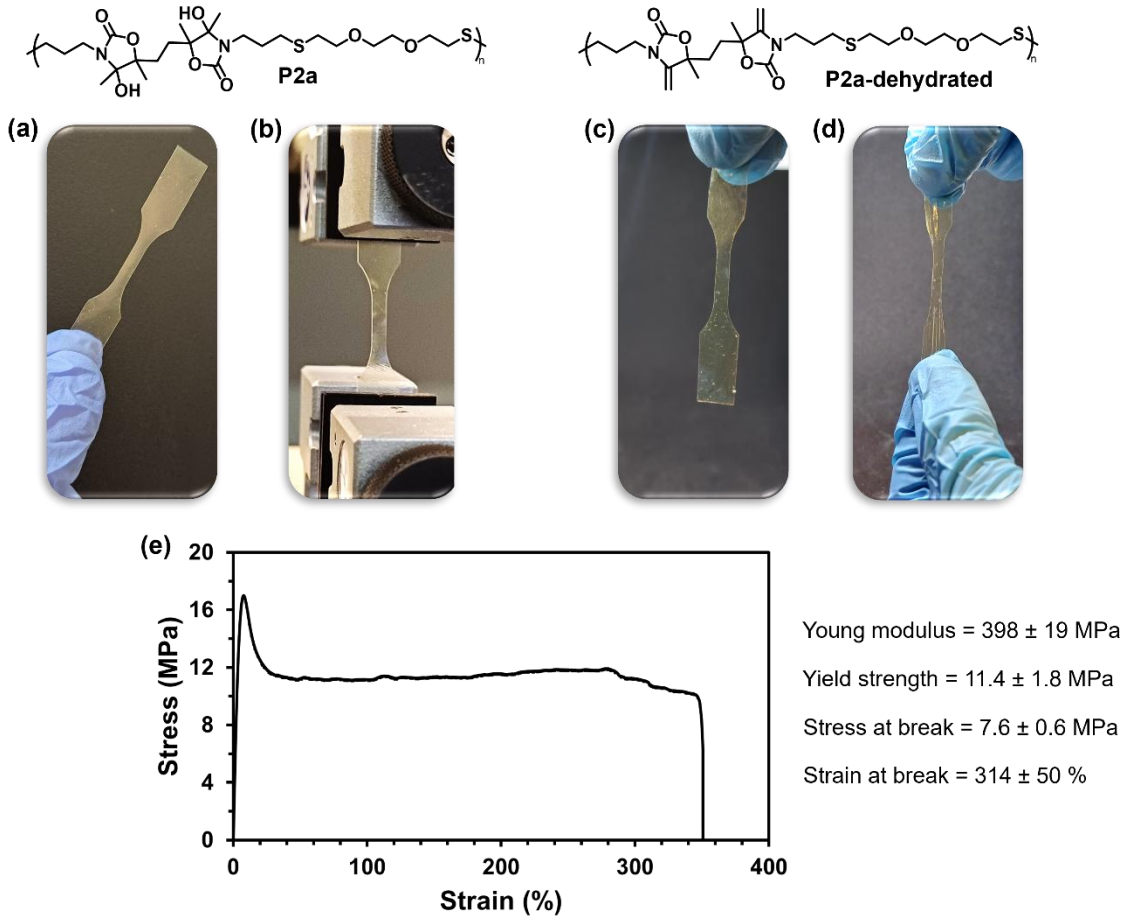

Figure 3. (a) Dog-bone shaped sample of **P2a**, (b) tensile strength experimental setup for **P2a**, (c) dog-bone shaped sample of **P2a-dehydrated**, (d) representative figure of **P2a-dehydrated**'s behavior when exposed to stress, (e) representative stress−strain curve of **P2a** and mechanical properties determined over five tests.

3.5 Chemical stability

The resistance of poly(oxazolidone)s to acidic and basic environments was assessed by immersing **P2a** in sulfuric acid and sodium hydroxide (NaOH) aqueous solutions of varying concentrations (0.1 M, 1 M and 5 M) at room temperature for a period of 48 h (Figure S111). The polymer has shown great stability in acidic conditions, with no apparent chain scission as determined by SEC (Figure S112). However, exposure to acid triggered partial dehydration, with a conversion in hydroxyl groups of 23 % at a concentration of 0.1 M and up to 71 % of conversion accompanied by some Wagner-Meerwein rearrangement of the resulting alkene at

a concentration of 5 M (Figure S113) [23]. In contrast, the polymer integrity was affected in basic conditions. In the 0.1 M NaOH aqueous solution, the polymer remained intact as determined by SEC and NMR (Figure S114 and Figure S115). Unexpectedly, the sample immersed in 1 M NaOH exhibited solubility and subsequent SEC analysis of the solution revealed a shift toward longer elution time, suggesting chain scission events. However, isolation of the product proved to be challenging and would necessitate further investigation on the stability of these polymers in alkaline conditions. Although the same result was expected when the polymer was introduced into the 5 M NaOH solution, SEC analysis didn't reveal any change in elution times and ^{1}H-NMR remained unchanged from the pure polymer. Overall, the poly(oxazolidone)s synthesized herein seemed stable in acidic conditions, although some dehydration of the hydroxyl group is expected with increasing acid content. However, the material integrity showed to be compromised in specific basic environments.

3.6 Post-polymerization modifications

All POxa were characterized by the presence of thioether linkages within their backbone, offering multiple possibilities for further modifications, notably by oxidation to sulfoxide or sulfone as well as by alkylation to sulfonium [36, 44]. The polymer **P2b** was selected as a representative polymer for all post-polymerization modifications.

3.6.1 Oxidation

We first explored the oxidation of the thioether linkages into sulfoxide or sulfone. The experiments were conducted at room temperature in DMF as solvent. Aqueous H_2O_2 (10 equiv *vs* thioether repeating unit) was used for the selective and quantitative mono-oxidation of **P2b** to sulfoxide (**P2b-Sulfoxide)**. Reaction completion was confirmed after 72 h by ^{1}H-NMR, where the characteristic resonance of the methylene ($\underline{CH_2}$-S-) of thioether at δ = 2.43-2.49 ppm totally disappeared. A new peak corresponding to the methylene protons adjacent to the sulfoxide groups (−SO-$\underline{CH_2}$) at δ= 2.57-2.81 ppm appeared [45, 46] (Figure S116 and Figure 4a-4b). To further confirm the quantitative sulfoxide formation, ^{1}H-NMR was also conducted in DMF-d_7 as typical signals of the thioether function overlapped with the peak attributed to

DMSO-d_6 (Figure S121, see ESI for more details). No peak attributed to sulfone groups were observed, confirming that overoxidation did not occur under these experimental conditions. As **P2b-Sulfoxide** was only soluble in DMF and DMSO, complete removal of residual solvent was not possible. The IR spectrum of **P2b-Sulfoxide** also revealed the appearance of sulfoxides (SO) stretching band at ~998 cm^{-1} (Figure S122) [45]. The SEC chromatogram presented the same pattern as **P2b** with only a slight decrease in elution time, suggesting no chain scission events **(**Figure S123).

Tirelli et al. used a diphenyldiselenide (DPDS) catalyst in combination with H_2O_2 for the double oxidation of poly(propylene sulfide) to poly(propylene sulfone) [37]. Herein, we adopted the same methodology to oxidize the thioether linkages into sulfones. This was achieved by using 3 equiv of H_2O_2 per thioether repeating unit and 0.025 equiv of DPDS as the catalyst, in DMF at RT. By monitoring the oxidation over time by ^{1}H-NMR, it appeared that the thioethers were fully oxidized to sulfone after 48 h of reaction, and that partial dehydration of the hydroxyoxazolidone moieties (10 mol% of functions) was observed (Figure S124).

P2b-Sulfone was purified by precipitation of the reaction mixture in diethyl ether, followed by drying under vacuum at 40 °C for 24 h. As the amount of residual DMF remaining in the polymer was high, the polymer was further dried at 60 °C under vacuum for 16 h. This mild thermal treatment was however enough to fully dehydrate the polymer. Moreover, a Wagner-Meerwein rearrangement was observed following the second thermal treatment resulting in the formation of β-alkylidene oxazolidone linkages (20 mol% of oxazolidone) (Figure S125). For further details and in-depth information regarding this rearrangement, we recommend referring to the article published by our group [23]. The complete oxidation of **P2b** to **P2b-Sulfone** was characterized similarly using NMR and FTIR. ^{1}H-NMR in DMSO-d_6 indicated that the thioether peak at δ= 2.43-2.49 ppm completely disappeared and a new downfield peak attributed to protons adjacent to sulfone at δ= 3.01-3.20 ppm appeared (Figure 4c and S125) [47]. The proton signals corresponding to the tertiary alcohol group, observed at δ = 5.95-6.1 ppm, vanished entirely, while the distinctive resonance of exocyclic olefinic protons emerged within the range of δ = 4.11-4.44 ppm, confirming the complete dehydration of the polymer. The olefinic proton associated to β-alkylidene oxazolidone linkage was observed at δ= 4.59-4.66 ppm, in alignment with the chemical shift observed in analogous structures investigated in a prior study [23]. To corroborate the quantitative formation of sulfone groups, an additional verification was conducted using ^{1}H-NMR in DMF-d_7 as the solvent (Figure S130, see ESI for more details). The two sulfone stretching frequencies could be observed by FTIR as two peaks

at ~1200 cm^{-1}, and ~1278 cm^{-1} as shown in Figure S131. No signal correlated to the sulfoxide were observed in ^{1}H-NMR nor FTIR, indicating that double oxidation of the thioether to sulfones was selective. The SEC trace for **P2b-Sulfone** showed a shift to lower molar mass after oxidation (Figure S132). This might be the result of different hydrodynamic volumes of the polymers before and after modification (dehydration and oxidation of the thioether) or some chain scission.

TGA was also employed to assess the thermal stability of the two oxidized polymers, which were both characterized by a multi-step degradation pattern (Figure S133). The initial weight reduction observed between 100 and 200 °C, was attributed to the evaporation of residual DMF and dehydration of the polymer. However, it is obvious that the thermal stability of **P2b-Sulfoxide** is lower than **P2b** as already observed in other sulfoxide-containing polymers [36, 45, 47]. Whereas **P2b** and **P2b-sulfoxide** were completely decomposed at 600 °C, sample **P2b-sulfone** produced 15 wt% of char at that temperature. We did not perform DSC analyses as remaining DMF within the polymers might have a drastic plasticizing effect on chain mobility.

3.6.2 S-Alkylation

As thioethers are reactive towards alkyl halides and form hydrophilic sulfonium salts, we investigated this reaction for introducing sulfonium groups in POxa. We selected iodomethane (10 equiv *vs* **P2b** unit) for the S-alkylation of **P2b** in DMF at RT. After 48 h, the quantitative formation of the sulfonium group was confirmed by ^{1}H-NMR with the characteristic resonance of the methylene ($\underline{CH_2}$-S-) of thioether at δ = 2.43-2.49 ppm that disappeared at the benefit of two new resonances at δ = 3.12-3.29 ppm and 3 ppm for the methylene (CH_2-S^+) and the methyl (CH_3-S^+) of the sulfonium group, respectively (Figure 4d, Figure S134). A partial dehydration (50 mol% of hydroxyoxazolidone) was also observed with the characteristic resonance of exocyclic olefinic protons at δ = 4.18-4.48 ppm. To our delight, the polymer has shown to be soluble in water, being the first water-soluble POxa reported so far. Further confirmation of quantitative *S*-alkylation was performed using ^{1}H-NMR characterization in D_2O (Figure S139, see ESI for more details). A multistep degradation pattern for **P2b-Sulfonium** was observed by TGA (Figure S140) that should correspond to dehydration (between 100 and 200 °C) and backbone degradation. However, a comprehensive elucidation of the degradation pathway falls beyond the scope of this study.

DSC characterization (Figure S141) showed a T_g at 35 °C, as well as an endotherm at around 120 °C. The latter might be attributed to the dehydration of the remaining hydroxyoxazolidone moieties that occurred in this temperature range (Table 3).

3.7 Renewability and sustainability considerations

An important aspect to consider in the context of sustainability is the renewability of both the starting monomers and the resulting polymers. In this work, the use of CO_2-sourced BisαCC introduces a degree of carbon renewability, as these intermediates valorize a greenhouse gas into functional building blocks. However, the other starting materials employed, such as allylamine and dithiols, are presently petrochemical in origin. Allylamine, for example, is industrially produced from allyl chloride and ammonia [48]- both derived from fossil resources- which limits the renewable fraction of the overall system. Similarly, the dithiols used (**2a-2e**) are typically produced from petrochemical feedstocks: while some aliphatic diols and diacids serving as precursors (e.g., succinic acid, 1,4-butanediol, adipic acid) are already available from bio-based processes, the thiolation step still relies on petrochemical sulfur chemistry, and aromatic dithiols (e.g., **2e**) remain essentially non-renewable. In this study the commercially available dithiols was employed. Future efforts could therefore explore biomass-derived amines or thiols to improve the renewable content of these polymers. Moreover, DMF was employed as a solvent during polymerization. However, DMF is well-known for its toxicity, particularly its hepatotoxic effects [49]. Occupational exposure has been associated with liver dysfunction, skin absorption hazards, and potential reproductive risks, making its use undesirable from a sustainability and safety perspective [49]. Consequently, the development of solvent-free or alternative green-solvent polymerization routes represents an important direction to improve the environmental and toxicological profile of the syntheized polymers. From the polymer perspective, the poly(oxo-carbonate)s display full chemical recyclability under mild conditions, demonstrating promising circularity. In contrast, the poly(oxazolidone-*co*-thioether)s obtained after thiol-ene polymerization exhibit enhanced thermal and chemical stability, but their end-of-life recovery is less straightforward. While this stability is advantageous for long-term performance applications, it currently limits renewability at the polymer stage. Importantly, beyond molecular design, life cycle assessment (LCA) will be essential to evaluate the overall sustainability of these chemical recycling

processes, as it enables a quantitative comparison of environmental trade-offs and helps to identify hotspots in energy, solvents, and auxiliary chemicals. Overall, this strategy demonstrates a partially renewable approach that integrates CO_2 valorization with functional polymer synthesis, while underscoring future opportunities in the use of renewable amines and thiols, as well as in developing recycling routes for the resulting polymers, to further enhance both the bio-based content and the circularity of polyoxazolidones.

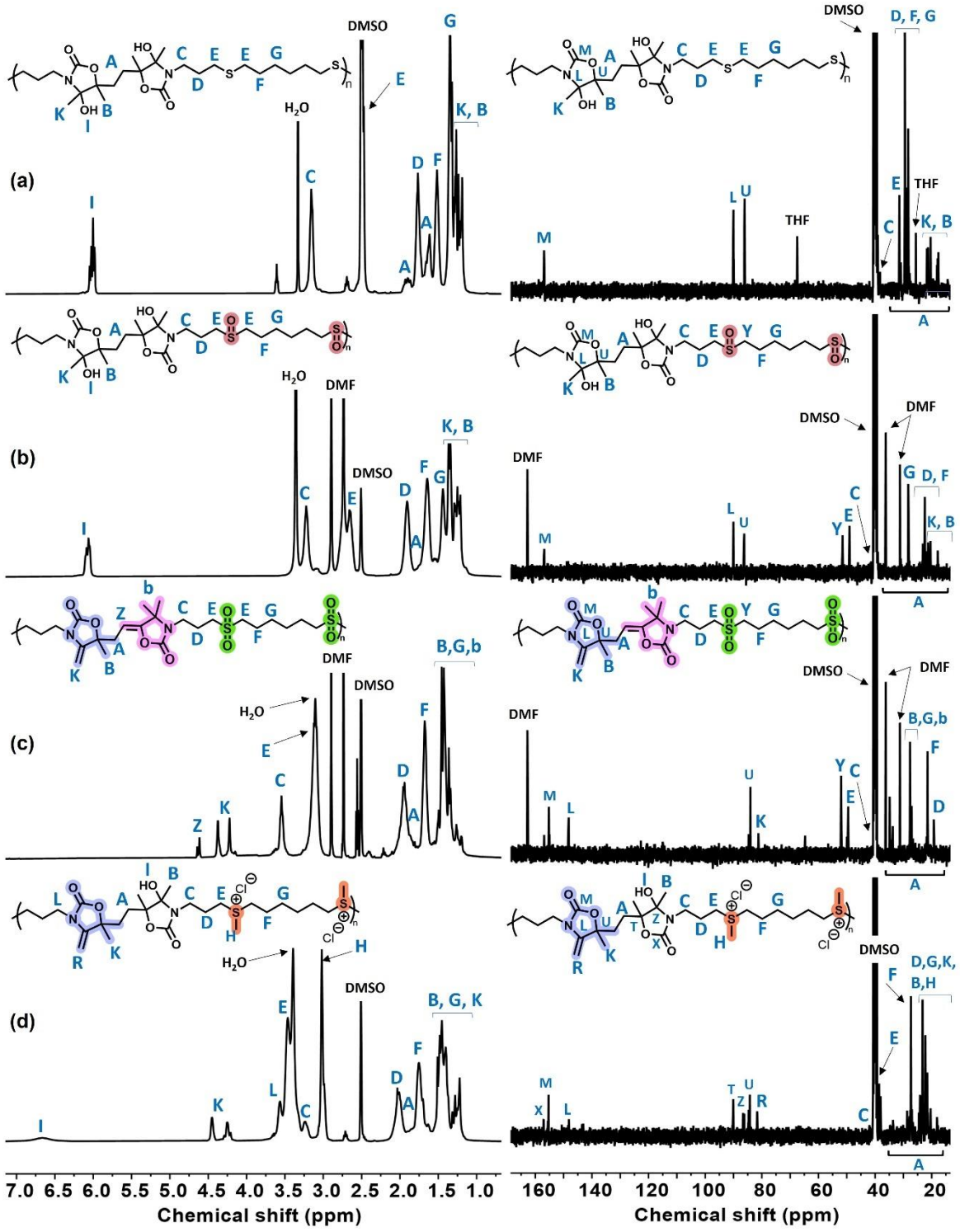

Figure 4. ^{1}H-NMR spectra (left, 400 MHz, DMSO-d_6) and ^{13}C-NMR spectra (right, 100 MHz, DMSO-d_6) of (a) **P2b**, (b) **P2b-Sulfoxide** (c) **P2b-Sulfone** (d) **P2b-Sulfonium**.

4 CONCLUSION

In this study, the chemical recycling of CO_2-sourced poly(*oxo*-carbonate)s was achieved under mild condition through aminolysis with allylamine, resulting in the recovery of a new bis(hydroxyoxazolidone) monomer featuring allyl functional groups. This monomer was copolymerized with various commercially available dithiols *via* photoinitiated thiol-ene click reaction at room temperature, delivering elusive poly(oxazolidone)-type polymers containing thioether functions, i.e. poly(oxazolidone-*co*-thioether)s. Optimal reaction conditions were investigated through solvent, initiator, and reaction time adjustments, leading to poly(oxazolidone)-type copolymers with a M_w of up to 101,000 g/mol. All the polymers exhibited an amorphous nature with a T_g spanning from 7 to 39 °C. These polymers displayed a two-step thermal decomposition pattern, with the first step associated with polymer dehydration in the temperature range of 120-140 °C, and the second step attributed to the degradation of the polymer's backbone within the range of 324-364 °C. Following a straightforward thermal treatment at the dehydration temperature for 2 h, the polymers underwent complete dehydration, resulting in the formation of polyoxazolidones enriched with exocyclic olefin moieties. This dehydration occurred at the solid state and did not require any solvent nor dehydrating agent, rendering the process facile and easily upscalable. The dehydrated polymers presented a high degradation temperature (305-361 °C) and a single T_g spanning from 2 to 53 °C. The post-modification of poly(oxazolidone-*co*-thioether)s was further assessed, focusing on the selective single or double oxidation of thioether linkages into sulfoxide or sulfone, as well as the alkylation of thioether to yield sulfonium derivatives. The introduction of sulfonium moieties delivered the first example of a water-soluble poly(oxazolidone). This research exemplifies the strategic utilization of functional monomers derived from the degradation of polycarbonates for the synthesis of a diverse range of novel functional poly(oxazolidone)-type polymers, whose properties have now to be investigated in a forthcoming work. Importantly, the allyl-functional bis(hydroxyoxazolidone) needed for their synthesis can also be quantitatively produced by reacting allylamine with the CO_2-sourced bis(alkylidene cyclic carbonate), offering perspective for facile upscaling.

Electronic supplementary information (ESI) available: Materials and instrumentation, additional information about optimization reactions, solubility tables, NMR spectra, SEC chromatograms, TGA & DSC analyses, FT-IR spectra, setup for the photopolymerization reaction.

5 REFERENCES

1. Deng, Y., et al., *Reviewing the thermo-chemical recycling of waste polyurethane foam.* Journal of environmental management, 2021. **278**: p. 111527.

2. Akindoyo, J.O., et al., *Polyurethane types, synthesis and applications–a review.* Rsc Advances, 2016. **6**(115): p. 114453-114482.

3. Engels, H.W., et al., *Polyurethanes: Versatile materials and sustainable problem solvers for today's challenges.* Angewandte Chemie International Edition, 2013. **52**(36): p. 9422-9441.

4. Liu, S.-H., et al., *Improving thermal stability of polyurethane through the addition of hyperbranched polysiloxane.* Polymers, 2019. **11**(4): p. 697.

5. Delebecq, E., et al., *On the versatility of urethane/urea bonds: reversibility, blocked isocyanate, and non-isocyanate polyurethane.* Chemical reviews, 2013. **113**(1): p. 80-118.

6. Szycher, M., *Szycher's handbook of polyurethanes*. 1999: CRC press.

7. Sendijarevic, V., et al., *Polyoxazolidones for high temperature applications.* Journal of Elastomers & Plastics, 1996. **28**(1): p. 63-83.

8. Sendijarevic, V., et al., *Novel isocyanate-based matrix resins for high temperature composite applications.* Polymer composites, 1996. **17**(2): p. 180-186.

9. Pankratov, V.A., T.M. Frenkel, and A. Fainleib, *2-Oxazolidinones.* Russian Chemical Reviews, 1983. **52**(6): p. 576.

10. Kinjo, N., et al., *Synthesis and viscoelastic properties of new thermosetting resins having isocyanurate and oxazolidone rings in their molecular structures.* Journal of Applied Polymer Science, 1983. **28**(5): p. 1729-1741.

11. Pelzer, T., et al., *Toward polymers with oxazolidin-2-one building blocks through tetra-n-butyl-ammonium halides (Cl, Br, I) catalyzed coupling of epoxides with isocyanates.* European Polymer Journal, 2018. **107**: p. 1-8.

12. Kitayama, M., et al., *Synthesis and properties of polyoxazolidone elastomers from diepoxides and diisocyanates.* Rubber Chemistry and Technology, 1980. **53**(1): p. 1-13.

13. Bakry, A., et al., *Flexible aliphatic poly (isocyanurate–oxazolidone) resins based on poly (ethylene glycol) diglycidyl ether and 4, 4'-methylene dicyclohexyl diisocyanate.* Journal of Applied Polymer Science, 2016. **133**(19).

14. Azechi, M. and T. Endo, *Synthesis and property of polyoxazolidone having fluorene moiety by polyaddition of diisocyanate and diepoxide.* Journal of Polymer Science Part A: Polymer Chemistry, 2014. **52**(12): p. 1755-1760.

15. Altmann, H.J., et al., *Synthesis of Linear Poly (oxazolidin-2-one) s by Cooperative Catalysis Based on N-Heterocyclic Carbenes and Simple Lewis Acids.* Macromolecules, 2019. **52**(2): p. 487-494.

16. Gomez-Lopez, A., et al., *Trends in non-isocyanate polyurethane (NIPU) development.* Chemical Communications, 2021. **57**(92): p. 12254-12265.

17. Ehrenberg, L. and S. Hussain, *Genetic toxicity of some important epoxides.* Mutation Research/Reviews in Genetic Toxicology, 1981. **86**(1): p. 1-113.

18. Iwakura, Y., S.I. Izawa, and F. Hayano, *Polyoxazolidones prepared from bisurethans and bisepoxides.* Journal of Polymer Science Part A-1: Polymer Chemistry, 1966. **4**(4): p. 751-760.

19. Wu, Q., et al., *Copper (I)-Catalyzed Four-Component Coupling Using Renewable Building Blocks of CO2 and Biomass-Based Aldehydes.* European Journal of Organic Chemistry, 2018. **2018**(24): p. 3105-3113.

20. Teffahi, D., S. Hocine, and C.-J. Li, *Synthesis of oxazolidinones, dioxazolidinone and polyoxazolidinone (a new polyurethane) via a multi component-coupling of aldehyde, diamine dihydrochloride, terminal alkyne and CO2.* Letters in Organic Chemistry, 2012. **9**(8): p. 585-593.

21. Gennen, S., et al., *CO2-Sourced α-Alkylidene Cyclic Carbonates: A Step Forward in the Quest for Functional Regioregular Poly (urethane) s and Poly (carbonate) s.* Angewandte Chemie, 2017. **129**(35): p. 10530-10534.

22. Ngassam Tounzoua, C., B. Grignard, and C. Detrembleur, *Exovinylene Cyclic Carbonates: Multifaceted CO2-Based Building Blocks for Modern Chemistry and Polymer Science.* Angewandte Chemie International Edition, 2022. **61**(22): p. e202116066.

23. Habets, T., et al., *Advancing the synthesis of isocyanate-free poly (oxazolidones) s: Scope and limitations.* Macromolecules, 2020. **53**(15): p. 6396-6408.

24. Dabral, S., et al., *Synthesis and polymerisation of α-alkylidene cyclic carbonates from carbon dioxide, epoxides and the primary propargylic alcohol 1, 4-butynediol.* Green Chemistry, 2020. **22**(5): p. 1553-1558.

25. Wong, A.R., et al., *Improved Characterization of Polyoxazolidinones by Incorporating Solubilizing Side Chains.* Macromolecules, 2022. **55**(24): p. 11006-11012.

26. Habets, T., et al., *Facile construction of functional poly (monothiocarbonate) copolymers under mild operating conditions.* Polymer Chemistry, 2022. **13**(21): p. 3076-3090.

27. Habets, T., et al., *Covalent adaptable networks through dynamic N, S-acetal chemistry: toward recyclable CO2-based thermosets.* Journal of the American Chemical Society, 2023.

28. Siragusa, F., et al., *Access to biorenewable and CO2-based polycarbonates from exovinylene cyclic carbonates.* ACS Sustainable Chemistry & Engineering, 2021. **9**(4): p. 1714-1728.

29. Siragusa, F., et al., *Unifying Step-Growth Polymerization and On-Demand Cascade Ring-Closure Depolymerization via Polymer Skeletal Editing.* Macromolecules, 2022. **55**(11): p. 4637-4646.

30. Ngassam Tounzoua, C., et al., *A catalytic domino approach toward oxo-alkyl carbonates and polycarbonates from CO2, propargylic alcohols, and (mono-and di-) alcohols.* ACS Sustainable Chemistry & Engineering, 2020. **8**(26): p. 9698-9710.

31. Siragusa, F., C. Detrembleur, and B. Grignard, *The advent of recyclable CO 2-based polycarbonates.* Polymer Chemistry, 2023. **14**(11): p. 1164-1183.

32. Lanzi, M. and A.W. Kleij, *Recent advances in the synthesis and polymerization of new CO2-based cyclic carbonates.* Chinese Journal of Chemistry.

33. Zhang, Y.-F., et al., *Facile synthesis, structure and properties of CO 2-sourced poly (thioether-co-carbonate) s containing acetyl pendants via thio-ene click polymerization.* Polymer Chemistry, 2022. **13**(2): p. 201-208.

34. Ouhib, F., et al., *CO 2-sourced polycarbonates as solid electrolytes for room temperature operating lithium batteries.* Journal of Materials Chemistry A, 2019. **7**(16): p. 9844-9853.

35. Siragusa, F., et al., *Catalyst-Free Approach for the Degradation of Bio-and CO2-Sourced Polycarbonates: A Step toward a Circular Plastic Economy.* ACS Sustainable Chemistry & Engineering, 2022. **10**(27): p. 8863-8875.

36. Sarapas, J.M. and G.N. Tew, *Poly (ether–thioethers) by thiol–ene click and their oxidized analogues as lithium polymer electrolytes.* Macromolecules, 2016. **49**(4): p. 1154-1162.

37. El Mohtadi, F., et al., *Main chain polysulfoxides as active 'stealth'polymers with additional antioxidant and anti-inflammatory behaviour.* International Journal of Molecular Sciences, 2019. **20**(18): p. 4583.

38. Page, P.C.B., et al., *Chemoselective oxidation of sulfides to sulfoxides with urea–hydrogen peroxide complex catalysed by diselenide.* Synlett, 2015: p. 80-82.

39. Younes, G.R., et al., *Sugar-based thermoplastic polyhydroxyurethanes: effects of sorbitol and mannitol diastereomers on polymer properties and applications in melt blending.* ACS Applied Polymer Materials, 2022. **4**(7): p. 5161-5172.

40. Jaratrotkamjorn, R., et al., *Synthesis and characterization of elastomeric, biobased, nonisocyanate polyurethane from natural rubber.* Journal of Applied Polymer Science, 2017. **134**(42): p. 45427.

41. Bourguignon, M., B. Grignard, and C. Detrembleur, *Water-Induced Self-Blown Non-Isocyanate Polyurethane Foams.* Angewandte Chemie International Edition, 2022. **61**(51): p. e202213422.

42. Fortman, D.J., et al., *Mechanically activated, catalyst-free polyhydroxyurethane vitrimers.* Journal of the American Chemical Society, 2015. **137**(44): p. 14019-14022.

43. Younes, G.R. and M. Marić, *Bio-based thermoplastic polyhydroxyurethanes synthesized from the terpolymerization of a dicarbonate and two diamines: design, rheology, and application in melt blending.* Macromolecules, 2021. **54**(21): p. 10189-10202.

44. Yook, J., D. Jeong, and J.-C. Lee, *Synthesis of Citronellol-Derived Antibacterial Polymers and Effect of Thioether, Sulfoxide, Sulfone, and Ether Functional Groups on Their Bactericidal Activity.* Macromolecules, 2023.

45. Yan, B., et al., *Facile synthesis of ROS-responsive biodegradable main chain poly (carbonate-thioether) copolymers.* Polymer Chemistry, 2018. **9**(7): p. 904-911.

46. Dannecker, P.K., et al., *Fatty Acid–Derived Aliphatic Long Chain Polyethers by a Combination of Catalytic Ester Reduction and ADMET or Thiol-Ene Polymerization.* Macromolecular Chemistry and Physics, 2019. **220**(4): p. 1800440.

47. Infante Teixeira, L., K. Landfester, and H. Thérien-Aubin, *Selective Oxidation of Polysulfide Latexes to Produce Polysulfoxide and Polysulfone in a Waterborne Environment.* Macromolecules, 2021. **54**(8): p. 3659-3667.

48. Krähling, L., et al., *Allyl compounds.* Ullmann's Encyclopedia of Industrial Chemistry, 2000.

49. Hong, S.J., et al., *The potential health risks of N, N-dimethylformamide: An updated review.* Journal of Applied Toxicology, 2024. **44**(11): p. 1637-1646.

6 Supporting Information

6.1 Materials and instrumentation

6.1.1 Materials

1,4-Butanediol (97%), 1,8-Diazabicyclo[5.4.0]undec-7-ene (DBU, 99%), Allylamine (98%), 2,2′-(Ethylenedioxy)diethanethiol (95%), 1,4-Butanedithiol (97%), 2,2-Dimethoxy-2-phenyl acetophenone (DMPA, 99%), Hydrogen peroxide solution 30%, Iodomethane (99%), Diphenyldiselenid (98%), 1,4-Benzenedimethanethiol (98%), Sulfuric acid 98% were purchased from Sigma Aldrich. Ethylene Glycol Bis(3-mercaptopropionate) (98%) was purchased from TCI. 1,6-Hexanedithiol (97%) was purchased from Thermo Scientific. Sodium hydroxide (>99%, beads) was purchased from Carl Roth. The following were selected as mixtures of photoinitiators: a blend of 2-hydroxy-2-methylpropiophenone phenyl bis(2,4,6-trimethylbenzoyl)-phosphine oxide and ethylphenyl(2,4,6-trimethylbenzoyl) phosphinate (Omnirad 2022), a blend of ethyl phenyl(2,4,6-trimethylbenzoyl) phosphinate and phenyl bis(2,4,6-trimethylbenzoyl)-phosphineoxide (Omnirad 2100). All photoinitiators mixtures used were from IGM Resigns (Netherlands). The structures of free radical photoinitiators–mixtures are presented in Scheme S1. All other chemicals and reagents were purchased from commercial sources and used as received.

Dialysis membrane Spectra/Por 7 (MWCO 1 kD) was purchased from Repligen.

6.1.2 Instrumentation

6.1.2.1 Nuclear Magnetic Resonance (NMR) Spectroscopy

All NMR analyses were performed using a Bruker 400 MHz spectrometer at 25 °C in the Fourier transform mode. 16 scans for ^{1}H spectra and 512 scans for ^{13}C spectra were recorded.

6.1.2.2 Size exclusion chromatography (SEC)

Number-average molecular weight (M_n), weight-average molecular weight (M_w), and dispersity ($D= M_w/M_n$) of the polymers were assessed by using a size exclusion chromatography (SEC) with a polystyrene calibration in dimethylformamide (DMF) containing LiBr (0.025 M) at 55 °C (flow rate: 1 mL/min) with a Waters chromatograph equipped with three columns (PSS gram 1000Å (x2), 30 Å) and a precolumn, a dual absorbance detector (Waters 2487) and a refractive index detector (Waters 2414).

6.1.2.3 Thermogravimetric analysis (TGA)

TGA of the polymers were measured on TGA2 instrument from Mettler Toledo. To determine the mass loss of polymers, 4-7 mg of each sample were heated at 10 °C/min from 30 to 50 °C and flushed for 10 min at 50 °C and then heated at 20 °C/min until 600 °C under an N_2 atmosphere (20 mL/min). To assign the dehydration temperature, 4-7 mg of each sample were heated at 2 °C/min from 30 to 250 °C under N_2 atmosphere (20 ml/min).

6.1.2.4 Differential scanning calorimetry (DSC)

DSC of all samples was acquired using a DSC 250 (TA Instruments) with a liquid nitrogen cooling system and a N_2 sample flow rate of 50 mL/min. 3−5 mgs of each sample were loaded into aluminum pans, hermetically sealed, and run using a heat/cool/heat method. To determine the T_g of polymers with hydroxyoxazolidone linkages, samples were heated from 25 to 90 °C at a heating rate of 10 °C/min, cooled to −40 °C at a rate of 10 °C/min. The temperature modulated segment was set with an amplitude of 2 °C with a period of 60 seconds. Finally, the sample was heated again to 200 °C at a rate of 2 °C/min. The final heating curve was used for thermal property evaluation. To assign the T_g for dehydrated polymers, samples were heated to 140 °C at a heating rate of 10 °C/min, cooled to −80 °C at a rate of 10 °C/min, and finally heated again to 160 °C at a rate of 10 °C/min.

6.1.2.5 Fourier Transform Infrared Spectra (F-TIR)

FTIR was performed using a Nicolet IS5 spectrometer (Thermo Fisher Scientific) equipped with a diamond attenuated transmission.

6.1.2.6 Tensile tests

Tensile tests were conducted at room temperature using an Instron 34TM-10 equipped with a load cell of 500 N at a speed of 5 $mm.min^{-1}$. Measurements were repeated 5 times on dogbone-shaped samples (ASTM-D638-V) with a thickness of around 0.15 mm. The samples were prepared by compression molding and were cut at room temperature using a Qualitest die cutter.

6.1.2.7 Compression molding

Polymer samples were cut into little pieces and pressed between Teflon sheets over steel plates in a Carver press. **P2a** was pressed at a temperature of 70 °C for 3x15 min under a pressure of 6 ton force (around 24 MPa). The process was achieved in three steps to correctly eliminate air bubbles trapped in the polymer film. **P2a-dehydrated** was pressed at 50 °C for 15 min under a pressure of 6 ton force (around 24 MPa). The steel plates were then removed from the hot press and cooled rapidly in a press at room-temperature.

6.2 BisαCC synthesis and characterization

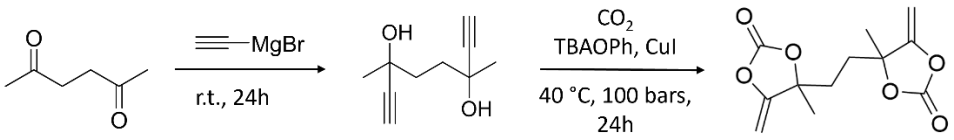

Figure S1. Synthesis route for BisαCC.

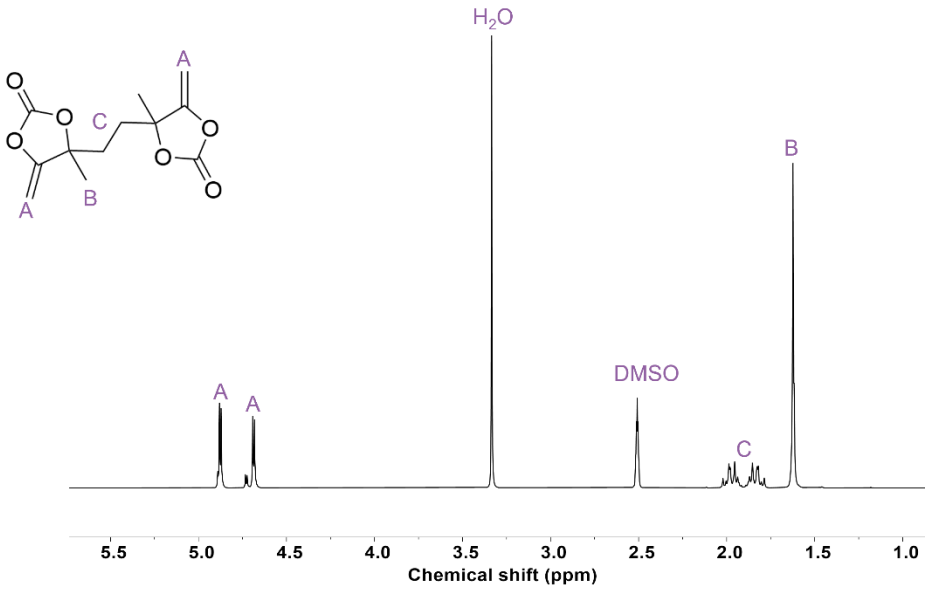

Figure S2. ^{1}H-NMR spectrum of BisαCC (400 MHz, DMSO-d_6).

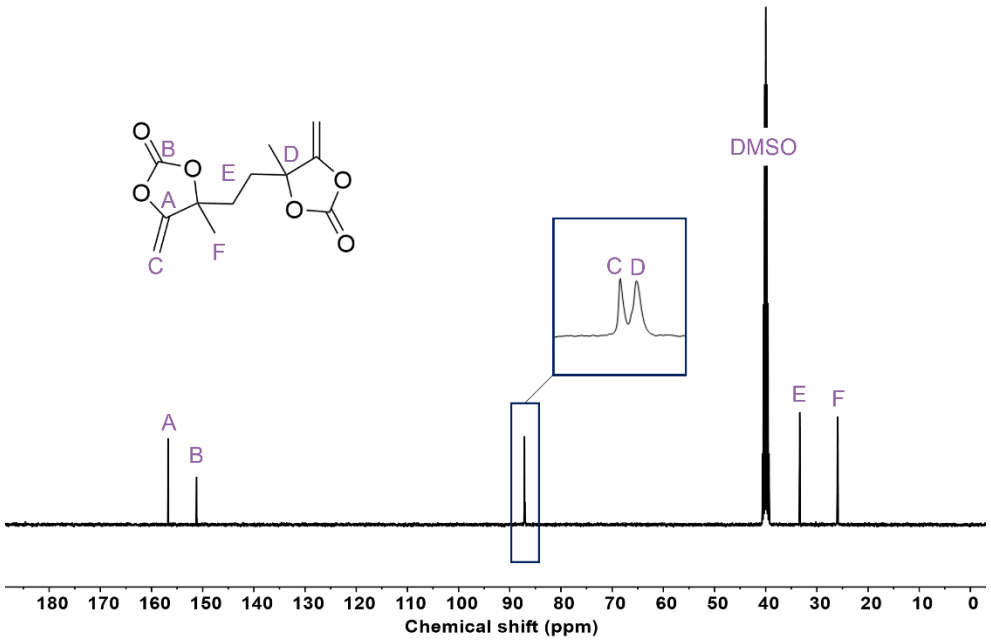

Figure S3. ^{13}C-NMR spectrum of BisαCC (100 MHz, DMSO-d_6).

6.3 Poly(*oxo*-carbonate)s characterizations

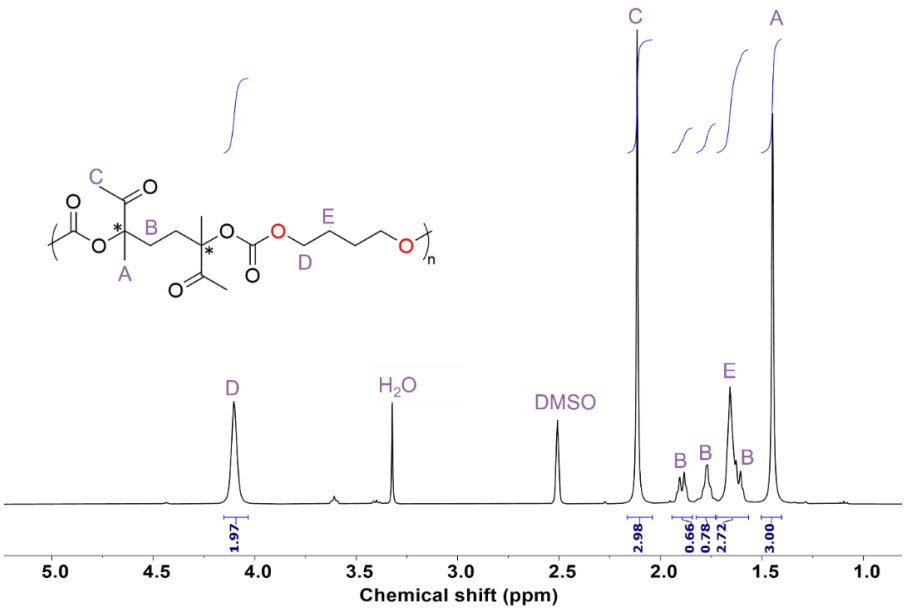

Figure S4. ^{1}H-NMR spectrum of pure PC (400 MHz, DMSO-d_6).

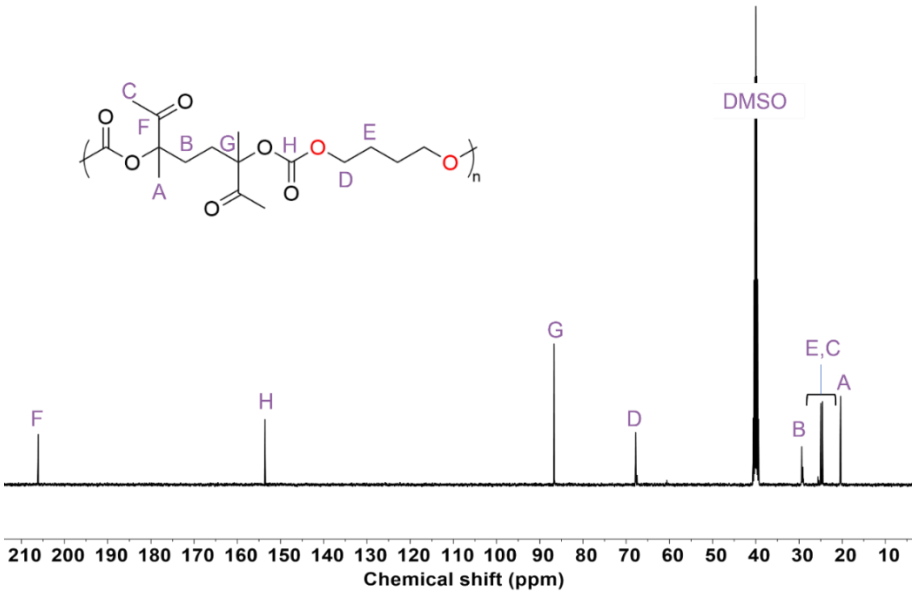

Figure S5. ^{13}C-NMR spectrum of pure PC (100 MHz, DMSO-d_6).

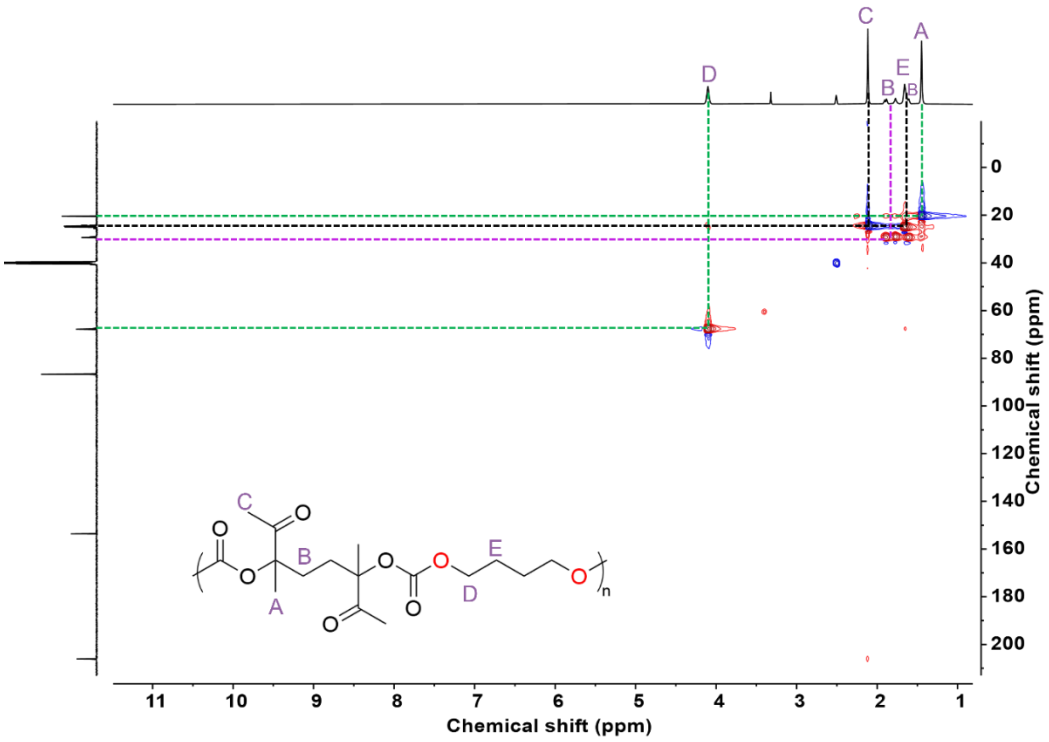

Figure S6. ^{1}H-^{13}C HSQC NMR spectrum of pure PC (400 MHz, DMSO-d_6).

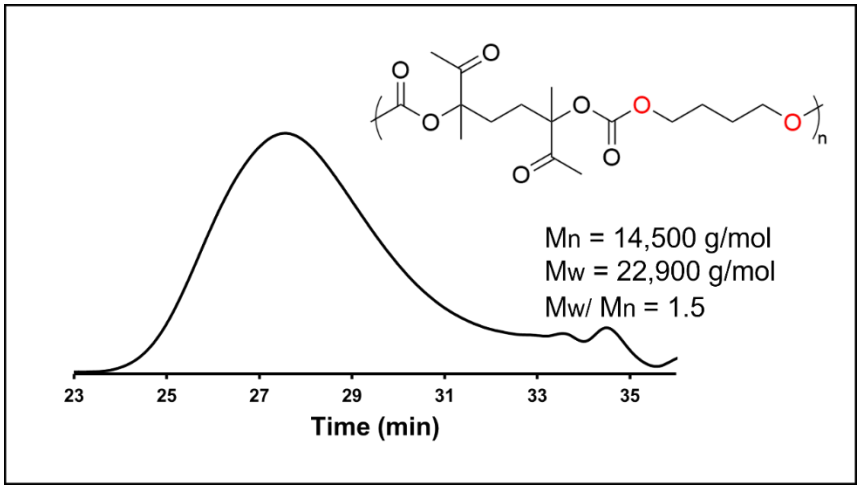

Figure S7. SEC chromatogram of poly(*oxo*-carbonate) PC (in DMF/LiBr).

6.4 Poly(*oxo*-carbonate)s degradation

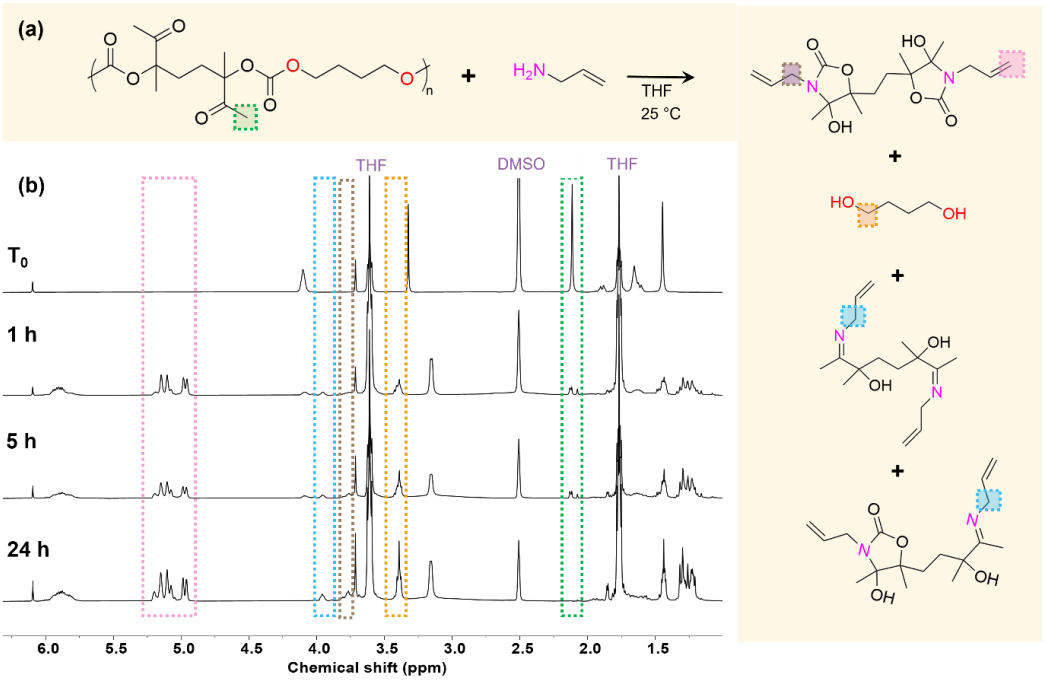

Figure S8. (a) Schematic of depolymerization of PC using allylamine and the degradation products; (b) Kinetic study of the PC depolymerization by ^{1}H-NMR spectroscopy using 1,3,5-trimethoxybenzene as internal standard (400 MHz, DMSO-d_6). T_0 was recorded before adding allylamine, since the amine is very reactive.

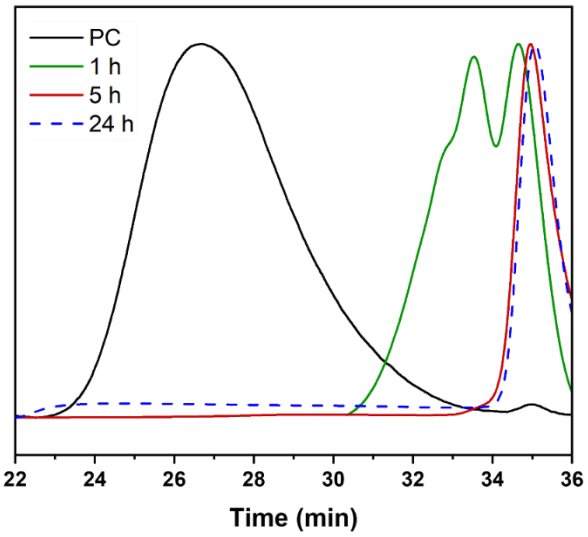

Figure S9. PC depolymerization along time by SEC (in DMF/LiBr).

6.5 Characterizations of bis(oxazolidone) with allyl functionality

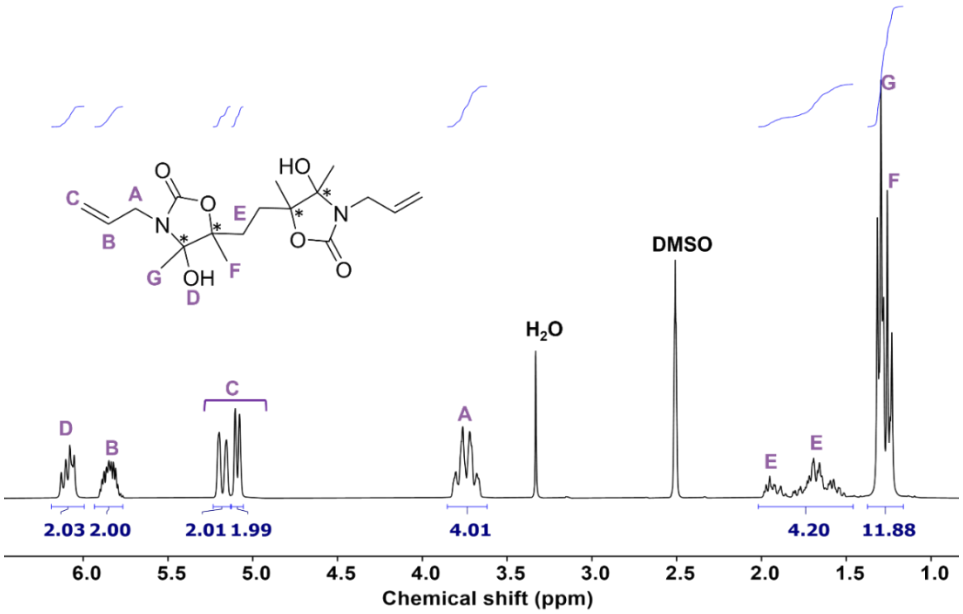

Figure S10. [1]H-NMR spectrum of monomer 1 (400 MHz, DMSO-d_6).

[1]H NMR (400 MHz, DMSO-d_6): δ = 6.09 ppm (m, 2H), δ = 5.84 ppm (m, 2H), δ = 5.18 (m, 2H), δ = 5.09 (m, 2H), δ = 3.73 (m, 4H), δ = 1.49-2.01 (m, 4H), δ = 1.16-1.37 (m, 12H).

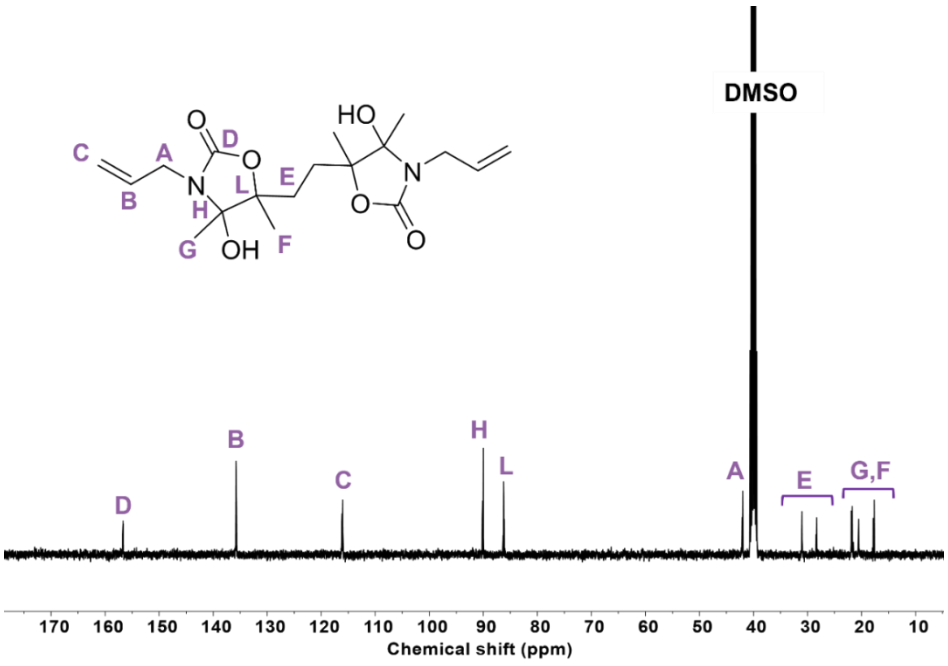

Figure S11. [13]C-NMR spectrum of monomer 1 (100 MHz, DMSO-d_6).

[13]C NMR (100 MHz, DMSO-d_6): δ = 156.7 ppm, δ = 135.7 ppm, δ = 116.1 ppm, δ = 90.1 ppm, δ = 86.2 ppm, δ = 42.1 ppm, δ = 31.03 ppm, δ = 28.3 ppm, δ = 21.8 ppm, δ = 20.6 ppm, δ = 17.7 ppm.

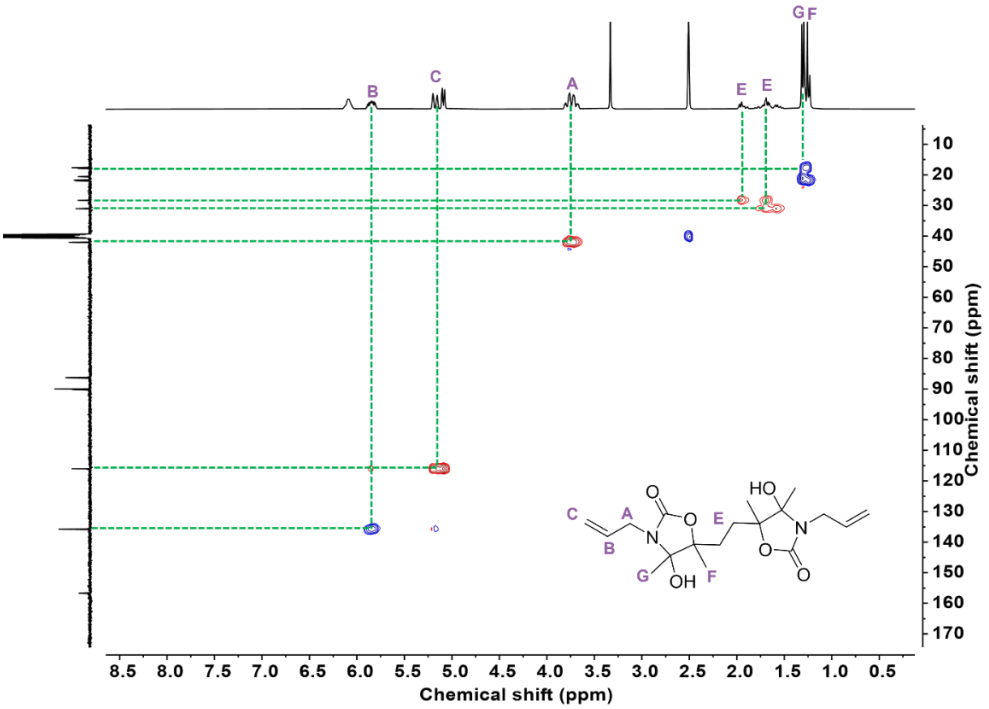

Figure S12. ^{1}H-^{13}C HSQC NMR spectrum of monomer 1 (400 MHz, DMSO-d_6).

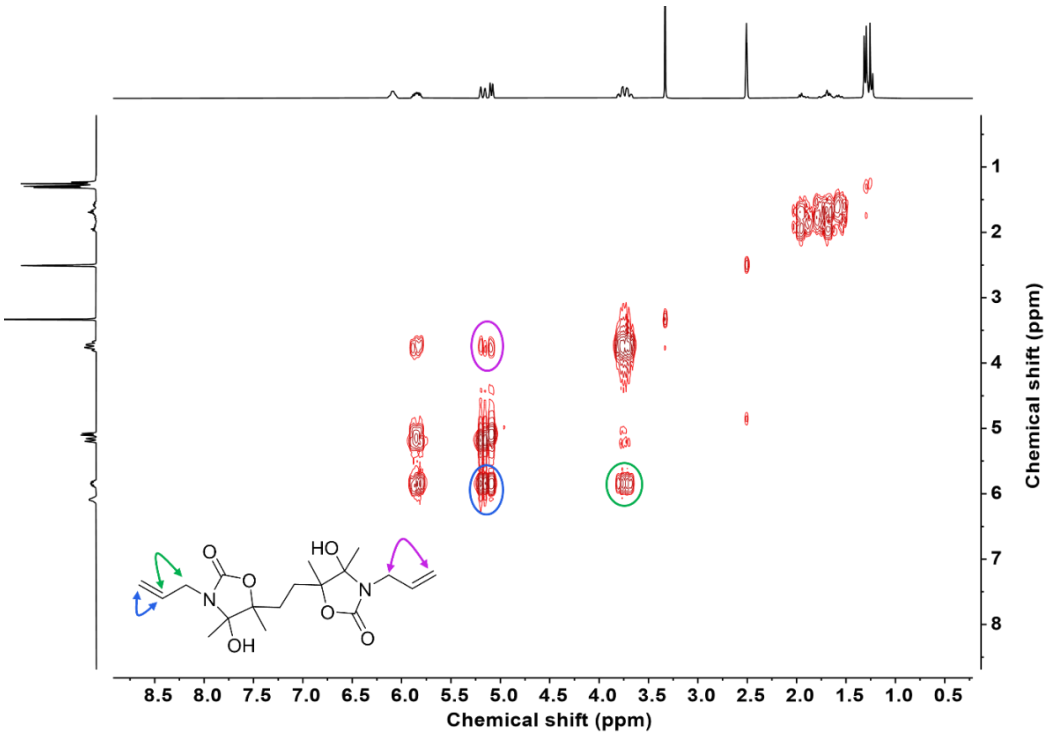

Figure S13. COSY NMR spectrum of monomer 1 (400 MHz, DMSO-d_6).

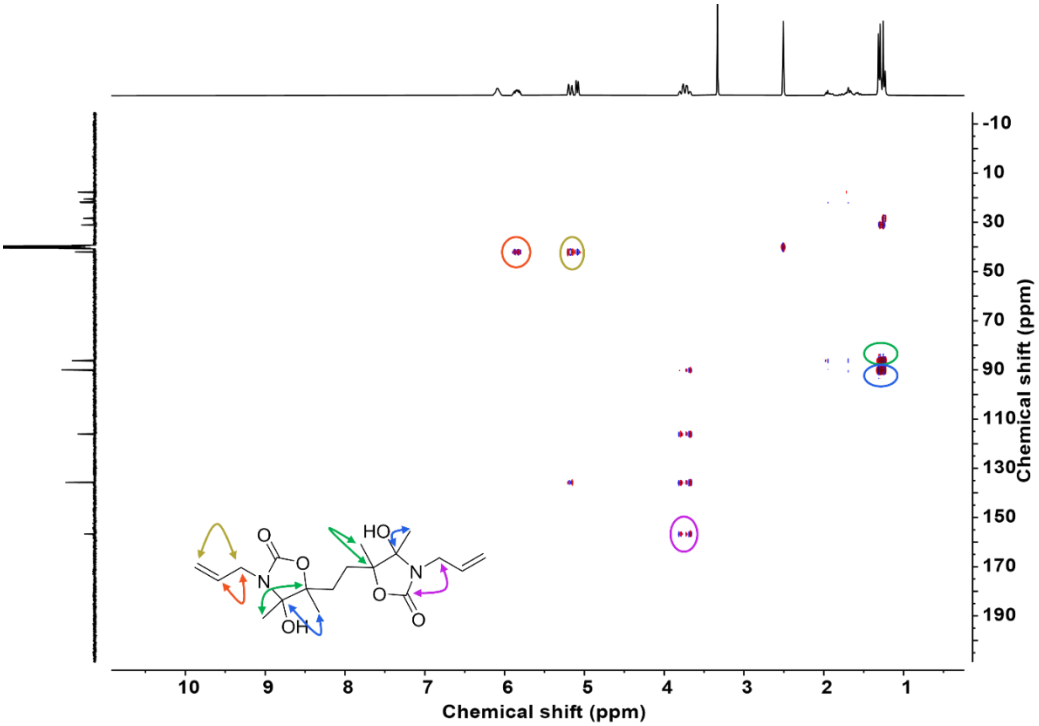

Figure S14. HMBC NMR spectrum of monomer 1 (400 MHz, DMSO-d_6).

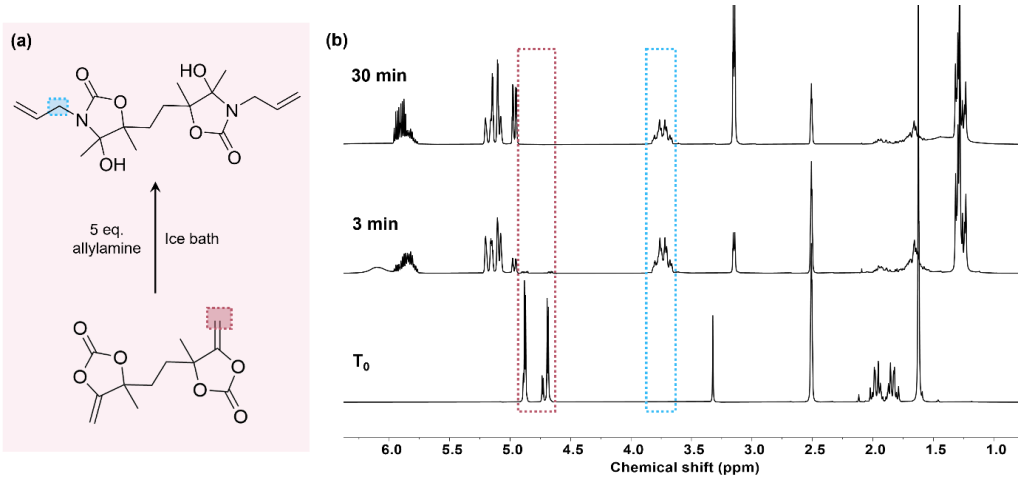

Figure S15. (a) The reaction between BisαCC and allylamine; (b) Kinetics of the reaction monitored by ^{1}H-NMR (400 MHz, DMSO-d_6), T_0 represents the time before addition of allylamine.

6.6 Polymerization experimental setup and optimization reactions

The reaction setup is displayed in Figure S16. However, as our setup does not include a temperature regulation system, we verified that the UV lamp did not generate too much heat during a reaction. We therefore monitored the reaction over 24h using a temperature probe. As shown in Figure S17, the temperature was measured to be of 23 °C over all the course of the experiment.

Figure S16. Photopolymerization setup using Omnicure series 2000, 200 W.

Figure S17. Photopolymerization apparatus, featuring an Omnicure series 2000, 200 W system integrated with a thermoset unit, (a) at the beginning ; (b) after 24 h of reaction

6.7 Optimization of the reaction conditions

To a glass vial, monomer 1 (400 mg, 1.08 mmol, 1 equiv) and 2,2′-(Ethylenedioxy)diethanethiol (2a, 1.08 mmol, 1 equiv) were added followed by the addition of the initiator (5 mol% vs monomer 1, 0.054 mmol, (13.9 mg for DMPA, 17.08 mg for Omnirad 2100, 22.5 mg for Omnirad 2022, see Scheme S1 for the structure of initiators). Then a specific amount of solvent was added to control the concentration of the mixture. The reaction mixture was then stirred under irradiation for 24 h. After that, a small amount of the crude product was withdrawn for 1H-NMR characterization to determine the monomer conversion and SEC analysis to investigate the relative molar mass of the polymers.

The conversion of monomer 1 was determined by comparison of the relative intensities of the peaks corresponding to allyl protons at 5.13 ppm of the monomer 1 and the methylene group of oxazolidones (N-CH2) at δ = 3.16 ppm of the produced polymer according to the equation:

$$Conv. = 1 - \left(\frac{I\,(5.13)/2}{\frac{I(5.13)}{2} + \frac{I(3.16)}{2}}\right) \qquad \text{(Eq.S1)}$$

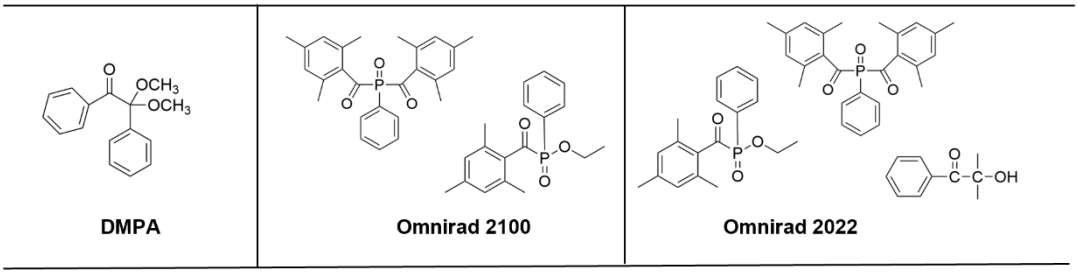

Scheme S1. Structure of the free-radical photoinitiators.

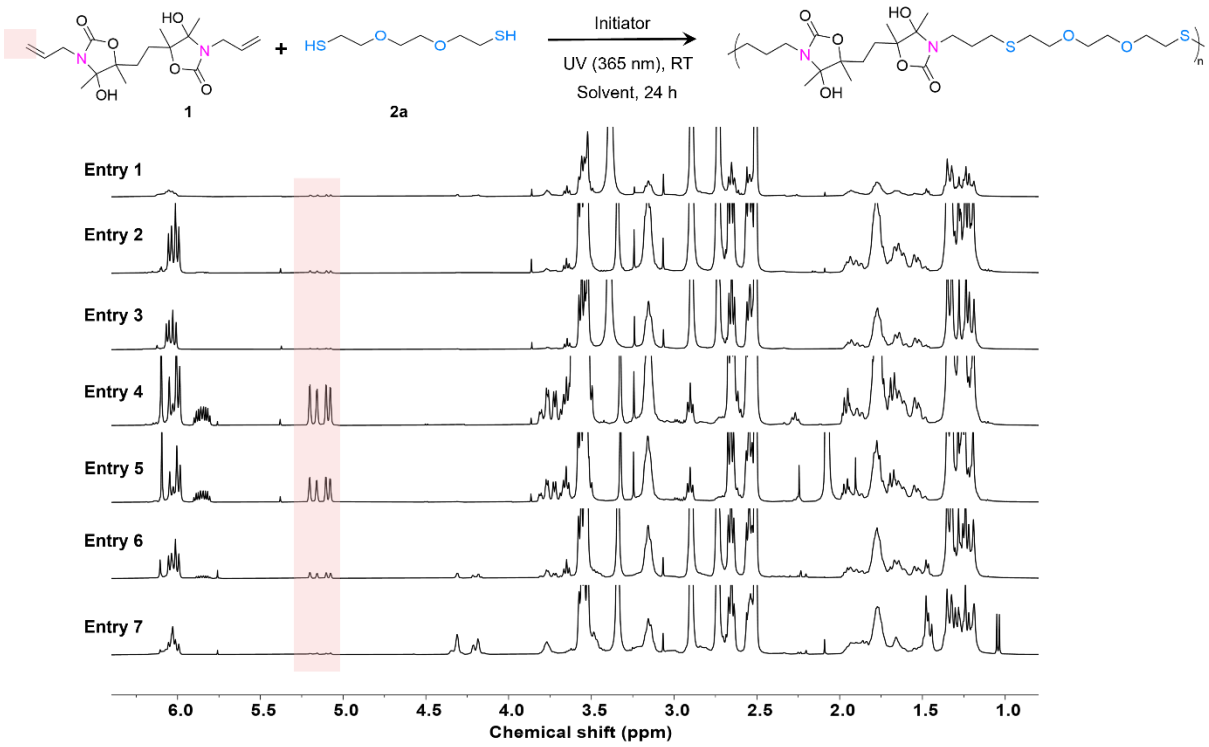

Figure S18. Thiol-ene photopolymerization of monomer 1 and dithiol 2a; ^{1}H-NMR spectrum of crude products of each optimization reaction (400 MHz, DMSO-d_6). Results are summarized in Table 1.

6.8 Kinetic of the polymerization reaction for P2b

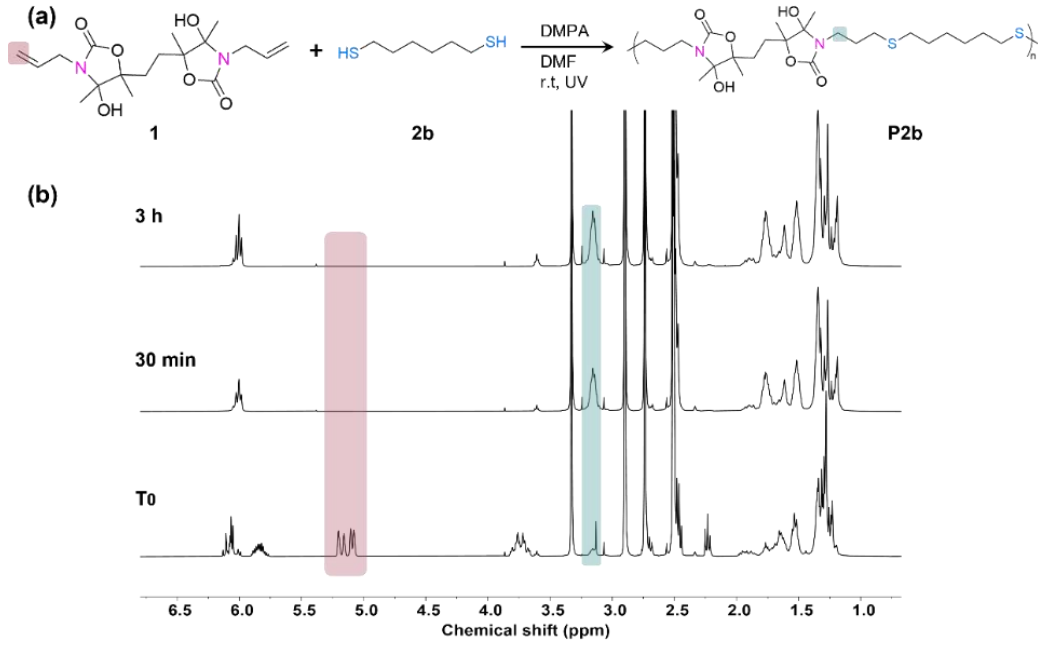

Figure S19. (a) Scheme of photopolymerization reaction between monomer 1 and dithiol 2b; (b) ^{1}H-NMR spectroscopy of photopolymerization of 1 and 2b along time (400 MHz, DMSO-d_6).

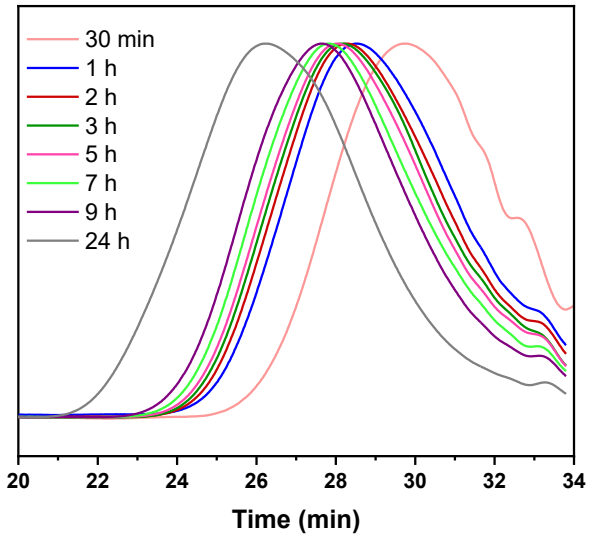

Figure S20. SEC chromatograms along time for thiol-ene polymerization of 1 and 2b (in DMF/LiBr).

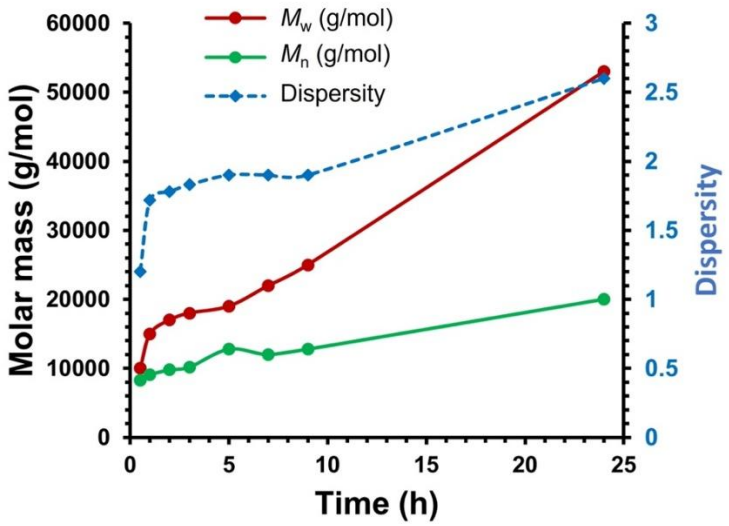

Figure S21. M_w and dispersity evolution for thiol-ene polymerization of 1 and 2b along time using SEC (in DMF/LiBr).

6.9 NMR of polymers (Table 2, entry 1-5)

For **P2a**, the conversion of monomer **1** was determined by comparison of the integrals of the peaks corresponding to allyl protons at 5.13 ppm of **1** and the oxazolidone linkages (N-$\underline{CH_2}$, δ = 3.15 ppm) of the produced polymer according to the equation:

$$Conv. = 1 - \left(\frac{I\,(5.13)/2}{\frac{I(5.13)}{2} + \frac{I(3.15)}{2}}\right) \qquad \text{(Eq.S2)}$$

For **P2b**, the conversion of monomer **1** was determined by comparison of the integrals of the peaks corresponding to allyl protons at 5.13 ppm of **1** and the oxazolidone linkages (N-$\underline{CH_2}$, δ = 3.16 ppm) of the produced polymer according to the equation:

$$Conv. = 1 - \left(\frac{I\,(5.13)/2}{\frac{I(5.13)}{2} + \frac{I(3.16)}{2}}\right) \qquad \text{(Eq.S3)}$$

For **P2c**, the conversion of monomer **1** was determined by comparison of the integrals of the peaks corresponding to allyl protons at 5.13 ppm of **1** and the ester moiety (O-$\underline{CH_2}$, δ = 4.25 ppm) of the produced polymer according to the equation:

$$Conv. = 1 - \left(\frac{I\,(5.13)/2}{\frac{I(5.13)}{2} + \frac{I(4.25)}{2}}\right) \qquad \text{(Eq.S4)}$$

For **P2d**, the conversion of monomer **1** was determined by comparison of the integrals of the peaks corresponding to allyl protons at 5.13 ppm of **1** and the the oxazolidone linkages (N-$\underline{CH_2}$, δ = 3.15 ppm) of the produced polymer according to the equation:

$$Conv. = 1 - \left(\frac{I\,(5.13)/2}{\frac{I(5.13)}{2} + \frac{I(3.15)}{2}}\right) \qquad \text{(Eq.S5)}$$

For **P2e**, the conversion of monomer **1** was determined by comparison of the integrals of the peaks corresponding to allyl protons at 5.13 ppm of **1** and thioether bond ($\underline{CH_2}$-S, δ = 2.41 ppm) of the produced polymer according to the equation:

$$Conv. = 1 - \left(\frac{I\,(5.13)/2}{\frac{I(5.13)}{2} + \frac{I(2.41)}{2}}\right) \qquad \text{(Eq.S6)}$$

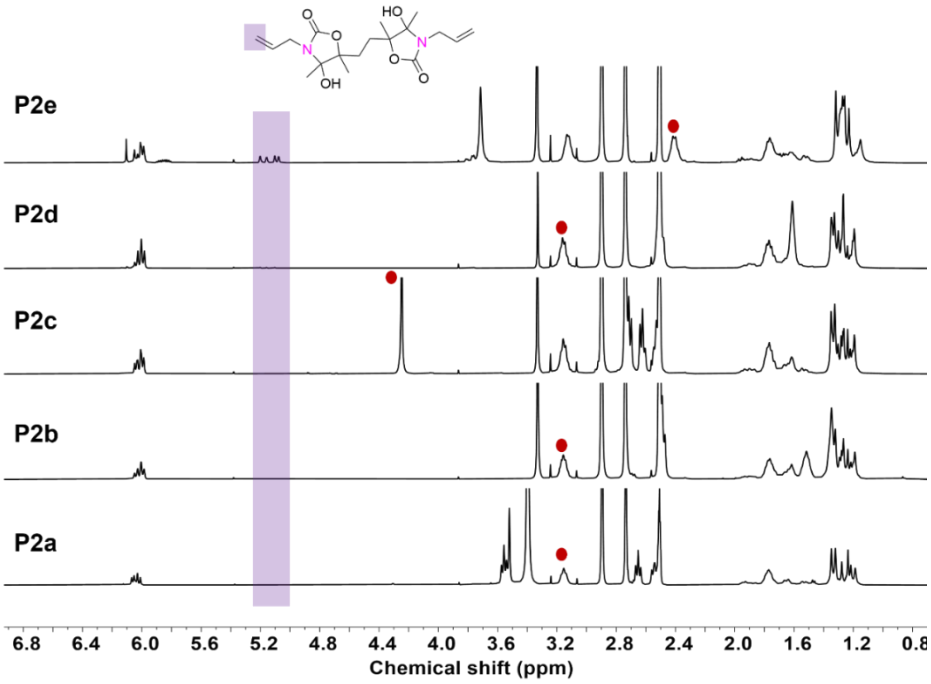

Figure S22. ^{1}H-NMR spectrum of crude hydrated polymers (400 MHz, DMSO-d_6).

6.10 SEC analyses of hydrated polymers

Table S1. Molecular characteristics of crude and pure copolymers

		Crude polymers			Pure polymers		
Entry	Polymer	M_n[a] (g/mol)	M_w[a] (g/mol)	Dispersity[a]	M_n[b] (g/mol)	M_w[b] (g/mol)	Dispersity[b]
1	P2a	27,000	116,000	4.2	31,000	101,000	3.2
2	P2b	19,000	71,000	3.7	20,000	57,000	2.7
3	P2c	18,000	54,000	2.9	21,000	64,000	3
4	P2d	22,000	55,000	2.5	23,000	69,000	3
5	P2e	7,000	19,000	2.7	8,000	20,000	2.5

[a]Determined on crude polymers, [b]Determined on pure polymers by SEC in DMF/LiBr calibrated with PS standards

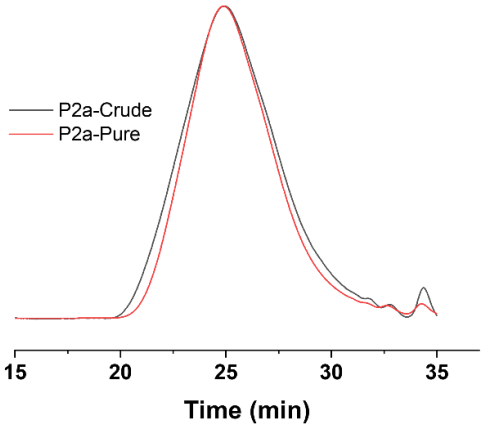

Figure S23. SEC chromatogram, overlay of crude and pure P2a (in DMF/LiBr).

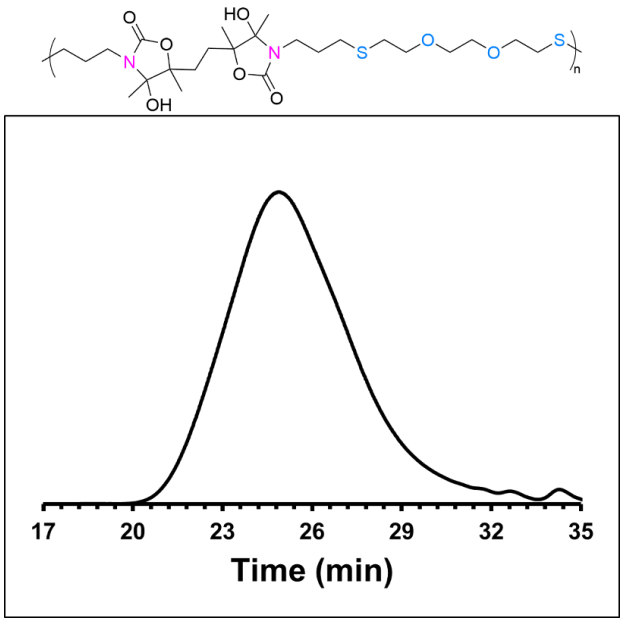

Figure S24. SEC chromatogram of purified P2a (in DMF/LiBr).

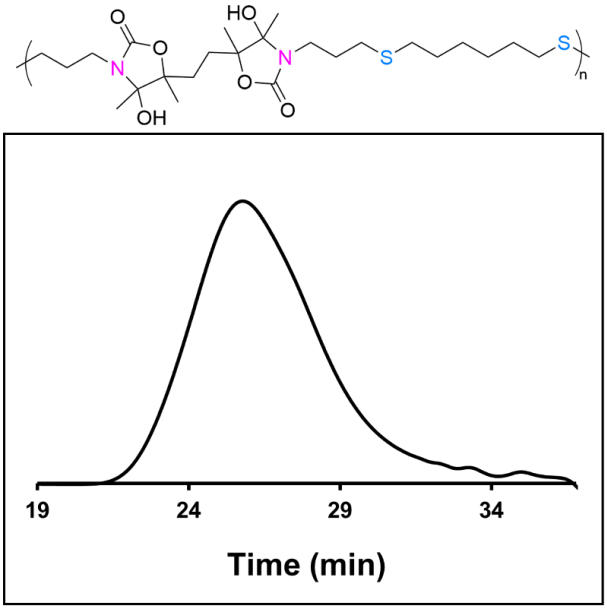

Figure S25. SEC chromatogram of purified P2b (in DMF/LiBr).

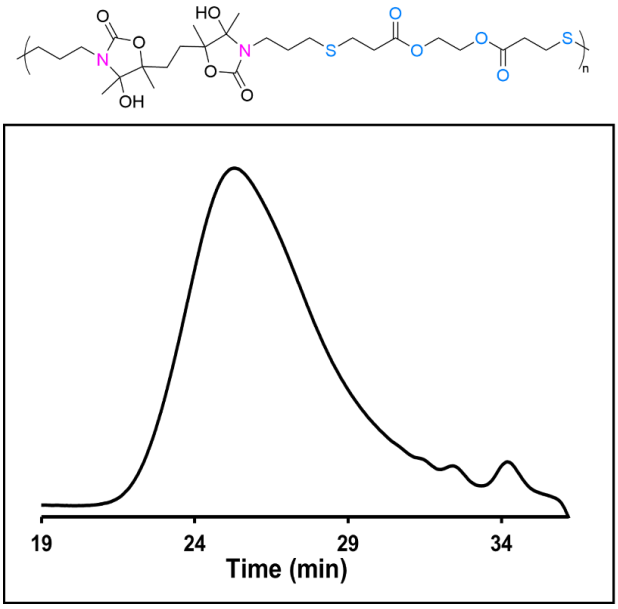

Figure S26. SEC chromatogram of purified P2c (in DMF/LiBr).

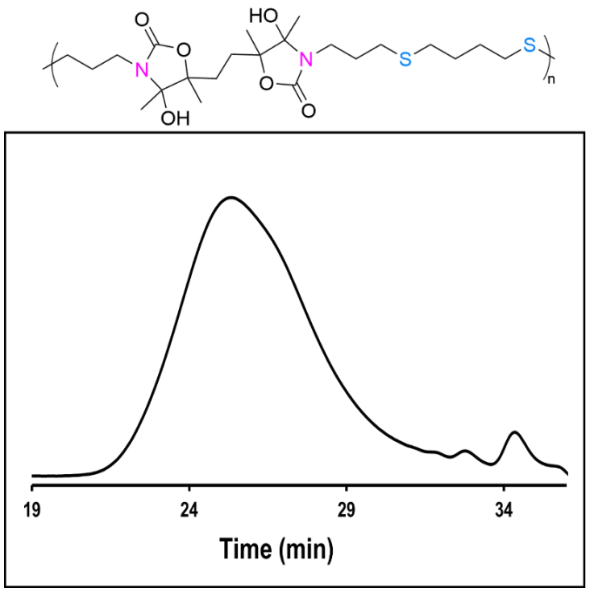

Figure S27. SEC chromatogram of purified P2d (in DMF/LiBr).

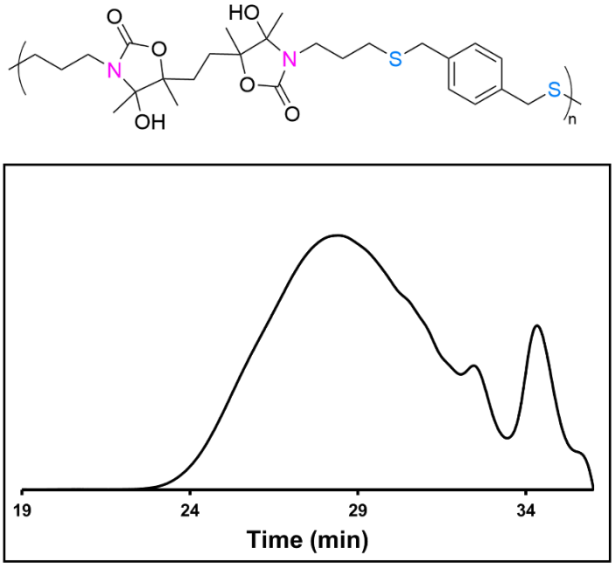

Figure S28. SEC chromatogram of purified **P2e** (in DMF/LiBr).

6.11 NMR characterizations of hydrated polymers (Table 2, entry 1-5)

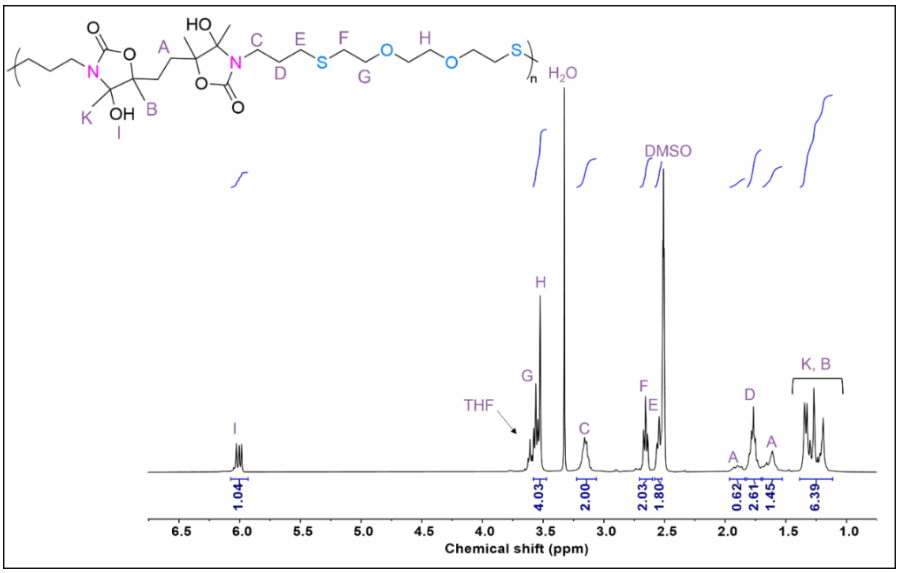

Figure S29. ^{1}H-NMR spectrum of purified P2a (400 MHz, DMSO-d_6).

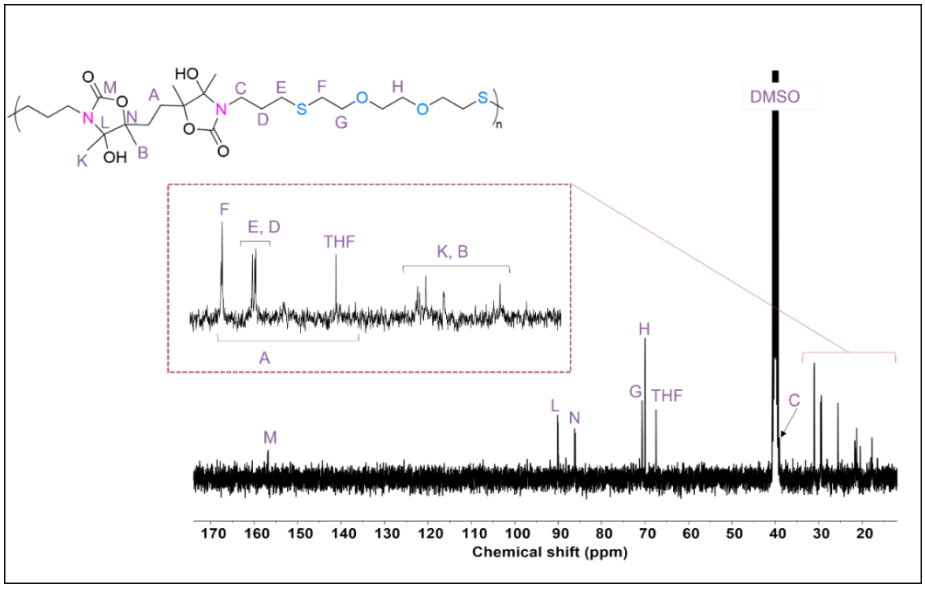

Figure S30. ^{13}C-NMR spectrum of purified P2a (100 MHz, DMSO-d_6).

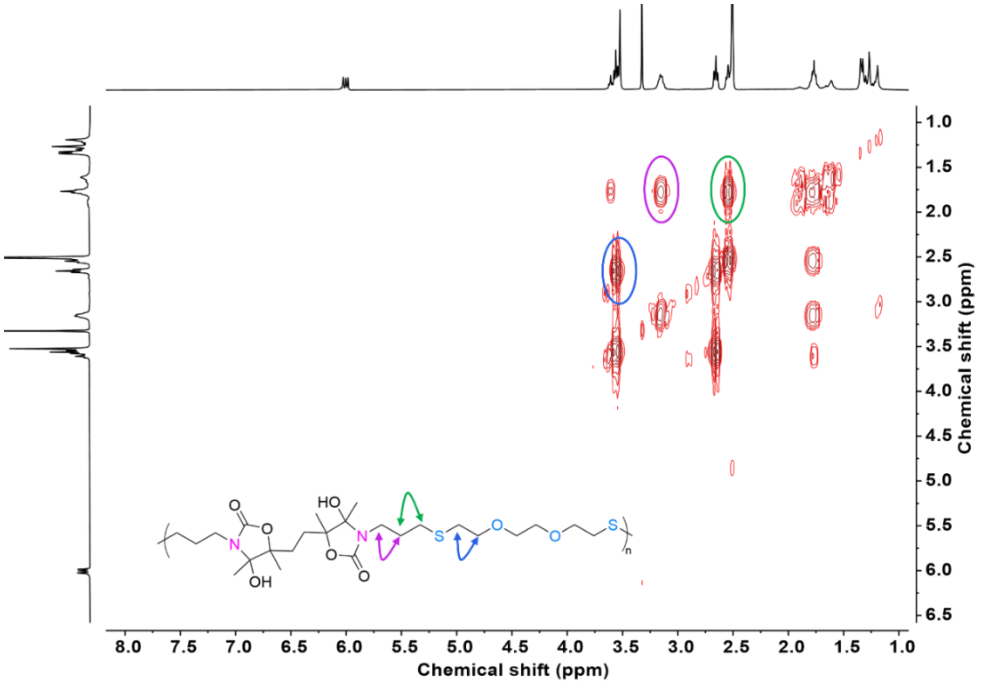

Figure S31. COSY NMR spectrum of purified P2a (400 MHz, DMSO-d_6).

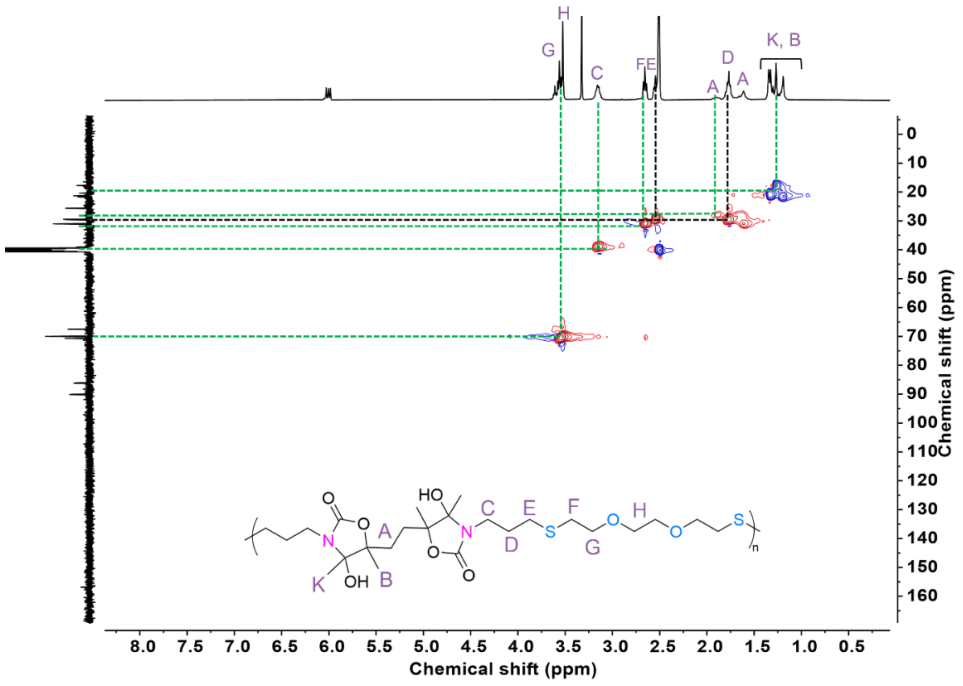

Figure S32. ^{1}H-^{13}C HSQC NMR spectrum of purified P2a (400 MHz, DMSO-d_6).

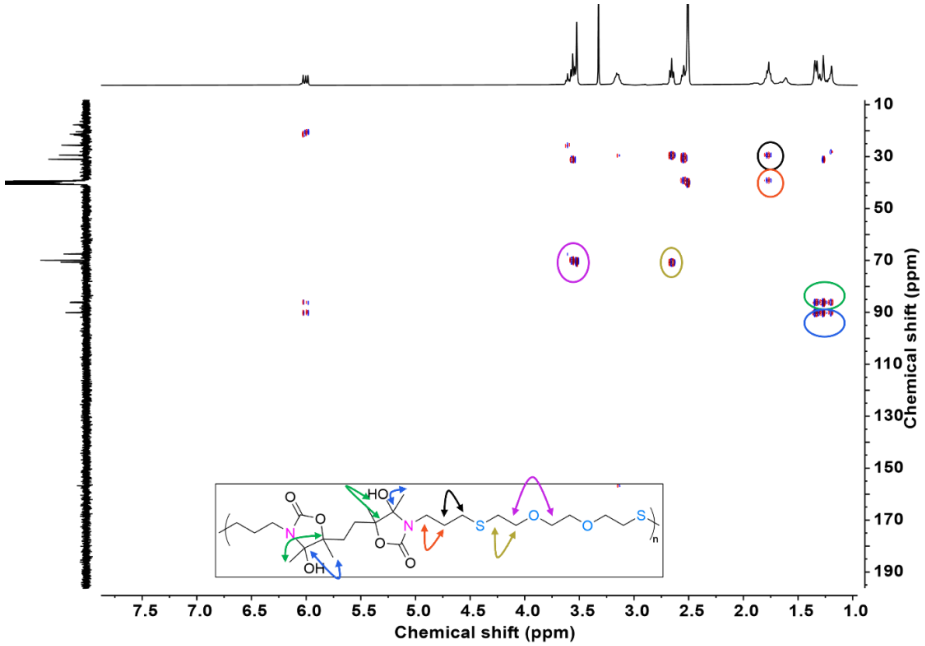

Figure S33. HMBC NMR spectrum of purified P2a (400 MHz, DMSO-d_6).

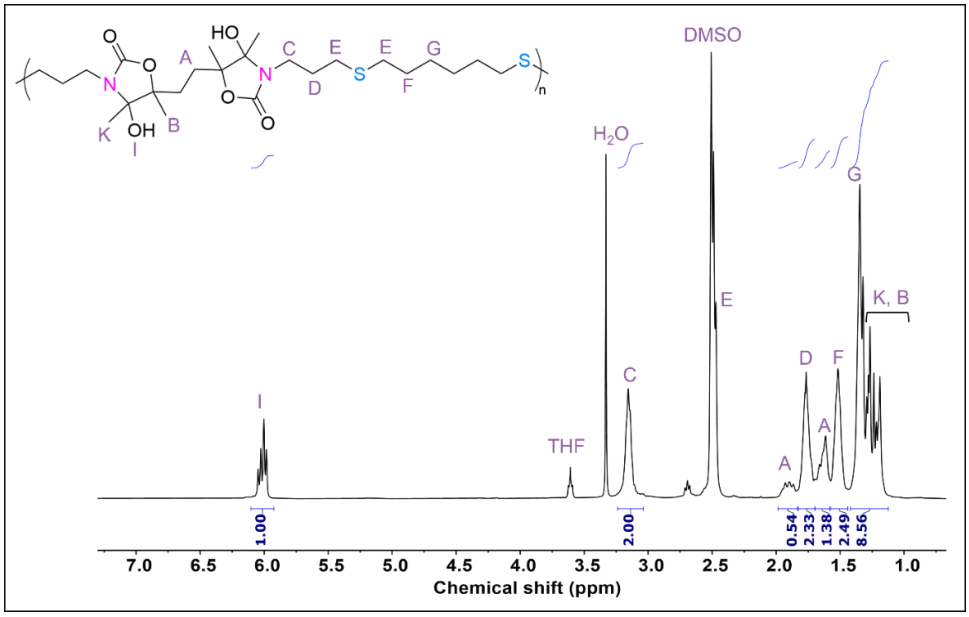

Figure S34. ^{1}H-NMR spectrum of purified P2b (400 MHz, DMSO-d_6).

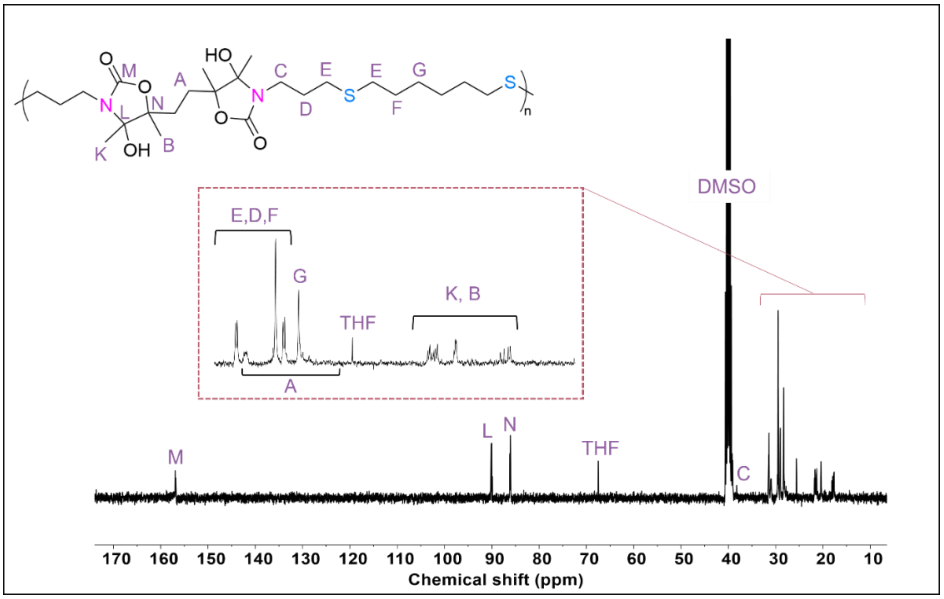

Figure S35. ^{13}C-NMR spectrum of purified P2b (100 MHz, DMSO-d_6).

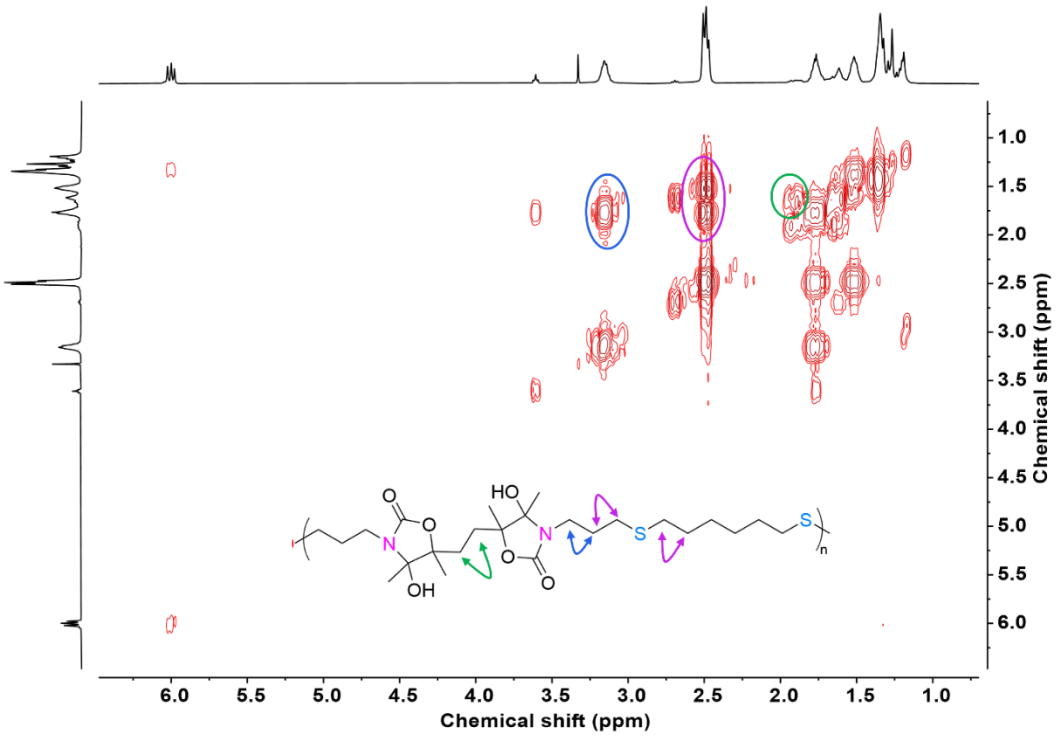

Figure S36. COSY NMR spectrum of purified P2b (400 MHz, DMSO-d_6).

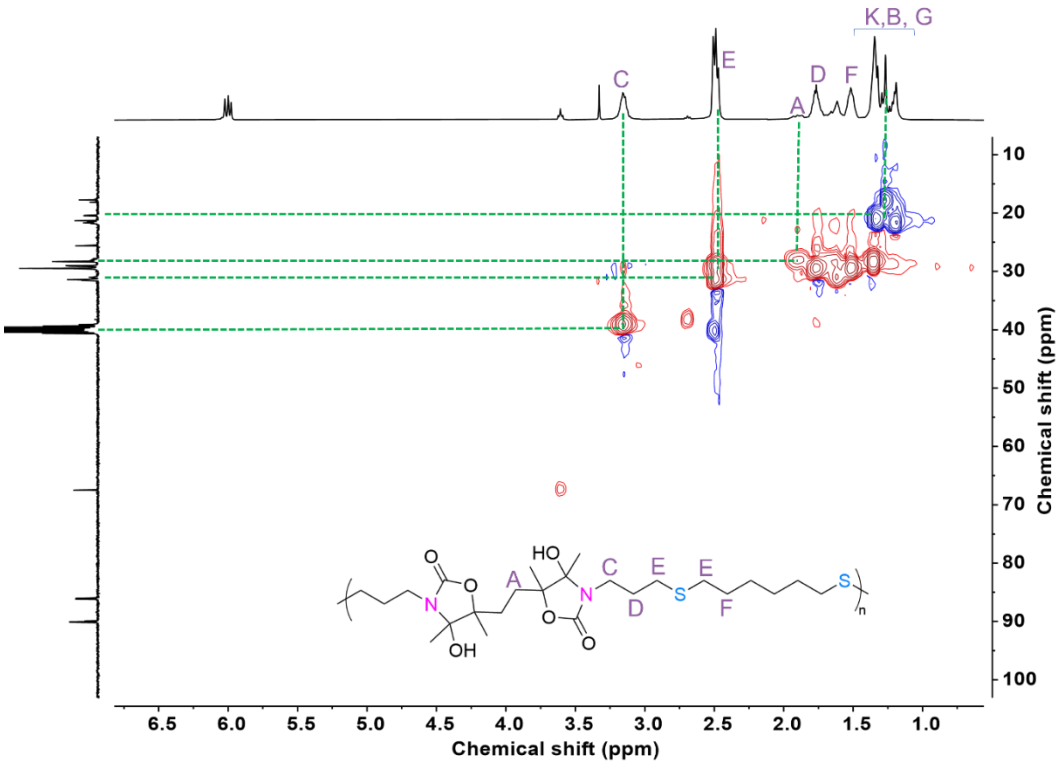

Figure S37. ^{1}H-^{13}C HSQC NMR spectrum of purified P2b (400 MHz, DMSO-d_6).

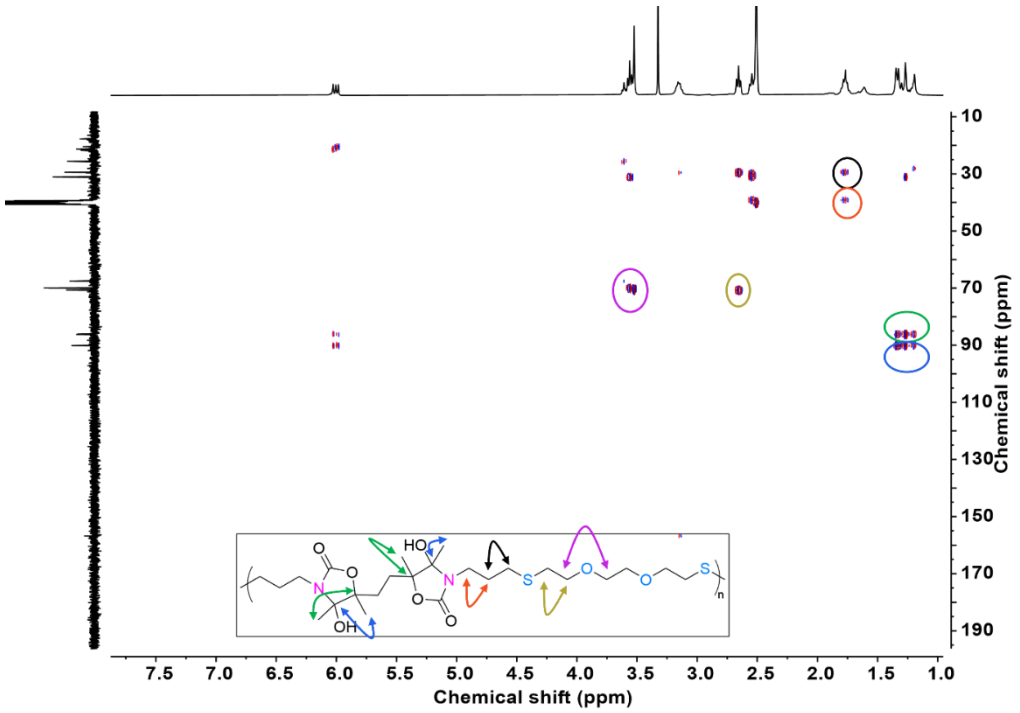

Figure S38. HMBC NMR spectrum of purified P2b (400 MHz, DMSO-d_6).

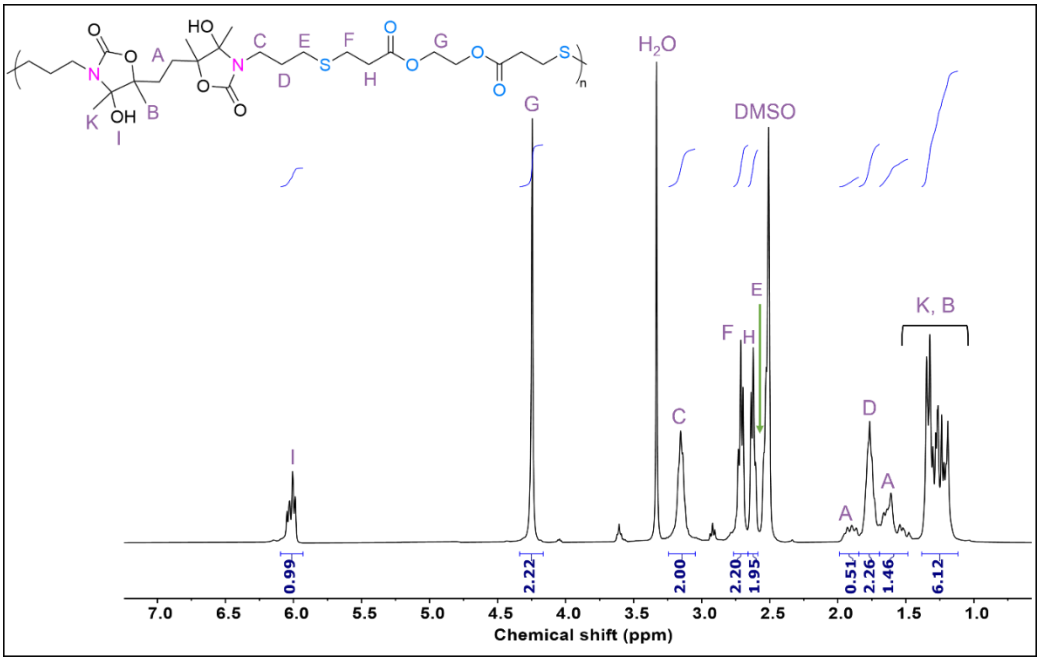

Figure S39. ^{1}H-NMR spectrum of purified P2c (400 MHz, DMSO-d_6).

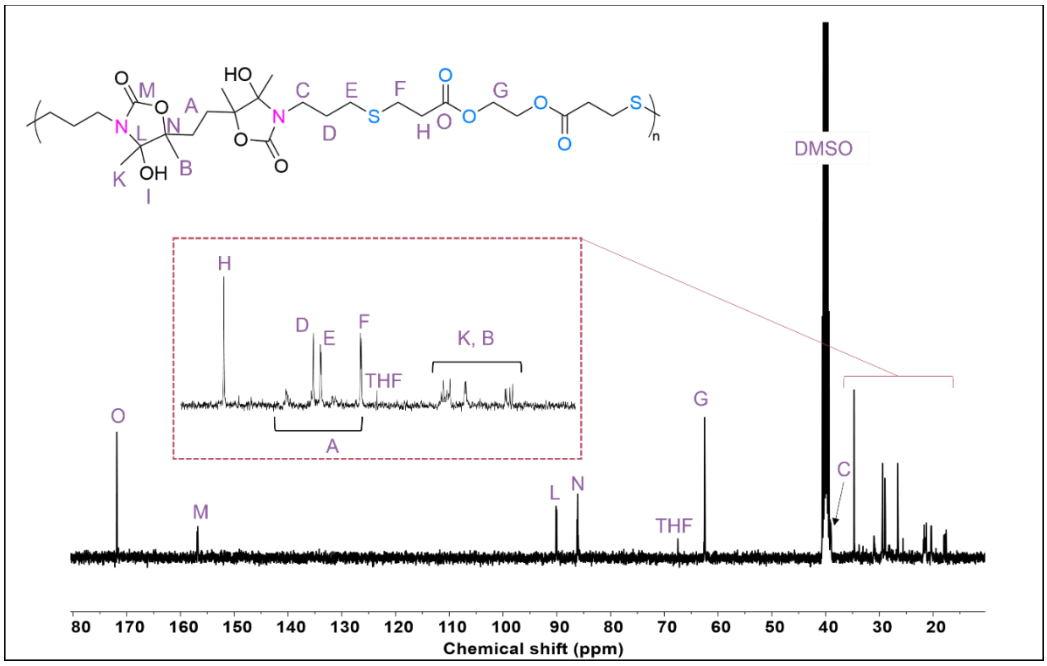

Figure S40. ^{13}C-NMR spectrum of purified P2c (100 MHz, DMSO-d_6).

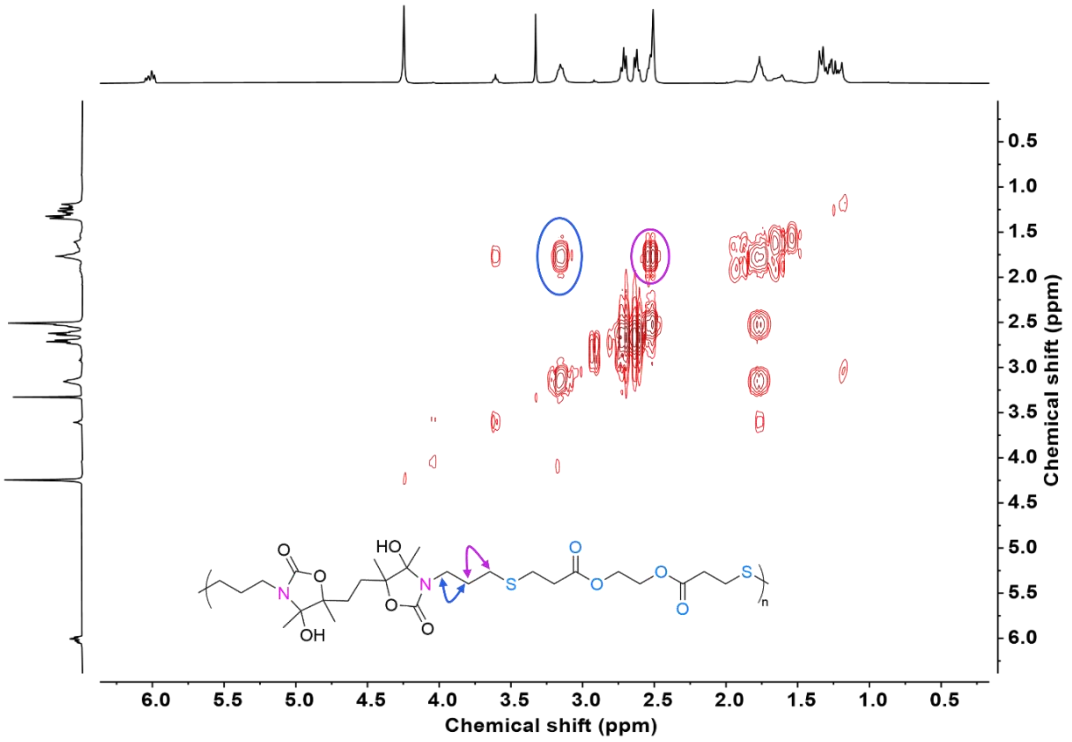

Figure S41. COSY NMR spectrum of purified P2c (400 MHz, DMSO-d_6).

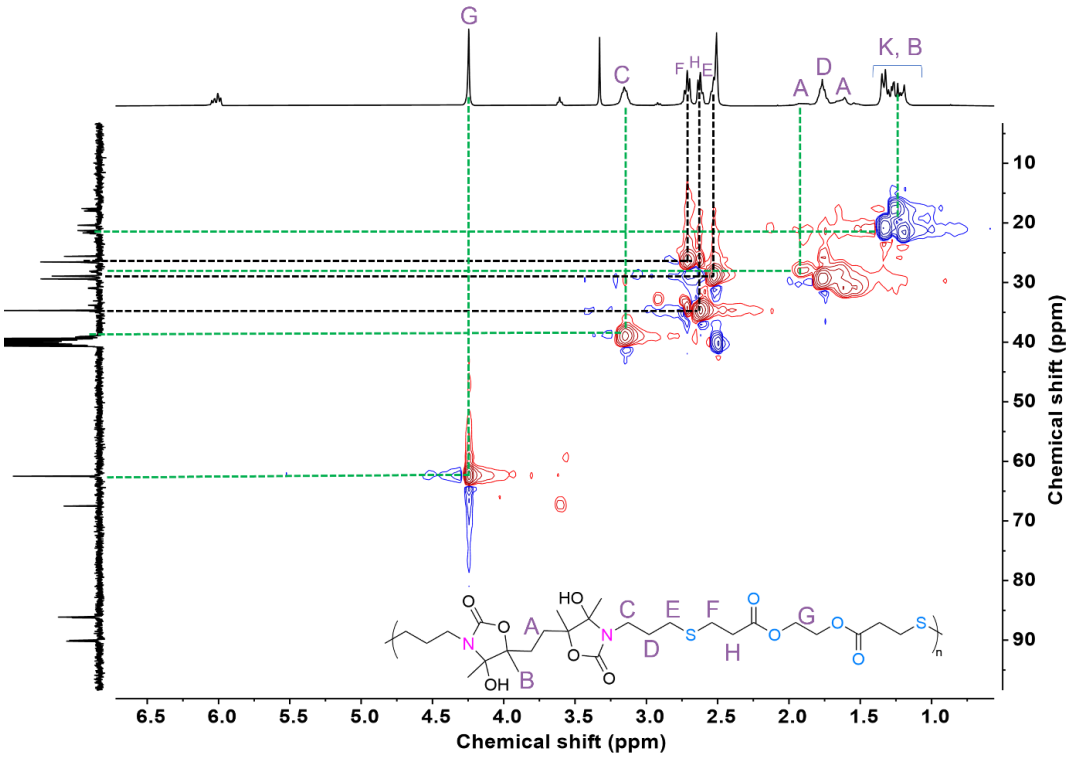

Figure S42. ^{1}H-^{13}C HSQC NMR spectrum of purified P2c (400 MHz, DMSO-d_6).

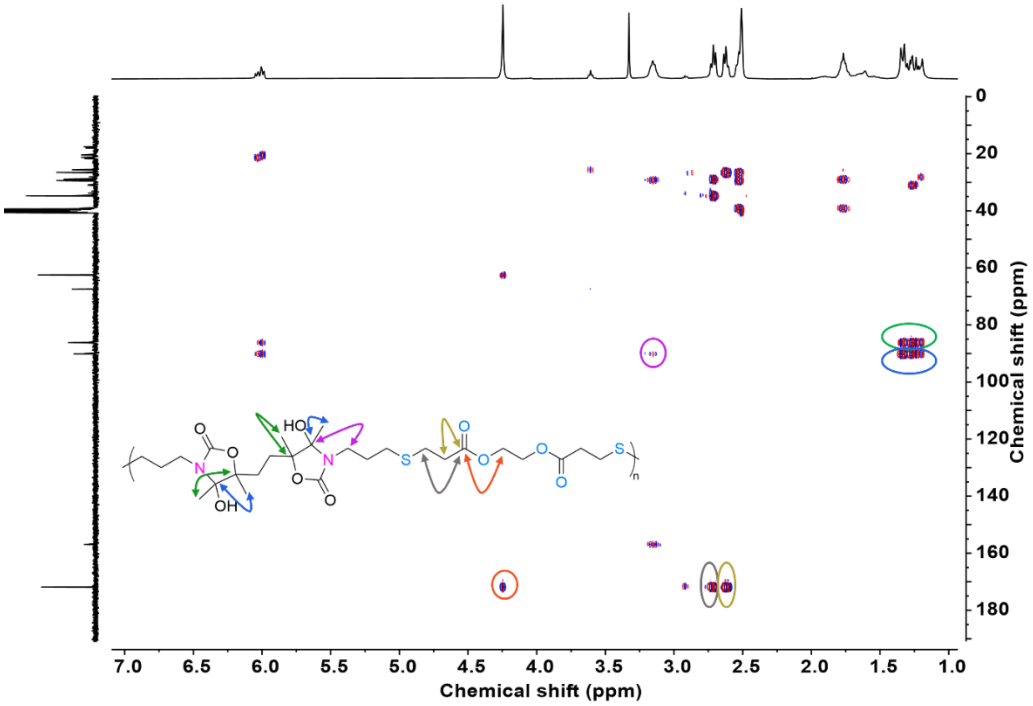

Figure S43. HMBC NMR spectrum of purified P2c (400 MHz, DMSO-d_6).

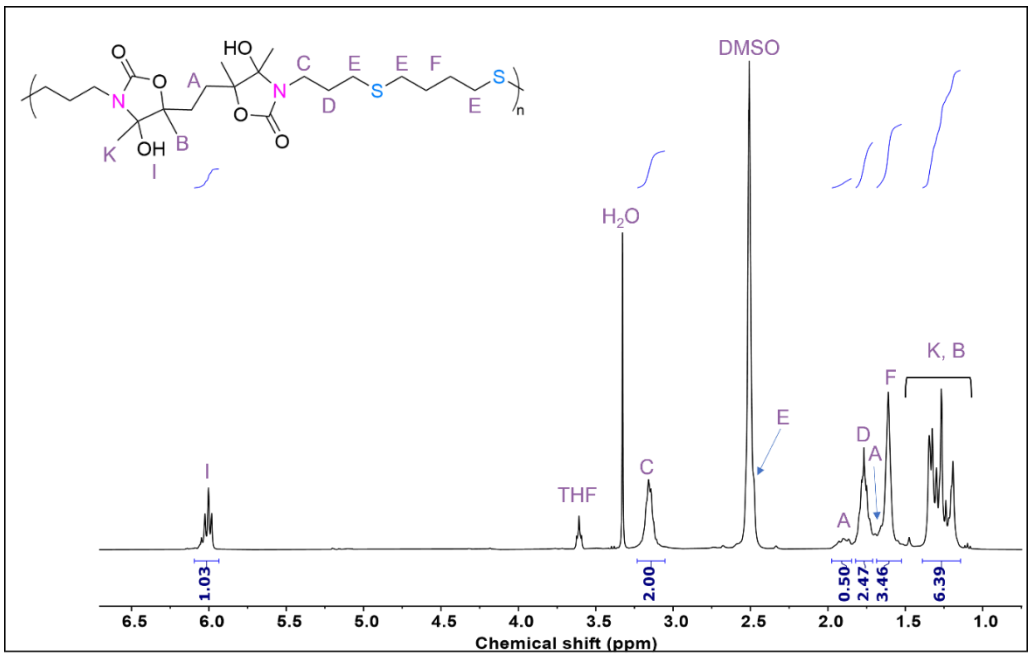

Figure S44. ^{1}H-NMR spectrum of purified **P2d** (400 MHz, DMSO-d_6).

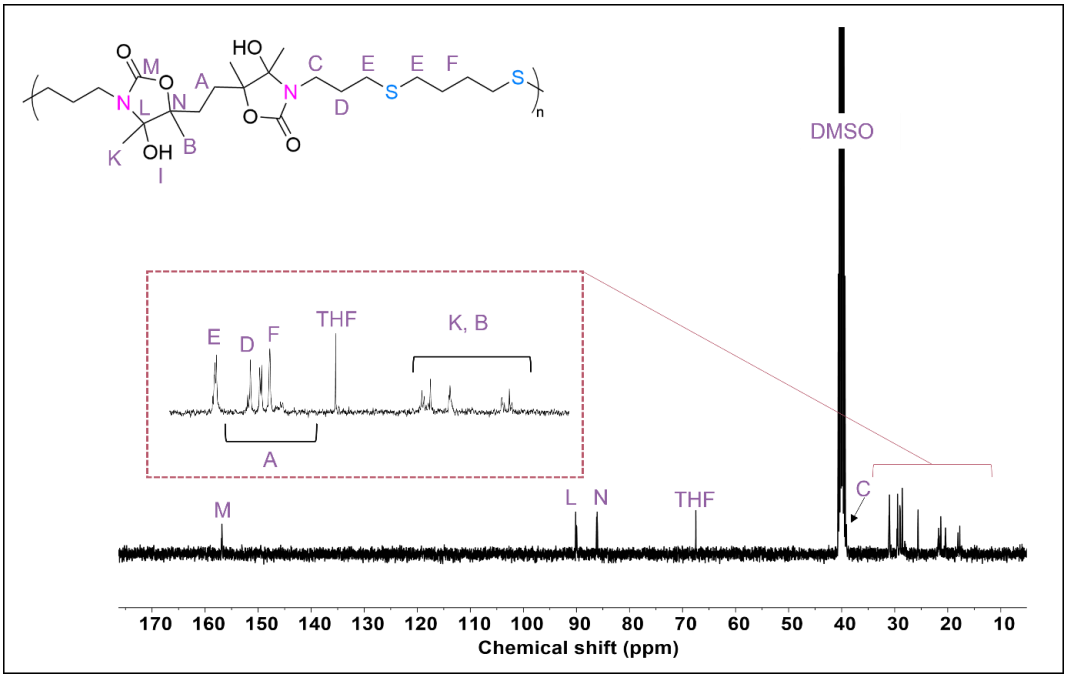

Figure S45. ^{13}C-NMR spectrum of purified P2d (100 MHz, DMSO-d_6).

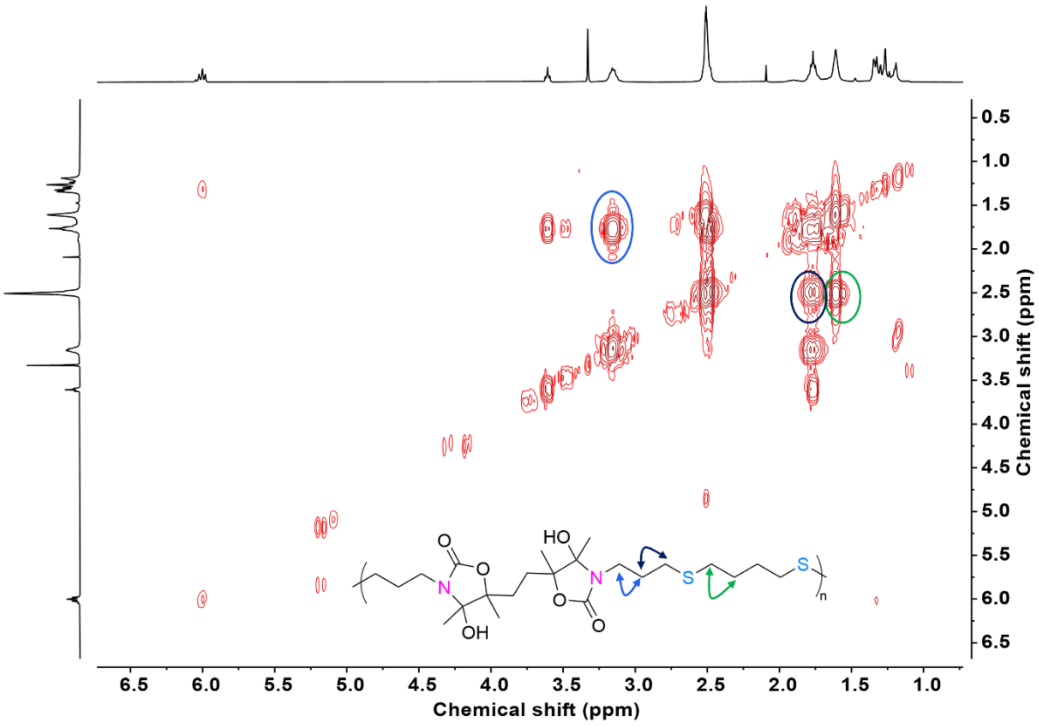

Figure S46. COSYNMR spectrum of purified P2d (400 MHz, DMSO-d_6).

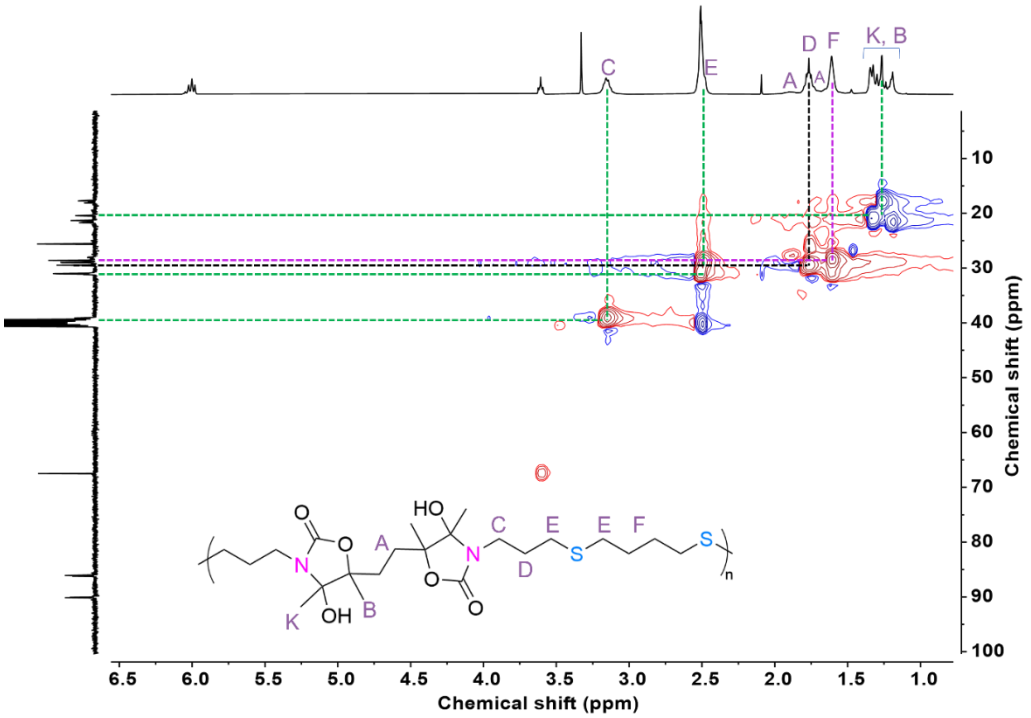

Figure S47. ^{1}H-^{13}C HSQC NMR spectrum of purified P2d (400 MHz, DMSO-d_6).

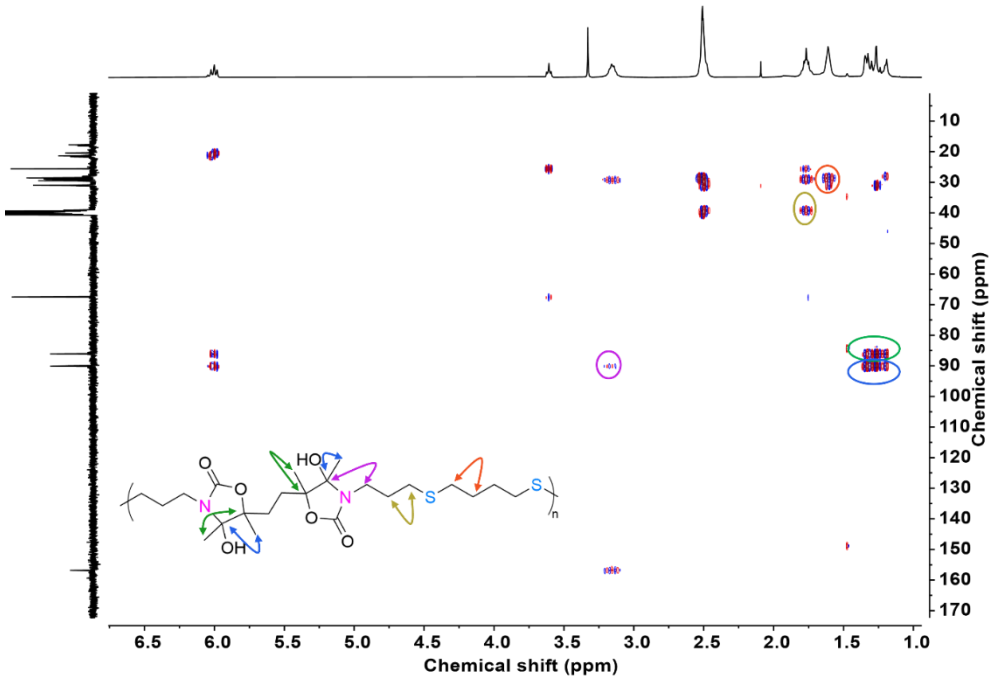

Figure S48. HMBC NMR spectrum of purified P2d (400 MHz, DMSO-d_6).

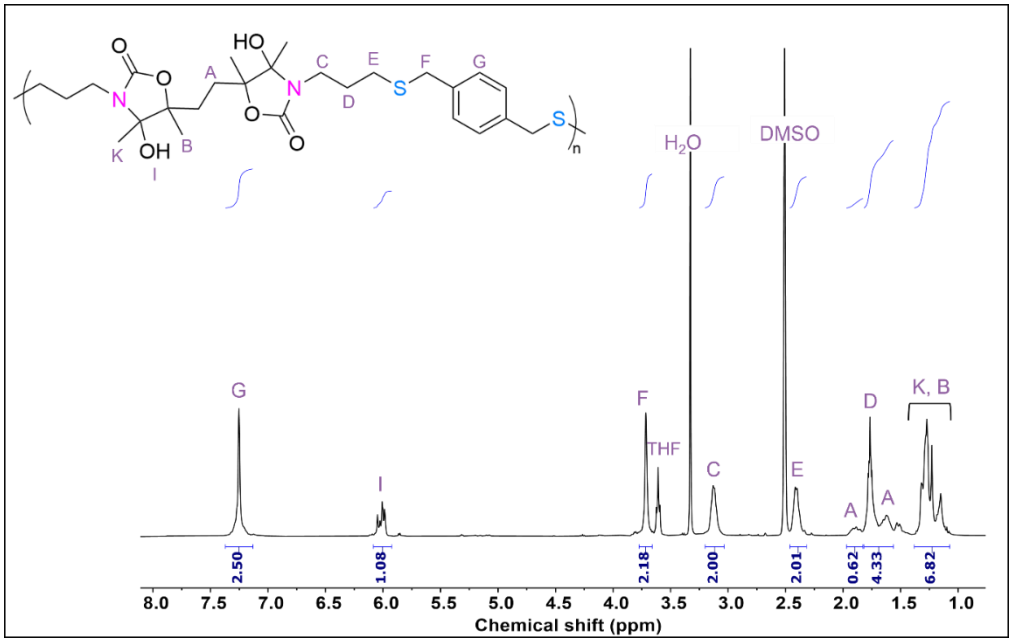

Figure S49. [1]H-NMR spectrum of purified P2e (400 MHz, DMSO-d_6).

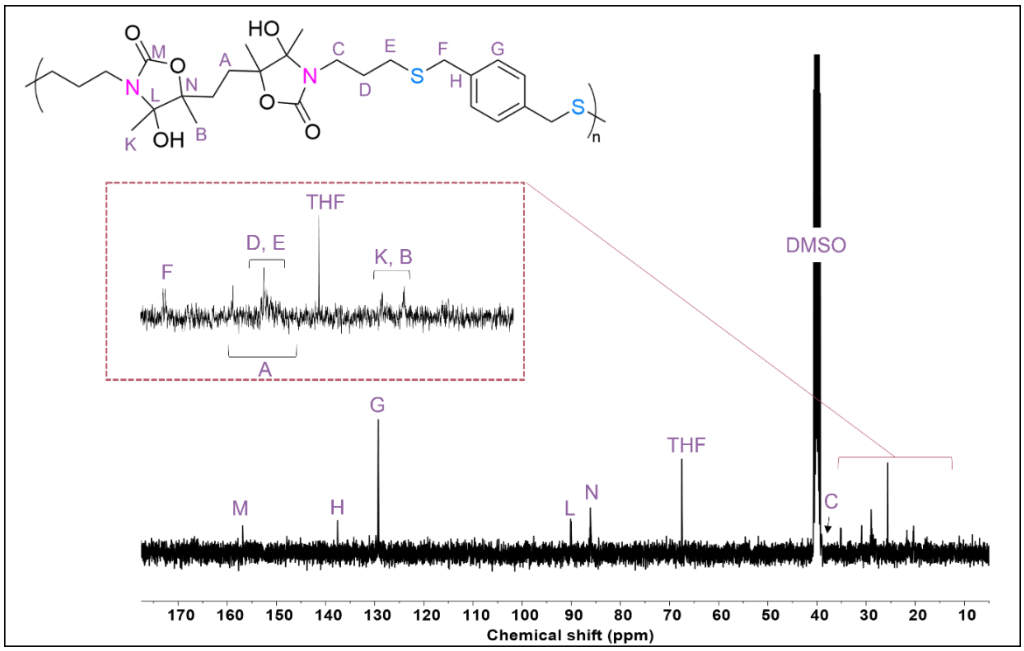

Figure S50. [13]C-NMR spectrum of purified P2e (100 MHz, DMSO-d_6).

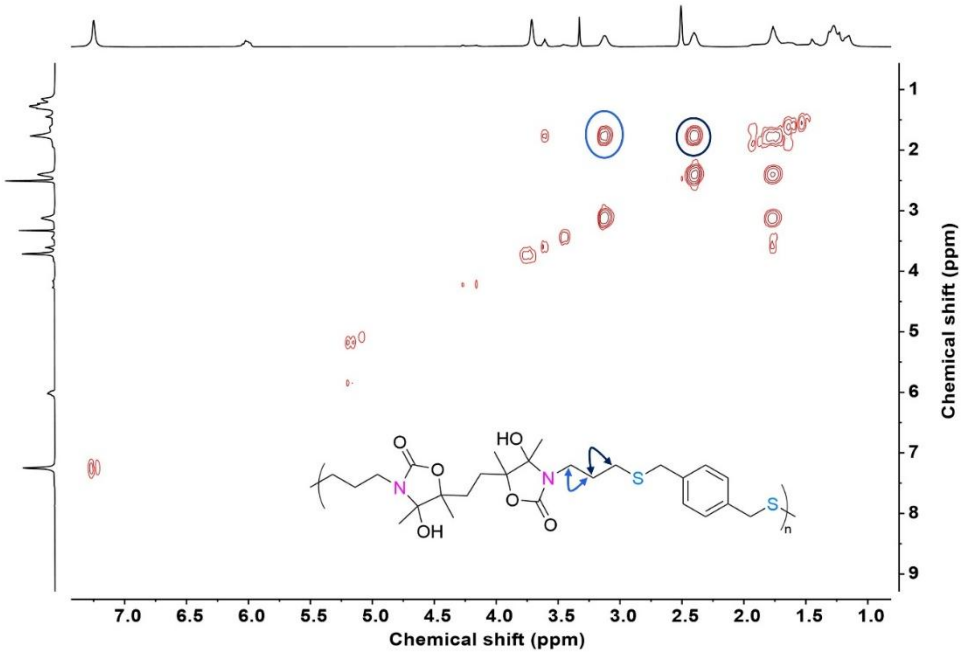

Figure S51. COSY NMR spectrum of purified P2e (400 MHz, DMSO-d_6).

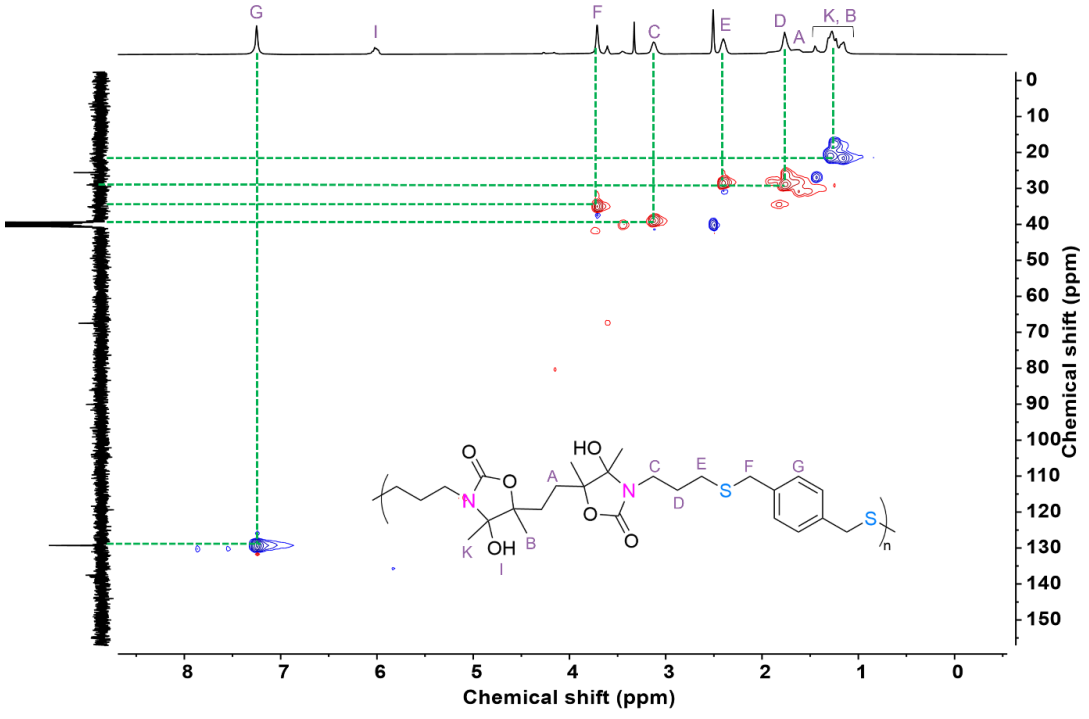

Figure S52. ^{1}H-^{13}C HSQC NMR spectrum of purified P2e (400 MHz, DMSO-d_6).

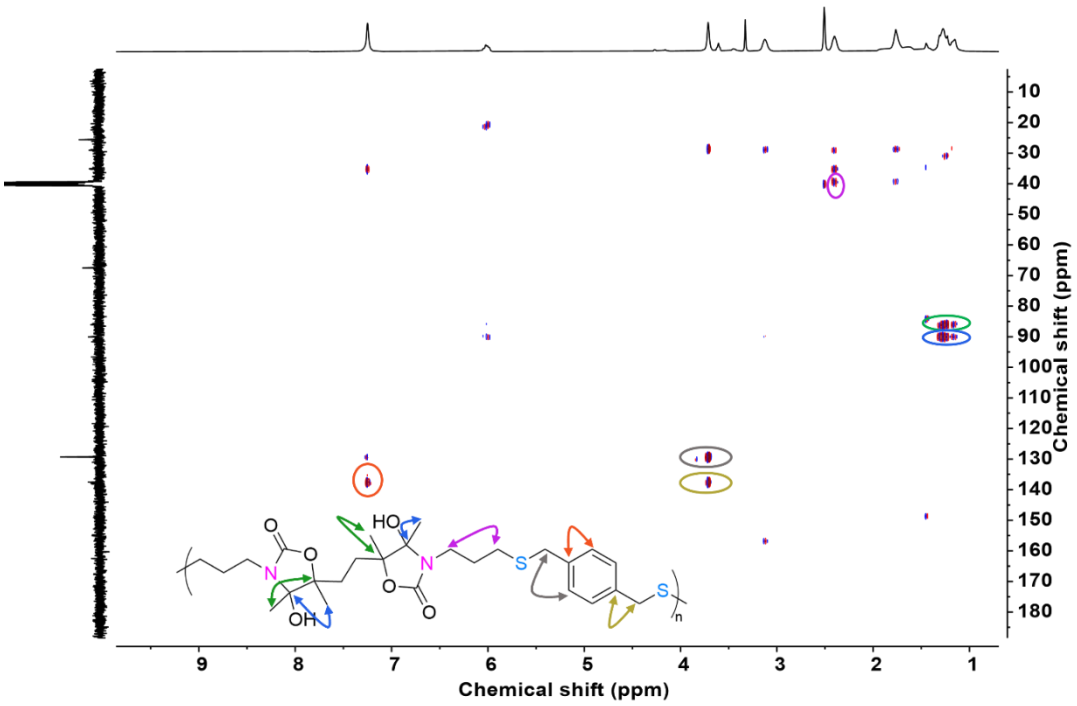

Figure S53. HMBC NMR spectrum of purified P2e (400 MHz, DMSO-d_6).

6.12 Solubility of all synthesized polymers

The polymer was cut into small pieces and 50 mg was immersed in DMF, DMSO, THF, and water for 48 h to determine solubility. Results are given in Table S2, categorizing them qualitatively as either soluble or not soluble.

Table S2. Solubility table of all synthesized polymers

		DMF	DMSO	THF	Water
Hydrated polymers	P2a	✓	✓	✓	✗
	P2b	✓	✓	✓	✗
	P2c	✓	✓	✓	✗
	P2d	✓	✓	✓	✗
	P2e	✓	✓	✓	✗
Dehydrated polymers	P2a-dehydrated	✓	✓	✓	✗
	P2b-dehydrated	✓	✓	✓	✗
	P2c-dehydrated	✓	✓	✓	✗
	P2d-dehydrated	✓	✓	✓	✗
	P2e-dehydrated	✓	✓	✓	✗
Post-modified polymers	P2b-Sulfoxide	✓	✓	✗	✗
	P2b-Sulfone	✓	✓	✗	✗
	P2b-Sulfonium	✗	✓	✗	✓

6.13 TGA characterization of pure polymers

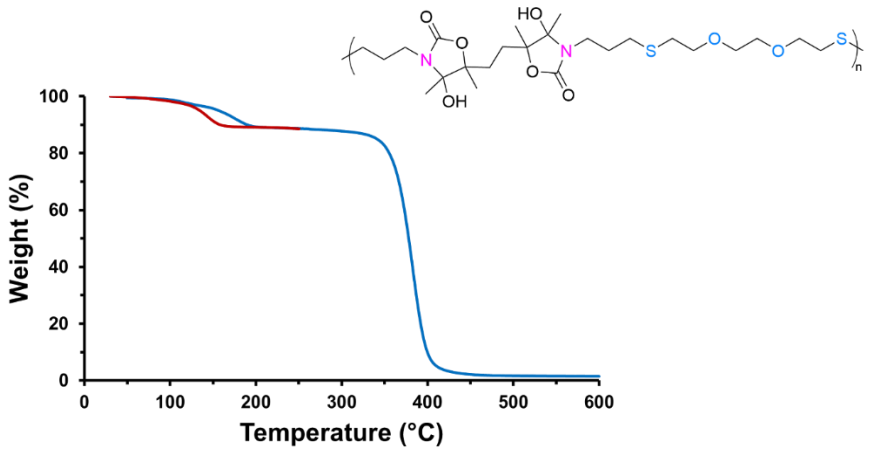

Figure S54. TGA thermogram of P2a at a heating rate of 20 K/min (blue) and 2 K/min (red)

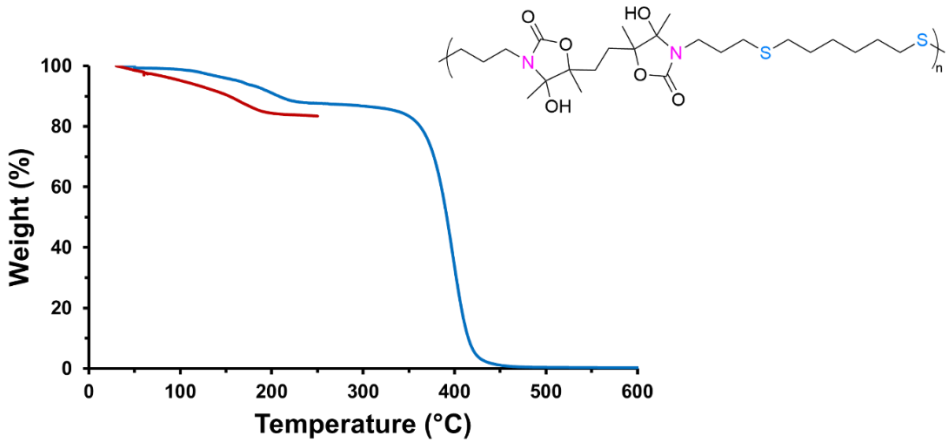

Figure S55. TGA thermogram of P2b at a heating rate of 20 K/min (blue) and 2 K/min (red)

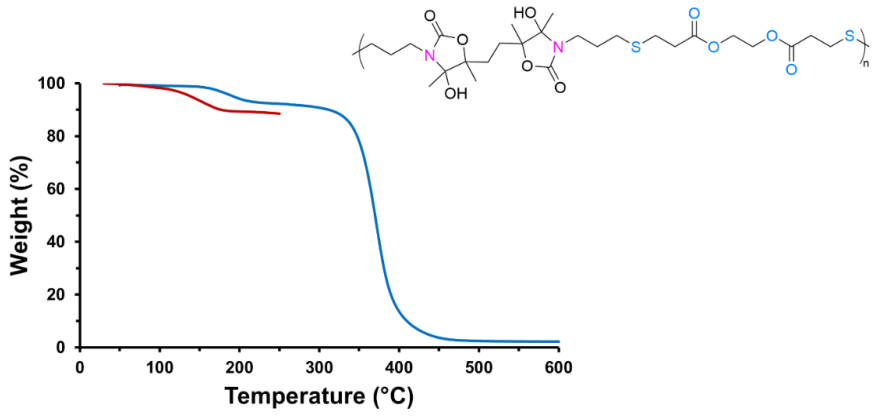

Figure S56. TGA thermogram of P2c at a heating rate of 20 K/min (blue) and 2 K/min (red)

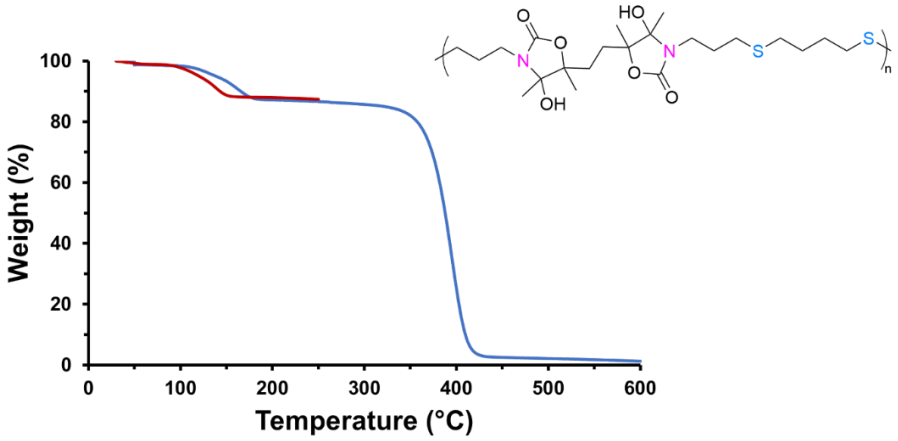

Figure S57. TGA thermogram of P2d at a heating rate of 20 K/min (blue) and 2 K/min (red)

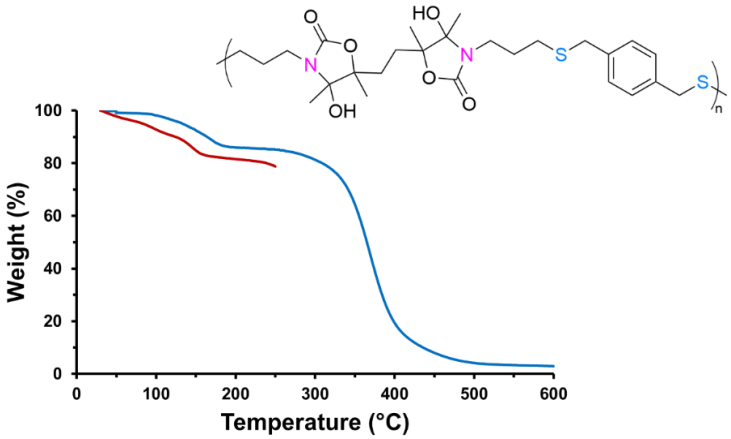

Figure S58. TGA thermogram of P2e at a heating rate of 20 K/min (blue) and 2 K/min (red)

6.14 Slow TGA characterization and derivative curves of pure polymers

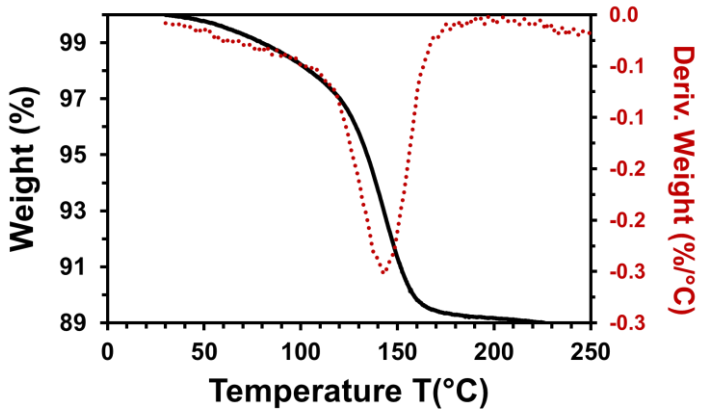

Figure S59. The slow TGA curve of P2a at the heating rate of 2 K/min and its derivative curve to determine the T_{dehy}.

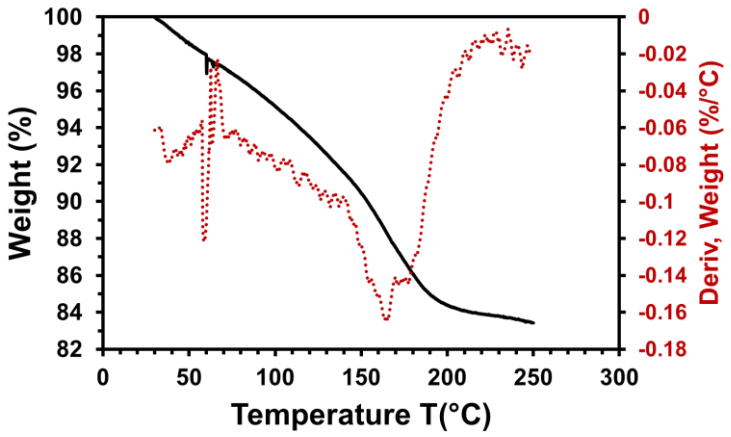

Figure S60. The slow TGA curve of **P2b** at the heating rate of 2 K/min and its derivative curve to determine the T_{dehy}.

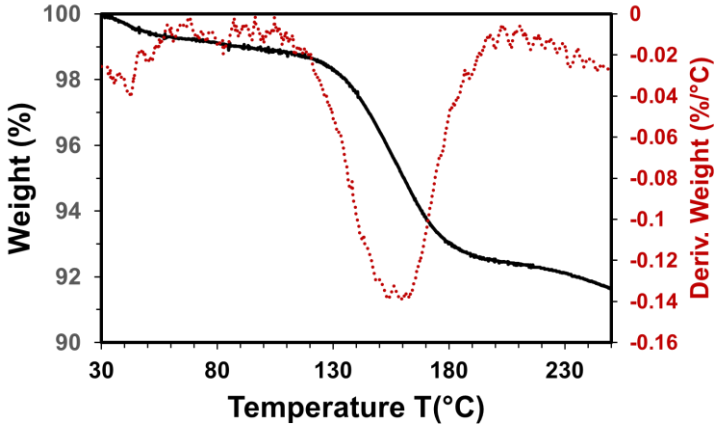

Figure S61. The slow TGA curve of **P2c** at the heating rate of 2 K/min and its derivative curve to determine the T_{dehy}.

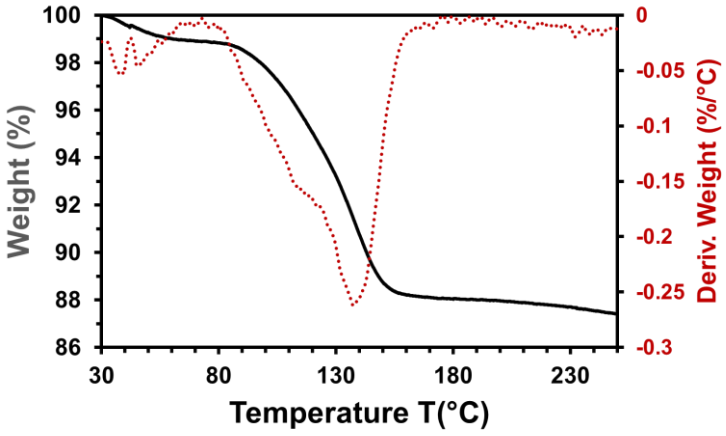

Figure S62. The slow TGA curve of P2d at the heating rate of 2 K/min and its derivative curve to determine the T_{dehy}

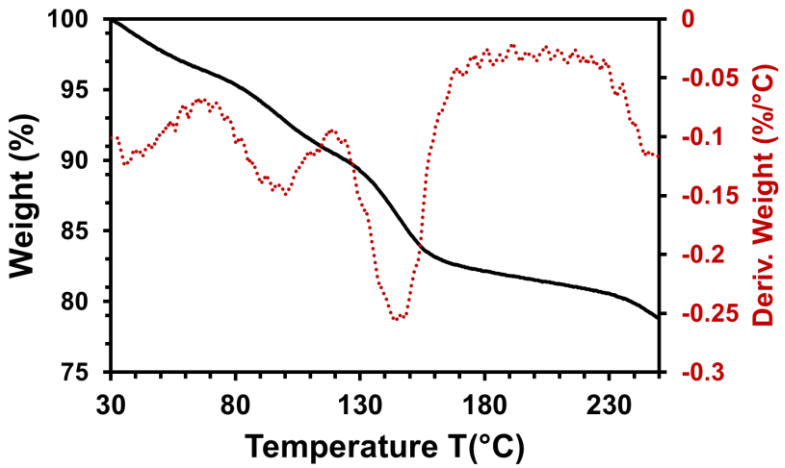

Figure S63. The slow TGA curve of P2e at the heating rate of 2 K/min and its derivative curve to determine the T_{dehy}

6.15 NMR spectra of dehydrated polymers

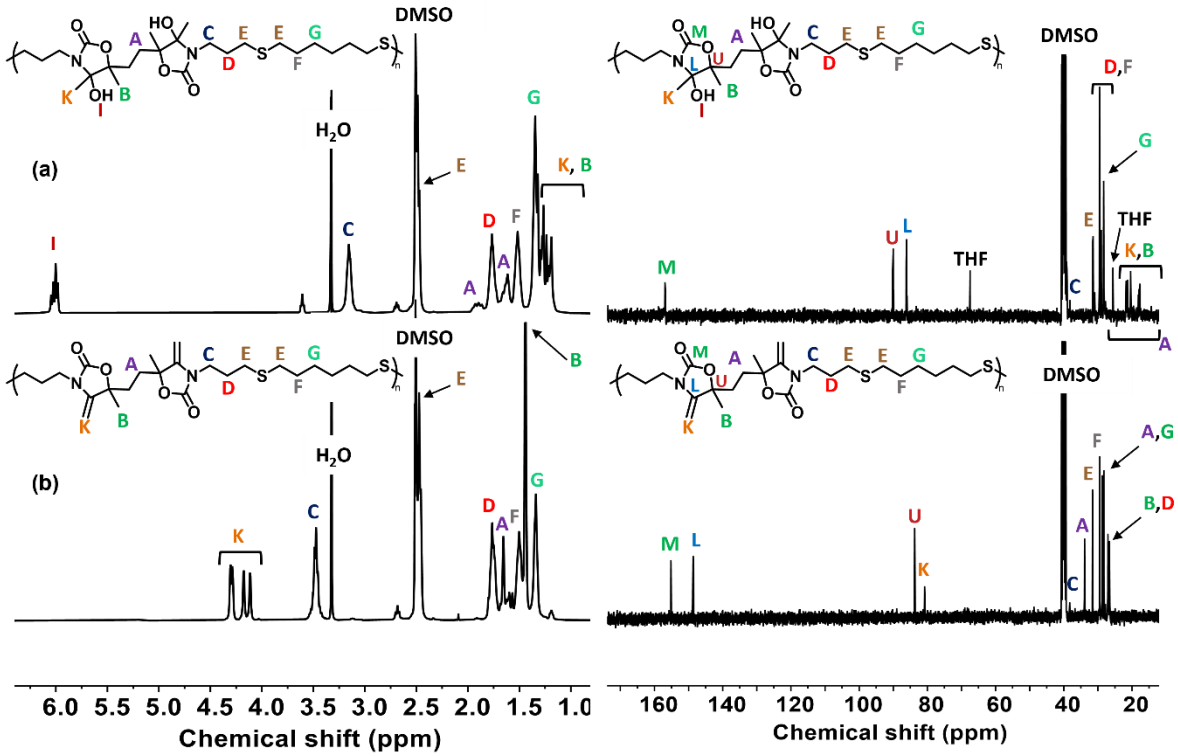

Figure S64. ^{1}H-NMR spectra (left, 400 MHz, DMSO-d_6) and ^{13}C-NMR spectra (right, 100 MHz, DMSO-d_6) of (a) **P2b** and (b) **P2b-dehydrated**.

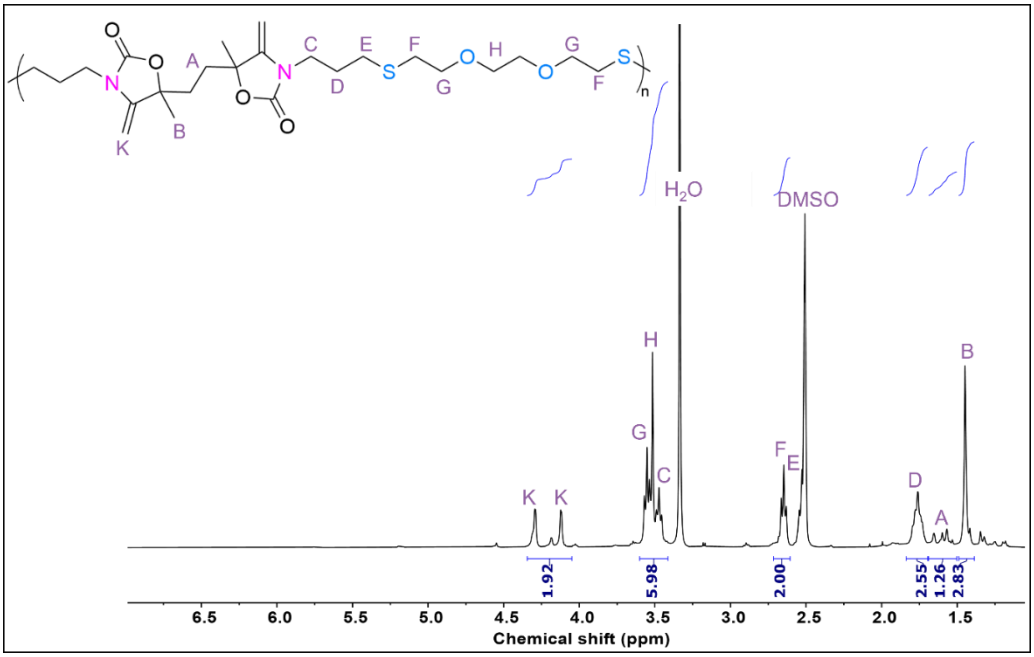

Figure S65. ^{1}H-NMR spectrum of P2a-dehydrated (400 MHz, DMSO-d_6).

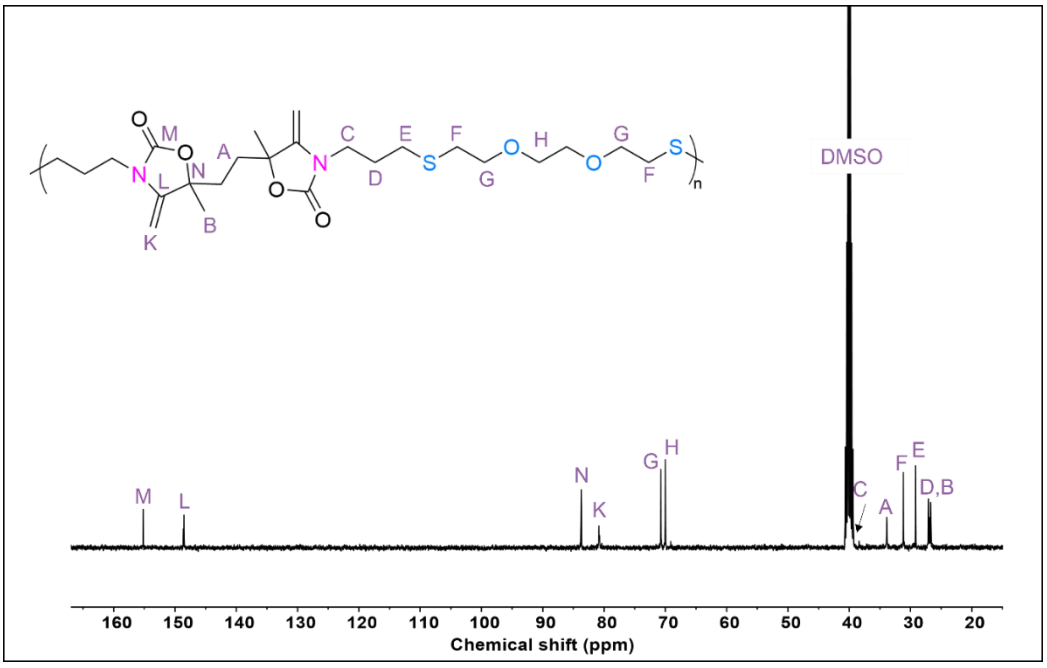

Figure S66. ^{13}C-NMR spectrum of P2a-dehydrated (100 MHz, DMSO-d_6).

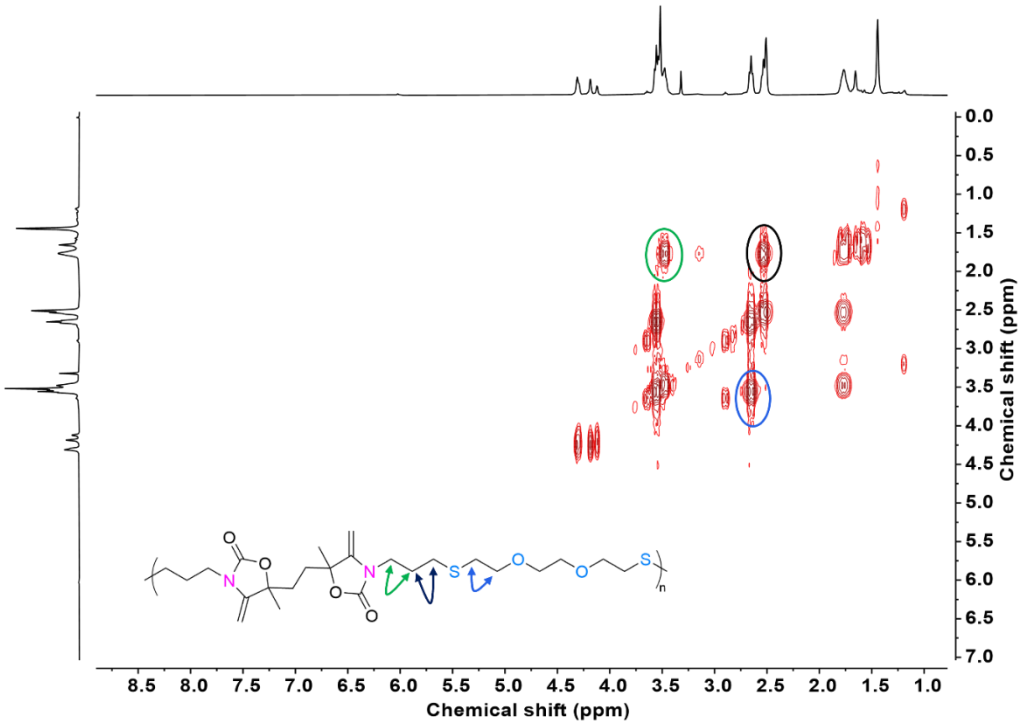

Figure S67. COSY NMR spectrum of P2a-dehydrated (400 MHz, DMSO-d_6).

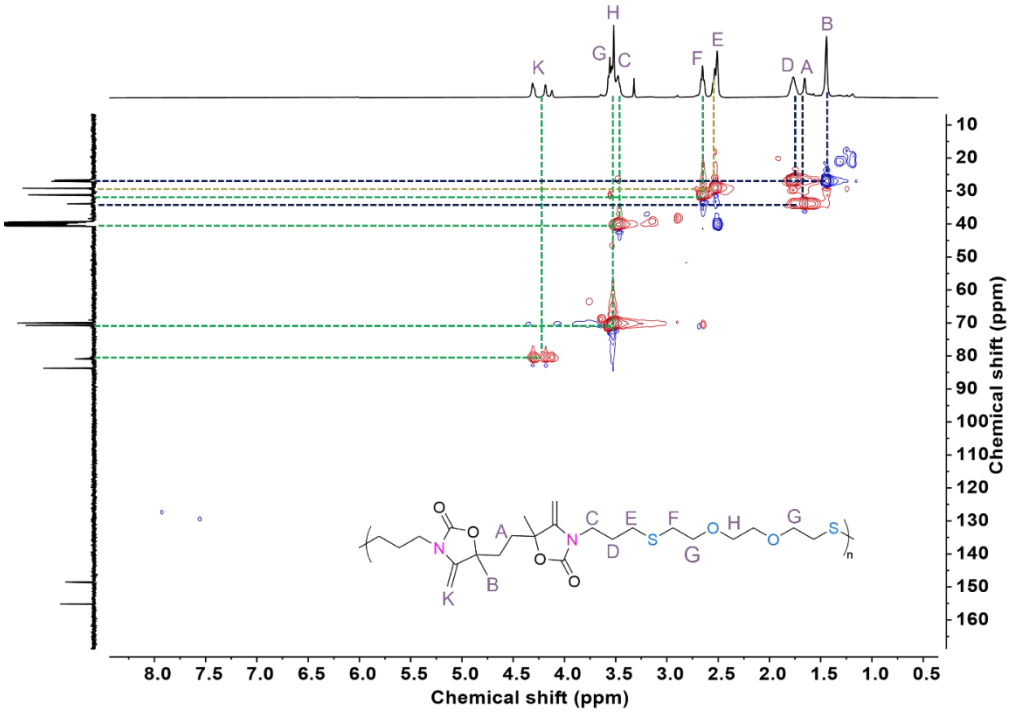

Figure S68. ^{1}H-^{13}C HSQC NMR spectrum of P2a-dehydrated (400 MHz, DMSO-d_6).

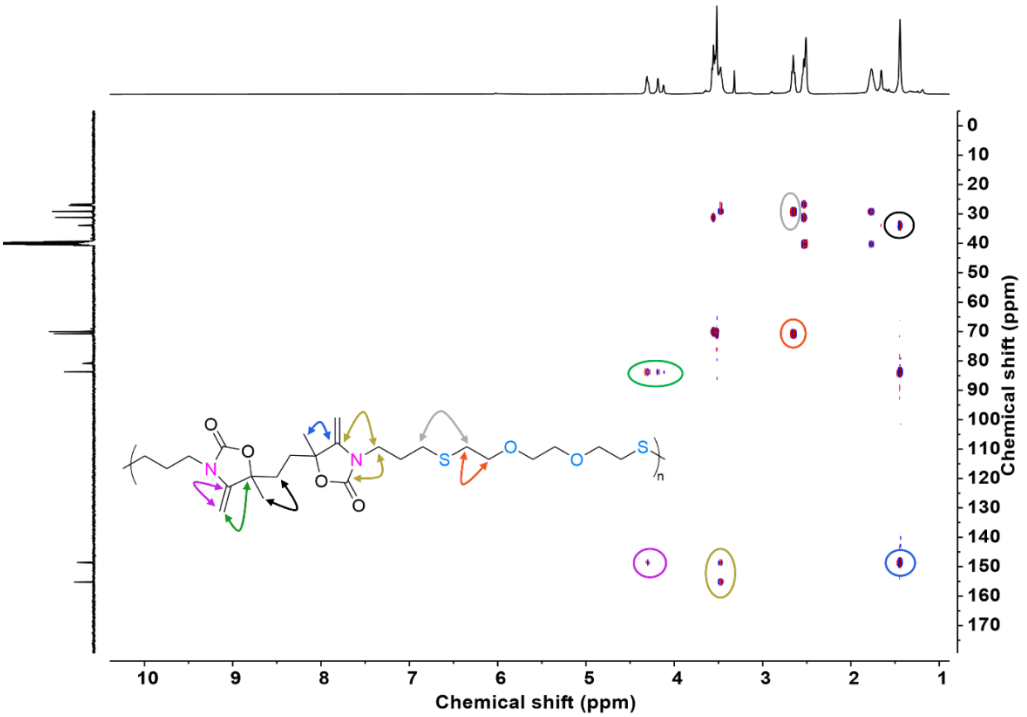

Figure S69. HMBC NMR spectrum of P2a-dehydrated (400 MHz, DMSO-d_6).

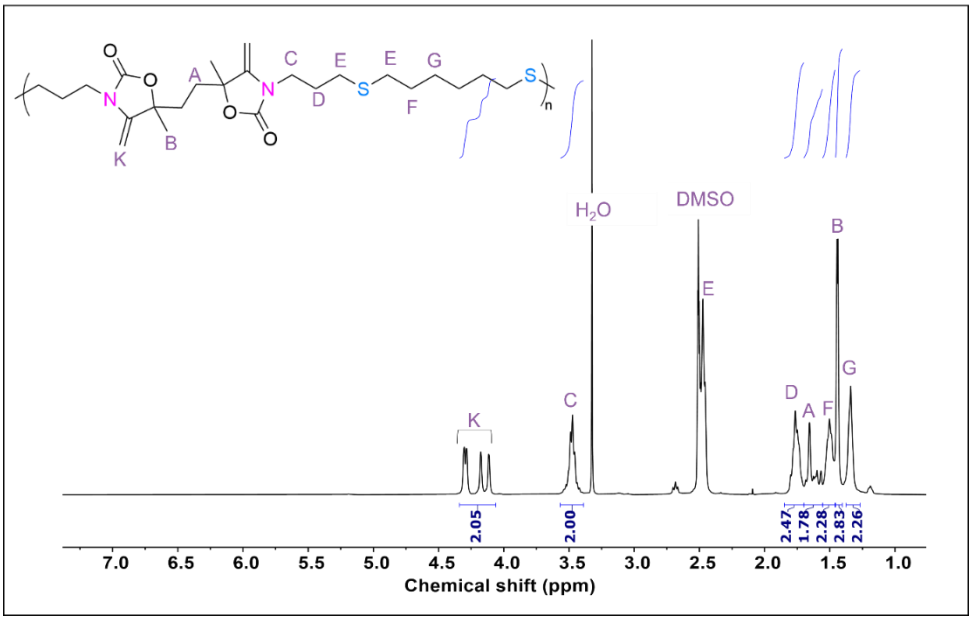

Figure S70. ^{1}H-NMR spectrum of P2b-dehydrated (400 MHz, DMSO-d_6).

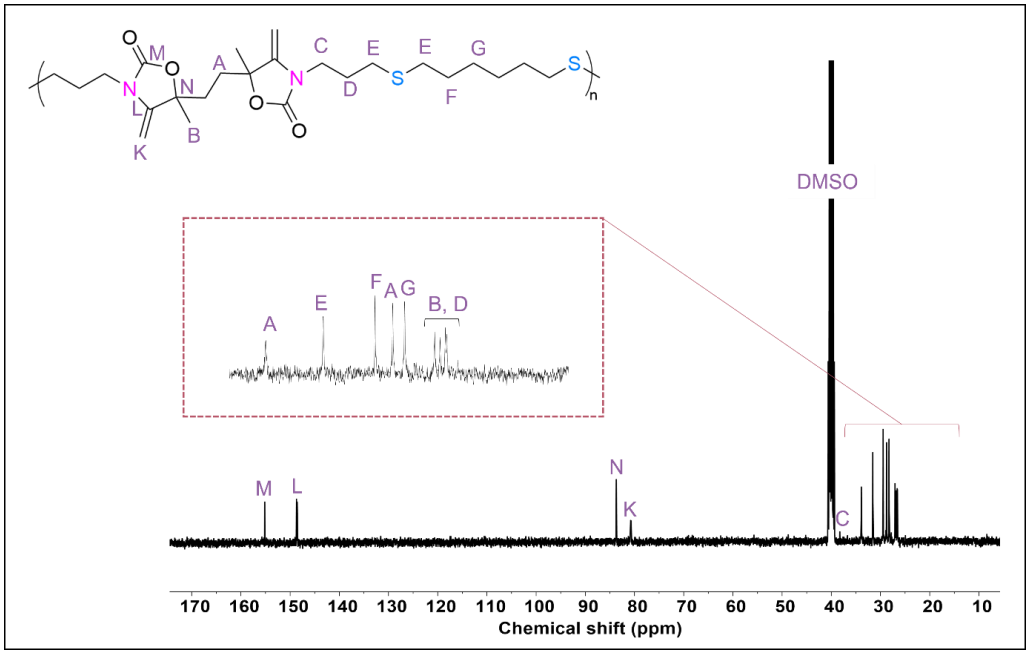

Figure S71. ^{13}C-NMR spectrum of P2b-dehydrated (100 MHz, DMSO-d_6).

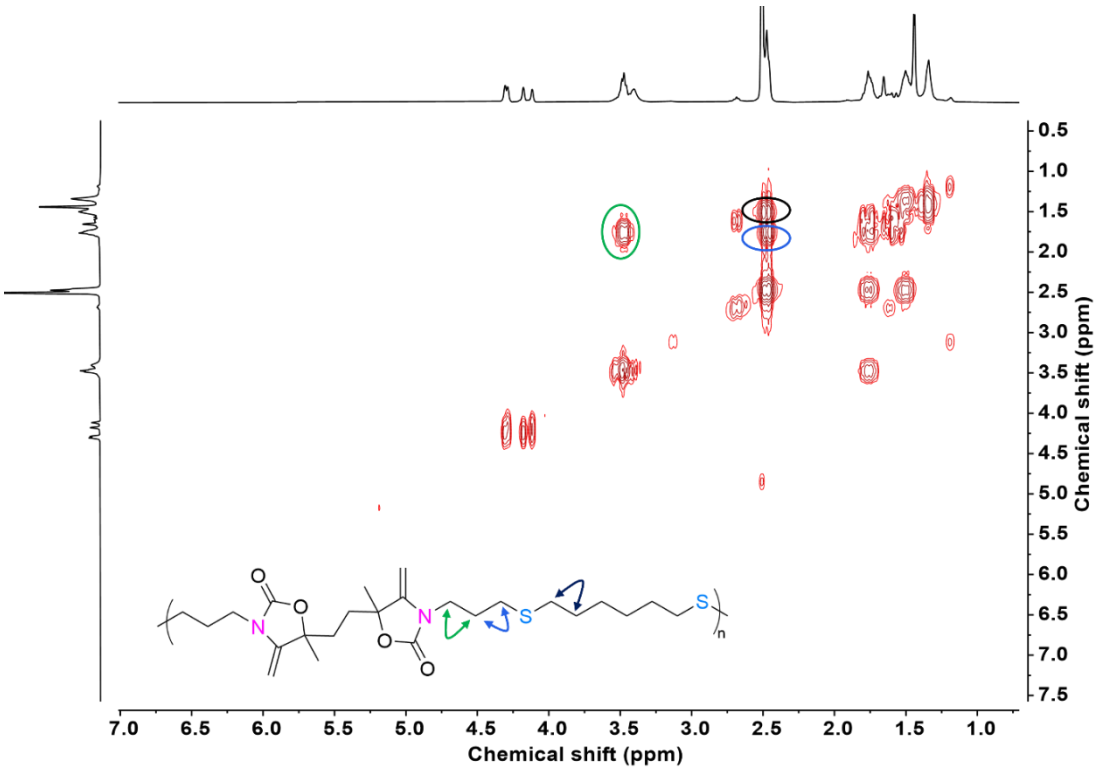

Figure S72. COSY NMR spectrum of P2b-dehydrated (400 MHz, DMSO-d_6).

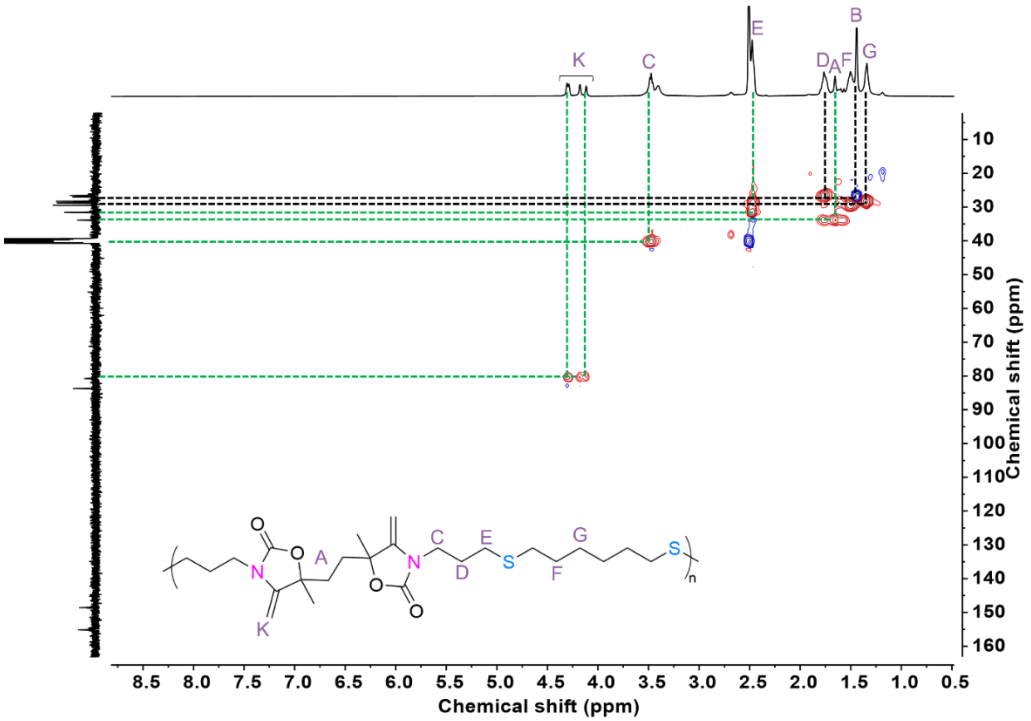

Figure S73. ^{1}H-^{13}C HSQC NMR spectrum of P2b-dehydrated (400 MHz, DMSO-d_6).

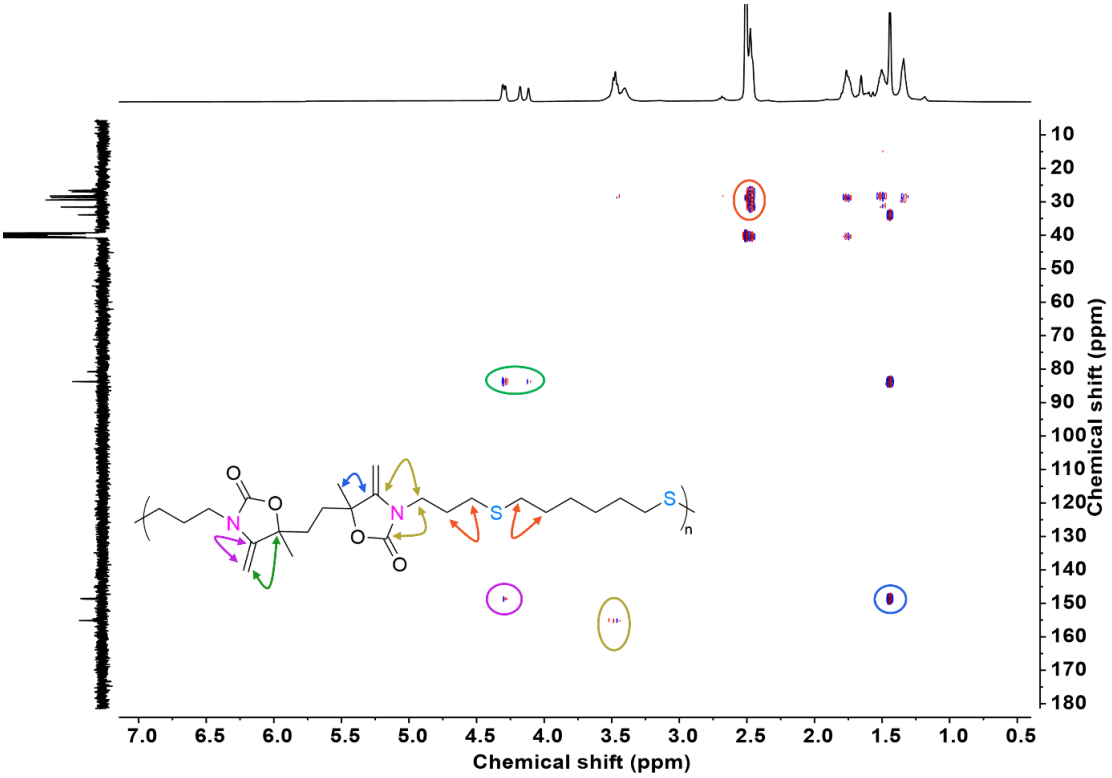

Figure S74. HMBC NMR spectrum of P2b-dehydrated (400 MHz, DMSO-d_6).

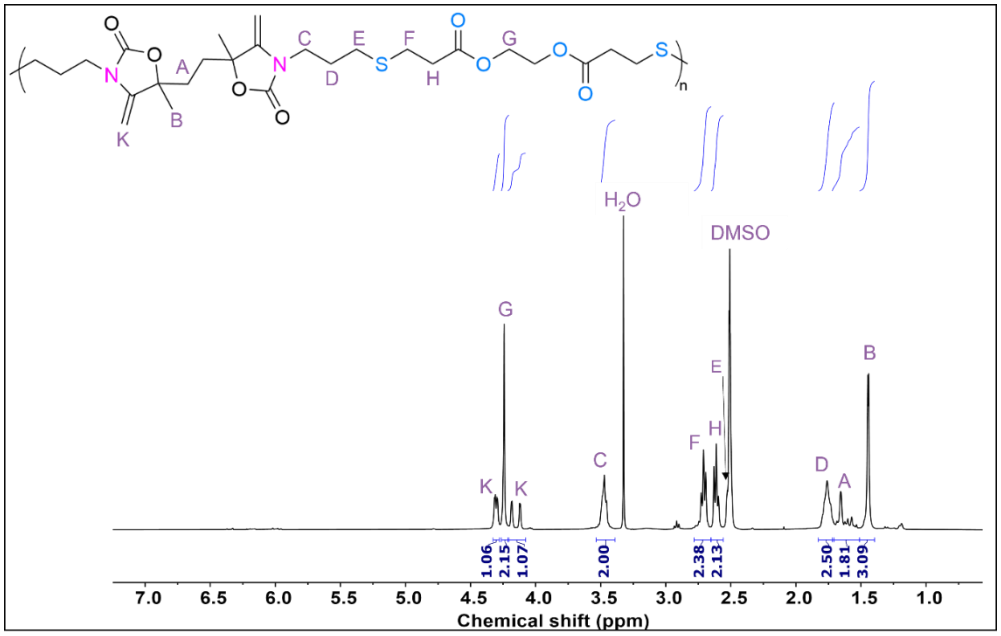

Figure S75. [1]H-NMR spectrum of P2c-dehydrated (400 MHz, DMSO-d_6).

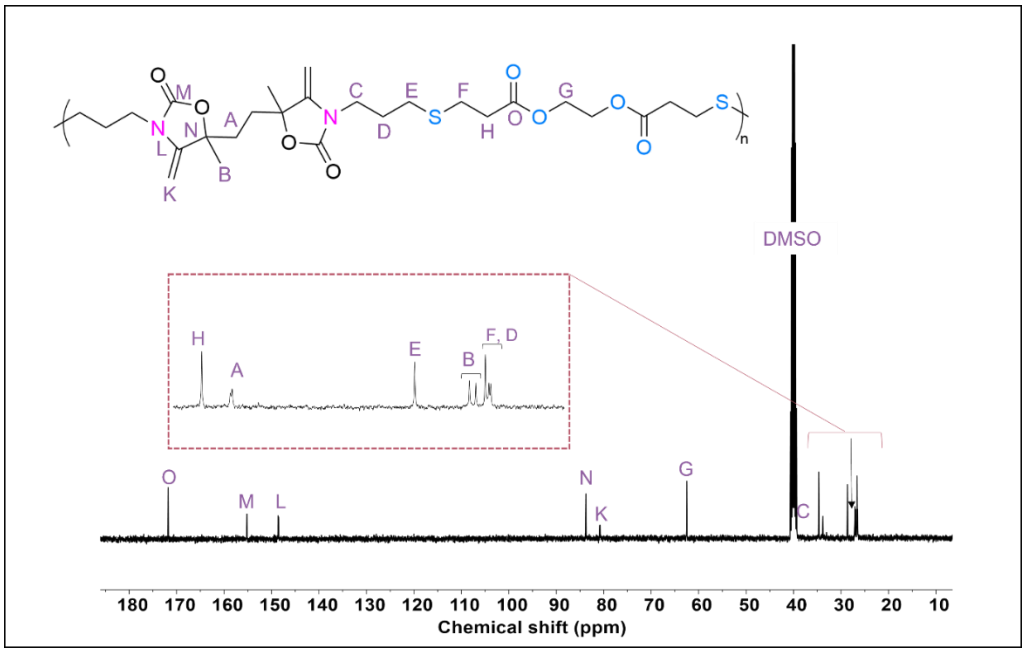

Figure S76. [13]C-NMR spectrum of P2c-dehydrated (100 MHz, DMSO-d_6).

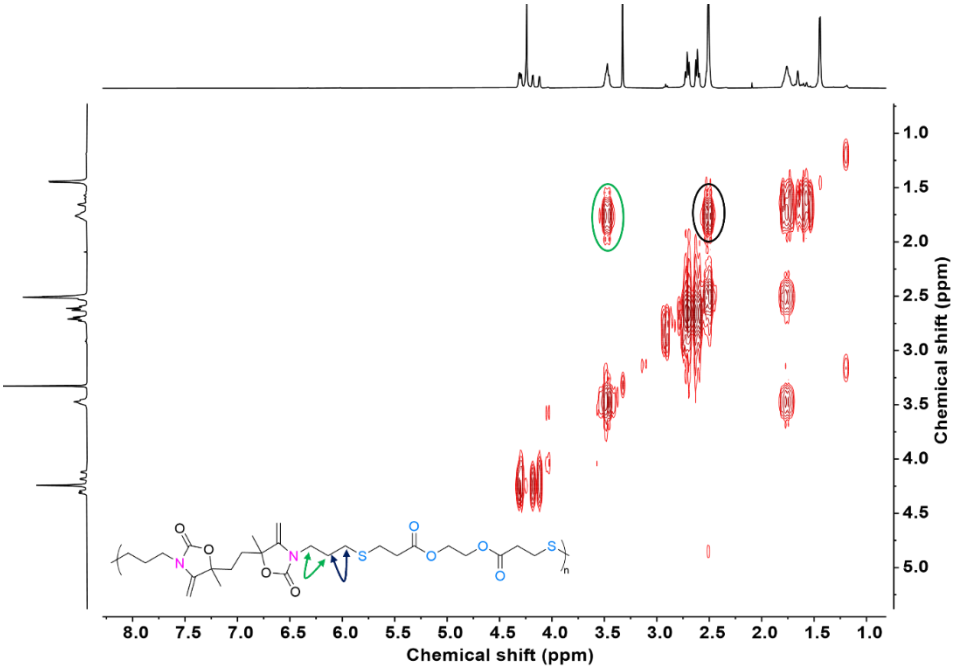

Figure S77. COSY NMR spectrum of P2c-dehydrated (400 MHz, DMSO-d_6).

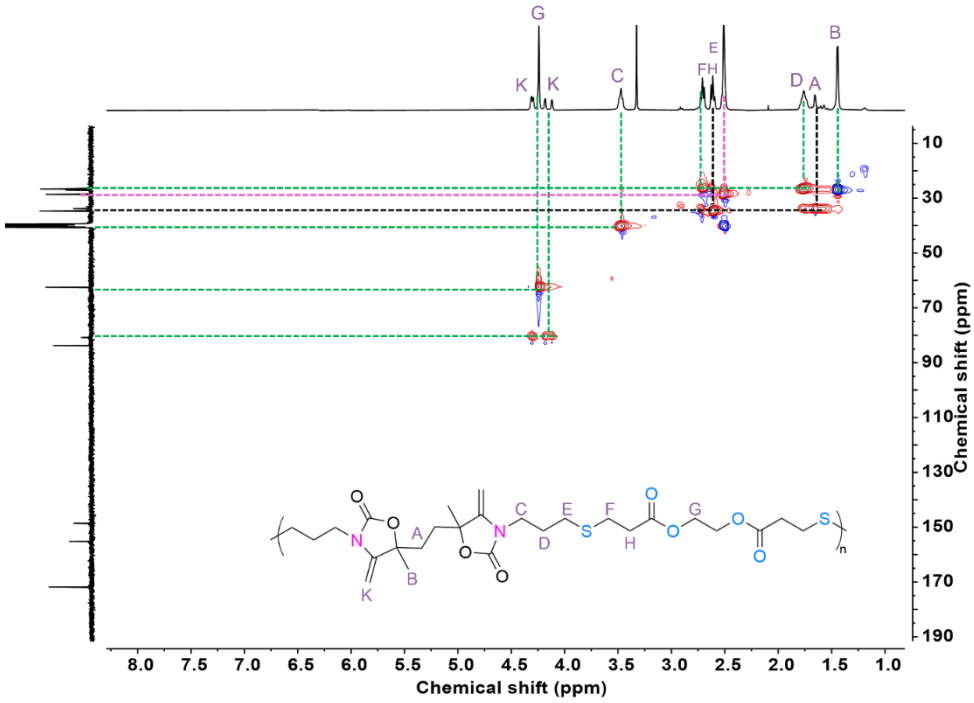

Figure S78. ^{1}H-^{13}C HSQC NMR spectrum of P2c-dehydrated (400 MHz, DMSO-d_6).

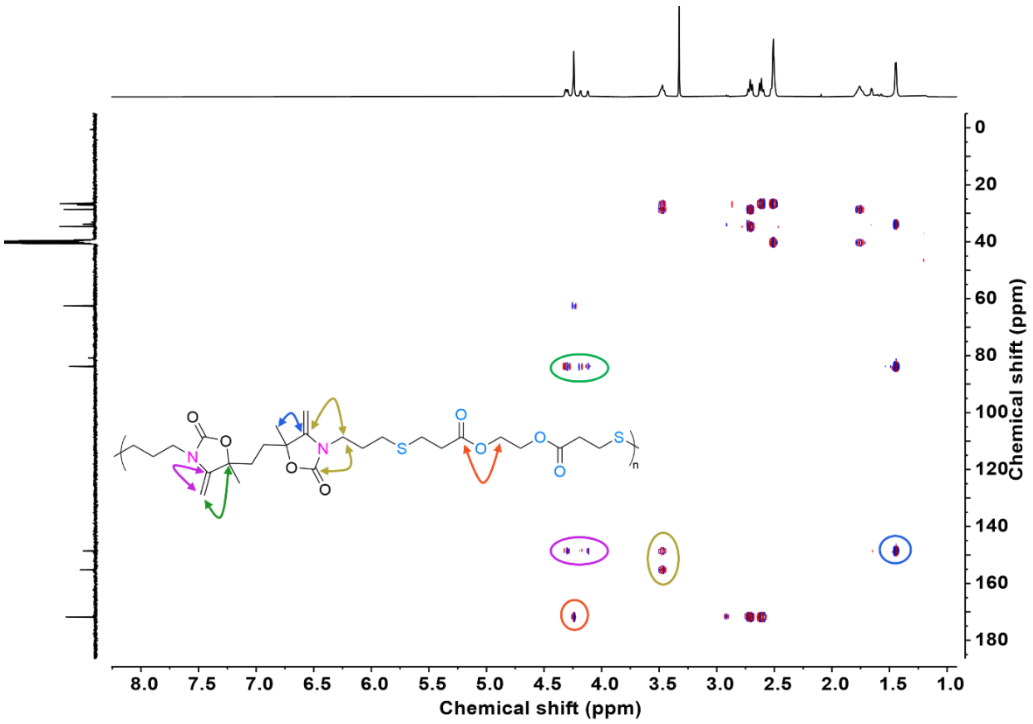

Figure S79. HMBC NMR spectrum of P2c-dehydrated (400 MHz, DMSO-d_6).

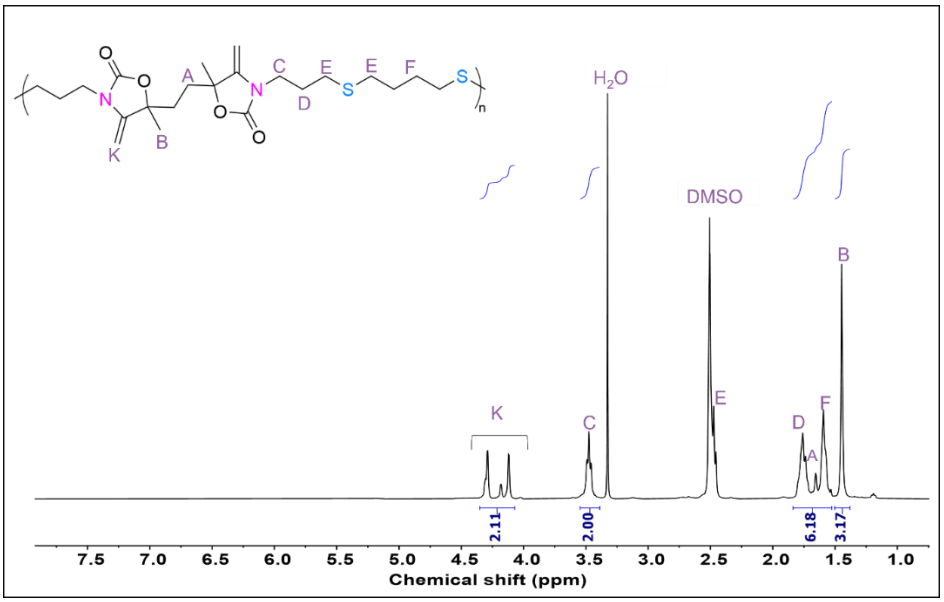

Figure S80. ^{1}H-NMR spectrum of P2d-dehydrated (400 MHz, DMSO-d_6).

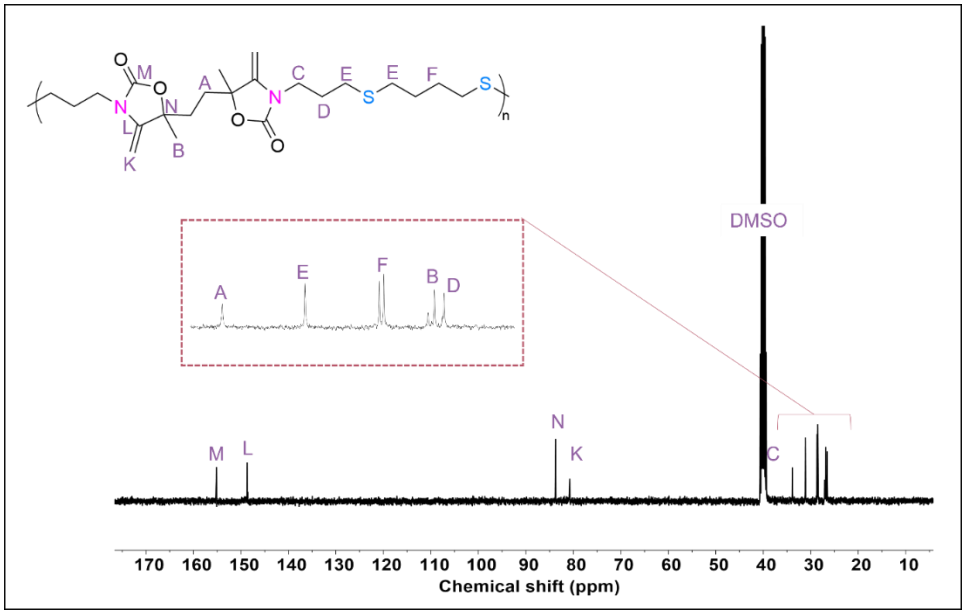

Figure S81. ^{13}C-NMR spectrum of P2d-dehydrated (100 MHz, DMSO-d_6).

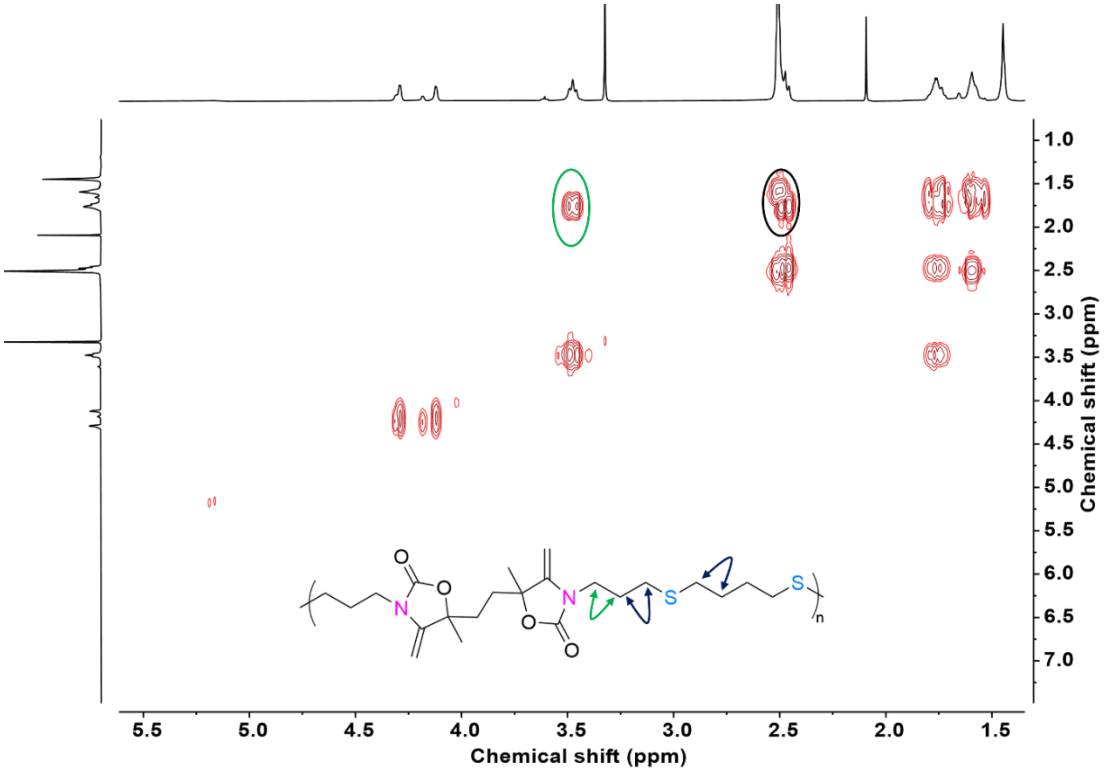

Figure S82. COSY NMR spectrum of P2d-dehydrated (400 MHz, DMSO-d_6).

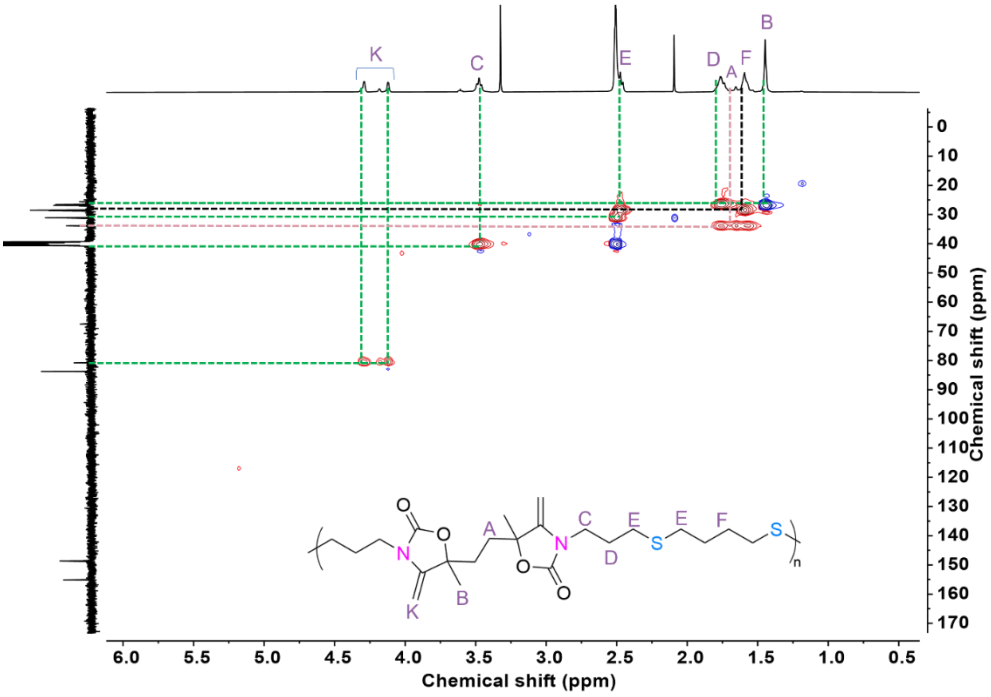

Figure S83. ^{1}H-^{13}C HSQC NMR spectrum of P2d-dehydrated (400 MHz, DMSO-d_6).

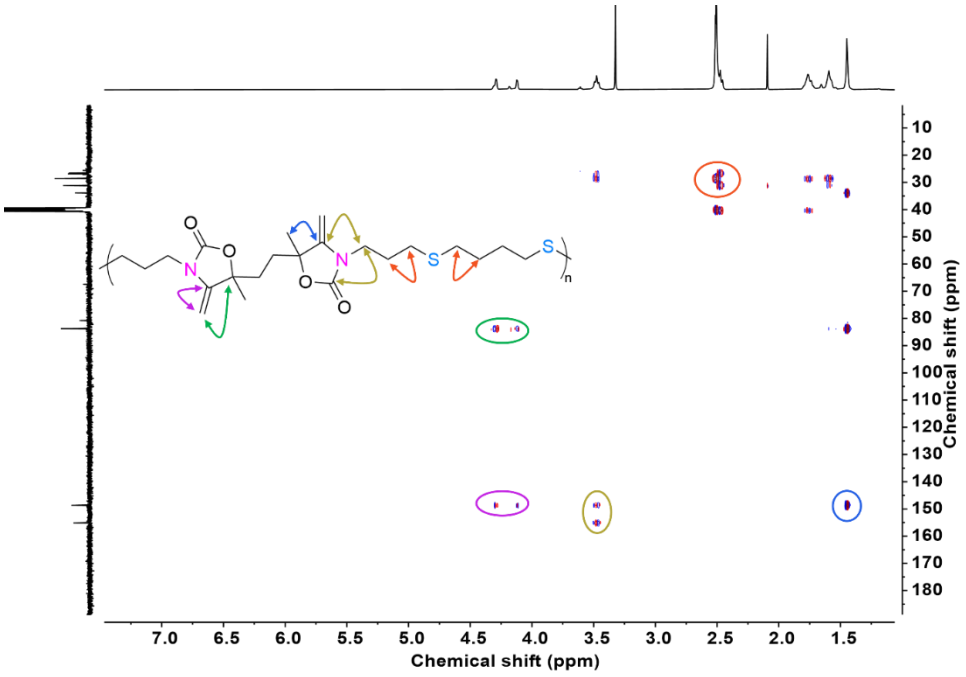

Figure S84. HMBC NMR spectrum of P2d-dehydrated (400 MHz, DMSO-d_6).

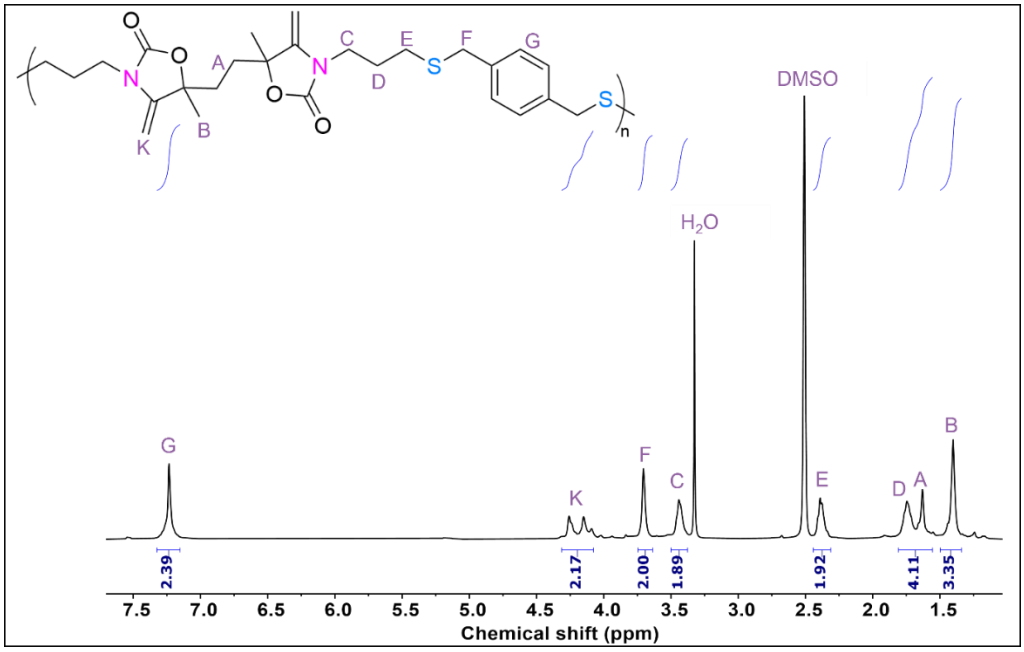

Figure S85. [1]H-NMR spectrum of P2e-dehydrated (400 MHz, DMSO-d_6).

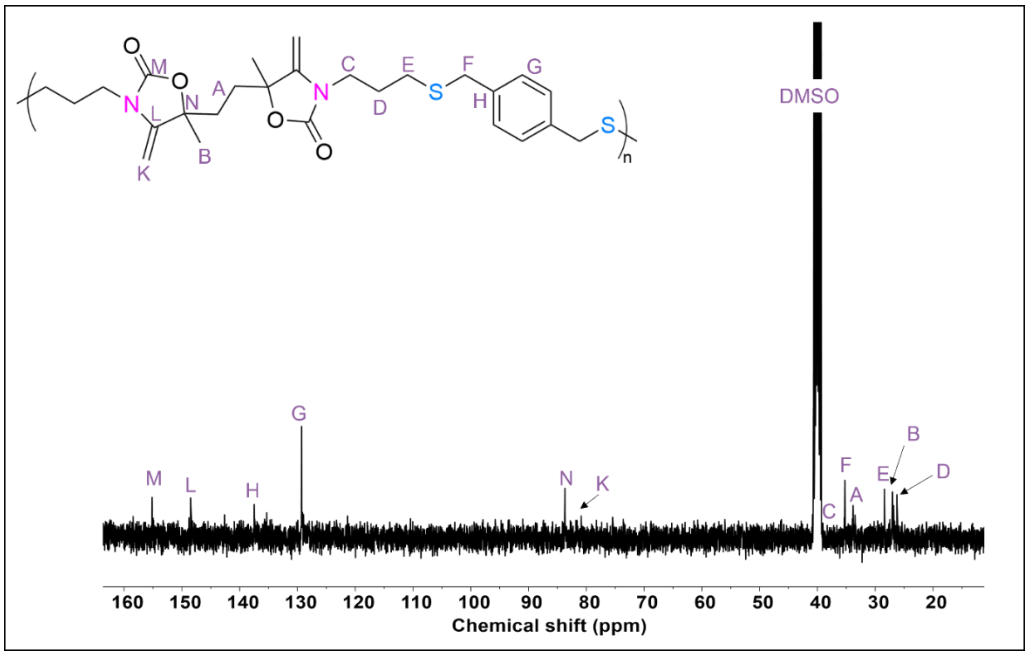

Figure S86. [13]C-NMR spectrum of P2e-dehydrated (100 MHz, DMSO-d_6).

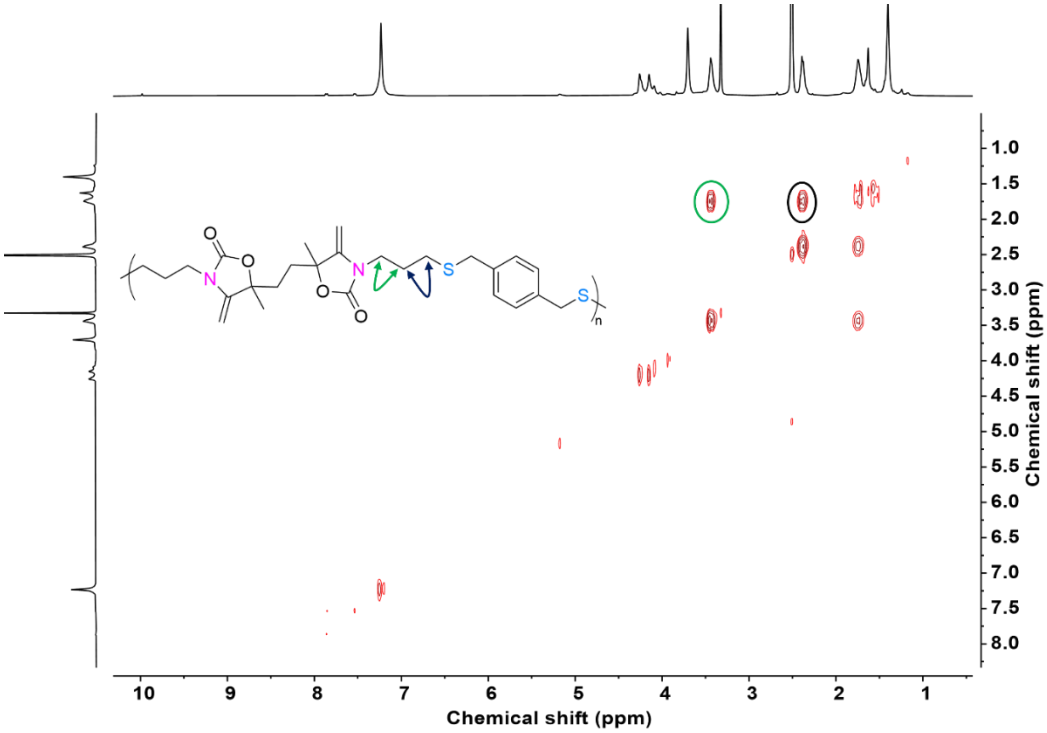

Figure S87. COSY NMR spectrum of P2e-dehydrated (400 MHz, DMSO-d_6).

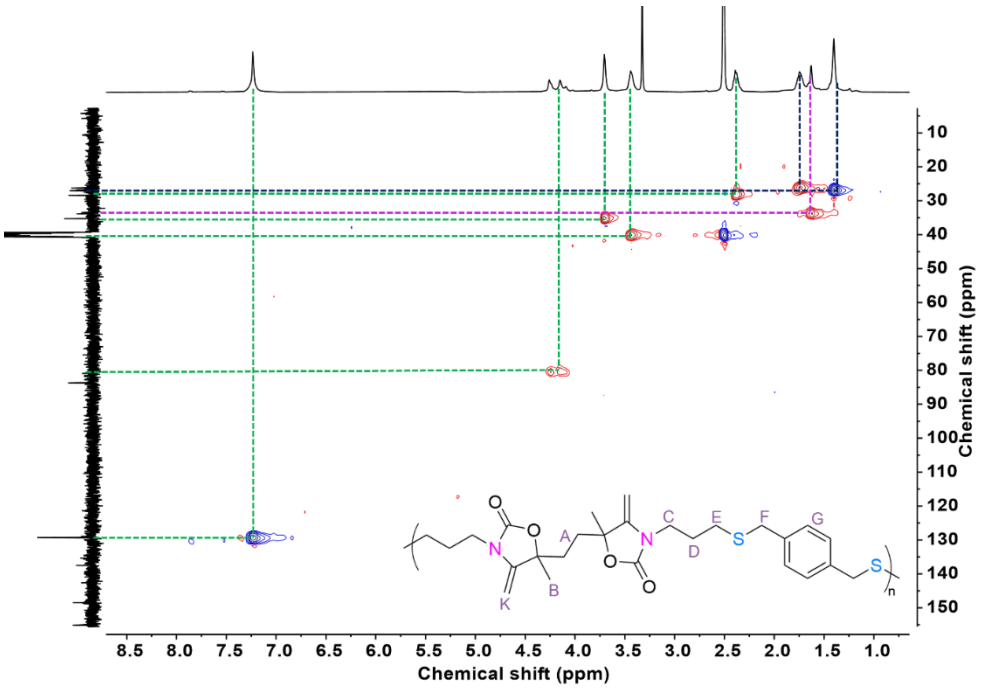

Figure S88. ^{1}H-^{13}C HSQC NMR spectrum of P2e-dehydrated (400 MHz, DMSO-d_6).

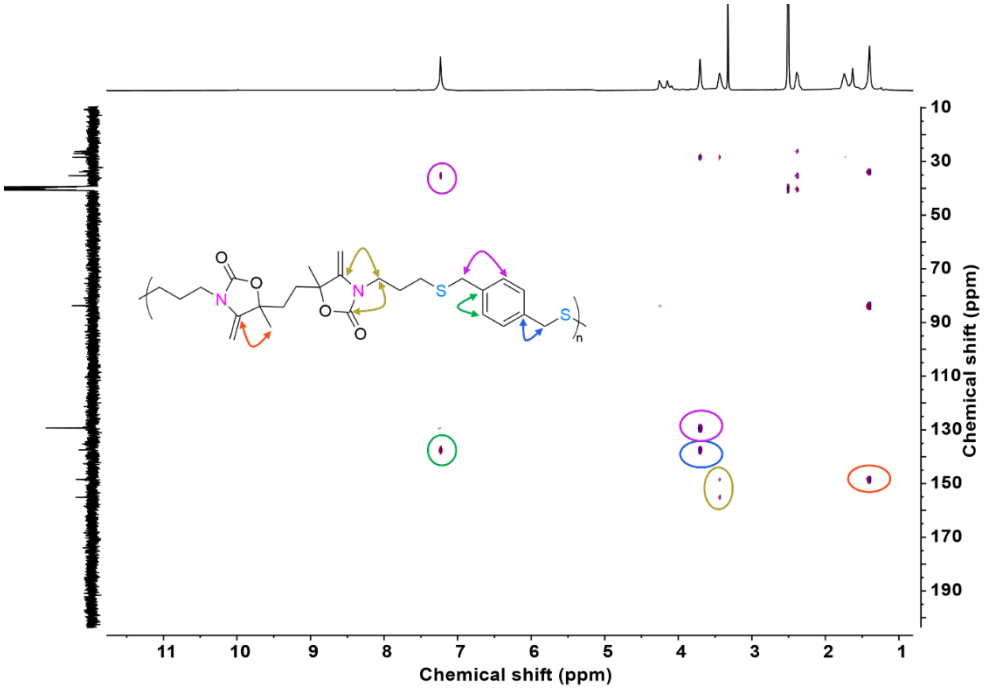

Figure S89. HMBC NMR spectrum of P2e-dehydrated (400 MHz, DMSO-d_6).

6.16 SEC chromatogram of dehydrated polymers

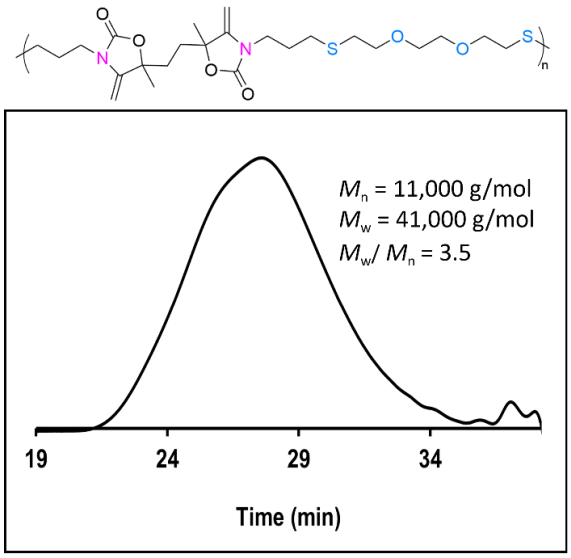

Figure S90. SEC chromatogram of P2a-dehydrated (in DMF/LiBr).

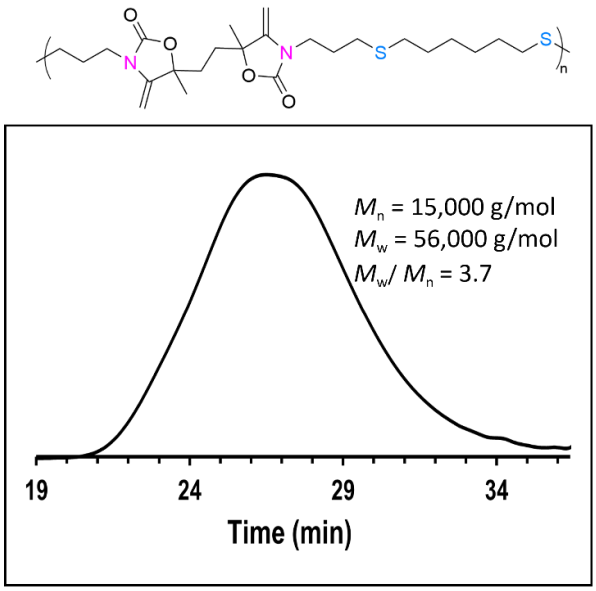

Figure S91. SEC chromatogram of P2b-dehydrated (in DMF/LiBr).

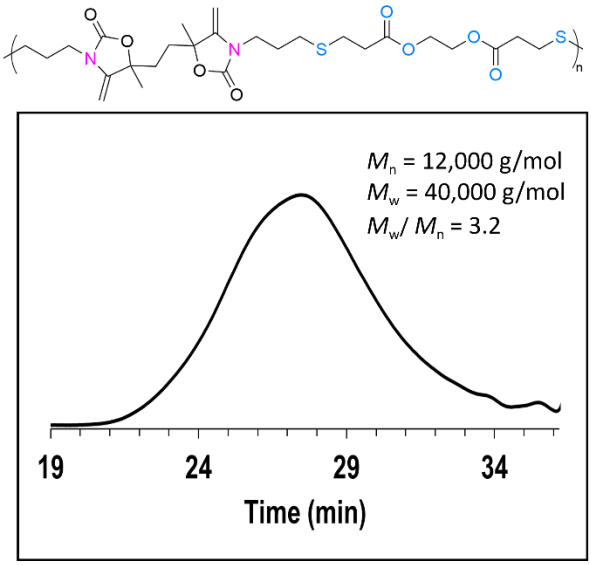

Figure S92. SEC chromatogram of P2c-dehydrated (in DMF/LiBr).

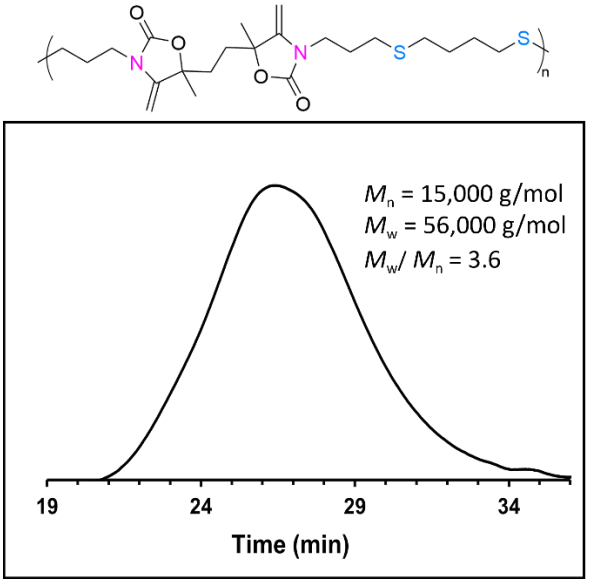

Figure S93. SEC chromatogram of P2d-dehydrated (in DMF/LiBr).

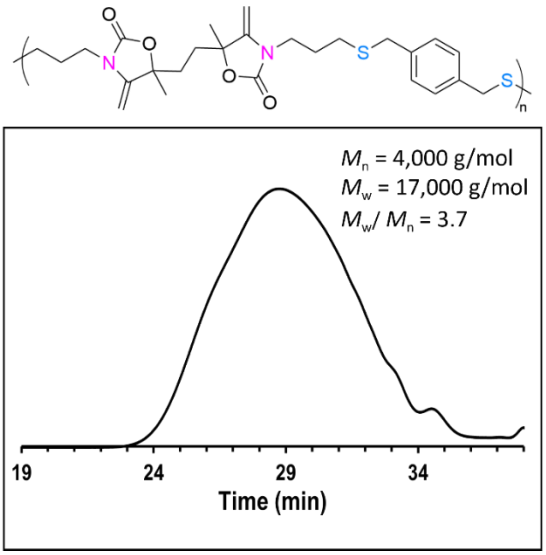

Figure S94. SEC chromatogram of P2e-dehydrated (in DMF/LiBr).

Table S3. Molecular characteristics of hydrated and dehydrated copolymers

		POxa-hydrated			POxa-dehydrated		
Entry	**Polymer**	M_n[a] (g/mol)	M_w[a] (g/mol)	Dispersity[a]	M_n[a] (g/mol)	M_w[a] (g/mol)	Dispersity[a]
1	**P2a**	**31,000**	**101,000**	**3.2**	**11,000**	**41,000**	**3.5**
2	**P2b**	**20,000**	**57,000**	**2.7**	**15,000**	**56,000**	**3.7**
3	**P2c**	**21,000**	**64,000**	**3.0**	**12,000**	**40,000**	**3.2**
4	**P2d**	**23,000**	**69,000**	**3.0**	**15,000**	**56,000**	**3.6**
5	**P2e**	**8,000**	**20,000**	**2.5**	**4,000**	**17,000**	**3.7**

[a] Determined on pure products by SEC in DMF/LiBr calibrated with PS standards

6.17 TGA of dehydrated samples

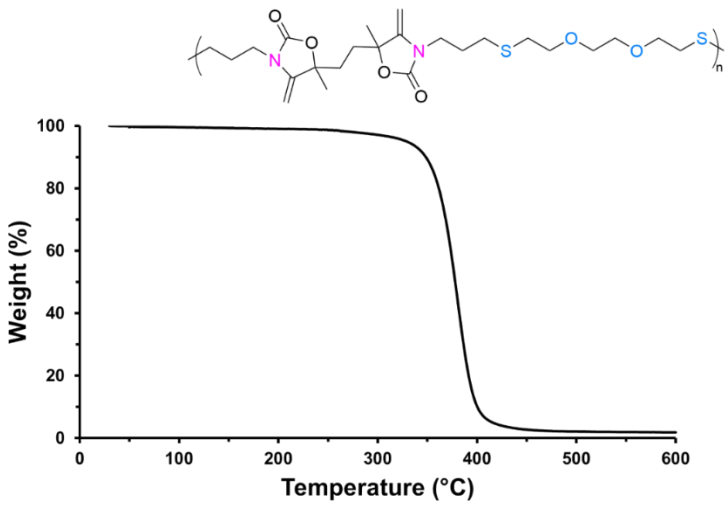

Figure S95. TGA thermogram of P2a-dehydrated

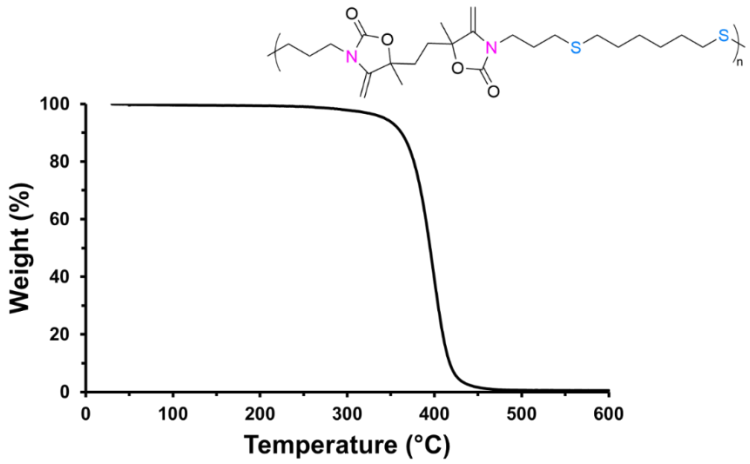

Figure S96. TGA thermogram of P2b-dehydrated

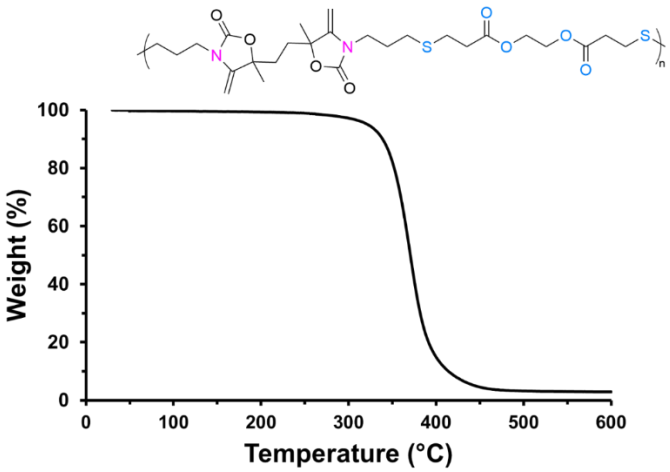

Figure S97. TGA thermogram of P2c-dehydrated

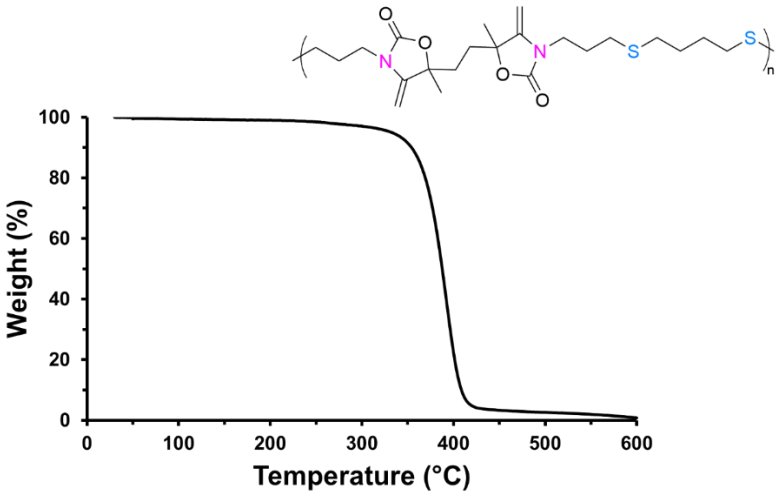

Figure S98. TGA thermogram of P2d-dehydrated

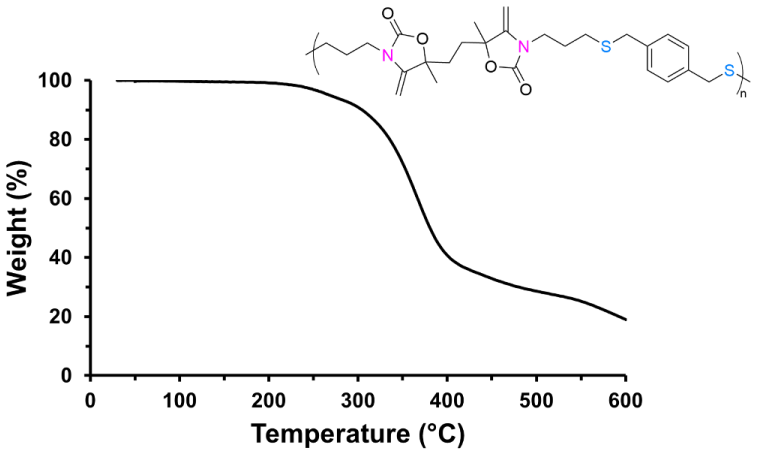

Figure S99. TGA thermogram of P2e-dehydrated

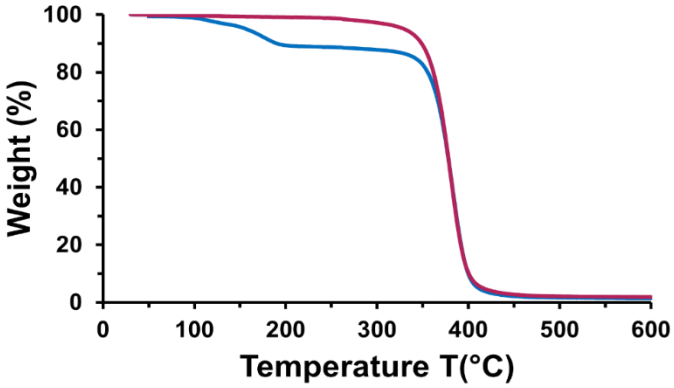

Figure S100. overlay of TGA curves for POxa (blue) and POxa-dehydrated (magenta); (samples P2b and P2b-dehydrated as a representative example)

6.18 DSC characterization of hydrated polymers

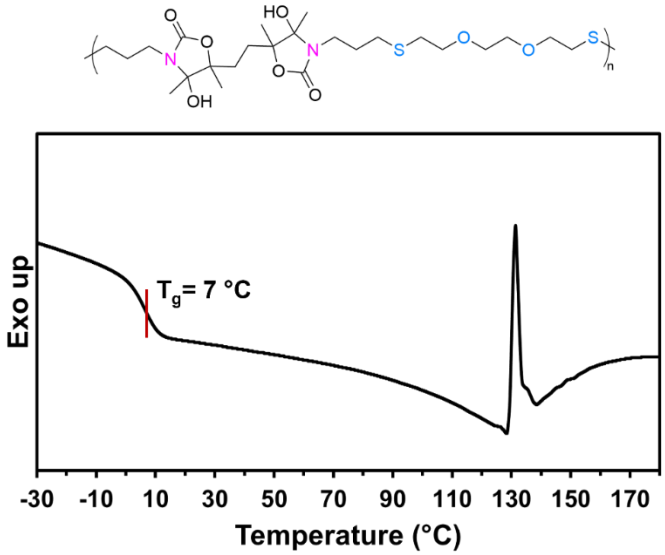

Figure S101. Reversing heat flow using modulated DSC of P2a

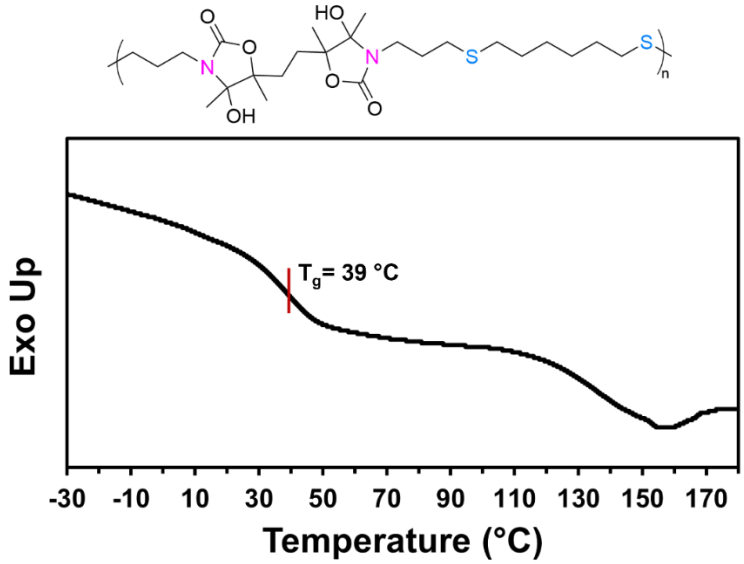

Figure S102. Reversing heat flow using modulated DSC of P2b

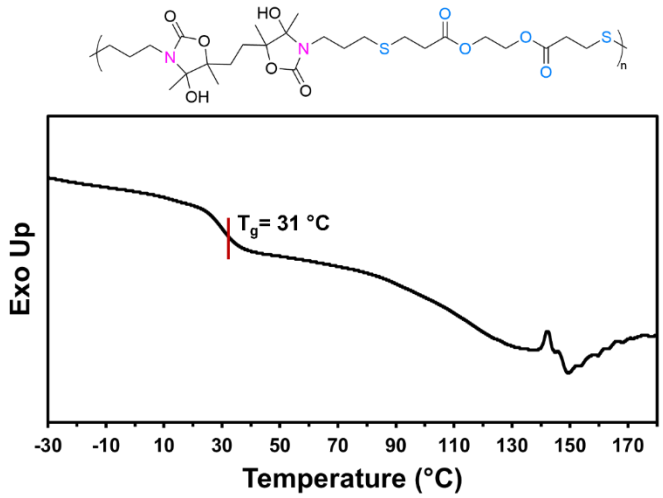

Figure S103. Reversing heat flow using modulated DSC of P2c

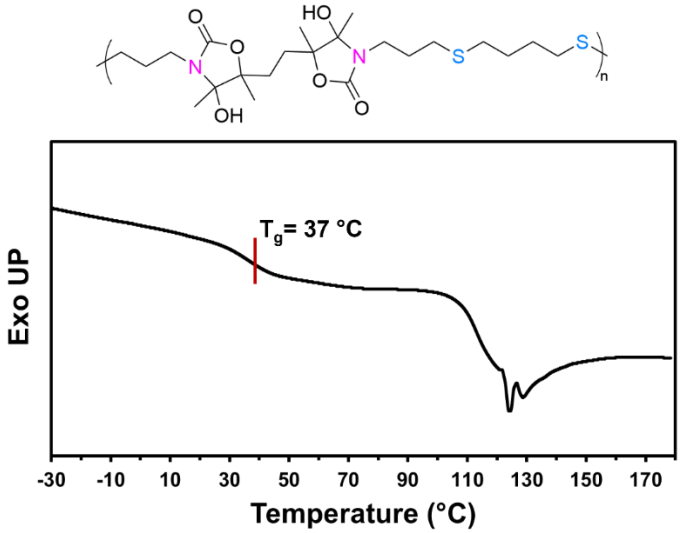

Figure S104. Reversing heat flow using modulated DSC of P2d

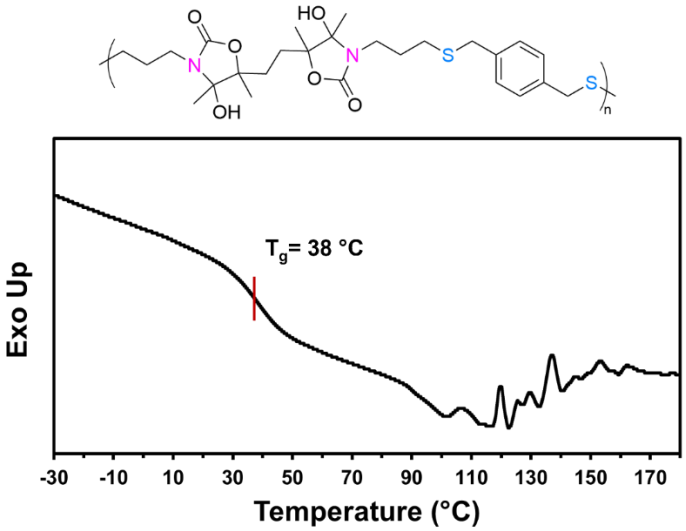

Figure S105. Reversing heat flow using modulated DSC of P2e

6.19 DSC characterization of dehydrated polymers

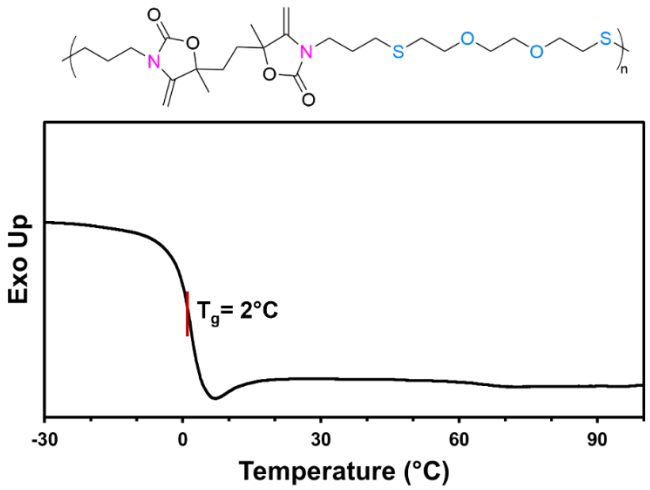

Figure S106. DSC characterization of P2a-dehydrated

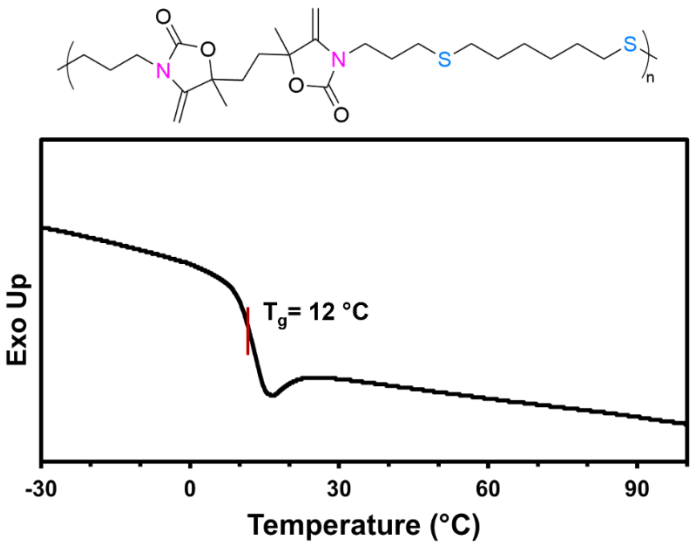

Figure S107. DSC characterization of P2b-dehydrated

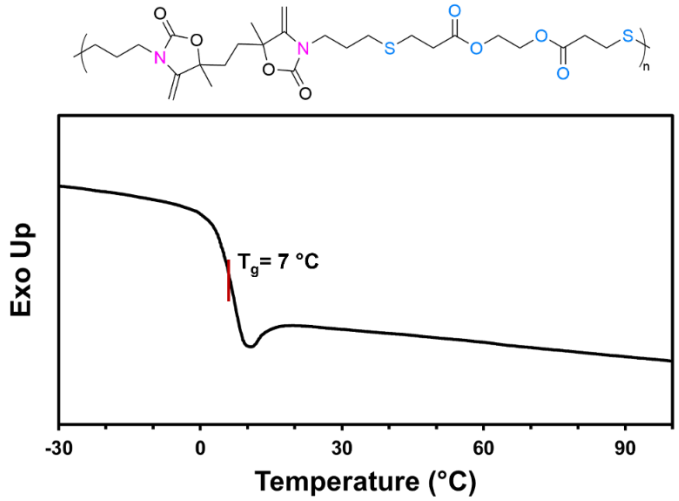

Figure S108. DSC characterization of P2c-dehydrated

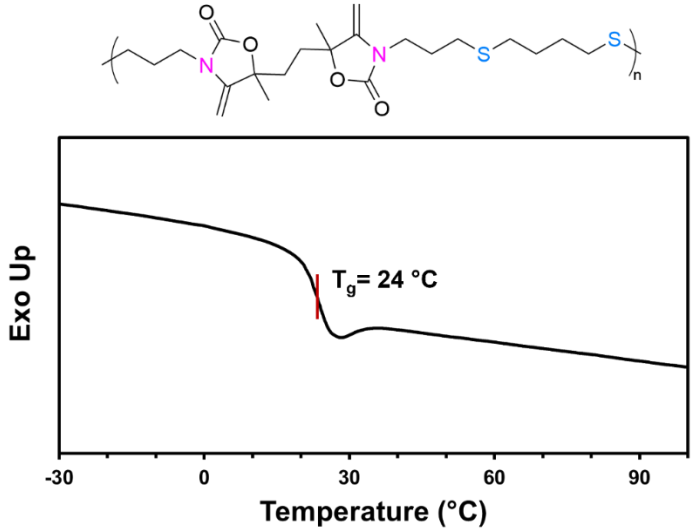

Figure S109. DSC characterization of P2d-dehydrated

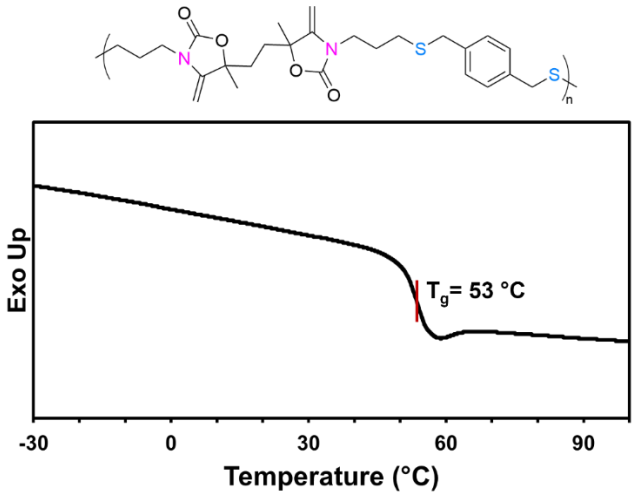

Figure S110. DSC characterization of P2e-dehydrated

6.20 Chemical stability

Pressed polymer films of **P2a** were cut into small pieces (50 mg) and immersed in 6 mL of sulfuric acid and sodium hydroxide aqueous solutions of different concentrations of (0.1 M, 1 M and 5 M) for 48 h. Except in the case of the 1 M NaOH solution, all polymers remained insoluble. The recovered solids were characterized by ^{1}H-NMR spectroscopy (Figure S113 and Figure S115) and by SEC (Figure S112 and Figure S114).

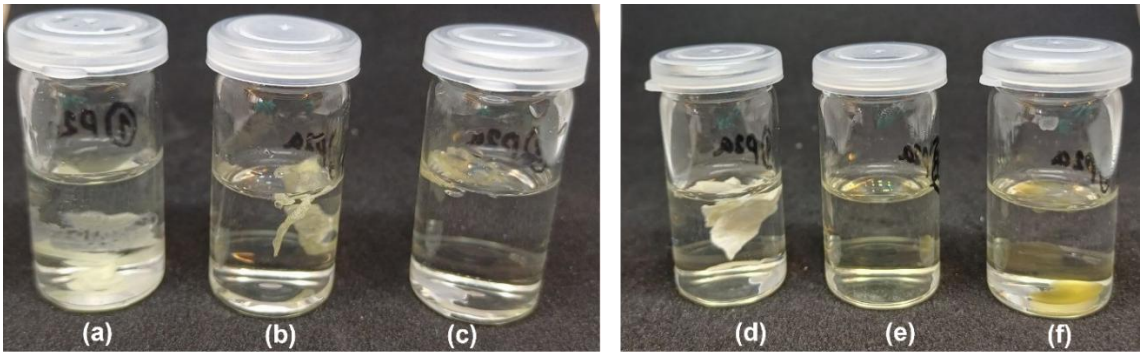

Figure S111. Comparative visual documentation of P2a polymer samples after 48 hours exposure to acidic and basic environments (a) in H_2SO_4 (0.1 M), (b) in H_2SO_4 (1 M), (c) in H_2SO_4 (5 M); (d) in NaOH (0.1 M), (e) in NaOH (1 M), (f) in NaOH (5 M)

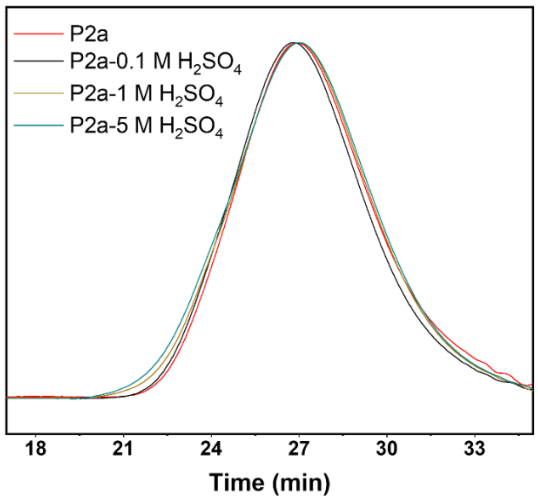

Figure S112. SEC chromatograms comparing P2a before and after a 48-hour immersion in an acidic environment, highlighting the polymer's stability (in DMF/LiBr).

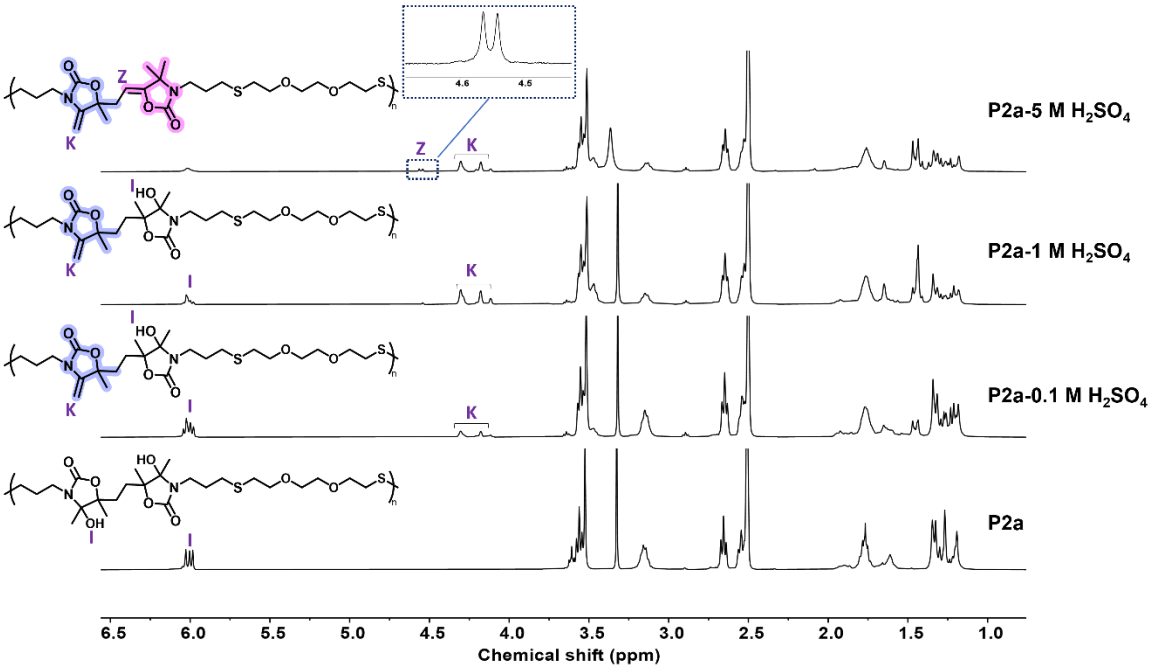

Figure S113. ^{1}H-NMR spectrum comparing P2a before and after a 48-hour immersion in an acidic environment (400 MHz, DMSO-d_6).

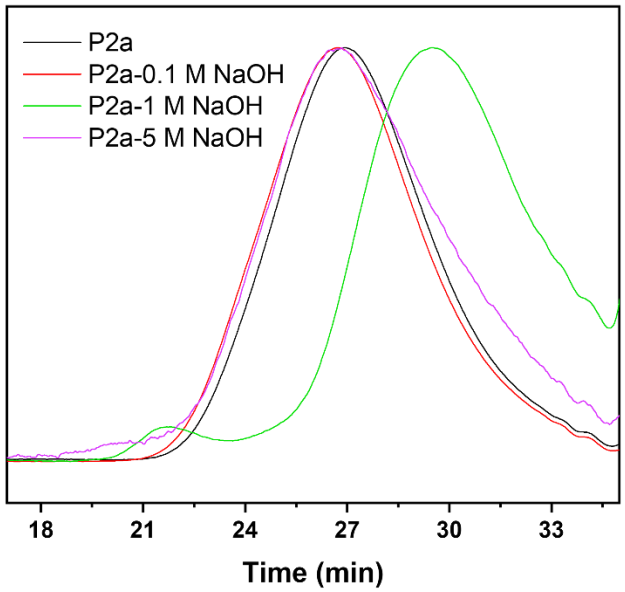

Figure S114. SEC chromatograms comparing **P2a** before and after a 48-hour immersion in basic environment, highlighting the polymer's stability (in DMF/LiBr).

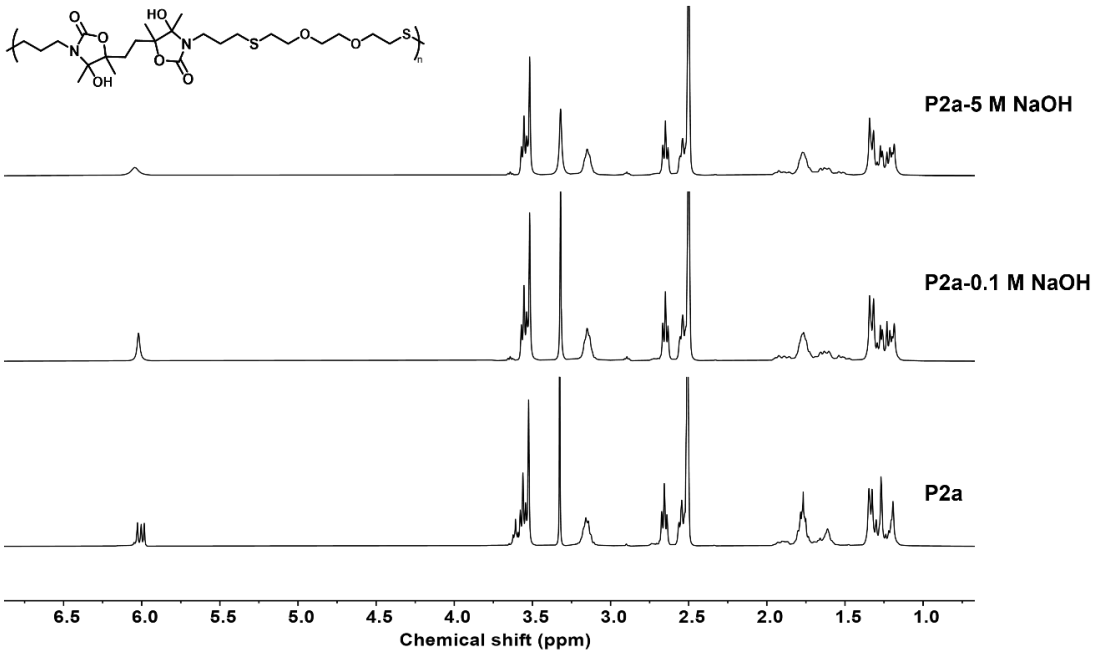

Figure S115. ^{1}H-NMR spectrum comparing P2a before and after a 48-hour immersion in basic environment (400 MHz, DMSO-d_6).

6.21 Structure characterizations of P2b-Sulfoxide (oxidation to sulfoxide)

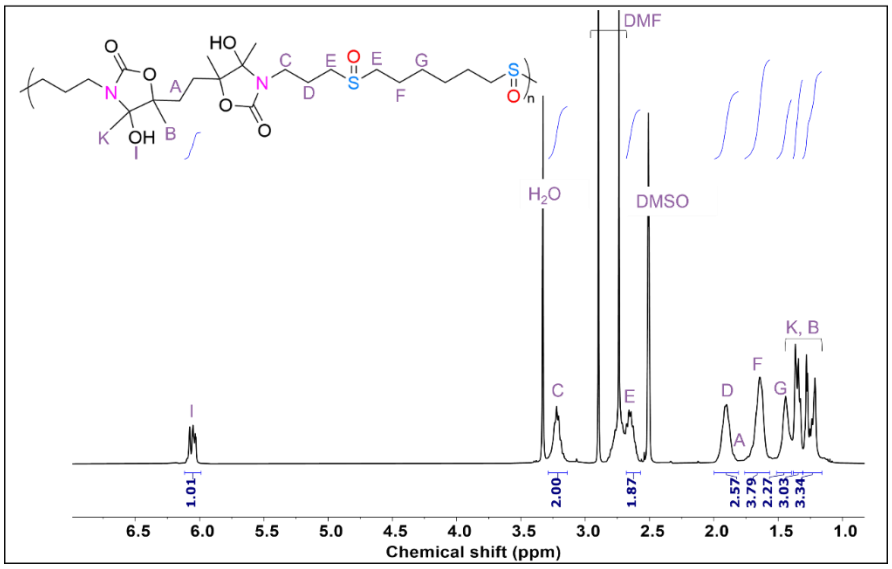

Figure S116. ^{1}H-NMR spectrum (400 MHz, DMSO-d_6) of P2b-Sulfoxide.

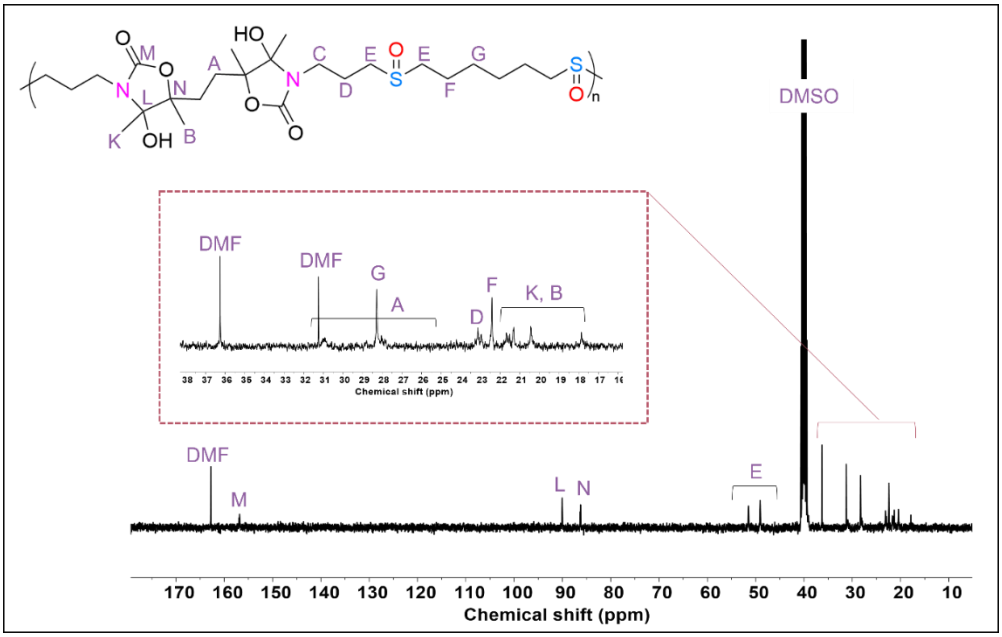

Figure S117. ^{13}C-NMR spectrum (100 MHz, DMSO-d_6) of P2b-Sulfoxide.

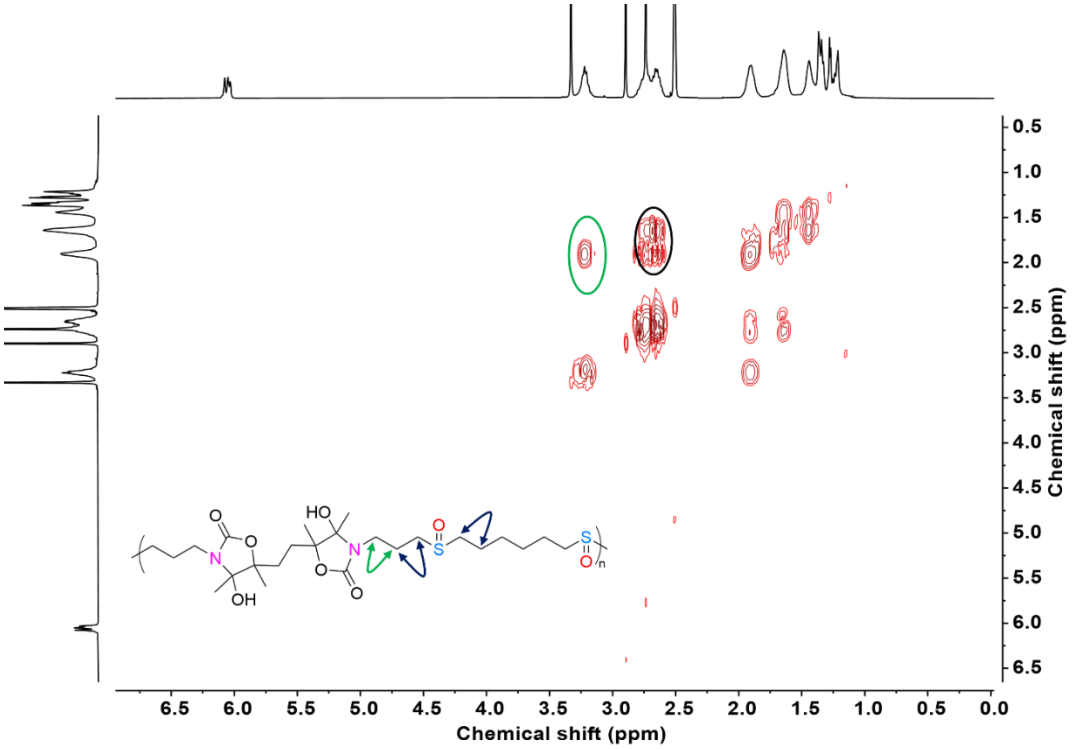

Figure S118. COSY NMR spectrum of P2b-Sulfoxide (400 MHz, DMSO-d_6).

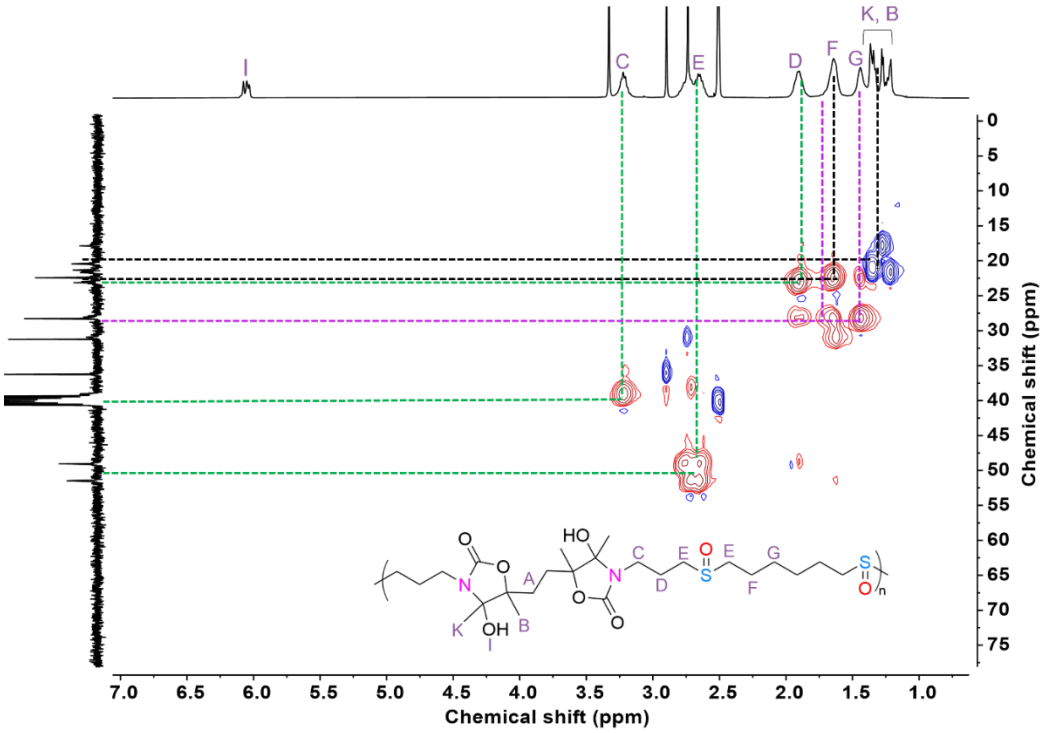

Figure S119. ^{1}H-^{13}C HSQC NMR spectrum of P2b-Sulfoxide (400 MHz, DMSO-d_6).

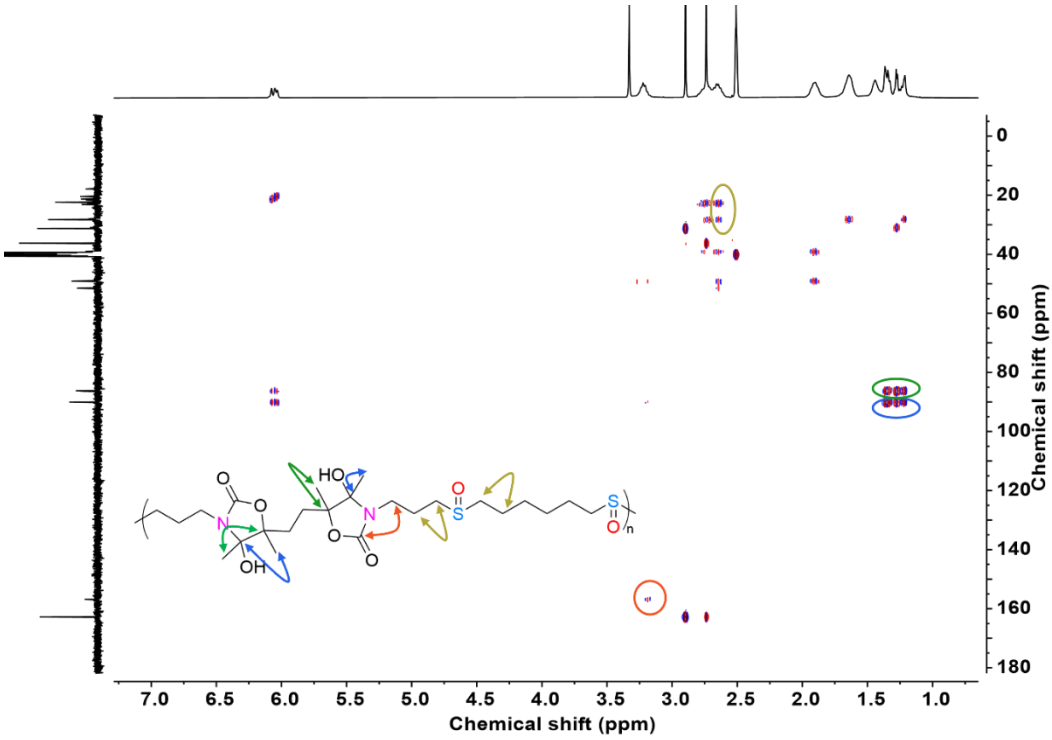

Figure S120. HMBC NMR spectrum of P2b-Sulfoxide (400 MHz, DMSO-d_6).

To further confirm the quantitative sulfoxide formation, ^{1}H-NMR was also conducted in DMF-d_7 as a solvent (Figure S121). It is verified that signals associated to protons adjacent to thioethers (δ=2.51-2.64 ppm) were vanished, substituted with a new downfield peak (δ=2.70-2.90 ppm) corresponding to the methylene protons adjacent to the sulfoxide groups (−$SOCH_2$).

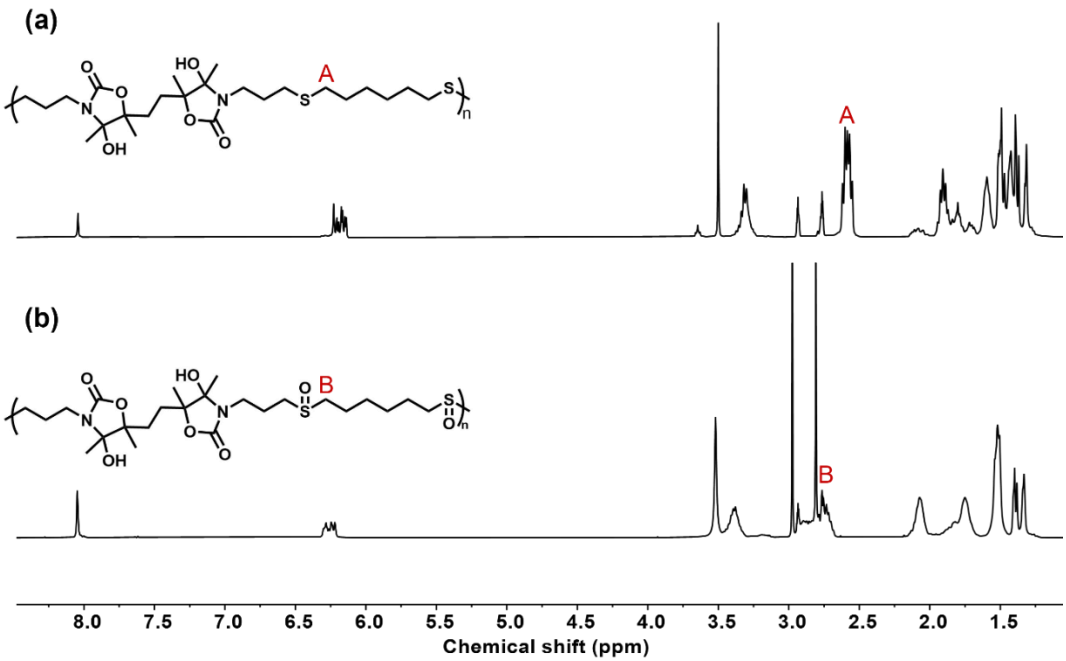

Figure S121. ^{1}H-NMR spectrum (400 MHz, DMF-d_7) of (a) P2b; (b) P2b-Sulfoxide

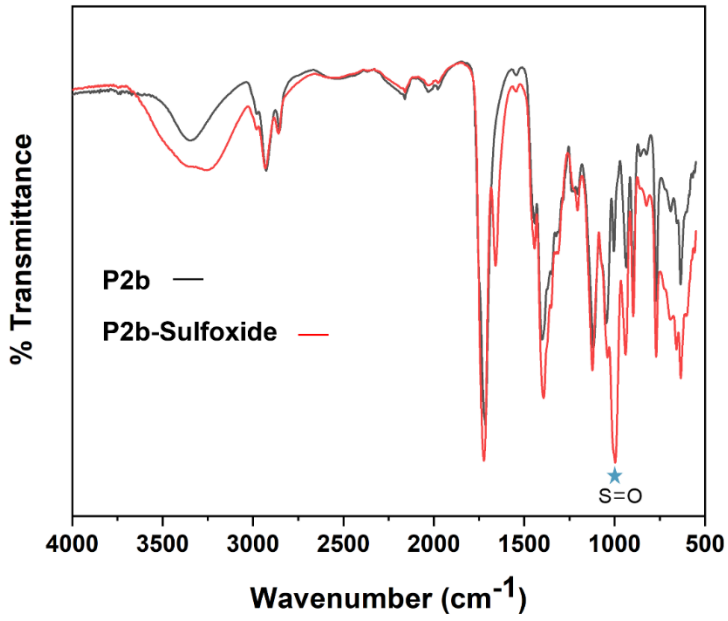

Figure S122. FT-IR spectra of P2b and P2b-Sulfoxide.

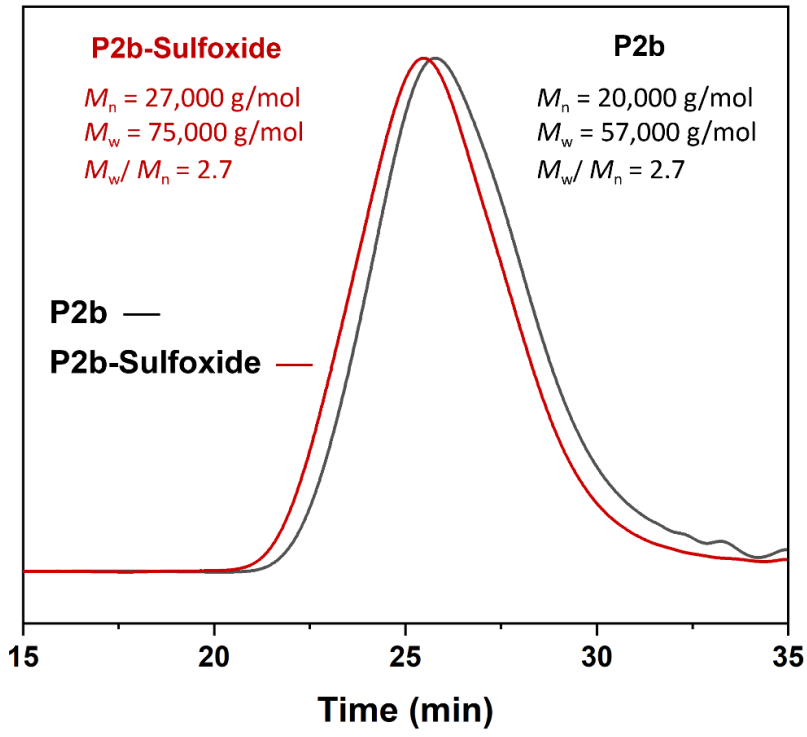

Figure S123. SEC chromatogram of P2b and P2b-Sulfoxide

6.22 Structure characterizations of P2b-Sulfone (oxidation to sulfone)

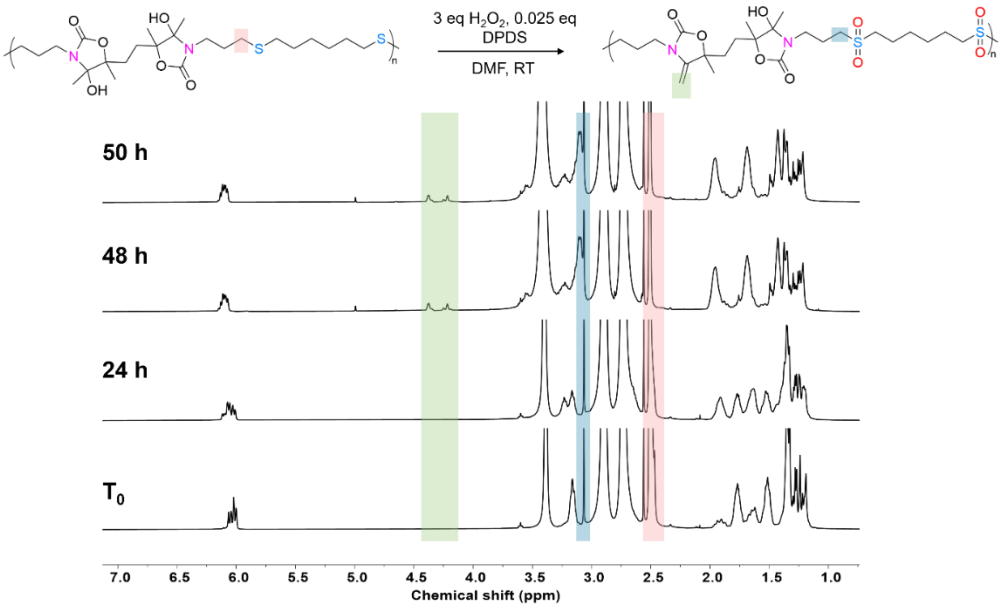

Figure S124. Kinetic study of oxidation of P2b to P2b-Sulfone containing sulfone groups using ^{1}H-NMR (400 MHz, DMSO-d_6).

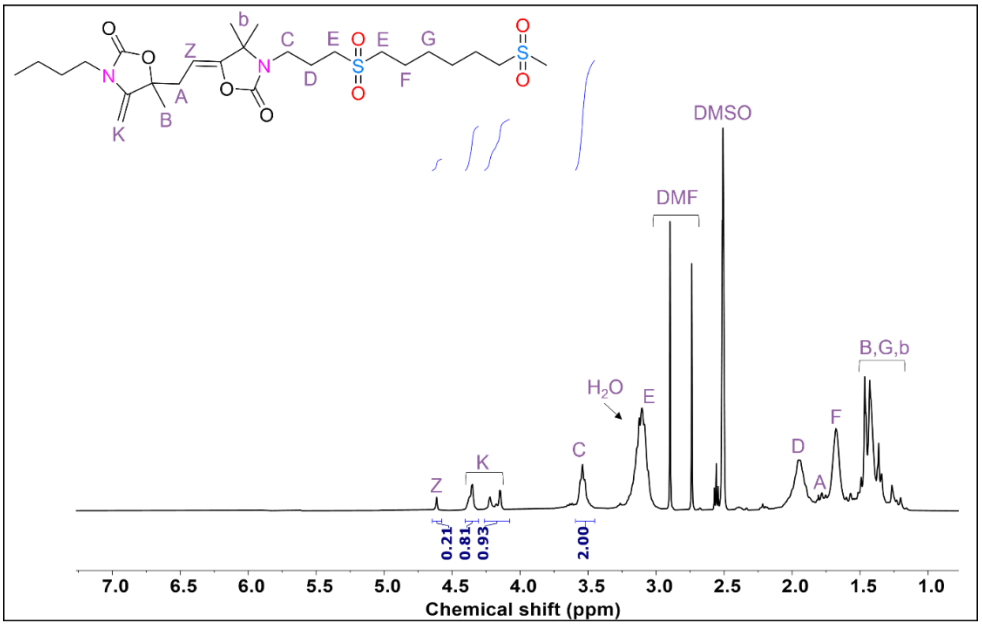

Figure S125. ^{1}H-NMR spectrum (400 MHz, DMSO-d_6) of P2b-Sulfone.

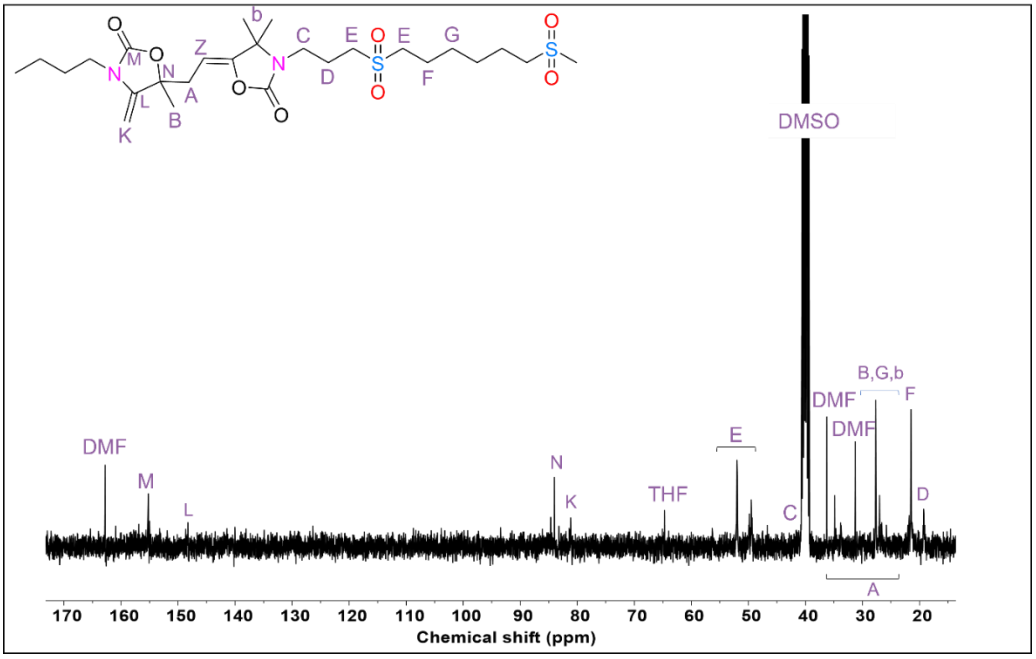

Figure S126. ^{13}C-NMR spectrum (100 MHz, DMSO-d_6) of P2b-Sulfone.

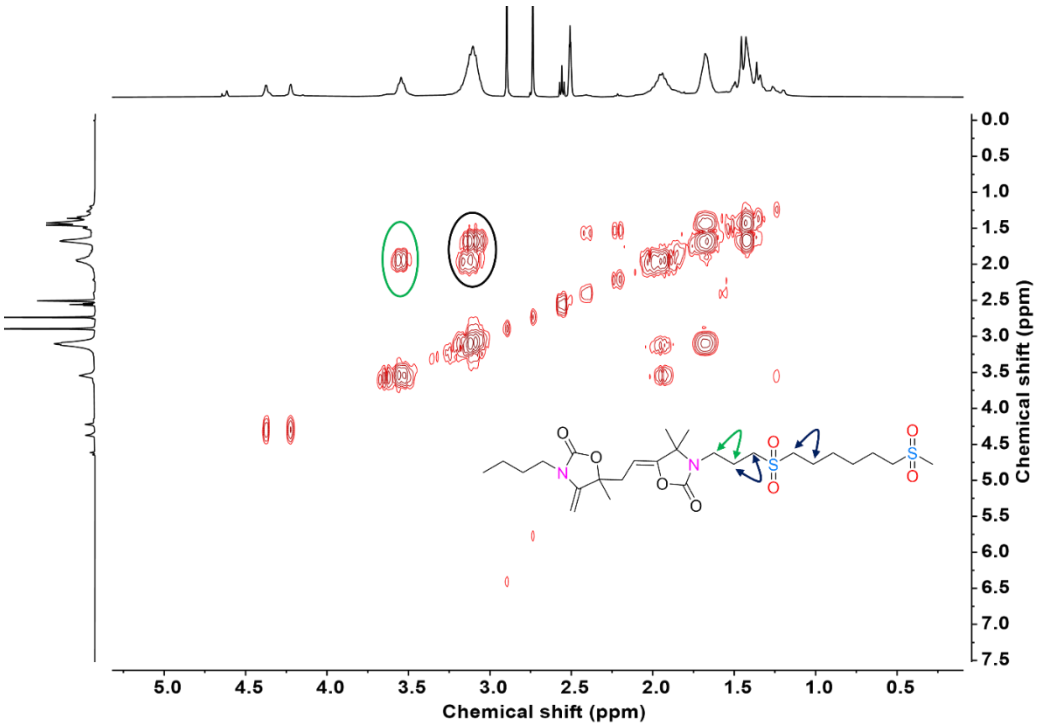

Figure S127. COSY NMR spectrum of P2b-Sulfone (400 MHz, DMSO-d_6).

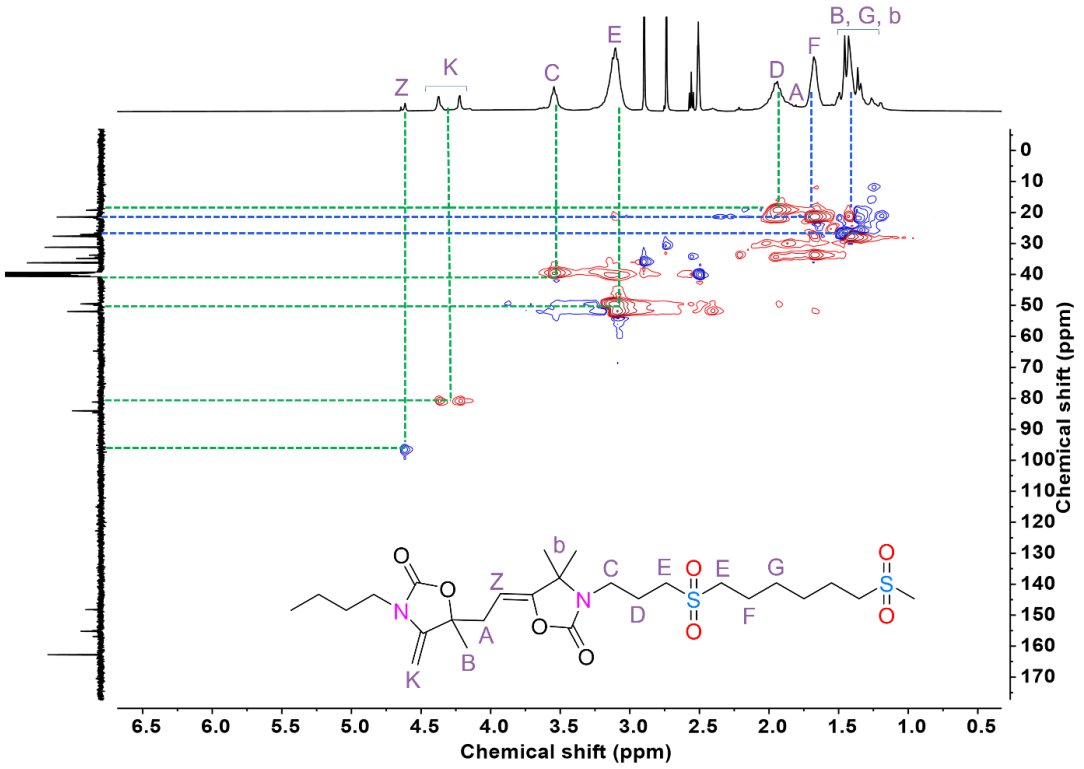

Figure S128. ^{1}H-^{13}C HSQC NMR spectrum of P2b-Sulfone (400 MHz, DMSO-d_6).

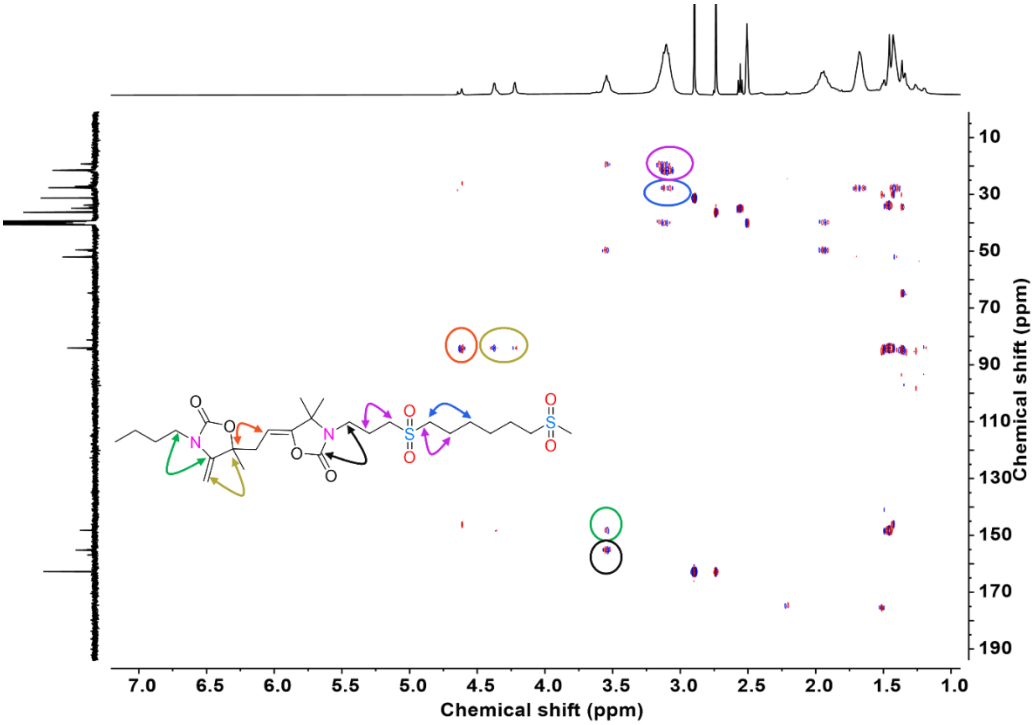

Figure S129. HMBC NMR spectrum of P2b-Sulfone (400 MHz, DMSO-d_6).

To corroborate the quantitative formation of sulfone groups, an additional verification was conducted using ^{1}H-NMR in DMF-d_7 as the solvent (Figure S130), which the peak associated to protons adjacent to thioethers (δ=2.51-2.64 ppm) were vanished, substituted with a new downfield peak (δ=3.27-3.52 ppm) corresponding to the methylene protons neighboring the sulfone groups (−SO_2CH_2).

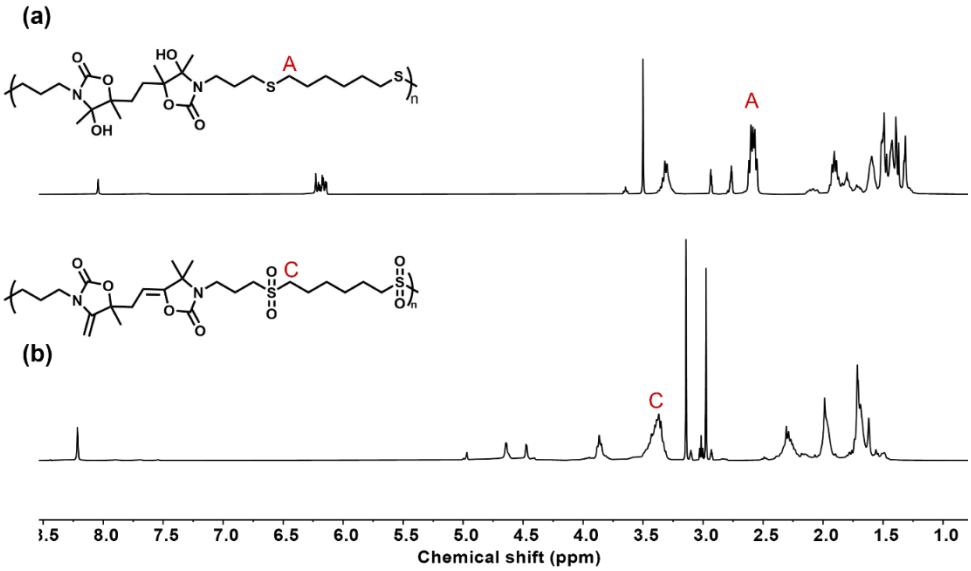

Figure S130. ^{1}H-NMR spectrum (400 MHz, DMF-d_7) of (a) P2b; (b) P2b-Sulfone.

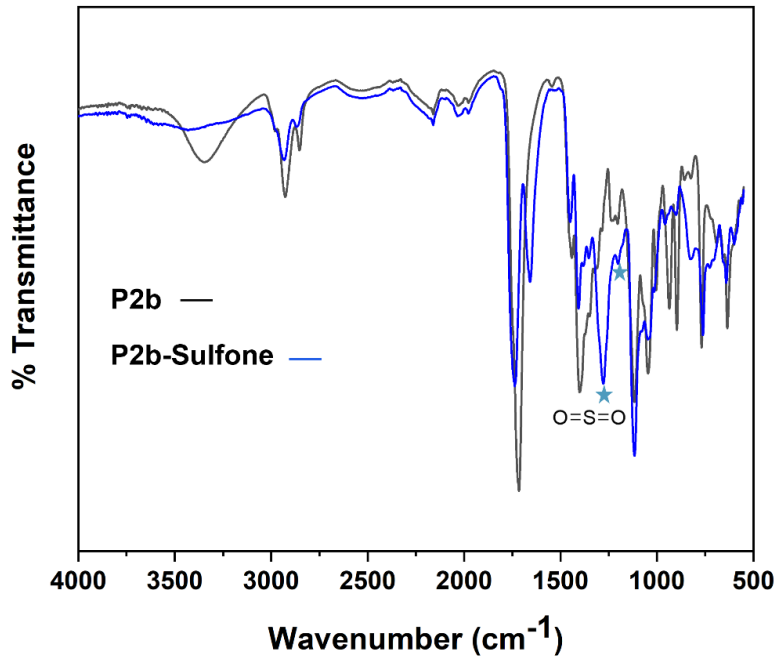

Figure S131. FT-IR spectra of P2b and P2b-Sulfone.

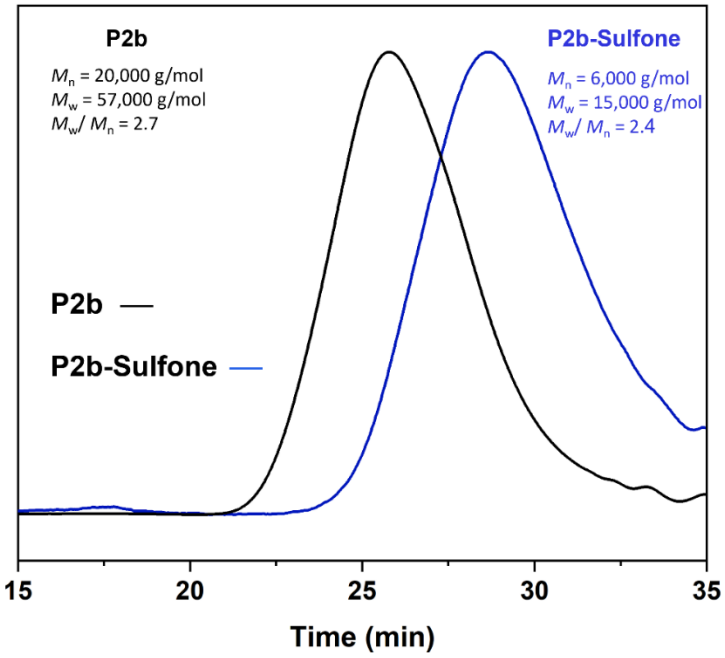

Figure S132. SEC chromatogram of P2b and P2b-Sulfone

6.23 TGA characterization of post-modified polymers

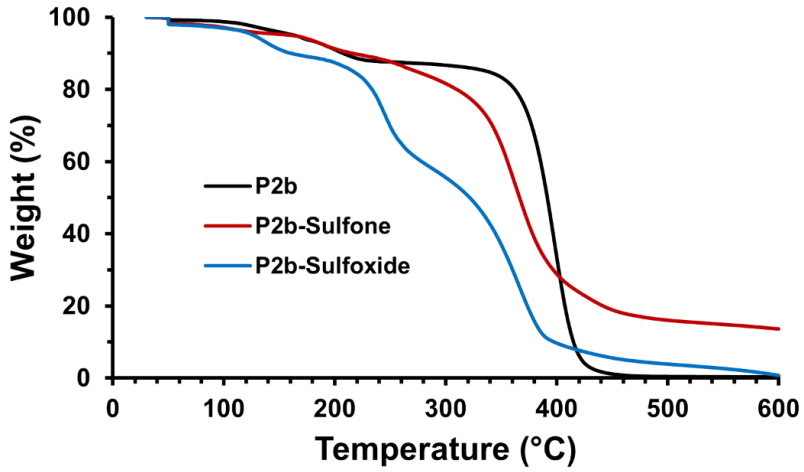

Figure S133. Overlay of TGA curves for polymers P2b, P2b-Sulfoxide, and P2b-Sulfone

6.24 Structure characterizations of P2b-Sulfonium (S-alkylated)

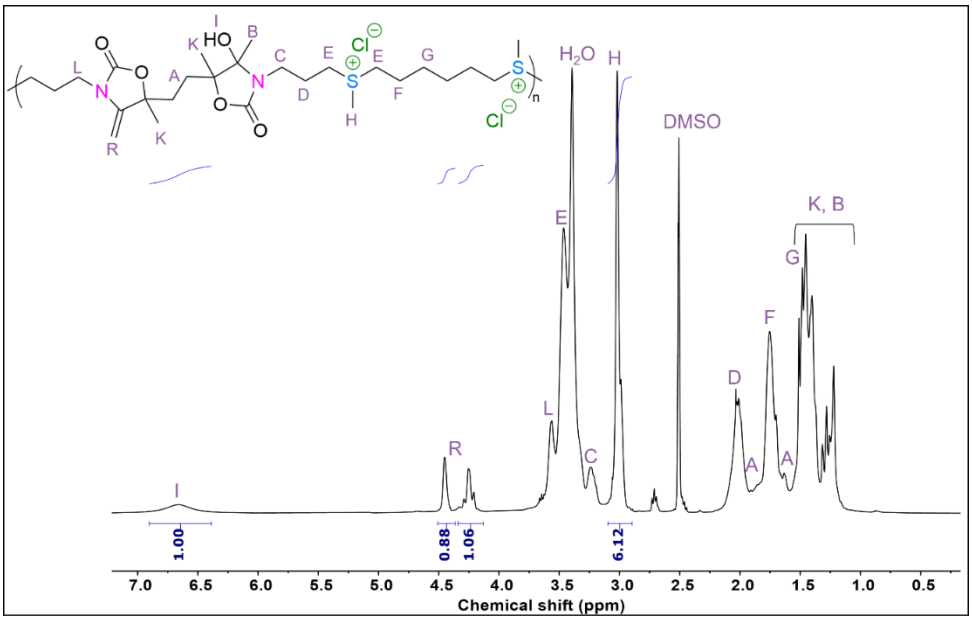

Figure S134. ^{1}H-NMR spectrum (400 MHz, DMSO-d_6) of P2b-Sulfonium.

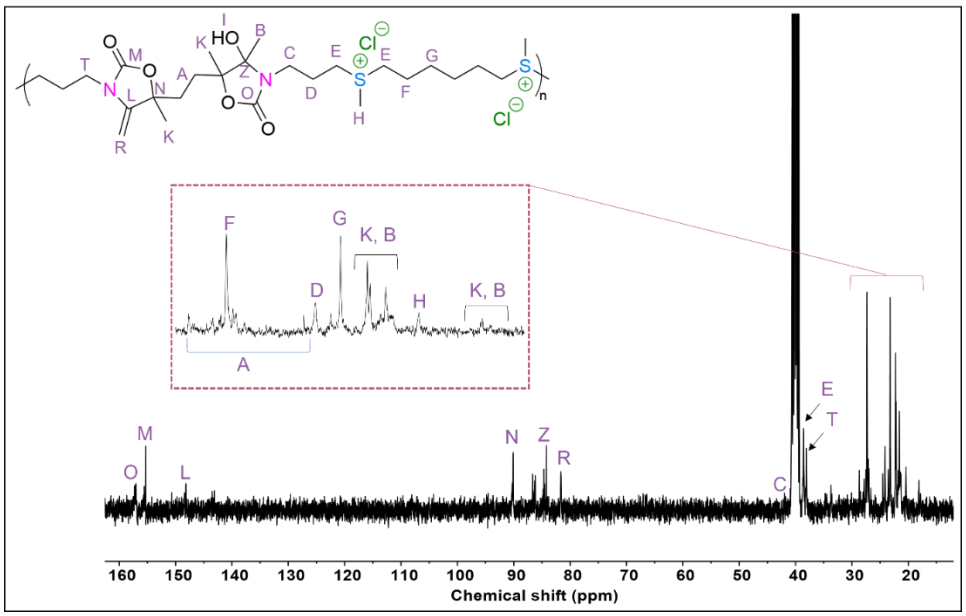

Figure S135. ^{13}C-NMR spectrum (100 MHz, DMSO-d_6) of P2b-Sulfonium.

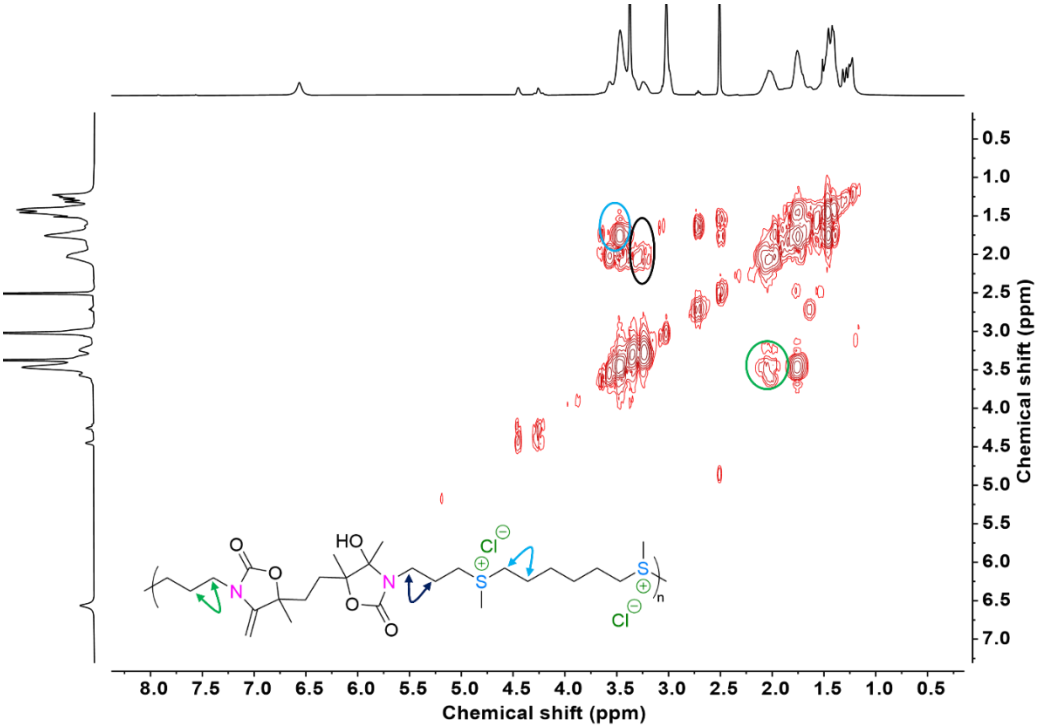

Figure S136. COSY NMR spectrum of P2b-Sulfonium (400 MHz, DMSO-d_6).

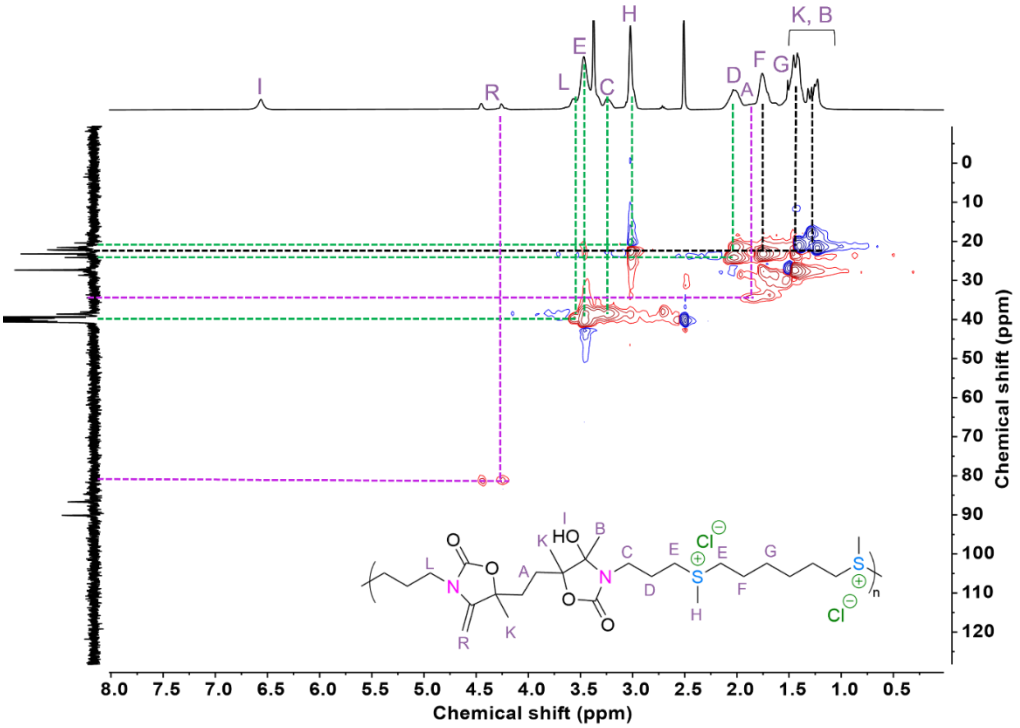

Figure S137. ^{1}H-^{13}C HSQC NMR spectrum of P2b-Sulfonium (400 MHz, DMSO-d_6).

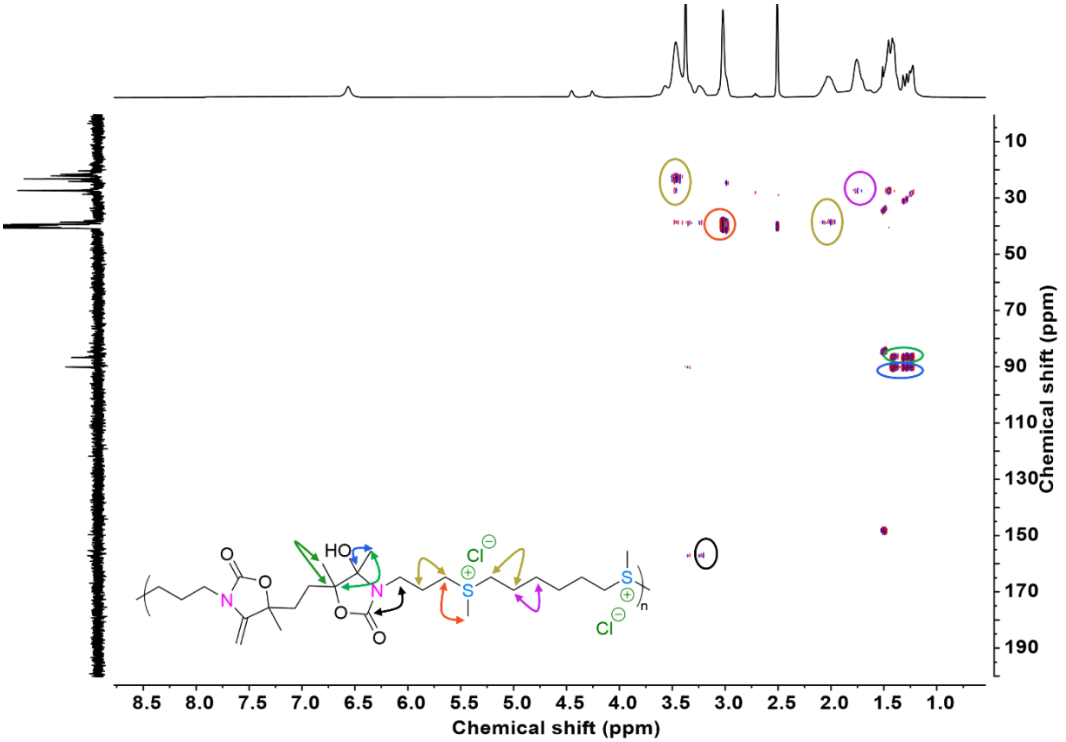

Figure S138. HMBC NMR spectrum of P2b-Sulfonium (400 MHz, DMSO-d_6).

To corroborate the quantitative formation of sulfonium groups, an additional verification was conducted using 1H-NMR in D2O as the solvent. As shown in S139, no resonance corresponding to protons adjacent to thioethers (δ=2.51-2.64 ppm) were detected, while two new distinctive downfield peaks emerged at δ=3.19-3.44 ppm and δ=2.81-2.89 ppm, signifying the presence of the methylene (CH2-S+) and the methyl (CH3-S+) groups of the sulfonium moiety.

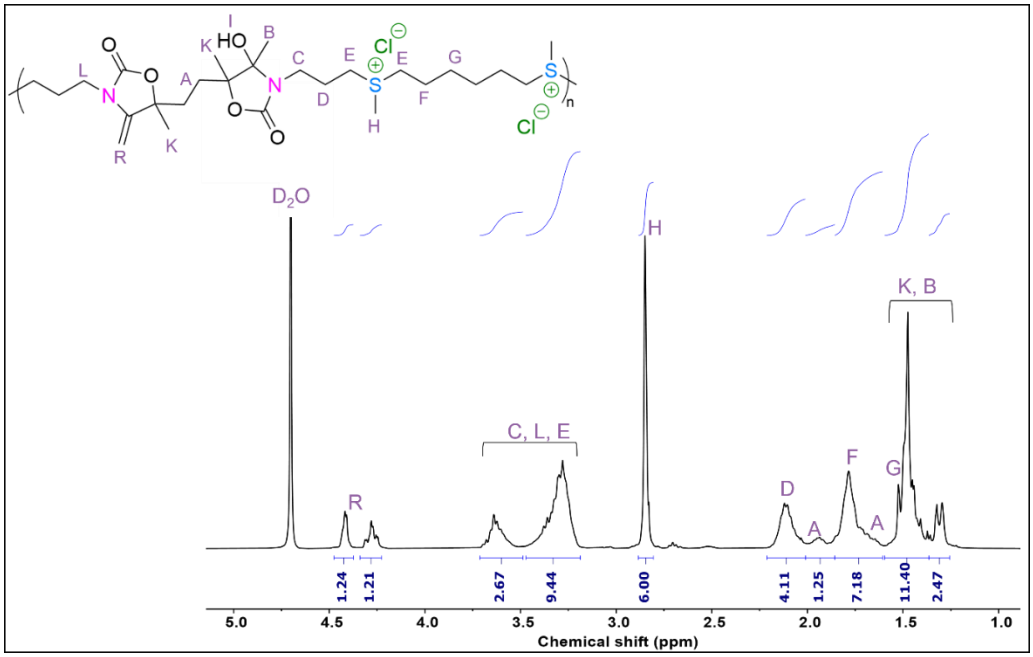

Figure S139. ^{1}H-NMR spectrum (400 MHz, D_2O) of P2b-Sulfonium.

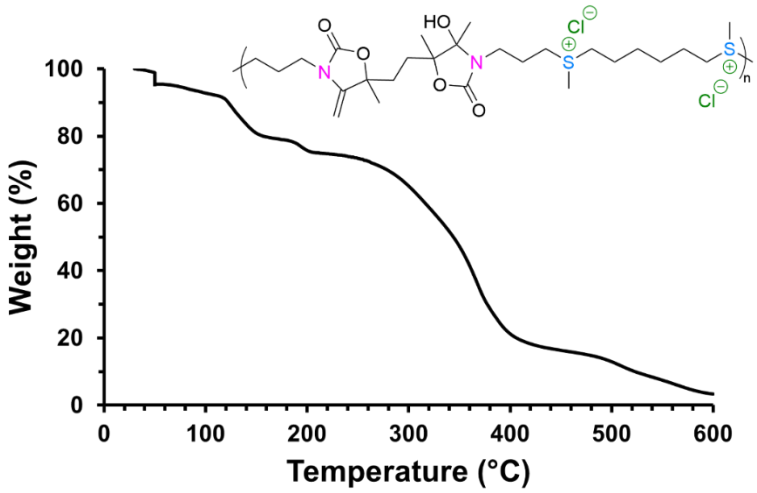

Figure S140. TGA thermogram for polymer P2b-Sulfonium

6.25 DSC characterization of alkylated polymer

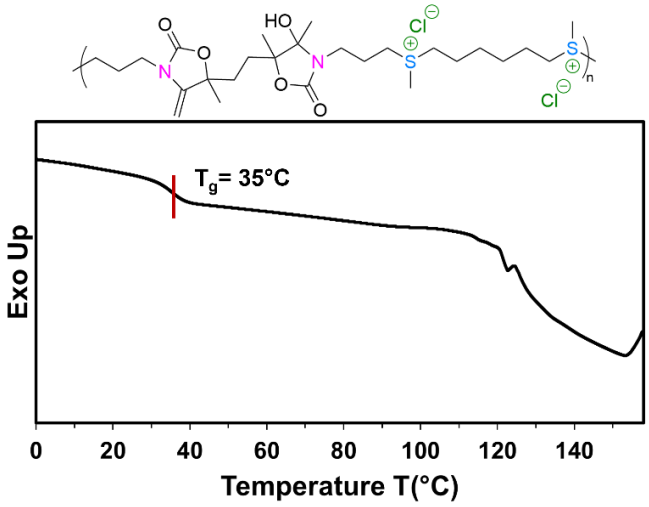

Figure S141. DSC trace of P2b-Sulfonium

Chapter 3. Non-Isocyanate Polyurethanes (NIPU)s Foam to Foam Recycling

Maliheh Razavi-Esfali, Marta Ximenis ,Gabriel Perli, Bruno Grignard, Christophe Detrembleur*, Haritz Sardon*

Abstract

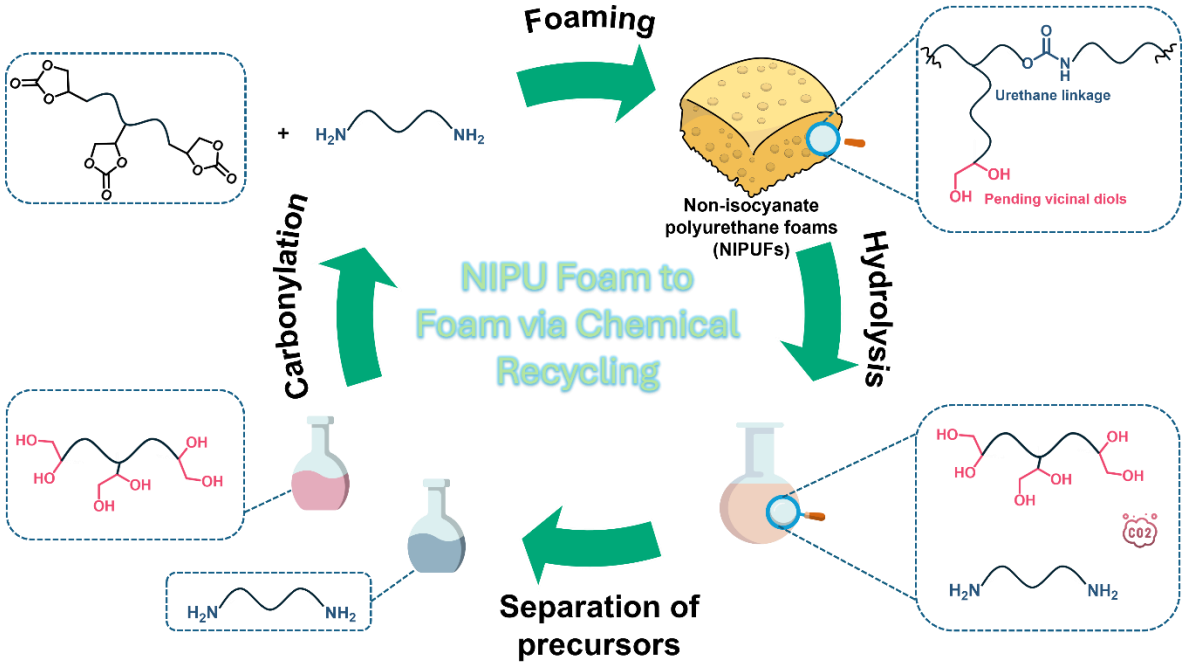

This study presents an efficient strategy for the chemical recycling of non-isocyanate polyurethane foams (NIPUFs) of the polyhydroxyurethane type through hydrolytic depolymerization under both alkaline and acidic conditions. Complete degradation of urethane linkages was achieved at 80 °C using 5 M NaOH and 5 M H_2SO_4 within 10 and 8 hours, respectively. NMR and FTIR analyses confirmed full bond cleavage and enabled the successful recovery of polyglycerol (PG) and diamine compounds (EDR-148 and *m*-XDA) with high purity and good yields. Remarkably, the depolymerization proceeded under significantly milder conditions compared to those required for conventional polyurethane recycling. PG was further valorized via a two-step carbonylation with dimethyl carbonate (DMC), yielding polyglycerol carbonate (PGC) with a cyclic carbonate functionality of 1.9-2.1. While PGC alone could not reproduce foams with native properties, its combination with virgin TMPTC enabled the fabrication of second-generation NIPUFs (r-NIPUFs) containing up to 63% recycled content. These r-NIPUFs retained comparable morphology, gel content, and thermal stability to the original materials. Overall, this work demonstrates a viable closed-loop recycling approach for NIPUFs and highlights the potential of small molecule recovery and reuse to advance circular economy practices in polyurethane chemistry.

1 Introduction

Polymeric foams are low-density materials consisting of a polymeric matrix incorporating a gaseous phase [1]. They are widely used across various application areas due to their ability to lower the total weight of products while allowing customization of mechanical and functional properties to meet particular requirements [2]. Among all the produced foams, polyurethane foams (PUFs) are extensively utilized across various industrial sectors, such as automotive, construction, packaging, medical devices, thermal insulation, cushions, furniture, and more. Their global market is projected to grow from USD 49.5 billion in 2023 to USD 67.8 billion by 2028 [3]. The broad usage of PUFs is attributed to their outstanding mechanical, thermal, and electrical properties, ease of processing, and low thermal and electrical conductivity [4]. These PUFs can be produced using either physical or chemical blowing agents. Physical blowing agents, such as cyclopentane and hydrofluorocarbons (HFCs), promote foam expansion through volatilization, an endothermic process [5]. In contrast, chemical blowing agents like water generate carbon dioxide via a reaction with isocyanates, resulting in foam expansion through an exothermic reaction [6]. The blowing agent, carbon dioxide (CO_2), is in-situ produced through the partial hydrolysis of sacrificial isocyanates during the formation of the PU matrix, ultimately resulting in self-blown PUFs **(Scheme 1A)**. In addition to gas formation, the hydrolysis produces amines, which further react with isocyanates to form urea linkages. These urea linkages significantly influence the properties of the PU network and impact its end-of-life management [7]. Moreover, secondary reactions involving the formation of biuret and allophanate linkages occur, leading to covalent cross-linking within the polymer matrix. Achieving the correct balance between these primary and secondary reactions is critical, as it governs the foam stability and enables the development of PUFs with tailored physical and mechanical properties [8].

Despite their numerous benefits, PUs face environmental, health, and legislative concerns that have been the subject of extensive research over the past decade. First, most PUs are derived from petroleum-based materials [9]. Second, most chemicals involved in PU synthesis, including isocyanates and dibutyltin dilaurate (DBTDL) -one of the most widely used catalysts for PU synthesis- are considered toxic even at low concentrations or upon inhalation. In certain cases, isocyanates may also be classified as carcinogenic, mutagenic, or reprotoxic (CMR) substances [10]. Additionally, they are industrially produced from highly toxic and hazardous reagents like phosgene, a gas that causes lung irritation and can be fatal when inhaled at

concentrations exceeding 4 ppm [11, 12]. Third, at the end of their lifespan, PUs are primarily disposed of through incineration or landfilling, leading to unfavorable environmental consequences, including land resource depletion and the release of toxic compounds and greenhouse gases. To date, post-consumer PU recycling is estimated to 5.5% [13-15].

Analysis of recycling strategies for PUFs indicates that thermoset PUs cannot be thermally reprocessed due to the high degree of cross-linking. Indeed, existing mechanical recycling methods for flexible foams are inadequate for handling current waste volumes. For example, compression molding yields PU materials of lower quality, resulting in limited market demand [13, 16]. An alternative strategy to improve the sustainability of PU production is chemical depolymerization. In principle, polymers with backbones linked by C-O and C-N bonds exhibit relatively low reaction barriers and nearly neutral reaction-free energies, making them suitable for chemical depolymerization. Consequently, the depolymerization of PUFs has been investigated through hydrolysis [17-19], acidolysis [20-24], glycolysis [25-28], and aminolysis [29-31]. This process allows for the partial recovery of polyols, which can be reused in the production of recycled PUs. In one study, a low-pressure superheated steam hydrolysis system was developed for the chemical recovery of PU foam components (**Scheme 1A**) [18]. In this process, PU foam waste is introduced into a reaction chamber and exposed to dry superheated steam at atmospheric pressure, with operating temperatures ranging from 232 °C to 316 °C. Under these conditions, the polyol fraction is released, separated from the reaction zone in a dry form, and directly reused without further purification. Meanwhile, the isocyanate moieties are hydrolyzed to corresponding diamines, which are extracted from the condensate. These diamines were discarded, as they could not be vaporized or easily reintegrated into the recycling loop. The recycled polyol was successfully used to produce new PU foams containing up to 20 wt% of reclaimed material.

While these recycling methods provide a renewed purpose for materials that would otherwise be discarded through incineration or landfilling, they are not truly circular, as they generate a secondary feed of inferior quality. Additionally, conventional PUFs present significant challenges due to the high reactivity of polyisocyanates, which lead not only to the formation of urea groups, but also allophanate, biuret, and isocyanurate linkages [32, 33]. Compared to urethane bonds, these thermodynamically stable groups are less susceptible to chemical cleavage. Additionally, commercial PUF formulations are highly complex, containing surfactants, flame retardants, UV stabilizers, and fillers, which further complicate chemical depolymerization [33]. Moreover, as most commercial flexible PUF products are composed of

co-polymers that often include various isocyanates and polyols, separating these components after depolymerization poses a greater challenge than identifying a suitable depolymerization method [24]. Also, in the hydrolysis of conventional PUFs, the recovered diamines need to be converted into isocyanates through a phosgene-based process, reducing its feasibility for true sustainability. Consequently, most studies on the chemical degradation of PUFs focus on depolymerizing PU rather than developing next-generation polymers from recycled monomers [13, 17].

These incentives are driving a renewed effort in both industry and academic sectors to **(1)** reconsider the production of PUs through an isocyanate-free approach, ideally utilizing raw materials derived from bio-renewable sources and/or gaseous waste emissions such as CO_2, and **(2)** to investigate the end-of-life recovery and recycling of these materials [34]. Within the framework of the production, poly(hydroxyurethane)s (PHUs) belong to the class of non-isocyanate polyurethanes (NIPUs) and are emerging as some of the most promising environmentally friendly alternatives to traditional PUs. They are synthesized through the copolymerization of polyamines with polycyclic carbonates, some of which originate from biobased and/or CO_2 sources [35-38]. When considering NIPU foams (NIPUFs), pioneering works exploited physical blowing agents such as supercritical CO_2 and solkane [39, 40], as well as chemical blowing agent such as citric acid combined with bicarbonate or reactive siloxanes [41, 42]. However, designing CO_2 self-foaming NIPU formulations mimicking the blowing process of conventional PUFs has required extensive research. To address this challenge, recent breakthrough discoveries have exploited the S-alkylation of cyclic carbonate monomers [43-46] or the hydrolysis of sacrificial cyclic carbonates to generate in-situ CO_2 as the blowing agent [47]. These innovative and straightforward chemistries enable the scalable manufacturing of NIPUFs based on aliphatic and aromatic amines, which feature minimal urea linkages and primarily urethane groups, opening perspectives for chemical depolymerization [48].

Despite extensive research on the synthesis of NIPUFs, their recyclability has remained largely unexplored. To date, only the work of Sternberg et al. [49] has reported a chemical recycling strategy for lignin-based NIPUFs using alkaline hydrolysis and ethylene glycol-assisted hydroglycolysis. By treating crushed foams with 0.1 M KOH, with or without 10% ethylene glycol (EG), at 200–220 °C, they selectively depolymerized the NIPU matrix and recovered lignin with up to 93% yield. Structural analyses confirmed EG insertion into lignin, enhancing its hydroxyl functionality and solubility for reuse. While the process focused on lignin recovery

rather than full monomer recovery, the upgraded lignin was successfully recycled into new NIPUFs with properties comparable to the originals. Additionally, the only reported downcycling strategies exploit the covalent adaptable network properties of PHUs, and rely on transcarbamoylation reactions and reversible urethane linkages formation to repurpose NIPUFs into films [45, 50]. The films obtained from downcycled NIPUFs can only be mechanically recycled a limited number of times due to progressive degradation of material properties, reduced dynamic bond efficiency, and accumulation of structural defects [51]. These factors collectively compromise performance and recyclability, making this strategy an incomplete solution that falls short of true closed-loop recycling. Additionally, studies on transcarbamoylation in PUs indicate that although this reaction facilitates recycling, the efficiency decreases over multiple cycles, limiting the material's reusability [52].

Thus, the opportunity for creating recycled NIPUFs materials with properties similar to the native foams is still unexplored. This represents a significant challenge regarding the recycling scenario of conventional PUFs for which the proportion of recycled material integrated into new formulations is often quite low (10-50%) [22, 53]. Overcoming these limitations is crucial for advancing truly sustainable and circular PU recycling techniques.

In this study, our goal is to design and chemically recycle CO_2 self-blown NIPUFs of the PHU-type through an efficient methodology employing hydrolysis under mild reaction conditions. Then, we will revalorize the decomposition products within a closed-loop process to reform new NIPUFs with analogue properties to the native materials. To examine this concept, we synthesized NIPUFs using the previously reported water-induced self-blowing strategy mimicking the foaming of conventional PUFs [47]. We next employed base- and acid-catalyzed hydrolysis of foams, achieving complete depolymerization under mild reaction conditions **(Scheme 1B)**. After isolation, purification and post-modification, these recyclates were effectively employed to regenerate NIPUFs demonstrating the feasibility of a more sustainable, closed-loop recycling process.

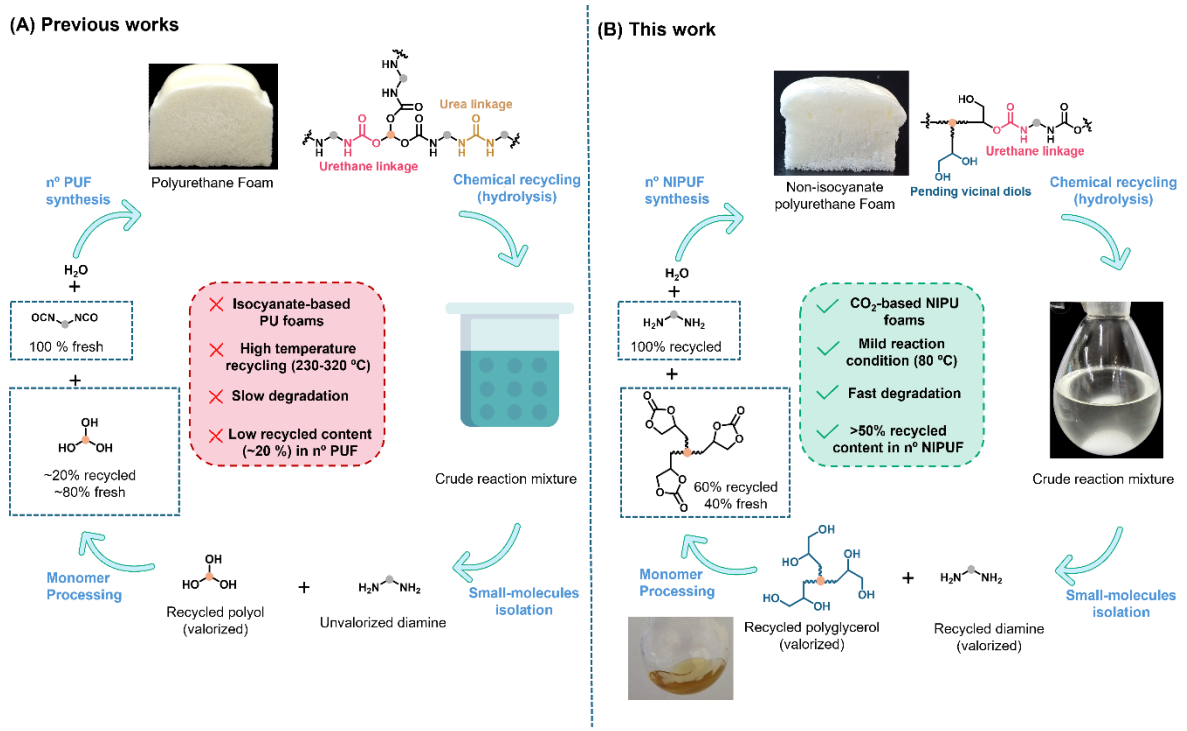

Scheme 1. Comparison of hydrolysis recycling cycles for (A) conventional isocyanate-based PUFs adapted from [18] and (B) CO_2-based NIPUFs. (A) Traditional PUF synthesis relies on isocyanates, requires high processing temperatures, degrades slowly, and results in limited recyclability (~20 % recycled content). (B) In contrast, NIPUFs are synthesized via CO_2-based chemistry under mild conditions, allowing for rapid degradation and significantly improved recyclability (>50% recycled content).

2 Experimental section

2.1 Materials

Trimethylol propane triglycidyl ether (TMPTE, Ipox Chemicals), *m*-Xylylene diamine (*m*-XDA, Sigma Aldrich, 99%), 1,2-Bis(2-aminoethoxy)ethane (EDR 148, TCI, >98%), tetrabutylammonium iodide (TBAI, Sigma Aldrich, 99%), 1,8-Diazabicyclo[5.4.0]undec-7-ene (DBU, Sigma Aldrich, 98%), Hydrotalcite ($Mg_6Al_2(CO_3)(OH)_{16}\cdot 4H_2O$, Sigma Aldrich), Sodium hydroxide (NaOH, Sigma Aldrich), Potassium hydroxide (KOH, Sigma Aldrich), 1-butanol (Sigma Aldrich, 99.9%), Dimethyl carbonate anhydrous, (DMC, Sigma Aldrich, ≥99%), Sulfuric acid (H_2SO_4, Sigma Aldrich, 95-98%), Diethyl ether (99%, Thermo Scientific), Toluene (Sigma Aldrich, 99.7%), Potassium carbonate (K_2CO_3, Thermo Scientific, anhydrous, 99%), Methanol (Thermo Scientific), Dichloromethane (DCM, 99%, Thermo Scientific).

2.2 Synthesis of trimethylolpropane tri-cyclic carbonate (TMPTC)

Trimethylolpropane triglycidyl ether (TMPTE, 20 g, 66 mmol) and tetrabutylammonium iodide (610 mg, 0.91 mmol) were introduced into an 80 mL high-pressure reactor. The system was equilibrated at 80 °C under 100 bar of CO_2 and stirred for 16 h. After completion, the reactor was depressurized, and the product was collected. Residual CO_2 was subsequently removed under vacuum at 60 °C for 16 h. The complete conversion of epoxide groups into cyclic carbonates was confirmed by ^{1}H-NMR spectroscopy in DMSO-d_6, evidenced by the disappearance of epoxide signals at 3.09, 2.72, and 2.54 ppm and the emergence of new resonances between 4.2 and 5.0 ppm, corresponding to the cyclic carbonate structure (**Fig. S1**). The process effectively yielded TMPTC functionalized with ~2.64 cyclic carbonate groups as evidenced by ^{1}H-NMR spectroscopy (**Fig. S2**).

2.3 Synthesis of non-isocyanate polyurethane foams (NIPUFs)

The foams were synthesized following a previously reported procedure [47]. For the preparation of EDR-based foams (denoted as **NIPUF-A**), TMPTC (5 g, 5CC = 30.38 mmol, 2.64 5CC per molecule), water (620 mg, 34.45 mmol), DBU (260 mg, 1.7 mmol), and EDR 148 (1.9 g, NH_2 = 25.7 mmol) were stepwise added into a square silicone mold (S = 16 cm^2). The mixture was stirred at room temperature for 1 min until a homogeneous mixture was obtained. The mixture was then placed in a preheated oven at 100 °C for 3 h. After cooling to room temperature, the foam was demolded and stored under ambient conditions. Foams based on aromatic diamine, *m*-XDA (denoted as **NIPUF-B**), were synthesized using the same procedure but with an adjusted composition consisting of TMPTC (5 g, 5CC = 30.38 mmol, 2.64 5CC per molecule), water (155 mg, 8.6 mmol), DBU (260 mg, 1.7 mmol), and *m*-XDA (1750 mg, NH_2 = 25.7 mmol). For hydrotalcite-embedded foams, TMPTC (5 g, 5CC = 30.38 mmol, 2.64 5CC per molecule) and hydrotalcite (600 mg) were sequentially added into an open square silicone mold (S = 16 cm^2). The mixture was stirred at room temperature for 1 min until an even, viscous mixture was formed. The rest of the reagents were added following the same method as described earlier. The formulation was subsequently heated at 100 °C for 3 h, cooled to room temperature, demolded, and stored under ambient conditions. All NIPUFs were

characterized by their chemical and thermal properties, as detailed in the SI, sections 6.3 and 6.4.

2.4 Hydrolysis of NIPUFs

For alkaline hydrolysis, 3.7 g of foam (cut into small cubes) was placed in a 500 mL round-bottom flask, followed by the addition of 150 mL of 5M NaOH solution. The mixture was stirred at 80 °C for 10 h. Similarly, for acidic hydrolysis, 3.7 g of foam (cut into small cubes) was placed in a 500 mL round-bottom flask with 150 mL of 5M H_2SO_4 solution. This mixture was stirred at 80 °C for 8 h. The reaction mixtures were lyophilized and characterized by ^1H NMR and FTIR spectroscopy (see **Fig. S15** and **Fig. 2D** and **Fig. S36-S37**).

2.5 Recovery of high-value products

2.5.1 Isolation of recyclates from NIPUF-A

Following the depolymerization of **NIPUF-A**, the reaction mixture was neutralized through the addition of H_2SO_4 solution (96%) until the pH reached 6. Polyglycerol (**PG**) was separated from the aqueous medium via liquid-liquid extraction using 1-butanol. Four sequential 200 mL extractions were performed to maximize the recovery yield of **PG** (see section 6.5.2 of SI for detailed explanation). The collected organic phases were dried over anhydrous magnesium sulfate ($MgSO_4$), filtered, and concentrated under reduced pressure to yield a pale-yellow oil (75% isolated yield, 1.53 g). The isolated precursor was characterized by ^1H and ^{13}C NMR and FT-IR spectroscopies (see **Fig. S17-S19**). The remaining aqueous phase was treated to isolate the diamine, EDR 148. Initially, approximately 0.5-1 g of KOH was added to the mixture and stirred for 1 h to deprotonate the diamine. Water was subsequently removed under reduced pressure using a rotary evaporator, yielding a concentrated residue. This residue was then mixed with 30 mL of diethyl ether and stirred for 2 h to extract the free diamine into the organic phase. The ether layer was dried over anhydrous $MgSO_4$, filtered, and concentrated, affording EDR 148 with a yield of 20% (190 mg). As a portion of the diamine was carbonated during the depolymerization process, the undissolved residue (retained on the filter)- corresponding to the remaining salt and amine-CO_2 carbamate- was refluxed in toluene for 3 h. After cooling, the

mixture was filtered and concentrated under vacuum, resulting in a light-yellow liquid (390 mg, 41% yield). The combined isolated yield of EDR 148 was 61% (579.5 mg). The product was characterized by ^{1}H and ^{13}C NMR spectroscopy (see **Fig. S20-S22**).

2.5.2 Isolation of recyclates from NIPUF-B

Depolymerization of **NIPUF-B** resulted in the formation of a two-phase solution (**Fig. S23**), with an upper yellow oil in the water phase, which was identified as an *m*-XDA carbamate salt formed via reaction of XDA with CO_2 (**Fig. S24**). This phase was separated from the reaction mixture by decantation, washed, dried and was characterized by ^{1}H and ^{13}C, COSY, HSQC, and HMBC NMR spectroscopy and FT-IR (see **Fig. S25-S30**). The remaining solution was neutralized to pH 4 by continuous addition of H_2SO_4 (96%). Like **NIPUF-A**, **PG** was selectively extracted from water by using four portions of 200 mL 1-butanol. The combined organic layers were dried over anhydrous $MgSO_4$, filtered, and concentrated under reduced pressure to yield **PG** (56% isolated yield, 1.14 g). The remaining aqueous phase was treated with an excess of KOH (~ 0.5-1 g) to deprotonate the *m*-XDA. Liquid-liquid extraction was then performed using dichloromethane (DCM) to selectively isolate the neat diamine. The organic phase was dried over $MgSO_4$, filtered, and concentrated under reduced pressure to yield purified *m*-XDA (30% isolated yield, 262 mg) and was characterized by ^{1}H and ^{13}C NMR spectroscopy (see **Fig. S31-S33**).

2.6 Isolation of recyclates from NIPUF-C and NIPUF-D

After the decomposition of NIPUFs synthesized with hydrotalcite as a filler (**NIPUF-C** and **NIPUF-D**), the reaction mixture became opaque due to the presence of insoluble hydrotalcite (see **Fig. S34**). Upon cooling to room temperature, the mixture was filtered to separate the hydrotalcite, which was then dried under vacuum at 40 °C for 8 h. The isolation yield of hydrotalcite exceeded 98%. The rest of the isolation steps and pathways remained identical to those observed for NIPUFs without fillers.

2.7 Synthesis of polyglycerol carbonate (PGC)

In a 50 mL round-bottom flask equipped with a magnetic stirrer and a reflux condenser, 1.5 g of branched polyglycerol (4.2 mmol, 1 equiv. of **PG** molecules; corresponding to 0.025 mol of hydroxyl groups, 6 OH per molecule, (OH index: 935 mg KOH/g)) was added. To this, dimethyl carbonate (DMC) (3.78 mL, 42 mmol, 10 equiv.), methanol (1 mL, 0.025 mol, 8 equiv.), and potassium carbonate (K_2CO_3, 4.5 mg, 0.3 wt.%) were introduced. The reaction mixture was stirred at 60 °C for 18 h under reflux. After 18 h, a small aliquot of the crude reaction mixture was withdrawn and analyzed via ^{1}H NMR spectroscopy (**Fig. S38-S39**), confirming the conversion of hydroxyl groups into cyclic carbonates. After this initial step, the reaction achieved a cyclic carbonate (CC) functionality of approximately 1.57 (see **Fig. S39**), with the partly modified **PG** becoming fully soluble in DMC. To further increase CC functionality, an excess of DMC (14.1 mL, 168 mmol, 40 equiv.), and TBD as a catalyst (29.2 mg, 0.21 mmol, 0.05 equiv.) was added to the reaction mixture. The temperature was maintained at 60 °C, and the reaction was conducted for an additional 4 h at the rotary evaporator at 500 mbar to facilitate the continuous removal of methanol. After completion, the final product exhibited a CC functionality of 1.9-2.1, as confirmed by ^{1}H NMR analysis (**Fig. S40**). Then, the excess DMC was recovered under rotary evaporation. The remaining residue was dissolved in 20 mL of dichloromethane (DCM), and the mixture was filtered to remove the catalyst. The solvent was then evaporated under reduced pressure, yielding a brownish liquid as the final product (87% isolated yield, 1.6 mg). The purified polyglycerol carbonate (**PGC**) was characterized using ^{1}H and ^{13}C NMR and FTIR spectroscopy to confirm the successful incorporation of CC groups (see **Fig. S40-S42** and **Fig. 5C** & **5D** and **Fig. 6**).

2.8 Non-isocyanate polyurethane foams from recycled monomers (NIPUF-R)

The second-generation of NIPUFs (NIPUF-R) were synthesized from the recycled monomers following modification of the previously reported procedure. For the preparation of EDR-based foams, TMPTC (2.31 g, 5CC =14.03 mmol, 2.64 5CC per molecule), recycled PGC (3.5 g, 5CC= 16.11 mmol, 1.9-2.1 5CC per molecule), water (620 mg, 34.45 mmol), DBU (260 mg, 1.7 mmol), and EDR 148 (1.9 g, NH_2 = 25.7 mmol) were sequentially added into a square

silicone mold (S = 16 cm^2). The mixture was stirred at room temperature for 1 min until a homogeneous consistency was obtained. The formulation was then placed in a preheated oven at 100 °C for 3 h. After cooling to room temperature, the foam was de-molded and stored under ambient conditions. The **NIPUF-R** were analyzed using FT-IR spectroscopy (**Fig. 7C**) and thermal properties to confirm their native-like properties (see section 6.11 of SI).

3 Results and Discussion

3.1 NIPUFs synthesis

NIPUFs were first synthesized using a water-induced CO_2 self-foaming formulation composed of TMPTC, diamines, water, and DBU as the catalyst. Initially, foams were synthesized without any filler. The foaming and curing were conducted at 100 °C for 3 h, employing a previously developed method [47] (**Fig. 1A**). During the foaming process, hydroxy-urethane linkages formed through the aminolysis of cyclic carbonate groups. At the same time, water hydrolyzed the cyclic carbonates, generating vicinal diol groups and releasing CO_2, which acted as the blowing agent. This foaming method was selected as it somehow mimics the self-foaming of conventional PUFs. Two distinct NIPUFs were synthesized using different diamines: EDR 148 was used as aliphatic diamine (the foam was denoted as **NIPUF-A**) and *m*-XDA was used as aromatic diamine (the foam was denoted as **NIPUF-B**), both synthesized without the addition of clays or surfactants. The two resulting NIPUFs were uniform with open-cell structures and cell sizes averaging 2 mm (**Fig. 1B** and **1C**). They also displayed similar densities of 191 kg/m^3 for **NIPUF-A** and 179 kg/m^3 for **NIPUF-B (Table 1)**. To further enhance foam homogeneity and reduce cell size, a synthetic clay was subsequently incorporated into the formulation. Hydrotalcite has been shown to promote nucleation, improve foam uniformity, and decrease cell size [47]. Additionally, its presence increases the viscosity of the prepolymer mixture, facilitating better gas entrapment and resulting in a more uniform and stable foam structure. Subsequently, **NIPUF-C** and **NIPUF-D** were synthesized using EDR 148 and *m*-XDA as the diamine components, respectively, and incorporating 12 wt% (relative to TMPTC) of hydrotalcite. The remainder of the synthesis followed the same procedure described above. The properties of the foams are summarized in **Table 1** and section 6.3 and 6.4 of SI. As shown in **Fig. 1**, with hydrotalcite present (**Fig. 1D** and **1E**), the cell morphology becomes distinctly finer and more uniform compared to foams without filler (**Fig. 1B** and **1C**), validating its

function in improving foam architecture without affecting too much the foam density (241 kg/m^3 for **NIPUF-C** and 186 kg/m^3 for **NIPUF-D (Table 1)**).

Moreover, the gel content above 92%, in combination with FT-IR spectra (**Fig. S3–S6**), provides clear evidence of the successful formation of the PHU network in all foams. Finally, the thermal properties of the NIPUFs equilibrated under ambient atmosphere for 48 h were characterized by DSC and TGA (**Table 1**). **NIPUF-A** showed a T_g of 1 °C that increased to 27 °C for **NIPUF-B**. As expected, the T_g's of dried materials- to eliminate moisture that plasticize the foam [54, 55]- increased to 3.5 °C and 38 °C, respectively for **NIPUF-A** and **NIPUF-B**. The incorporation of hydrotalcite into the foam formulation resulted in a decrease in the T_g of the foams and **NIPUF-C** showed a T_g of -13 °C and **NIPUF-D** of 17 °C. All foams demonstrated excellent thermal stability, with a 10% weight loss temperature ($T_{deg,10\%}$) above ~250 °C **(Table 1)**.

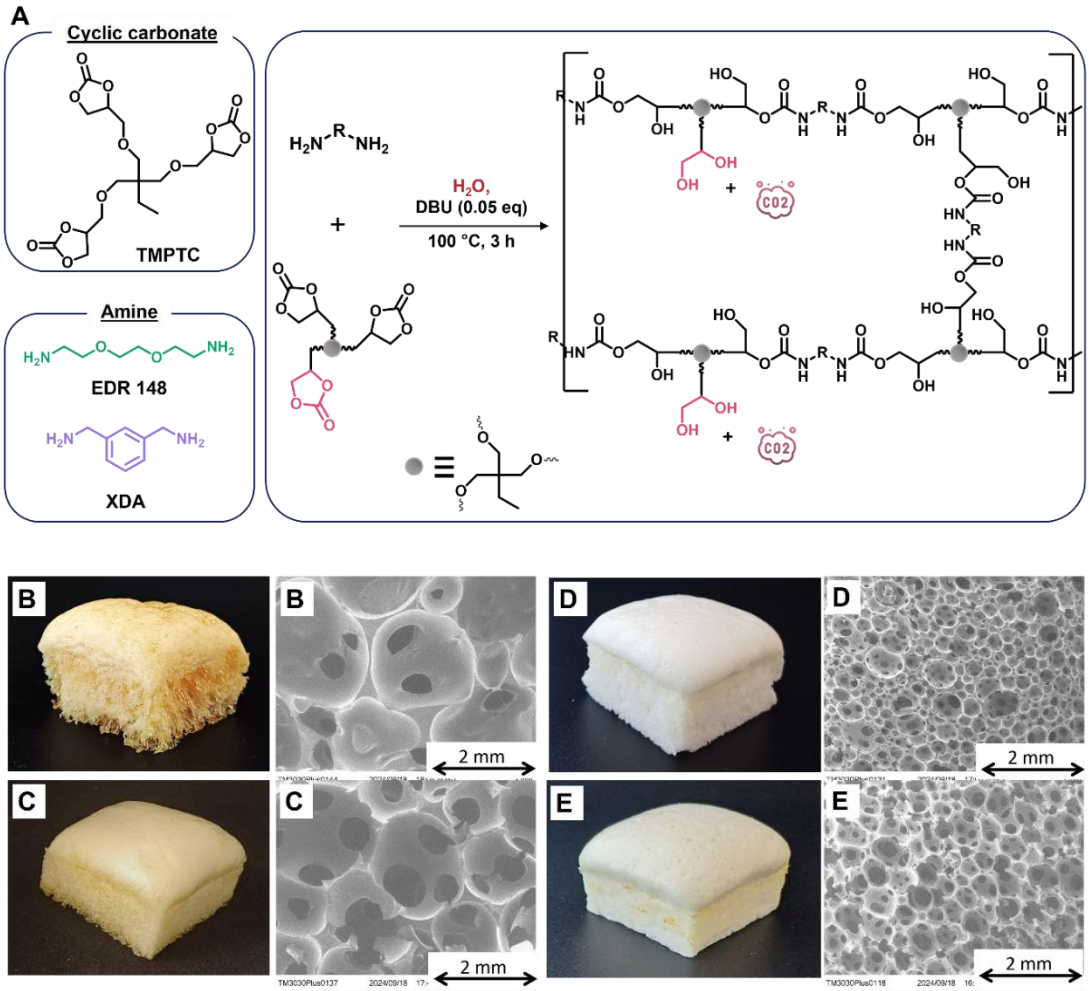

Fig. 1. (A) Reaction pathway illustrates the synthesis of NIPUFs from cyclic carbonates and different amines. Visual and SEM characterizations of the resulting foams: (B) **NIPUF-A**, (C) **NIPUF-B**, (D) **NIPUF-C**, and (E) **NIPUF-D**.

Table 1. Properties of water-induced self-blown NIPUFs.

Entry	Foam	Amine	Hydrotalcite (*vs* TMPTC)	Density [kg.m^{-3}]	Gel content [%]	T_g/T_g dried [°C]	$T_{deg,10\%}$ [°C]	Compression Modulus [MPa]
1	**NIPUF-A**	EDR 148	-	191 ± 10	92 ± 2	1/3	249	0.03 ± 0.01
2	**NIPUF-B**	*m*-XDA	-	179 ± 21	93 ± 3	27/38	260	7.48 ± 0.9
3	**NIPUF-C**	EDR 148	12 wt%	241 ± 30	98 ± 2	-13/-6	254	0.037 ± 0.006
4	**NIPUF-D**	*m*-XDA	12 wt%	186 ± 40	97 ± 1	17/30	268	8.25 ± 1.05

The mechanical resistance of the four equilibrated foams was evaluated by compression testing (**Fig. 2, Table 1**). It should be emphasized that the foams exhibited different densities, and therefore their mechanical properties cannot be directly compared. However, the foams prepared with *m*-XDA, which had the lowest densities (179 and 186 kg·m^{-3}) and more rigidity, displayed higher compression modulus of 7.48 MPa and 8.25 MPa. In contrast, the foams synthesized with EDR-148 showed significantly lower values of 0.03 MPa and 0.037 MPa, respectively.

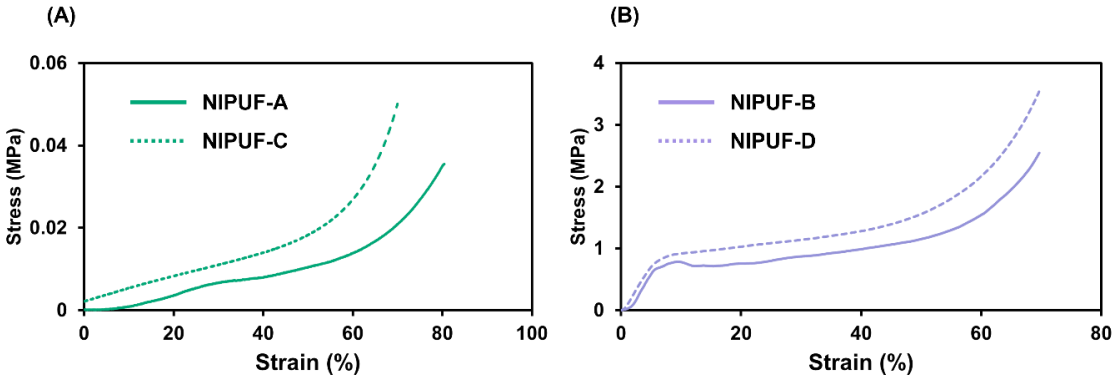

Fig. 2. Compressive curve of equilibrated foams (A) EDR-based foams; (B) *m*-XDA-based foams

Moreover, the thermomechanical properties of the synthesized NIPU foams were compared with two representative conventional PU foams (the characteristics of PUFs are summarized in **Table S1**, See Section 6.5 of the Supporting Information for more details on the comparison). Such comparisons should be interpreted with caution, since the formulations differ in terms of monomer structures, density, and cell morphology. Within these limitations, the thermal properties were found to be broadly comparable, whereas the mechanical properties of the rigid PU foam were significantly higher. This underlines a key challenge: while achieving highly rigid NIPU foams remains difficult at present, the preparation of flexible NIPUFs with

competitive performance is already much more straightforward, as also reflected in the present results and in other reports [56, 57].

3.2 Hydrolytic degradation of NIPUFs

Conventional PUs are prone to hydrolysis under alkaline or acidic conditions, further releasing polyols, amines and carbon dioxide [24, 58]. Capitalizing on these outcomes, hydrolysis was applied to the decomposition of NIPUFs. **NIPUF-A** was selected as a model foam to optimize the chemical depolymerization process. The foam was subjected to basic hydrolysis (**Table 2**). With the aim of developing a cost-effective and environmentally friendly process that avoids high temperatures, experiments were carried out at 80 °C. NaOH concentrations ranged from 1 to 5 M, with reaction times adjusted accordingly (**Table 2**). When the reaction was performed at 1 M NaOH, **NIPUF-A** exhibited an incomplete degradation, even after 24 h. This was shown by the presence of non-degraded pieces of foam in the reaction vessel. The extent of decomposition was quantified by weighing the remaining foam and estimated to ~90%. While increasing the NaOH concentration to 2 M reduced the amount of residual foam to ~5%, complete hydrolysis was still not attained. Contrarily, raising the NaOH concentration to 5 M resulted in complete foam decomposition within 10 h, indicating that the efficiency of hydrolysis is highly dependent on the base concentration. The images illustrating the decomposition of **NIPUF-A** at various hydrolysis durations are shown in **Fig. 3A**.

Table 2. Hydrolytic depolymerization conditions for NIPUFs.

Entry	Foam	Depolymerization condition			
		Solution	Concentration of solvent	Time (h)	Degree of degradation (%)[a]
1	NIPUF-A	NaOH	1M	24	90
2	NIPUF-A	NaOH	2M	24	95
3	NIPUF-A	NaOH	5M	10	100
2	NIPUF-B	NaOH	5M	10	100
3	NIPUF-A	H_2SO_4	5M	8	100
4	NIPUF-B	H_2SO_4	5M	8	100

[a]The chemical depolymerization of the foams were carried out in a round-bottom flask at 80 ºC.

Upon alkaline conditions, the hydrolysis of **NIPUF-A** proceeds via nucleophilic attack of the urethane linkages by hydroxide ions (OH^-). This reaction results in a transient carbamic acid intermediate, which undergoes spontaneous decarboxylation, generating EDR 148 with release of carbon dioxide, along with a polyglycerol (**PG**) (**Fig. 3B**).

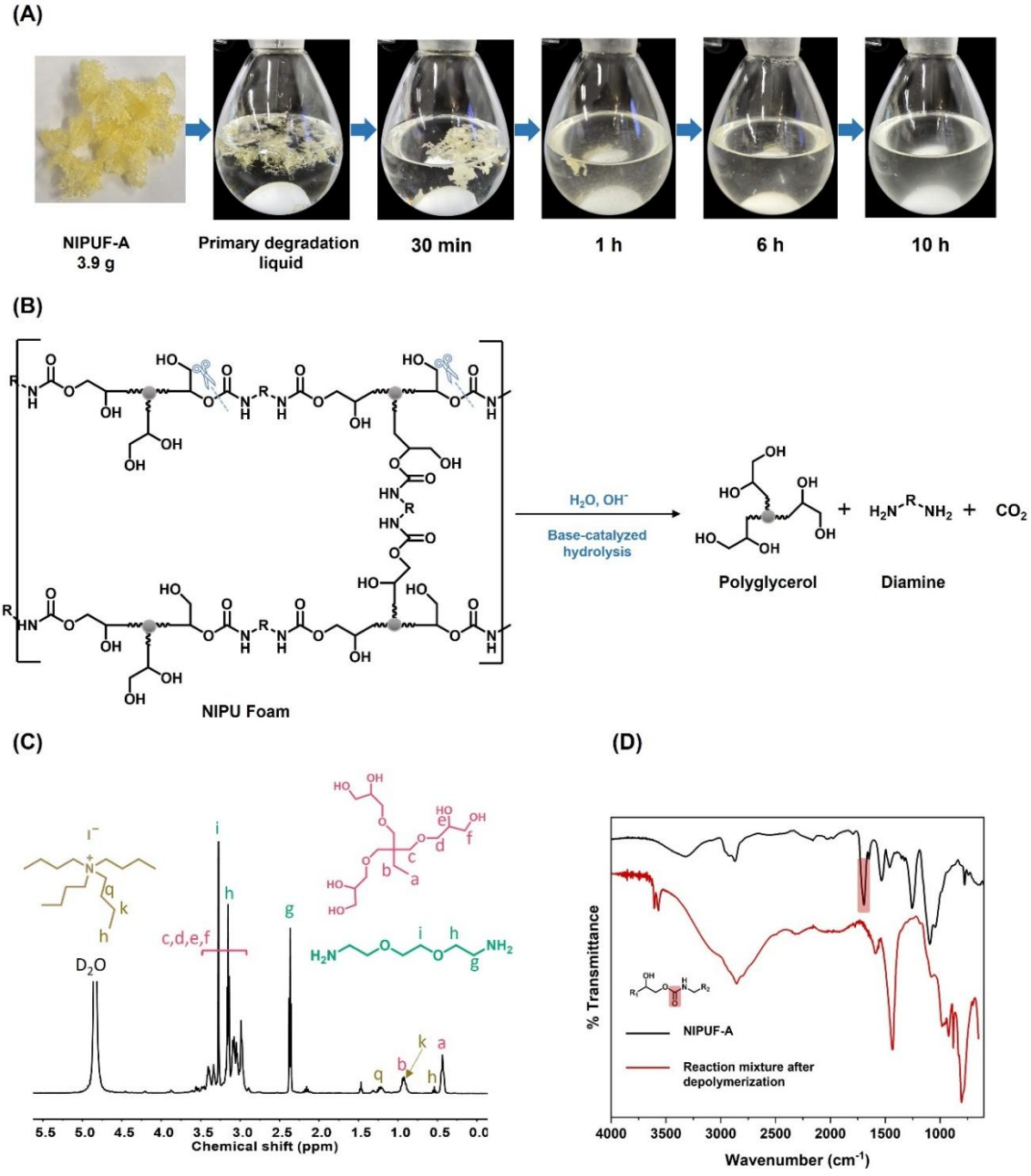

Fig. 3. (A) Time-lapse images of the depolymerization process of **NIPUF-A**; (B) Schematic illustration of selective urethane bond cleavage via base-catalyzed hydrolysis; (C) ^{1}H-NMR spectra (300 MHz, D_2O) of the crude reaction mixture after basic hydrolysis of **NIPUF-A**; (D) Comparative FTIR spectra of **NIPUF-A** and the lyophilized reaction mixture following hydrolysis.

To confirm the structure of the crude products formed after degradation, a small-scale hydrolysis experiment of **NIPUF-A** was performed in a 5 M NaOH solution using D_2O for 10 h. The crude reaction mixtures were then analyzed by ^{1}H-NMR spectroscopy (**Fig. 3C**). After complete decomposition, the ^{1}H-NMR spectra of the reaction mixtures presented the signals corresponding to **PG** and EDR 148, the signals of urethane linkages being no more detectable. For **PG**, the signal corresponding to the methyl group (CH_3-) at δ = 0.43-0.48 ppm, the ethyl group (CH_2-C) at δ = 0.92-0.96 ppm, and overlapping signals from ether linkages (CH_2-O) were detected at δ = 3.2-3.6 ppm. Moreover, the characteristic resonances associated with EDR 148 were detected, including signals at δ =2.37-2.43 ppm for terminal methylene groups (CH_2-NH_2) and at δ =3.15-3.17 ppm and δ =3.28-3.31 ppm for methylene protons adjacent to oxygens in the ether linkage (CH_2-O). Furthermore, residual tetrabutylammonium iodide (TBAI)- the catalyst employed to synthesize TMPTC from CO_2 and the corresponding epoxy precursor - was observed by the presence of specific peaks corresponding to methyl groups (CH_3-CH_2) at δ = 0.54-0.59 ppm, methylene groups (CH_2-CH_3) at δ = 0.92-0.96 ppm, and (CH_2-CH_2) at δ = 1.23-1.27 ppm. Since the polymers and oligomers containing urethane linkages are not soluble in water, the crude reaction mixture was lyophilized. The resulting material was then analyzed by ^{1}H-NMR in DMSO-*d*$_6$ (**Fig. S15**) and FTIR spectroscopy (**Fig. 3D**) to confirm the complete cleavage of urethane bonds. No resonances attributed to urethane linkages were detected in the ^{1}H-NMR spectra, and the characteristic urethane stretching frequencies were absent in the FTIR spectra.

Then, the degradation products were successfully separated and isolated using a stepwise procedure illustrated in **Fig. 4**. After adjusting the pH of the crude mixture to 6, **PG** was isolated with a yield of 75% via simple liquid-liquid extraction using 1-butanol. ^{1}H-NMR analysis confirmed the recovery of **PG** (**Fig. S16**) with a purity of 95%. Impurities consisted of residual TBAI that could be further removed by silica filtration (**Fig. 4A** and **Fig. S17-S19**). The remaining aqueous phase was then treated to isolate the diamine, EDR-148. First, the solution was basified to deprotonate the diamine, followed by water removal under reduced pressure using a rotary evaporator. After removing water, a residue containing Na_2SO_4 salt (formed after neutralization), excess of KOH, and EDR 148 remained. The resulting residue was mixed with diethyl ether and stirred for 2 h, then filtered and concentrated, affording free EDR-148 in 20% yield (190 mg). Since some of the diamine could have converted to carbamate salt during the process (as a result of the reaction of amine with CO_2), the residue retained on

the filter-comprising unextracted carbamate salt- was refluxed in toluene for 3 h to afford free EDR 148. After cooling, the mixture was filtered and concentrated under vacuum to yield a light-yellow liquid (390 mg, 41% yield). The overall isolated yield of EDR-148 was 61% (579.5 mg) (**Fig. S20-S22**). The comparison of ^{1}H-NMR spectra of the isolated and commercial EDR-148 confirms the purity of the recycled diamine (**Fig. 4B** and **Fig. S21**).

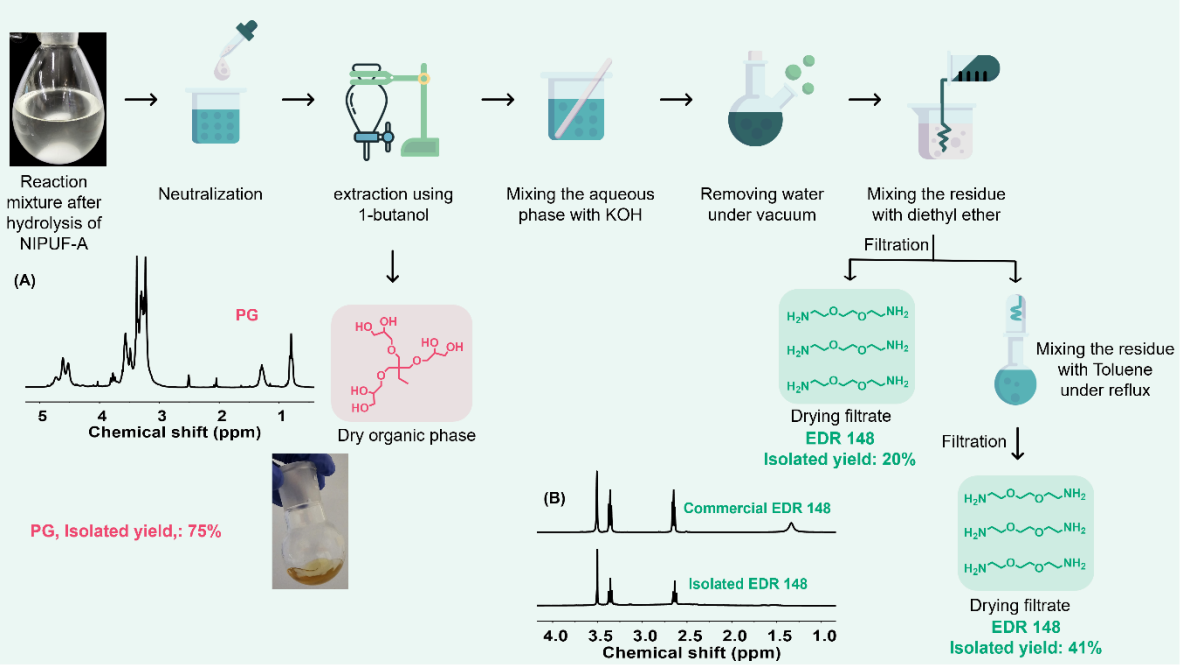

Fig. 4. Schematic representation of product isolation after depolymerization of **NIPUF-A**. The workflow comprises neutralization, phase extraction, reaction with KOH, solvent treatment, and final filtration and drying steps. The corresponding ^{1}H-NMR spectra are shown for (A) **PG**, and (B) an overlay of recycled and commercial EDR 148, recorded at 400 MHz in DMSO-d_6. *Full signal assignments and integrations are provided in ESI (Figures S17-S18 for **PG**, S20-S22 for EDR 148)*

Leveraging these outcomes, the degradation protocol of **NIPUF-A** was applied to **NIPUF-B** (5M NaOH, 80 °C, 10 h). The alkaline hydrolysis of **NIPUF-B** yielded a two-phase mixture, with a yellow viscous oil being immiscible to water (the reaction mixture is shown in **Fig. S23**). The crude oil was subsequently isolated and characterized using ^{1}H-NMR spectroscopy (**Fig. S24**). The characteristic signals corresponding to the free *m*-XDA (methylene protons adjacent to primary amine groups (CH_2-NH_2) at δ = 3.71-3.67 ppm), *m*-XDA carbamate salt (methylene protons adjacent to secondary amine groups (CH_2-NH) at δ = 4.14-4.32 ppm) and **PG** (methyl group (CH_3-) at δ = 0.76–0.85 ppm, the ethyl group (CH_2-C) at δ = 1.2–1.42 ppm) were observed. Because the crude oil was insoluble in water, it was repeatedly washed with water

to remove impurities, then dried under vacuum at 40 °C prior to characterization by NMR and FT-IR spectroscopy (**Fig. S25-S30**). The formation of *m*-XDA carbamate salt (**Fig. 5A**) was evidenced by resonances of the methylene adjacent to a carbamate group at δ = 4.21-4.28 ppm and further confirmed by ^{13}C by the presence of the carbonyl signal of the carbamate group at ~ 160 ppm (**Fig. S26**). The formation of *m*-XDA carbamate salt was further confirmed by COSY, HSQC, and HMBC NMR spectra (**Fig. S27-S29**). Additionally, as shown in **Fig. S30**, which presents the overlay of the FTIR spectra of *m*-XDA and its corresponding carbamate salt, a new band appeared in the 1520-1600 cm^{-1} region for the carbamate salt. This band is attributed to the carbamate anion.

After removal of the carbamate salt, the pH of the aqueous phase was adjusted to pH 4 and subjected to 1-butanol extraction, mirroring the procedure used for **NIPUF-A** (**Fig. 5**). The isolated yield of **PG** reached 56% (**Fig. 5B**). Then, the aqueous phase was basified and *m*-XDA further extracted by liquid-liquid extraction with DCM, leading to the recovery of pure amine with a yield of 30% and purity > 98% (**Fig. S31-S33**). The overlay of ^{1}H-NMR spectra in DMSO-d_6 of the isolated *m*-XDA and the commercial version confirms the purity of the recycled diamine (**Fig. 5C** and **Fig. S32**). The isolation yields of recovered monomers obtained after hydrolysis depolymerization of NIPUFs were summarized in **Table 3**.

In this work, we further explored the depolymerization of **NIPUF-C** and **NIPUF-D**, which contained hydrotalcite as a filler. After 10 h under basic condition, the foams were fully decomposed demonstrating that the presence of hydrotalcite did not hinder the depolymerization process (**Fig. S34** shows the image of reaction mixture after degradation). The hydrotalcite was simply recovered by filtration ((isolation yield >98%) see **Fig. S34**), leaving the remaining depolymerization products and pathways identical to those observed for NIPUFs without fillers. These results indicate that the clay filler does not significantly impact the breakdown kinetics or hinder monomer recovery.

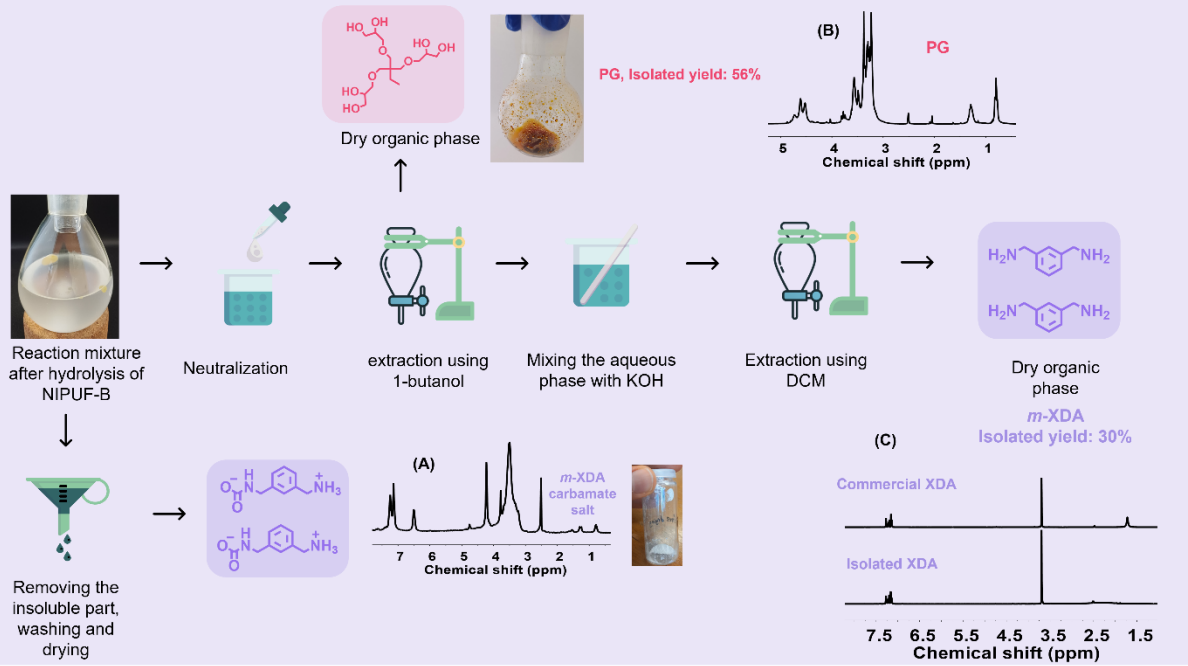

Fig. 5. Schematic representation of product isolation after depolymerization of **NIPUF-B**. The workflow comprises neutralization, phase extraction, reaction with KOH, solvent treatment, and final filtration and drying steps. The corresponding ^{1}H-NMR spectra are shown for (A) *m*-XDA carbamate salt, (B) **PG**, and (C) an overlay of recycled and commercial XDA, recorded at 400 MHz in DMSO-d_6. *Full signal assignments and integrations are provided in ESI (Figures S17-S18 for **PG**, S25-S29 for m-XDA carbamate salt, and S31-S33 for m-XDA).*

The NIPUFs decomposition was then examined via acid-catalyzed hydrolysis. The reaction was performed on both **NIPUF-A** and **NIPUF-B** at 80 °C replacing NaOH by a 5M H_2SO_4 solution. This process resulted in a slightly faster decomposition of 8 h. Both the foams based on aliphatic and aromatic diamines were fully decomposed, producing a homogeneous solution (the reaction mixture is shown in **Fig. S35**). To further confirm the complete depolymerization of urethane bonds, the crude reaction mixture was lyophilized to remove water, ensuring that the samples were suitable for analysis. The dried samples were then characterized by ^{1}H-NMR in DMSO (**Fig. S36** and **S37**). The absence of proton signals corresponding to urethane linkages in the ^{1}H-NMR spectra confirmed the complete hydrolysis of NIPUF.

The resulting degradation products were subsequently separated and isolated through a stepwise procedure. Initially, the reaction mixture was neutralized using NaOH pellets to achieve a pH of 6 for **NIPUF-A** and pH 4 for **NIPUF-B**. For **NIPUF-A**, once the neutralization step reached pH 6, the subsequent isolation steps followed the same procedure as in the base-catalyzed hydrolysis pathway. This included liquid-liquid extraction with 1-butanol, basification with an excess of KOH to deprotonate the diamine, and recovery of the amine by

diethyl ether extraction followed by reflux in toluene. However, the isolation yields for **PG** and EDR 148 were comparatively lower, at 42% and 30%, respectively. In the case of **NIPUF-B**, neutralization immediately led to the formation of an insoluble oily phase containing the carbamate salt, which was subsequently separated by decantation. These results indicate that under acidic conditions, amine protonation occurs more rapidly than CO_2 capture. However, upon increasing the pH and deprotonating the amines, the carbamate salt readily forms. After removing the carbamate salt, the remaining aqueous phase was subjected to the same isolation steps as the base-catalyzed hydrolysis method, yielding **PG** and *m*-XDA at 36% and 24%, respectively. These results underscore the effectiveness of both acid- and base-catalyzed approaches in facilitating the depolymerization of NIPUFs.

Table 3. Isolation yields of various monomers obtained after hydrolysis depolymerization of NIPUFs

Entry	Foam	Hydrolytic depolymerization	PG yield (%) [a]	Diamine yield (%) [a]
1	**NIPUF-A**	Base-catalyzed [b]	75	61
2	**NIPUF-B**	Base-catalyzed [b]	56	30
3	**NIPUF-A**	Acid-catalyzed [c]	42	30
4	**NIPUF-B**	Acid-catalyzed [c]	36	24

[a] Yield is the ratio of recovered precursor to initial precursor (in mol).

[b] reaction condition: 5 M NaOH, 80 ºC, 10 h

[c] reaction condition: 5 M H_2SO_4, 80 ºC, 8 h

3.3 Carbonation of polyglycerol into poly(glycerol-carbonate)

Recycled **PG** can be further converted into polyglycerol-carbonate (**PGC**) via reaction with a suitable carbonation agent in the presence of a catalyst. Direct carbonation of vicinal diols, alike those present in **PG**, with CO_2 presents an attractive route. However, Brege et al. pointed out significant limitations of this technique, including extensive side reactions and wastes generation, low selectivity, and poor isolation yields when metal-free dual activating systems were used [59]. As an indirect CO_2 valorization route, the transesterification of glycerol to glycerol carbonate using a carbonation agent - dimethyl carbonate - has been selected for the carbonation of **PG** (**Scheme 2**) [60]. The success of this reaction is highly dependent on several factors, including reaction temperature, time, molar ratio of reactants and solvent choice which impact both conversion and selectivity of the reaction [61].

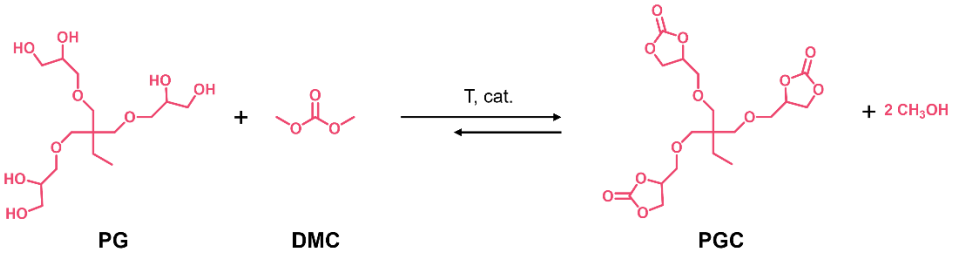

Scheme 2. Schematic representing the synthesis of polyglycerol carbonate (**PGC**).

To investigate the conversion of **PG** into **PGC**, various reaction conditions and parameters were systematically examined, as summarized in **Table S2**. Crude reaction mixtures were analyzed by ^{1}H-NMR spectroscopy to determine the cyclic carbonate (CC) functionality. Initially, a widely used literature approach was attempted, utilizing dimethyl carbonate (DMC) as the carbonylation agent and potassium carbonate (K_2CO_3) as the base catalyst [62]. However, a major challenge was the poor solubility of **PG** in DMC. It was observed that without using a solvent, **PG** became soluble in DMC only after 72 h at 60°C, achieving a CC functionality of 1.5-1.6 (**Table S2**, entry 1). A possible explanation for this limited conversion is that, In conventional glycerol carbonate synthesis, the reaction equilibrium Is driven toward product formation by continuously removing methanol as a by-product [63]. However, the limited initial solubility of **PG** in DMC prompted us to introduce methanol as a co-solvent to enhance **PG** solubility and shorten the reaction time. While this modification allowed the reaction to proceed under homogeneous conditions, the presence of methanol hindered the full carbonation of **PG**, resulting in CC functionality of 1.5 after 18 h of reaction at 60 °C (**Table S2**, entry 2). Further increasing the reaction temperature to 80 °C exacerbated this effect, leading to a significant drop in CC functionality to 0.43 (**Table S2**, entry 3). Methanol was also replaced with alternative solvents, including 1-butanol and 1-methylimidazole, to improve the carbonation efficiency. However, the CC functionality remained low, reaching only 0.65 and 1.4, respectively (**Table S2**, entries 4 and 5). Furthermore, diphenyl carbonate (DPC) was chosen as an alternative carbonyl source using different catalysts (DBU, $MgCl_2$, NaO^tBu) at 100 °C. ^{1}H-NMR of crude reaction mixture confirmed the highest CC functionality of 2 when TBD was used as a catalyst compared to $MgCl_2$ and NaO^tBu (**Table S2**, entries 6-8 and **Fig. 6A**). The use of DPC Improved cyclic carbonate functionality but presents some concerns, primarily the formation of phenol by-product that is hard to remove and raises environmental issues. To address these challenges, inspired from a research by Meier et. Al [63] we developed an

efficient two-step process to enhance CC functionality (**Fig. 6A** and **B**). In the first step, methanol was used to solubilize **PG**, and the reaction was conducted in DMC with K_2CO_3 as a catalyst at 60 °C **(Table S2, entry 2)**. After 18 h, a CC functionality of 1.5 was achieved, with the product becoming fully soluble in DMC (**Fig. S38-S39**). The second step involved adding an excess of DMC, TBD catalyst, and conducting the reaction at 60 °C under rotary evaporation at 500 mbar, which facilitated continuous removal of methanol and shifted the equilibrium toward product formation. This optimized process successfully led to **PGC** with CC functionalization of 1.9-2.1. The chemical structures of **PGC** were elucidated using NMR and FTIR spectroscopy. ^{1}H-NMR analysis (**Fig. 6C & S40**) confirmed the successful synthesis of **PGC**, as evidenced by characteristic signals corresponding to the methyne/methylene protons of the 5-membered carbonate ring within the range of 4.0–5.0 ppm (**Fig. S40**). However, signals corresponding to hydroxyl protons were also observed at δ = 4.73 ppm. The overlay of ^{1}H-NMR spectra of **PGC** and TMPTC is depicted in **Fig. 6C** which further confirms the successful incorporation of CC rings into the **PG** structure. The ^{13}C-NMR spectra of **PGC** and its overlay with **PG** shown in **Fig. S41-S42**, further confirm the successful CC functionalization through the presence of a characteristic carbonate linkage signal at 155 ppm. Moreover, the overlay of the ^{13}C-NMR spectra of **PG**, **PGC**, and TMPTC (**Fig. 7**) reveals signals at δ = 59–60 ppm in the spectrum of **PGC** and **PG**, corresponding to carbons adjacent to hydroxyl groups. This observation is consistent with the presence of hydroxyl functionalities in the **PGC** structure.

FT-IR analysis supported these findings, with a prominent carbonyl elongation observed at approximately 1790 cm^{-1} (**Fig. 6D**). Additionally, the presence of unreacted hydroxyl (OH) groups in **PGC** was indicated by a broad, intense band around 3300 cm^{-1}.

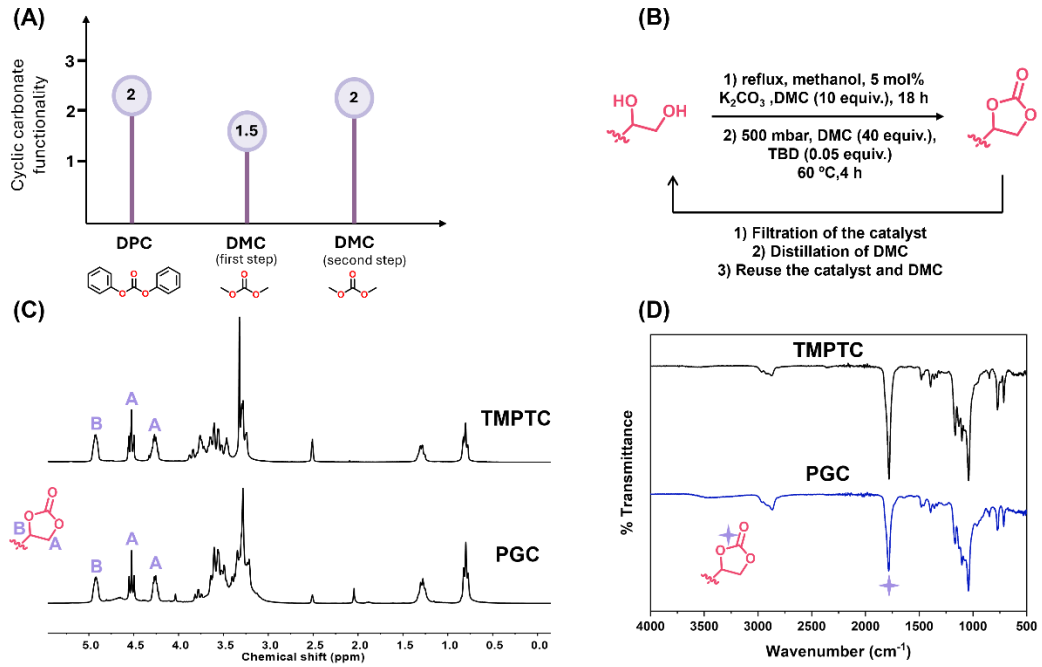

Fig. 6. (A) Cyclic carbonate functionalities using different carbonation agents, (B) General reaction scheme for the conversion of **PG** to **PGC**, illustrating the filtration-based separation of the pure product and the reuse of the reaction mixture for subsequent cycles, (C) ^{1}H-NMR spectra of TMPTC and **PGC**, confirming the structural transformation (recorded at 300 MHz in DMSO-d_6), (D) Overlay of FTIR spectra of TMPTC and **PGC**.

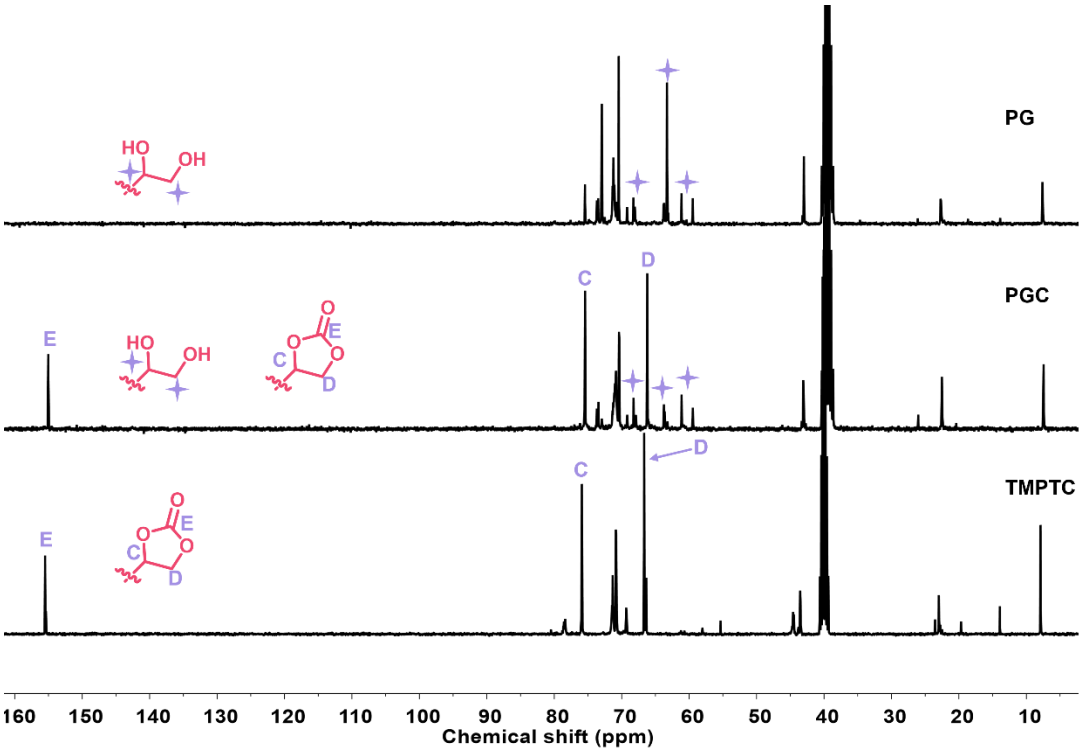

Fig. 7. Overlay of ^{13}C-NMR spectrum of purified **PG**, **PGC**, and TMPTC (100 MHz, DMSO-d_6).

3.4 NIPUFs from recycled chemicals (r-NIPUFs)

Foaming is a highly complex procedure that requires a precise balance between PHU network formation and the timing of gas generation. For the first-generation NIPUFs, an optimal [NH_2]/[5CC] ratio of 0.85 was employed, leaving 15 mol% of the CC moieties available for decarboxylation and CO_2 generation. Nevertheless, considering the reduced number of reactive sites in **PGC**, it was necessary to adapt the conditions to achieve adequate cross-linking and ensure foam stability.

To begin with, formulation was developed using **PGC** (with ~2.1 5CC functionality) as the primary component, along with EDR 148, water, and DBU as a catalyst (see **Table S3** for all formulations). The ratio of [amine]/[cyclic carbonate] ([NH_2]/[5CC]) was adjusted from 0.6 to 0.8 to leave the remaining CC available for hydrolysis. The designed formulations resulted in inhomogeneous foam structures, with the foam collapsing during cooling as a result of excessive hydrolysis and insufficient cross-linking. This compromised the structural integrity of r-NIPUFs (**Fig. S43**). To enhance the foam stability, tris(2-aminoethyl)amine (TREN) was incorporated in the formulation with EDR 148. The [NH_2]/[5CC] ratio was set at 0.75, ensuring sufficient crosslinking while preserving unreacted CC for hydrolysis. The formulation consisted of **PGC**, TREN (NH_2/5CC ratio of 0.4), and EDR 148 (NH_2/5CC ratio of 0.35). To induce CO_2 generation, water (1 equiv. *vs* 5CC) was added, using DBU as the catalyst (**Table S3**, entry D). Upon foaming, the structure exhibited limited expansion (**Fig. S43D**). The observed rough surface and varying bubble sizes indicate uneven CO_2 release and possibly phase separation during curing. Advancing the process could include adjusting the water ratio, extending the curing time, or modifying the TREN-to-EDR 148 ratio.

To further enhance the foam's structure and address previous stability issues, fresh TMPTC was incorporated at approximately 20 wt.% in combination with **PGC**. This modification aimed to increase the crosslinking density and improve foam homogeneity. However, upon foaming, the structure showed limited expansion (**Table S3**, entry E, **Fig. S43E**). Subsequently, the TMPTC content was increased by 40%, resulting in a blend of approximately 40 wt.% TMPTC and 60 wt.% **PGC**. The remaining formulation components included recycled EDR-148 (NH_2/5CC ratio of 0.85), DBU catalyst (0.056 equiv. relative to 5CC), and water (1.14 equiv. relative to 5CC) (**Table S3**, entry F). This adjustment led to a significantly improved

foam (denoted **NIPUF-R**, **Fig. 8B**) featuring a uniform, well-expanded structure with a density of 356 kg/m^3 and open cells sized approximately 1-2 mm.

The addition of TMPTC significantly enhanced crosslinking, yet probably slightly affecting the evolution of the viscosity of the material when CO_2 is released. Consequently, this formulation successfully prevented shrinkage and collapse, enabling the creation of the first NIPUF composed of 63% of recycled content. FT-IR spectra comparison of the native **NIPUF-A** and recycled **NIPUF-R** shows close similarity (**Fig. 8C**). The other characteristics, such as the T_g's values of the dried foams, $T_{deg,10\%}$ and the GC remained similar to those of the native NIPUF (**Fig. 8D-7F**, **Table 4**). The drop in compression modulus (0.03 MPa for **NIPUF-A**, and 0.01 MPa for **NIPUF-R**) is likely attributed to the differences in cell morphology (**Fig. S48, Table 4).**

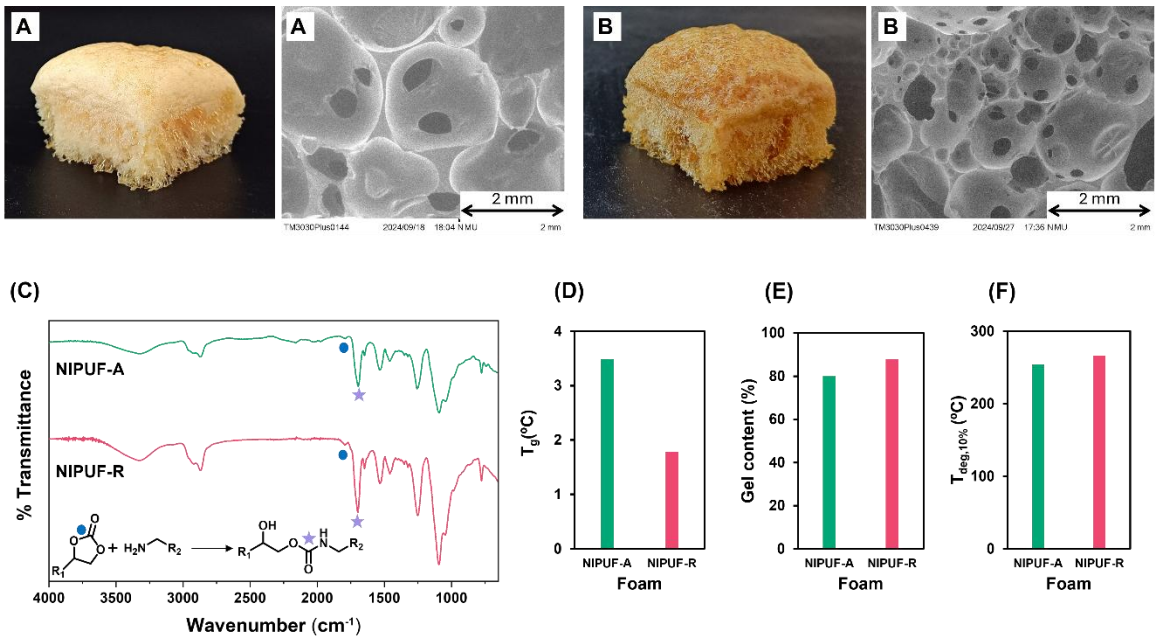

Fig. 8. Actual foam photographs and morphological characterizations of (A) **NIPUF-A** and (B) **NIPUF-R**; (C) comparative FTIR spectra of **NIPUF-A** and **NIPUF-R**, along with (D) comparative glass transition temperature (T_g), I gel content (GC), and (F) $T_{deg,10\%}$ of **NIPUF-A** and **NIPUF-R.**

Table 4. Reaction conditions and characterization of the native and recycled NIPUFs.

Entry	Foam	T/time	T_g/T_g dried [°C]	$T_{deg,10\%}$ [°C]	Gel content (% in THF)	Density [kg/m^3]	Compression Modulus [MPa]
1	NIPUF-A	100 °C/3 h	1.2/3.3	254	80	191 ± 10	0.03 ± 0.01
2	NIPUF-R	100 °C/3 h	-10.6/1.4	266	89	356 ± 34	0.01 ± 0.02

4 Conclusion

This study presents an efficient approach for the chemical recycling of NIPUFs of the polyhydroxyurethane-type via hydrolytic depolymerization under both alkaline and acidic conditions. Complete degradation of the urethane linkages was achieved using 5 M NaOH and 5 M H_2SO_4 at 80 °C within 10 and 8 hours, respectively. NMR and FTIR analyses confirmed the full cleavage of urethane bonds, resulting in the successful recovery of **PG** and diamine compounds with high purity and good isolated yields. Notably, the depolymerization proceeded under significantly milder conditions compared to those typically required for conventional polyurethanes. Recovered diamines, including EDR 148 and XDA, were structurally and spectroscopically equivalent to their commercial counterparts. Polyglycerol was further valorized via a two-step carbonylation process using dimethyl carbonate (DMC) in the presence of a catalytic amount of potassium carbonate. This method yielded polyglycerol carbonate (**PGC**) with a cyclic carbonate (CC) functionality of 1.9–2.1, which is lower than that of original TMPTC (2.64), as confirmed by NMR and FTIR analyses. Consequently, using **PGC** alone was insufficient to reproduce foams with the same morphology and thermal properties. However, a formulation combining **PGC** and TMPTC enabled the successful fabrication of second-generation recycled NIPUFs (r-NIPUFs) with virgin-like characteristics, including gel content, thermal stability, and morphology. These r-NIPUFs incorporated up to 63% recycled content, marking a significant advancement in the development of recyclable polyurethane systems.

At the same time, a realistic evaluation highlights both opportunities and limitations. From a renewability standpoint, the system is only partially renewable: while the cyclic carbonate precursors incorporate CO_2 as a renewable carbon source, their glycidyl ether intermediates (e.g., TMPTE) and the diamines employed (*m*-XDA and EDR-148) are petrochemical. Moreover, although DMC is often considered a “green” reagent, its large-scale production is still primarily fossil based. Thus, significant progress toward bio-based diamines and renewable epoxide precursors will be needed to achieve fully renewable NIPUF formulations.

With respect to recyclability, hydrolytic depolymerization achieved complete urethane bond cleavage under mild aqueous conditions and enabled the recovery of polyglycerol and diamines with usable purity. However, the isolated yields remain moderate (56–75 % for **PG** and 30–61 % for diamines) which will be addressed in the next chapters.

In terms of performance, the recycled foams (r-NIPUFs) retained comparable thermal stability, gel content, and network integrity to virgin foams, but they displayed higher densities and less uniform cell morphology and slightly lower mechanical performance. Improving crosslinking balance, gas release control, and blowing uniformity will therefore be critical to approach the performance of commercial PU foams.

Taken together, this study provides one of the first holistic demonstrations of closed-loop NIPU foam recycling. While the results establish a solid proof-of-concept, they also underline that further optimization in feedstock renewability, recycling efficiency, and foam performance is required for NIPUFs to emerge as truly sustainable, high-performance alternatives to conventional polyurethanes.

5 References

1. Costeux, S. and L. Zhu, *Low density thermoplastic nanofoams nucleated by nanoparticles.* Polymer, 2013. **54**(11): p. 2785-2795.

2. Lohtander, T., et al., *Lightweight lignocellulosic foams for thermal insulation.* Cellulose, 2022. **29**(3): p. 1855-1871.

3. *Fortune Business Insights. (n.d.). Polyurethane (PU) market size, share & COVID-19 impact analysis.* March 13, 2025; Available from: https://www.fortunebusinessinsights.com/industry-reports/polyurethane-pu-market-101801.

4. Madbouly, S.A., *Novel recycling processes for thermoset polyurethane foams.* Current Opinion in Green and Sustainable Chemistry, 2023. **42**: p. 100835.

5. Choe, K.H., et al., *Properties of rigid polyurethane foams with blowing agents and catalysts.* Polymer journal, 2004. **36**(5): p. 368-373.

6. Petrovic, Z.S., *Polyurethanes*, in *Handbook of Polymer Synthesis*. 2004, CRC Press. p. 515-552.

7. Peyrton, J. and L. Averous, *Structure-properties relationships of cellular materials from biobased polyurethane foams.* Materials Science and Engineering: R: Reports, 2021. **145**: p. 100608.

8. Dworakowska, S., et al., *The role of catalysis in the synthesis of polyurethane foams based on renewable raw materials.* Catalysis today, 2014. **223**: p. 148-156.

9. Delavarde, A., et al., *Sustainable polyurethanes: toward new cutting-edge opportunities.* Progress in Polymer Science, 2024: p. 101805.

10. Karol, M.H. and J.H. Dean, *Respiratory effects of inhaled isocyanates.* CRC critical reviews in toxicology, 1986. **16**(4): p. 349-379.

11. Razavi-Esfali, M., et al., *Design of functional isocyanate-free poly (oxazolidone) s under mild conditions.* Polymer Chemistry, 2024. **15**(19): p. 1962-1974.

12. Pauluhn, J., *Phosgene inhalation toxicity: update on mechanisms and mechanism-based treatment strategies.* Toxicology, 2021. **450**: p. 152682.

13. Rossignolo, G., G. Malucelli, and A. Lorenzetti, *Recycling of polyurethanes: where we are and where we are going.* Green Chemistry, 2024. **26**(3): p. 1132-1152.

14. Liang, C., et al., *Material flows of polyurethane in the United States.* Environmental science & technology, 2021. **55**(20): p. 14215-14224.

15. Di, J., et al., *United States plastics: Large flows, short lifetimes, and negligible recycling.* Resources, Conservation and Recycling, 2021. **167**: p. 105440.

16. Kemona, A. and M. Piotrowska, *Polyurethane recycling and disposal: methods and prospects. Polymers 12 (8): 1752*. 2020.

17. Mahoney, L.R., S.A. Weiner, and F.C. Ferris, *Hydrolysis of polyurethane foam waste.* Environmental Science & Technology, 1974. **8**(2): p. 135-139.

18. Campbell, G.A. and W.C. Meluch, *Polyurethane foam recycling. Superheated steam hydrolysis.* Environmental Science & Technology, 1976. **10**(2): p. 182-185.

19. Motokucho, S., et al., *Hydrolysis of aromatic polyurethane in water under high pressure of CO2.* Journal of Polymer Science Part A: Polymer Chemistry, 2017. **55**(12): p. 2004-2010.

20. Gama, N., et al., *Recycling of polyurethane by acidolysis: The effect of reaction conditions on the properties of the recovered polyol.* Polymer, 2021. **219**: p. 123561.

21. Godinho, B., et al., *Recycling of polyurethane wastes using different carboxylic acids via acidolysis to produce wood adhesives.* Journal of Polymer Science, 2021. **59**(8): p. 697-705.

22. He, H., et al., *Chemical recycling of waste polyurethane foams: Efficient acidolysis under the catalysis of zinc acetate.* ACS Sustainable Chemistry & Engineering, 2023. **11**(14): p. 5515-5523.

23. Gama, N., et al., *Recycling of polyurethane scraps via acidolysis.* Chemical Engineering Journal, 2020. **395**: p. 125102.

24. Bech, T.B., et al., *Chemical separation of polyurethane via acidolysis–combining acidolysis with hydrolysis for valorisation of aromatic amines.* Green Chemistry, 2024. **26**(14): p. 8395-8404.

25. Nikje, A., et al., *"Split-phase" glycolysis of flexible PUF wastes and application of recovered phases in rigid and flexible foams production.* Polymer-Plastics Technology and Engineering, 2007. **46**(3): p. 265-271.

26. Molero, C., et al., *Glycolysis of flexible polyurethane wastes using stannous octoate as the catalyst.* Journal of material cycles and waste management, 2009. **11**: p. 130-132.

27. Murai, M., et al., *Glycolysis of rigid polyurethane foam under various reaction conditions.* Journal of cellular plastics, 2003. **39**(1): p. 15-27.

28. Wu, C.-H., et al., *Glycolysis of waste flexible polyurethane foam.* Polymer Degradation and Stability, 2003. **80**(1): p. 103-111.

29. Grdadolnik, M., et al., *Chemical recycling of flexible polyurethane foams by aminolysis to recover high-quality polyols.* ACS sustainable chemistry & engineering, 2023. **11**(29): p. 10864-10873.

30. Chen, X., et al., *Reprocessable polyhydroxyurethane networks exhibiting full property recovery and concurrent associative and dissociative dynamic chemistry via transcarbamoylation and reversible cyclic carbonate aminolysis.* Polymer Chemistry, 2017. **8**(41): p. 6349-6355.

31. Bhandari, S. and P. Gupta, *Chemical depolymerization of polyurethane foam via ammonolysis and aminolysis*, in *Recycling of Polyurethane Foams*. 2018, Elsevier. p. 77-87.

32. Lapprand, A., et al., *Reactivity of isocyanates with urethanes: Conditions for allophanate formation.* Polymer degradation and stability, 2005. **90**(2): p. 363-373.

33. Fonseca, L.P., et al., *Reducing the carbon footprint of polyurethanes by chemical and biological depolymerization: Fact or fiction?* Current Opinion in Green and Sustainable Chemistry, 2023. **41**: p. 100802.

34. Perli, G., H. Sardon, and F. Vidal, *Reaction: Is a circular economy for chemicals and materials possible?* Chem, 2024. **10**(7): p. 1961-1962.

35. Maisonneuve, L., et al., *Isocyanate-free routes to polyurethanes and poly (hydroxy urethane) s.* Chemical reviews, 2015. **115**(22): p. 12407-12439.

36. Grignard, B., et al., *Advances in the use of CO 2 as a renewable feedstock for the synthesis of polymers.* Chemical Society Reviews, 2019. **48**(16): p. 4466-4514.

37. Bobbink, F.D., A.P. van Muyden, and P.J. Dyson, *En route to CO 2-containing renewable materials: catalytic synthesis of polycarbonates and non-isocyanate polyhydroxyurethanes derived from cyclic carbonates.* Chemical Communications, 2019. **55**(10): p. 1360-1373.

38. Gomez-Lopez, A., et al., *Trends in non-isocyanate polyurethane (NIPU) development.* Chemical Communications, 2021. **57**(92): p. 12254-12265.

39. Grignard, B., et al., *CO 2-blown microcellular non-isocyanate polyurethane (NIPU) foams: from bio-and CO 2-sourced monomers to potentially thermal insulating materials.* Green Chemistry, 2016. **18**(7): p. 2206-2215.

40. Blattmann, H., M. Lauth, and R. Mülhaupt, *Flexible and bio-based nonisocyanate polyurethane (NIPU) foams.* Macromolecular Materials and Engineering, 2016. **301**(8): p. 944-952.

41. Cornille, A., et al., *Room temperature flexible isocyanate-free polyurethane foams.* European Polymer Journal, 2016. **84**: p. 873-888.

42. Dong, T., et al., *Assessment of plant and microalgal oil-derived nonisocyanate polyurethane products for potential commercialization.* ACS Sustainable Chemistry & Engineering, 2021. **9**(38): p. 12858-12869.

43. Detrembleur, C., B. Grignard, and F. Monie, *Self-blowing isocyanate-free polyurethane foams*. 2023.

44. Monie, F., et al., *Chemo-and regioselective additions of nucleophiles to cyclic carbonates for the preparation of self-blowing non-isocyanate polyurethane foams.* Angewandte Chemie, 2020. **132**(39): p. 17181-17189.

45. Monie, F., B. Grignard, and C. Detrembleur, *Divergent aminolysis approach for constructing recyclable self-blown nonisocyanate polyurethane foams.* ACS Macro Letters, 2022. **11**(2): p. 236-242.

46. Purwanto, N.S., et al., *Rapidly synthesized, self-blowing, non-isocyanate polyurethane network foams with reprocessing to bulk networks via hydroxyurethane dynamic chemistry.* Polymer, 2023. **272**: p. 125858.

47. Bourguignon, M., B. Grignard, and C. Detrembleur, *Water-Induced Self-Blown Non-Isocyanate Polyurethane Foams.* Angewandte Chemie International Edition, 2022. **61**(51): p. e202213422.

48. Bakkali-Hassani, C., et al., *Polyhydroxyurethane covalent adaptable networks: looking for suitable catalysts.* Polymer Chemistry, 2023. **14**(31): p. 3610-3620.

49. Sternberg, J. and S. Pilla, *Chemical recycling of a lignin-based non-isocyanate polyurethane foam.* Nature Sustainability, 2023. **6**(3): p. 316-324.

50. Bourguignon, M., B. Grignard, and C. Detrembleur, *Cascade exotherms for rapidly producing hybrid nonisocyanate polyurethane foams from room temperature formulations.* Journal of the American Chemical Society, 2023. **146**(1): p. 988-1000.

51. Kamarulzaman, S., et al., *Covalent adaptable networks from renewable resources: Crosslinked polymers for a sustainable future.* Chem, 2023. **9**(10): p. 2771-2816.

52. Bakkali-Hassani, C., et al., *Transcarbamoylation in polyurethanes: underestimated exchange reactions?* Macromolecules, 2022. **55**(18): p. 7974-7991.

53. Miguel-Fernández, R., et al., *Recovery of Green Polyols from Rigid Polyurethane Waste by Catalytic Depolymerization.* Polymers, 2022. **14**(14): p. 2936.

54. Trojanowska, D., et al., *Valorization of waste biomass for the fabrication of isocyanate-free polyurethane foams.* Green Chemistry, 2024. **26**(14): p. 8383-8394.

55. Makarov, M., et al., *Advancing Non-isocyanate Polyurethane Foams: exo-Vinylene Cyclic Carbonate–Amine Chemistry Enabling Room-Temperature Reactivity and Fast Self-Blowing.* Macromolecules, 2025.

56. Chaudhary, M.L. and R.K. Gupta, *Non-Isocyanate Polyurethanes-Based Foams*, in *Non-Isocyanate Polyurethanes: Chemistry, Progress, and Challenges*. 2025, ACS Publications. p. 199-219.

57. Rayung, M., N. Abd Ghani, and N. Hasanudin, *A review on vegetable oil-based non isocyanate polyurethane: towards a greener and sustainable production route.* RSC advances, 2024. **14**(13): p. 9273-9299.

58. Le Gac, P.-Y., D. Choqueuse, and D. Melot, *Description and modeling of polyurethane hydrolysis used as thermal insulation in oil offshore conditions.* Polymer testing, 2013. **32**(8): p. 1588-1593.

59. Brege, A., et al., *The coupling of CO2 with diols promoted by organic dual systems: Towards products divergence via benchmarking of the performance metrics.* Journal of CO2 Utilization, 2020. **38**: p. 88-98.

60. Teng, W.K., et al., *A review on the performance of glycerol carbonate production via catalytic transesterification: Effects of influencing parameters.* Energy conversion and management, 2014. **88**: p. 484-497.

61. De Caro, P., et al., *Recent progress in synthesis of glycerol carbonate and evaluation of its plasticizing properties.* Frontiers in Chemistry, 2019. **7**: p. 308.

62. Parzuchowski, P.G., M. Kiźlińska, and G. Rokicki, *New hyperbranched polyether containing cyclic carbonate groups as a toughening agent for epoxy resin.* Polymer, 2007. **48**(7): p. 1857-1865.

63. Dannecker, P.-K. and M.A. Meier, *Facile and sustainable synthesis of erythritol bis (carbonate), a valuable monomer for non-isocyanate polyurethanes (NIPUs).* Scientific Reports, 2019. **9**(1): p. 9858.

6 Supporting Information

6.1 Instrumentation

6.1.1 Nuclear Magnetic Resonance (NMR) Spectroscopy

All NMR spectra were recorded using a Bruker (300 and 400 MHz) spectrometer using dimethyl sulfoxide (DMSO), or D_2O as the solvent at 25 °C in the Fourier transform mode. 16 scans for ^{1}H spectra and 512 scans for ^{13}C spectra were recorded.

6.1.2 Thermogravimetric analysis (TGA)

Thermo-gravimetric analyses (TGA) of all resulting polymers were measured on a TGA2 instrument from Mettler Toledo. To determine the mass loss of polymers, 4-7 mg of each sample was heated at 10 °C/min from 30 to 50 °C and flushed for 10 min at 50 °C and then heated at 20 °C/min until 600 °C under an N_2 atmosphere (20 ml/min).

6.1.3 Differential scanning calorimetry (DSC)

DSC analyses were performed in a DSC25 from TA instruments. The samples were analyzed at a heating rate of 10 °C/min over a temperature range from -50 to 80 °C in non-hermetic pan. To measure the T_g of dried samples, the foam was first dried under vacuum at 50 °C for 16 hours and then stored in a desiccator. The dried sample was placed in a non-hermetic pan and subjected to a pre-conditioning ramp from room temperature to 80 °C, followed by a 10-minute isothermal hold at 80 °C. Subsequently, a second heating cycle was applied from -40 °C to 80 °C at 10 °C/min to determine T_g of dried foams.

6.1.4 Fourier Transform Infrared Spectra (FT-IR)

FTIR was performed using a Nicolet IS50 spectrometer (Thermo Fisher Scientific) equipped with a diamond attenuated total reflection (ATR) accessory.

6.1.5 Scanning electron microscopy (SEM)

The cell size and morphology of the foams were analyzed using a scanning electron microscope (SEM, Hitachi TM 3030).

6.1.6 Compression tests

Compression tests were conducted using an INSTRON universal testing machine at a rate of 1 mm/min on cubic foam specimens with a volume of approximately 1 cm^3. The compression modulus was determined from the initial linear region of the stress-strain curve, corresponding to 1-8% strain.

6.2 Characteristics of precursor to synthesize foams

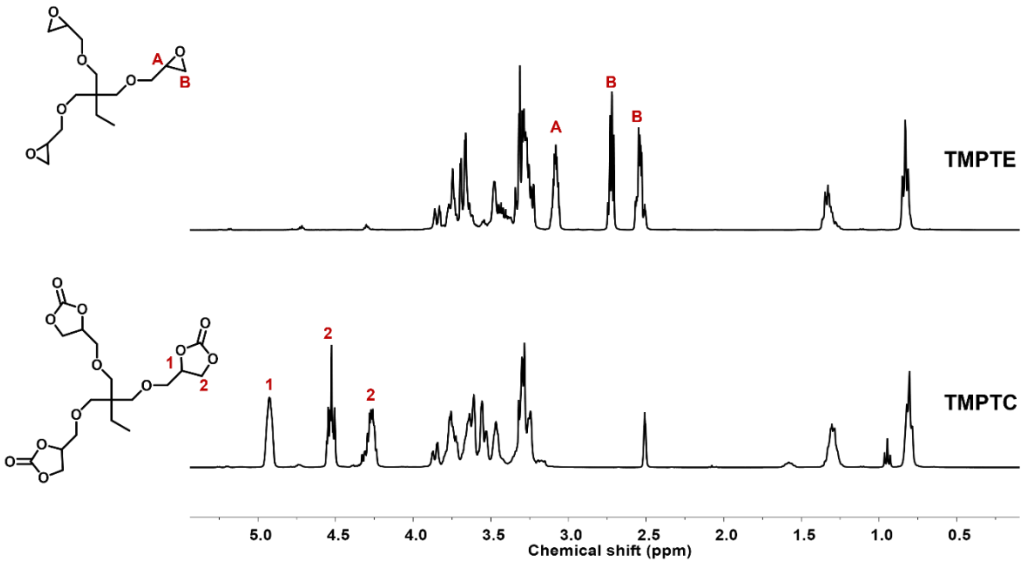

Fig. S1. ^{1}H-NMR spectrum of TMPTE and TMPTC (300 MHz, DMSO-d_6).

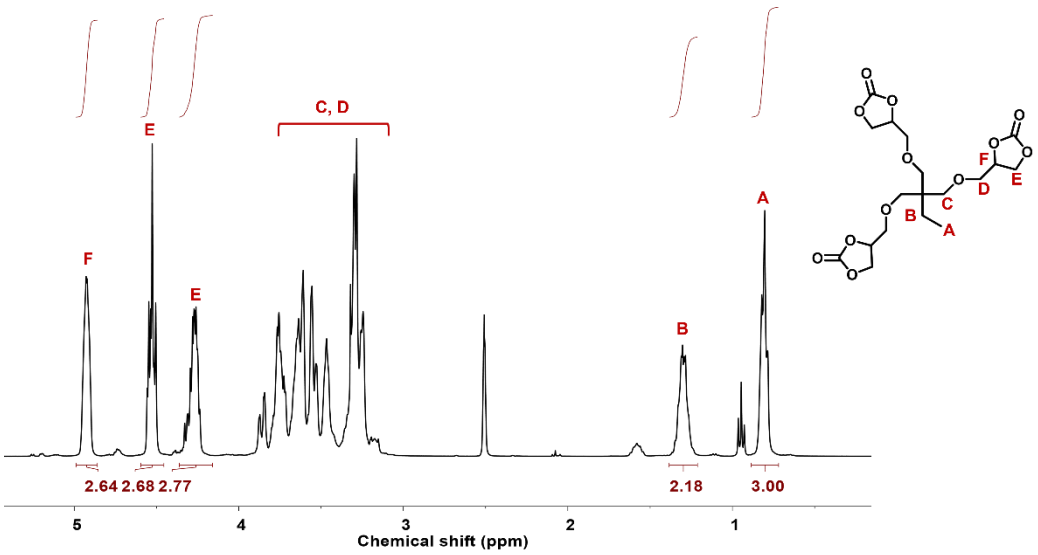

Fig. S2. ^{1}H-NMR spectrum of TMPTC (300 MHz, DMSO-d_6).

6.3 Characteristics of native NIPUFs

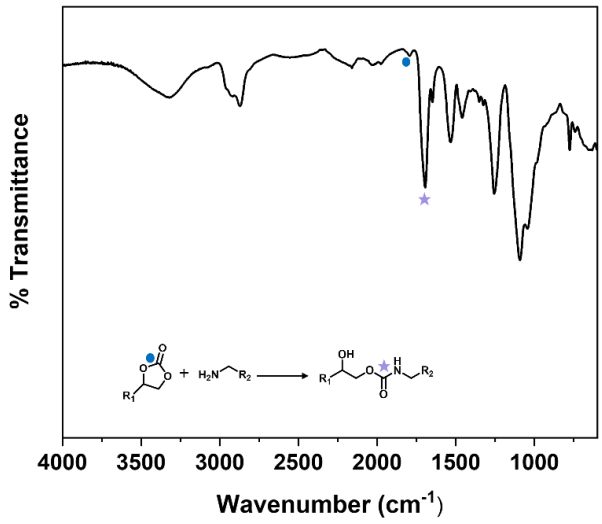

Fig. S3. FTIR spectra of NIPUF-A.

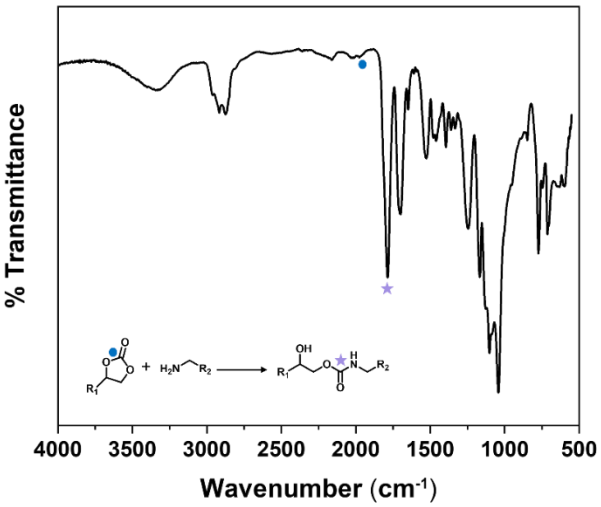

Fig. S4. FTIR spectra of NIPUF-B.

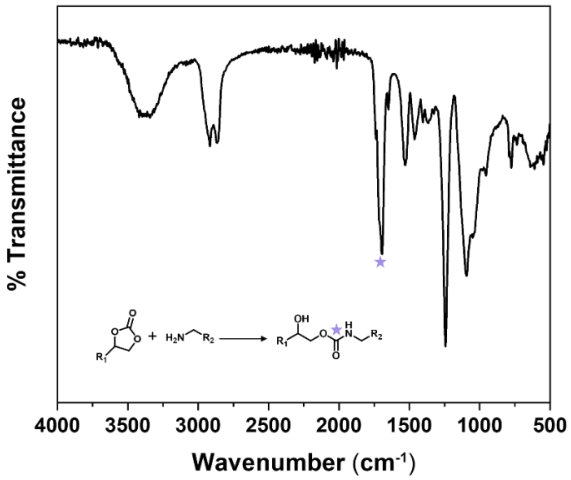

Fig. S5. FTIR spectra of NIPUF-C.

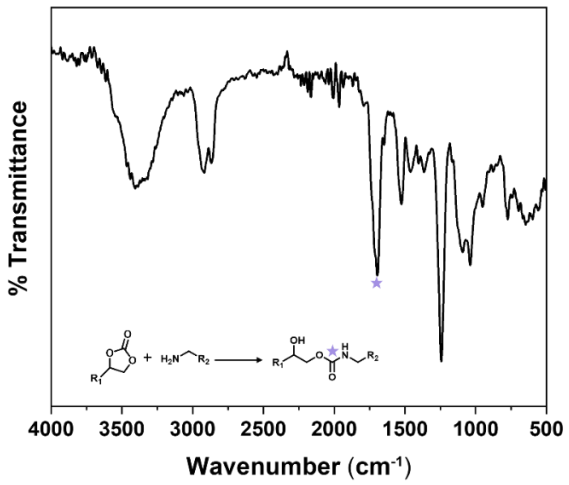

Fig. S6. FTIR spectra of NIPUF-D.

6.4 Thermal properties of native NIPUFs

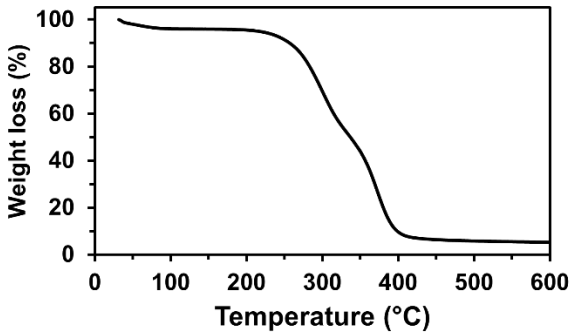

Fig. S7. TGA thermogram of NIPUF-A.

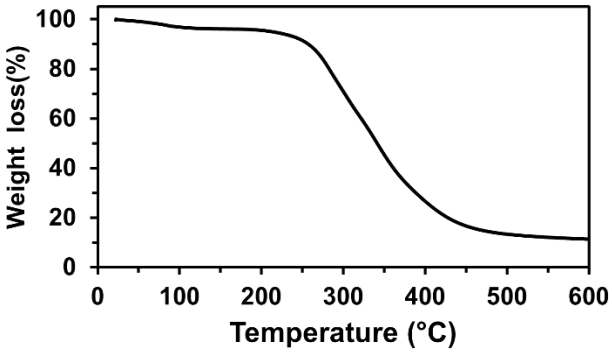

Fig. S8. TGA thermogram of NIPUF-B.

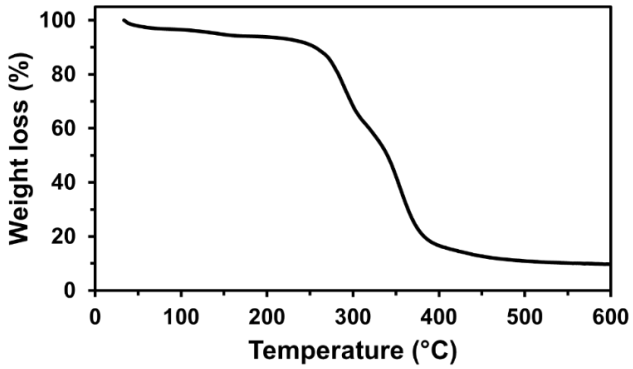

Fig. S9. TGA thermogram of NIPUF-C.

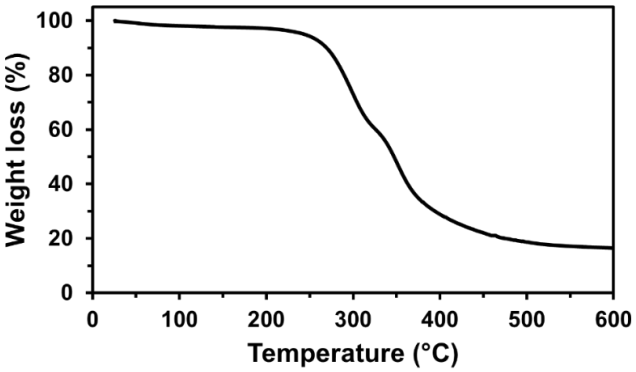

Fig. S10. TGA thermogram of NIPUF-D.

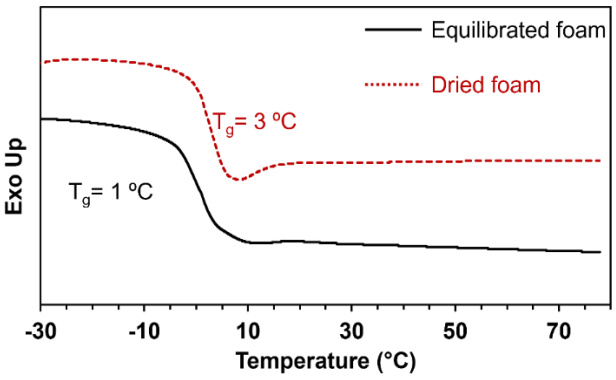

Fig. S11. DSC characterization of NIPUF-A.

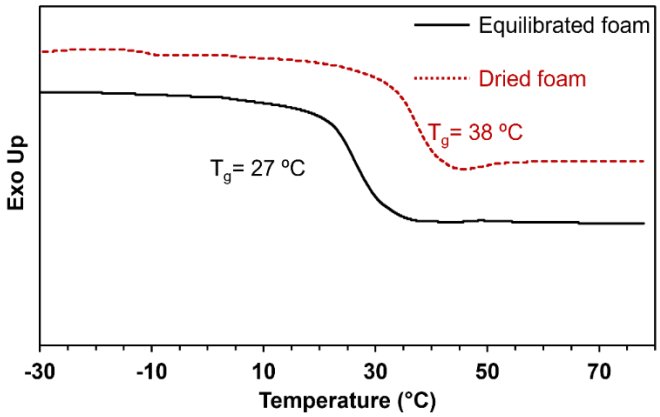

Fig. S12. DSC characterization of NIPUF-B.

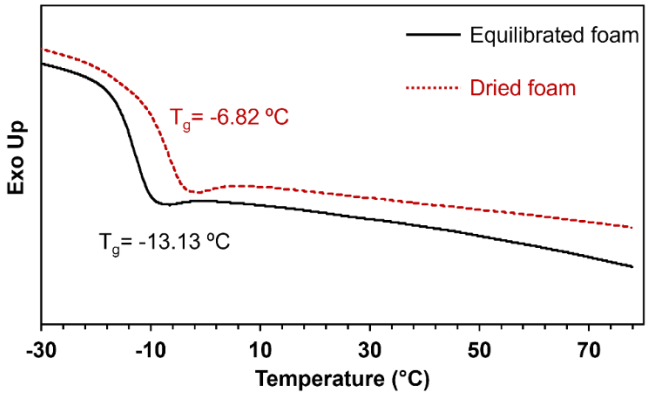

Fig. S13. DSC characterization of NIPUF-C.

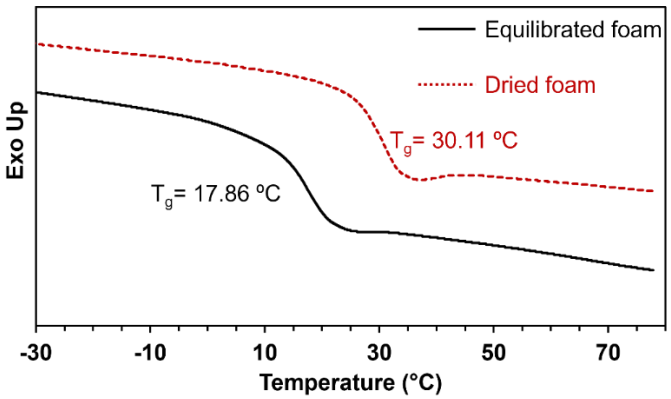

Fig. S14. DSC characterization of NIPUF-D.

6.5 Benchmarking of synthesized PHU foams and selected conventional PUFs

To contextualize the performance of our NIPUFs, we benchmarked them against two conventional PU foams of similar density (~200 kg·m^{-3}): a rigid PU foam (here denoted as **PUF1**) prepared from renewable and recycled polyester polyols [1], and a flexible PU foam (here denoted as **PUF2**) containing grafted lignin as a bio-based polyol substitute [2]. While the underlying chemistries differ, their synthesis routes explain much of the divergence in mechanical and thermal properties.

Composition of the foams:

PUF1 was based on a mixture of three renewable polyols and two aromatic polyester polyols, combined with polymeric MDI (pMDI, isocyanate index 160). Water acted as the chemical blowing agent, yielding a closed-cell rigid foam with load-bearing character. **PUF2** represented a flexible PU system formulated from PEG2000 and lignin derivatives (mainly PEG-grafted alkali lignin, with one sample containing pristine lignin) in combination with hexamethylene diisocyanate (HDI, index 0.95–1.1). Water was again used as the blowing agent, producing an open-cell flexible foam with high resilience and elastic recovery.

In comparison, our NIPUFs are produced via cyclic carbonate-amine chemistry, and water as blowing agent, entirely avoiding isocyanates. Their network density and rigidity are tuned through amine selection, rather than isocyanate index.

Mechanical properties:

As expected from its aromatic, crosslinked chemistry, **PUF1** showed the highest stiffness (Table : compressive modulus 51-82 MPa at ~200 kg·m^{-3}. **PUF2**, in contrast, is optimized for elasticity and cushioning, with a compression modulus of ~0.27 MPa, consistent with open-cell flexible foams. Our NIPUFs bridge these extremes. NIPUF-A/C are very soft (0.03-0.037 Mpa), even lower than **PUF2** in stiffness. NIPUF-B/D reach 7.5–8.3 MPa, more rigid than **PUF2** and falling into a semi-rigid regime, though still well below **PUF1**'s modulus. Thus, while rigid PU remains mechanically superior, NIPUFs demonstrate formulation-dependent tunability.

Thermal properties:

PUF1 displayed glass transition temperatures (T_g) of 113-145 °C and onset degradation ($T_{deg,5\%}$) at 191-203 °C. It should be noted that the $T_{deg,5\%}$ values of the foams (191-203 °C) appear lower than typical for rigid PU foams. However, according to the reference [1], this first mass loss step mainly corresponds to the release of additives (e.g., flame retardant TCPP), unreacted isocyanate/polyols, and moisture, rather than degradation of the polymer backbone. The actual decomposition of the polyurethane network begins later, around 245-300 °C for soft segments and 430-450 °C for hard segments, consistent with literature reports on rigid PUFs. Flexible PU (**PUF2**) exhibited a multi-step degradation, with the first significant weight loss beginning around 200-220 °C due to urethane and polyether breakdown. In contrast, our NIPUFs showed 5% weight loss temperatures ($T_{deg,5\%}$) of 145-230 °C, i.e., a comparable thermal onset stability with both PUF1 and PUF2. However, NIPUFs generally show lower T_g values compared to rigid PU, reflecting greater segmental mobility. T_g values of PUF2 were not reported.

Taken together, these comparisons show that rigid PU foams (**PUF1**) remain the benchmark in terms of stiffness, a direct consequence of their aromatic polyol backbone, high isocyanate index, and molded closed-cell structure. Flexible PU foams (**PUF2**), designed around polyether soft segments and lignin-derived polyols, provide excellent resilience and elastic recovery but only modest modulus. Our NIPUFs, by contrast, span a wide mechanical spectrum: formulations such as NIPUF-A and C fall below the stiffness of flexible PU, while NIPUF-B and D exceed it significantly and approach semi-rigid behavior, though without yet reaching the strength levels of PUF1. In thermal properties (degradation temperature), however, NIPUFs are comparable with both PUF references. This balance of intermediate mechanical properties and thermal stability, combined with the advantage of an isocyanate-free and potentially bio-based synthesis route, positions NIPUFs as promising sustainable alternatives.

Table S1. Thermomechanical properties of selected conventional polyurethane foams.

Entry	Density [kg.m^3]	T_g [°C]	Thermal stability [$T_{deg,5\%}$]	Compression modulus [MPa]	Reference
PUF1	202.6 ±1.0	142	191	50.4 ±2.1	[1]
	203.3 ±2.2	145	201	66.4 ±0.7	
	203.1 ±1.3	136	195	67.8 ±6.6	
	207.8 ±1.2	113	203	81.7 ±1.1	
	209.6 ±1.2	134	196	64.7 ±0.7	
tPUF2	206.7	-*	305	0.021	[2]
	119.9	-*	301	0.0883	
	129.7	-*	296	0.0907	
	200.9	-*	287	0.273	
	343.9	-*	278	0.016	

* T_gs were not reported.

6.6 Alkaline hydrolysis degradation of NIPUFs

6.6.1 NIPUF-A

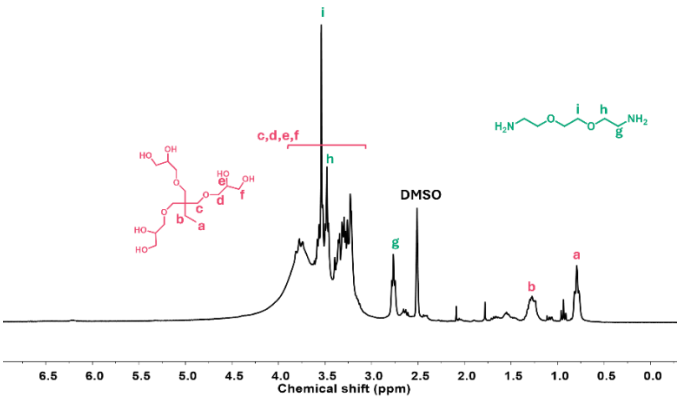

Fig. S15. ^{1}H-NMR spectrum of the crude mixture of **NIPUF-A** after base-catalyzed hydrolysis and subsequent lyophilization (300 MHz, DMSO-d_6).

6.6.2 Partition coefficient experiment

To figure out the most effective method for isolating polyglycerol (**PG**) from an aqueous medium, a partition coefficient experiment was carried out. The reaction mixture containing **PG** was subjected to a liquid-liquid extraction process using 1-butanol as the organic solvent. Following proper mixing, the system was given time to phase separate into aqueous and organic layers. The efficiency of phase separation was assessed by measuring the distribution of **PG** between the aqueous and organic phases. The concentration of **PG** in each layer was determined, and the partition coefficient was calculated using the eq. S1.

$$Partition\ coefficient = \frac{Concentration\ of\ solute\ in\ the\ organic\ phase}{Concentartion\ of\ solute\ in\ the\ aqueous\ phase} \qquad \text{eq. S1}$$

From the obtained results, the calculated partition coefficient was 0.78, indicating that **PG** has a higher affinity for water compared to the organic solvent. This suggests that a single extraction step may not be sufficient for optimal **PG** recovery. To enhance the yield of isolated **PG**, multiple extraction cycles should be performed. Repeating the extraction process increases the overall transfer of **PG** from the aqueous phase into the organic solvent, thereby improving the efficiency of isolation.

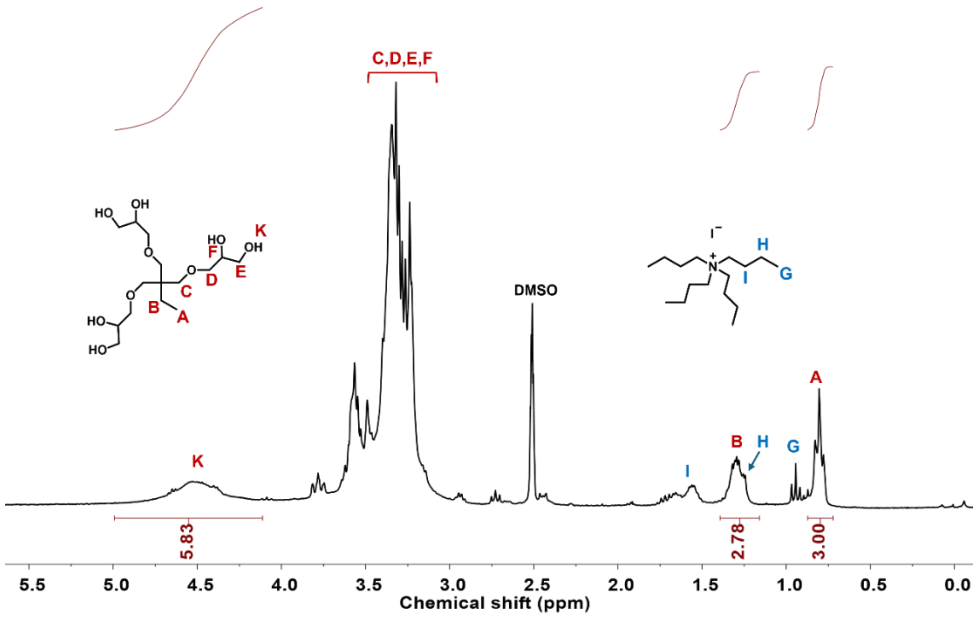

Fig. S16. ^{1}H-NMR spectrum of **PG** (300 MHz, DMSO-d_6).

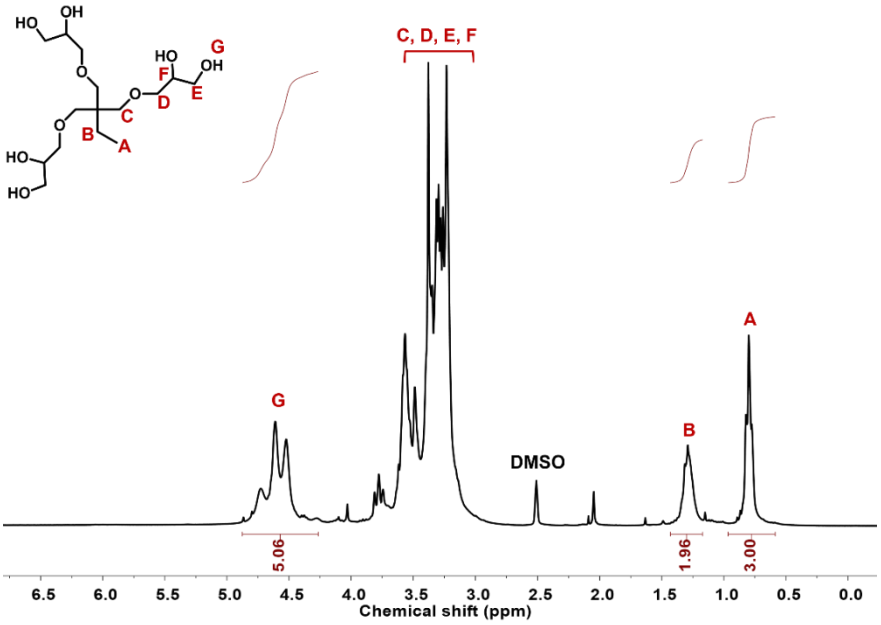

Fig. S17. ^{1}H-NMR spectrum of **PG** (after silica filtration) (300 MHz, DMSO-d_6).

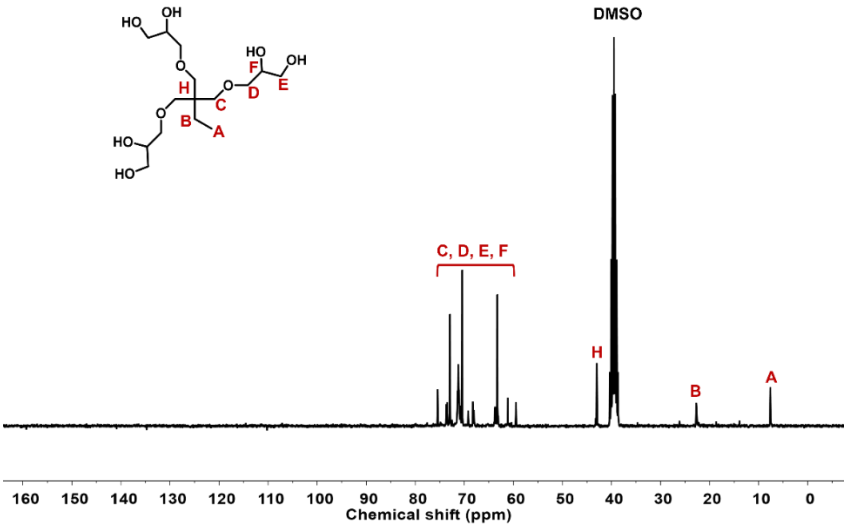

Fig. S18. ^{13}C-NMR spectrum of **PG** (100 MHz, DMSO-d_6)

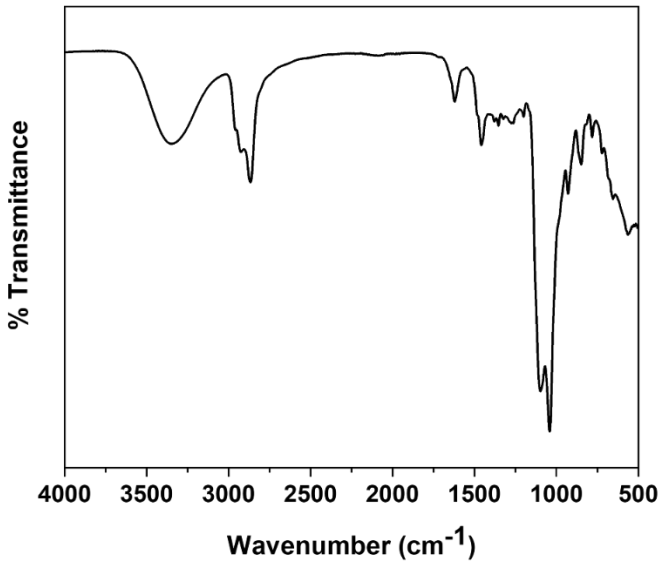

Fig. S19. FTIR spectra of **PG**.

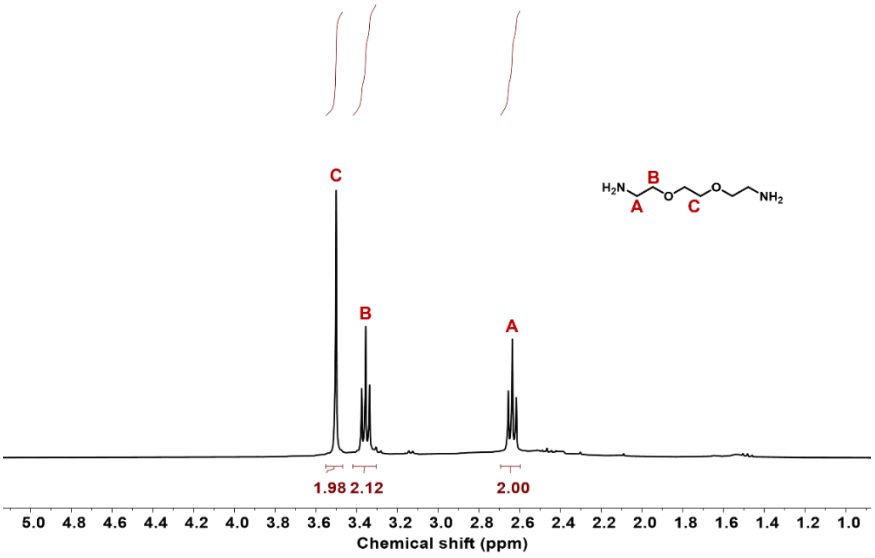

Fig. S20. ^{1}H-NMR spectrum of purified Recycled EDR 148 (400 MHz, DMSO-d_6).

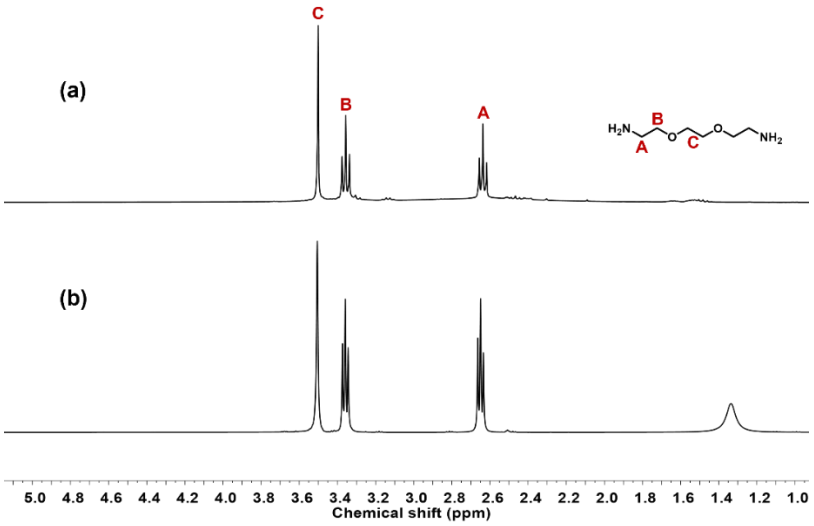

Fig. S21. ^{1}H-NMR spectrum of (a) purified Recycled EDR 148 and (b) commercial EDR 148 (400 MHz, DMSO-d_6).

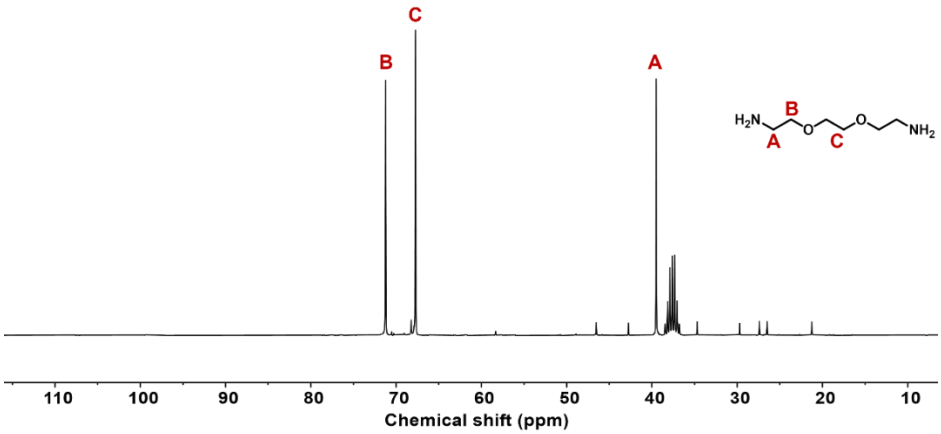

Fig. S22. ^{13}C-NMR spectrum of purified Recycled EDR 148 (100 MHz, DMSO-d_6).

6.7 NIPUF-B

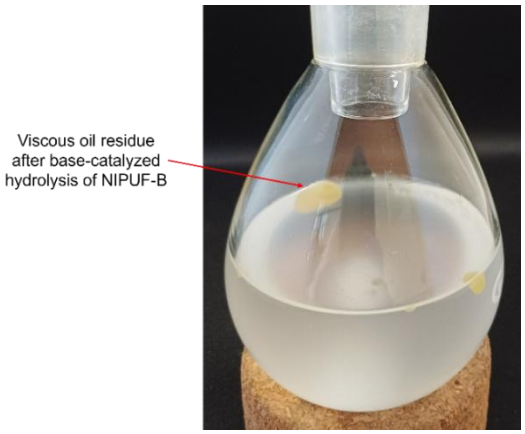

Fig. S23. Images showing the reaction mixture after the base-catalyzed depolymerization of **NIPUF-B**

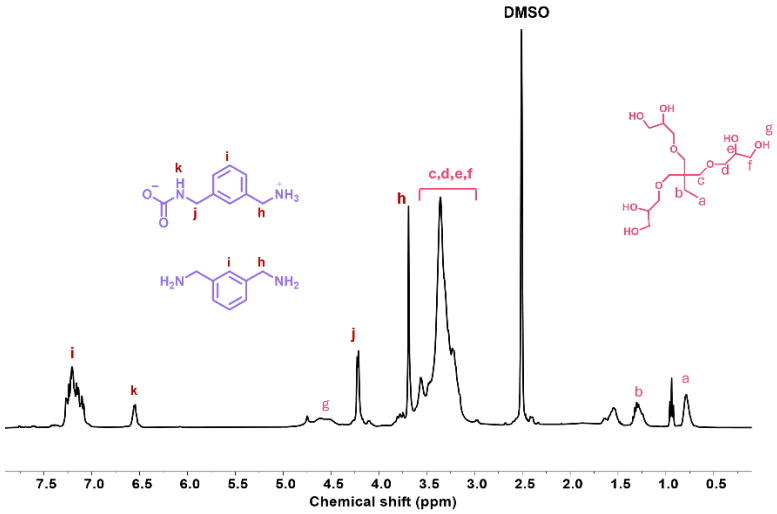

Fig. S24. ^{1}H-NMR spectrum of the separated crude oil from depolymerized **NIPUF-B** after base-catalyzed hydrolysis (300 MHz, DMSO-d_6).

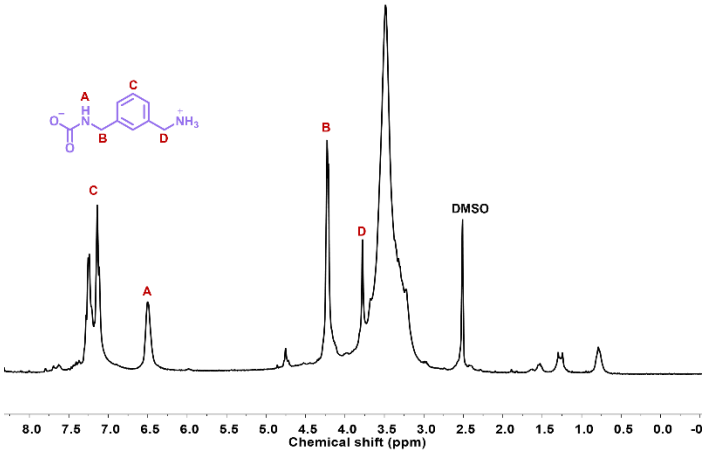

Fig. S25. ^{1}H-NMR spectrum of the *m*-XDA carbamate salt (300 MHz, DMSO-d_6).

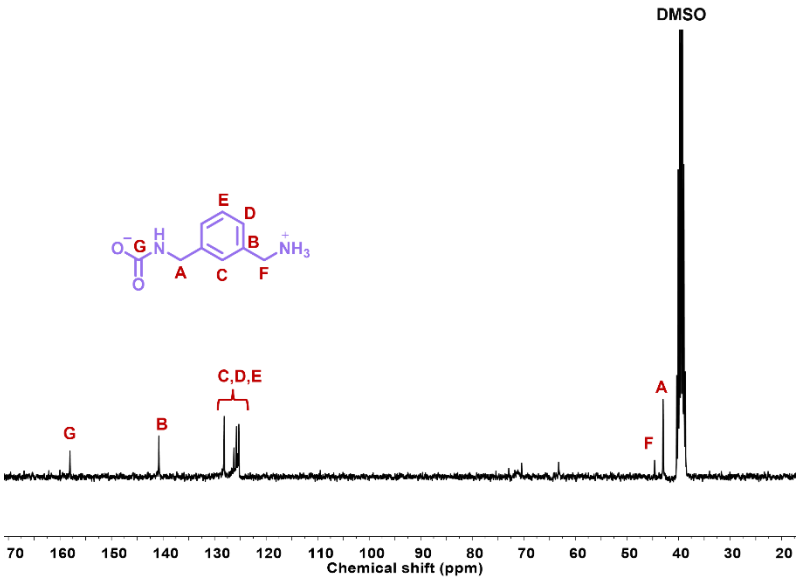

Fig. S26. ^{13}C-NMR spectrum of the *m*-XDA carbamate salt (100 MHz, DMSO-d_6).

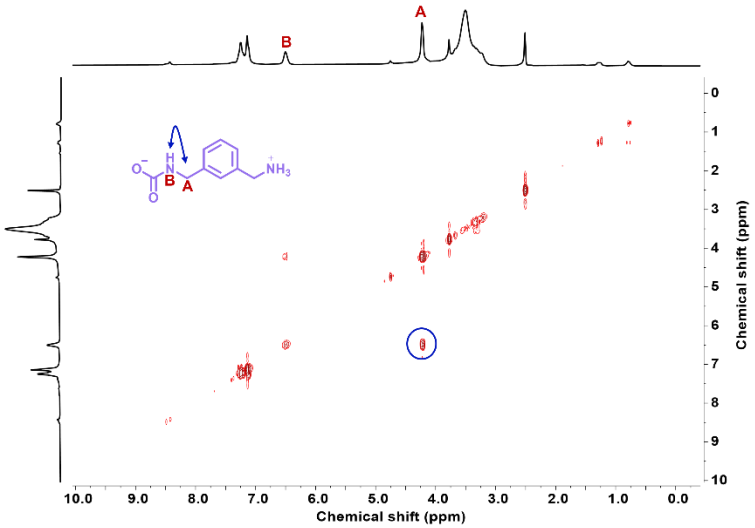

Figure S27. COSY NMR spectrum of *m*-XDA carbamate salt (300 MHz, DMSO-d_6).

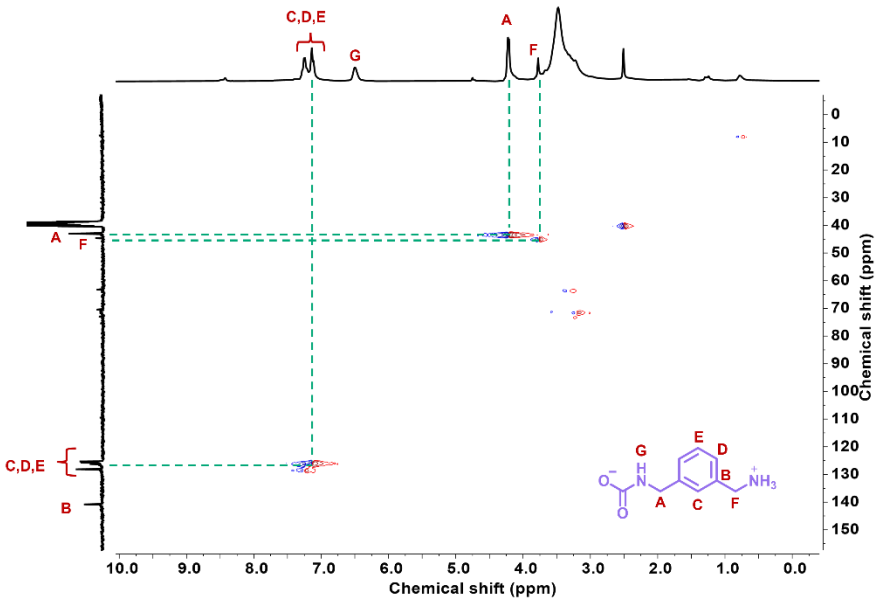

Fig. S28. ^{1}H-^{13}C HSQC NMR spectrum of *m*-XDA carbamate salt (300 MHz, DMSO-d_6).

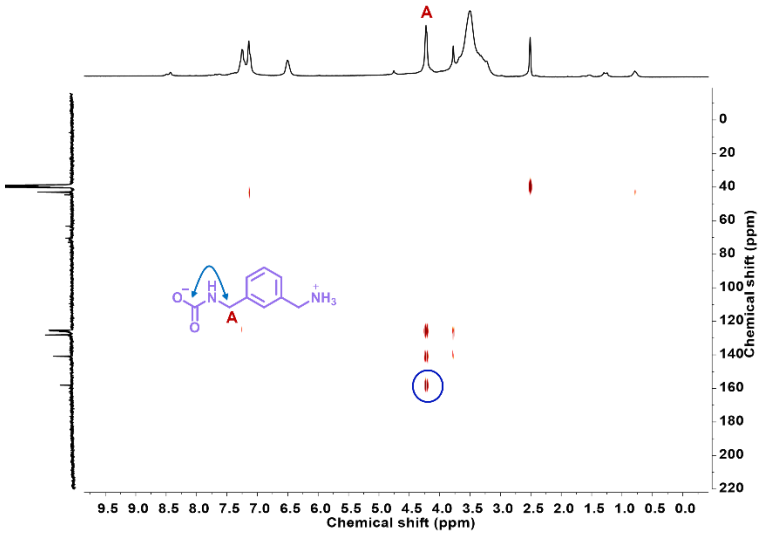

Figure S29. HMBC NMR spectrum of *m*-XDA carbamate salt (300 MHz, DMSO-d_6).

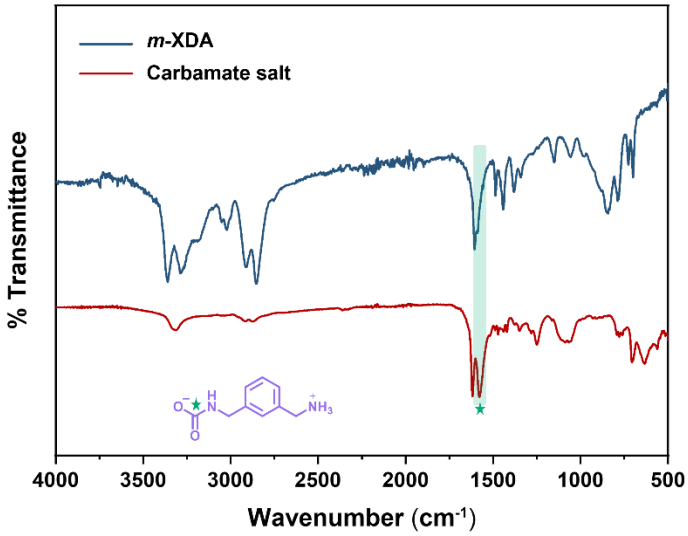

Fig. S30. Overlay of FTIR spectra of *m*-XDA and carbamate salt

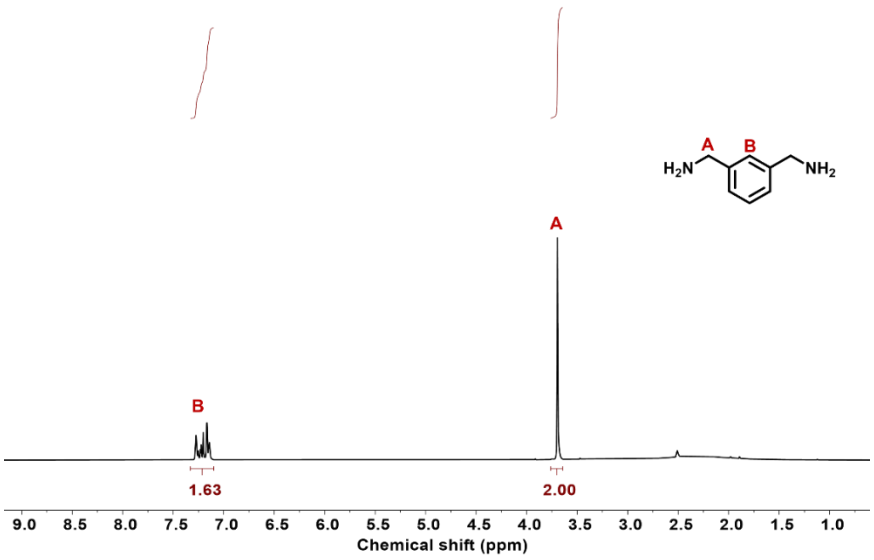

Fig. S31. ^{1}H-NMR spectrum of purified Recycled *m*-XDA (400 MHz, DMSO-d_6).

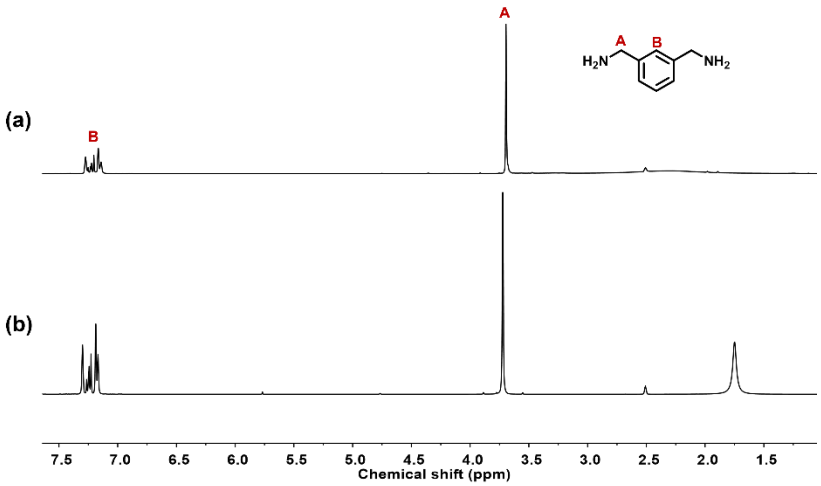

Fig. S32. ^{1}H-NMR spectrum of (a) purified Recycled *m*-XDA, and (b) commercial *m*-XDA (400 MHz, DMSO-d_6).

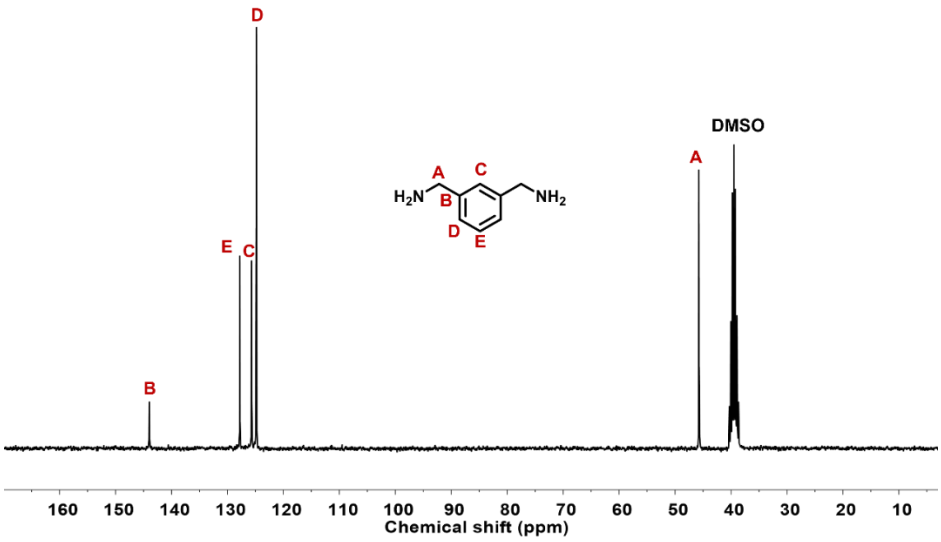

Fig. S33. ^{13}C-NMR spectrum of purified Recycled *m*-XDA (100 MHz, DMSO-d_6).

6.8 Degradation of foam synthesized using filler

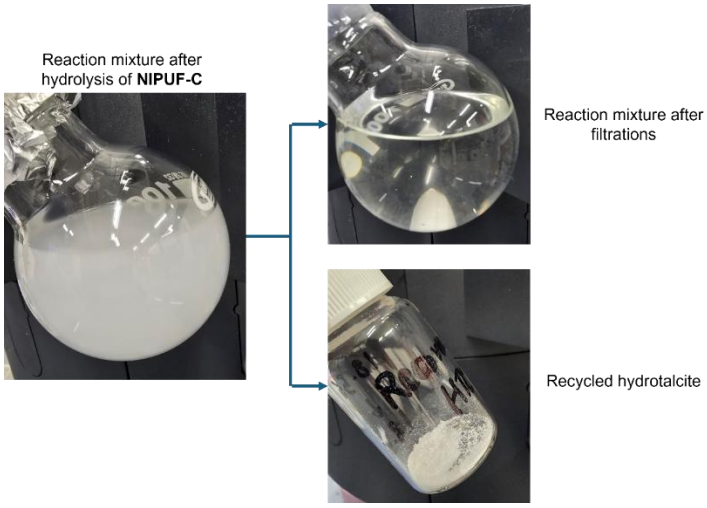

Fig. S34. Images showing the reaction mixture after the alkaline depolymerization of **NIPUF-C** and subsequent filtration to recover hydrotalcite.

6.9 Acid-catalyzed hydrolysis depolymerization of NIPUFs

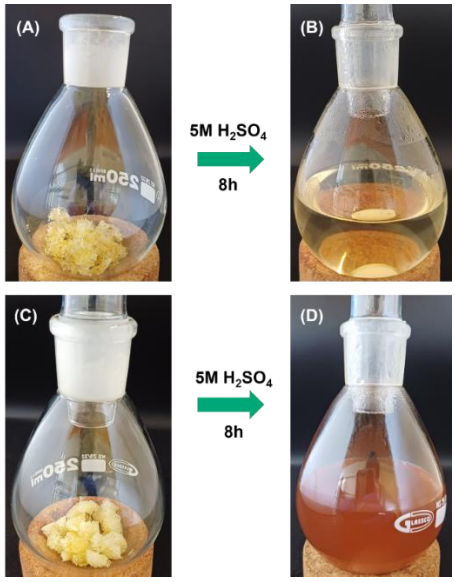

Fig. S35. Images of (A) **NIPUF-A** before starting the reaction, (B) the reaction mixture after the acid-catalyzed depolymerization of **NIPUF-A**, (C) **NIPUF-B** before starting the reaction, (D) the reaction mixture after the acid-catalyzed depolymerization of **NIPUF-B**

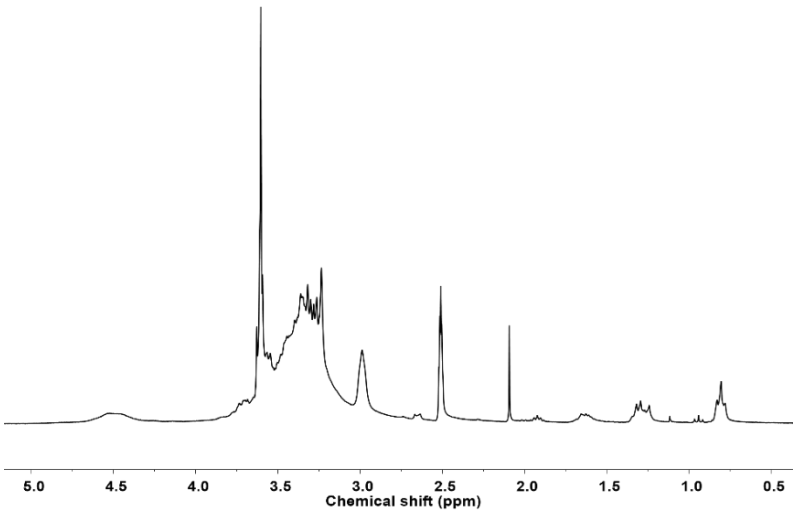

Fig. S36. ^{1}H-NMR spectrum of the crude mixture of **NIPUF-A** after acid-catalyzed hydrolysis and subsequent lyophilization (300 MHz, DMSO-d_6).

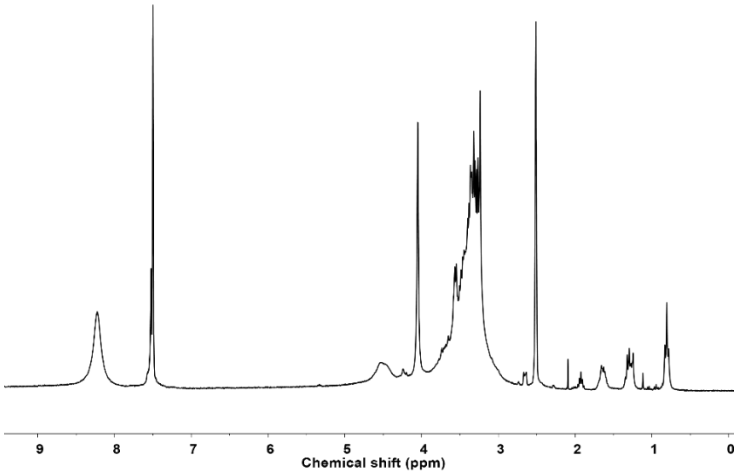

Fig. S37. ^{1}H-NMR spectrum of the crude mixture of **NIPUF-B** after acid-catalyzed hydrolysis and subsequent lyophilization (300 MHz, DMSO-d_6).

6.10 Conversion of PG to PGC

Table S2. Reaction conditions for the cyclization of **PG** to **PGC**

Entry	Carbonyl source	Catalyst[a]	Solvent	T (°C)	t (h)	CC functionality	Reaction condition
1	DMC (10 equiv *vs* **PG**)	K_2CO_3	No solvent	60	72	1.5	--
2	DMC (10 equiv *vs* **PG**)	K_2CO_3	Methanol	60	18	1.5	--
3	DMC (10 equiv *vs* **PG**)	K_2CO_3	Methanol	80	24	0.43	Under reflux
4	DMC (10 equiv *vs* **PG**)	K_2CO_3	1-Butanol	60	24	0.65	--
5	DMC (10 equiv *vs* **PG**)	K_2CO_3	1-methylimidazole	60	24	1.4	--
6	DPC (12 equiv *vs* **PG**)	TBD	No solvent	100	24	2.02	Under N_2
7	DPC (12 equiv *vs* **PG**)	$MgCl_2$	No solvent	100	24	1.36	Under N_2
8	DPC (12 equiv *vs* **PG**)	NaOt-Bu	No solvent	100	24	1.60	Under N2

[a] 5 mol% *vs* **PG**

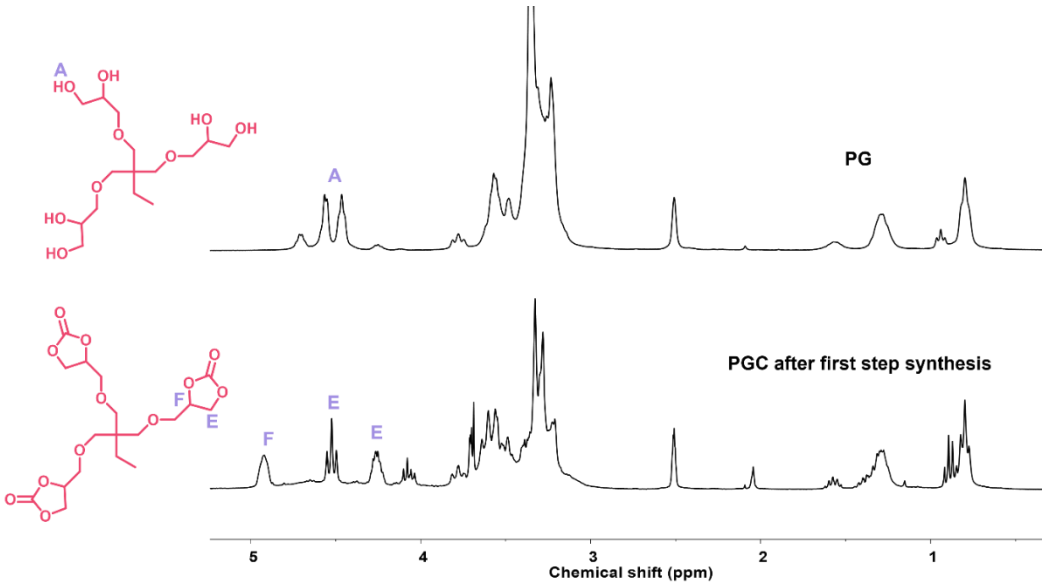

Fig. S38. [1]H-NMR spectrum of crude **PG** and **PGC** after first step cyclization (400 MHz, DMSO-d_6).

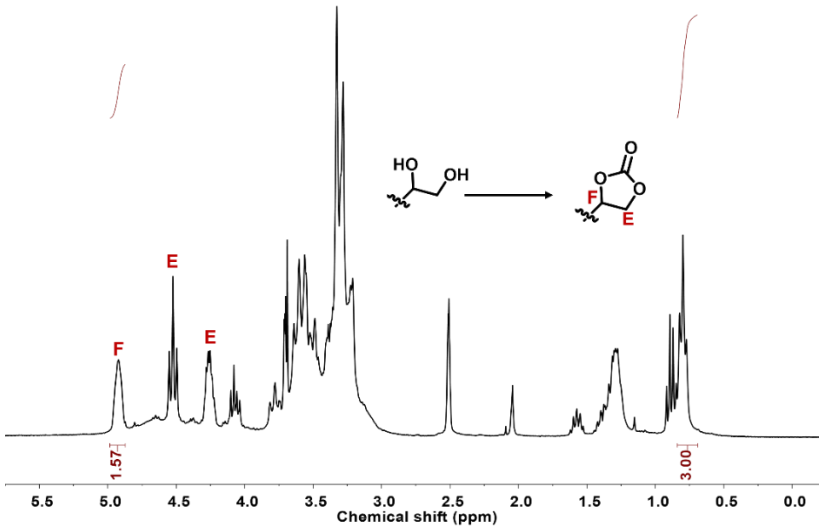

Fig. S39. [1]H-NMR spectrum of crude **PGC** after first step cyclization (300 MHz, DMSO-d_6).

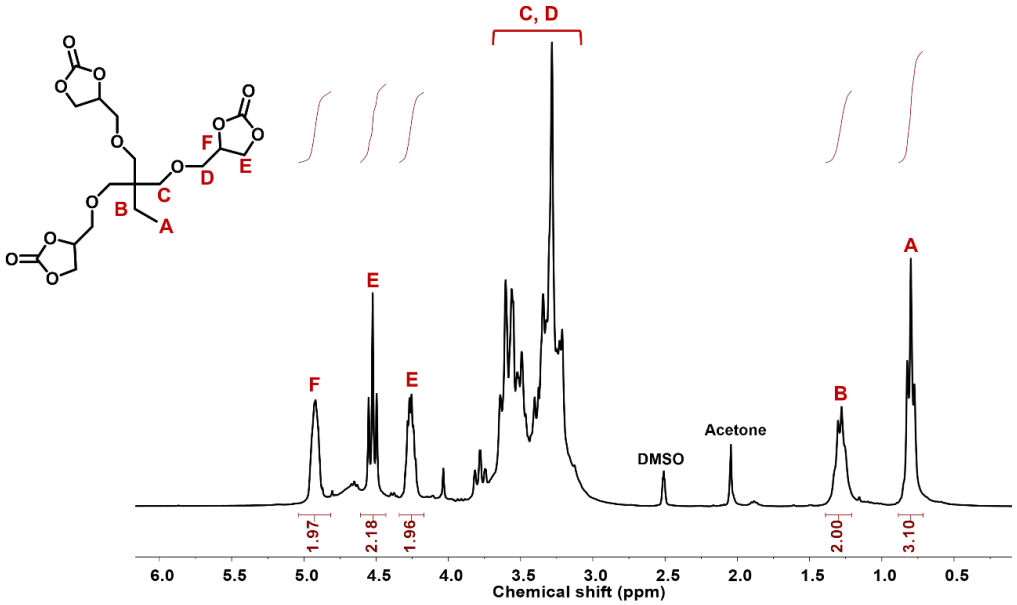

Fig. S40. ^{1}H-NMR spectrum of pure **PGC** after second step cyclization (300 MHz, DMSO-d_6).

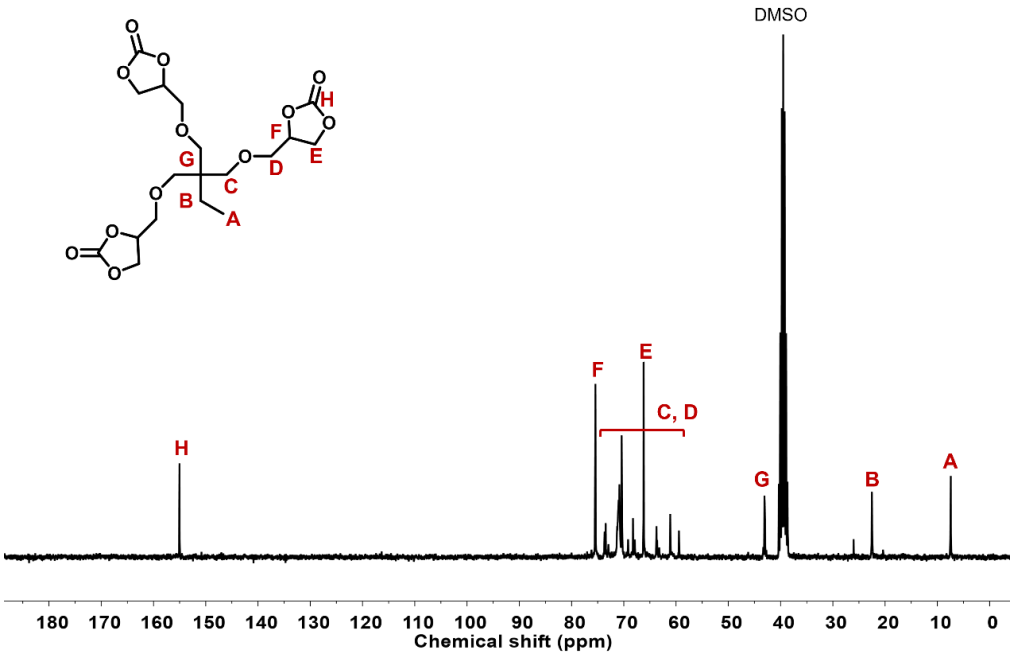

Fig. S41. ^{13}C-NMR spectrum of purified **PGC** (100 MHz, DMSO-d_6).

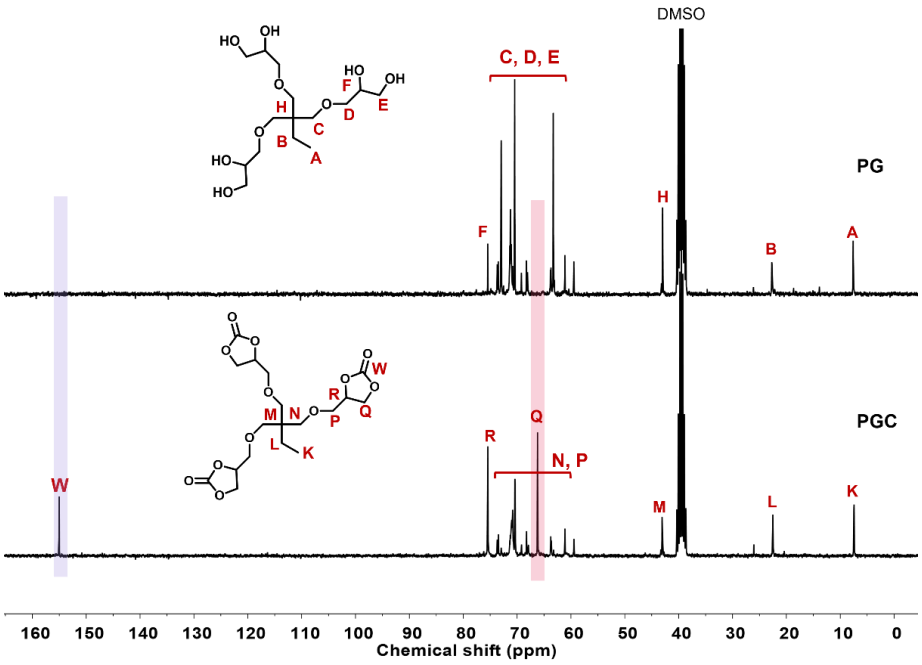

Fig. S42. Overlay of ^{13}C-NMR spectrum of purified **PG** and **PGC** (100 MHz, DMSO-d_6).

6.11 Preparation of water-induced self-blown foams (r-NIPUF) using recycled PGC

Table S3. Formulations of the different foams.

Entry	PGC[a]	TMPTC[b]	Amine (NH_2/5CC ratio)	Foaming agent (equiv. vs 5CC)	Catalyst (equiv. vs 5CC)
A	2.5 g (5CC= 11.5 mmol)	–	EDR 148/ 640 mg (0.75 equiv.)	H_2O/207.17 mg (1 equiv.)	DBU/87.5 mg (0.05 equiv.)
B	2.5 g (5CC= 11.5 mmol)	–	EDR 148/ 511.7 mg (0.6 equiv.)	H_2O/207.17 mg (1 equiv.)	DBU/87.5 mg (0.05 eqiov.)
C	2.5 g (5CC= 11.5 mmol)	–	EDR 148/ 682.3 mg (0.8 equiv.)	H_2O/207.17 mg (1 equiv.)	DBU/87.5 mg (0.05 equiv.)
D	2.5 g (5CC= 11.5 mmol)	–	EDR 148 (0.35 equiv.)/298.5 mg & TREN/224.4 mg (0.4 equiv.)	H_2O/207.17 mg (1 equiv.)	DBU/87.5 mg (0.05 equiv.)
E	4 g (5CC= 18.41 mmol)	1 g (5CC= 5.9 mmol)	EDR 148/1530 mg (0.85 equiv.)	H_2O/438 mg (1 equiv.)	DBU/185 mg (0.05 equiv.)
F	3.5 g (5CC= 16.11 mmol)	2.31 g (5CC= 14.3 mmol)	EDR 148/1900 mg (0.85 equiv.)	H_2O/620 mg (1.14 equiv.)	DBU/ 260 mg (0.056 equiv.)

[a] Considering 2 functionality of 5CC, [b] considering 2.6 functionality of 5CC

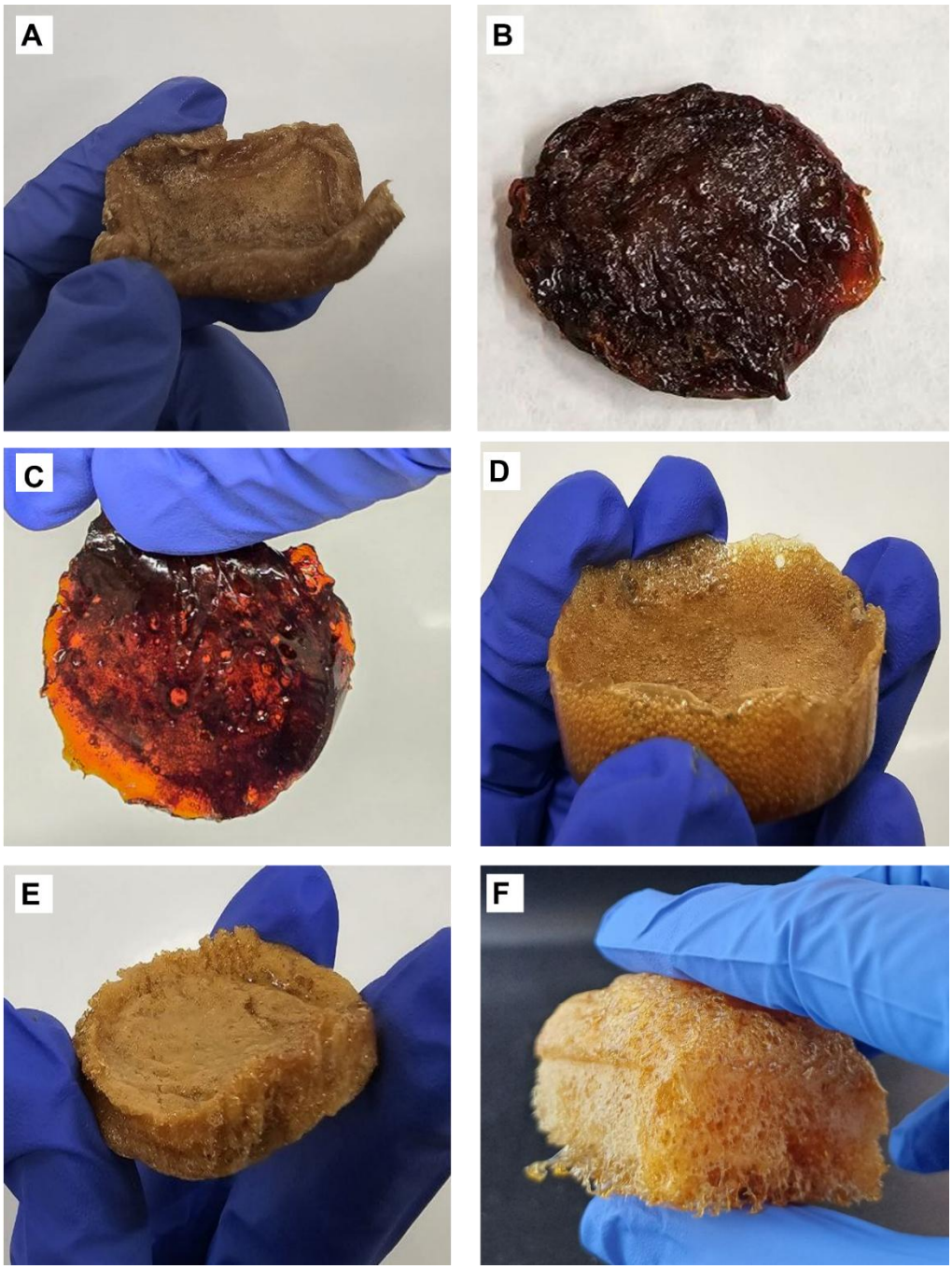

Fig. S43. Images of experimental trials for synthesizing second-generation NIPUFs. The formulation details are provided in **Table S2**.

6.12 Thermal properties of NIPUF-R (recycled NIPUF)

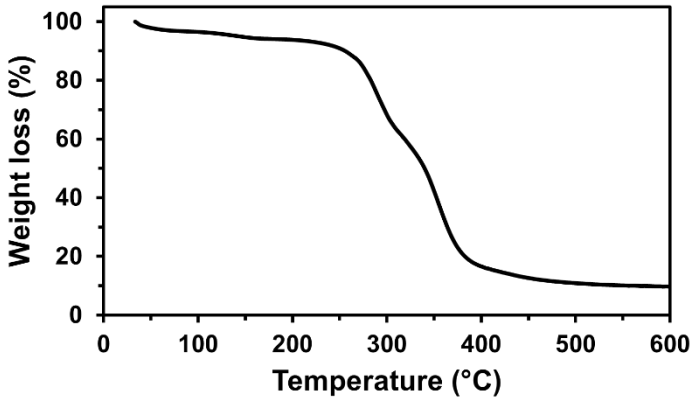

Fig. S44. TGA thermogram of **NIPUF-R**

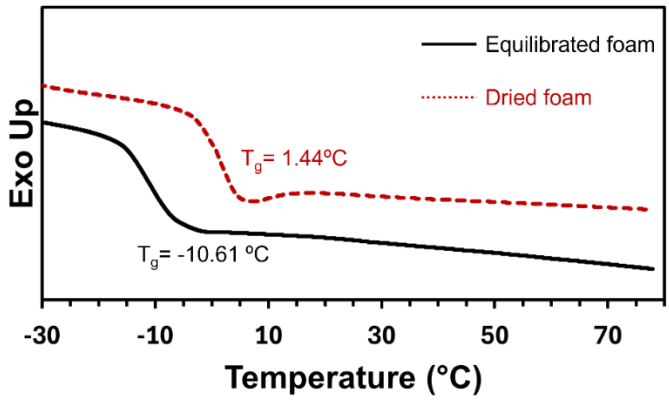

Fig. S45. DSC characterization of NIPUF-R

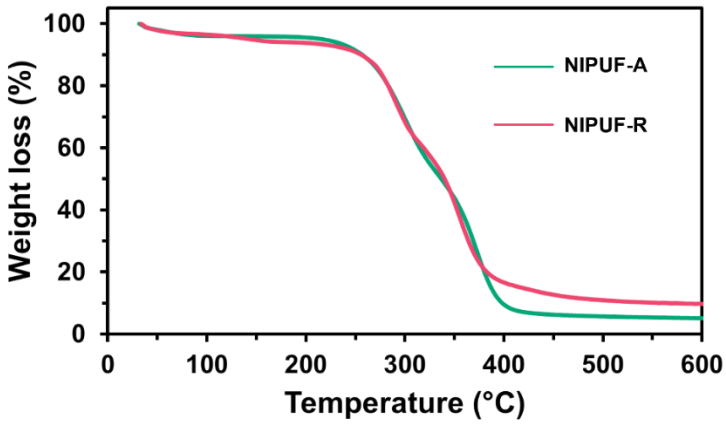

Fig. S46. Overlay of TGA thermogram of **NIPUF-A** and **NIPUF-R**

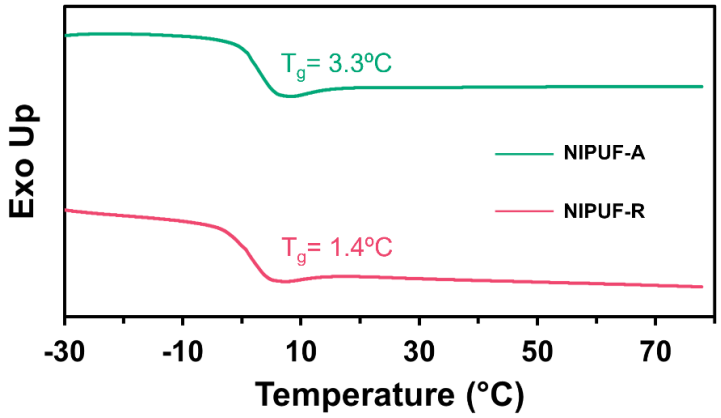

Fig. S47. Overlay of DSC characterization of **NIPUF-A** and **NIPUF-R** (in equilibrium).

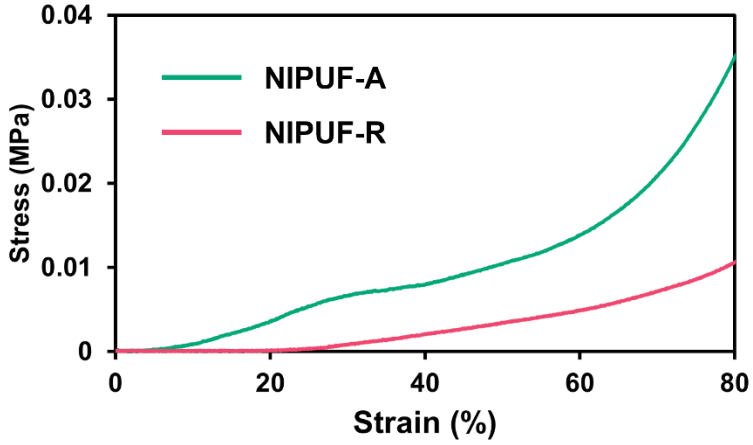

Fig. S48. Overlay of compressive curve of foam **NIPUF-A** and **NIPUF-R** (in equilibrium). Compression modulus is discussed in the main manuscript and depicted in Table 4.

6.13 References

1. Kirpluks, M., et al., *Mechanical and thermal properties of high-density rigid polyurethane foams from renewable resources.* Journal of Renewable Materials, 2016. **4**(1): p. 86-100.

2. Wang, S., et al., *Highly resilient lignin-containing polyurethane foam.* Industrial & Engineering Chemistry Research, 2018. **58**(1): p. 496-504.

Chapter 4. Non-Isocyanate Polyurethane Foams in a Circular Economy: A Life Cycle Assessment-Based Evaluation of Chemical Recycling

Maliheh Razavi-Esfali, Olivier Talon, Bruno Grignard, Christophe Detrembleur*, Haritz Sardon*

Abstract

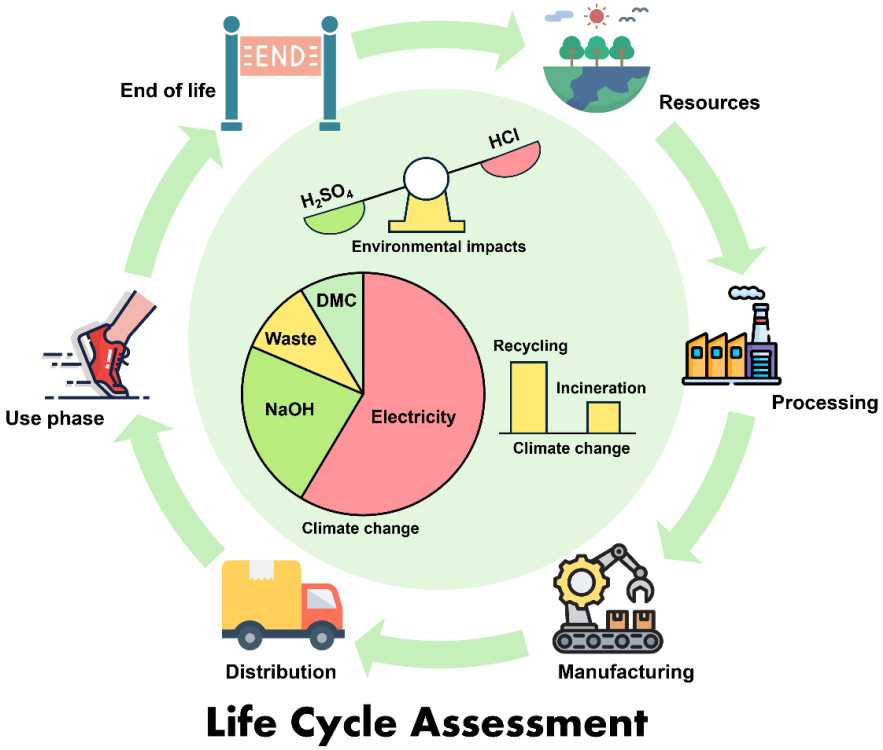

This chapter presents one of the first cradle-to-grave life cycle assessments (LCAs) of non-isocyanate polyurethane foams (NIPUFs), based on experimentally validated hydrolysis-based recycling and regeneration pathways. By integrating lab-scale data on depolymerization and second-generation NIPUF synthesis, the study offers a realistic evaluation of circularity in these emerging materials. Results show that, under current conditions, chemical recycling does not outperform incineration in overall environmental impact. Categories such as global warming potential (GWP), fossil resource use, and human toxicity remain higher for the recycling route due to energy-intensive recovery steps and solvent use. Contribution analysis identified electricity, sulfuric acid, sodium hydroxide, DMC, and waste generation as key impact drivers. Sensitivity analysis further revealed the strong influence of electricity source- Norwegian renewable-based electricity significantly reduced GWP and fossil resource impacts- and confirmed sulfuric acid as the most environmentally favorable neutralization agent. Despite limitations of lab-scale modeling, this study provides valuable insight into the environmental trade-offs of circular strategies for NIPUFs. The LCA framework developed here offers a foundation for future optimization and supports more sustainable design in green polymer chemistry.

1 Introduction

Plastics serve as essential materials for many industrial and production systems, but they pose important environmental problems due to ineffective recycling procedures combined with heavy dependence on landfill solutions and dangerous additive use. This leads to the release of macro- and microplastics in ecosystems affecting terrestrial and aquatic systems [1-3]. To tackle these issues, the circular economy (CE) concept was introduced which focuses on keeping products, materials, and resources within the economic system for extended periods to improve resource efficiency while reducing waste. The European Commission revealed its initial Circular Economy Action Plan in 2015 to promote circular business models in key sectors with plastics as the main emphasis [2]. The updated Action Plan of 2020 maintained plastics as a strategic focus area because of their considerable environmental impact and their circular innovation opportunities [4, 5]. A subsequent public consultation addressed two critical messages: the importance of delivering clear information regarding the potential environmental impacts of plastics and the necessity of addressing these impacts at the earliest stages of the life cycle, particularly during the design and development phases [6]. Within the Circular Economy Action Plan, special emphasis was placed on exploring various strategies to promote the sustainable use and production of plastics through the utilization of biobased and/or recycled feedstocks. Nonetheless, the commission acknowledged that the environmental benefits of such approaches require further comprehensive and quantitative evaluation [7].

Among the various categories of plastics, polyurethanes- particularly in the form of foams- represent a critical case due to their widespread use, complex chemical structure, and limited recyclability, underscoring the urgent need for sustainable innovation in this area. The chemistry underlying polyurethane foams (PUFs)- including their formulation strategies, reactivity, foaming mechanisms, and recyclability-has been described in detail in the previous chapters. It was emphasized that conventional PUFs present notable environmental issues throughout their entire life cycle despite their extensive practical applications. The combination of petrochemical-based feedstocks and toxic isocyanates along with their thermoset structure makes conventional PUFs challenging to recycle and poses significant environmental risks when they reach end-of-life (EoL) [8]. This has prompted increasing interest in developing safer and more sustainable alternatives such as non-isocyanate polyurethane foams (NIPUF)s [9-11], as was discussed comprehensively in previous chapters.

Although the PU to NIPU transition brings benefits including toxicity reduction and renewable material use, sustainability claims require careful evaluation. True sustainability extends beyond the practice of simply replacing harmful components in products. Consequently, the study of NIPUs in terms of their environmental performance remains incomplete with regards to resource demands and recyclability as well as emissions despite their synthesis routes being compatible with green chemistry principles [12, 13]. Particularly within the framework of a circular economy- that emphasizes material reuse through recovery and reintegration processes - it is essential to examine not only the chemical aspects but also overarching system-level effects.

In chapter 3, we introduced a hydrolysis-based closed-loop recycling technique for foams based on aliphatic (EDR 148) and aromatic (*m*-XDA) diamine (water-born NIPUFs in the form of poly(hydroxyurethane), PHU). The system allowed the recovery of small molecules that were subsequently processed for second-generation PHU foam synthesis. This innovation of chemical circularity stands as a major achievement, but we cannot automatically conclude that these recycling strategies offer environmental benefits. A rigorous approach based on quantifiable metrics must evaluate profiles and measure impacts throughout the entire material system life cycle to confirm sustainability claims and guide future material design [12].

Life cycle assessment (LCA) establishes a structured approach with quantitative metrics to measure environmental impacts and analyze trade-offs throughout a product's entire life span including raw material extraction and production until EoL scenarios [14]. It provides comprehensive insights by quantifying key metrics such as carbon footprint, energy use, and resource depletion, while assessing a broad spectrum of impact categories, including climate change, human toxicity, and ecosystem damage [15].

Several prior LCA studies have examined various forms of isocyanate-based PU materials including panels [16], aerogels [17], dispersions [18], bio-based coatings [19], and foams [6, 20, 21] by evaluating raw material sourcing, energy demands, toxicity, and EoL scenarios. More recently, LCA investigations have expanded into NIPU systems, particularly PHUs, highlighting both the environmental implications of original materials and the benefits of reprocessing. These studies underscore the critical influence of factors such as monomer origin, cyclic carbonate ring size, solvent use, and recyclability on the overall sustainability profile of NIPUs [12, 22, 23].

Despite increasing interest in LCA studies on NIPUs, comprehensive cradle-to-grave LCA on NIPUFs remain scarce- particularly those that incorporate experimentally verified recycling and regeneration pathways. This chapter fills this research gap by delivering a system-wide LCA that covers the entire life cycle of NIPUFs beginning with native foam production and concluding with EoL management. Two EoL scenarios were compared: (i) material recovery through hydrolysis and regeneration, and (ii) conventional incineration without recovery. Standardized system boundaries and a unified functional unit ensured robust and equitable comparison across scenarios. Afterwards, a contribution analysis was performed to identify key environmental hotspots across both the initial production of NIPUF and the regeneration loop. The study assesses the contribution of key elements (materials and energy-consumption) across several major impact categories, including global warming potential (GWP), fossil resource depletion, human toxicity (both carcinogenic and non-carcinogenic), and particulate matter formation. Influential parameters including electricity mix and chemical choice were also systematically assessed. By combining real experimental recycling data with quantitative LCA modeling, this study provides one of the first holistic environmental assessments of NIPUFs, delivering actionable insights for the development and scaling of circular polyurethane materials.

2 Methodological framework

In the present study, the LCA models were developed in accordance with the international standards ISO 14040 and ISO 14044 [24, 25]. The LCA was performed using SimaPro 9.6, a widely recognized LCA software developed by Pré Sustainability (The Netherlands). This tool enabled a comprehensive and transparent assessment of environmental impacts across all life cycle stages. When primary data was unavailable, background data were sourced from the Ecoinvent 3.10 database (in the Cut-Off version as provided in SimaPro 9.6), which offers high-quality, peer-reviewed datasets for raw materials, energy production, and emissions, thereby ensuring consistency and reliability in the modeling process.

2.1 Goal and scope

As described in the previous chapter, a lab-scale hydrolysis-based degradation approach was developed to recycle NIPUFs, enabling the recovery of small molecules that were subsequently used to synthesize second-generation NIPUFs (2º NIPUFs). The purpose of this research is to assess the potential environmental impacts associated with this chemical recycling process and the subsequent upcycling. LCA methods were applied to quantify these impacts and to identify opportunities for improvement in the recycling and upcycling processes, supporting further process development and scale-up. To this end, two comparative scenarios involving different EoL options for NIPUFs were evaluated (**Fig. 1-2**).

The first scenario (**Scenario 1**) incorporates recycling, wherein NIPUF based on EDR is synthesized using a water-induced formulation [9]. Upon reaching the end of its initial use phase, the foam undergoes hydrolysis degradation, and the recovered monomers are subsequently used in the production of 2º NIPUFs. After its utilization phase, the regenerated foam is incinerated. In the second scenario (**Scenario 2**), NIPUF is produced, used, and incinerated without recycling, with this cycle repeated once.

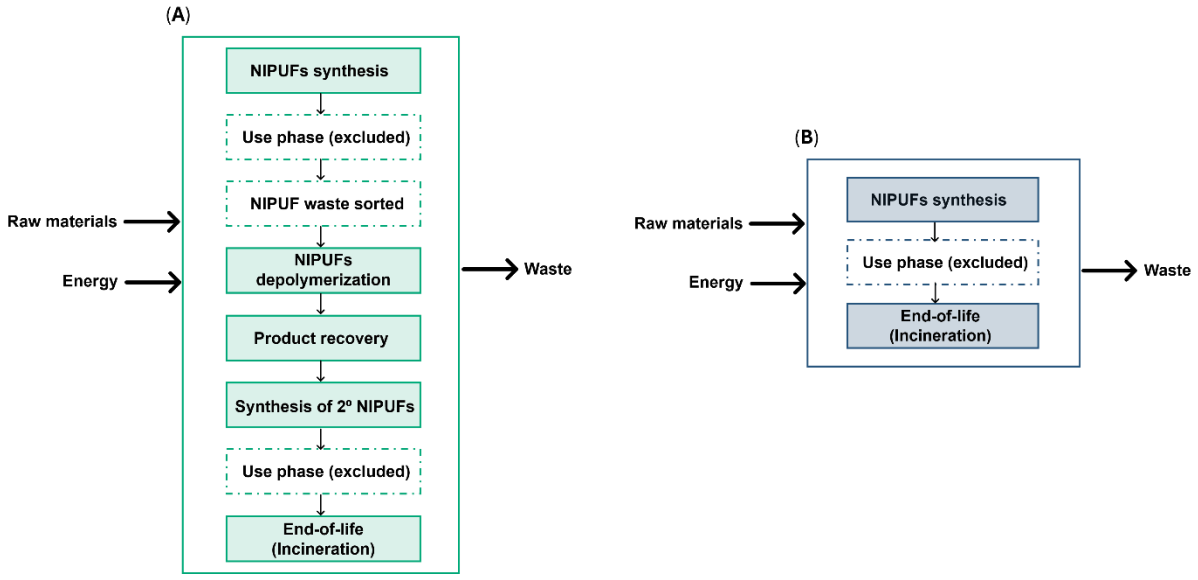

Fig 1. Comparative life cycle system boundaries for NIPUs considering (A) recycling and resynthesis (**Scenario 1**) and (B) linear EoL (**Scenario 2**). The left (green) pathway represents a recycling approach involving NIPU waste sorting, chemical recycling via depolymerization, product recovery, and re-synthesis of secondary NIPUs. The right (blue) pathway depicts a linear scenario where NIPUs are incinerated at EoL. In both cases, the use phase is excluded from the system boundaries.

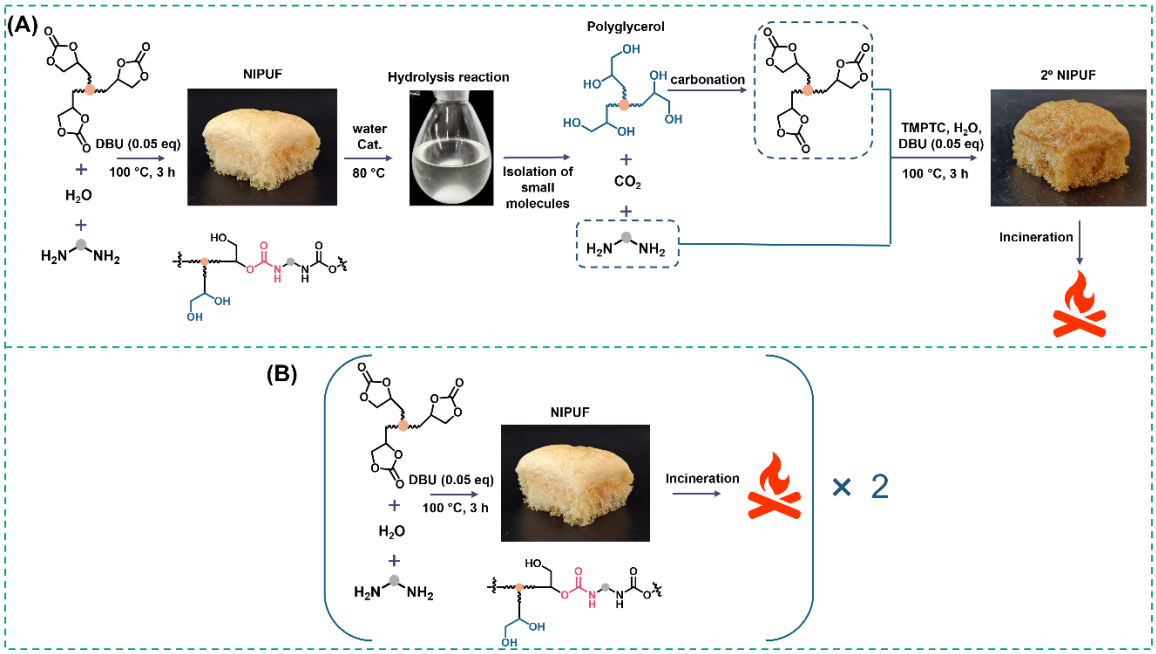

Fig 2. Schematic comparison of the recycling process versus conventional single-use EoL treatment for NIPUFs. (A) **Scenarios 1**, the NIPUF is chemically hydrolyzed into its monomeric components, which are recovered and reused to synthesize new foam, reducing waste and material consumption. (B) **Scenario 2** involves the disposal of used foams via incineration, requiring the consumption of fresh raw materials for each production cycle.

The study finally attempts to recognize which EoL treatment results in higher environmental impacts. In addition, this research seeks to reveal which stages of the NIPUF recycling process contribute the most to the total environmental impact. By doing so, it emphasizes the possible optimization techniques and assesses how close current NIPUF recycling methods are to fulfilling a comprehensive model emphasizing sustainability, circularity, and upcycling. The outcomes of this LCA are anticipated to play a role in the advancement of future studies in material development, recycling process design, and sustainable policymaking in the NIPU field.

Functional unit. The functional unit is defined as 1 kg of NIPUF produced, used, and disposed of or recycled, ensuring equivalent performance and service life.

System boundaries. This study employs a 'cradle-to-grave' with an EoL approach LCA model, focusing on the prepared NIPUFs as the final product. The assessment covers the impacts of feedstocks, NIPUF synthesis, and EoL waste treatment. The use phase of NIPUF was excluded from the analysis, as it does not involve the consumption of energy, materials, or other environmentally significant flows [26].

Impact categories. **Table 1** presents the recommended life cycle impact assessment (LCIA) methods and corresponding indicators for each environmental impact category, as established by the Joint Research Centre (JRC) of the European Commission [27]. In the comparative assessment, all 16 impact categories were considered to ensure a comprehensive evaluation. However, for the contribution analysis, four key categories-climate change, fossil resource use, human toxicity (cancer and non-cancer combined), and particulate matter- were selected. These categories were chosen based on their relevance to polymer production and recycling processes, as well as their significance in environmental and human health contexts.

Table 1. Recommended life cycle impact assessment methods and their indicators, as outlined by the Joint Research Centre of the European Commission [27]

Impact Category	Acronym	Unit	Indicator
Climate Change	CC	Kg CO_2 eq	Radiative forcing as Global Warming Potential (GWP100)
Ozone Depletion	ODP	kg CFC-11eq	Ozone Depletion Potential (ODP)
Particulate Matter	PM	Disease incidences	Human health effects associated with exposure to PM2.5
Ionizing Radiation	IR	kBq U235	Human exposure efficiency relative to U235
Photochemical ozone formation	POF	kg NMVOC eq	Tropospheric ozone concentration increase
Acidification	AC	mol H^+eq	Accumulated Exceedance (AE)
Eutrophication, freshwater	FE	kg Peq	Fraction of nutrients reaching freshwater end compartment (P)
Eutrophication, marine	ME	kg Neq	Fraction of nutrients reaching marine end compartment (N)
Eutrophication, terrestrial	TE	mol Neq	Accumulated Exceedance (AE)
Water use	WAT	m3 world eq. deprived water	User deprivation potential (deprivation-weighted water consumption)
Land use	LU	Dimensionless (pt)	Soil quality index
Resource use, fossils	RES-f	MJ	Abiotic resource depletion – fossil fuels (ADP-fossil)
Resource use, minerals and metals	RES-m	kg Sbeq	Abiotic resource depletion (ADP ultimate reserves)
Human toxicity, cancer	HT-c	CTUh	Comparative Toxic Unit for humans (CTUh)
Human toxicity, non-cancer	HT-nc	CTUh	Comparative Toxic Unit for humans (CTUh)
Ecotoxicity, freshwater	FWT	CTUe	Comparative Toxic Unit for ecosystems (CTUe)

3 Data collection

In this LCA, priority was given to primary data obtained from laboratory-scale experiments. The data used were categorized by source, as described here:

Primary data were obtained from laboratory-scale experiments conducted by our research group. This applies to both the synthesis and hydrolytic degradation of NIPUFs, as well as the isolation of small molecules and preparation of 2º NIPUFs. Given the importance of accurate energy consumption data, electricity usage was measured directly using laboratory equipment during the syntheses according to a procedure described before [28]. Details of electricity consumption are provided in SI.

Secondary data modeled from the literature (similar LCAs, existing protocols in articles, patents, etc.) or from former LCA projects carried out by partner Materia Nova were used for some chemicals specific to this study, including benzyl triethylammonium chloride, trimethylolpropane triglycidyl ether (TMPTE), and TMPTC. All these data were derived from laboratory-scale experiments. In this step, data were based on experiments conducted at pilot-plant scale, with electricity consumption estimated accordingly (see section 4 for detailed explanation).

Secondary data from the Ecoinvent 3.10 database (Ecoinvent Center, St. Gallen, Switzerland) were used for basic chemicals such as solvents, acids, bases, inorganic salts, and similar substances. These data were sourced from the European market, or when unavailable, from the global market to ensure greater representativeness for the context of this study. Similarly, data for electricity production were based on BE energy at medium voltage.

For some chemicals not available in the Ecoinvent database or literature, alternative substances with equivalent functions were used: EDR 148 was replaced by hexamethylenediamine; trimethylolpropane by pentaerythritol; tetrabutyl ammonium iodide by benzyl triethylammonium chloride; 1,8-Diazabicyclo(5.4.0)undec-7-ene (DBU) by pyridine. Such approximations are common practice in LCA when exact datasets are lacking, and proxies are generally chosen based on criteria such as molecular similarity, chemical origin, or production process. Once the inventory is modeled, the contribution of each proxy to the overall impacts should be evaluated to determine whether further refinement is necessary.

It is true that these substances are not identical and may differ in properties or toxicological profiles. However, in this study the substituted compounds appeared as minor or marginal contributors to the overall environmental impacts. Consequently, the approximations did not significantly influence the conclusions. Importantly, in LCA one must also distinguish between a substance used as a material input and the same substance considered as an emission. While emissions are directly linked to toxicological and ecotoxicological indicators, inputs are primarily assessed through their production pathways. In this case, the proxy substitutions concerned inputs rather than emissions, and therefore their different toxicity profiles do not bias the results.

4 Life cycle inventory (LCI)

All intermediate inventories are made available in the following section to ensure reproducibility of the study.

4.1 Chemical and precursor synthesis

4.1.1 Trimethylolpropane triglycidyl ether (TMPTE)

Trimethylolpropane triglycidyl ether (TMPTE) serves as the precursor for the synthesis of cyclic carbonates. As TMPTE is not available in the database, its synthesis was modeled analogously to that of diglycidyl ether of bisphenol A (DGEBA)- readily available in the Ecoinvent database- based on a previously reported method [23, 29] (**Table 2**). Under basic conditions, TMPTE is typically synthesized via the reaction of trimethylolpropane (TMP) with epichlorohydrin (ECH) [29] using a large molar excess of ECH to drive the reaction to completion. In industrial practice, this excess ECH is assumed to be recovered and recycled. Sodium hydroxide (NaOH) is then introduced (3 equiv. per TMP molecule) as a stoichiometric base to facilitate ring closure and the formation of the epoxy functionality following the initial glycidylation step. Benzyltriethylammonium chloride (TEBAC) is employed as a phase-transfer catalyst to promote the reaction between TMP and ECH. As TEBAC is not included in

the database, its synthesis was modeled according to a previously published protocol (Table 3) [22]. Since TMP is also unavailable in the database, pentaerythritol was selected as a proxy due to its structural similarity and comparable synthetic pathway.

Table 2. Life cycle inventory of Trimethylolpropane triglycidyl ether (adapted from [23]).

Production of TMPTE					
Process/product flow	**Unit**	**Input**	**Output**	**Database name**	**Geography**
Trimethylolpropane	g	443.7	-	Pentaerythritol market for	GLO
Benzyltriethylammonium chloride	g	37	-	NFM - benzyltriethylammonium chloride	-
Epichlorohydrin	g	918	-	Epichlorohydrin market for	GLO
Sodium hydroxide	g	793	-	Sodium hydroxide, without water, in 50% solution state market for	RER
Water	m^3	8E-3	-	Water, cooling, unspecified natural origin	RER
Water	m^3	5E-4	-	Water, river	RER
Water	m^3	4E-4	-	Water, well	RER
Heat	MJ	1.059	-	Heat, district or industrial, natural gas, market for	RER
Heat	MJ	0.117	-	Heat, from steam, in chemical industry, market for	RER
Electricity	kWh	0.39	-	Electricity, medium voltage market group for	BE
Emissions in air, water	m^3	-	0.001	Water/m^3	RER
Emission in water, chloride	kg	-	0.361	Chloride	
Emission in water, Sodium	kg	-	0.397	Sodium (I)	
Emission in water, water	m^3	-	4E-4	Water	RER
Waste	m^3	-	3E-8	Wastewater, average, market for	CH
Waste	m^3	-	1E-6	Wastewater, average, market for	Europe without Switzerland
Trimethylolpropane triglycidyl ether (TMPTE)	kg	-	1	NFM - Trimethylolpropane triglycidyl ether	-

4.1.2 Benzyl triethylammonium chloride (TEBAC)

The synthesis of benzyl triethylammonium chloride (TEBAC) was explained by Chen et al. [22, 30] and is synthesized through the quaternization reaction of benzyl chloride with

trimethylamine, using a mixed solvent system of ethyl acetate and acetonitrile (**Table 3**). The reactants are used in a molar ratio of 1.15:1 (benzyl chloride to trimethylamine), and the solvents are combined in a mixture where ethyl acetate constitutes 23.6% by mass. The overall solvent-to-trimethylamine mass ratio is 1.68:1. After the reaction, the crude product undergoes filtration and drying to yield TEBAC with a high purity of 99% and a yield of 98%. During purification, 95% of the solvents are recovered and reused, while 5% is considered as a loss.

Table 3. Life cycle inventory of benzyl triethylammonium chloride (adapted from [22]).

Production of benzyl triethylammonium chloride (TEBAC)					
Process/product flow	**Unit**	**Input**	**Output**	**Database name**	**Geography**
Benzyl chloride	kg	0.390	-	Benzyl chloride market for	RER
Triethyl amine	kg	0.283	-	Triethyl amine market for	GLO
Ethyl acetate	kg	0.006	-	Ethyl acetate market for	GLO
Acetonitrile	kg	0.018	-	Acetonitrile market for	GLO
Waste	kg	-	0.053	Hazardous waste, for incineration market for	Europe without Switzerland
Benzyl triethylammonium chloride (TEBAC)	kg	-	0.66	NFM - benzyltriethylammonium chloride	-

4.1.3 Trimethylolpropane tri-cyclic carbonate (TMPTC) synthesis

A CO_2-based synthesis route was employed for the synthesis of trimethylolpropane tri-cyclic carbonate (TMPTC), in line with methodologies described in various research studies [9, 23] (**Table 4**). TMPTC was obtained using TMPTE as the epoxy precursor. The typical synthesis is performed at kilogram scale in a 2 L high-pressure stainless-steel reactor. The catalyst for this reaction is typically tetrabutyl ammonium iodide, however in this model, TEBAC is applied as a model catalyst. After mixing the precursors, CO_2 is then pressurized into the reactor and heat is applied. During supercritical CO_2 conditions the system is maintained at 100-110 °C for 24 h at 100 bar. The reaction usually continues from 15 to 24 h, leading to yields approaching quantitative. This requires no solvents and no purification after the reaction.

Table 4. Life cycle inventory of Trimethylolpropane tri-cyclic carbonate (adapted from [23]).

Production of Trimethylolpropane tri-cyclic carbonate (TMPTC)					
Process/product flow	**Unit**	**Input**	**Output**	**Database name**	**Geography**
Carbon dioxide	g	505	-	Carbon dioxide, liquid, market for	RER
Trimethylolpropane triglycidyl ether (TMPTE)	kg	1.157	-	NFM- Trimethylolpropane triglycidyl ether	-
tetrabutyl ammonium iodide	g	35.29	-	NFM - benzyltriethylammonium chloride	-
Electricity	kWh	3.3	-	Electricity, medium voltage market group for	BE
TMPTC	kg		1.6	NFM - TMPTC - ULiege Synthesis	-

4.2 NIPUF synthesis and recycling

Fig. 3 illustrates the various steps involved in the synthesis, recycling, and upcycling of NIPUF. Each step is explained in the following sections.

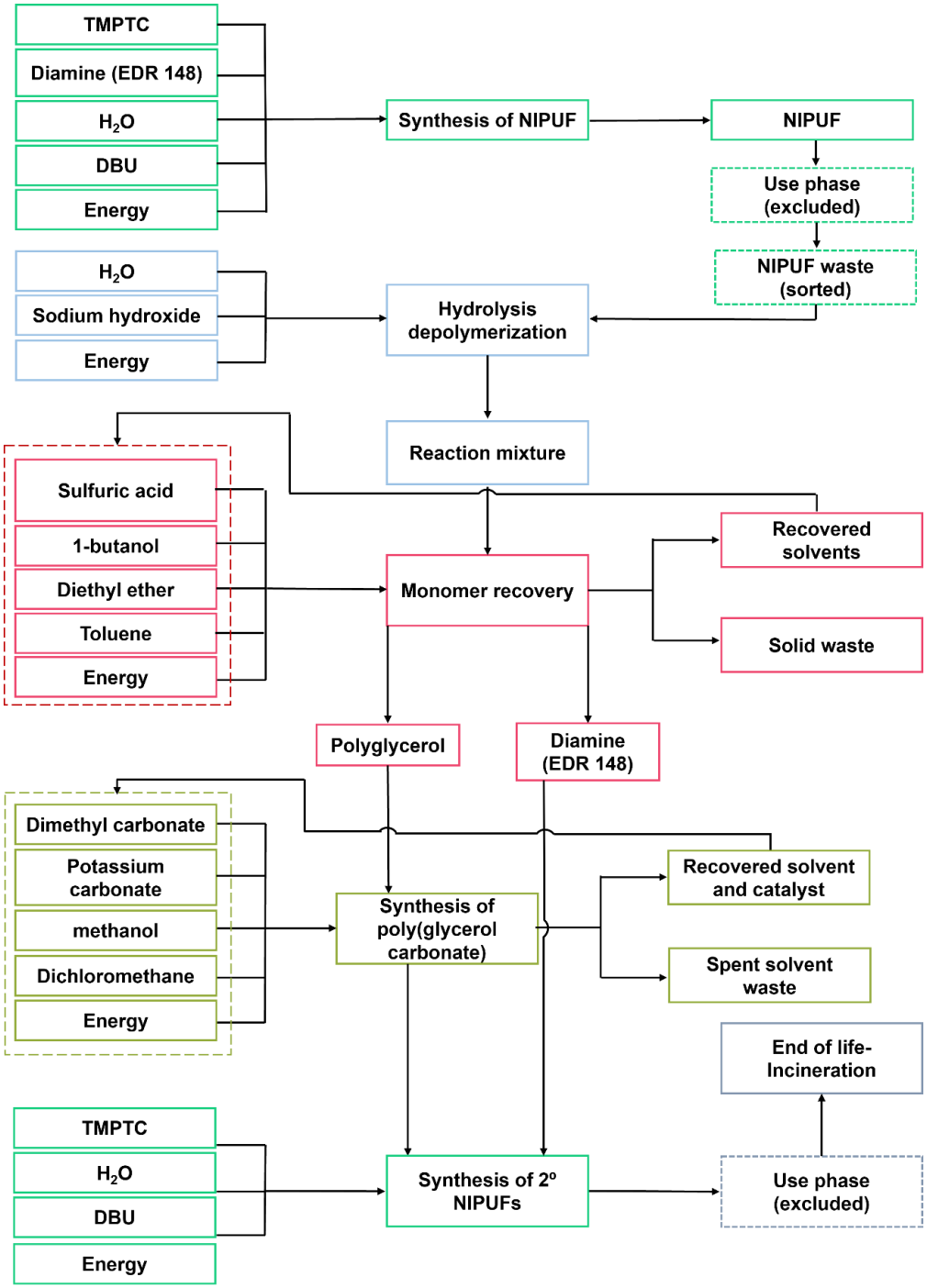

Fig 3. Schematic flow diagram illustrates the synthesis, depolymerization, and recycling of NIPUF representing material, energy and emission flows associated with the various stages in the life cycle of NIPUF.

4.2.1 Production of NIPUF

The native NIPUF was initially synthesized using TMPTC, EDR 148, water, and DBU at 100 °C for 3 h. Detailed experimental conditions are provided in Chapter 3, Section 2.3. As background data for EDR 148 was not available in the Ecoinvent database,

hexamethylenediamine was used as a proxy due to its structural and functional similarity. Similarly, in the absence of DBU in the database, pyridine was selected as an approximate substitute, given the comparable heterocyclic structure. The LCI for the synthesis process is summarized in **Table 5**.

Table 5. Life cycle inventory of NIPUF.

Production of NIPUF					
Process/product flow	**Unit**	**Input**	**Output**	**Database name**	**Geography**
TMPTC	g	5	-	NFM-TMPTC	-
Water	mg	620	-	Water, deionized, market for	Europe without Switzerland
EDR	mg	1900	-	Hexamethylenediamine, market for	GLO
DBU	mg	260	-	Pyridine, market for	GLO
Electricity	Wh	3	-	Electricity, medium voltage, market	BE
NIPU foam-NIPUF-A	g	-	7.5	NFM-NIPU foam-NIPUF-A	-

4.2.2 Hydrolysis depolymerization of NIPUF and recovery of small molecules

Following the use phase, NIPUF underwent a recycling process via hydrolysis in 5 M NaOH at 80 °C for 10 h. LCI for the hydrolysis process is presented in **Table 6**.

Upon completion of the decomposition, two primary products, polyglycerol (**PG**) with an isolated yield of 65% and diamine EDR 148 (isolated yields: 61%) were recovered through a multistep purification procedure (see section 2.5.1 of chapter 3 for details). LCI for the whole process is presented in **Table 7**. The solvents used for extraction and purification are considered to be fully recovered using electricity as energy input for solvent recovery process. A mass allocation approach was applied to divide the environmental burdens of the recycling process between the two co-products- polyglycerol (PG) and EDR 148- based on their isolated masses. This means that environmental impacts (e.g., energy and material use) were allocated proportionally: 73% to PG and 27% to EDR 148, corresponding to their respective shares in the total recovered mass.

Table 6. Life cycle inventory of NIPUF hydrolysis process.

Hydrolysis of NIPUF					
Process/product flow	**Unit**	**Input**	**Output**	**Database name**	**Geography**
NIPUF	g	3.8	-	NFM- NIPU foam	-
Water	g	150	-	Water, deionized, market for	Europe without Switzerland
Sodium hydroxide	g	30	-	Neutralising agent, sodium hydroxide-equivalent, market for	RER
Electricity	kWh	0.015	-	Electricity, medium voltage, market for	BE
Hydrolyzed reaction mixture	g	-	183.8	NFM-Hydrolysis of NIPUF	BE

Table 7. Life cycle inventory of recycled polyglycerol and diamine.

Recycled polyglycerol and diamine					
Process/product flow	**Unit**	**Input**	**Output**	**Database name**	**Geography**
Hydrolyzed reaction mixture	g	183.8	-	NFM-Hydrolysis of NIPUF	-
Sulfuric acid	g	36.8	-	Sulfuric acid, market for	RER
1-butanol	g	648*	648*	1-butanol, market for	GLO
Diethyl ether	g	143*	143*	Diethyl ether, without water, in 99.95% solution state	RER
Toluene	g	90*	90*	Toluene, liquid, market for	RER
Water	g	-	150*	Water, deionized, market for	Europe without Switzerland
Electricity	kWh	0.3	-	Electricity, medium voltage, market for	BE
Waste	g	-	52	Municipal solid waste, market for	BE
Recycled polyglycerol (**PG**)[a]	g	-	1.53	NFM-recycled polyglycerol	-
Recycled diamine (EDR 148) [b]	mg	-	580	NFM-recycled diamine (EDR 148)	-

* The solvents used for extraction and purification are considered to be fully recovered using electricity as energy input. [a] mass allocation of 73 %, and [b] mass allocation of 27%.

4.2.3 Carboxylation of PG to PGC

Subsequently, **PG** underwent carboxylation using dimethyl carbonate (DMC) and K_2CO_3 as a catalyst to produce polyglycerol carbonate (**PGC**) (see section 2.7 chapter 3 for further details).

Methanol was used to solubilize **PG**, and dichloromethane (DCM) was used to isolate the catalyst and **PG**. LCI for the synthesis process is presented in **Table 8**. No waste except methanol was generated during the purification and cyclization stages as DMC, DCM and K_2CO_3 were recovered and reused after the product isolation.

Table 8. Life cycle inventory of polyglycerol carbonate.

Production of polyglycerol carbonate					
Process/product flow	**Unit**	**Input**	**Output**	**Database name**	**Geography**
Recycled polyglycerol	g	1.53	-	NFM-Recycled polyglycerol	-
Dimethyl carbonate	g	46*	45*	Dimethyl carbonate, market for	GLO
Potassium carbonate	mg	255*	255*	Potassium carbonate, market for	GLO
Methanol	g	1.5	-	Methanol, market for	RER
Dichloromethane	g	42*	42*	Dichloromethane, market for	RER
Electricity	kWh	0.011	-	Electricity, medium voltage, market	BE
Waste	g	-	2	Spent solvent mixture, market for	Europe without Switzerland
Polyglycerol carbonate (PGC)	g	-	1.7	NFM- Polyglycerol carbonate	-

* The solvents used for purification and excess of DMC are considered to be fully recovered using electricity as energy input.

4.2.4 Production of second generation NIPUF (2º NIPUF)

The isolated **PGC** and diamine EDR 148 were then incorporated into 2º NIPUF, along with fresh TMPTC, H_2O as the blowing agent, and DBU as the catalyst, under the same reaction conditions as native NIPUF (100 °C for 3 h). LCI for the whole process is presented in **Table 9**.

Table 9. Life cycle inventory of 2º NIPUF.

Production of NIPUF-second generation					
Process/product flow	**Unit**	**Input**	**Output**	**Database name**	**Geography**
Polyglycerol carbonate (PGC)	g	3.5	-	NFM- Polyglycerol carbonate	-
TMPTC	g	2.3	-	NFM-TMPTC	-
Water	mg	620	-	Water, deionised market for	Europe without Switzerland
Recycled diamine EDR 148	mg	1900	-	NFM- Recycled diamine	-
DBU	mg	260	-	Pyridine, market for	GLO
Electricity	Wh	3		Electricity, medium voltage, market for	BE
Second generation of NIPUF	g	-	8.3	NFM-Second generation of NIPUF	-

4.2.5 Acids used for neutralizing the reaction medium after hydrolysis

One step in the isolation of small molecules following hydrolysis depolymerization involved the neutralization of these molecules (see section 2.5 chapter 3 for more details). Four different acids were considered for this purpose: sulfuric acid, nitric acid, hydrochloric acid, and acetic acid. The environmental impacts of these acids were compared, considering the quantities required to achieve complete neutralization of the reaction mixture to pH 6. The LCI data for different acids are presented in **Table 10**.

Table 10. Life cycle inventory of different acids.

Different acids					
Process/product flow	**Unit**	**Input**	**Output**	**Database name**	**Geography**
Sulfuric acid	g	37.5	-	Sulfuric acid, market for	RER
Nitric acid	g	94.6	-	Nitric acid, without water, in 50% solution state, market for	RER w/o RU
Hydrochloric acid	g	91.2	-	Hydrochloric acid, without water, in 30% solution state, market for	RER
Acetic acid	g	46.1	-	Acetic acid, without water, in 98% solution state, market for	GLO

4.2.6 Energy sources for producing 2° NIPUFs

The LCI data for the various energy sources used across Europe in the production of 1 kg of 2° NIPUF are presented in **Table 11**.

Table 11. Life cycle inventory of different energy sources.

Different energy sources			
Process/product flow	**Unit**	**Database name**	**Geography**
Electricity (BE)	kWh	Electricity, medium voltage, market group for	BE
Electricity (ES)	kWh	Electricity, medium voltage, market group for	ES
Electricity (FR)	kWh	Electricity, medium voltage, market group for	FR
Electricity (NL)	kWh	Electricity, medium voltage, market group for	NL
Electricity (NO)	kWh	Electricity, medium voltage, market group for	NO
Electricity (EU)	kWh	Electricity, medium voltage, market group for	EU

4.3 Energy consumption calculation

The energy consumption for each step of material synthesis, depolymerization, and re-synthesis was calculated following the framework and methodology outlined by Piccinno et al. [28]. Their research provides a detailed procedure for simulating industrial-scale production using data obtained from laboratory-scale experiments. Three primary types of energy consumption were involved in the reactions: reaction energy (Qreact, Eq.1), stirring energy (Estir, Eq.2), and drying energy which refers to the energy required to remove solvents from the reaction mixture (Qdry, Eq.3). The details of experimental process are reported in chapter 3, and the details of energy consumption data for each process are presented in the SI.

$$Q_{react} = \frac{Q_{heat}+Q_{loss}}{\eta_{heat}} = \frac{C_p * m_{mix} * (T_r - T_0) + A * \frac{k_a}{s} * (T_r - T_{out}) * t}{\eta_{heat}} \quad \text{(Eq.1)}$$

$$E_{stir}[J] = \frac{N_p * \rho_{mix} * N^3 * d^5 * t}{\eta_{stir}} \quad \text{(Eq.2)}$$

$$Q_{dry} = \frac{C_{p,liq} * m_{liq} * (T_{boil} - T_0) + \Delta H_{vap} * m_{vap}}{\eta_{dry}} \quad \text{(Eq.3)}$$

The definition of each variable in the above equations is described in **Table 12**.

Table 12. Summary and definitions of variables used in energy consumption calculations

Variable (unit)	Description
Q_{heat}(J)	Energy for raising the temperature
Q_{loss}(J)	Heat loss on the reactor surface
η_{heat}	Efficiency of the heating device
C_p(J/kg.K)	Specific heat capacity
m_{mix}(Kg)	Mass of the reaction mixture
T_r (K)	Reaction temperature
T_0 (K)	Starting temperature
A*k_a/s(W/K)	Rate of heat loss per Kelvin
T_{out}(K)	Temperature outside of the reactor
t (s)	Time of the reaction
N_p	Type of the impeller
ρ_{mix} (kg/m^3)	Density of the reaction mixture
N (s^{-1})	Rotational velocity of stirring
d (m)	Diameter of the impeller
η_{stir}	Efficiency of stirring
T_{boil} (K)	Boiling temperature
ΔH_{vap}(J/kg)	Enthalpy of vaporization
η_{dry}	Drying efficiency

5 Life cycle impact assessment results

5.1 Comparative study of NIPUF considering two EoL scenarios (recycling and incineration)

The comparative results of **Scenario 1** and **Scenario 2** across 16 impact categories are presented in **Fig. 4**, where **Scenario 1** is shown in green and **Scenario 2** in blue. The results

indicate that **Scenario 1** exhibits higher environmental impacts across all categories compared to **Scenario 2**. In many impact categories, such as climate change, ozone depletion, acidification, resource use, and human toxicity, **Scenario 1** reaches 100% impact (used as the reference), while **Scenario 2** ranges between approximately 5–50% of that impact. This result suggests that, in its current form, the recycling and reproduction process used in **Scenario 1** introduces additional environmental burdens compared to incineration.

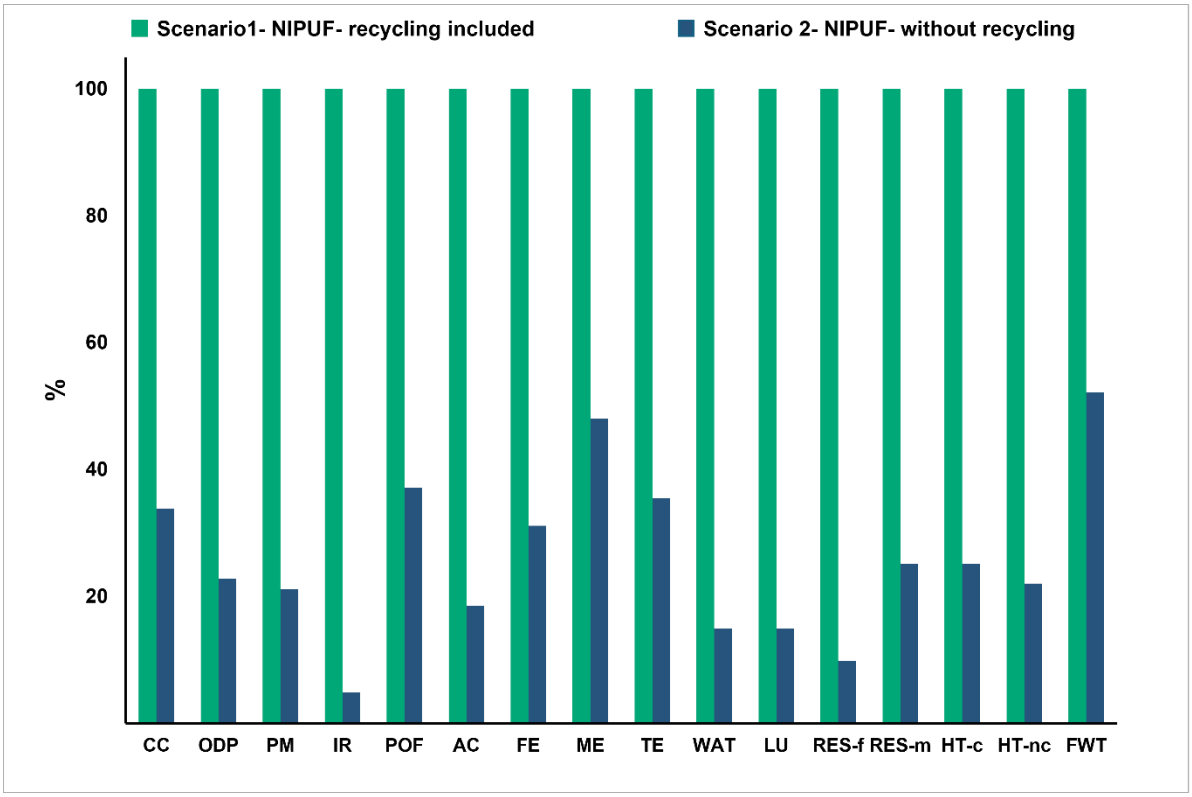

Fig. 4. LCA comparative cradle-to-grave impact assessment results for **Scenario 1** and **Scenario 2**.

A stepwise contribution analysis was carried out to evaluate the environmental performance of the hydrolytic recycling process. The study evaluated the environmental impact of producing 1 kg of 2º NIPUF through a model that incorporated multiple interconnected subprocesses. These subprocesses included: (i) hydrolysis of native NIPUF (**Fig. 5**); (ii) isolation and recovery of small molecules (**PG**) and diamine EDR 148 (**Fig. 6**); (iii) conversion of **PG** into the cyclic carbonate precursor **PGC** (**Fig. 7**); and (iv) synthesis of 2º NIPUF from **PGC** and recovered diamine (**Fig. 8**). The LCA models for each subprocess were created independently which enabled detailed evaluations of their separate environmental impact contributions. This modular approach ensured that the impact assessment accounted not only for the production of

the final product but also for the key upstream subprocesses, providing a comprehensive and transparent understanding of the life cycle impacts.

In the hydrolysis process applied to native NIPUF (**Fig. 5**), the consumption of sodium hydroxide and electricity was identified as the dominant contributors to environmental impacts. In the subsequent isolation and recovery process of **PG** and EDR 148 (**Fig. 6**), electricity consumption, sulfuric acid usage, and waste generation were the primary sources of environmental burden. The environmental impact of **PGC** production (**Fig. 7**) was mainly attributed to the use of recycled **PG** and dimethyl carbonate (DMC) as the cyclocarbonation agent, with particularly notable contributions to climate change, human toxicity, and resource depletion categories. In the overall life cycle of 2º NIPUF production, **PGC** and diamine emerged as the most significant contributors across all environmental impact categories, respectively (**Fig. 8**), primarily due to the multi-step synthesis routes, high energy inputs, and the use of solvents and reagents required for their production and recovery.

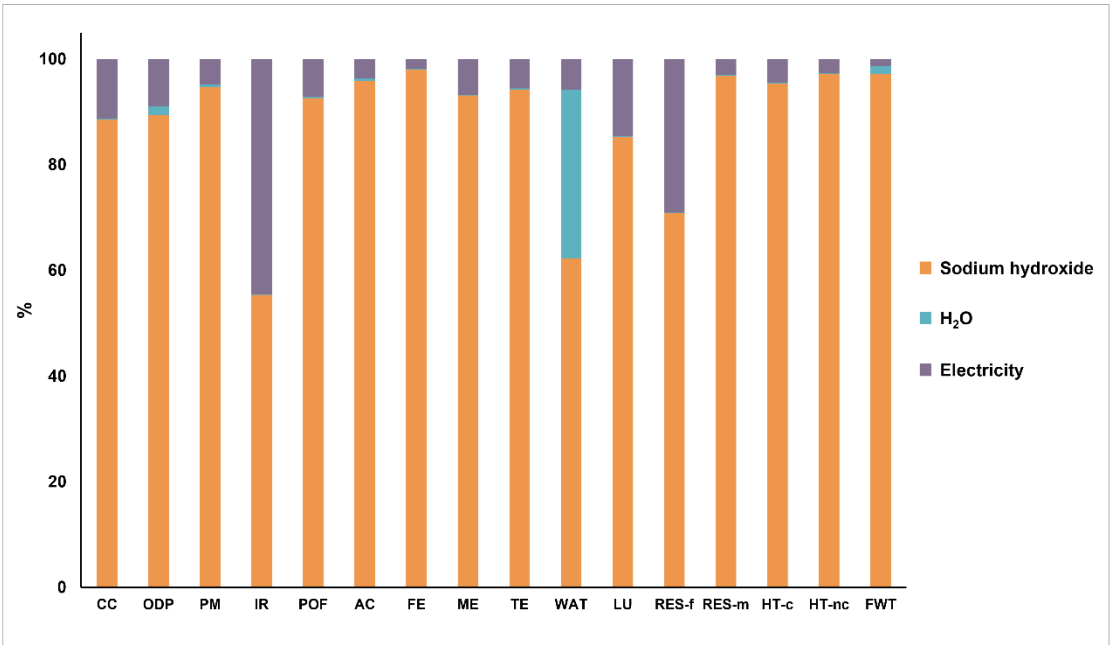

Fig. 5. Impact assessment of hydrolysis reaction across 16 environmental impact categories, contribution analysis. The electricity contribution reflects the energy consumed during the hydrolysis process of native NIPUF.

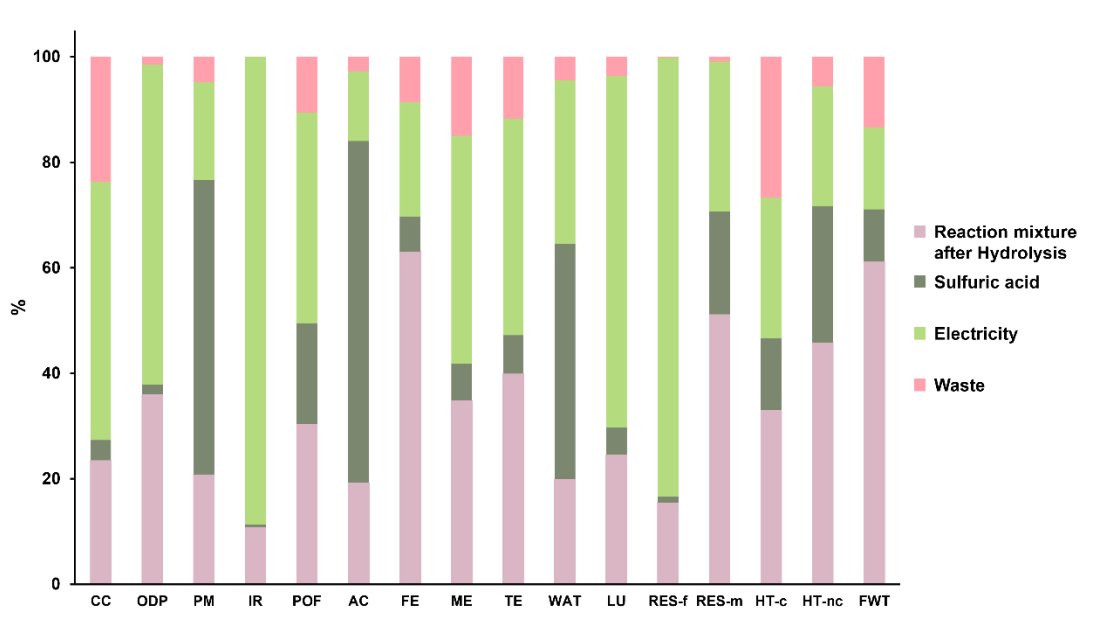

Fig. 6. Impact assessment of recovered **PG** and diamine (EDR 148) across 16 environmental impact categories: contribution analysis. The electricity contribution reflects the energy consumed during purification and isolation of **PG** and EDR 148. The waste contribution corresponds to the produced salt after neutralization.

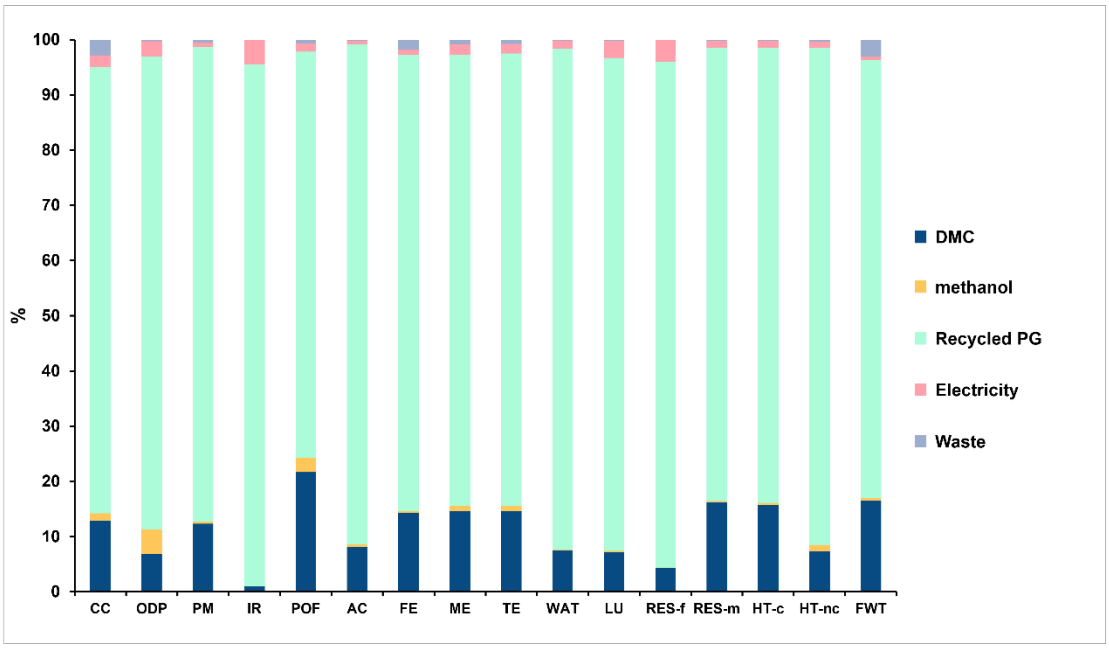

Fig. 7. Impact assessment of **PGC** across 16 environmental impact categories: contribution analysis. The electricity contribution reflects the energy consumed during the synthesis and purification stages of PGC. The waste contribution corresponds to spent solvent that could not be recovered during **PGC** synthesis.

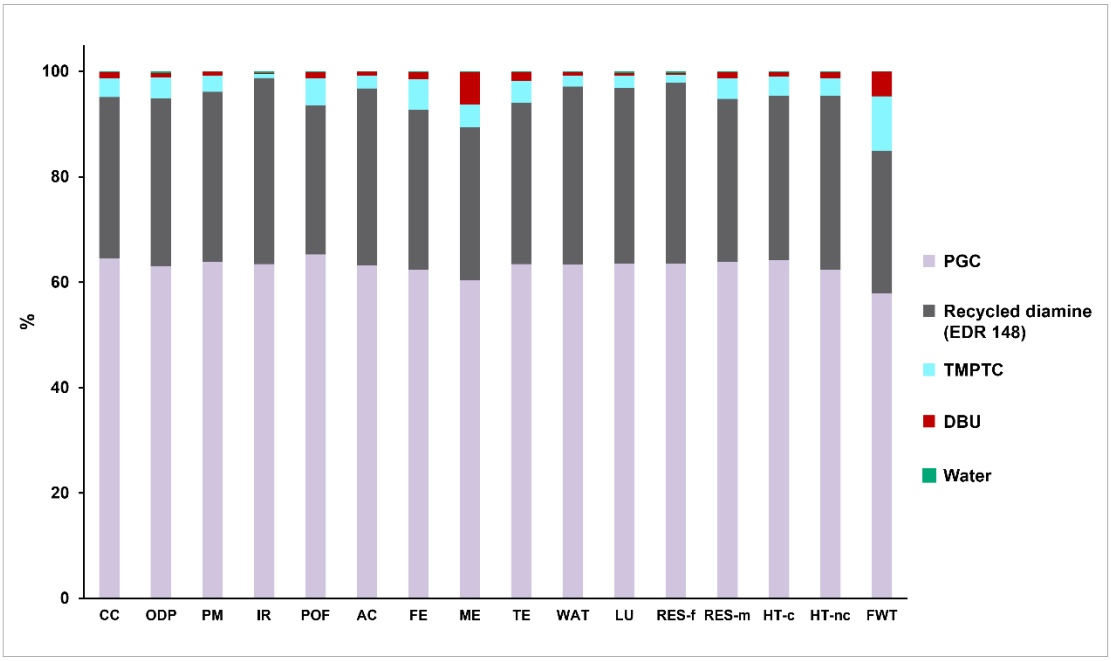

Fig. 8. Impact assessment of 2º NIPUF production across 16 environmental impact categories, contribution analysis.

5.2 Contribution analysis of environmental impacts in the production of 2° NIPUF

Finally, to quantify the cumulative environmental burdens of individual substances across the entire recycling and upcycling process and identify the overall dominant impact sources, an aggregated contribution analysis was performed (for producing 1 kg of 2º NIPUF). The impacts of each input- electricity, and materials- were summed across all subprocesses, including hydrolysis, isolation and recovery of monomers, **PGC** production, and the final synthesis of 2º NIPUF. For example, the total impact of electricity accounted for its use in all relevant subprocesses. The resulting relative contributions were evaluated across four key environmental impact categories: climate change, fossil resource use, human toxicity (cancer and non-cancer combined), and particulate matter and is discussed in the following section.

5.2.1 Climate change

The climate change impact category reflects the contribution of greenhouse gas (GHG) emissions- such as carbon dioxide, methane, and nitrous oxide- to global warming, measured in kilograms of CO_2 equivalents. These gases trap infrared radiation in the atmosphere, increasing the Earth's radiative forcing and leading to rising global temperatures that disrupt ecosystems, human health, and infrastructure [31, 32]. As depicted in **Fig. 9**, in terms of climate change, electricity consumption emerges as the predominant contributor (42%), highlighting the carbon-intensive nature of energy production, particularly when derived from fossil-based sources (e.g., coal or natural gas) [1]. Waste generation (20%) and the use of sodium hydroxide (15%) and dimethyl carbonate (DMC, 8%) also contribute significantly owing to their upstream emissions. Water (H_2O) usage accounts for 7%, while sulfuric acid and TMPTC each contribute 3%. Other minor contributors (DBU, methanol) collectively represent 2% of the total impact.

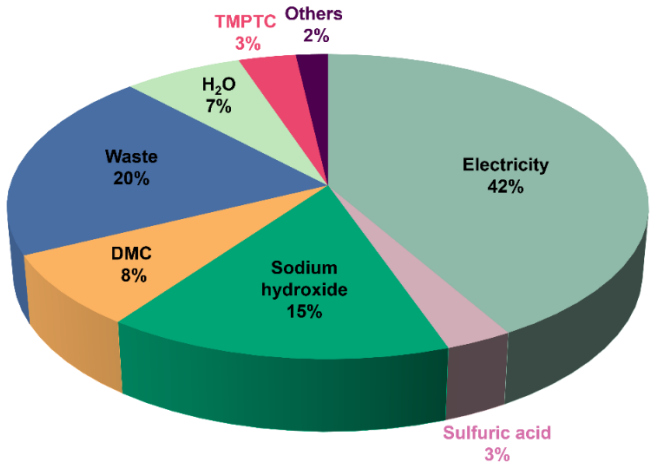

Fig. 9. Contribution distribution for the Climate change environmental impact category. The environmental impacts are associated with the production of 1 kg of 2º NIPUF. Contributions below 3% (DBU, methanol) are gathered in the category of Others. Unit: kg CO_2 equivalent (kg CO_2-eq)

5.2.2 Resource use, fossils

The resource use, fossils impact category quantifies the depletion of non-renewable fossil resources such as crude oil, natural gas, and coal, which are extensively utilized for both

material synthesis and energy production [33]. As shown in **Fig. 10**, electricity accounts for an overwhelming 84% of fossil resource consumption, reflecting the energy-intensive nature of the process and the dependency on fossil-fuel-based power generation. However, this result is based on the Belgian electricity mix and is highly dependent on the regional energy supply, particularly the share of fossil-based versus low-carbon sources. This highlights the need to consider geographic variability when interpreting energy-related impacts in LCA. Sodium hydroxide contributes 10%, followed by DMC and TMPTC, each contributing 3%. All other inputs- including DBU, methanol, water, sulfuric acid, and waste- collectively account for just 1% and are grouped under the category "Others."

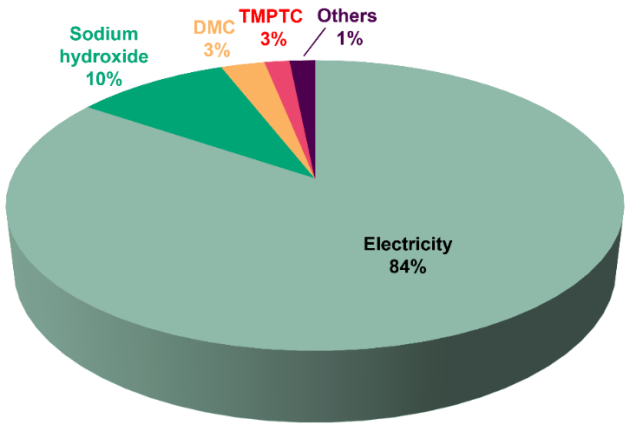

Fig. 10. Contribution distribution for the Resource use, fossils environmental impact category. The environmental impacts are associated with the production of 1 kg of 2º NIPUF. Minor contributors-including DBU, methanol, water, sulfuric acid, and waste- each account for less than 3% of the total impact and are aggregated under the category “Others.” Unit: MJ

5.2.3 Human toxicity

The human toxicity impact category evaluates the effects of chemical emissions during a product's life cycle on human health. This category covers both cancer and non-cancer effects while considering exposure pathways including inhalation, ingestion, and skin contact [34]. As demonstrated in **Fig 11**, sodium hydroxide contributes the largest share (30%) to human toxicity, due to its caustic nature and the hazardous emissions associated with its energy-intensive chlor-alkali production process [35, 36]. Electricity follows closely (24%), reflecting the indirect release of toxic pollutants- including heavy metals and particulates- during fossil-

fuel-based electricity generation [37, 38]. Sulfuric acid (16%), DMC (8%), and TMPTC (4 %) further contribute to toxicity burdens due to their high reactivity and involvement in potentially hazardous synthesis and disposal pathways. Additionally, waste streams account for 17% of the impact, highlighting the health risks related to improper treatment or incineration of residuals containing harmful substances. This distribution emphasizes the need for stringent management of toxic inputs and emissions along the life cycle, as well as a shift toward cleaner energy sources and safer chemical alternatives to minimize public health risks. All other inputs collectively (DBU, methanol, water) represent 1% and are grouped under "Others."

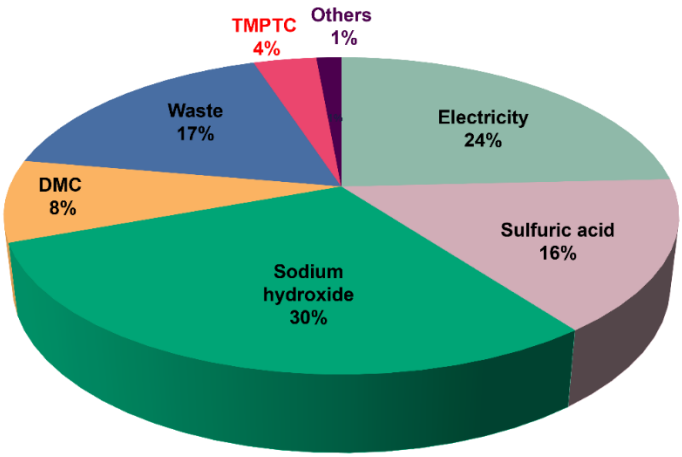

Fig. 11. Contribution distribution for the Human toxicity (Cancer and non-cancer) environmental impact category. The environmental impacts are associated with the production of 1 kg of 2º NIPUF. Minor contributors-including DBU, methanol, and water- each account for less than 3% of the total impact and are aggregated under the category "Others." Unit: Comparative Toxic Unit for humans (CTUh)

5.2.4 Particulate matter

The particulate matter (PM) formation impact category assesses the emission of fine particles ($PM_{2.5}$ and PM_{10}) and their precursors, which pose significant risks to human health, particularly by increasing the incidence of respiratory and cardiovascular diseases [39]. As shown in **Fig. 12**, sulfuric acid is the largest contributor (49%), primarily due to its production process, which emits sulfur oxides (SO_x) that act as precursors to secondary inorganic aerosols- a key component of fine particulate matter in atmospheric chemistry [40]. Electricity use (18%) also contributes notably, especially when derived from coal or heavy fuel oil, which emit particulates directly along with precursor gases like NO_x and SO_x [38, 41]. Sodium hydroxide (16%) and DMC (8%) further influence PM formation, stemming from emissions associated

with raw material extraction, combustion, and chemical synthesis [42]. Waste generation (5%) and other minor inputs, including TMPTC (3%) and Others (including DBU, methanol, and water, 1%), also contribute to the overall burden, though to a lesser extent. This analysis emphasizes the need for mitigation strategies targeting both primary emissions and secondary particle precursors, particularly through cleaner electricity sources and emissions controls within chemical production.

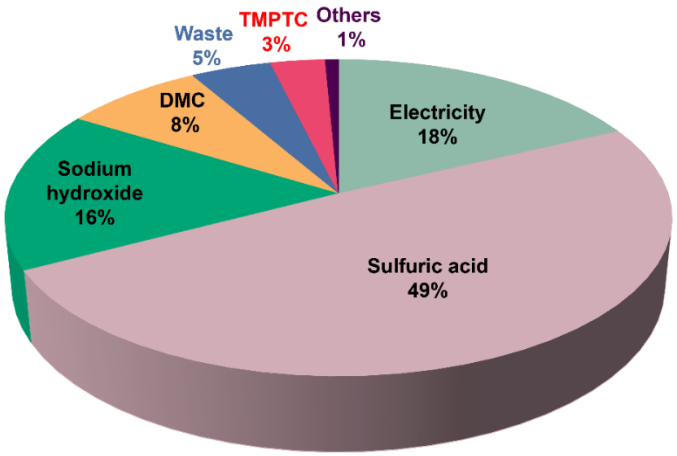

Fig. 12. Contribution distribution for the Particulate matter environmental impact category. The environmental impacts are associated with the production of 1 kg of 2º NIPUF. Minor contributors-including DBU, methanol, and water each account for less than 3% of the total impact and are aggregated under the category "Others." Unit: kg $PM_{2.5}$ equivalent (kg $PM_{2.5}$-eq)

5.3 Key impact contributors

The results in section 5.2 prompted a closer investigation into why each of these contributors is impactful, followed by a breakdown of their respective roles in the process and potential areas for improvement.

5.3.1 Electricity

Electricity usage is the most dominant impact driver, especially during hydrolysis, purification, and solvent evaporation steps. The three solvents that contributed most significantly to electricity consumption were 1-butanol, water, and toluene. Their relatively high boiling points necessitate substantial energy input for evaporation, as a result, the distillation and solvent recovery steps become particularly energy-intensive, making electricity a key contributor to the overall environmental burden. Electricity production, which relies on a mix of sources (such as coal, natural gas, nuclear, hydroelectric, wind, solar, etc.), results in diverse environmental effects depending on whether the source is renewable or nonrenewable [43, 44]. The extraction of fossil fuels [45] or uranium [46] generates environmental concerns, particularly due to the depletion of fossil resources, water usage, and the release of greenhouse gases (GHGs). After electricity is generated- an activity that itself emits GHGs [47]- the infrastructure required for its transmission also adds to the environmental burdens, because of its construction (as well as biodiversity loss from land use) and maintenance [48, 49]. As this study was based on laboratory-scale experiments, all energy consumption was attributed solely to electricity. It is important to note that this differs from industrial-scale operations, where energy inputs are typically derived from a combination of sources, including thermal energy (e.g., through heat exchangers or steam networks). Moreover, energy consumption at the laboratory scale is generally higher on a per-unit-product basis compared to optimized industrial processes, due to lower efficiencies, smaller batch sizes, and the absence of energy recovery systems [50].

Several factors contribute to this discrepancy: 1) In laboratory-scale reaction development, researchers typically prioritize parameters such as yield, selectivity, and chemical feasibility, while electricity consumption remains largely unaddressed. Consequently, early-stage LCAs often reveal elevated energy-related environmental impacts, as these processes have not been optimized for energy efficiency. 2) Laboratory equipment typically consumes more energy during start-up, raising the average energy demand per unit of product. 3) Most critically, industrial-scale equipment is significantly more energy-efficient than its laboratory counterparts. These differences underscore the importance of scale in LCA, particularly regarding equipment and energy efficiency. They further emphasize the need to include electricity consumption in initial research phases.

5.3.2 Sodium hydroxide (NaOH)

NaOH was used in the process mainly for the hydrolysis of urethane bonds, which impacted both the system's functionality and environmental footprint. Despite having crucial function in cleaving urethane linkages and enabling degradation, NaOH causes significant upstream environmental damage particularly in human toxicity impact category. Industrial production of NaOH via the chlor-alkali process demands extensive electricity usage specifically in membrane and diaphragm cell technologies which leads to environmental impacts in climate change and fossil resource depletion along with human toxicity categories [36]. NaOH in water creates alkaline waste which requires neutralization before disposal or reuse thereby increasing downstream treatment requirements. These waste streams generate freshwater ecotoxicity when mismanaged and demand extra materials like sulfuric acid to neutralize them, which raises the total environmental impact. Therefore, while NaOH played a critical functional role in the reaction step, both its upstream sourcing and downstream management are relevant contributors to the life cycle impacts of the process.

5.3.3 Sulfuric acid (H_2SO_4)

Sulfuric acid plays an essential role as a chemical input for neutralization and pH adjustment following NIPUF hydrolytic degradation. H_2SO_4 remains widely used across industrial processes because of its beneficial performance characteristics and affordability but generates major environmental impacts because its production demands considerable energy input. Industrial sulfuric acid is typically produced via the contact process, which involves the catalytic oxidation of sulfur dioxide to sulfur trioxide, followed by absorption in water [51]. The production steps for sulfuric acid necessitate high temperatures which lead to significant electricity and heat consumption thereby positioning H_2SO_4 as a major environmental impact driver within the system. Moreover, the production process emits sulfur oxides (SO_x), that cause acidification and contribute to air pollution [52].

5.3.4 Dimethyl carbonate (DMC)

DMC stood out as a primary reagent in **PGC** production. Although its contribution was less than other inputs, DMC usage emerged as one of the prominent contributors to the overall environmental impact. DMC is frequently labeled as a green reagent, yet its upstream production demands substantial energy input which affects the process's total energy requirements [53]. The synthesis of this compound demands high temperature and pressure conditions together with extensive separation and purification steps [42, 54].

5.3.5 Waste generation (solvent loss, residues)

While most solvents including 1-butanol, toluene, water, diethyl ether, and dichloromethane (DCM) were successfully recovered during isolation, some spent solvents persisted and increased the environmental impact of the procedure. The purification and post-reaction work-up steps produced the bulk of solid residues which included unrecyclable materials, leftover catalysts, and salts created during the neutralization process. The disposal methods for these wastes involve incineration or landfilling processes which produce emissions and require energy while posing possible long-term ecological risks. Spent solvents, particularly those contaminated beyond recovery, also add significantly to the waste load. The treatment of these substances through high-temperature burning or chemical removal systems creates significant energy demands and adds to environmental problems such as climate change and human health risks along with resource depletion [55]. In sum, the process showed effective solvent recovery, but the inevitable production of both solid and solvent-based wastes underscores that waste minimization and closed-loop design are essential to enhance process sustainability.

In summary, electricity, sodium hydroxide, sulfuric acid, DMC, and waste generation are key areas of concern in the environmental profile of 2º NIPUF production. Opportunities for improvement include optimizing energy efficiency, increasing solvent recovery, substituting or minimizing high-impact reagents, and integrating renewable electricity sources.

6 Sensitivity analysis

6.1 Comparison between different acids

One of the critical downstream steps in the synthesis route involves the neutralization of the reaction mixture, which contains 5M NaOH. When neutralization processes are implemented at industrial scales, they become environmentally significant because strong acids needed for these processes add substantial life cycle impacts. To evaluate the environmental impacts associated with the neutralization of aqueous NaOH, a comparative impact assessment was conducted for four different acids: sulfuric acid, nitric acid, hydrochloric acid, and acetic acid. We established the functional unit by determining the volumes of different acids needed to neutralize 150 mL of 5 M NaOH until the solution reached a pH of 6 and adjusted each acid's amount accordingly (see **Table 10** for details). The methodology achieves equitable comparisons between acids by standardizing measures based on their neutralization potential rather than their weight. The environmental impacts of the four acids in 16 different categories are presented in **Table 13**.

Nitric acid showed elevated impacts in acidification and eutrophication, terrestrial, respectively. Hydrochloric acid demonstrated higher impacts in ozone depletion, ionizing radiation, resource use, minerals and metals, and human toxicity. Notably, acetic acid- despite being an organic acid- showed significantly higher values in most of the categories such as climate change, particulate matter formation, and eutrophication. The reason behind this is likely to stem from its biomass production route that uses energy-intensive fermentation techniques along with agricultural feedstocks. In addition, a higher mass is needed for each neutralization unit when acetic acid is used compared to stronger mineral acids. Earlier LCA research on organic acid production documented similar patterns [56]. Sulfuric acid showed the smallest environmental impact among these four acids across most categories including climate change and fossil resource use, making it the best choice for NaOH neutralization in this research. Our study shows that even routine chemical steps such as pH adjustments can produce measurable environmental impacts, and LCA is essential for selecting suitable reagents during green chemistry design. The high contribution of this step to the overall footprint of the process shows that the amount of NaOH and acid used here should be carefully optimized.

Table 13. Heat map of absolute values of environmental impacts (LCA results) of the neutralization process with different reagents (acids).

Impact category	Unit	Sulfuric acid	Nitric acid	Hydrochloric acid	Acetic acid
Climate change	kg CO2 eq	4.64E-03	9.80E-02	5.89E-02	1.52E-01
Ozone depletion	kg CFC11 eq	7.70E-11	2.07E-09	9.28E-09	2.84E-09
Particulate matter	disease inc.	3.19E-09	4.31E-09	3.02E-09	7.32E-09
Ionising radiation	kBq U-235 eq	5.59E-04	2.13E-03	1.18E-02	1.04E-02
Photochemical ozone formation	kg NMVOC eq	5.03E-05	2.32E-04	1.82E-04	5.70E-04
Acidification	mol H+ eq	5.00E-04	8.56E-04	4.24E-04	6.01E-04
Eutrophication, freshwater	kg P eq	1.91E-06	9.08E-06	2.99E-05	4.27E-05
Eutrophication, marine	kg N eq	5.49E-06	6.88E-05	4.91E-05	1.15E-04
Eutrophication, terrestrial	mol N eq	5.98E-05	3.49E-03	4.88E-04	1.19E-03
Water use	m3 depriv.	3.25E-02	4.26E-02	3.71E-02	7.88E-02
Land use	Pt	3.38E-02	1.59E-01	2.56E-01	3.65E-01
Resource use, fossils	MJ	2.41E-02	9.14E-02	4.15E-01	9.43E-01
Resource use, minerals and metals	kg Sb eq	1.62E-07	9.59E-07	1.02E-06	6.58E-07
Human toxicity, non-cancer	CTUh	1.61E-10	6.86E-10	9.04E-10	3.69E-09
Human toxicity, cancer	CTUh	1.61E-10	2.44E-10	4.68E-10	3.18E-10
Ecotoxicity, freshwater	CTUe	8.31E-02	2.34E-01	8.16E-01	1.35E+00

The functional unit was defined as the amount of each acid required to neutralize 150 mL of 5 M NaOH solution, adjusting the quantity of each acid to achieve a final pH of 6 (see **Table 10** for details).

6.2 Comparison between different sources of energy

Electricity consumption was identified as the largest contributor to the environmental impact of 2º NIPUF synthesis, based on the current BE electricity. Given this significant influence, alternative electricity sourcing scenarios were also evaluated using electricity data representative of six regions: Belgium (BE), Spain (ES), France (FR), Netherlands (NL), Norway (NO), and the EU-28 average according to Ecoinvent v3.10 (see **Table 11** for LCI). The impact results associated with the production of 1 kg of 2° NIPUF, are presented on **Fig. 13** for two key impact categories: climate change (left) and fossil resource use (right). For the climate change impact, the Netherlands exhibited the highest emissions, followed by the EU average and Belgium. This is attributed to a higher share of fossil fuels in their electricity generation mix. In contrast, France and Norway showed the lowest climate change impacts, thanks to their heavy reliance on nuclear and hydroelectric power, respectively [57]. Spain also showed relatively lower emissions due to its higher share of renewables in the grid.

In terms of fossil resource depletion, France showed the highest impact, with Belgium and the EU average following closely. Norway again ranked lowest in this category, reinforcing the environmental advantage of low-carbon electricity sources. Spain and Netherlands displayed moderate impact, consistent with its balanced energy mix.

These findings demonstrate that the choice of electricity source- defined by regional energy mixes- can significantly alter the environmental footprint of NIPUF production, particularly in energy-intensive steps such as solvent recovery and hydrolysis. Consequently, selecting electricity from low-carbon grids, such as those in Norway, can contribute substantially to reducing both greenhouse gas emissions and fossil resource depletion.

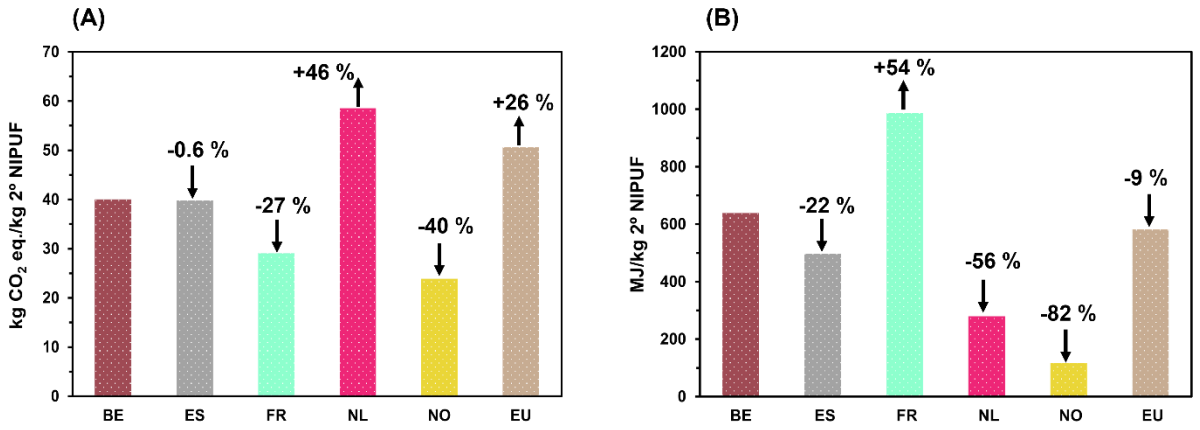

Fig. 13. (A) Climate change and (B) fossil resource use impacts associated with the production of 1 kg of second-generation NIPUF, based on the electricity mixes of six countries/regions: Belgium (BE), Spain (ES), France (FR), Netherlands (NL), Norway (NO), and EU-28 average (EU). Results highlight the significant influence of national electricity profiles on the overall environmental performance, with lower impacts observed on low-carbon energy mixes (e.g., NO). The percentages at the top of the columns are based on BE reference case.

7 How could the environmental profiles of the 2° NIPUF be improved?

Following the evaluation of the environmental profiles of the 2° NIPUFs and a detailed contribution analysis of each inventory component, several improvement strategies are proposed to reduce the environmental impacts identified across the assessed categories. These recommendations aim to guide researchers and stakeholders in prioritizing areas for further optimization in NIPUF recycling and upcycling processes. The analysis revealed five major environmental hotspots: (i) the use of sodium hydroxide (NaOH) as the hydrolysis catalyst, (ii) sulfuric acid (H_2SO_4) as the neutralizing agent, (iii) dimethyl carbonate (DMC) as the cyclocarbonation agent, (iv) process-related waste generation, and (v) high energy demand- particularly electricity consumption- as the dominant contributors to overall impacts. The environmental footprint would decrease significantly from optimizing these steps. For instance, using more diluted NaOH solutions, that can further minimize the H_2SO_4 needed for neutralization and cut down on waste production.

In terms of energy consumption, several opportunities exist to improve the environmental performance of NIPUF recycling processes. A primary strategy would involve transitioning to renewable energy sources or integrating biomass in a cogeneration system to simultaneously supply both electricity and heat. Additionally, operational energy consumption can be reduced

by selecting energy-efficient process equipment and using proper insulation to decrease thermal losses.

Another key factor influencing overall energy demand is the duration of thermal operations such as hydrolysis, drying, and re-polymerization. These stages that need several hours to finish make a substantial impact on electricity and heat consumption during process. Researchers should direct future work towards decreasing reaction durations by applying process intensification techniques and optimizing catalysts to obtain better energy and time efficiencies. Additionally, by choosing solvents with lower boiling points for small-molecule recovery operations, we can achieve considerable energy savings. These proposed measures form the basis for the next chapter, which explores process modifications to enhance the environmental sustainability of NIPUF recycling.

8 Conclusion

This chapter presents orientational cradle-to-grave LCAs of NIPUFs, that relies on experimentally validated recycling and regeneration pathways. By integrating laboratory data on hydrolysis-based depolymerization and the synthesis of second-generation NIPUFs, the study delivers a realistic and quantifiable assessment of circularity within this new class of materials.

The comparative study revealed that, under current laboratory conditions, the hydrolysis-based recycling and regeneration of NIPUFs did not outperform incineration in terms of overall environmental impact. Key categories such as global warming potential, fossil resource use, and human toxicity remained higher for the recycling route, mainly because of the energy-intensive recovery steps and solvent-related burdens. Nevertheless, the research deepens comprehension of the environmental trade-offs associated with circular strategies for NIPUFs. A contribution analysis was performed for the production of 1 kg of 2° NIPUF, focusing on key impact categories such as global warming potential, fossil resource depletion, human toxicity, and particulate matter formation. Electricity, sulfuric acid, sodium hydroxide, DMC and waste generation emerged as the primary factors affecting the overall environmental footprint of 2° NIPUF production.

The sensitivity analysis further demonstrated that the electricity source significantly impacted the overall results. For instance, electricity sourced from Norway achieved significantly reduced environmental impacts in two impacts categories of global warming potential, and fossil resource use, because it mainly comes from renewable sources. In addition, sensitivity analysis revealed that sulfuric acid was found to be the most environmentally favorable choice among the tested neutralization agents.

Despite the limitations of lab-scale modeling, this work provides meaningful insights into how process adjustments and material choices can influence sustainability outcomes. The LCA framework developed here serves as a useful tool for guiding future optimization and scale-up efforts in the field of green polymer chemistry. Looking ahead, future research should explore alternative methods to reduce the environmental footprint of the current recycling approach. This may include meticulous solvent selection and reduction, the use of more sustainable chemicals, and the optimization of small molecule isolation steps to minimize energy use. Overall, this study reinforces the value of LCA as a powerful instrument for identifying environmental trade-offs and guiding the development of safer, greener, and more circular polymer systems from the earliest stages of innovation.

9 References

1. Nielsen, T.D., et al., *Politics and the plastic crisis: A review throughout the plastic life cycle.* Wiley Interdisciplinary Reviews: Energy and Environment, 2020. **9**(1): p. e360.

2. Eisenriegler, S., *The circular economy in the European Union*. 2020: Springer.

3. Löhr, A.J. and F. Van Belleghem, *Sustainable development goals to reduce and prevent marine litter.* Life Below Water, 2020: p. 1-12.

4. Wuttke, J., *The Circular Economy Package of the European Union*, in *Factor X: Challenges, Implementation Strategies and Examples for a Sustainable Use of Natural Resources*. 2017, Springer. p. 251-262.

5. Plan, C.E.A., *For a cleaner and more competitive Europe.* European Commission (EC): Brussels, Belgium, 2020. **28**.

6. Marson, A., et al., *Life cycle assessment of polyurethane foams from polyols obtained through chemical recycling.* ACS omega, 2021. **6**(2): p. 1718-1724.

7. Jürgens, M. and H.-J. Endres, *Environmental impacts of circular economy practices for plastic products in Europe: Learnings from life cycle assessment studies.* Procedia CIRP, 2024. **122**: p. 312-317.

8. Lim, C.C.N.D., et al., *Emerging Trends in Nonisocyanate Polyurethane Foams: A Review.* ACS Engineering Au, 2024. **4**(6): p. 493-518.

9. Bourguignon, M., B. Grignard, and C. Detrembleur, *Water-Induced Self-Blown Non-Isocyanate Polyurethane Foams.* Angewandte Chemie International Edition, 2022. **61**(51): p. e202213422.

10. Bourguignon, M., B. Grignard, and C. Detrembleur, *Cascade exotherms for rapidly producing hybrid nonisocyanate polyurethane foams from room temperature formulations.* Journal of the American Chemical Society, 2023. **146**(1): p. 988-1000.

11. Monie, F., B. Grignard, and C. Detrembleur, *Divergent aminolysis approach for constructing recyclable self-blown nonisocyanate polyurethane foams.* ACS Macro Letters, 2022. **11**(2): p. 236-242.

12. Liang, C., et al., *Techno-economic analysis and life cycle assessment of biomass-derived polyhydroxyurethane and nonisocyanate polythiourethane production and reprocessing.* ACS Sustainable Chemistry & Engineering, 2024. **12**(32): p. 12161-12170.

13. Beena Unni, A. and T. Muringayil Joseph, *Enhancing polymer sustainability: eco-conscious strategies.* Polymers, 2024. **16**(13): p. 1769.

14. Horne, R., T. Grant, and K. Verghese, *Life cycle assessment: principles, practice, and prospects*. 2009: Csiro Publishing.

15. Guinée, J.B., *Handbook on life cycle assessment: operational guide to the ISO standards*. Vol. 7. 2002: Springer Science & Business Media.

16. Guolo, E., et al. *Environmental impacts for polyurethane panels*. in *E3S Web of Conferences*. 2019. EDP Sciences.

17. Aldaghi, S.A., et al., *Environmental Impact of Polyurethane-Based Aerogel Production: Influence of Solvents and Solids Content.* Resources, 2024. **13**(10): p. 138.

18. Klug, V., et al., *Comparative life cycle assessment of different production processes for waterborne polyurethane dispersions.* ACS Sustainable Chemistry & Engineering, 2021. **9**(27): p. 8980-8989.

19. Wray, H.E., et al., *Life cycle environmental impact considerations in the design of novel biobased polyurethane coatings.* ACS Sustainable Chemistry & Engineering, 2023. **11**(21): p. 8065-8074.

20. Recupido, F., et al., *Rigid composite bio-based polyurethane foams: From synthesis to LCA analysis.* Polymer, 2023. **267**: p. 125674.

21. Silva, R., A. Barros-Timmons, and P. Quinteiro, *Life cycle assessment of fossil-and bio-based polyurethane foams: a review.* Journal of Cleaner Production, 2023. **430**: p. 139697.

22. Bron, P., et al., *Comparative Life Cycle Assessment of Recyclable Polyhydroxyurethanes Synthesized from Five-and Six-Membered Carbonates.* Macromol, 2025. **5**(1): p. 12.

23. Seychal, G., et al., *Can polyhydroxyurethane-derived covalent adaptable networks provide environmental benefits in composite applications?* 2025.

24. Standard, I., *Environmental management-Life cycle assessment-Requirements and guidelines.* London: ISO, 2006.

25. Finkbeiner, M., et al., *The new international standards for life cycle assessment: ISO 14040 and ISO 14044.* The international journal of life cycle assessment, 2006. **11**: p. 80-85.

26. Jang, H., et al., *Comparative life cycle assessment of marine insulation materials.* Journal of Marine Science and Engineering, 2021. **9**(10): p. 1099.

27. Andreasi Bassi, S., et al., *Updated characterisation and normalisation factors for the Environmental Footprint 3.1 method.* Publications Office of the European Union: Luxembourg, 2023.

28. Piccinno, F., et al., *From laboratory to industrial scale: a scale-up framework for chemical processes in life cycle assessment studies.* Journal of Cleaner Production, 2016. **135**: p. 1085-1097.

29. Spadlo, M. and E. Dziwinski, *Glycidylation of trimethylolpropane with epichlorohydrin.* PRZEMYSL CHEMICZNY, 2007. **86**(9): p. 905-910.

30. Chen, B., et al., *Environmental Sustainability of π-Electron Donor-Based Deep Eutectic Solvents for Toluene Absorption: A Life-Cycle Perspective.* ChemSusChem, 2024. **17**(4): p. e202301310.

31. Chomkhamsri, K., M.-A. Wolf, and R. Pant, *International reference life cycle data system (ILCD) handbook: Review schemes for life cycle assessment.* Towards life cycle sustainability management, 2011: p. 107-117.

32. Change, I.P.O.C., *Climate change 2007: the physical science basis.* Agenda, 2007. **6**(07): p. 333.

33. Smurthwaite, M., L. Jiang, and K.S. Williams, *A review of the LCA literature investigating the methods by which distinct impact categories are compared.* Environment, Development and Sustainability, 2024. **26**(8): p. 19113-19129.

34. Egemose, C.W., et al., *Human toxicological impacts in life cycle assessment of circular economy of the built environment: a case study of Denmark.* Buildings, 2022. **12**(2): p. 130.

35. Garcia-Herrero, I., et al., *Environmental challenges of the chlor-alkali production: Seeking answers from a life cycle approach.* Science of the Total Environment, 2017. **580**: p. 147-157.

36. Garcia-Herrero, I., et al., *Life Cycle Assessment model for the chlor-alkali process: A comprehensive review of resources and available technologies.* Sustainable Production and Consumption, 2017. **12**: p. 44-58.

37. Rosenbaum, R.K., *USEtox-The UNEP-SETAC toxicity model: recommended characterisation factors for human.* Info: Lawrence Berkeley National Laboratory, 2010.

38. Barros, M.V., et al., *Life cycle assessment of electricity generation: a review of the characteristics of existing literature.* The International Journal of Life Cycle Assessment, 2020. **25**: p. 36-54.

39. Fantke, P., et al., *Global effect factors for exposure to fine particulate matter.* Environmental science & technology, 2019. **53**(12): p. 6855-6868.

40. Boogaard, P., et al., *Review of recent health effect studies with sulphur dioxide.* Concawe Rep., 2016: p. 1-89.

41. Van Zelm, R., et al., *European characterization factors for human health damage of PM10 and ozone in life cycle impact assessment.* Atmospheric Environment, 2008. **42**(3): p. 441-453.

42. Garcia-Herrero, I., et al., *Environmental assessment of dimethyl carbonate production: comparison of a novel electrosynthesis route utilizing CO2 with a commercial oxidative carbonylation process.* ACS Sustainable Chemistry & Engineering, 2016. **4**(4): p. 2088-2097.

43. Gagnon, L., C. Belanger, and Y. Uchiyama, *Life-cycle assessment of electricity generation options: The status of research in year 2001.* Energy policy, 2002. **30**(14): p. 1267-1278.

44. Spellman, F.R., *Environmental impacts of renewable energy*. 2014: CRC press.

45. Dincă, C., A. Badea, and T. Apostol, *Life cycle impact assessment of fossil fuels.* Natural gas, 2010. **9**(25.3): p. 9.5.

46. Nian, V., et al., *Life cycle analysis on carbon emissions from power generation–The nuclear energy example.* Applied energy, 2014. **118**: p. 68-82.

47. Motuzienė, V., et al., *A review of the life cycle analysis results for different energy conversion technologies.* Energies, 2022. **15**(22): p. 8488.

48. Caetano, N.S., F.F. Martins, and G.M. Oliveira, *Life cycle assessment of renewable energy technologies.* The Renewable Energy-Water-Environment Nexus, 2024: p. 37-79.

49. Fthenakis, V. and H.C. Kim, *Land use and electricity generation: A life-cycle analysis.* Renewable and Sustainable Energy Reviews, 2009. **13**(6-7): p. 1465-1474.

50. Constable, D.J., A.D. Curzons, and V.L. Cunningham, *Metrics to 'green'chemistry—which are the best?* Green Chemistry, 2002. **4**(6): p. 521-527.

51. Mousavinezhad, S., S. Kadivar, and E. Vahidi, *Comparative life cycle analysis of critical materials recovery from spent Li-ion batteries.* Journal of Environmental Management, 2023. **339**: p. 117887.

52. Marwa, M., et al., *An environmental life cycle assessment of an industrial system: case of industrial sulfuric acid.* International Journal of Energy, Environment and Economics, 2017. **25**(4): p. 255-268.

53. Huang, H., et al., *Greener production of dimethyl carbonate by the Power-to-Fuel concept: a comparative techno-economic analysis.* Green Chemistry, 2021. **23**(4): p. 1734-1747.

54. Lee, Y.G., et al., *Design of dimethyl carbonate (DMC) synthesis process using CO2, techno-economic analysis, and life cycle assessment.* Korean Journal of Chemical Engineering, 2024. **41**(1): p. 117-133.

55. Amelio, A., et al., *Guidelines based on life cycle assessment for solvent selection during the process design and evaluation of treatment alternatives.* Green Chemistry, 2014. **16**(6): p. 3045-3063.

56. Salazar-Sogamoso, L.M., M.-Á. Gómez-García, and I. Dobrosz-Gómez, *Comparative life cycle assessment of sequential chemical and electrochemical processes for the treatment of industrial textile wastewater.* Journal of Solid State Electrochemistry, 2024: p. 1-21.

57. Delgove, M.A., et al., *A prospective life cycle assessment (LCA) of monomer synthesis: comparison of biocatalytic and oxidative chemistry.* ChemSusChem, 2019. **12**(7): p. 1349-1360.

10 Supplementary Information

10.1 Details of energy-consumption calculations

The numerical values for each step of energy consumption- including stirring, heating, and drying- are presented in **Tables S1-S3**. Since the available dimensional data refer to reactors of 100 L or larger, the energy consumption for stirring and heating was initially estimated using a 100 L reactor as the basis. These values were subsequently scaled down to reflect the actual volume of the laboratory-scale reaction vessels used as inputs in the LCA. The efficiency of the heating element depends on several factors, including its type, construction material, the nature of the heated fluid, and the operating temperature. For consistency, we standardized the efficiency at 72% for a 100 L reactor, based on the reference procedure [28]. Drying efficiency (η_{dry}) is defined as the ratio between the heat required to vaporize the removed liquid and the total heat supplied. In this context, only the energy needed to heat the liquid to its vaporization point is considered, while heat losses are implicitly accounted for within the efficiency value. An efficiency of 90% was selected as a standard estimate.

Table S1. Details of Energy calculations, definition of abbrevioations

Abbreviation	Definition
E1	Energy for hydrolysis depolymerization of NIPUFs (heating and stirring energies)
E2	Energy for neutralization of solution using acid (stirring energy)
E3	Energy for mixing the residue with diethyl ether (stirring energy)
E4	Energy for deprotonation of amine (stirring energy)
E5	Energy for mixing with Toluene (heating and stirring energy)
E6	Energy for removing 1-Butanol (Drying energy)
E7	Energy for removing diethyl ether (Drying energy)
E8	Energy for removing Toluene (Drying energy)
E9	Energy for removing water (Drying energy)
E10	Energy for cyclo-carbonation step (heating and stirring energy)
E11	Energy for removing DMC (Drying energy)
E12	Energy for removing DCM (Drying energy)

Table S2. Detailed Energy Calculations for Stirring, Heating, and Drying Steps.

	E1	E2	E3	E4	E5	E6	E7
Parameter	For a 100 L reactor	For a 100 L reactor	For a 100 L reactor	For a 100 L reactor	For a 100 L reactor	For 800 mL solvent	For a 200 mL solvent
C_p (J/kg.k)	3980	-	-	-	1710	2420	2370
m_{mix} (kg)	90	-	-	-	90	0.65	0.178
T_r (K)	353.15	-	-	-	393.15		
T_0 (K)	298.15	-	-	-	298.15	298.15	298.15
A*ka/s (W/K)	0.712	-	-	-	0.712	-	-
T_{out} (K)	298.15	-	-	-	298.15	-	-
t (s)	36000	900	7200	3600	7200	-	-
η_{heat}	0.72	-			0.72	-	-
N_p	0.79	0.79	0.79	0.79	0.79	-	-
ρ_{mix} (kg/m3)	1200	1200	1100	1200	867	-	-
N (s^{-1})	3.052	3.052	3.052	3.052	3.052	-	-
d (m)	0.173	0.173	0.173	0.173	0.173	-	-
η_{stir}	0.9	0.9	0.9	0.9	0.9	-	-
$m_{solvent}$ (kg)	90	-	-	-	90	0.64	0.143
T_{boil} (K)	-	-	-	-	383.75	390.85	307.75
ΔH_{vap} (J/kg)	-	-	-	-	360200	586,900	440000
Q_{heat} (J)	19701000	-	-	-	14620500	-	-
Q_{loss} (J)	1409760	-	-	-	487008	-	-
Q_{react}(J)	29320500	-	-	-	20982650	-	-
E_{react}(KWh)	8.1445	-	-	-	5.828	-	-
E_{Stirr} (J)	167052	4176.307	30626	16705	24139	-	-
E_{Stirr} (KWh)	0.04640	0.0011	0.0085	0.004	0.0067	-	-
η_{dry}	-	-	-	-	-	0.9	0.9
Q_{dry}	-	-	-	-	-	579370.1111	74410.95111
E_{dry} (KWh)	-	-	-	-	-	0.160	0.0206

Table S3. Detailed Energy Calculations for Stirring, Heating, and Drying Steps.

	E8	**E9**	**E10**	**E11**	**E12**
Parameter	For a 100 mL solvent	For a 150 mL solvent	For a 100 L reactor	For a 100 L reactor	For a 100 L reactor
C_p (J/kg.k)	1710	4180	2500	2100	1326
m_{mix} (kg)	0.217	0.2	90	0.05	0.05
T_r (K)	-		338.15		
T_0 (K)	298.15	298.15	298.15	298.15	298.15
A*ka/s (W/K)	-	-	0.712	-	-
T_{out} (K)	-	-	298.15	-	-
t (s)	-	-	68400	-	-
η_{heat}	-	-	0.72	-	-
N_p	-	-	0.79	-	-
ρ_{mix} (kg/m3)	-	-	792	-	-
N (s^{-1})	-	-	3.052	-	-
d (m)	-	-	0.173	-	-
η_{stir}	-	-	0.9	-	-
$m_{solvent}$ (kg)	0.174	0.16	90	0.042	0.042
T_{boil} (K)	383.75	373.15	337.85	363.15	312.75
ΔH_{vap} (J/kg)	378000	2260000	-	347500	337900
Q_{heat} (J)	-	-	9000000	-	-
Q_{loss} (J)	-	-	1948032	-	-
Q_{react}(J)	-	-	15205600	-	-
E_{react}(KWh)	-	-	4.223777778	-	-
E_{Stirr} (J)	-	-	209483.571	-	-
E_{Stirr} (KWh)	-	-	0.058189881	--	-
η_{dry}	0.9	0.9	-	0.9	0.9
Q_{dry}	108372.88	471444.4444	-	23800	16844.2
E_{dry} (KWh)	0.03	0.13	-	0.0066	0.004

10.2 List of abbreviations

Table S4. Comprehensive list of abbreviations in alphabetical order.

Abbreviation	Definition
2° NIPUF	second-generation non-isocyanate polyurethane foam
AC	Acidification
BE	Belgium
CC	Climate change
CO_2	Carbon dioxide
DBU	1,8-Diazabicyclo(5.4.0)undec-7-ene
DCM	Dichloromethane
DMC	Dimethyl carbonate
ECH	epichlorohydrin
EDR 148	2,2′-(Ethylenedioxy)bis(ethylamine)
EoL	End of life
ES	Spain
EU	Europe
FE	Eutrophication, freshwater
FR	France
FU	Functional unit
FWT	Ecotoxicity, freshwater
g	Gram
GHG	Greenhouse gas
GLO	Dataset refers to global worldwide relevant data
HT-c	Human toxicity, cancer
HT-nc	Human toxicity, non-cancer
ILCD	International Life Cycle Data System
IR	Ionizing radiation
K_2CO_3	Potassium carbonate
kWh	kilowatt-hour
LCA	Life cycle assessment
LCI	Life cycle inventory
LCIA	Life cycle impact assessment
LU	Land use
ME	Eutrophication, marine
NaOH	Sodium hydroxide
NIPU	Non-isocyanate polyurethane
NIPUF	Non-isocyanate polyurethane foam
NL	Netherland
NO	Norway
ODP	Ozone depletion
PG	Polyglycerol
PGC	Polyglycerol carbonate

PHU	Polyhydroxyurethane
PM	Particulate matter
PM2.5	Particles with a diameter of less than 2.5 μm
POF	Photochemical ozone formation
PU	Polyurethane
PUF	Polyurethane foam
RER	Datasets refer to Europe-relevant data
RES-f	Resource use, fossils
RES-m	Resource use, minerals and metals
RoW	Rest-of-World-relevant data
SI	Supplementary Information
TE	Eutrophication, terrestrial
TEBAC	Benzyltriethylammonium chloride
TMP	Trimethylolpropane
TMPTC	Trimethylolpropane triglycidyl carbonate
TMPTE	Trimethylolpropane triglycidyl ether
WAT	Water use

Chapter 5. Process Optimization of Non-Isocyanate Polyurethane (NIPU) Foam Recycling, Guided by Life Cycle Assessment

Maliheh Razavi-Esfali, Mahammad Anas, Olivier Talon, Bruno Grignard, Christophe Detrembleur*, Haritz Sardon*

Abstract

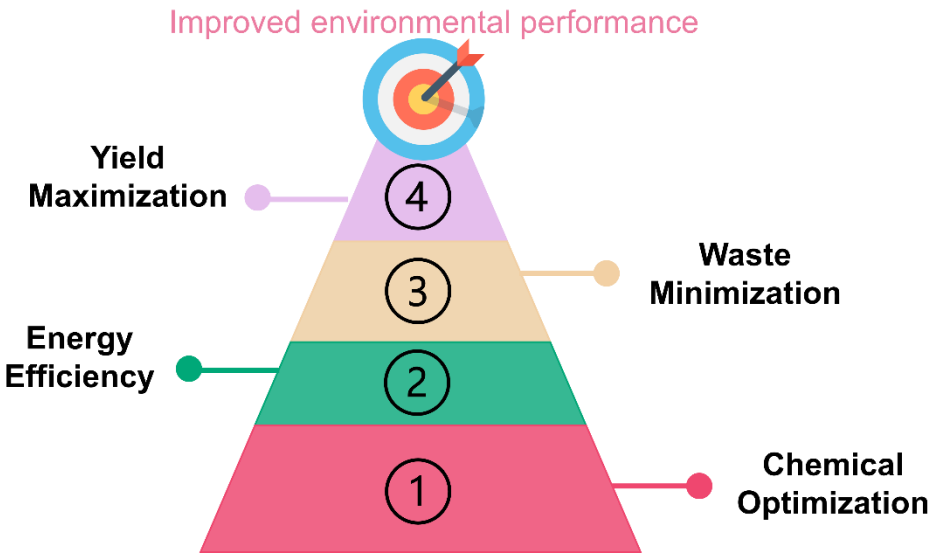

This chapter presents a life cycle assessment-driven optimization of a chemical recycling process for non-isocyanate polyurethane foams, with the dual aim of improving environmental performance and ensuring technical feasibility. A baseline hydrolytic depolymerization process was assessed in the previous chapter, highlighting key environmental hotspots related to the use of sodium hydroxide and sulfuric acid, solvent recovery, and electricity consumption. Informed by these insights, an alternative process was developed in this chapter, incorporating milder conditions (1 M NaOH instead of 5 M), lower-boiling solvents, and reduced reagent inputs. Despite these modifications, high monomer recovery yields were maintained (75% for polyglycerol and 80% for diamines, following foam degradation). The LCA results demonstrated substantial environmental improvements: climate change impacts associated with main hotspots of electricity, NaOH, and H_2SO_4 were reduced by 66%, 88%, and 90%, respectively, while chemical waste generation decreased by 90%. These enhancements were achieved without compromising monomer purity or process reliability. Overall, this work illustrates how the integration of green chemistry principles and prospective LCA can guide the early-stage development of circular, environmentally optimized recycling strategies for polyurethane-based materials.

1 Introduction

Recycling polymers is an essential aspect of sustainable materials management; however, it is equally important to assess the environmental impacts connected to the recycling processes themselves. Without such an assessment, it is possible to overlook hidden burdens that may compromise the overall sustainability of recycling technologies. Life cycle assessment (LCA) offers a comprehensive framework to quantify these impacts across the entire value chain, from material recovery to reprocessing and reuse. Integration of LCA into polymer recycling not only enables a meaningful comparison with conventional end-of-life scenarios such as incineration or landfill but also reveals the specific steps within the recycling process that contribute most significantly to environmental burdens. Detecting these hotspots is important for targeted process optimization and for moving toward a fully sustainable, closed-loop material system.

In the previous chapters of this thesis, a circular strategy for non-isocyanate polyurethane foams (NIPUFs) was developed, combining chemical recycling with upcycling to generate second-generation foams. Chapter 3 described the design of the degradation process for NIPUFs based on aliphatic and aromatic diamines (EDR and *m*-XDA), employing hydrolytic conditions and recovering key building blocks- primarily diamines and polyglycerol (**PG**). These small molecules were then treated and repolymerized into new NIPUFs, demonstrating the technical feasibility of a closed-loop foam-to-foam recycling.

To assess the sustainability of this approach, Chapter 4 presented a cradle-to-grave LCA of the full process chain, covering the synthesis, depolymerization, recovery of small molecules, and upcycling steps. This evaluation revealed five primary contributors to the overall environmental impact of the second-generation foams: 1) Electricity consumption, particularly during solvent evaporation steps involving high-boiling solvents like 1-butanol. 2) Sodium hydroxide (NaOH), used as a catalyst in the depolymerization stage. 3) Sulfuric acid (H_2SO_4), required for neutralizing the depolymerization mixture. 4) Generation and treatment of waste streams, including aqueous and organic residues. 5) Dimethyl carbonate (DMC), employed in the carbonylation reaction to produce cyclic carbonates.

These findings formed the foundation for a process optimization strategy with a goal of mitigating environmental hotspots without compromising material quality or yield. Several modifications were introduced considering the LCA results: the replacement or reduction of

energy-intensive solvents, minimization of chemical input (especially NaOH and H_2SO_4), improved separation techniques, and refined purification workflows to reduce solvent and waste volumes.

This chapter presents the results of this iterative, LCA-guided optimization. A revised LCA was conducted to quantify the improvements in environmental performance, offering a direct comparison between the original and optimized processes. By integrating sustainability metrics into experimental design, this work demonstrates a practical methodology for coupling chemical innovation with environmental responsibility. The approach aligns with broader goals in green chemistry and circular economy, offering a model for developing polymer systems that are not only recyclable, but also environmentally optimized across their lifecycle.

2 Experimental

2.1 Chemicals

Trimethylol propane triglycidyl ether (TMPTE, Ipox Chemicals), 1,2-Bis(2-aminoethoxy)ethane (EDR 148, TCI, >98%), tetrabutylammonium iodide (TBAI, Sigma Aldrich, 99%), 1,8-Diazabicyclo[5.4.0]undec-7-ene (DBU, Sigma Aldrich, 98%), Hydrotalcite ($Mg_6Al_2(CO_3)(OH)_{16}\cdot 4H_2O$, Sigma Aldrich), Sodium hydroxide (NaOH, Sigma Aldrich), Dimethyl carbonate anhydrous, (DMC, Sigma Aldrich, ≥99%), Sulfuric acid (H_2SO_4, Sigma Aldrich, 95-98%), Isopropanol (Sigma Aldrich, ≥99%), Dichloromethane (DCM, 99%, Thermo Scientific), Chloroform (Sigma Aldrich, ≥99%).

2.2 Synthesis of trimethylolpropane tri-cyclic carbonate (TMPTC)

The synthesis of TMPTC was carried out following the same procedure described in Chapter 3, Section 2.2. The process effectively yielded TMPTC functionalized with ~2.64 cyclic carbonate groups as evidenced by ^{1}H-NMR spectroscopy (see **Fig. S2**, Section 6.2, chapter 3).

2.3 Synthesis of native NIPUFs

The synthesis of NIPUFs was carried out following the same procedure described in Chapter 3, Section 2.3. All the properties and characterizations of the foams are explained in section 3.1 of Chapter 3.

2.4 Hydrolysis of NIPUFs

A sample of EDR-based NIPU foam, 7.1 g of foam (cut into very small cubes) was placed in a 250 mL round-bottom flask, followed by the addition of 150 mL of 1M NaOH solution. The mixture was stirred at 80 °C for 10 h.

2.5 Recovery of high-value products

Following the depolymerization of EDR-based foam (denoted as **NIPUF-A**), the aqueous solution was filtered to remove any undissolved residue (it was negligible and could not be quantified). The filtrate was concentrated to dryness under reduced pressure using a rotary evaporator. To the resulting solid mixture, 100 mL of DCM was added and stirred at rt overnight. The DCM layer was then separated by filtration (the remaining solid residue was retained for subsequent **PG** extraction) and were dried over anhydrous magnesium sulfate ($MgSO_4$), filtered, and concentrated under reduced pressure to yield EDR 148 (light-yellow liquid, ~80% isolated yield, 1.55 g). The isolated precursor was characterized by ^{1}H and ^{13}C NMR spectroscopies (see **Fig. S1** and **S2**). The solid residue retained from the amine extraction step was dissolved in 50 mL of Milli-Q water. The reaction mixture was neutralized through the addition of H_2SO_4 solution (96%) until the pH reached 6. Water was then filtered and removed under reduced pressure to yield a solid residue. To this residue, 70 mL of iPrOH was added, and the mixture was stirred at 60 °C overnight. Upon cooling to rt, the iPrOH layer was filtered and dried over anhydrous $MgSO_4$. Insoluble NaCl was discarded. The yellow, **PG** fraction was isolated by filtering the iPrOH solution and removing the solvent via rotary evaporation (75% isolated yield, ~2.9 g). The product was characterized by ^{1}H and ^{13}C NMR spectroscopy (see **Fig. S3** and **S4**).

3 LCA methodological frameworks

In the present study, the LCA models were developed in accordance with the international standards ISO 14040 and ISO 14044 [1, 2]. The LCA was performed using SimaPro 9.6, a widely recognized LCA software developed by Pré Sustainability (The Netherlands). This tool enabled a comprehensive and transparent assessment of environmental impacts across all life cycle stages. When primary data was unavailable, background data were sourced from the Ecoinvent 3.10 database (in the Cut-Off version as provided in SimaPro 9.6), which offers high-quality, peer-reviewed datasets for raw materials, energy production, and emissions, thereby ensuring consistency and reliability in the modeling process.

3.1 Goal and scope

The goal of this study is to compare the environmental impacts associated with the recovery of small molecules- specifically polyglycerol (**PG**) and diamines- following the hydrolytic degradation of NIPUFs using two process routes (**Fig. 1**). The baseline approach (**Method-1**), described in previous chapters, employs hydrolysis under standard conditions using 5 M sodium hydroxide (NaOH) at 80 °C for 10 hours. The optimized process (**Method-2**) introduces several key improvements, including a reduction in NaOH concentration to 1 M, the substitution of high-boiling-point solvents with lower-boiling alternatives, and energy-efficient solvent recovery techniques.

This LCA is designed to evaluate and compare the environmental performance of **PG** recovery in both methods, based on standardized LCA methodology. The ultimate objective is to quantify the environmental benefits achieved through the optimization process.

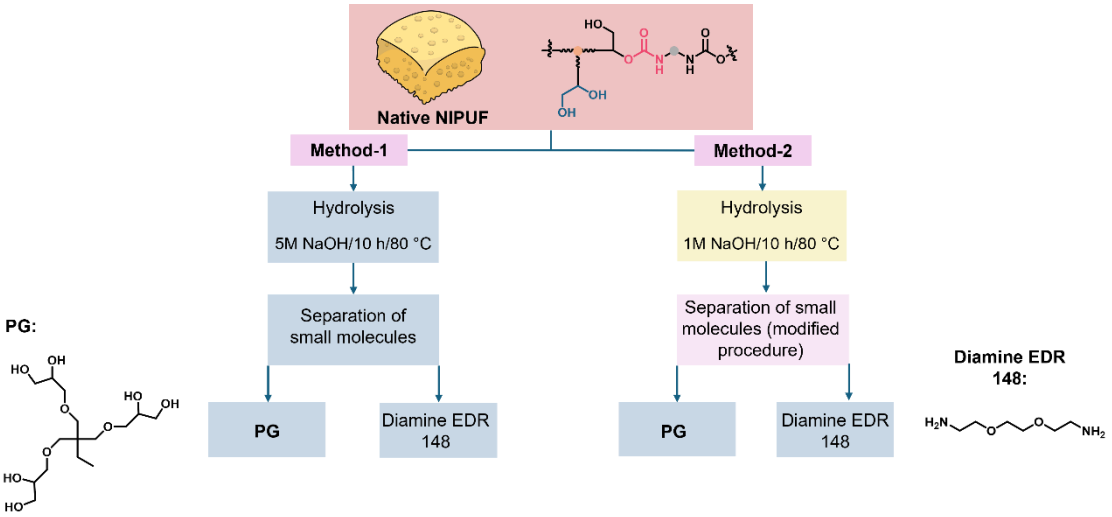

Fig 1. Schematic comparison of the recycling process through **Method-1** and **Method-2**; the NIPUF is chemically hydrolyzed into its monomeric components, which are recovered and isolated.

The second part of this study investigates the environmental benefits of using the optimized recycling method as a circular end-of-life strategy for NIPUFs, compared to conventional linear disposal through incineration. To do so, three scenarios were defined:

Scenario-A, one time recycling via **Method-1** (**Fig. 2A**): NIPUF is initially produced as described before by using a water-induced CO_2 self-foaming formulation composed of TMPTC, diamines, water, and DBU as the catalyst. After its first use, it is chemically recycled via **Method-1**. The recovered monomers are used to produce second generation NIPUF, which is incinerated at the end of its use.

Scenario-B, one time recycling via **Method-2** (**Fig. 2B**): Similar to **Scenario-A**, but the recycling is performed using **Method-2** (modified method), which enables the production of second generation NIPUF. This foam is also incinerated after its life.

Scenario-C, Linear Incineration (**Fig. 2C**): A baseline case where NIPUF is produced as described before by using a water-induced CO_2 self-foaming formulation composed of TMPTC, diamines, water, and DBU as the catalyst, used, and subsequently incinerated. The cycle is repeated once without any recycling.

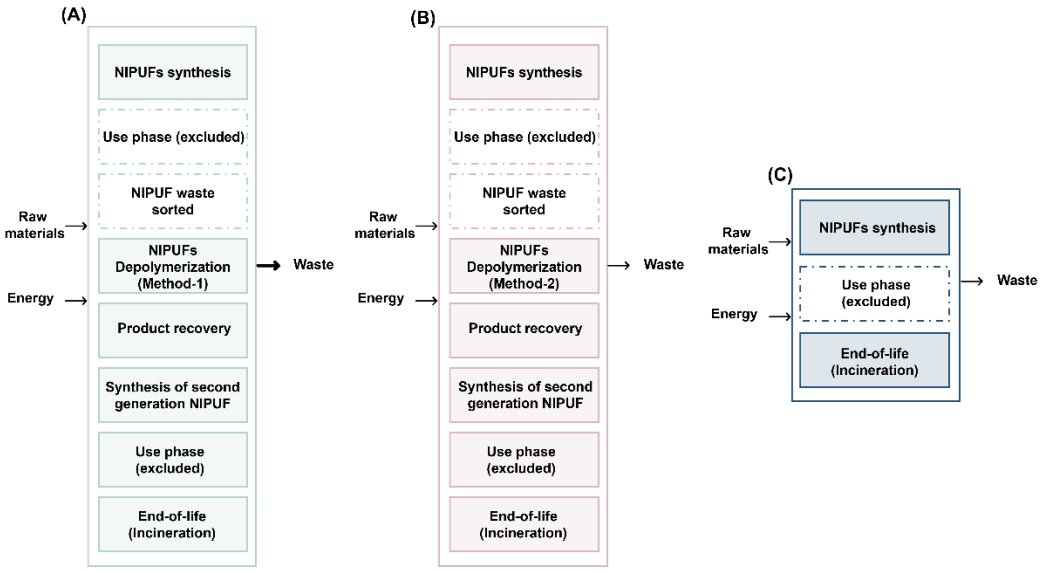

Fig 2. Comparative life cycle system boundaries for NIPUs considering (A) recycling and resynthesis using **Method-1** (**Scenario- A**); and (B) recycling and resynthesis using **Method-2** (**Scenario-B**); and (C) linear EoL (**Scenario-C**). In all cases, the use phase is excluded from the system boundaries.

Functional unit. For the comparison between **Method-1** and **Method-2**, the functional unit is defined as 1 kg of polyglycerol isolated through each recycling process. In the evaluation of different end-of-life (EoL) scenarios, the functional unit is defined as 1 kg of NIPUF produced, used, and subsequently either disposed of or recycled, assuming equivalent performance characteristics and service life across all scenarios.

System boundaries. The comparative study between **Method-1** and **Method-2** adopts a cradle-to-gate life cycle assessment (LCA) approach, focusing on the recovery of small molecules, with the isolated compounds (e.g., polyglycerol and diamines) defined as the final products. The assessment encompasses environmental impacts associated with feedstock production, NIPUF synthesis, and hydrolytic chemical degradation. The use phase of NIPUFs is excluded from the system boundaries, as it does not involve significant energy or material consumption, nor does it generate emissions relevant to the selected impact categories [3]. In contrast, the comparative analysis of different EoL scenarios follows a cradle-to-grave LCA approach, as it evaluates the complete life cycle- including production, use, and final disposal or recycling and upcycling of NIPUF.

4 Life cycle inventory (LCI)

All synthesis inventories are made available in the following section to ensure reproducibility of the study.

4.1 Native NIPUF production

The native NIPUF was initially synthesized using TMPTC, EDR 148, water, and DBU at 100 °C for 3 h. Detailed experimental conditions are provided in chapter 3, section 2.3. The LCI for the synthesis process is summarized in **Table 5**, Section 4.2.1 of Chapter 4.

4.2 NIPUF recycling

4.2.1 Hydrolysis depolymerization of NIPUF and recovery of small molecules (Method-1)

The recycling and upcycling of NIPUFs based on **Method-1** is presented in chapter 3, section 2.4. The LCI of the whole process are presented in **Table 6**, section 4.2.2 of Chapter 4.

4.2.2 Hydrolysis depolymerization of NIPUF and recovery of small molecules (Method-2)

Following the use phase, NIPUF underwent a recycling process via hydrolysis in 1 M NaOH at 80 °C for 10 h. LCI for the hydrolysis process is presented in **Table 1**.

Table 1. Life cycle inventory of NIPUF hydrolysis process (modified procedure).

Hydrolysis of NIPUF (modified procedure)					
Process/product flow	**Unit**	**Input**	**Output**	**Database name**	**Geography**
NIPUF	g	7.1	-	NFM- NIPU foam	-
Water	g	150	-	Water, deionized, market for	Europe without Switzerland
Sodium hydroxide	g	6	-	Neutralizing agent, sodium hydroxide-equivalent, market for	RER
Electricity	kWh	0.015	-	Electricity, medium voltage, market for	BE
Hydrolyzed reaction mixture	g	-	163.1	NFM-Hydrolysis of NIPUF	BE

Upon completion of the decomposition, two primary products, polyglycerol (**PG**) with an isolated yield of 75% and diamine EDR 148 (isolated yields: 80%) were recovered through a multistep purification procedure (see Section 2.5 for details). LCI for the whole process is presented in **Table 2**. The solvents used for extraction and purification are considered to be fully recovered using electricity as energy input for solvent recovery process. To allocate the environmental burdens of the recycling process to the two recovered small molecules (**PG** and diamine), a mass allocation approach was applied. The allocation factors were calculated based on the isolated yields of each product (66% for **PG** and 34% for EDR 148).

Table 2. Life cycle inventory of recycled **PG** and diamine (modified procedure)

Recycled polyglycerol and diamine					
Process/product flow	**Unit**	**Input**	**Output**	**Database name**	**Geography**
Hydrolyzed reaction mixture	g	163.1	-	NF2M-Hydrolysis of NIPUF	-
Sulfuric acid	g	7.507	-	Sulfuric acid, market for	RER
Dichloromethane	g	133*	133*	Dichloromethane, market for	RER
Isopropanol	g	55*	55*	Isopropanol, market for	RER
Water	g	50*	200*2	Water, deionized, market for	Europe without Switzerland
Waste	g	-	11	Municipal solid waste, market for	BE
Electricity	kWh	0.18	-	Electricity, medium voltage, market for	BE
Recycled polyglycerol (**PG**)[a]	g	-	2.9	NFM-recycled polyglycerol	-
Recycled diamine [b]	g	-	1.55	NFM-Recycled diamine	-

* The solvents used for extraction and purification are considered to be fully recovered using electricity as energy input. *2 The total water output accounts for the sum of the water used during processing and the amount employed in the hydrolysis reaction which is recovered here. [a] mass allocation of 66%, and [b] mass allocation of 34%.

5 Results and discussion

5.1 Hydrolytic degradation of NIPUFs

As demonstrated in Chapter 3, water-induced self-blown NIPUFs (based on aliphatic and aromatic diamine) were successfully degraded under acidic and basic hydrolytic conditions. Specifically, degradation was achieved using 5 M NaOH at 80 °C for 10 h (basic hydrolysis), and 5 M H_2SO_4 at 80 °C for 8 h (acidic hydrolysis). Following depolymerization, the main degradation products- polyglycerol (**PG**) and diamines- were recovered via multistep isolation and purification. The recovered **PG** was subsequently converted into polyglycerol carbonate (**PGC**), enabling the synthesis of next-generation NIPU foams from recycled monomers.

Chapter 4 presented an LCA of this process, focusing on the basic hydrolysis of a representative NIPUF sample (based on aliphatic diamine-EDR). The results revealed that sodium hydroxide (NaOH) was a dominant contributor to the environmental impacts, particularly in categories such as global warming potential and human toxicity. Additionally, the use of sulfuric acid (H_2SO_4) for neutralization and high-boiling-point solvents (e.g., 1-butanol, toluene) during the isolation steps significantly increased the overall energy demand. These findings highlighted the need for process optimization to reduce the environmental burden of the chemical recycling route. By decreasing the concentration of NaOH from 5 M to 1 M, it was possible to achieve >98% degradation efficiency within 10 h at 80 °C for NIPUFs. This adjustment not only maintained high depolymerization yields but also substantially reduced chemical consumption and the associated life cycle impacts.

Following complete hydrolytic depolymerization of **NIPUF-A**, the resulting aqueous reaction mixture was subjected to sequential separation steps to isolate the two major degradation products: diamines and **PG** (**Fig. 3**). The solution was first filtered to remove any insoluble residues and unreacted foams. The clear filtrate was then concentrated to dryness under reduced pressure using a rotary evaporator. The resulting solid residue was treated with dichloromethane (DCM, 100 mL) and stirred at room temperature overnight to extract the amine-rich fraction. The DCM phase was separated by filtration, dried over anhydrous magnesium sulfate ($MgSO_4$), filtered again, and concentrated under reduced pressure to yield a light-yellow liquid. This fraction, attributed to the diamine product, was obtained in

approximately 80% isolated yield (1.55 g) and was characterized by both ^{1}H and ^{13}C NMR spectroscopy (see **Fig. S1-S2**).

The solid residue retained after amine extraction was then redissolved in Milli-Q water (50 mL). The solution was neutralized with concentrated sulfuric acid (96%) until reaching pH 6. Water was subsequently removed under reduced pressure to afford a crude solid, which was treated with isopropanol (iPrOH, 70 mL) and stirred at 60 °C overnight. Upon cooling to room temperature, the mixture was filtered to separate the iPrOH-soluble **PG** fraction. The organic phase was dried over anhydrous $MgSO_4$, filtered, and concentrated under reduced pressure. Insoluble salts (primarily NaCl) were discarded. **PG** was obtained as a sticky yellow solid in 75% isolated yield (~2.9 g), and its structure was confirmed by ^{1}H and ^{13}C NMR spectroscopy (see **Fig. S3-S4**).

This optimized isolation protocol enabled the efficient recovery and purification of both diamine and **PG** building blocks under mild conditions, with minimal solvent loss and high purity, supporting their subsequent reuse in the synthesis of second-generation NIPU foams.

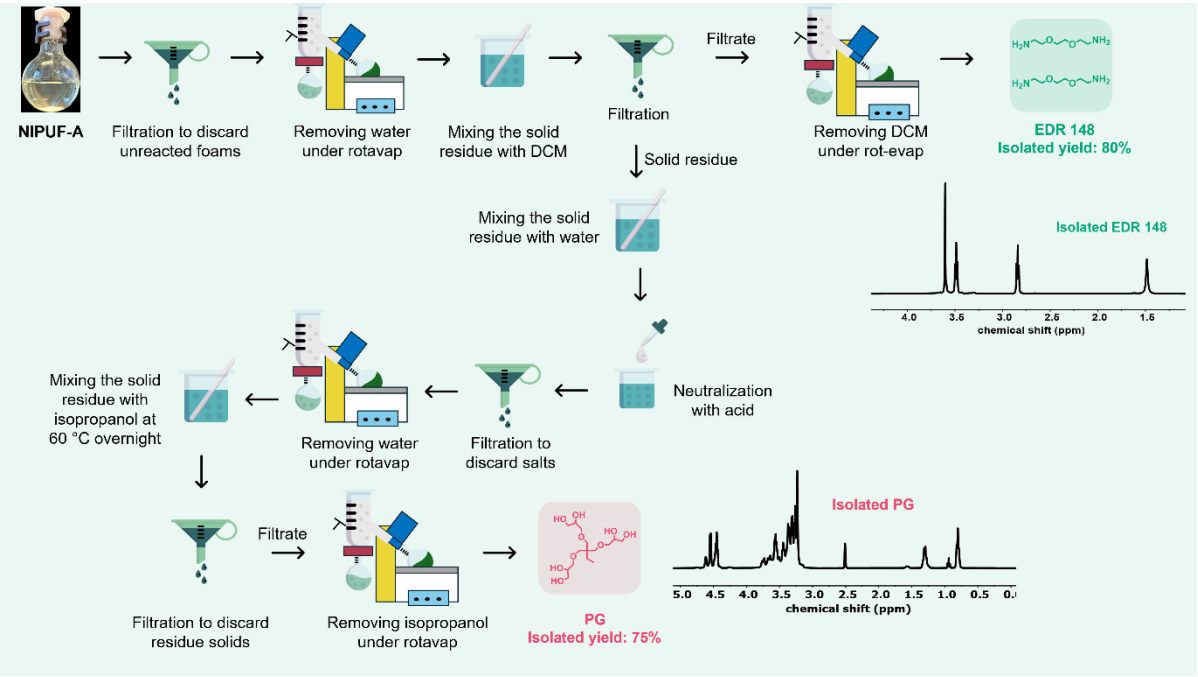

Fig. 3. Schematic representation of product isolation after depolymerization of **NIPUF-A**. The workflow comprises several steps of filtration, neutralization, phase extraction, solvent treatment, and final filtration and drying steps. The corresponding ^{1}H-NMR spectra are shown for **PG**, and recycled EDR 148 recorded at 400 MHz in DMSO-d_6. *Full signal assignments and integrations are provided in ESI (Fig. S1-S2 for EDR 148, and S3-S4 for **PG**).*

5.2 Life cycle impact assessment results

5.2.1 Comparative environmental assessment of two hydrolytic recycling methods for NIPUFs

Fig. 4 presents a comparative evaluation of two methods relative to the functional unit (which is 1 kg of **PG** product isolated). Each method involves alkaline hydrolysis of the native NIPUF, followed by isolation of the resulting small molecules. In **Method-1**, hydrolysis was performed using 5 M NaOH at 80 °C for 10 h. **Method-2** employed milder conditions- 1 M NaOH at 80 °C for 10 h-coupled with an optimized recovery protocol designed to minimize chemical consumption and waste generation (see sections 2.4 and 2.5 for more details). Notably, **Method-2** yielded a favorable environmental performance across all 16 impact categories evaluated. This improvement can be primarily attributed to the streamlined upstream chemical inputs- particularly the reduced use of base and catalyst-thereby decreasing both neutralization acid requirements and downstream waste. Additionally, in **Method-2**, the total energy demand across the isolation stages was reduced by approximately 40% relative to **Method-1**, further enhancing its sustainability profile.

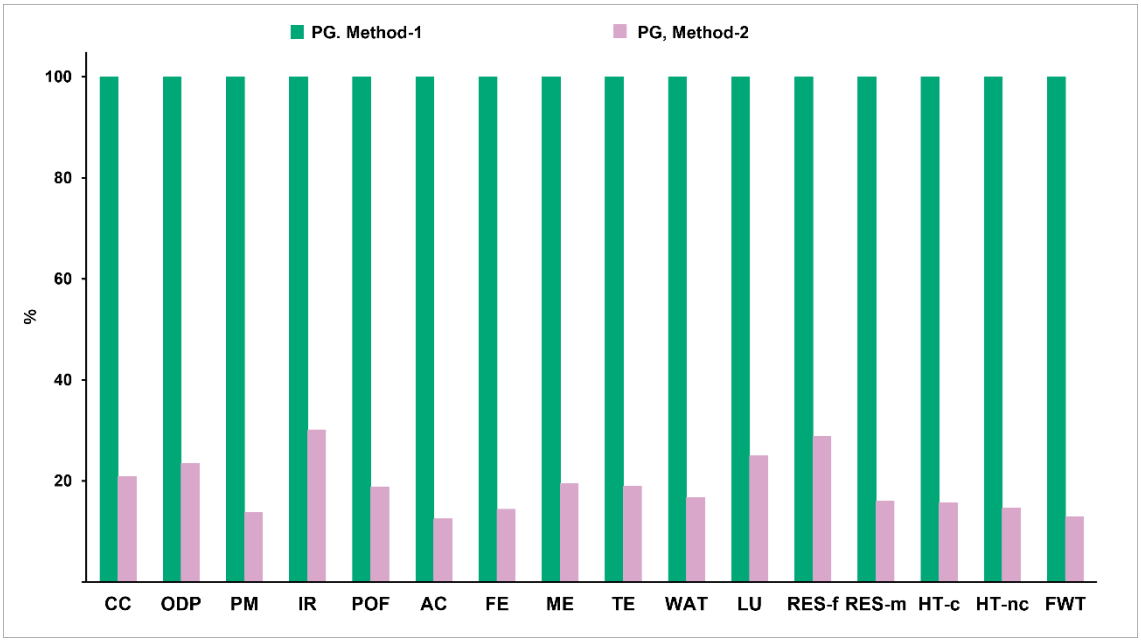

Fig. 4. LCA comparative cradle-to-gate impact assessment results in the production of 1 kg **PG** using **Method-1** and **Method-2.**

To quantify the cumulative relative environmental burdens of individual inputs throughout the recycling process of both methods, an aggregated contribution analysis was conducted, considering the production of 1 kg of **PG** as the functional unit (**Fig. 5**). This analysis accounted for all relevant material and energy flows- including electricity, chemicals, and solvents- across each subprocess involved in hydrolysis, isolation, and monomer recovery. The environmental contribution of each input was calculated by summing its impacts across all applicable stages. For example, the total electricity impact incorporated its consumption during heating, stirring, evaporation, and drying operations throughout the entire process chain. The focus was placed on the climate change impact category, which measures the global warming potential (GWP) of greenhouse gas (GHG) emissions- including carbon dioxide (CO_2), methane (CH_4), and nitrous oxide (N_2O)-expressed in kilograms of CO_2-equivalents. These emissions contribute to radiative forcing by trapping infrared radiation in the atmosphere, thereby accelerating global temperature rise and causing wide-ranging disruptions to ecosystems, public health, and infrastructure [4, 5].

As illustrated in **Fig. 5A**, the optimized process (**Method-2**) resulted in a reduction of over 60% in climate change impact associated with electricity consumption, compared to the initial process (**Method-1**). This improvement is primarily attributed to the replacement of high-boiling-point solvents (e.g., 1-butanol, toluene) with lower-boiling alternatives such as isopropanol, thereby substantially reducing the thermal energy required for solvent recovery. In addition, the concentration of sodium hydroxide (NaOH) was reduced fivefold in **Method-2**, leading to an 88% decrease in its contribution to the overall climate change impact (**Fig. 5B**). Although complete foam degradation was not achieved under these milder conditions, the residual undegraded fraction was negligible and had no meaningful effect on either recovery efficiency or environmental performance.

The reduced NaOH input also lowered the demand for sulfuric acid (H_2SO_4), which was previously required in stoichiometric amounts for neutralization. As a result, the climate change impact associated with acid usage decreased by 90% (**Fig. 5C**). Moreover, the overall consumption of reagents was significantly reduced, leading to a 90% decrease in impact associated with waste relative to **Method-1** (**Fig. 5D**). Collectively, these optimizations in **Method-2** translated into substantial environmental benefits, particularly in terms of climate change mitigation.

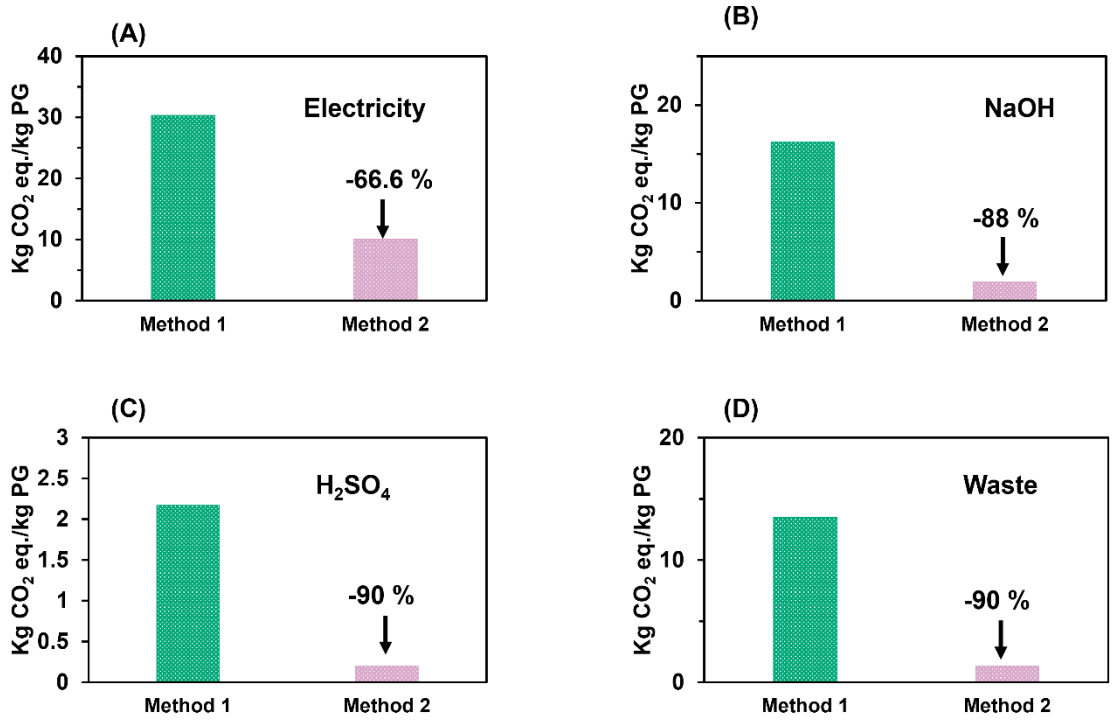

Fig. 5. Comparative contribution distribution in **Method-1** and **Method-2** for the Climate change environmental impact category showing four main hotspots of (A) electricity, (B) NaOH, (C) sulfuric acid, and (D) waste .The environmental impacts are associated with the production of 1 kg of **PG**. Unit: kg CO_2 equivalent (kg CO_2-eq).

5.2.2 Comparative study of NIPUF considering two EoL scenarios (recycling and incineration)

The comparative results of **Scenario-A** (green), **Scenario-B** (pink), and **Scenario-C** (blue) across 16 environmental impact categories are presented in **Fig. 6**. **Scenario-A** involves a single recycling step using recyclates obtained via **Method-1** to produce next-generation NIPUF, followed by incineration after use. Similarly, **Scenario-B** includes one recycling cycle using **Method-2** to produce NIPUF, which is also incinerated at end-of-life. In contrast, **Scenario-C** represents a conventional linear pathway without recycling, where NIPUF is produced and incinerated twice during the system lifespan. The results show that **Scenario-B** yields lower environmental impacts than **Scenario-A** across all categories but remains slightly more impactful than **Scenario-C**. Although the recycling and reprocessing steps in **Scenario-B** introduce additional environmental burdens, the differences with **Scenario-C** are relatively small in certain categories- such as marine eutrophication and freshwater ecotoxicity- ranging

from approximately 3% to 7%. These findings suggest that the process improvements in **Method-2**- namely, the reduced NaOH concentration and the use of a lower boiling point solvent- significantly contributed to lowering the environmental footprint, thereby advancing the recycling approach toward greater sustainability.

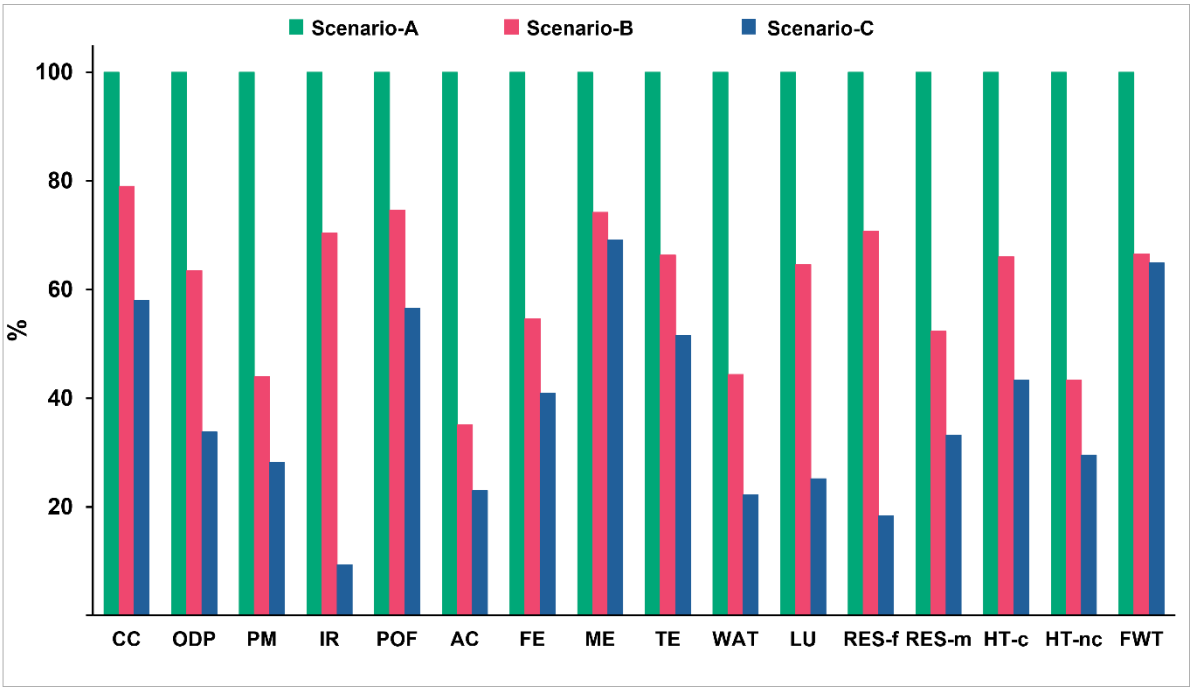

Fig. 6. LCA comparative cradle-to-grave impact assessment results for **Scenario-A** (which considers NIPUF recycling using **Method-1**), **Scenario-B** (which considers NIPUF recycling using **Method-2**-modified method), and **Scenario-C** (which considers no recycling).

6 Conclusion

This chapter demonstrates a practical and sustainability-driven approach to the chemical recycling of non-isocyanate polyurethane foams (NIPUFs) through hydrolytic depolymerization and recovery of valuable monomers. By integrating life cycle assessment (LCA) into the experimental workflow, environmental hotspots in the initial recycling method (**Method-1**) were identified- most notably the high impacts associated with sodium hydroxide usage, sulfuric acid during neutralization, solvent evaporation, and energy consumption.

Informed by these insights, a series of targeted process optimizations were implemented in **Method-2**. These included reducing the concentration of NaOH, replacing high-boiling-point solvents with lower-boiling alternatives, and minimizing reagent usage throughout the isolation

and purification steps. The resulting process not only maintained high yields of key building blocks- polyglycerol (75%) and diamines (80%)- but also achieved significant reductions in environmental burdens. Climate change impacts associated with electricity, NaOH, and H_2SO_4 were reduced by 60%, 88%, and 90%, respectively, while chemical waste impacts decreased by 90% compared to **Method-1**. The comparative cradle-to-gate LCA clearly illustrates the effectiveness of combining chemical innovation with environmental assessment to advance greener materials processing.

Moreover, the comparative study revealed that, under current laboratory conditions, the hydrolysis-based recycling and regeneration of NIPUFs using **Method-2** outperformed **Method-1** but did not surpass incineration in terms of overall environmental impact. Nevertheless, the research provides valuable insight into the environmental trade-offs associated with circular strategies for NIPUFs. Notably, the difference in environmental impact between **Method-2**-based recycling and regeneration and the conventional incineration pathway was substantially reduced- and even negligible in certain categories- highlighting a promising trajectory toward sustainability. This also underscores the potential for further optimization and improvement of recycling processes in future developments.

This research offers a model for developing closed-loop recycling strategies for NIPUs that are both technically feasible and environmentally optimized. The findings contribute to the broader goals of green chemistry and circular economy, reinforcing the importance of embedding sustainability metrics into the design and implementation of polymer recycling technologies.

7 References

1. Standard, I., *Environmental management-Life cycle assessment-Requirements and guidelines.* London: ISO, 2006.

2. Finkbeiner, M., et al., *The new international standards for life cycle assessment: ISO 14040 and ISO 14044.* The international journal of life cycle assessment, 2006. **11**: p. 80-85.

3. Jang, H., et al., *Comparative life cycle assessment of marine insulation materials.* Journal of Marine Science and Engineering, 2021. **9**(10): p. 1099.

4. Chomkhamsri, K., M.-A. Wolf, and R. Pant, *International reference life cycle data system (ILCD) handbook: Review schemes for life cycle assessment.* Towards life cycle sustainability management, 2011: p. 107-117.

5. Change, I.P.O.C., *Climate change 2007: the physical science basis.* Agenda, 2007. **6**(07): p. 333.

8 Supplementary information

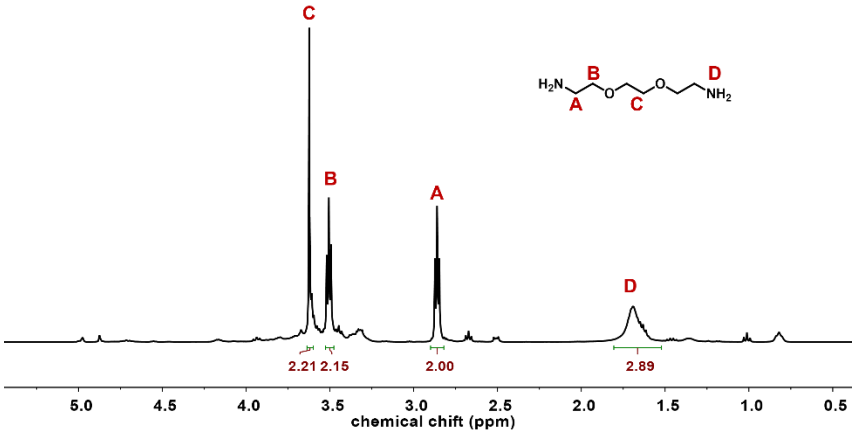

Fig. S1. ^{1}H-NMR spectrum of purified Recycled EDR 148 (400 MHz, DMSO-d_6).

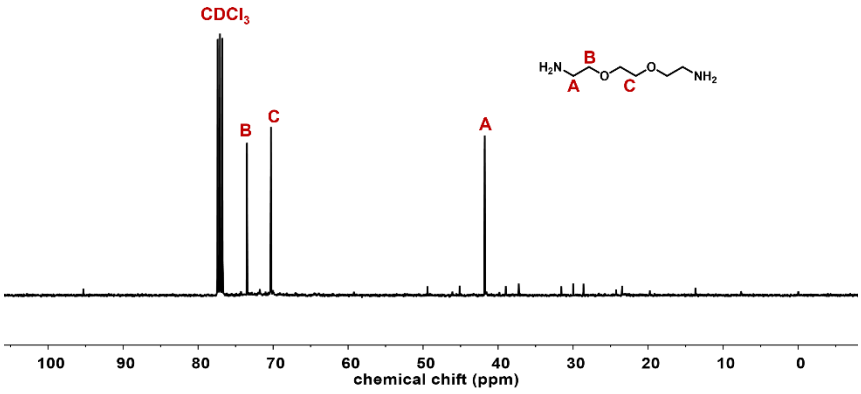

Fig. S2. ^{13}C-NMR spectrum of purified Recycled EDR 148 (100 MHz, DMSO-d_6).

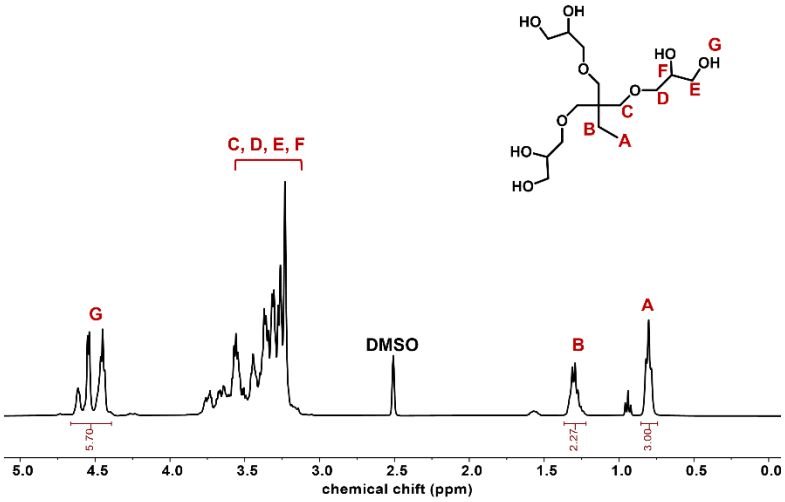

Fig. S3. ^{1}H-NMR spectrum of **PG** (400 MHz, DMSO-d_6).

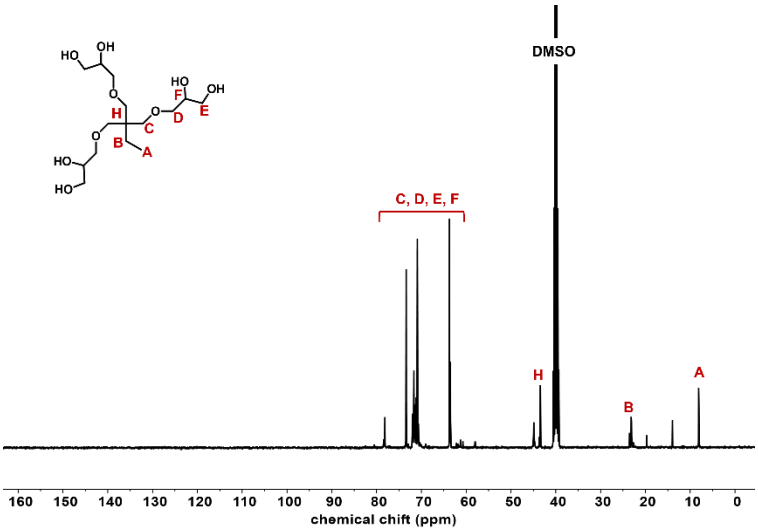

Fig. S4. ^{13}C-NMR spectrum of **PG** (100 MHz, DMSO-d_6)

Chapter 6. Conclusions and Perspectives

1 Conclusions

This thesis was driven by two growing concerns in the field of polyurethane (PU) science: the need to eliminate toxic isocyanates from polymer production, and the limited development of robust, scalable recycling strategies for non-isocyanate polyurethanes (NIPUs). In Chapter 1, we explained the concept of circular thinking (**Scheme 1**). While NIPUs have emerged as safer alternatives to conventional PUs- particularly due to their compatibility with CO_2-derived building blocks- most recycling efforts to date have focused on mechanical reprocessing using dynamic covalent bonds, which typically allow only a limited number of reuse cycles and result in progressive loss of material properties. In contrast, chemical recycling especially approaches that recover monomers or functional intermediates- holds greater potential for achieving material circularity. However, such strategies remain rare and technically challenging for NIPU systems. The central objective of this thesis was to develop and evaluate chemical recycling methods to produce NIPUs out of polymer waste that enable high degrees of material recovery and reintegration.

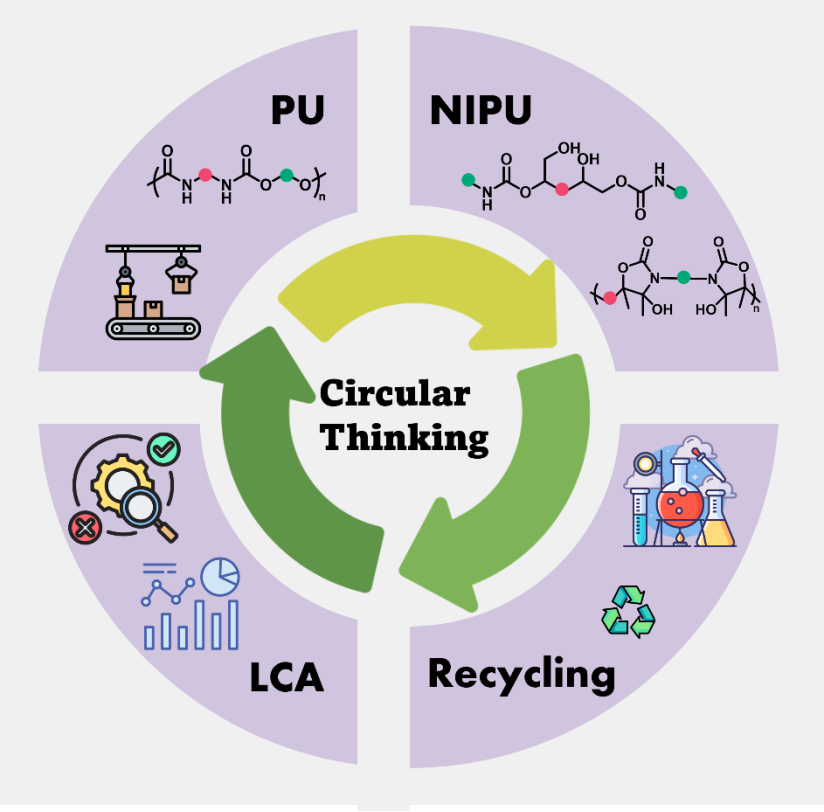

Scheme 1. Schematic representation of the main concepts discussed in Chapter 1.

The second chapter of this research focused on a novel class of NIPUs, namely polyoxazolidones (POxas), which feature cyclic urethane (cyclic carbamate) linkages and are recognized for their outstanding thermal stability (**Scheme 2**). These high-performance polymers were accessed through a sustainable and catalyst-free upcycling strategy using CO_2-based poly(oxo-carbonates) as precursors. Specifically, aminolysis of poly(oxo-carbonates) with allylamines at room temperature led to complete depolymerization and the formation of an allyl-functionalized bis(oxazolidone) monomer. This monomer was subsequently copolymerized with various dithiols via UV-initiated thiol-ene click chemistry, yielding poly(oxazolidone-*co*-thioether) copolymers with molecular weights of up to 101,000 $g \cdot mol^{-1}$. The incorporation of thioether linkages into the polymer backbone enabled extensive structural tunability and post-polymerization functionalization. The resulting materials exhibited excellent thermal properties, with $T_{deg,10\%}$ reaching up to 360 °C, and T_g tunable between 2 and 53 °C. Moreover, the poly(oxazolidone-*co*-thioether) copolymers could be further modified through a range of post-polymerization reactions. Thermal dehydration in the solid state (120–140 °C) generated exocyclic vinylene moieties; thiol oxidation led to sulfoxide or sulfone derivatives; and S-alkylation enabled the creation of water-soluble analogues- marking the first report of water-soluble polyoxazolidones. This work establishes a versatile and modular platform for the synthesis of functional POxa materials that are not accessible via traditional isocyanate chemistry. Importantly, it also illustrates a promising open-loop chemical recycling approach that transforms CO_2-derived waste polymers into advanced, structurally diverse NIPUs. By combining mild reaction conditions, tunable functionality, and strong environmental relevance, this strategy contributes to the development of next-generation sustainable polymer systems.

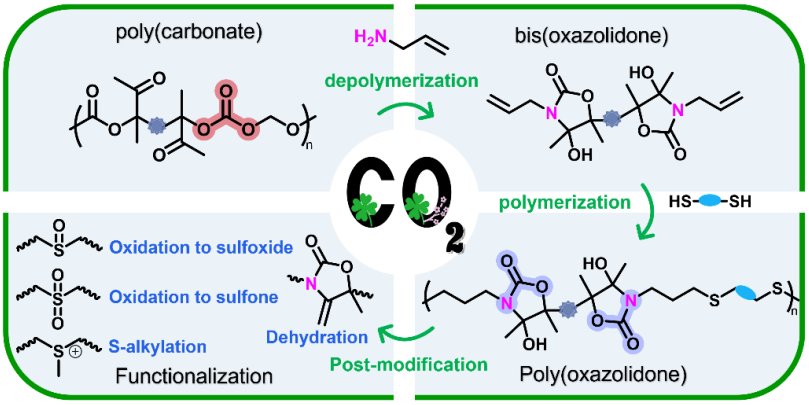

Scheme 2. General scheme showing the design of functional poly(oxazolidone)s through upcycling of polycarbonates (Chapter 2)

In the third chapter, attention turned to the chemical recycling of polyhydroxyurethane-type NIPU foams (NIPUFs) (**Scheme 3**). This study established a closed-loop strategy based on hydrolytic depolymerization under both acidic and alkaline conditions. Using 5 M NaOH/ 5 M H_2SO_4 at 80 °C, complete degradation of urethane linkages was achieved within 10 and 8 hours, respectively. FTIR and NMR analyses confirmed full cleavage of urethane bonds, and the two key building blocks- polyglycerol (PG) and diamines such as EDR-148 and XDA- were recovered with high purity and good yields. Notably, the depolymerization proceeded under significantly milder conditions than those required for conventional PU recycling, highlighting the intrinsic recyclability of these NIPUs. Recovered PG was further valorized via a two-step carbonylation process using dimethyl carbonate (DMC) and catalytic K_2CO_3, yielding polyglycerol carbonate (PGC) with a cyclic carbonate functionality of 1.9–2.1 (lower than the original TMPTC value of 2.64). Although foams prepared solely from PGC lacked sufficient crosslinking, blending PGC with TMPTC enabled the fabrication of second-generation recycled NIPUFs (r-NIPUFs) that matched the original materials in gel content, morphology, and thermal stability. These r-NIPUFs incorporated up to 63% recycled content, providing strong evidence that true chemical foam-to-foam recycling is achievable for this class of materials. Importantly, the use of DMC as a benign carbonylation agent contributes to the improved environmental profile of the recycling process. Altogether, this study provided a scalable platform for the recovery, purification, and reintegration of NIPU monomers, marking a key milestone in the transition toward circular PU materials.

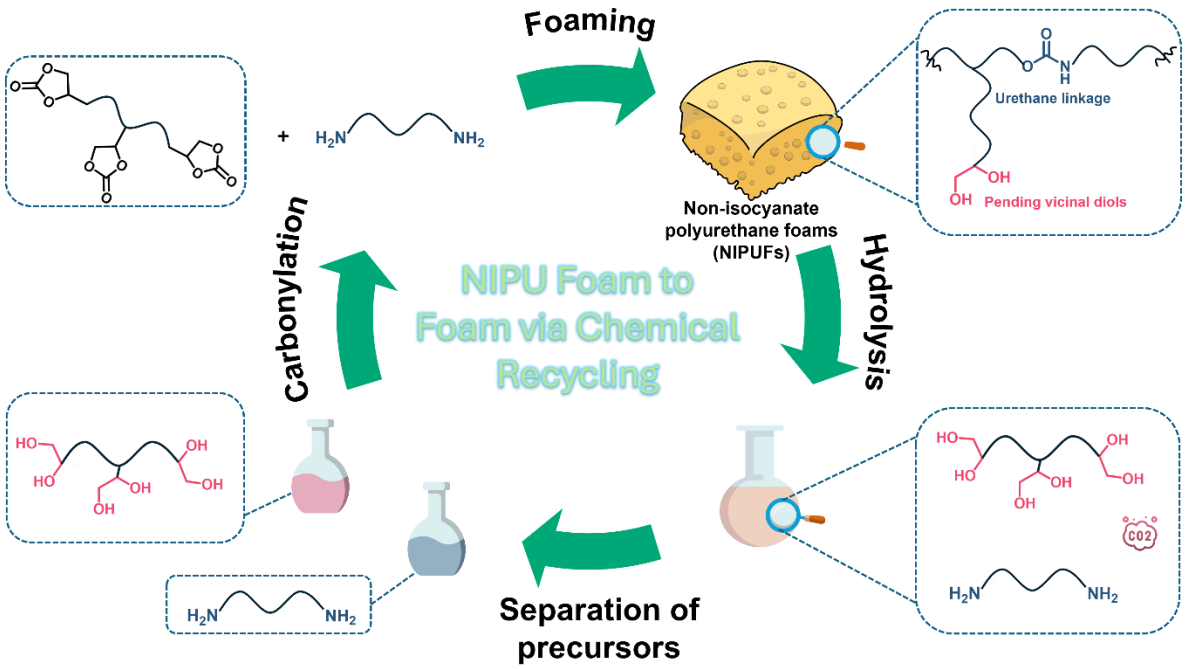

Scheme 3. General scheme showing showing NIPU foam to foam via hydrolytic chemical recycling (Chapter 3)

To evaluate the sustainability of this strategy, in the fourth chapter, a comprehensive cradle-to-grave life cycle assessment (LCA) was performed- one of the first to rigorously assess chemically recyclable NIPUFs based on experimentally validated depolymerization and regeneration pathways (**Scheme 4**). By integrating laboratory-scale data on hydrolysis and foam re-synthesis, the LCA provided a realistic and quantifiable picture of the environmental trade-offs in NIPUF circularity. The comparative results revealed that, under current laboratory conditions, the hydrolysis-based recycling route did not outperform incineration in all impact categories, including global warming potential, fossil resource use, and human toxicity. These drawbacks were mainly attributed to energy-intensive solvent recovery and reagent usage. A contribution analysis showed that electricity, sulfuric acid, sodium hydroxide, DMC, and waste generation were the main contributors to the environmental footprint of 1 kg of second-generation NIPUF. Meanwhile, sensitivity analyses revealed promising directions for improvement. For instance, using Norwegian electricity, sourced largely from renewables, significantly reduced the impacts in climate change and fossil depletion categories. Among tested neutralization agents, sulfuric acid was identified as the most environmentally favorable option. Although the current approach does not yet surpass conventional disposal routes in all impact categories, it offers valuable insights into how process conditions, reagent selection, and energy sourcing can strongly influence the sustainability profile of circular polymers. More importantly, the work illustrates that while innovative chemistry and recycling pathways can

enhance circularity, their true sustainability must be evaluated using systematic and quantifiable methods. As shown here, LCA remains an indispensable tool to navigate the complex trade-offs between material performance, environmental burden, and economic feasibility.

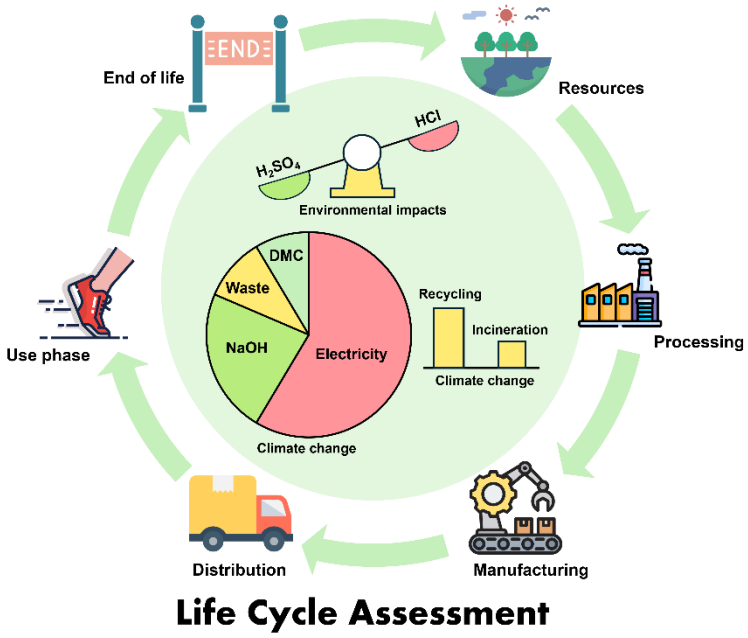

Scheme 4. General scheme showing Life cycle assessment of NIPU foam to foam chemical recycling (Chapter 4)

The insights gained through the LCA conducted in Chapter 4 were strategically applied in Chapter 5 to enhance the environmental performance of the NIPU foam recycling process (**Scheme 5**). This chapter underscores the value of coupling experimental optimization with environmental assessment to advance truly closed-loop recycling strategies. Building on the LCA findings, which identified critical environmental hotspots- including high electricity consumption, solvent evaporation, and the use of sodium hydroxide and sulfuric acid- a refined process was developed. This optimized workflow reduced chemical and energy inputs while maintaining high recovery yields of polyglycerol and diamines. The improved method resulted in significant reductions in environmental burdens, including up to 90% decreases in chemical waste and acid/base-related emissions in the climate change impact category. These outcomes clearly demonstrate that environmental and technical performance can be enhanced simultaneously. This work exemplifies how principles of green chemistry, when combined with systems-level evaluation, can guide the development of recycling strategies that are not only

effective but also environmentally sound. Overall, this chapter offers a compelling case for embedding sustainability thinking into the design and implementation of polymer recycling processes. It reinforces the broader vision of this thesis: that the realization of truly sustainable polymer materials depends not only on molecular innovation, but also on rigorous life cycle evaluation and continuous process improvement.

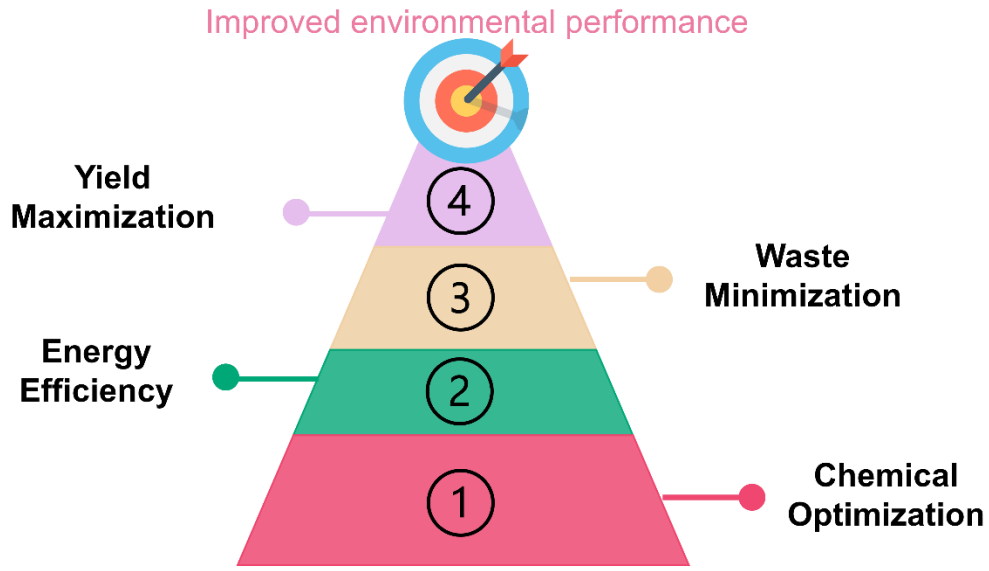

Scheme 5. General scheme showing strategies to enhance the environmental performance of the NIPU foam recycling process (Chapter 5)

In conclusion, this thesis delivers a holistic, experimentally grounded strategy for the design of NIPUs from recycling other polymers, closed-loop recycling, and sustainability assessment of NIPU foams. It demonstrates that isocyanate-free materials can be regenerated with high efficiency under mild conditions, while LCA-driven insights guide their optimization for minimal environmental impact. This integrative approach unites polymer synthesis, depolymerization, and systems-level analysis into a cohesive model for advancing truly sustainable materials.

2 Perspectives

2.1 Opportunities for future exploration- poly(oxazolidone)-based NIPUs

Although this study introduced a promising and modular route to functional poly(oxazolidone) materials through the upcycling of CO_2-based poly(oxo-carbonates), several opportunities remain open for further investigation. Notably, the chemical recyclability of the resulting poly(oxazolidone)s was not explored. Due to the inherent thermal and chemical stability of oxazolidone linkages, conventional urethane bond cleavage approaches are unlikely to be effective. However, in this work, we strategically introduced labile ester moieties within the polymer backbone to enable potential degradation pathways under selective conditions (**Scheme 6**). This opens the door to future studies aimed at developing depolymerization strategies tailored for otherwise robust POxa structures.

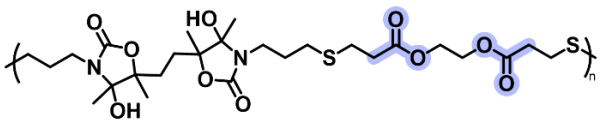

Scheme 6. Structure of poly(oxazolidone-*co*-thioether) containing ester linkage.

Moreover, we demonstrated that the synthesized copolymers could be selectively dehydrated to furnish exovinylene-functionalized poly(oxazolidone)s (**Scheme 7**). These unsaturated moieties offer a versatile platform for post-polymerization cross-linking, which may enable the formation of thermoset materials with tunable properties. The potential to create cross-linked networks from these POxa backbones could significantly broaden their application space, especially in areas demanding dimensional stability and solvent resistance, such as coatings, adhesives, or high-performance composites. Future efforts could capitalize on this functionality to explore network formation (for expample through cationic thiol-ene reaction), mechanical performance, and thermal behavior of these exovinylene-derived thermosets.

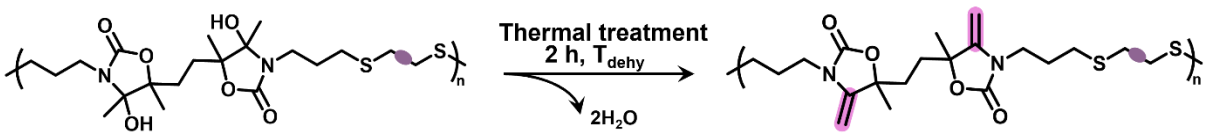

Scheme 7. Structure of poly(oxazolidone-*co*-thioether)s dehydration to furnish exovinylene-functionalized poly(oxazolidone)s.

In summary, while the current study established an effective upcycling route and outlined the structural tunability of POxa-based materials, further investigation into depolymerization pathways and functional applications-including thermoset fabrication and end-of-life scenarios- remains a rich area for future exploration.

2.2 Toward smarter design and greener regeneration pathways

Building upon the synthetic innovations of the first study, the following chapters demonstrated that complete chemical degradation of water-induced PHU-based NIPU foams is achievable under relatively mild acidic and basic conditions. This finding marks a significant step toward circularity for NIPU systems, as the urethane bonds were fully cleaved, enabling the recovery of both diamines and polyglycerol-based polyols. The integration of life cycle assessment (LCA) provided an additional layer of insight, identifying critical environmental hotspots such as energy use during isolation, solvent-intensive purification, and the consumption of sulfuric acid, sodium hydroxide, and dimethyl carbonate. These burdens guided process improvements in the final chapter, leading to higher yields and increased recycled content in regenerated foams.

Yet, despite these advances, several aspects remain ripe for optimization. From the synthesis aspect, a key distinction between NIPUFs and conventional PUFs lies in their hydrophilicity. Whereas conventional PUFs are relatively hydrophobic, NIPUFs readily absorb water due to their polar backbone. This susceptibility to hydroplasticization can lower compressive strength and long-term dimensional stability. Addressing this intrinsic feature will be crucial for the commercial success of NIPUFs. As formulation strategies evolve, mitigating water sensitivity will be central to positioning NIPUFs as viable and sustainable alternatives.

From the recycling aspect, compared to the depolymerization of conventional isocyanate-based PU foams- where spontaneous phase separation often simplifies the recovery of components- the hydrolysis of NIPUFs results in single-phase aqueous mixtures, necessitating complex and energy-intensive isolation steps. A promising future direction would be the rational design of NIPUFs that phase-separate upon degradation, for instance by tuning the polarity or

hydrophobicity of the building blocks, or by incorporating cleavable units that promote immiscibility. Such strategies could significantly reduce processing burdens and improve material recovery.

In addition, although encouraging yields of monomer recovery were achieved, we believe that further optimization of the isolation protocols could push the recovery rates of both polyglycerol and diamines beyond 90%, thereby enhancing the material circularity and resource efficiency of the process. These strategies could also be extended beyond the current formulation: exploring the depolymerization and regeneration of other classes of NIPUFs, synthesized from different carbonate or amine precursors, may offer new insights into structural influences on recyclability and regeneration performance.

Furthermore, the upcycling of polyglycerol into polyglycerol carbonate (PGC) remains a key area for further development (**Scheme 8**). While this transformation enabled the synthesis of second-generation NIPU foams, its current environmental footprint- primarily due to the use of dimethyl carbonate (DMC) and catalytic systems- was found to be higher than that of virgin TMPTC production. In addition, the resulting PGC exhibited a lower average cyclic carbonate functionality (approximately 2.0 CC groups per molecule) compared to TMPTC (2.65 CC groups per molecule), which limited its performance in foam formulations. Enhancing the cyclic carbonate content of PGC is therefore critical for improving the quality and sustainability of recycled NIPUs. Future research should explore strategies to increase carbonylation efficiency, such as the use of greener or bio-based catalysts, solvent-free processes, or optimized reaction conditions. These efforts would contribute to reducing the environmental burden of this crucial upcycling step and further close the loop in NIPU foam recycling.

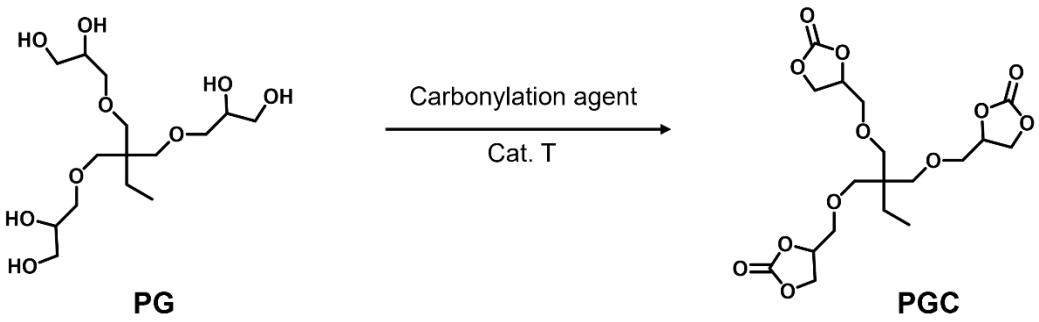

Scheme 8. Structure of polyglycerol and polyglycerol carbonates.

2.3 The role of metrics in designing truly sustainable polymers

While significant progress has been made in designing and regenerating NIPU foams through novel chemical pathways, it has become increasingly evident that performance alone is not a sufficient measure of sustainability. Durability, recyclability, and mechanical integrity are essential, but without a comprehensive understanding of the associated environmental impacts, such innovations risk falling short of their sustainability promise. This thesis has shown that LCA is an indispensable tool for navigating this complexity. It provides a quantitative framework to assess trade-offs between environmental burden and functional performance- bringing visibility to hidden costs such as solvent recovery, chemical usage, and energy sourcing.

The LCA developed in this work- one of the first cradle-to-grave assessments for NIPU foams based on experimentally validated recycling pathways- enabled data-driven process optimizations that enhanced both material yields and environmental performance.

Going forward, it is clear that future innovations in polymer science must integrate design-for-recyclability and quantitative sustainability analysis from the earliest stages of material development. Just as molecular structure influences degradation chemistry, process design and systems thinking must guide decisions on feedstock sourcing, synthetic routes, and end-of-life strategies. By embedding LCA into the research-development loop, we can move toward materials that are not only high-performing and recyclable but also optimized for minimal environmental impact across their entire life span.

2.4 Long-Term Vision

The vision that emerges from this work extends beyond polymer chemistry and material science. It points toward a future in which the design, use, and regeneration of materials are fully synchronized with environmental responsibility and circularity principles. We envision a next generation of NIPUs that are not only structurally advanced and high-performing, but also inherently designed for closed-loop lifecycles, leveraging smart molecular design, renewable feedstocks, and digitally integrated sustainability tools such as real-time LCA. By uniting molecular innovation with process engineering and systems-level thinking, the field can move

decisively toward the realization of a circular polymer economy- an economy where waste becomes resource, materials flow in regenerative cycles, and sustainability is embedded as a core criterion in every stage of polymer development.

At the same time, industrial translation requires further steps beyond the molecular design demonstrated here. A key priority will be the selection of monomers with low toxicity, thereby avoiding problematic amines or other hazardous intermediates, to ensure safe large-scale implementation. Moreover, the scaling-up of synthesis routes must address cost-efficiency, robustness under industrial processing conditions, and compatibility with existing PU manufacturing infrastructure. Finally, regulatory alignment and certification, coupled with partnerships between academia, industry, and policy makers, will be essential to accelerate adoption. In this sense, the present work should be viewed as an enabling step: it demonstrates the feasibility of greener NIPUs, while pointing clearly to the next challenges that must be solved before their widespread industrial uptake.

Dissemination & Communication

Parts of this thesis have been published or are intended for future publication. Below is a list of the related publications:

Razavi-Esfali, M., Habets, T., Siragusa, F., Grignard, B., Sardon, H. and Detrembleur, C., 2024. Design of functional isocyanate-free poly (oxazolidone) s under mild conditions. Polymer Chemistry, 15(19), pp.1962-1974.

Furthermore, these works are submitted or programmed to be submitted in the near future.

Razavi-Esfali, M., Talon, O., Ximenis. M., Perli, G. Grignard, B., Sardon, H. and Detrembleur. Closed-Loop Recycling of Non-Isocyanate Polyurethane Foams: Process Optimization and Environmental Evaluation via LCA

Acid-Catalyzed and In Situ Functionalization of CO_2-Derived Foams with High Mechanical Performance. Gabriel Perli, Guillem Seychal, Maliheh Razavi-Esfali, Lucas Polo, Bruno De Almeida Piscelli, Rodrigo Cormanich, Xabier Pariza, Jon Aystaran, Christhophe Detrembleur, Bruno Grignard, Haritz Sardon

Participation in the congress.

Recycling and Upcycling of Non-isocyanate Polyurethanes by Chemical and Mechanical Approaches, GEP-SLAP conference, San sebastian, Spain, May 8-12 2022, (Poster presentation), **won the best poster prize**.

Facile Synthesis of Functional Poly(oxazolidone)s via Thiol-ene Click Polymerization, Annual meeting of the Belgian polymer group (BPG 2024), Blankenberg, Belgium, May 30-31 2024, (Oral presentation), **won the best oral presentation prize**.

Facile synthesis of oxazolidone-containing polymers with high molar mass and tunable properties via thiol-ene click polymerization, IUPAC 2024, Warwick, UK, July 1-4, (Oral presentation).

Poly(oxazolidone-thioether) copolymers with tunable properties prepared from upcycling of CO_2-based polycarbonates, Department day, University of Liege, Liege, Belgium, 30 June 2022, (Poster presentation).

Construction poly(oxazolidones) from recycling and upcycling of polycarbonates, PhD day, UPV/EHU, Donistia (San Sebastian), Spain, 19 April 2024, (Poster presentation)